SYNER-G: Typology Definition and Fragility Functions for Physical Elements at Seismic Risk

GEOTECHNICAL, GEOLOGICAL AND EARTHQUAKE ENGINEERING

Volume 27

For further volumes:
http://www.springer.com/series/6011

K. Pitilakis • H. Crowley • A.M. Kaynia
Editors

SYNER-G: Typology Definition and Fragility Functions for Physical Elements at Seismic Risk

Buildings, Lifelines, Transportation Networks and Critical Facilities

Springer

Editors
K. Pitilakis
Department of Civil Engineering
Aristotle University
Thessaloniki, Greece

H. Crowley
European Centre for Training and Research
in Earthquake Engineering (EUCENTRE)
Pavia, Italy

A.M. Kaynia
Norwegian Geotechnical Institute (NGI)
Oslo, Norway

Department of Structural Engineering
Norwegian University of Science
and Technology (NTNU)
Trondheim, Norway

Additional material can be downloaded from http://extras.springer.com

ISBN 978-94-024-0690-0 ISBN 978-94-007-7872-6 (eBook)
DOI 10.1007/978-94-007-7872-6
Springer Dordrecht Heidelberg New York London

Preface

Modern societies and economies become more complex and at the same time more sophisticated. Still, the experience from earthquakes reveals that even the developed societies are quite vulnerable, although the provisions against seismic hazards have been considerably improved. Their exposure to seismic risk in prone seismic areas rely on an *integrated seismic risk approach*, which should define accurately the physical seismic risk and the socio-economic vulnerability and resilience. *Physical seismic risk* is defined with the probability of damages and loss to structures and people due to an earthquake of any intensity. *Socio-economic vulnerability* is the expected impact of a given earthquake on the society and the economy. *Resilience* is the capacity of a society and economy to cope with earthquake events. The physical risk assessment depends on the *seismic hazard*, which expresses the probability of ground shaking and induced phenomena i.e. liquefaction, fault crossing, landslides due to earthquakes, the *exposure* of the different assets and the *physical vulnerability* of the exposed elements at risk, which is the vulnerability of structures, their occupants and services to seismic hazard.

A critical component of this chain of seismic risk assessment is the definition and evaluation of the so-called *fragility functions* or *fragility curves*. They provide the necessary link between seismic hazard assessment at a site and the corresponding effects on any kind of exposed structures i.e. buildings, infrastructures, utilities, lifelines and industrial facilities. The majority of currently available approaches to assess the potential losses for a wide group of exposed elements rely on the availability of relevant fragility curves. In the past decades, the field of seismic risk assessment has witnessed remarkable developments.

SYNER-G is a research project funded by European Commission in the frame of FP7 Theme 6: Environment. The objective of SYNER-G is to develop an integrated methodology and the necessary tools for the systemic seismic vulnerability and risk analysis of complex systems exposed to earthquake hazard, like buildings, and aggregates in urban scale, lifelines, transportation and utility networks, gas and electric power systems, critical facilities, and infrastructures. Interactions between different components and systems are considered in the analysis, as they may increase considerably the global vulnerability and risk of the systems or the system

of systems. SYNER-G methodology encompasses in an integrated way all aspects in the chain, from hazard to the physical vulnerability and loss assessment of components and systems and to the socio-economic impacts of earthquakes, accounting for all relevant uncertainties within an efficient quantitative simulation scheme, modeling interactions between the multiple components and systems.

In the frame of this large collaborative project, an extensive literature review of fragility functions for all elements at risk has been made. Based on a new taxonomy and typology that considers the distinctive European features, existing fragility curves and associated uncertainties have been critically reviewed and new or existing fragility curves have been proposed.

The book presents in a comprehensive way the latest developments on the fragility functions encompassing the work done in SYNER-G and in some other parallel projects, as for example in case of masonry buildings. It is organized in several chapters devoted to different systems. For each system, the new taxonomy and classification scheme is presented and then, after a review of the existing fragility functions, the most relevant fragility functions, new ones and selected from the international literature, for the different components are highlighted. Uncertainties are discussed throughout the book and in particular at the beginning, where the framework of the treatment of uncertainties in view of the construction of fragility functions is outlined. Recommendations are also provided for the selection of the most adequate fragility functions. A special tool has been also developed in the frame of SYNER-G to store, visualize and manage a large number of fragility function sets. The tool can store functions for a wide range of elements at risk, and has features that allow these functions to be harmonized in terms of intensity measure type and limit state. The tool is provided, together with a collection of European fragility functions for buildings, as an electronic supplement to this book (extras.springer.com).

The ambition is to offer to the European and international scientific and engineering community a standard reference book of the present state of the art in fragility models for the seismic risk analysis of most elements at risk, and at the same time to highlight the remaining gaps and the necessary future developments on this important topic. The present book is the first of the two volumes that present the main achievements and results of SYNER-G. The second one entitled *Systemic Seismic Vulnerability and Risk Assessment of Complex Urban*, *Utility*, *Lifeline Systems and Critical Facilities. Methodology and Applications*, demonstrates the integrated methodological framework of SYNER-G, which is applied in selected case studies, also using fragility curves that are included in the present book.

The Editor would like to acknowledge the contributors to the individual chapters who are listed under each chapter. Most of them actively participated in SYNER-G. In particular special acknowledgement to Sergio Lagomarsino, Serena Cattari, Tiziana Rossetto and Dina D'Ayala, who without being partners in SYNER-G accepted the invitation to contribute to this volume.

Finally, the support of the two co-editors, Helen Crowley and Amir M. Kaynia, and in particular the devotion and hard work of Dr. Sotiris Argyroudis to the preparation of this volume is gratefully acknowledged.

Thessaloniki, Greece K. Pitilakis

Contents

1 Introduction 1
Kyriazis Pitilakis, Helen Crowley, and Amir M. Kaynia

2 Modeling and Propagation of Uncertainties 29
Paolo Emilio Pinto

3 Evaluation of Existing Fragility Curves 47
Tiziana Rossetto, Dina D'Ayala, Ioanna Ioannou, and Abdelghani Meslem

4 Epistemic Uncertainty in Fragility Functions for European RC Buildings 95
Helen Crowley, Miriam Colombi, and Vitor Silva

5 Fragility Functions of Masonry Buildings 111
Sergio Lagomarsino and Serena Cattari

6 Fragility Functions of Electric Power Stations 157
Francesco Cavalieri, Paolo Franchin, and Paolo Emilio Pinto

7 Fragility Functions of Gas and Oil Networks 187
Pierre Gehl, Nicolas Desramaut, Arnaud Réveillère, and Hormoz Modaressi

8 Fragility Functions of Water and Waste-Water Systems 221
Kalliopi Kakderi and Sotiris Argyroudis

9 Fragility Functions of Road and Railway Bridges 259
Georgios Tsionis and Michael N. Fardis

10 Fragility Functions of Highway and Railway Infrastructure 299
Sotiris Argyroudis and Amir M. Kaynia

11 Fragility Functions of Harbor Elements 327
Kalliopi Kakderi and Kyriazis Pitilakis

12 Component Fragilities and System Performance of Health Care Facilities 357
Alessio Lupoi, Francesco Cavalieri, and Paolo Franchin

13 Fragility Function Manager Tool 385
Vitor Silva, Helen Crowley, and Miriam Colombi

14 Recommendations for Future Directions in Fragility Function Research 403
Kyriazis Pitilakis and Helen Crowley

Subject Index 415

List of Acronyms

AC	Asbestos cement
AC	Alternating current
BCL	Bars-connecting line
BDG	Buildings
BN	Bayesian networks
BS	Bar systems
C	Concrete
CI	Cast iron
CIDH	Cast-in-drilled-holes
CCD	Central composite design
CoV	Coefficient of variation
CSM	Capacity spectrum method
DBV	Displacement based vulnerability
DI	Ductile iron
DM	Damage state
DS	Damage state
DVE	Damage value
EC2	Eurocode 2
EC8	Eurocode 8
EDP	Engineering demand parameter
EMS98	European Macroseismic Scale
EPN	Electric power network
EPG	Emergency power generator
EQL	Equivalent linear analysis
FE	Finite element
FFM	Fragility function manager
ffs	Fragility function set
FS	Factor of safety
FOSM	First order second moment method
GEM	Global earthquake model
GMICEs	Ground motion to intensity conversion equations

GMPE	Ground motion prediction equations
GIS	Geographical information systems
GMPGV	Geometric mean of PGV
HDPE	High density polyethylene
IDA	Incremental dynamic analysis
IGMCEs	Intensity to ground motion conversion equations
IM	Intensity measure
IML	Intensity measure level
IMT	Intensity measure type
ISDR	Inter-story drift ratio
IO	Immediate Occupancy
JMA	Japan Meteorological Agency
LHS	Latin hypercube sampling
LN	Lognormal
LS	Limit state
MBSR	Matrix-based system reliability methods
MC	Monte Carlo
MCS	Mercalli-Cancani-Sieberg intensity scale
MDOF	Multi degree of freedom
MDPE	Medium density polyethylene
MMI	Modified Mercalli intensity
MSK81	Medvedev-Sponheuer-Karnik Intensity Scale
MV-LV	Medium voltage – low voltage
MRI	Mean return interval
NDA	Nonlinear dynamic analysis
NSA	Nonlinear static analysis
NLTHA	Non-linear time history analysis
OLE	Operating level earthquake
PBVA	Performance based vulnerability assessment
PI	Performance indicator
PGA	Peak ground acceleration
PGD	Permanent ground deformation
PGV	Peak ground velocity
PGS	Peak ground strain
PE	Polyethylene
PLS	Performance limit states
POSA	Push over static analysis
PSI	Parameterless scale of intensity
PVC	Polyvinyl chloride
RC or R/C	Reinforced concrete
RMS	Root mean square of the acceleration
SCADA	Supervisory control and data acquisition
SDOF	Single degree of freedom
SM	Simplified method

SSWP	Strong spandrels weak piers
TGD	Transient ground deformation
ULS	Ultimate limit state
UPS	Uninterruptible power system
WS	Welded steel
WSSP	Weak spandrels strong piers
WSAWJ	Welded-steel arc-welded joints
WSCJ	Welded-steel caulked joints
WSGWJ	Welded-steel gas-welded joints

List of Symbols

A_u	Ultimate spectral acceleration
A_y	Spectral acceleration at yielding
ASI	Acceleration spectrum intensity
C_i	Capacity of RC structural elements
C	Number of casualties as percentage of the population
C_{YY}	Covariance matrix
CL	Connectivity loss
Γ_X	Participation factor of the equivalent SDOF system
D_{YY}	Standard deviation matrix
D	Displacement
D_{LS}	Limit state threshold of displacement
D_u	Ultimate spectral displacement
D_y	Spectral displacement at yielding
DI	Damage index
DV	Vector of decision variables
DM	Vector of random damage measures
E	Modulus of elasticity
G	Shear modulus
G_o	Initial shear modulus
HTC	Hospital treatment capacity
HTD	Hospital treatment demand
I	Macroseismic intensity
IM	Intensity measure
IM_{LS}	Median value of the lognormal distribution of the intensity measure im_{LS} that produces the LS threshold
IQR	The inter-quartile range of the normal distribution
K	Corrective factor
K_1	Corrective factor
K_2	Corrective factor
L	Length
M	Bending moment

M_{Rd}	Design value of bending moment capacity
N	Axial force
N	Number of stories
N_{T1+T2}	Number of severely injured people
N_{T3}	Number of lightly injured people
N_{T4}	Number of deaths
N_{cas}	Total number of casualties
N_{pop}	Population
$P(\cdot)$	Probability
Q	Ductility index
R_{YY}	Correlation matrix
RR	Repair rate
R^2	Coefficient of determination
S_1	Medical severity index
S_2	Injuries severity index
S_a	Spectral acceleration
$S_a(T)$	Spectral acceleration at period T
$S_d(T)$	Spectral displacement at period T
SI	Spectrum intensity
T	Period
T_e	Elastic fundamental-mode period
T_{LS}	Inelastic period corresponding to a specific limit state
T_y	Elastic period
$T_{1.0}$	1-second period
V	Vulnerability index
V_{s30}	Shear wave velocity in the upper 30 m of the soil profile
V_s	Shear wave velocity
X	Vector of probabilistically qualified random quantities
c	Apparent wave propagation velocity
c_v	Coefficient of variation
h	Height
f_{cm}	Mean material strength for concrete
f_{ym}	Mean material strength for steel
f_X	Base shear at ground floor for unity gross area
k	Parameter in casualties model
k_y	Yield acceleration coefficient
m	Median of normal distribution
m_X^*	Equivalent mass of the equivalent SDOF system
q	Behaviour factor
t_m	Mean duration of a surgical operation
v_p	Peak horizontal particle velocity
Δ	Drift
Φ	Standard cumulative probability function
α	Factor accounting for the efficiency of the hospital emergency plan

α_g	Peak ground acceleration
β	Standard deviation of lognormal distribution
β	Factor accounting for the quality, training and preparation of hospital operators
β_{tot}	Total standard deviation or total uncertainty
β_C	Uncertainty in capacity
β_D	Uncertainty in demand
β_{ME}	Dispersion in mechanical parameters
β_{GE}	Dispersion in geometric parameters
β_{ST}	Dispersion in structural detailing
β_{MO}	Dispersion in numerical modeling
β_{RE}	Dispersion in record to record
β_a	Dispersion in attenuation laws
β_{LS}	Dispersion of the LS
β_H	Uncertainty in the derivation of the hazard curve
β_T	Uncertainty in the definition of the Limit State threshold
γ	Shear strain
γ_1	Number of functioning operating theatres
γ_2	System-survival Boolean function
γ_c	Unit weight of concrete
γ_m	Partial safety factor for the resistance
δ	Displacement
$\varepsilon_{q,d}$	Design shear strain due to translational movements
$\varepsilon_{t,d}$	Total nominal design strain
ε_c	Error in element capacity model
ε_{cas}	Error in casualties model
ζ	Factor accounting for the proportion of patients that require surgical attention
$\eta(\xi_{LS})$	Damping correction factor
θ	Rotation
θ_{max}	Maximum interstory drift ratio
λ	Logarithmic mean
μ	Median value
μ_D	Mean damage grade
ξ_0	Initial damping
ξ_H	Maximum hysteretic damping
σ_X	Average vertical compressive stress at the middle height of the first level masonry piers
τ_X	Masonry shear strength at the ground level
φ	Curvature

Chapter 1
Introduction

Kyriazis Pitilakis, Helen Crowley, and Amir M. Kaynia

Abstract This chapter outlines the main components, parameters and methods to derive fragility functions, which can be used in seismic risk assessment of different engineering systems and components at urban and regional scale. It provides the means of understanding the main factors governing this topic, introducing the subjects that will be extensively described and discussed in the subsequent chapters, where the fragility curves for buildings and all important components of the systems and infrastructures will be described in detail.

1.1 Background

Seismic risk assessment can be defined is the estimation of the probability of expected damages and losses due to seismic hazards. The majority of currently available approaches to assess the potential losses for a wide group of exposed elements rely on the availability of relevant fragility curves. In the past decades, the field of seismic risk assessment has witnessed remarkable developments. A detailed

K. Pitilakis (✉)
Department of Civil Engineering, Aristotle University, P.O.Box. 424,
54124 Thessaloniki, Greece
e-mail: kpitilak@civil.auth.gr

H. Crowley
European Centre for Training and Research in Earthquake Engineering (EUCENTRE),
Via Ferrata 1, 27100 Pavia, Italy
e-mail: helen.crowley@eucentre.it

A.M. Kaynia
Norwegian Geotechnical Institute (NGI), Ullevål Stadion, N-0806,
P.O. Box. 3930 Oslo, Norway

Department of Structural Engineering, Norwegian University of Science
and Technology (NTNU), 7491 Trondheim, Norway
e-mail: Amir.M.Kaynia@ngi.no

K. Pitilakis et al. (eds.), *SYNER-G: Typology Definition and Fragility Functions for Physical Elements at Seismic Risk*, Geotechnical, Geological and Earthquake Engineering 27,
DOI 10.1007/978-94-007-7872-6_1,

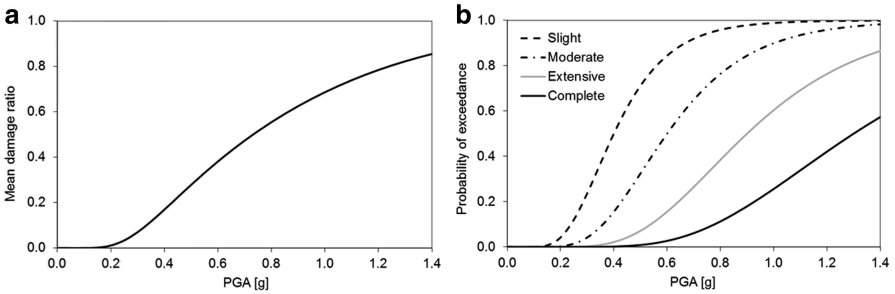

Fig. 1.1 Examples of (**a**) vulnerability function and (**b**) fragility function

review of this subject is presented among others in the state-of-the-art paper by Calvi et al. (2006). The level of vulnerability of a structure is described in all engineering-relevant approaches using vulnerability functions and/or fragility functions.

There are a number of definitions of vulnerability and fragility functions; one of these describes vulnerability functions as the probability of losses (such as social or economic losses) given a level of ground shaking, whereas fragility functions provide the probability of exceeding different limit states (such as physical damage or injury levels) given a level of ground shaking. Figure 1.1 shows examples of vulnerability and fragility functions. The former relates the level of ground shaking with the mean damage ratio (e.g. ratio of cost of repair to cost of replacement) and the latter relates the level of ground motion with the probability of exceeding the limit states. Vulnerability functions can be derived from fragility functions using consequence functions, which describe the probability of loss, conditional on the damage state.

Fragility curves constitute one of the key elements of seismic risk assessment. They relate the seismic intensity to the probability of reaching or exceeding a level of damage (e.g. minor, moderate, extensive, collapse) for the elements at risk. The level of shaking can be quantified using different earthquake intensity parameters, including peak ground acceleration/velocity/displacement, spectral acceleration, spectral velocity or spectral displacement. They are often described by a lognormal probability distribution function as in Eq. 1.1, although it is noted that this distribution may not always be the best fit.

$$P_f\left(ds \geq ds_i | IM\right) = \Phi\left[\frac{1}{\beta_{tot}} \cdot \ln\left(\frac{IM}{IM_{mi}}\right)\right] \tag{1.1}$$

where $P_f(\cdot)$ denotes the probability of being at or exceeding a particular damage state, DS, for a given seismic intensity level defined by the earthquake intensity measure, IM (e.g. peak ground acceleration, PGA), Φ is the standard cumulative probability function, IM_{mi} is the median threshold value of the earthquake intensity measure IM required to cause the i_{th} damage state and β_{tot} is the total standard

deviation. Therefore, the development of fragility curves according to Eq. 1.1 requires the definition of two parameters, IM_{mi} and β_{tot}.

The development of fragility functions for seismic risk assessment is a fairly new subject as it started in the early 90s. Following the 1971 San Fernando earthquake in USA, where catastrophic damages observed in almost every type of lifeline, many efforts were launched to better understand the causes of the seismic failures and identify ways to mitigate future earthquake damages and losses. Major earthquakes that followed, such as the 1985 Mexico, 1989 Loma Prieta, 1994 Northridge, 1995 Kobe, 1999 Chi-Chi and Turkey, and more recently the 2010 Chile, 2011 New Zealand and Tohoku events, revealed important lessons for developing new methods for estimating risk and reducing potential losses.

HAZUS (NIBS 2004) is the first comprehensive methodology that contains models for estimating potential losses from natural hazards. It is implemented in the geographic information system platform (GIS) developed by the Federal Emergency Management Agency (FEMA). Its first edition was released in 1997 (HAZUS 97); the current version is HAZUS-MH v2.0, which estimates the risk due to earthquakes, floods and hurricanes. Fragility curves for buildings, utility and transportation networks are provided in HAZUS methodology. In the first editions, the majority of the fragility functions were relied on the methodology and data that were presented in ATC-13 (ATC 1985) and ATC-25 (ATC 1991) reports following an expert judgement approach. Analytical studies have been later considered for bridges and buildings.

Another important effort for reducing risks to lifelines from hazards initiated in 1998 by American Lifelines Alliance, a public-private partnership. Guidelines and fragility curves for seismic hazard are provided for lifeline components such as for water systems (ALA 2001), telecommunication or electric power facilities. Other major projects in the US include the PEER lifelines program, which has the objective of improving seismic safety and reliability of lifeline systems, primarily funded by the California Department of Transportation and the Pacific Gas & Electric Company. Also, the MCEER's Highway Project with the overall aim of improving the seismic performance and reliability of the national highway system, was initiated in the fall of 1992 under Federal Highway Administration (FHWA) funds. Finally, the Mid-America Earthquake (MAE) Center and the National Center for Supercomputing Applications (NCSA) developed MAEviz platform which is an open-source software that integrates spatial information, data and visual information to perform risk assessment and analysis (MAEviz; Mid-America Earthquake Center 2009).

In Europe, the first initiative to establish a methodology for the seismic risk assessment of buildings and lifeline elements include the RISK-UE (2004) project followed by LESSLOSS (2007) both funded by European Commission framework programmes for Research and Technological Development. Fragility curves for buildings and some lifeline components were proposed by establishing a new taxonomy appropriate for the European context.

Several research efforts have been made at a national level in Europe, aiming to propose adequate fragility curves for buildings, lifeline and transportation

infrastructure. Representative examples include the SRM-LIFE (2007) and AsProGe (2007) projects in Greece, and the RELUIS projects in Italy. Finally, numerous other research efforts have been performed worldwide, developing fragility functions and methods for the vulnerability assessment of different physical assets.

Among the latest developments is SYNER-G (2013). The following section gives an overview of this model, and specific details are presented in the other chapters of this book.

1.2 The SYNER-G Project

SYNER-G is a European collaborative research project funded by the European Commission in the Seventh Framework Program, Theme 6: Environment. The main objective of SYNER-G is to develop an integrated methodology for the systemic seismic vulnerability and risk analysis of buildings, lifelines, infrastructures, transportation and utility systems and critical facilities, taking into account the interactions between the different components and systems, which generally increase the seismic impact. SYNER-G developed an innovative framework to assess the physical and socio-economic seismic vulnerability and risk at urban and regional level (Franchin 2013). The complex systems within the urban or regional fabric were modeled according to a detailed taxonomy, grouped into the following categories: buildings, transportation and utility networks, and critical facilities (Hancilar and Taucer 2013). Each category may have several types of components and systems; for example, a road system comprises bridges, tunnels, road embankments, etc.

The framework encompasses in an integrated way all aspects in the chain, from hazard to the physical damage assessment of components and systems to the socio-economic impacts of an earthquake, accounting for all relevant uncertainties within an efficient quantitative simulation scheme. The most innovative part of the project is the modeling of interactions between the multiple components of a system and between systems. The whole methodology has been implemented in an open source software tool (Schäfer and Bosi 2013) and has been applied and validated in selected case studies at urban and regional scale (Pitilakis and Argroudis 2013). The case studies have included the city of Thessaloniki in Greece, and Vienna in Austria, the harbor of Thessaloniki, the gas system of L'Aquila in Italy, the electric power network in Sicily, a roadway network and hospital facility again in Italy. The research consortium has relied on the active participation of 12 entities from Europe, 1 from USA and 1 from Japan. The consortium has included partners from academia, research institutions, the consulting sector, and the insurance industry. The results of the research work are intended to meet the needs of researchers, professionals, stakeholders of different systems, civil protection, public services, and the insurance industry involved in seismic risk assessment and management.

One of the aims in SYNER-G has been to develop a unified approach for modelling socio-economic impacts caused by earthquake damage, which integrates social vulnerability in the physical system modelling approaches (Cavalieri et al. 2012). In most earthquake loss estimation models socio-economic losses are computed as linear damage-consequence functions without consideration of social vulnerability. Contributing to the challenge of integrating social vulnerability with physical damage/performance models is realisation of the fact that social vulnerability is a second order phenomenon and not something that can be directly observed and measured.

In SYNER-G, social losses (e.g., casualties and number of displaced people) are computed as integrated functions of hazard intensity, vulnerability of physical systems (through fragility curves) and the social vulnerability of the population at risk (Khazai 2013). The integrated approach proposed in SYNER-G provides a framework to link the degree of damage and performance of physical systems to vulnerabilities and coping capacities in society to assess: (1) Impacts on displaced populations and their shelter needs, and (2) Health impacts on exposed populations and their health-care needs. This way of conceptualizing the integrated framework emphasizes the importance of understanding the interrelations between physical and social systems and the associated and interrelated damages and losses. In other words, how direct physical losses can potentially aggravate existing vulnerabilities in society and how vulnerabilities in society can ultimately lead to greater impacts from physical damage and loss.

Thus, one of the main objectives has been the adoption of an indicator system and common nomenclature, which posits social vulnerability in relation to the vulnerability of the physical system. For example, the number of displaced persons is not computed as a function of damaged buildings alone, rather derived as a function of the habitability of buildings (defined by the tolerance to utility loss for different levels of building damage and weather conditions) and a set of key socio-economic indicators influencing a population to leave their homes and seek or not seek public shelter.

In the framework of SYNER-G a comprehensive review has been carried out of fragility curves for most important elements at risk. Moreover, new fragility curves have been developed where necessary, considering the distinctive features of European elements (Kaynia 2013). The result of these studies is presented in this book. A second book, in the same series, will follow with the SYNER-G systemic methodology and the representative applications.

1.3 Elements at Risk

The elements at risk are commonly categorized as populations, communities, built environment, natural environment, economic activities and services, which are under the threat of disaster in a given area (Alexander 2000). In the present book, the elements at risk within the built environment are examined. They are classified

in four main categories: buildings, utility networks, transportation infrastructures and critical facilities. In each category there are several sets of fragility curves that have been developed considering the taxonomy and their typological characteristics. In that sense there are numerous typologies for reinforced concrete (RC) or masonry buildings, numerous typologies for bridges and numerous typologies for all other element at risk of all systems considered in this book. The development of a homogenous taxonomy for all engineering element at risk exposed to seismic hazard and the recommendation of adequate fragility functions for each one, considering also the European context, is a significant contribution to the reduction of seismic risk in Europe and worldwide.

1.4 Derivation of Fragility Functions

There are several methods available and used in the literature to derive fragility functions for different elements exposed to seismic hazard and in particular to transient ground motion and permanent ground deformations due to ground failure. Conventionally, they are classified into four categories: empirical, expert elicitation, analytical and hybrid. All these approaches have their strengths and weaknesses as will be highlighted and discussed in the following chapters of this book. However, analytical methods, validated with large-scale experimental data and observations from recent strong earthquakes have become more popular in recent years. The main reason is the considerable improvement of computational tools, methods and skills, which allows comprehensive parametric studies covering all possible typologies, to be undertaken. A complementary, equally important, reason, is the better control of several of the associated uncertainties, e.g. material properties. In the following we will make a short overview of the different methods, which will be presented and further discussed in Chap. 3. Before outlining the essentials of the four categories it is important to present the main methodological parameters involved in the derivation of the fragility functions. Many of the epistemic uncertainties are related to the ontology and definition of these parameters, namely:

- Taxonomy, typology, classification
- Performance levels and damage states
- Intensity measures

1.4.1 Taxonomy, Typology, Classification

The key assumption in the vulnerability assessment of buildings, infrastructures and lifeline is that structures and components of systems, having similar structural characteristics, and being in similar geotechnical conditions (e.g. a bridge of a given typology), are expected to perform in the same way for a given seismic

excitation. Within this context, damage is directly related to the structural properties of the elements at risk. Taxonomy and typology are thus fundamental descriptors of a system that are derived from the inventory of each element and system. Geometry, material properties, morphological features, age, seismic design level, anchorage of the equipment, soil conditions, and foundation details are among usual typology descriptors/parameters. RC buildings, masonry buildings, monuments, bridges, pipelines (gas, fuel, water, waste water), tunnels, road embankments, harbour facilities, road and railway networks, have their own specific set of typologies and different taxonomy.

The knowledge of the inventory of a specific structure in a region and the capability to create classes of structural types (for example with respect to material, geometry, design code level) are among the main challenges when carrying out a general seismic risk assessment for example at a city scale, where it is practically impossible to perform this assessment at building level. It is absolutely necessary to classify buildings, and other elements at risk, in "as much as possible", homogenous classes presenting more-or-less similar response characteristics to ground shaking. Thus, the derivation of appropriate fragility curves for any type of structure depends entirely on the creation of a reasonable taxonomy that is able to classify the different kinds of structures and infrastructures in any system exposed to seismic hazard. In SYNER-G a great effort is paid to create a coherent and comprehensive taxonomy from which European typologies for the most important elements at risk are defined (Hancilar and Taucer 2013). Previous taxonomies and typologies in Europe (e.g. RISK-UE and LESSLOSS EU projects) and USA (e.g. HAZUS or ALA), have been reviewed and updated in order to develop a unique SYNER-G typology for all elements at risk, which is proposed to be the reference from now on in Europe. In the subsequent chapters dealing with the various structures under consideration the proposed SYNER-G taxonomy and typologies are presented in a comprehensive way.

For the purpose of summarising the taxonomy, all the systems, components and their sub-components considered in the infrastructure are reported with their tags in Table 1.1.

1.4.2 Performance Levels and Damage States

In seismic risk assessment, the performance levels of a structure, for example a RC building belonging in a specific class, can be defined through damage thresholds called *limit states*. A limit state defines the boundary between two different damage conditions often referred to as *damage states*. Different damage criteria have been proposed depending on the typologies of elements at risk and the approach used for the derivation of fragility curves. The most common way to define earthquake consequences is a classification in terms of the following damage states: No damage; slight/minor; moderate; extensive; complete. This qualitative approach requires an agreement on the meaning and the content of each damage state.

Table 1.1 SYNER-G infrastructure taxonomy

System	Component (and sub-components)
BDG: buildings	Force Resisting Mechanism (FRM1), FRM Material (FRMM1), Plan (P), Elevation (E), Cladding (C), Detailing (D), Floor System (FS), Roof System (RS), Height Level (HL), Code Level (CL)
EPN: electric power network	EPN01: electric power grid
	EPN02: generation plant
	EPN03: substation
	EPN04: distribution circuits
	EPN05-09: substation macro-components (autotransformer line; line without transformer; bars-connecting line; bars; cluster)
	EPN10-23: substation micro-components (circuit breaker; lightning arrester or discharger; horizontal disconnect switch or horizontal sectionalizing switch; vertical disconnect switch or vertical sectionalizing switch; transformer or autotransformer; current transformer; voltage transformer; box or control house; power supply to protection system; coil support; bar support or pothead; regulator; bus; capacitor tank)
	EPN24: transmission or distribution line
GAS: natural gas system	GAS01: production and gathering facility (onshore, offshore)
	GAS02: treatment plant
	GAS03: storage tank
	GAS04: station (compression, metering compression/metering, regulator/metering)
	GAS05: pipeline
	GAS06: SCADA
OIL: oil system	OIL01: production and gathering facility (onshore, offshore)
	OIL02: refinery
	OIL03: storage tank farm
	OIL04: pumping plant
	OIL05: pipeline
	OIL06: SCADA
WSS: water-supply network	WSS01: source (springs, rivers, natural lakes, impounding reservoirs, shallow or deep wells)
	WSS02: treatment plant
	WSS03: pumping station
	WSS04: storage tank
	WSS05: pipe
	WSS06: tunnel
	WSS07: canal
	WSS08: SCADA system
WWN: waste-water network	WWN01: waste-water treatment plant
	WWN02: pumping (lift) station
	WWN03: pipe
	WWN04: tunnel
	WWN05: SCADA system

(continued)

Table 1.1 (continued)

System	Component (and sub-components)
RDN: road network	RDN01: bridge (material, type of deck, deck structural system, pier to deck connection, type of pier to deck connection; type of section of the pier, spans, type of connection to the abutments, skew, bridge configuration, foundation type, seismic design level)
	RDN02: tunnel
	RDN03: embankment (road on)
	RDN04: trench (road in)
	RDN05: unstable slope (road on, or running along)
	RDN06: road pavement (ground failure)
	RDN07: bridge abutment
RWN: railway network	RWN01: bridge
	RWN02: tunnel
	RWN03: embankment (track on)
	RWN04: trench (track in a)
	RWN05: unstable slope (track on, or running along)
	RWN06: track
	RDN07: bridge abutment
	RWN07: station
HBR: harbour	HBR01: waterfront components (gravity retaining structures; sheet pile wharves; piers; breakwaters mooring and breasting dolphins)
	HBR02: earthen embankments (hydraulic fills and native soil material)
	HBR03: cargo handling and storage components (cranes, tanks, etc)
	HBR04: buildings (sheds, warehouse, offices, etc)
	HBR05: liquid fuel system (as per the OIL system)
HCS: health-care system	HCS01: organisational
	HCS02: human
	HCS03: physical
	HCS03-1: structural elements (of the buildings within the complex/ facility)
	HCS03-2: non-structural elements
	HCS03-3: architectural (walls, ceilings, windows etc)
	HCS03-4: basic installations (generation/distribution)
	HCS03-5: basic installations/medical gases
	HCS03-6: basic installations/power system
	HCS03-7: basic installations/water system
	HCS03-8: basic installations/conveying system
	HCS03-9: building contents
FFS: fire-fighting system	FFS01: fire-fighters station
	FFS02: pumping station
	FFS03: storage tank
	FFS04: fire-hydrant
	FFS05: pipe

The number of damage states is variable and is related with the functionality of the components and/or the repair duration and cost. In this way the total losses of the system (economic and functional) can be estimated. In particular, physical damages are related to the expected serviceability level of the component (i.e. fully or partial

operational or inoperative) and the corresponding functionality (e.g. power availability for electric power substations, number of available traffic lanes for roads, flow or pressure level for water system). These correlations provide quantitative measures of the component's performance, and can be applied for the definition of specific Performance Indicators (PIs), which are introduced in the systemic analysis of each network. Therefore, the comparison of a demand with a capacity quantity, or the consequence of a mitigation action, or the accumulated consequences of all damages (the "impact") can be evaluated. The restoration cost, when provided, is given as the percentage of the replacement cost. These thresholds are qualitative and are given as general outline; the user could modify them accordingly, considering the particular conditions of the network or component under study.

Methods for deriving fragility curves generally model the damage on a discrete damage scale. In empirical procedures, the scale is used in reconnaissance efforts to produce post-earthquake damage statistics and is rather subjective. In analytical procedures the scale is related to limit state mechanical properties that are described by appropriate indices, such as for example displacement capacity in the case of buildings or pier bridges. For other elements at risk the definition of the performance levels or the limit states may be more vague and follow other criteria related, for example in the case of pipelines, to the limit strength characteristics of the material used in each typology.

It will be shown later that the definition and consequently the selection of the damage thresholds, i.e. limit states, are among the main sources of uncertainties. For this reason a considerable effort has been made in SYNER-G to homogenize the criteria as much as possible, while also discussing the different approaches or assumptions made by different researchers. In the subsequent chapters the performance levels and limit states for every type of structure are presented and discussed in order to offer to the user of the proposed fragility functions, the means to make most suitable selection according to the specific needs.

1.4.3 Intensity Measures

A main issue related to the fragility curves is the selection of an appropriate earthquake *Intensity Measure* (IM) that characterizes the strong ground motion and best correlates with the response of each element, for example, building, pipeline or harbour facilities like cranes. Several measures of the strength of ground motion (IMs) have been developed. Each intensity measure may describe different characteristics of the motion, some of which may be more adverse for the structure or system under consideration. The use of a particular IM in seismic risk analysis should be guided by the extent to which the measure corresponds to damage to the components of a system or the system of systems. Optimum intensity measures are defined in terms of practicality, effectiveness, efficiency, sufficiency, robustness and computability (Cornell et al. 2002; Mackie and Stojadinovic 2003, 2005).

Practicality refers to the recognition that the IM has some direct correlation to known engineering quantities and that it "makes engineering sense" (Mackie and Stojadinovic 2005; Mehanny 2009). The practicality of an IM may be verified analytically via quantification of the dependence of the structural response on the physical properties of the IM such as energy, response of fundamental and higher modes, etc. It may also be verified numerically by interpretation of the response of the structure under non-linear analysis using existing time histories.

Sufficiency describes the extent to which the IM is statistically independent of ground motion characteristics such as magnitude and distance (Padgett et al. 2008). A sufficient IM is one that renders the structural demand measure conditionally independent of the earthquake scenario. This term is more complex and is often at odds with the need for computability of the IM. Sufficiency may be quantified via statistical analysis of the response of a structure for a given set of records.

The *effectiveness* of an IM is determined by its ability to evaluate its relation with an engineering demand parameter (EDP) in closed form (Mackie and Stojadinovic 2003), so that the mean annual frequency of a given decision variable exceeding a given limiting value (Mehanny 2009) can be determined analytically.

The most widely used quantitative measure from which an optimal IM can be obtained is *efficiency*. This refers to the total variability of an engineering demand parameter for a given IM (Mackie and Stojadinovic 2003, 2005).

Robustness describes the efficiency trends of an IM-EDP pair across different structures, and therefore different fundamental period ranges (Mackie and Stojadinovic 2005; Mehanny 2009).

In general, IMs are grouped in two general classes: empirical intensity measures and instrumental intensity measures. With regards to the empirical IMs, different macroseismic intensity scales could be used to identify the observed effects of ground shaking over a limited area. In the instrumental IMs, which are by far more accurate and representative of the seismic intensity characteristics, the severity of ground shaking can be expressed as an analytical value measured by an instrument or computed by analysis of recorded accelerograms.

The selection of the intensity parameter is also related to the approach that is followed for the derivation of fragility curves and the typology of element at risk. The identification of the proper Intensity Measure (IM) is determined from different constraints, which are first of all related to the adopted hazard model, but also to the element at risk under consideration and the availability of data and fragility functions for all different exposed assets.

Empirical fragility functions are usually expressed in terms of the macroseismic intensity defined according to the different Macroseismic Scales, namely, EMS, MCS, and MM. Analytical or hybrid fragility functions are, on the contrary, related to instrumental IMs, which are related to parameters of the ground motion (PGA, PGV, PGD) or of the structural response of an elastic SDOF system (spectral acceleration S_a or spectral displacement S_d, for a given value of the period of vibration T). Sometimes, integral IMs can be useful, which consider a specific integration of a motion parameter, for example Arias Intensity I_A or of a spectral value like the Housner Intensity I_H. When the vulnerability of elements due to

ground failure is examined (i.e. liquefaction, fault rupture, landslides) permanent ground deformation (PGD) is the most appropriate IM.

In the subsequent chapters the most adequate IMs are selected for every asset under consideration in this book, while in the Fragility Manager Tool (see Chap. 13) a correlation is made among different IMs used by different researchers specifically for buildings, in order to derive homogenous fragility functions.

1.4.4 Treatment of Uncertainties

Several uncertainties are introduced in the process of constructing a set of fragility curves of a specific element at risk. They are associated to the parameters of fragility curves, and to the derivation methodology, as well as in the relationship between physical damage state and the performance (PI) of the element at risk. The uncertainties are usually categorized in aleatory and epistemic. Aleatory uncertainty is one that is presumed to be due to the intrinsic randomness of a phenomenon. An epistemic uncertainty is one that is considered to be caused by lack of knowledge, which is usually related to the method or the available data. The reason that it is convenient to have this distinction within an engineering analysis model is that the lack-of-knowledge-part of the uncertainty can be represented in the model by introducing auxiliary non-physical variables. These variables capture information obtained through gathering of more data or use of more advanced scientific principles (DerKiureghian and Ditlevsen 2009).

In general, the uncertainty of the fragility parameters is estimated through the standard deviation, β_{tot}, that describes the total variability associated with each fragility curve. Three primary sources of uncertainty are usually considered, namely, the definition of damage states, β_{DS}, the response and resistance (capacity) of the element, β_{C}, and the earthquake input motion (demand), β_{D}. In particular, damage state definition uncertainties are due to the fact that the thresholds of the damage indexes or parameters used to define damage states are not known. Capacity uncertainty reflects the variability of structure properties as well as the fact that the modelling procedures are not perfect. Demand uncertainty reflects the fact that IM is not exactly sufficient, so different records of ground motion with equal IM may have different effects on the same structure (Selva et al. 2013). The total variability is modelled by the combination of the three contributors, assuming that they are stochastically independent and lognormally distributed random variables, by Eq. 1.2:

$$\beta_{tot} = \sqrt{\beta_{Ds}^2 + \beta_C^2 + \beta_D^2} \tag{1.2}$$

The general framework of the treatment of uncertainties in the derivation of the fragility functions is presented in Chap. 2 of this book, while detailed discussion is carried out for each element at risk in the respective chapters.

1.4.5 Methodologies for Deriving Fragility Functions

Several approaches are used to establish fragility functions. They are grouped in four general categories: empirical, judgmental or expert elicitation, analytical and hybrid. *Empirical methods* are based on post-earthquake surveys and observations of actual damage. They are specific to particular sites and seismotectonic, geological and geotechnical conditions, as well as the properties of the damaged structures. Consequently, the use of these functions in different regions is always questionable. *Expert judgment* fragility curves are based on expert opinion and experience. Therefore, they are versatile and relatively fast to establish, but their reliability is questionable because of their dependence on the experiences of the experts consulted. *Analytical fragility curves* adopt damage distributions simulated from the analyses of structural models under increasing earthquake loads. In general they result in a reduced bias and increased reliability of the vulnerability estimates for different structures compared to expert opinion and thus they are becoming ever more attractive in terms of the ease and efficiency by which data can be generated. *Hybrid methods* combine any of the above-mentioned techniques in order to compensate for their respective drawbacks.

Finally, the fragility functions of complex components that consist of different sub-components (e.g. hospital facilities, water or waste water treatment plants and pumping stations) are derived based on *fault tree* analyses. The fault trees analysis schematically depicts the sub-components and their functional interrelationship. A basic combination of components consists of a tree-like relationship where the top component is related to its contributing components by "AND" and "OR" gates. An "AND" gate means that the top component is functional (survival state) if all the contributing components are functional (series arrangement), whereas an "OR" gate indicates that the top component is functional if at least one of the contributing components is functional (parallel arrangement). In this way the fragility curves of all sub-components are used to obtain the global fragility function of complex components, such as pumping plants.

The above methods are further described and discussed in Chap. 3. The following sections are devoted to their general description with respect to the typology of the exposed structure, along with first order critical assessment of their qualities and flaws.

1.4.5.1 Empirical Methods

The study of past earthquakes and the field surveys of actual damages on exposed elements lead to extensive statistics on the damage states of various typologies under earthquake loading. For instance, the study by Spence et al. (1992) based on a survey of 70,000 buildings subjected to 13 different earthquakes has led to fragility curves for 14 classes of buildings, expressed as functions of macroseismic intensity. Rossetto and Elnashai (2003) developed empirical fragility functions for various

typologies of RC buildings (moment-resisting frames, infill walls, shear walls) from a database of 340,000 buildings exposed to 19 earthquakes worldwide. Sabetta et al. (1998) have also developed empirical fragility curves for the Italian building typologies after studying data of 50,000 damaged buildings in Italy. The probability of exceeding a damage state is expressed with respect to PGA or spectral response parameters, which are converted from the observed macroseismic intensity. However, it is widely recognized that correlations of this type include a large number of high uncertainties.

Empirical relations are also widely used to assess the vulnerability of components that are less amenable to analytical methods, e.g. pipeline segments (ALA 2001; O'Rourke et al. 2012) or tunnels (ALA 2001; Corigliano 2007) and highway embankments (Maruyama et al. 2010).

Empirical methods have the advantage of being based on real observed data, thus successfully account for various effects such as soil-structure interaction, site effects, and variability in the structural capacity of a group of buildings and the mechanisms, which govern the failure modes. However, this may also provide a drawback, as the empirically derived fragility curves remain specific to a given area with particular conditions of site effects, earthquake parameters (magnitude, depth, etc.) and structural capacity of buildings. Available data are often based on low-magnitude events with limited damage, which lead to fragility curves that may be unreliable for greater magnitude events (i.e. the portions of the curves corresponding to high seismic levels). It has also been noted that undamaged buildings after an event are not properly accounted for in the survey. This leads to a large uncertainty on the actual total number of elements exposed to the event. Finally, another difficulty often lies in the lack of knowledge of the exact ground motion in the immediate vicinity of the damaged buildings. Estimation must then be made with macroseismic intensity or through the extrapolation of the recorded signals from close stations.

Further insight on empirical methods is provided in Chap. 3, whilst Rossetto et al. (2013) provide an extensive review of the state-of-art in the construction of empirical fragility functions for buildings.

1.4.5.2 Expert Judgment

This procedure entirely relies on the judgment of appointed experts who are asked to provide an estimate of the mean loss or probability of damage of a given element at risk for different levels of seismic loading. Some of the fragility curves proposed in HAZUS (e.g. roads and tunnels) are developed using this approximate and subjective method. The traditional procedure is described in the ATC13 (ATC 1985) documents. A similar approach is to estimate vulnerability indexes based on a visual diagnostic (expert opinion-based) of a group of buildings. Several characteristics can be observed: force-resisting mechanism and material, floor types, building height, soft stories, quality of construction, irregularities, non-structural elements, age of building, etc. With this technique the vulnerability

is defined through a vulnerability index V_i varying between 0 and 1 based on the observed characteristics of the element (RISK-UE project, Milutinovic and Trendafiloski 2003).

These techniques have the advantage of not being affected by the lack of extensive damage data (empirical approaches) or the reliability or the structural model used in analytical developments. However, the results rely solely on the individual experience of the experts consulted. The potential bias in the curves can be reduced by extending the number of experts and by assigning appropriate weight to their estimations, based on their expertise level (Porter et al. 2007). These methods are, however, always useful to calibrate, together with the empirical methods, the resulting fragility functions from the analytical methods. Even more importantly, they are necessary in areas with poor data from past earthquake damages, or low level of engineering expertise. Their main weakness remains the difficulty to extrapolate their results in other countries with different engineering and construction practice.

A recent effort to revive the use of expert opinion for the derivation of fragility function has been carried out within the Global Earthquake Model (www.globalquakemodel.org) and further information on this activity is provided in Chap. 3.

1.4.5.3 Analytical Methods

Analytical methods are based on the estimation of the damage distributions through the simulation of an element's structural response subjected to seismic action. The seismic input can be represented by a response spectrum (static methods) or an acceleration time-history (dynamic methods).

Numerical models need to be developed and a compromise has to be made between the accuracy of the representation of the nonlinear behavior and the robustness and cost-efficiency of the model. For the case of buildings, two widely used methods to model the nonlinear structural behavior are plastic hinge modeling (i.e. concentrated inelasticity) and fiber element modeling (i.e. distributed plasticity). An important choice is also related to the representation of the building in 3D or 2D. For structures that are regular in plan, the torsion effects can often be ignored and 2D analyses lead to fairly accurate results.

Regarding the analytical approaches, a distinction can also be made between direct methods that yield fragility curves as functions of intensity measure types, IMT (e.g. PGA, PGV, $S_a(T)$, etc.) and the "indirect" ones that estimate the damage probability with respect to structural response parameters (e.g. spectral displacement at the inelastic period). The latter approach is used for instance in the framework of HAZUS (NIBS 2004).

In the following we shortly describe and discuss the two more popular analytical methods, namely, the Capacity Spectrum Method (CSM) and the general Dynamic Analysis and the more recent developments with the Incremental Dynamic Analysis (IDA).

1.4.5.3.1 Capacity Spectrum Method (CSM)

The use of mechanical models and capacity curves to assess the vulnerability of an element at risk (i.e. RC building) is described in detail in the HAZUS methodology (NIBS 2004) and the RISK-UE Level 2 approach. Each typology (based on code level, height class, force-resisting mechanism and material) is defined by a bilinear capacity curve for an equivalent SDOF system, which is developed from a static pushover analysis.

The HAZUS methodology treats 36 building typologies, which are identified based on the structural type (force-resisting mechanism and material) and the height class (low-, mid- and high-rise). The different typologies are associated with various building capacity parameters, such as:

- T_e, true "elastic" fundamental-mode period of building;
- h, typical roof height;
- α_2, fraction of building height at location of push-over mode displacement.

For different levels of seismic code (pre-code, low-, moderate- and high-level code) and for each typology, the HAZUS methodology defines bilinear capacity curves based on two control points: the yield (D_y, A_y), and the ultimate capacity (D_u, A_u). Yield capacity represents the true lateral strength of the building, whereas ultimate capacity represents the maximum strength of the building when the global structural system has reached a fully plastic state. The capacity curves, expressed in the spectral acceleration – spectral displacement (S_a-S_d) format, are used to obtain the performance point of the structural element (depending on the seismic response spectrum) and to deduce the spectral displacement, which corresponds to a given damage level.

For a building within a given typology, the probability of reaching or exceeding damage state DS can then be expressed as a cumulative lognormal function with respect to the spectral displacement at the performance point:

$$P(DS|S_d) = \phi\left[\frac{1}{\beta_{DS}}\ln\left(\frac{S_d}{\overline{S_{d,DS}}}\right)\right] \tag{1.3}$$

where $\overline{S_{d,DS}}$ is the median value of spectral displacement at which the building reaches the threshold of the damage state DS, β_{DS} is the standard deviation of the natural logarithm of spectral displacement of damage state DS, and Φ is the standard normal cumulative distribution function.

The median values of structural component fragility are determined based on building drift ratios Δ_{DS} that describe the threshold of the following damage states: slight, moderate, extensive and complete. The conversion of the damage state drift ratios to spectral displacement S_d values can be obtained as:

$$\overline{S_{d,DS}} = \Delta_{DS} \cdot \alpha_2 \cdot h \tag{1.4}$$

The various uncertainties are taken into account through the log-standard deviation parameter β_{DS}, which describes the total dispersion related to each fragility curve. Usually three primary sources of uncertainty contribute to the total variability for any given damage state namely the uncertainty associated with the definition of the damage state value $\beta_{M(DS)}$, the structural response of the element β_C (capacity curve) and the seismic demand β_D (response spectrum). The standard deviation β_{DS} can be estimated according to the following equation:

$$\beta_{DS} = \sqrt{(\mathrm{CONV}[\beta_C, \beta_D])^2 + \left(\beta_{M(DS)}\right)^2} \tag{1.5}$$

The convolution procedure between β_C and β_D is extensively described in Gencturk (2007). The HAZUS manual advocates the value $\beta_{M(DS)} = 0.4$ for all damage states. Some values are also recommended for the variability on the capacity curve: $\beta_{C(Au)} = 0.25$ for code-compliant elements and $\beta_{C(Au)} = 0.3$ for pre-code constructions. Taking into account the various uncertainties, the spectral displacement S_d for the threshold of damage state DS is expressed as $S_d = \overline{S_{d,DS}} \cdot \varepsilon_{DS}$, where $\overline{S_{d,DS}}$ is the median value of S_d for damage level DS, and ε_{DS} is a log normally-distributed variable with standard deviation β_{DS}.

The HAZUS methodology for the building damage estimation based on the CSM is represented schematically in Fig. 1.2

In Europe, the EU-funded research project RISK-UE was the first attempt to collect various studies, and develop a taxonomy for buildings adapted to the European context, and propose specific capacity curves by applying the CSM following the HAZUS procedure consisting of:

- typological classification of the elements;
- development of capacity curves;
- determination of the performance point based on the seismic level;
- assessment of the probabilities to reach or exceed the different damage states.

The two approaches obviously diverge in terms of input data. The damage state definitions in RISK-UE rely on interstory drift ratio (ISDR) values that are identified based on the capacity curve, which means that the drift values are structure-specific, as opposed to HAZUS, which recommends fixed values for each typology. Table 1.2 (from RISK-UE approach) gives threshold values for each damage state as a function of yielding and ultimate capacity points.

It has to be noted that nonlinear static analyses can also be used to generate "direct" fragility curves that do not necessarily rely on the structural response parameter. The response spectrum can be used to associate each estimated performance point with the equivalent intensity measure (e.g. PGA) of the seismic records that are used (NIBS 2004). Therefore, the fragility curves can be used as stand-alone function to directly estimate the damage probability, without going through the capacity curve.

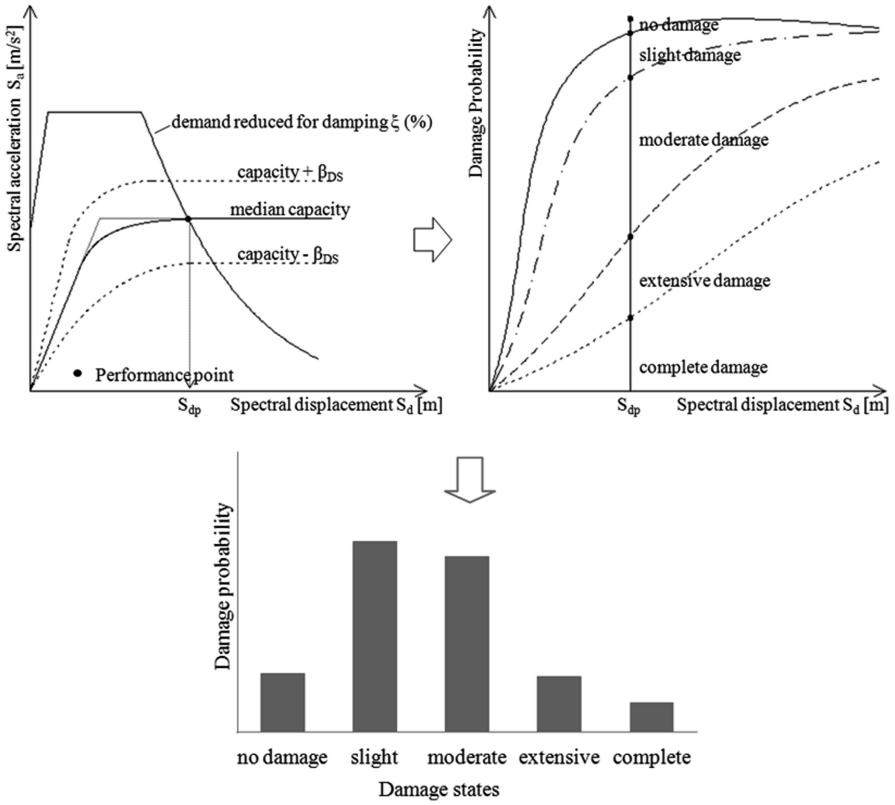

Fig. 1.2 HAZUS procedure for building damage estimation based on CSM

Table 1.2 Damage state definitions

	Damage state	Drift limit	Spectral displacement limit
DS1	No damage	$\Delta < 0.7\Delta_y$	$D < 0.7Dy$
DS2	Slight	$0.7\Delta_y < \Delta < 0.7\Delta_y + 0.05\Delta_{uy}$	$0.7D_y < D < D_y$
DS3	Moderate	$0.7\Delta_y + 0.05\Delta_{uy} < \Delta < 0.7\Delta_y + 0.2\Delta_{uy}$	$D_y < D < D_y + D_{uy}$
DS4	Extensive	$0.7\Delta_y + 0.2\Delta_{uy} < \Delta < 0.7\Delta_y + 0.5\Delta_{uy}$	$D_y + D_{uy} < D < D_u$
DS5	Very heavy	$0.7\Delta_y + 0.5\Delta_{uy} < \Delta < 0.7\Delta_y + \Delta_{uy}$	$D_u < D$
With: $\Delta_{uy} = 0.9\Delta_u - 0.7\Delta_y$ and $D_{uy} = 0.25(D_u - D_y)$			

Adapted from RISK-UE

Since then the library of fragility functions derived using the CSM has been considerably increased. Different researchers proposed fragility functions for a variety of typologies of structures in addition to buildings and bridges. In several cases they use different standard deviation values according to various criteria. In the different chapters of this book the reader will have the opportunity to explore most of these differences and applications of the CSM to derive fragility curves.

1.4.5.3.2 Dynamic Analyses

This approach resides essentially in numerous non-linear dynamic analyses of structural models with a series of acceleration time-histories. Various statistical procedures (maximum likelihood or linear least squares-based) are then used to develop fragility curves that can directly be used for earthquake risk assessment.

The dynamic analyses are quite straightforward in the case of individual elements (e.g. specific buildings) allowing the aleatory variability associated with the earthquake ground motion to be modeled. However, when analytical fragility curves are developed for a typology or a class of buildings, it is necessary to account for a large variability in the structural response. Therefore uncertainties should also be introduced in the mechanical and morphological/geometrical properties. The first enable to account for the variability in the quality of the construction techniques (e.g. wall-floor continuity, amount of reinforcement in RC frames, concrete type, etc.), while the second ones to represent the whole range of possibilities of buildings included in a given typology. Several building models have to be analyzed that are able to span the whole typology in terms of, for instance, number of storeys, horizontal dimensions, ratio of openings in the walls, irregularities, etc. Other sources of uncertainty could also be addressed in the dynamic analyses concerning the impact of deterioration of the material properties caused by aging effects (e.g. Pitilakis et al. 2013) or cumulative earthquake damage under successive earthquake shocks. Such effects may adversely affect the seismic performance and fragility of the as-built structures.

For a given typology, the number of models to analyze can grow dramatically, which leads to a significant number of dynamic analyses. In such studies, sampling techniques, such as Latin Hypercube Sampling (McKay et al. 1979), enable a wide range of uncertainties inside a typology to be modeled while keeping a reasonable number of simulations.

The use of response surfaces (Towashiraporn et al. 2008) – i.e. a polynomial regression between the building response and some structural parameters such as Young modulus, yield strength or damping ratio – is also a potential solution. Depending on the quality and the specificity of the studied elements, it could be possible to use a response surface to adapt the parameters of the fragility curves. The use of a complete time-history, rather than its spectral representation, can lead to the development of fragility models based on a wide range of ground motion parameters, and vector-valued parameters (Seyedi et al. 2010).

Dynamic analyses are often used to derive fragility functions for roadway/railway elements such as abutments or embankments/cuts (Argyroudis et al. 2013) and bridges (Kim and Shinozuka 2004), because the static procedures, such as pushover approaches, are less adapted to these types of components. For roadway or railway elements, the whole geotechnical system (i.e. accounting for soil-structure interaction) has to be considered and the uncertainties in the soil profiles have to be introduced.

The choice of representative ground-motion records is of paramount importance for the reliable evaluation of the seismic response. The quantity and the distribution

of intensity measures in the sample of records have indeed a great influence on the fragility parameters (both the standard deviation and the median). The studied typology is usually restricted to a given geographical area, which allows adequate time-histories based on specified intervals of magnitude, source-to-site distance and possibly other scenario characteristics, such as focal depth and mechanism to be selected (e.g. Bommer and Acevedo 2004). Special software and strong ground motion recordings from European and international databases can be used for this purpose, as for example REXEL (Iervolino et al. 2010) and REXEL-DISP (Smerzini et al. 2012). In the record selection and analysis processes it is important to consider records with possible special features, such as near-source directivity pulses. Such records must be appropriately accounted for, since the results can be significantly different than those for records further from the source. When soil-foundation-structure interaction (SSI) is taken into consideration, modeling both soil and structure in a coupled system, the input motion is normally introduced at the seismic bedrock and therefore it should refer to rock conditions, as the SSI model directly captures site effects.

1.4.5.3.3 Incremental Dynamic Analysis

Incremental dynamic analysis (IDA) is a promising computer-intensive method, which has recently risen to offer comprehensive evaluation of the seismic performance of structures. IDA procedure involves the performing of a series of nonlinear dynamic analyses under a suite of multiple scaled ground motion records whose intensities should be ideally selected to cover the whole range from elasticity to global dynamic instability (Vamvatsikos and Cornell 2002). IDA curves of the structural response, which provide a relationship between a damage measure quantity (i.e. engineering demand parameter EDP) and an intensity measure (IM) of the applied scaled accelerograms, are then constructed by interpolating the resulting EDP-IM discrete points.

The reliability of the procedure generally relies primarily on the proper formation of the nonlinear structural model, the compilation of a suite of records, as well as on the selection of efficient EDPs and IMs.

A representative set of input ground motions should consist of approximately 15–30 ordinary records assuming that a relatively efficient IM, like $Sa(T_1,5\ \%)$, is used and that peculiar features in the records (e.g. ground motions containing pulses due to effects such as forward-directivity, fling step, basin effects and site effects) that could potentially bias structural response are eliminated.

In addition, care should be taken in the selection of the scaling levels for each record and in the post processing of the IDA analysis results. The scaling of the records may provide good estimates of the distribution of EDP given IM provided that their statistical relationship is effectively independent of magnitude M and source-to-site distance R in the range of interest. An advanced tracing algorithm, such as the hunt & fill (Vamvatsikos and Cornell 2002, 2004), which ensures that

the records are properly scaled, with the minimum required computational effort is recommended to perform the IDA.

A monotonic scalable intensity measure should be used such as the Peak Ground Acceleration (PGA) or the 5 %-damped spectral acceleration at the fundamental period of the structure [Sa(T_1,5 %)]. The latter is generally found to be both adequately efficient and sufficient for first-mode dominated, moderate period structures (Shome and Cornell 1999). Further reduction in record-to-record variability may be achieved employing a single optimal spectral value or a vector of 2 or a scalar combination of several spectral values (Vamvatsikos and Cornell 2005).

The engineering demand parameter EDP is an observable response parameter that can be extracted from IDA. A typically adopted EDP is the maximum interstory drift ratio, θ_{max}, which is known to relate well to dynamic instability and structural damage.

Subsequently, limit-states (e.g., for Immediate Occupancy IO or collapse prevention CP) can be defined on the IDA curve and the corresponding capacities can be calculated. Finally, the results of the IDA (e.g. Sa(T_1,5 %) − θ_{max} discrete values) could be used to derive fragility curves for the already specified (on the IDA curve) damage limit states.

Figure 1.3a presents indicative plots of 15 continuous IDA curves derived by interpolation of the Sa(T_1,5 %) − θ_{max} pairs for each individual record and the associated CP limit-state capacities for a nine-story reinforced concrete moment resisting frame building whereas Fig. 1.3b illustrates the corresponding summarized across all records IDA curves at 16, 50 and 84 % fractiles.

Despite the relatively large computational efforts involved, the fragility functions developed by means of dynamic analyses or IDA are able to reproduce most accurately in most cases the seismic response of typical civil engineering structures.

Inelastic analyses, either static (pushover) or dynamic (time-history) are the most appropriate approach to investigate the deformation capacity of the structure and to provide estimate of their seismic vulnerability. The use of time-history analyses, however, requires several assumptions regarding the selection of the suite of earthquake ground motions and is also generally time-consuming because of the high number of calculations involved (fib 2007).

As a general remark, the method that is followed for the derivation of analytical fragility curves is related to the nature of each element at risk, the availability of resources and the reliability of the analytical tools.

1.4.5.4 Hybrid Methods

Hybrid fragility curves are the result of a combination of methods, using for instance both analytical and observational data, or completed by expert judgment. The main advantage is that they compensate for the lack of observational data for the deficiencies of structural models and for the subjectivity in expert opinion data. For instance, analytical fragility curves can be modified and improved by integrating post-seismic observations that are made available after their initial

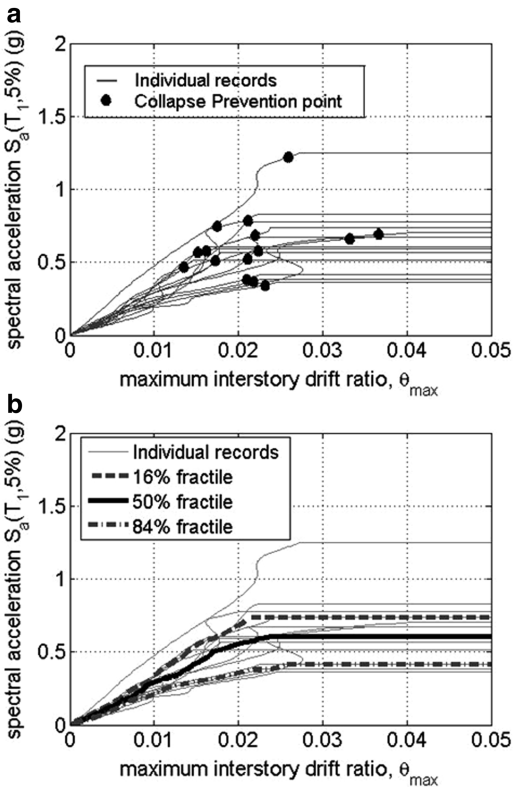

Fig. 1.3 (**a**) IDA curves for the individual records and the estimation of the associated limit-state capacities for CP limit state and (**b**) summarization of the 15 IDA curves into their 16, 50 and 84 % fractiles

development. This kind of approach enables one to calibrate the analytical results (which are usually based on more or less justified assumptions) or to fill-in some blanks due to scarce data at high seismic levels (Calvi et al. 2006). The addition of empirical data to analytical curves can be done through Bayesian updating, resulting in new estimations of the median and standard deviation of the initial lognormal distribution (Singhal and Kiremedjian 1998). The work by Kappos et al. (2006), where fragility curves for RC and unreinforced masonry buildings are derived using both statistical data from earthquake-damaged Greek buildings and results from nonlinear static or dynamic analyses is a typical example of a hybrid method. Recent attempts to produce hybrid fragility functions are described further in Chap. 3.

1.5 In Summary

The main contribution of SYNER-G, which is provided in this book, is the compilation of the existing fragility curves/functions and the development of new functions for all the system elements based on the taxonomy/typology that has been

derived in the framework of the SYNER-G project. A literature review on the typology, the fragility functions (analytical/empirical/expert judgment/hybrid), damage scales, intensity measures and performance indicators has been performed for all the elements. The fragility functions are based on new analyses and collection/review of the results that are available in the literature. In some cases, the selection of the fragility functions has been based on validation studies using damage data from past and recent earthquakes mainly in Europe. In case of linear elements such as the pipelines the fragility functions are provided in terms of the repair rate, expressed as repairs per km, which is correlated with the IM, as for example with the PGVor PGD. Moreover, the damage and serviceability states have been defined accordingly. Appropriate adaptations and modifications have been made to the selected fragility functions in order to satisfy the distinctive features of the presented taxonomy and to respect as close as possible the European distinctive features of the construction practice. In other cases new fragility functions have been developed based on numerical solutions or by using fault tree analysis together with the respective damage scales and serviceability rates in the framework of European typology and hazard.

A fragility function manager tool[1] has been developed for buildings and bridges and is connected with the SYNER-G software platform. This tool is able to store, visualize, harmonize and compare a large number of fragility functions sets. For each fragility function set, the metadata of the functions, representative plots and the parameters of the functions can be visualized in an appropriate panel or window. Once the fragility functions are uploaded, the tool can be used to harmonize and compare the curves. The harmonization module allows one to harmonize the curves using a target intensity measure type and a number of limit states of reference (as described further in Chap. 13). After the harmonization, the comparison module can be used to plot together and to compare different functions, which can then be extracted and the mean and dispersion of the parameters of the curves can be calculated. In Fig. 1.4 the screenshot of the main window of the tool is presented together with a brief description of its principal panels.

1.6 Outline of the Book Organization

In the next chapters, the fragility functions and the associated dependencies, as shortly presented above, are described for buildings, utility networks, gas networks, transportation infrastructures and critical facilities. Based on the review of state-of-the-art fragility functions for each component, either the existing functions are adopted or improved and new fragility functions for the individual components are

[1] The fragility function manager tool is provided with the present volume at http://extras.springer.com.

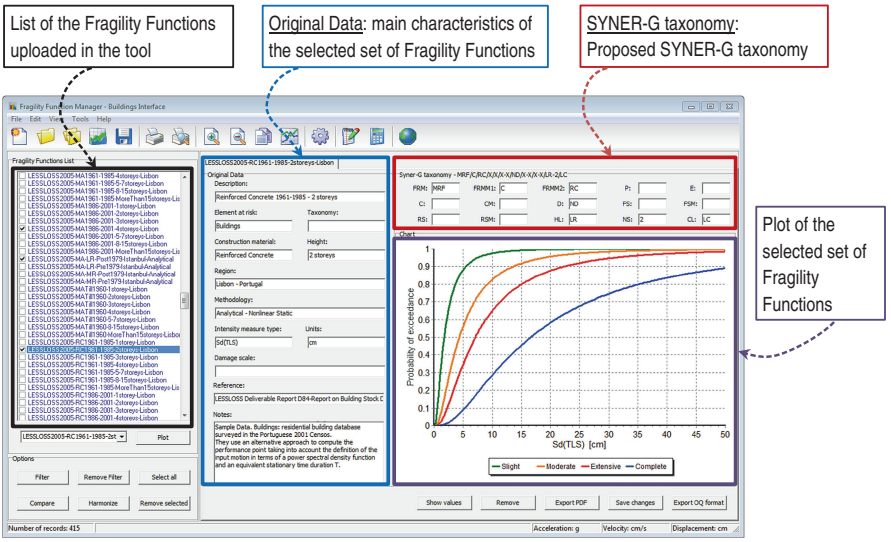

Fig. 1.4 Screenshot of the main window of the Fragility Function Manager tool

proposed. For the proposed fragility functions, the following parameters are provided:

- typology classification of each component;
- damage state definition;
- intensity measure (IM);
- fragility curve parameters, for each damage state and typology.

Each chapter is written by a different group of experts and contains the following issues:

- outline the principles and main issues related to fragility functions;
- classify the available methods for deriving fragility curves;
- review the available fragility functions for each element and system;
- present fragility functions for each element and system of SYNER-G taxonomy.

In particular, in Chap. 2, the propagation of the uncertainties in complex systems is discussed and the current state-of-the art on the treatment of uncertainties is presented. The existing methods for constructing fragility curves together with the factors influencing the reliability of resulting fragility functions are reviewed in Chap. 3. Additionally, the selection of the most appropriate fragility curves and the concept of combining different fragility curves or including new empirical data are discussed in the same Chapter focusing on buildings. The work carried out under the auspices of the SYNER-G project to collect, harmonize and compare fragility functions for European RC buildings in summarized in Chap. 4. An overview of existing methods along with recommendations for deriving fragility curves is presented in Chap. 5 for masonry buildings. Chapter 6 deals with the fragility models for the components of electric power networks, including the main

characteristics and typologies, the main works on fragility functions and the most suited models for use in the European context. Chapter 7 presents and reviews fragility curves and associated parameters for the components of gas and oil systems such as buried pipelines, storage tanks and processing facilities. The state-of-the-art on the fragility models for the vulnerability assessment of the water and waste water networks components together with their main characteristics and typologies, damage mechanisms and failure modes, as well as the most suitable fragility functions for use in the European context are presented in Chap. 8. Chapter 9 presents a literature review of fragility functions for reinforced concrete road and railway bridges considering the main issues in fragility analysis. Recent developments that examine special issues such as damaged and retrofitted bridges, the effects of corrosion, skew, spatial variability of the seismic action and liquefaction are also described and a method for rapid fragility analysis of regular bridges is presented. Appropriate fragility functions for roadway and railway components other than bridges are proposed in Chap. 10. A general procedure for the derivation of analytical fragility curves that was followed in SYNER-G is described and applied for the fragility assessment of tunnels in alluvial soils, embankments, cuttings and bridge abutments due to ground shaking. Existing fragility curves and improved methods for the seismic vulnerability assessment of harbor elements such as waterfront structures, cargo handling and storage components and other infrastructures are proposed and discussed in Chap. 11. The fragilities and system performance of health care facilities are presented in Chap. 12. In particular, the global fragility of the physical component is estimated based on the fragilities of a large variety of elements following a fault tree analysis. The SYNER-G Fragility Function Manager, which has been developed to store, visualize, harmonize and manage a large number of fragility function sets is presented in Chap. 13. Finally, the general recommendations, gaps and needs for future research are summarized in Chap. 14.

References

Alexander D (2000) Confronting catastrophe: new perspectives on natural disasters. Oxford University Press, New York, p 282

American Lifelines Alliance, ALA (2001) Seismic fragility formulations for water systems. Part 1 – Guidelines, ASCE-FEMA, p 104

Applied Technology Council, ATC (1985) Earthquake damage evaluation data for California. Report No. ATC-13, Applied Technology Council, Redwood City, CA

Applied Technology Council, ATC (1991) Seismic vulnerability and impact of disruption of life lines in the conterminous United States. Report No. ATC-25, Applied Technology Council, Redwood City, CA

Argyroudis S, Kaynia AM, Pitilakis K (2013) Development of fragility functions for geotech-nical constructions: application to cantilever retaining walls. Soil Dyn Earthq Eng 50:106–116

ASPROGE (2007) Aseismic protection of bridges. Research project, General Secretariat for Research and Technology, Greece

Bommer JJ, Acevedo AB (2004) The use of real earthquake accelerograms as input to dynamic analysis. J Earthq Eng 8:43–91

Calvi GM, Pinho R, Magenes G, Bommer JJ, Restrepo-Velez LF, Crowley H (2006) Development of seismic vulnerability assessment methodologies over the past 30 years. J Earthq Technol 43 (3):75–104

Cavalieri F, Franchin P, Gehl P, Khazai B (2012) Quantitative assessment of social losses based on physical damage and interaction with infrastructural systems. Earthq Eng Struct Dyn 41 (11):1569–1589

Corigliano M (2007) Seismic response of deep tunnels in near-fault conditions. Ph.D. dissertation, Politecnicodi Torino, Italy, p 222

Cornell CA, Jalayer F, Hamburger RO, Foutch DA (2002) Probabilistic basis for 2000 SAC/FEMA steel moment frame guidelines. J Struct Eng 1284:26–533

DerKiureghian A, Ditlevsen O (2009) Aleatory or epistemic? Does it matter? Struct Saf 31:105–112

fib (2007) Seismic bridge design and retrofit – structural solutions: State-of-art report, fib Bulletin No. 39, International Federation for Structural Concrete (fib). ISBN 978-2-88394-079-6, p 300

Franchin P (ed) (2013) Methodology for systemic seismic vulnerability assessment of buildings, infrastructures, networks and socio-economic impacts. SYNER-G Reference Report 1, Publications Office of the European Union. ISBN 978-92-79-28975-0

Gencturk BE (2007) Fragility relationships for populations of buildings based on inelastic response. MS thesis, Department of Civil and Environmental Engineering, University of Illinois at Urbana-Champaign, Urbana

Hancilar U, Taucer F (eds) (2013) Guidelines for typology definition of European physical assets for earthquake risk assessment. SYNER-G Reference Report 2, Publications Office of the European Union. ISBN 978-92-79-28973-6

Iervolino I, Galasso C, Cosenza E (2010) REXEL: computer aided record selection for code-based seismic structural analysis. Bull Earthq Eng 8:339–362

Kappos AJ, Panagopoulos G, Penelis G (2006) A hybrid method for the vulnerability assessment of R/C and URM buildings. Bull Earthq Eng 4(4):391–413

Kaynia AM (ed) (2013) Guidelines for deriving seismic fragility functions of elements at risk: buildings, lifelines, transportation networks and critical facilities. SYNER-G Reference Report 4, Publications Office of the European Union. ISBN 978-92-79-28966-8

Khazai B (ed) (2013) Guidelines for the consideration of socio-economic impacts in seismic risk analysis. SYNER-G Reference Report 5, Publications Office of the European Union. ISBN 978-92-79-28968-2

Kim SH, Shinozuka M (2004) Development of fragility curves of bridges retrofitted by column jacketing. Probab Eng Mech 19:105–112

LessLoss (2007) Risk mitigation for earthquakes and landslides, Research project, European Commission, GOCE-CT-2003-505448

Mackie K, Stojadinovic B (2003) Seismic demands for performance-based design of bridges. PEER Report 2003/16, Pacific Earthquake Engineering Research Center, University of California, Berkeley, CA

Mackie K, Stojadinovic B (2005) Fragility basis for California highway overpass bridge seismic decision making. PEER Report 2005/12, Pacific Earthquake Engineering Research Center, University of California, Berkeley, CA

MAEviz software tool. http://mae.cee.illinois.edu/software_and_tools/maeviz.html

Maruyama Y, Yamazaki F, Mizuno K, Tsuchiya Y, Yogai H (2010) Fragility curves for ex-pressway embankments based on damage datasets after recent earthquakes in Japan. Soil Dyn Earthq Eng 30:1158–1167

McKay MD, Beckman RJ, Conover WJ (1979) A comparison of three methods for selecting values of input variables in the analysis of output from a computer code. Technometrics 21 (2):239–245

Mehanny SSF (2009) A broad-range power-law form scalar-based seismic intensity measure. Eng Struct 31:1354–1368

Mid-America Earthquake Center (2009) Impact of New Madrid seismic zone earthquakes on the central USA. MAE Center Report No. 09-03

Milutinovic ZV, Trendafiloski WS (2003) WP4: vulnerability of current buildings, Handbook of RISK-UE research project, September 2003

National Institute of Building Sciences (NIBS) (2004) HAZUS-MH: users's manual and technical manuals. Report prepared for the Federal Emergency Management Agency, Washington, DC

O'Rourke TD, Jeon SS, Toprak S, Cubrinovski M, Jung JK (2012) Underground lifeline system performance during the Canterbury earthquake sequence. In: Proceedings of the 15th world conference on earthquake engineering, Lisbon, Portugal

Padgett JE, Nielson BG, DesRoches R (2008) Selection of optimal intensity measures in probabilistic seismic demand models of highway bridge portfolios. Earthq Eng Struct Dyn 37:711–725

Pitilakis K, Argroudis S (eds) (2013) Systemic seismic vulnerability and loss assessment: validation studies. SYNER-G Reference Report 6, Publications Office of the European Union. ISBN 978-92-79-30840-6

Pitilakis KD, Karapetrou ST, Fotopoulou SD (2013) Consideration of aging and SSI effects on seismic vulnerability assessment of RC buildings. Bull Earthq Eng (accepted)

Porter K, Kennedy R, Bachman R (2007) Creating fragility functions for performance-based earthquake engineering. Earthquake Spectra 23(2):471–489

RELUIS (2003–2013) Retedei Laboratori Universitaridi Ingegneria Sismica. http://www.reluis.it/

RISK-UE (2004) An advanced approach to earthquake risk scenarios with applications to different European towns. Research project, European Commission, DG XII2001-2004, CEC: EVK4-CT-2000-00014

Rossetto T, Elnashai A (2003) Derivation of vulnerability functions for European-type RC structures based on observational data. Eng Struct 25:1241–1263

Rossetto T, Ioannou I, Grant DN (2013) Existing empirical fragility and vulnerability relationships: compendium and guide for selection. GEM Technical Report 2013-X, GEM Foundation, Pavia, Italy, April 2013, p 62

Sabetta F, Goretti A, Lucantoni A (1998) Empirical fragility curves from damage surveys and estimated strong ground-motion. In: 11th European conference on earthquake engineering, Paris, France

Schäfer D, Bosi A (2013) Systemic seismic vulnerability assessment software user's manual. SYNER-G reference report 7. Publications Office of the European Union. ISBN 978-92-79-30839-0

Selva J, Argyroudis S, Pitilakis K (2013) Impact on loss/risk assessments of inter-model variability in vulnerability analysis. Nat Hazards 67(2):723–746. doi:10.1007/s11069-013-0616-z

Seyedi D, Gehl P, Douglas J, Davenne L, Mezher N, Ghavamian S (2010) Development of seismic fragility surfaces for reinforced concrete buildings by means of nonlinear time-history analysis. Earthq Eng Struct Dyn 39(1):91–108

Shome N, Cornell CA (1999) Probabilistic seismic demand analysis of nonlinear structures. RMS Report-35, Reliability of Marine Structures Group, Stanford University, Stanford

Singhal A, Kiremedjian AS (1998) Bayesian updating of fragilities with application to RC frames. J Struct Eng 124(8):922–929

Smerzini C, Galasso C, Iervolino I, Paolucci R (2012) Engineering ground motion selection based on displacement-spectrum compatibility. In: Proceedings of 15WCEE, Lisboa, PT. Paper No. 2354

Spence RJS, Coburn AW, Pomonis A (1992) Correlation of ground motion with building damage: the definition of a new damage-based seismic intensity scale. In: Proceedings of 10th world conference on earthquake engineering structure, Balkema, Rotterdam

SRMLIFE (2007) Development of a global methodology for the vulnerability assessment and risk management of lifelines, infrastructures and critical facilities. Application to the metropolitan

area of Thessaloniki. Research project, General Secretariat for Research and Technology, Greece

SYNER-G (2013) Systemic seismic vulnerability and risk analysis for buildings, lifeline networks and infrastructures safety gain. Research project, European Commission, ENV-2009-1-244061

Towashiraporn P, Duenas-Osorio L, Craig JI, Goodno BJ (2008) An application of the response surface metamodel in building seismic fragility estimation. In: Proceeding of 14th world conference on earthquake engineering, Beijing, China

Vamvatsikos D, Cornell CA (2002) Incremental dynamic analysis. Earthq Eng Struct Dyn 31:491–514

Vamvatsikos D, Cornell CA (2004) Applied incremental dynamic analysis. Earhq Spectra 20 (2):523–553

Vamvatsikos D, Cornell CA (2005) Developing efficient scalar and vector intensity measures for IDA capacity estimation by incorporating elastic spectral shape information. Earthq Eng Struct Dyn 34(13):1573–1600

Chapter 2
Modeling and Propagation of Uncertainties

Paolo Emilio Pinto

Abstract The basic problem dealt within this chapter consists in finding the distribution of a scalar quantity Y which is a function of a vector **X** of probabilistically qualified random quantities. The dependence of Y on **X** is not explicit, requiring algorithms for its determination. An approach that facilitates the solution of the problem was first adopted in problems of nuclear safety, and consists in expressing the probability of Y exceeding a given value (if Y has a monetary connotation), or a given structural Limit-State of a whole system, as a multiple integral of a Markov chain of conditional probability functions. This approach is described in this chapter with reference to buildings, but the approach can be equally applied to various industrial systems. A crucial step in the chain is the passage from the intensity of the action, in the present case the intensity of the ground motion, to the vector of the structural response variables on which the state of the system, and ultimately Y, depend. This passage involves consideration of the variability of the action, in the form of different samples of ground motion together with all the uncertainties inherent in the numerical determination of the response, which include those related to the selection of the structural model and the uncertainties of its parameters. A number of approximate techniques for dealing with this problem are presented, starting from the simple but inadequate FOSM method, to the approach based on the use of a Response Surface in the space of the structural variables, and concluding with the potentially more accurate Latin Hypercube Sampling technique, underlining however its practical limits due to the computational effort required for large number of uncertain quantities.

P.E. Pinto (✉)
Department of Structural Engineering and Geotechnics, University of Rome 'La Sapienza', Via Gramsci 53, 00197 Rome, Italy
e-mail: pinto@uniroma1.it

K. Pitilakis et al. (eds.), *SYNER-G: Typology Definition and Fragility Functions for Physical Elements at Seismic Risk*, Geotechnical, Geological and Earthquake Engineering 27,
DOI 10.1007/978-94-007-7872-6_2,

2.1 On the Nature of the Uncertainties

It is usual to separate the uncertainties affecting all human activities into two categories, namely, *aleatoric* or *epistemic*. A common definition of the first category includes the uncertainties related to events whose outcome cannot be known before an experiment is made, as for example the outcome of a fair throwing of a fair dice, even if the associated phenomenon is completely understood. The definition above is, however, not exhaustive: there exist in nature phenomena that are, or are considered to be, inherently random, and others for which the idea of experiments is not applicable.

The second category includes uncertainties deriving from our incomplete knowledge of the corresponding phenomenon. Uncertainties of this nature are in principle reducible concurrently with improved understanding of the relevant process.

The distinction between the two categories appears at first quite clear and well founded. To blur somewhat the picture, one might argue that in a deterministic view of the world where every fact occurs as a consequence of precise laws, all uncertainties would reflect ignorance, hence, they would all belong to the epistemic class. At the opposite end, in a view of the world represented as a huge stochastic process, all the uncertainties would be represented in the model, hence they would be classified as aleatoric, while the parameters of the process, in case they would be only partially known, would be epistemic in nature.

This brief introduction is meant to establish a terminological basis. In probabilistic applications to actual problems, like for example the risk analyses that have been carried out within SYNER-G, the two types of uncertainty coexist, and there is no conceptual difference between the two, except for the following one. The aleatoric uncertainties are describable, in the majority of cases, by means of continuous probability distributions; on the other hand, the epistemic ones are often of the discrete type, and the associated probabilities are to be assigned subjectively on the basis of experience. Exceptions occur in both cases with discrete aleatoric variables, e.g. the variable describing which seismic source is generating an event, among the finite set of sources affecting the area, or continuous epistemic variables, such as those describing the uncertainty in model parameters.

2.2 The "Propagation" of the Uncertainties in Complex Systems

2.2.1 General

The SYNER-G project includes a number of individual systems (buildings, power stations, bridges, electric networks, etc.) connected to each other so as to form what could be called a "live" super-system (since the functioning of the whole depends

on the proper interaction amongst all the functioning components), and aims at evaluating the risk of different levels of reduced performance of the whole super-system in consideration of a spatially distributed seismic hazard.

All components of the super-system are in themselves complex systems which are made up in general of a large number of elements, each one performing a specific function and exposed to being damaged by a seismic event.

In general, the functional logic of complex systems cannot be described by means of an explicit functional relationship linking the response of the system to the state of its elements. Further, the states of the elements are generally of the continuous type, evolving from complete functionality to complete loss of it, and also the particular state of any component has an influence on that of the others. Under these conditions, the classical system theory based on elements having only binary behaviour is of no use for a probabilistic analysis of the types of complex systems.

A further issue is relevant regarding the use of the two different types of uncertainties, aleatoric and epistemic. It is customary to proceed by first assigning values to, or making choices for, the epistemic variables, evaluate then the risk conditional on all the possible combinations of values/choices of these variables, and then to make use of the total probability theorem to de-condition the previously determined conditional probabilities. This way of proceeding lends itself to a graphical illustration called "logic tree", of which a simple example is given in Sect. 2.2 (Fig. 2.1). Different techniques can be employed to evaluate the conditional probabilities in each branch of the logic tree.

A full blown Monte Carlo (MC) approach would be perfectly suited for the purpose, but even enhanced with the modern variance reduction techniques it would result in an unrealistic computational effort.

The few applications that can be found in the structural engineering literature use a mixture of MC simulations for some steps of the procedure and First Order-Second Moment (FOSM) methods for others. While the MC procedure is asymptotically exact, application of FOSM leads to acceptable approximations in cases of linear or approximately linear relationships among the variables involved (Lee and Mosalam 2005; Baker and Cornell 2008). If the relation is not originally linear, a first-order Taylor expansion can be used:

$$Y = g(\mathbf{X}) \cong g(\mathbf{X}_0) + \nabla g|_{\mathbf{X}_0}(\mathbf{X} - \mathbf{X}_0) \tag{2.1}$$

where Y is a scalar quantity dependent on the vector $\mathbf{X}$ collecting the N variables X_i, $g(\bullet)$ is a generic function of $\mathbf{X}$ and ∇g is its gradient with respect to $\mathbf{X}$, that can be obtained either analytically or numerically (through perturbation) depending on whether g($\mathbf{X}$) is known in explicit or algorithmic form. If the expansion is centred at the mean value of $\mathbf{X}$, owing to linearity one gets for the mean and the variance of Y:

$$\mu_Y = g(\mu_{\mathbf{X}}) \tag{2.2}$$

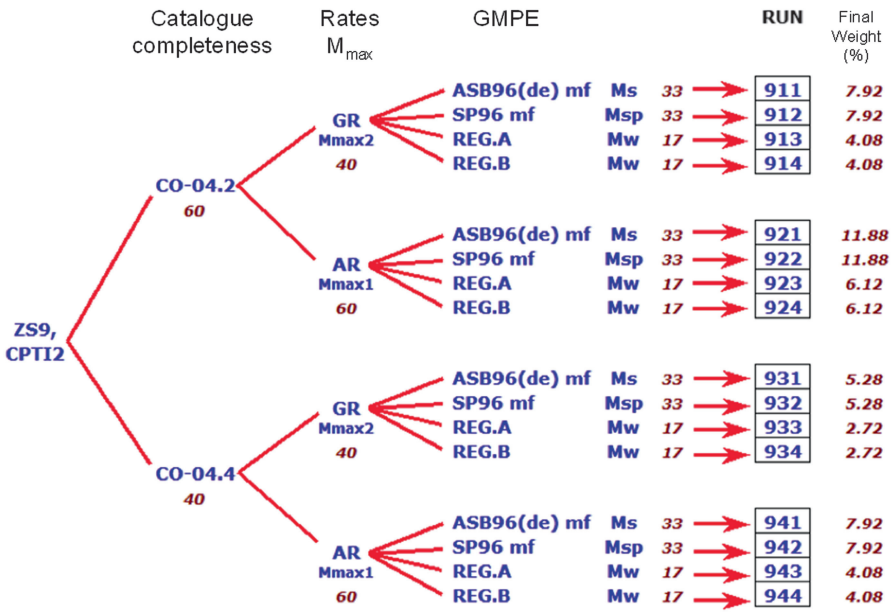

Fig. 2.1 Logic tree employed in the latest Italian seismic hazard map derivation to handle epistemic uncertainty. The weights are the product of the weights of the branches leading to the RUN (e.g. RUN 911 has weight $0.6 \cdot 0.4 \cdot 0.33 = 0.0792$). RUN numbers are composed of Seismic Zonation number (9), catalogue-M_{max} combination number (1–4) and employed GMPE (1–4)

$$\sigma_Y^2 = \nabla g|_{\mu_\mathbf{X}} \mathbf{C_{XX}} \nabla g^T\big|_{\mu_\mathbf{X}} \tag{2.3}$$

where $\mathbf{C_{XX}}$ is the known covariance matrix of $\mathbf{X}$. The expression above shows an example of how the variability of N variables can be condensed into that of a single one.

An approach that has been shown to offer practical advantages in probabilistic risk assessments dates back to early studies of seismic safety of nuclear plants in the 1950s of the last century. It consists in expressing the risk (defined, for example, as the annual rate of exceedance of a chosen measure of loss, functional or economic) in the form of a multiple integral of a Markovian chain of conditional probability functions. This approach has been adopted in recent years by the Pacific Earthquake Engineering Research (PEER) Center (Yang et al. 2009; fib 2012) with reference to buildings, and its presentation given in the following uses quantities that are meaningful for this class of structures, but the approach is general, and it can be adapted to other types of systems, such as industrial plants, hospitals, electric transformation/distribution systems, etc. Hospital systems, in particular, have been treated in SYNER-G with an approach having common points with the PEER approach.

2.2.2 The PEER Approach

2.2.2.1 Nomenclature

List of the terms used in this chapter:

- IM = Intensity Measure: a parameter expressing the intensity of seismic action, such as the peak ground acceleration, and the spectral acceleration at the fundamental period of the system.
- $\lambda(im)$ = the hazard function, or mean annual frequency of exceedance of $IM = im$
- **EDP** = Engineering Demand Parameter: a vector of response variables used for assessing the degree of damage to all structural and non-structural elements. The full characterization of the vector in probabilistic terms, i.e. in terms of a joint distribution function, is obtained from a number of dynamic response analyses.
- **DM** = Damage Measure: a vector having as many components as the number of structural and non structural elements. The passage from **EDP** = **edp** to **DM** = **dm** is obtained using "fragility curves" relative to different states of damage.
- DV = decision variable: a scalar quantity, monetary, as in the case of PEER, or a suitable performance index in the case of a generic system. The passage from **DM** = **dm** to $DV = dv$ is obtained through the so-called "loss curves" giving the probability of loss dv as function of the damage level **dm**. The number of the loss curves is given by the product of the number of damage levels times the different groups of damageable elements.
- $\lambda(dv)$ = the mean annual exceedance rate of $DV = dv$, unconditional from all previous variables.

2.2.2.2 Formulation

Using the symbols defined in the previous section the annual rate of exceedance of $DV = dv$ can be written as:

$$\lambda(dv) = \int_{\mathbf{DM}} \int_{\mathbf{EDP}} \int_{IM} G(dv|\mathbf{dm}) f(\mathbf{dm}|\mathbf{edp}) d\mathbf{dm} f(\mathbf{edp}|im) d\mathbf{edp} |d\lambda(im)| \qquad (2.4)$$

where $G(\bullet)$ indicates the complementary distribution function of the argument and $|d\lambda(im)|$ is the absolute value of the derivative of the hazard function.

The above equation is valid in the assumption of a Markovian dependence between the successive functions in the chain: for example, it implies that $f(\mathbf{dm}|\mathbf{edp})$ is the same as $f(\mathbf{dm}|\ \mathbf{edp}, im)$, that is, **dm** is only dependent on **edp** and not on im.

Equation (2.4) identifies four stages of the performance assessment: hazard analysis, response analysis, damage analysis and consequence analysis. This arrangement is convenient since it subdivides the total task into subtasks each one requiring a specific field of competence, starting from seismology to cost analysis.

2.2.2.3 Development

2.2.2.3.1 Hazard Analysis

This stage requires availability of the *hazard curve* appropriate for the site together with a *set of accelerograms* needed for the structural response analysis.

The hazard curve, which is definitely the most important element in risk analysis, is the result of a process disseminated with epistemic uncertainties, such as the subdivision in homogeneous seismic sources, their spatial dimension, their activity in terms of magnitudes and frequencies, the functional form of the attenuation laws, etc.

These uncertainties are accounted for by having recourse to the "logic tree", whose branches have as many nodes as the uncertainties considered, and at each node two or more choices are made for a particular uncertainty, with a subjective probability attached to each of them. Each branch is then characterized by a probability value, which is the product of the probabilities assigned at all choices defining the branch.

These probabilities are associated with the hazard evaluated using the choices along the branches, so that a discrete probability distribution of the hazard curves is obtained.

In order to reduce the burden of calculating the system risk using the different hazard curves and then convolving the risks so obtained with the probability of the hazard, in order to de-condition the system risk from the hazard uncertainty, current practice adopts the simplification of using the mean hazard obtained from the logic tree.

Figure 2.1 shows an example of the logic tree used to handle the epistemic uncertainty in the evaluation of the latest version of the seismic hazard of Italy (Stucchi et al. 2004) using a spatial grid of sides of 5×5 km. Discrete variables were used to describe uncertainty in the following issues: seismic catalogue completeness (two levels), upper bound magnitude in the G&R recurrence law (two levels), and attenuation laws (four different laws), resulting in 16 different combinations. Subjectively assigned probabilities are given in percent in the figure.

A number of accelerograms, typically between 20 and 40, is generally adequate, depending on the structure and in particular on the number of significant modes of vibration.

The selection can be made using the hazard de-aggregation procedure, by which one gets the triplet of M, r and ε that gives the major contribution to a selected value of the local exceedance rate of the intensity measure utilized. Records are then selected based on this triplet, more frequently on the values of M and r alone. Whether the records should also be compatible with a uniform hazard spectrum (characterized by a specified mean return period), or the choice should be made according to other, finer criteria, is still debated.

2.2.2.3.2 From *im* to **edp**

The response of the structure to each individual accelerogram is obtained, as already indicated, through non-linear time history analysis (NLTHA). The resulting **edp** vectors (one vector for each accelerogram and for each value of its intensity) collect all the response variables that will be needed in the next stage for passing from response to damage. These normally include the (maximum) values of the nodal displacements, the relative displacements and distortions of the elements, the accelerations at various points, and internal forces for brittle elements.

Once the NLTHAs are completed for the whole set of accelerograms at a given intensity level, statistical analysis is carried out on the response variables, and estimates of the parameters of their joint density function conditional on the intensity; i.e. mean values and covariance matrix, are obtained.

As the dynamic analysis phase is computationally the more demanding task of the whole risk determination procedure, often an artifice that involves the following steps is used to increase the number of correlated response values in the **edp** vector beyond those directly obtained through the NLTHAs.

In the first place the common assumption is accepted that the **edp** variables are jointly lognormally distributed, so that their logarithms are jointly normal.

Denoting by $\mathbf{X}$ the initial **edp** vectors, their logarithms are taken, denoted by $\mathbf{Y}$, and the mean μ_Y and covariance matrix $C_{\mathbf{YY}} = \mathbf{D_{YY}R_{YY}D_{YY}}$ are constructed, where $\mathbf{D_{YY}}$ indicates the diagonal matrix of the standard deviations of $\mathbf{Y}$ and $\mathbf{R_{YY}}$ its correlation matrix.

Use is then made of the fact that a vector $\mathbf{Z}$, having mean value μ_Y, standard deviation matrix $\mathbf{D_{YY}}$, and correlation matrix $\mathbf{R_{YY}}$ can be obtained from the expression:

$$\mathbf{Z} = \mu_{\mathbf{Y}} + \mathbf{D_{YY}L_{YY}U} \tag{2.5}$$

with $\mathbf{U}$ being a standard normal vector and $\mathbf{L_{YY}}$ the lower triangular decomposition of the correlation matrix ($\mathbf{R_{YY}} = \mathbf{L_{YY}L_{YY}}^{\mathrm{T}}$).

Based on the relationship above one can generate samples of $\mathbf{U}$, obtain the vector $\mathbf{Z}$, and finally compute a vector $\mathbf{X}$ by taking the exponential of $\mathbf{Z}$.

This simulation procedure of creating additional **edp** vectors having the proper statistical structure is very efficient, so that large numbers of these vectors can be generated with a minimal computational effort.

It is important to recall that in order to follow these steps one needs random vectors of **edp** for several levels of the intensity.

In the discussion thus far, related to the passage from *im* to **edp**, attention has focused on the variability of the response due to the variability of the ground motion, given a measure of its intensity. Though it is generally recognized that this variability is quite possibly the main contributor to the total uncertainty, this does not allow ignoring further sources of uncertainty of different nature whose relevance varies from case to case, and sometimes can be of significant importance.

As discussed in the following, the further sources are two, and are different in nature.

In order to determine **edp** from *im* a model of the structure has to be set up. Here the term model is used in a wide sense; it includes the structural modelling, e.g., whether and how certain elements have been included and their behaviour described, as for example the beam-column joints, or whether account has been taken of the shear–flexure interaction, whether beam-column elements are of the distributed or concentrated plasticity type, etc.

Various combinations of the above mentioned features are clearly possible. None of the existing models can be said to be perfect, and it is not guaranteed that the most "sophisticated" ones give the most accurate response.

One clearly recognizes the above situation as one where the uncertainty is of the epistemic type, whose solution could consist of the following steps: selecting two (or more) models, all of them considered in principle as valid candidates, running the whole procedure of risk analysis, and assigning the weight (degree of confidence) attributed to each of the models to the risks values computed. In this particular instance of application of the logic tree all models would have the same weight, it would make in fact little sense to use a model considered as less reliable than the others. The final value of the risk would clearly be the weighted average of the different risk values.

The second source of uncertainty can be of both aleatoric and epistemic type, and is related to the parameters of the models, for example the mechanical properties of the reinforced concrete components (if there are doubts on other aspects, such as the exact layout of the reinforcement, they would belong to the previous category). The mechanical properties of the materials are random variables whose distributions must be assumed as known. Correlations exist between some of them (as for ex strength and ultimate deformability of concrete), as well as spatial correlations of the same variable at different locations.

It has been observed that for structures designed according to modern codes, and for not extreme ranges of the response, the variability of these quantities has normally a reduced effect on the variability of the dynamic response, and its relevance becomes quite modest in consideration of the other major uncertainties affecting the whole procedure (see following steps). In view of their reduced importance their effect is treated in an approximate way, consisting in sampling all the variables from their distributions as many times as is the number of the dynamic runs, and in associating to each run (i.e. to each accelerogram) a different model having the properties of the corresponding sample.

In the last few years, however, much research has been devoted to obtain models suitable for describing the degrading behaviour of existing, non code-conforming structural elements, down to their total loss of vertical load carrying capacity. These models are of completely empirical derivation, with a rather restricted experimental base. As a consequence, their parameters are characterized by large dispersions, inducing a variability of the response of the same order of magnitude of that due to ground motion variability. The developing state of such models leads to consider the variability of the parameters as belonging to the epistemic class.

The simplified PEER approach is not suited for these cases, and a review of the techniques that have been recently proposed to deal with them is presented at the end of this section.

Continuing with the PEER approach, the stage of progress reached thus far is the one characterized by the largest number of variables: a number of 100/200 edp vectors (each one having the dimension necessary to describe the state of the structure), necessary for the need of the simulation procedure to follow, times the number of levels of the intensity to be considered (usually around ten). The subsequent steps will need to gradually condense this large vector down to the final one, where a single variable (or possibly a small number of alternative variables in the form of performance indexes) will express the risk of the system.

2.2.2.3.3 From **edp** to **dm**

Real systems are made up of a very large number of individual components that can be broadly classified into two categories: the *structural* components, into which one may include, for convenience, both *load-resisting elements* (beams, columns, floors,. . .), and the so-called *architectural component*s like partition walls, ceilings, glazing, etc., and *functional* components, i.e. those allowing each particular system to operate.

The focus of risk analysis varies with the type of the system. For ordinary buildings the risk is normally defined in terms of the total economic loss, while for a hospital the definition is in terms of its continued operability, and for an electric generation/transformation station the risk is in terms of the number of lines that remain active and of the quantity and quality of the power that can be delivered, etc.

Whatever the adopted definition of risk, each particular **edp** vector determines a particular state of the system, involving both structural and functional components according to the functional logic of the system.

The PEER procedure, which is exemplified in this chapter, has been developed with reference to buildings, so the risk refers to the total monetary cost.

In order to reduce the variables of the problem, elements are divided into groups with the criterion that the members belonging to one group are (approximately) attributed to the same fragility function. Fragilities are available for discrete states of damage, frequently three for structural elements and two for architectural elements.

The states of damage for structural elements are described in qualitative terms, as for example light, moderate and severe, having in mind that to each term and for each type of element there should be associated (in probabilistic terms) a cost of repair.

The passage from edp to dm is illustrated with reference to Fig. 2.2, showing three fragility curves relative to interstorey drift ratio. Damage State 1 (DS1) corresponds to negligible damage and is not represented in the figure, DS2 corresponds to slight damage requiring superficial repair, DS3 represents severe damage

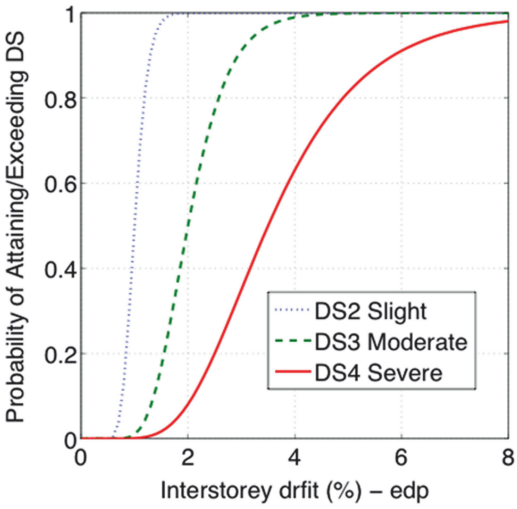

Fig. 2.2 Fragility curves for increasing damage states

requiring substantial repair, and DS4 is for damage requiring a cost of repair equal to that of replacement.

It is recalled that each fragility curve expresses (in this case) the probability that the damage of the element (or group of elements) is equal or larger than that relative to the specified curve for a given value of *edp* (the component of the **edp** vector that influences the state of the element/group). The vertical distance between two curves (e.g. DS2 and DS3) provides the probability of being in the damage state corresponding to the higher curve (DS2).

The passage from the probability of **edp** to that of **dm** is thus the following:

- an **edp** vector is chosen from the collection relative to a specific intensity level.
- each group of elements is considered in turn and its damage level is determined using the appropriate fragility curve. This is done by sampling a uniform random number (in the interval 0–1) and checking where it falls in the intervals defined by the fragility curves at the current *edp* value.
- the operation is repeated for all **edp** vectors, and the distribution of the **dm** vector (for a particular intensity level) is thus obtained.

2.2.2.3.4 From **dm** to *dv*

The passage from ***dm*** to *dv* is accomplished by introducing the so-called "loss functions", which give for each group of elements the probability of the cost associated with each level of damage. An example of such types of functions is given in Fig. 2.3.

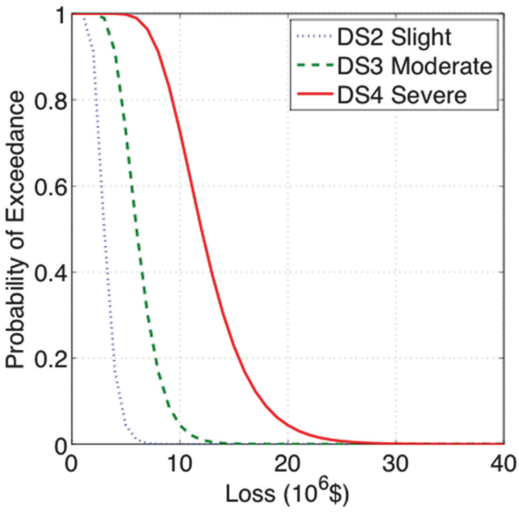

Fig. 2.3 Probability of exceedance of economic loss thresholds as a function of damage state

The passage from the probability of **dm** to that of the total *dv* is as follows:

- for each group, the probability that the value $DV = dv$ is exceeded is obtained as the sum of the products of the probability of *dv* conditional to the generic value of damage *dm* (loss curve), times the probability of that damage.
- the operation above is repeated for all the desired values of *dv* and for all levels of damage *dm*.
- since damage levels are mutually exclusive, the total probability (complementary distribution) of *DV* exceeding any given value *dv* is obtained as the sum of the probabilities over all groups and all damage levels.

2.2.2.3.5 Consideration of Collapse

In the developments thus far, structural and non-structural elements have been considered to be susceptible to damages of various severity.

However, the integrity of the whole system, i.e. its ability to continue sustaining its own weight, has not been considered. Yet the total physical collapse of a building is an event that has a weight in the post-earthquake decisions, and for this reason the probability of its occurrence and the associated DV are often included in the overall procedure. This is simply done as follows.

Starting from a certain intensity level, in some of the simulations the integrity of the structure is so seriously endangered as to suggest the use of the term "collapse".

These cases should be considered separately from the "non collapse" states and, for any given intensity, a probability of collapse should be approximately evaluated as the ratio between the number of simulations where collapse has occurred to the total number of simulations. The complement of this probability, namely, the "non

collapse probability", is the one to be associated to the computation of damages as previously described.

It is important to note, however, that the question of how to define this extreme state of a structure is not yet completely settled, and different approaches are in use.

The first and still widely adopted proposal consists in looking at collapse in a global way, and defining this state as the one when the calculated dynamic displacements tend to increase indefinitely for an infinitesimal increase of the intensity (so-called dynamic instability). This approach does not look directly at the state of the individual structural elements, some of which may well have exceeded their individual deformation capacity and be in the post-peak negative stiffness branch of response. Rather, the approach relies on the ability of the model to correctly reflect the effect of the local damage at the global level.

As in the passage from *im* to **edp**, models have been developed in the last few years to describe the degrading behaviour of reinforced concrete beam-column elements subjected to cyclic normal force, bending and shear down to the exhaustion of their vertical load bearing capacity.

Availability of these models, however, even when they will have become more accurate and robust, will not per se provide a unique solution to the problem of defining the collapse of an entire structure, since collapse can occur involving the failure of a variable number of elements depending on structural topology and robustness.

The frequent choice of considering a structure as a series system whose failure is made to depend on the first complete failure of a single element can be in many cases a rather conservative approach. Attempts to overcome this conservatism include for instance a floor-level comparison between gravity load demand and capacity (to account for vertical load redistribution), as done for instance in Baradaran Shoraka et al. (2013).

2.2.2.3.6 Evaluation of Risk

The complementary distribution of *DV* calculated as above is a function of the intensity of the seismic action. As such, it may be already sufficiently informative for those in charge of taking decisions if, for instance, the interest is in knowing the loss associated with a given "design" action (e.g. earthquake with 1,000 years return period).

If, on the contrary, the interest is in knowing the total risk contributed by all possible intensities, one should simply integrate the product of the probability of *DV* conditional on $IM = im$ times the mean annual rate of the *IM*. In performing this integration, collapse and non-collapse cases must be kept separate and weighted with the corresponding probabilities:

$$\lambda(dv) = \int_{IM} [G(dv|im, NC)P_{NC}(im) + G(dv|C)P_C(im)]|d\lambda(im)| \qquad (2.6)$$

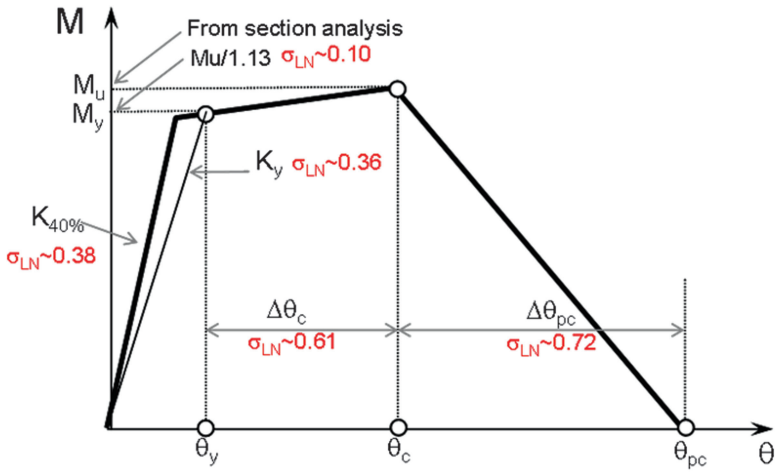

Fig. 2.4 Section degrading moment-rotation curve with indication of parameter dispersion (Models by Haselton and Deierlein 2007)

2.2.3 Treatment of "Epistemic" Model Uncertainties

As mentioned before, models have been recently developed which are capable of describing progressively degrading states of reinforced concrete elements down to their complete loss of bearing capacity. It has also been observed that the parameters of these models are affected by large variability whose final effect is that of a significant increase of the variance of the Limit State fragilities (Ibarra et al. 2005; Ibarra and Krawinkler 2005; Goulet et al. 2007).

Figure 2.4 shows a monotonic envelope of a moment-chord rotation relationship typical of this class of models used in a demonstration study by Liel et al. (2009). The logarithmic standard deviations attributed to the corner points of the diagram are 0.6 and 0.7 for the rotations up to and post peak, and 0.5 to a parameter which regulates the cyclic degradation. These values are much higher than, for example, the values adopted for the beam or column strength (0.19) or stiffness (0.36 ÷ 0.38).

A standard procedure for introducing model uncertainties into a seismic fragility function does not exist. All methods available in the literature are approximate, and every improvement in approximation is paid with a rapidly increasing amount of additional computations.

The simplest and perhaps most widely used method is FOSM which was briefly described in Sect. 2.2.1. It is applicable to any type of LS fragility, from light damage to collapse, including all intermediate LSs. As explained earlier, the method consists of deriving a linear relationship $g(\mathbf{X})$ between the LS of interest and the variables (in this case the epistemic quantities) whose influence on the LS is sought (an expression involving response and capacity, as a function of the

variables **X**). Linearity implies that the mean value of the distribution of the LS is unchanged with respect to that obtained by using the mean values of the epistemic variables, $\mu_g = g(\mu_{\mathbf{X}})$, while the variance of the fragility due to the variability of these variables is (approximately) evaluated.

FOSM has two limitations: the linear dependence can become grossly inadequate as the considered LS moves towards the collapse state and, second, the mean value of the fragility remains unchanged, a fact that is shown to be untrue by more elaborate approaches.

A second approach, described in Liel et al. (2009), makes use of a *response surface* in the space of model uncertainties, combined with a MC procedure. Response surfaces can be set up to give the log-mean and the log-standard deviation of the LS capacity (IM that induces the LS), in the form of complete second order polynomial functions of **X**. This allows one to capture both direct effects of the variables, up to their squared values, and the interactions between any two of them on the quantity of interest.

With four random variables, each polynomial function contains 15 coefficients. This gives already an idea of the number of "experiments" to be carried out, since this number must be significantly larger than the number of the coefficients to be estimated in order to reduce the variance of the "error term".

For a complete quadratic form of the function the so-called Central Composite Design of (numerical) experiments is appropriate (Pinto et al. 2004). This plan requires a complete two-level factorial design involving experiments for all the $2^4 = 16$ combinations of the (4) variables complemented by the addition of two further "star" points located along each of the variable axes and a "centre" point, for an additional $2 \times 4 + 1 = 9$ points, which makes a total of 25 "experiments".

Each "experiment" consists in performing an incremental dynamic analysis on one particular model out of the 25 ones using an adequate set of accelerograms (in the order of 20–30), and in calculating log-mean and log-standard deviation values of the selected LS capacity. When all the experiments are concluded, standard Least Square method is used to obtain the numerical values of the coefficients of the two response surfaces $\mu_{\ln IM}(\mathbf{X})$ and $\beta(\mathbf{X}) = \sigma_{\ln IM}(\mathbf{X})$.

Once the response surfaces are created, a MC procedure is used to sample a large number of sets of the modelling variables from their distributions, which yield the fragility parameters through the fitted surfaces. The unconditional fragility function, accounting both for record-to-record variability and epistemic model uncertainty, is obtained by averaging over all the samples. Results generally show a decrease in the median and an increase in the dispersion, more pronounced for LS closer to collapse due to the fact that the uncertainty affecting ultimate deformation is larger than that associated with elastic or low-ductility response.

Figure 2.5 shows the collapse fragility obtained by both the response surface (left) and the FOSM approach (right), including or neglecting the modelling epistemic uncertainty. The curves show that the median collapse capacity is influenced by the epistemic uncertainty.

A further alternative to account for the effect of both the ground motion variability and all other types of uncertainty on the structural fragility has been

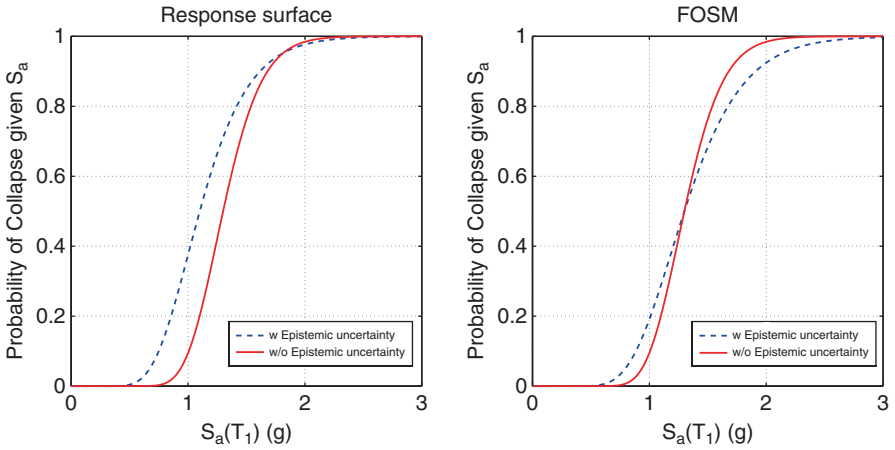

Fig. 2.5 Fragility curves with and without epistemic uncertainty, as obtained by the response surface (*left*) and the FOSM (*right*) procedures (Adapted from Liel et al. 2009)

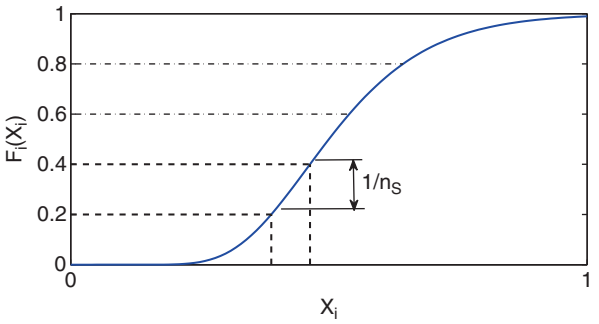

Fig. 2.6 Equal probability values obtained by stratified sampling (Adapted from Vořechovský and Novák 2009)

adopted in a number of recent publications, e.g. Fragiadakis and Vamvatsikos (2010) and Dolšek (2012). The procedure is conceptually the same as described in Sect. 2.2.2.3 for the passage from *im* to **edp**, but made more efficient and potentially accurate through the use of the so-called Latin Hypercube Sampling (LHS) technique (Helton and Davis 2003) for the sampling of the random variables describing the modelling uncertainties. This technique is much more efficient than ordinary (random) MC. While random sampling produces standard errors that decrease with the number N of simulations according to $\sqrt{N}$, the error with LHS goes down at a much faster rate, approaching $\sqrt[3]{N}$ for linear functions.

According to Helton and Davis (2003) LHS operates in the following way to generate a sample of size n_S from a random vector $\mathbf{X} = (X_1, X_2, \ldots X_{nX})$, consistently with the marginal distributions of the X_i's. The range of each variable X_i is exhaustively divided into n_S intervals of equal probability content as shown in Fig. 2.6, and one value is sampled at random from each interval. The n_S values thus

obtained for X_1 are paired at random without replacement with the n_S values obtained for X_2. These n_S pairs are combined in a random manner with the n_S values of X_3, and the process continues until a set of n_S n_X-tuples is formed. The resulting matrix of n_S rows by n_X columns constitutes the LHS sample, and the values contained in each row represent a possible model for the structure.

The obtained LHS sample, however, is characterized by a correlation matrix that is not the one specified by the analyst according to the specific features of the structure, and hence needs to be modified. This can be achieved according to a procedure proposed in Helton and Davis (2003) and Vořechovský and Novák (2009), which is based on rearranging the values on the individual columns of the original matrix.

The LSH technique is in principle applicable for any size n_X of the vector of the modelling variables. However, the number of variables that can practically be treated is limited by computational considerations. Although there are no fixed rules, the sample size n_S, i.e., the number of different models, must be a multiple (of the order of, say, two) of the size n_X of the vector **X**. Since each model must be subjected to dynamic analyses under the full set of the selected accelerograms, and for different intensity levels, the total number of models should not be exceedingly large.

To reduce the number of variables under consideration (the components of vector **X**), correlations can be assumed between the variables within each structural member and among the members in the structure. For example, within a RC member, variables related to strength, such as stiffness and yield moment could be assumed as perfectly correlated, and similarly for the deformation parameters (see Fig. 2.4). At the system level, all elements having the same properties could also be assumed as perfectly correlated. In the examples found in the literature, e.g. Fragiadakis and Vamvatsikos (2010) and Dolšek (2012), the dimension of vector **X** does not exceed 12. It is noted that in the mentioned literature the components of the vector **X** are all indicated as epistemic, though they include both the material properties such as, for ex., concrete and steel strength, which are usually categorized as aleatoric, as well as the other parameters of the model such as those shown in Fig. 2.4. All the components of **X** are however represented by continuous variables, i.e. they do not include epistemic variables such as the consideration of alternative models, alternative methods of analysis, etc., for which the logic tree approach remains necessary and appropriate.

References

Baker JW, Cornell CA (2008) Uncertainty propagation in probabilistic seismic loss estimation. Struct Saf 30(3):236–252

Baradaran Shoraka M, Yang TY, Elwood KJ (2013) Seismic loss estimation of non-ductile reinforced concrete buildings. Earthq Eng Struct Dyn 42(2):297–310

Dolšek M (2012) Simplified method for seismic risk assessment of buildings with consideration of aleatory and epistemic uncertainty. Struct Infrastruct Eng 8(10):939–953

Fragiadakis M, Vamvatsikos D (2010) Fast performance uncertainty estimation via pushover and approximate IDA. Earthq Eng Struct Dyn 39:683–703

Goulet CA, Haselton CB, Mitrani-Reiser J, Beck JL, Deierlein GG, Porter KA, Stewart JP (2007) Evaluation of the seismic performance of a code-conforming reinforced-concrete frame building—from seismic hazard to collapse safety and economic losses. Earthq Eng Struct Dyn 36(13):1973–1997

Haselton CB, Deierlein GG (2007) Assessing seismic collapse safety of modern reinforced concrete moment frame buildings. John Blume Center technical report 156

Helton JC, Davis FJ (2003) Latin hypercube sampling and the propagation of uncertainty in analyses of complex systems. Reliab Eng Syst Saf 81:23–69

Ibarra LF, Krawinkler H (2005) Global collapse of frame structures under seismic excitations. John Blume Center technical report 152

Ibarra LF, Medina RA, Krawinkler H (2005) Hysteretic models that incorporate strength and stiffness deterioration. Earthq Eng Struct Dyn 34(12):1489–1511

International Federation of Structural Concrete (fib) (2012) Bulletin 68. Probabilistic performance-based seismic design

Lee TH, Mosalam KM (2005) Seismic demand sensitivity of reinforced concrete shear-wall building using FOSM method. Earthq Eng Struct Dyn 34(14):1719–1736

Liel AB, Haselton CB, Deierlein GG, Baker JW (2009) Incorporating modeling uncertainties in the assessment of seismic collapse risk of buildings. Struct Saf 31:197–211

Pinto PE, Giannini R, Franchin P (2004) Seismic reliability analysis of structures. IUSS Press, Pavia. ISBN 88-7358-017-3

Stucchi M, Akinci A, Faccioli E, Gasperini P, Malagnini L, Meletti C, Montaldo V, Valensise G (2004) Derivation of the seismic hazard map for Italy – final report to the Department of Civil Protection (in Italian)

Vořechovský M, Novák D (2009) Correlation control in small-sample Monte Carlo type simulations I: a simulated annealing approach. Probab Eng Mech 24:452–462

Yang TY, Moehle J, Stojadinovic B, Der Kiureghian A (2009) Seismic performance evaluation of facilities: methodology and implementation. ASCE J Struct Eng 135(10):1146–1154

Chapter 3
Evaluation of Existing Fragility Curves

Tiziana Rossetto, Dina D'Ayala, Ioanna Ioannou, and Abdelghani Meslem

Abstract There is a wealth of existing fragility curves for buildings and infrastructure. The main challenge in using these curves for future applications is how to identify and, if necessary, combine suitable fragility curves from a pool of curves with different characteristics and, often unknown, reliability. The present chapter aims to address this challenge by developing a procedure which identifies suitable fragility curves by firstly assessing their representativeness to the needs of the future application and then assessing the reliability of the most relevant relationships. The latter is based on a novel procedure which involves the assessment of the most significant factors affecting the robustness and quality for each fragility assessment methodology, also presented here. In addition, a decision-tree approach is adopted in order to combine more than one suitable fragility curves. The proposed selection and combination procedures are illustrated here with a simple case study which appraises the impact of different weighting schemes and highlights the importance of a deep understanding of the existing fragility curves and their limitations.

3.1 Introduction

Fragility curves are important components of seismic risk assessments, providing the link between the seismic hazard assessment at a site and the effects of the predicted ground motions on the built environment. To date, significant work has been carried out in the field of fragility with numerous fragility curves having been proposed for components of the built environment (assets) in different countries (e.g. see Rossetto et al. 2013a; D'Ayala and Meslem 2013). However, a range of

T. Rossetto (✉) • D. D'Ayala • I. Ioannou • A. Meslem
Department of Civil, Environmental and Geomatic Engineering, University College London, Gower Street, WC1E 6BT London, UK
e-mail: t.rossetto@ucl.ac.uk; d.d'ayala@ucl.ac.uk; Ioanna.ioannou@ucl.ac.uk; a.meslem@ucl.ac.uk

K. Pitilakis et al. (eds.), *SYNER-G: Typology Definition and Fragility Functions for Physical Elements at Seismic Risk*, Geotechnical, Geological and Earthquake Engineering 27, DOI 10.1007/978-94-007-7872-6_3,

methods have been adopted in the literature to produce fragility curves resulting in curves with different, and often unknown, reliability. The central questions this Chapter aims to answer are:

- How do I choose suitable set/s of fragility curves for the asset class and location in my seismic risk assessment?
- What approaches can I take to combining the selected fragility curve sets?

First, the main methods for constructing fragility curves are reviewed. Next, for each predominant method the factors influencing the reliability of resulting fragility functions are discussed in greater detail. On the basis of this discussion a rating system is proposed for empirical and analytical fragility functions. A procedure is proposed for rationally selecting the most useful and appropriate fragility curves from the literature for application in a future seismic risk assessment. Given that it is often very difficult to decide which existing fragility function is the "best" for an assessed asset and location, within this Chapter possible methods for combining fragility functions, in cases where more than one set of suitable fragility curves exist, are explored. The concept of combining fragility functions in seismic risk assessments is relatively new in the academic literature, even though it is commonly used in probabilistic seismic hazard assessment. In the latter assessment, ground motion prediction equations are combined through the use of logic trees which accounts for the confidence of the users in the suitability of each equation to the needs of the hazard assessment. The investigated approaches to combining fragility functions are therefore tested for the case of mid-rise masonry buildings in Italy to assess their influence on the final mean curves. Furthermore, approaches for including new empirical data with the existing fragility functions are also investigated. It is emphasised that, as this is a single case, the results of the application are deemed indicative. Further research is required to make definite conclusions on the adequacy of the different approaches for other sites, assets and additional empirical datasets.

3.2 Review of Existing Methods for Constructing Fragility Curves

In recognition of the diverse response of different components of the built environment to seismic excitation, fragility curves are typically defined for specific and well-constrained asset classes (e.g. particular types of buildings or infrastructure). They express continuous relationships between the probability that the specified asset class will reach or exceed predefined damage states, for a range of earthquake ground motion intensities. Mathematically they can be expressed as:

$$P\left(DS \geq ds_i \middle| IM\right) \quad \text{for} \quad IM_{\min} \leq IM \leq IM_{\max} \tag{3.1}$$

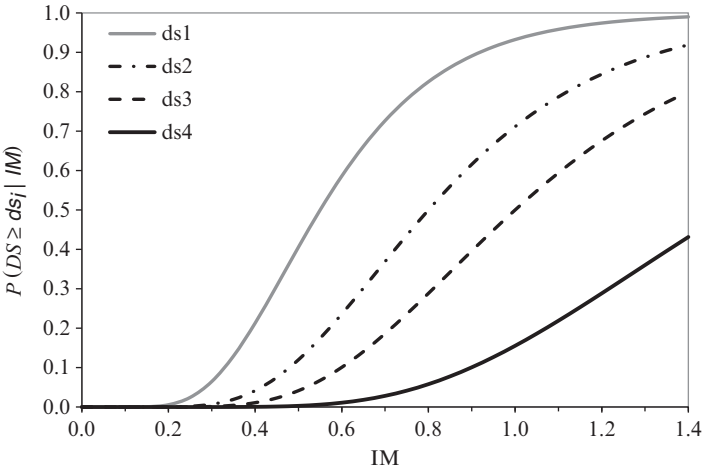

Fig. 3.1 Example fragility curve set

where DS is the damage state of the asset class being assessed, ds_i is a particular predefined state of damage and IM is the parameter used to define the ground motion, which takes a minimum and maximum value IM_{min} and IM_{max}, respectively. Where, in the same study and for the same asset class, fragility curves have been defined for several damage states they are termed a set of fragility curves, e.g. Fig. 3.1. In this case, the difference in exceedance probabilities defined by consecutive fragility functions at the same value of IM, represents the probability that the asset class will be in the lower of the two damage states, i.e.:

$$P\left(DS \geq ds_i \middle| IM\right) = \begin{cases} 1 - P\left(DS \geq ds_i \middle| im_j\right) & i = 0 \\ P\left(DS \geq ds_i \middle| im_j\right) - P\left(DS \geq ds_{i+1} \middle| im_j\right) & 0 < i < n \\ P\left(DS \geq ds_i \middle| im_j\right) & i = n \end{cases} \tag{3.2}$$

where, n is the number of damage states adopted.

Conversely, the damage state probability of an asset class can be used to construct a fragility function. And this is what is most commonly done in the literature, with the source of the asset damage statistics defining the four major categories of fragility curves (modified from Rossetto and Elnashai 2003):

- Post-earthquake surveys – Empirical fragility curves.
- Expert elicitation – Expert Elicitation fragility curves.
- Simulations of the earthquake response of the asset class – Analytical fragility curves.
- A combination of the above sources – Hybrid fragility curves.

The main approaches for constructing fragility functions within each category are presented in the following sections.

3.2.1 Overview of Empirical Fragility Approaches

Post-earthquake damage surveys of asset classes are commonly regarded as the most reliable source from which to construct fragility curves. This is due to the fact that they are real observations of damage and intrinsically account for the influence on the strong ground motion and asset damage of the earthquake source, path, site, exposure, structural and non-structural components. Rossetto et al. (2013a) provide an extensive review of the state-of-art in the construction of empirical fragility functions for buildings. They highlight that there is a large variation in the empirical fragility assessment procedures presented in the literature, which result from differences in the damage observation databases used, functional forms chosen to fit to the data, the selected ground motion intensity measure, and the statistical modelling technique used.

In general, an empirical fragility function is constructed from a database of damage data collected following one or more earthquake events. The quality and completeness of the database are extremely important in determining the reliability of the resulting empirical fragility function, and are often linked to the method of collection of the empirical data. As shown in Table 3.1, high reliability of data is often associated with survey methods that produce small numbers of damage observations (sample sizes). These small sample sizes are not ideal for fragility assessments as they result in large confidence bounds being associated with the constructed curves. If the empirical fragility curves are based on data obtained from a single earthquake event, the range of intensity measure values covered by the damage observations may also be limited, moreover, the fragility curves may not appropriately account for the variability in structural response from aleatory uncertainty in the ground shaking (e.g. number of cycles, frequency content) at any given intensity measure value. Despite these observations, the majority of existing empirical fragility functions are derived solely from single event damage databases (e.g. Karababa and Pomonis 2010; Liel and Linch 2012).

Large damage databases from rapid post-earthquake surveys and inferred from change analysis of satellite images (remotely sensed) have also been used for the construction of fragility functions (e.g. Hancilar et al. 2011). However, these databases are associated with very broad building classes and there is a larger probability that buildings in the database have been assigned to the wrong damage state. Ioannou and Rossetto (2013) have shown that these misclassification errors can have a large influence on the resulting mean fragility curves.

In order to cover a larger range of intensity measure levels and maintain a higher quality of damage database, some studies have developed fragility functions by combining post-earthquake damage surveys from several events that have affected the same building class (e.g. Rota et al. 2008; Gűlkan et al. 1992). However, even in these cases, due to the infrequency of large earthquake events near urban areas, the data are still seen to be highly clustered in the low-damage, low ground motion intensity range. Furthermore, implicit in the studies is the assumption that the uncertainty in the seismic performance of individual buildings for a given earthquake

Table 3.1 Empirical damage data sources and data characteristics

Survey method	Typical sample sizes	Typical building classes	No. of damage states	Reliability of observations	Typical issues
Rapid surveys	Large	All buildings	2–3	Low	Safety not damage evaluations
Detailed engineering surveys	Medium to small	Detailed classes	5–6	High	Possibility of unrepresentative samples
Surveys by reconnaissance teams	Very small	Detailed classes	5–6	High	Possibility of unrepresentative samples
Remotely sensed	Very large	All buildings	3–5	Low	Only collapse or very heavy damage states may be reliable. Misclassification errors

Adapted from Rossetto et al. (2013a)

(intra-event variability) is larger than the uncertainty in the building performance when subjected to different earthquakes (inter-event variability). This assumption has not yet been addressed anywhere in the literature (Rossetto et al. 2013a).

To construct a fragility curve from building damage observations, these must be associated with a ground motion intensity measure level. Ideally, ground motion recordings would be available across the area of damage observations. However, ground motion recording instruments are scarce and it is unlikely that there would be multiple instruments in the same area. The majority of existing empirical studies therefore evaluate their adopted intensity measure from damage data (i.e. macroseismic intensity measures) or ground motion prediction equations (GMPE). Modern GMPEs are based on numerous ground motion recordings and account for differences in focal mechanisms and soil types. However, modern GMPEs may not be available for the particular country assessed and adopted from regions with similar tectonic environments, or the study may pre-date the derivation of reliable GMPEs for the particular intensity measure and site (Rossetto et al. 2013a). In terms of the intensity measure used, peak ground acceleration (PGA) and peak ground velocity (PGV) are the most commonly used parameters. This mirrors their dominance in GMPE availability. As GMPEs have been recently developed for spectral values, some empirical fragility functions have been developed in terms of spectral acceleration and spectral displacement but constitute a minority of empirical studies (e.g. Rossetto and Elnashai 2003; Amiri et al. 2007; Colombi et al. 2008).

In the literature a functional form is fit to the empirical data through the use of a statistical model. The vast majority of existing studies select a cumulative log-normal distribution to represent the shape of the fragility function, with a few studies adopting the cumulative normal distribution (e.g. Spence et al. 1992) and a minority an exponential function (e.g. Rossetto and Elnashai 2003). These

parametric functions are fit to the data via three main statistical modelling approaches: nonlinear, linear and generalised linear. Fitting these models to a set of data requires the estimation of their unknown parameters through an optimisation procedure. The reader is referred to Rossetto et al. (2013b) for a detailed description of the methods and to Sect. 3.3.1 for a discussion of the validity of these models in the context of post-earthquake damage data and fragility curves.

The main assumption in the development of empirical fragility curves is that damage that has occurred in the past to a particular asset class is representative of the damage that might happen in the future to a similar asset class subjected to a similar earthquake. In practice, this assumption essentially limits the applicability of empirical fragility functions to the assessments of locations and buildings in geographical proximity to where the empirical data was collected. This poses a problem for their use for seismic risk assessments in some countries as there is not an equal distribution of fragility functions for buildings worldwide. For example in the case of buildings, the vast majority of empirical fragility curves have been derived for Greece, Italy, Japan, Turkey and USA (Rossetto et al. 2013a).

Empirical fragility curves have been also developed for individual (often critical) components of common infrastructure systems, such as electric microcomponents or substations in electric power networks (e.g. Anagnos 1999; Giovinazzi and King 2009), pipelines in water distribution systems (e.g. ALA 2001), bridges, tunnels or highway embankments in transportation networks (Elnashai et al. 2004; Corigliano et al. 2011; Maruyama et al. 2010). The same approaches as applied for buildings are relevant to the construction of empirical fragility functions for infrastructure components, with the added complexity that some of the infrastructure components (in particular pipelines and bridges) have an extended length and so care must be taken to consider this in the evaluation of a single value of intensity measure at the damaged component sites. An overview of fragility functions for infrastructure components is provided in Kaynia (2013). It is interesting to note that although many of these fragility functions are developed for several damage states, typically only the collapse or failure damage state fragility curve is adopted in system earthquake impact studies, which are mainly based on assessing network connectivity. This is mainly due to the level of data and computation required to carry out a serviceability analysis of systems affected by earthquakes, for which damage states other than collapse/failure would be useful.

3.2.2 Overview of Analytical Fragility Approaches

Analytical methods for constructing fragility curves frame the problem of seismic vulnerability in structural engineering terms, defining a direct mechanical relationship between construction characteristics, structural response to seismic action and damage effects.

The development of ground motion prediction equations (GMPE) for specific seismic regions and corresponding derivation of seismic hazard maps in terms of

spectral ordinates as opposed to macroseismic intensity or peak ground acceleration (PGA), (the most common ground motion parameters adopted in empirical approaches), has given impetus to the development of analytical methods for fragility assessment (see Stafford 2013, for an overview of GMPE derivation methods). These methods tend to feature more explicit assessment algorithms with direct physical meaning. In the development of analytical fragility functions three predominant approaches can be identified:

1. Correlation between damage index and damage states.
2. Correlation between acceleration/displacement capacity curves (for buildings) and spectral response curves.
3. Correlation between acceleration/displacement capacity curves (for buildings) and acceleration time histories.

Approach (1) has been widely used in the past decade within simplified models. The damage indices can be either global (for the entire structure) or local (determined for each structural element) or global damage indices determined from a combination of local indices. Threshold values of the indices are correlated to damage states defined by a damage scale. The most commonly used local damage index is that by Park and Ang (1985), which is defined as the linear combination of the maximum displacement and the dissipated energy in a reinforced concrete structural element. Park and Ang (1985) also define a global damage index that can be determined from a weighted summation of the local damage index values. A major limitation of approach (1) is the need to adopt indices that are extensively validated with experiments. Few such damage indices exist, and those that exist do not cover all building types. Furthermore, in order to ensure robustness of the fragility curves derived using damage indices, attention should be paid to the consistency between the damage model/damage index and the level of complexity of the structural model, the type of analysis, and the damage indicator to which the damage level is correlated. For example, the Park and Ang (1985) damage index requires a 2D or 3D model of the structure to be built and is more appropriate for use in damage evaluation from non-linear time history analyses than pushover analyses due to the dissipated energy component of the index.

Approach (2) is at the basis of the well-known HAZUS-M (FEMA 2003) or N2 methods (Fajfar 2000). The capacity spectrum approach is based on running a pushover nonlinear static analysis for a given structure, producing a capacity curve, i.e. a bilinear or multilinear acceleration-displacement curve which describes the global behaviour of the structure when subjected to gravity loads and laterally pushed, to simulate statically the seismic action. Various methodologies of pushover analysis are available in literature, relating to possible distribution of lateral acceleration with height, and to the possibility of adapting the lateral load to the response as the analysis progress (Antoniou and Pinho 2004). The actual pushover curve is then usually idealised to be reduced to a series of linear branches of constant stiffness and expressed in the pseudoacceleration/displacement spectral space. The capacity curve is then intersected with an appropriate spectral curve representing the demand in order to determine the performance point, i.e. the point

in the Sa/Sd plane which represents the response of the structure when subjected to a seismic action of a given intensity represented through the non-linear spectrum. The process of determining the performance point is usually iterative as the nonlinear spectrum chosen to define the intersection with the capacity curve is a function of the ductility demand, and this depends on the position of the performance point relative to the elastic limit performance for the structure. Methods for the calculation of the performance points are proposed by various authors and included in EC8 and FEMA 440, for instance. A performance point for a structure can be calculated for each level of intensity, from which fragility curves can then be constructed. Following this approach, numerous analytical procedures to define seismic vulnerability of buildings structures have been developed in the past decade to the extent that several platforms are available to the risk analyst to determine building losses in urban contexts. Among the most commonly used are HAZUS-MH (FEMA 2003), SELENA (Molina et al. 2009), and ELER V3.0 (Demircioglu et al. 2010). In these approaches the fragility curve is associated to a specific structural typology, usually defined by the lateral resisting system, divided into subclasses by use of secondary indicators, believed to sufficiently characterise the global response. While HAZUS and ELER relay on predetermined sets of capacity curves, SELENA has the flexibility of accommodating for user defined capacity curves, and site specific response spectra.

Recently substantial work has been developed within the framework of the European projects PERPETUATE (D'Ayala 2013; Lagomarsino and Cattari 2013) and SYNER-G (see Chap. 5) to develop robust fragility functions for masonry structures in historic centres using a performance point based approach.

Approach (3) is adopted in the simplified version of incremental dynamic analysis proposed by Vamvatsikos and Cornell (2002) and the procedure proposed by Rossetto and Elnashai (2005). Both procedures allow the performance and hence damage of a structure to be determined for a suite of records, in the former case defining a performance function rather than a performance point. Approaches (2) and (3) define their seismic assessment methods for existing buildings following the same framework of performance-based design that is used in the case of new buildings (EC8 (CEN 2005), FEMA 356 (FEMA 356 2000), ATC-58, ATC-63 (ATC 2007), etc).

Within approaches (2) and (3) the basic required analysis steps are:

(a) Classification of buildings by typology and seismic design.
(b) Definition of damage states.
(c) Assignment of capacity curves or back bone curves (for dynamic analysis).
(d) Choice of response spectra (associated with return periods and performance targets) or choice of a set of ground motion records to perform dynamic response history analysis.
(e) Evaluation of building response in terms of performance points or performance function.

The two latter approaches, when applied to large sets of buildings, allow the derivation of fragility curves and damage scenarios for given sites and strong motion return periods. The damage states or damage levels are directly correlated

to an engineering demand parameter (EDP), usually expressed in terms of lateral capacity, displacement or drift.

As the fragility curves are commonly developed on the basis of a lognormal distribution, once the typologies have been defined, it is not necessary to have a detailed knowledge of the building stock to use these methods in the seismic risk assessment of an urban area. What is required are the parameters defining the capacity curve for each building typology, the damage thresholds, and the number of buildings belonging to each typology within the urban area. Moreover, as ground motion intensity measures and exposure are also usually represented probabilistically by a lognormal distribution then the seismic risk for a specific facility at a specific location can be expressed according to Cornell and Krawinkler (2000) as a triple integral to analytically compute the annual total repair cost, constrained to a given intensity measure (IM), a given damage value (DVE) and a given damage state (DM) correlated to an engineering demand parameter (EDP):

$$G_{TC|IM}(z|x) = \iiint G_{TC|DVE}(z|u) f_{DVE|DM}(u|v) f_{DM|EDP}(u|y) f_{EDP|IM}(y|x)\, du dv dy \tag{3.3}$$

Although this theoretical framework is sound and in line with the probabilistic performance based displacement procedures used for the design of new structures, the epistemic uncertainty associated with its applications means that some simplifying assumptions are necessary to calculate the integral in Eq. (3.3) in closed form, by assuming independence among the three variables of integration and using the total probability theorem. Strategies for the solution of the triple integral are presented, for instance, by Baker and Cornell (2003), Solberg et al. (2008) and Yang (2013). Moreover, a common assumption is that much of the variance in the loss measure is associated with the uncertainty relating to the IM hazard curve (Baker and Cornell 2008), and hence it is inherently aleatoric and well represented by a lognormal function. While this can to an extent be the case for engineered structures, this has proven not to be correct for low-engineered or non-engineered structures, which constitute a high proportion of the building stock in European urban centres and large urban conurbation in developing countries. A more in depth discussion of the factors affecting the reliability of fragility curves in analytical approaches for buildings is included in Sect. 3.3.2.

Analytical fragility functions associated to building typologies have the limitation of being difficult to calibrate with experimental work and propagate inherent uncertainty due to the limited real applicability of a prototype building. As an alternative, the component approach has the advantage of overcoming the strict definition of a building type as the loss function can be aggregated for any building through the summation of the losses for each of its components, however it requires greater computational effort and a broader and more detailed database. The approach, initially proposed by the PEER group (Moehle and Deierlein 2004) and standardised in ATC-58-1 (ATC 2012), is particularly suited to the assessment of

single buildings; ATC-58, besides including a useful database of structural, non-structural and content components fragility curves, also provides tabulated values for a range of uncertainty parameters, to be used as default when a tailored uncertainty evaluation cannot be performed.

A components' approach also characterises vulnerability studies for infrastructure and utility networks. Normally an infrastructure is defined as a system of systems that provides a flow of goods, services or people from a point in space time to another. The spatial temporal relationship of the components within the system is a critical parameter for the definition of the system vulnerability, as it is the space-temporal distribution of the hazard. Fragility is described in terms of flow capacity along linear elements and flow interruption at point-like elements or critical connections (also called critical facilities). Vulnerability might be computed in terms of down-time, loss of connectivity, or satisfied demand (flow rate). A simplified approach usually entails defining the fragility of specific components in a binary fail/safe form. The system is then made up of components in serial or parallel arrangement leading to reduced flow rate depending on damage distribution on single components. Vulnerability assessments of systems simulated with the latter approach are typically conducted using matrix-based system reliability (MBSR) methods (Song and Kang 2009). Within the SYNER-G project (Kaynia 2013) a systemic methodological approach for the derivation of fragility curves for utility networks and transportation infrastructure is proposed. Although drawing largely from adaptation of existing fragility functions, the project also proposes some new functions for specific components, based on numerical solutions or by using fault tree analysis. A more detailed presentation of this methodology from the various types of networks is contained in several chapters of this book.

A complete performance based probabilistic assessment can be performed using Bayesian Networks (BN) which have the advantage of seamlessly simulating qualitative, quantitative and incomplete data within the same framework. Results are sensitive to the dependency and cause-effect relationship among components; hence a detailed description of the connectivity is essential, usually accomplished through graphical methods and connectivity trees. Computational loads become very high for realistic systems (Bensi et al. 2011) so applications are so far limited. In prospective the main advantage of BN is the possibility of conducting near real-time analysis and considering in detail many scenarios that might be affected, not only by external events, but also by decision making processes. Bensi et al. (2011) propose an application of BN to the California speed rail system.

The seismic risk associated to rail and road networks is highly dependent on the fragility of tunnels, embankments, trenches, slopes, tracks, bridges and abutments. Although the components are common to both systems, damage thresholds for performance requirement might be substantially different leading to diverse vulnerability functions. Relatively little work on analytical seismic fragility is available for many of the network components; one example being the analytical fragility functions for tunnels proposed by Argyroudis and Pitilakis (2012). Bridges are usually treated as subsystems, composed of a number of components with diverse seismic vulnerability. Approaches similar to the Performance Based

Vulnerability Assessment (PBVA) for buildings structures are used and several authors have proposed full Push Over Static Analysis (POSA) or Incremental Dynamic Analysis (IDA) for bridge piers, decks and whole bridge structures (Hwang et al. 2001; Bhuiyan and Alamb 2012). Among others, Nielson and Des Roches (2007) propose a component approach for bridges. The study shows that the bridge as a system is more fragile than any one of the individual components, and that considering only the piers leads to gross underestimation of fragility.

3.2.3 Overview of Expert Elicitation Fragility Approaches

Expert elicitation can be used to provide either the damage statistics for deriving fragility functions or the fragility functions themselves. Fragility functions based on expert elicitation can be particularly useful where there is little empirical information on the asset damage from past earthquakes or where the asset is difficult to model numerically or analytically. In all expert elicitation approaches a panel of experts is chosen, recruited and trained in the adopted elicitation approach (Jaiswal et al. 2012). Different approaches exist for the collection of the expert elicitation data and its combination, but in general, the procedures adopted in the fragility literature can be classified into the two broad categories of mathematical and behavioural approaches (Clemen and Winkler 1999).

In the mathematical approach each expert provides their estimate of an uncertain quantity as a subjective probability. The experts do not interact. After the elicitation the estimates of the unknown quantity provided by each expert are combined mathematically, typically using either a technique for weighting each expert's estimates (e.g. Cooke 1991) or through use of Bayesian statistics (e.g. Morris 1977). Such approaches have been adopted in various financial and environmental risk assessment exercises, for example in the estimation of volcanic risk (Aspinall and Cooke 1998) or in seismic hazard estimation (e.g. see Klügel 2011). Within the fragility literature Cooke's classical method (Cooke 1991) is currently being used by Jaiswal et al. (2012) for the construction of fragility curves for the collapse limit state of reinforced concrete and masonry buildings expressed as a function of peak ground acceleration (PGA). It is noted that the elicitation carried out by Jaiswal et al. (2012) is being carried out as part of the Global Earthquake Model (GEM, www.globalearthquakemodel.org) and has yet to publish its results. In Cooke's method each expert's estimates of the unknown quantity/ies of interest are weighted according to their performance in answering a set of "seed" questions. These seed questions are a set of questions relevant to the topic of interest that are unambiguously worded and have a unique and known numerical answer value. The seed questions are asked at the start of the elicitation process, with each expert providing their best estimate answer as well as upper and lower bounds to their answers (assumed to correspond to the 5th and 95th percentile). The responses to the seed questions are used to assign a "calibration" and "information" score to each expert, which are then used to weight the expert's responses in the main elicitation process

for the quantity of interest. In this process, the calibration score is the statistical likelihood that the expert's quantile assessment contains the true answer, whilst the information score measures the degree to which the expert's distribution is concentrated, relative to a reference distribution (e.g. uniform). The responses from all experts are adopted and the weightings of each expert are not revealed to participants in the process. The method is implemented in a free software, EXCALIBUR (Cooke 2001).

Behavioural approaches differ from the mathematical approaches in that they attempt to achieve some level of consensus amongst the group of experts on the unknown quantity to be estimated. In such methods, the experts may interact and share their assessments (Ouchi 2004). The Delphi approach (Dalkey 1969) is probably the best known such method. In this approach experts first provide an estimate of the unknown quantity and are then asked to anonymously assess the estimates made by other experts. Each expert may then revise their original estimate, if they so wish, to take into account the estimates by the other experts that they have reviewed. The process is repeated until a degree of agreement/consensus is reached between the expert estimates. In theory, the anonymity of the reviews should avoid expert reputations or personality traits having an effect on the results. The most important example of where a behavioural approach has been used in building fragility analysis is ATC-13 (Applied Technology Council 1985). Within this study a modified-Delphi method is applied to construct Damage Probability Matrices (DPM) expressing the likelihood of particular damage factors (ratios of repair to replacement costs) being achieved over a range of Modified-Mercalli Intensity (MMI) values, for 78 different building types in California. The "modification" in the approach consists in asking the experts to rate their experience and level of confidence in their estimates, and using these self-ratings to weight their answers in the combination of estimates of the value of interest by different experts. In general, this is seen to result in experts that self-rate highly in terms of confidence and experience being attributed a higher weight (Jaiswal et al. 2012).

There is much debate in the literature as to the reliability of behavioural approaches. For example, Cooke (1991) observes that more extreme probability estimates seem to result from use of the Delphi method, and Scheibe et al. (1975) observes that the fact that experts can see the response of others may have a significant influence in swaying expert's initial judgements towards conformity rather than an agreement. Overall, mathematical approaches to expert elicitation are regarded to be more reliable, reproducible and fair than behavioural approaches in aggregating expert opinions (Cooke 1991; Clemen and Winkler 1999; Jaiswal et al. 2012).

3.2.4 Overview of Hybrid Fragility Approaches

Examples of systematic approaches to define hybrid fragility functions for buildings are actually rather sparse, and usually focus on the combination of empirical and analytical data. Within these approaches the analytical curve is typically used

as the prior within a Bayesian approach, and is updated with a typically limited amount of empirical data.

One rare example of hybridization between analytical, empirical and expert opinion was attempted by the EERI-WHE study group in support of the PAGER project (Jaiswal and Wald 2010). The exercise aimed at defining the proportion of collapses for a given building type given a shaking intensity expressed in EMS-98 Intensity (Grünthal 1998) for as many nations worldwide as voluntary expert could be contacted. The hybridization took the format of a comparative analysis by building types and then comparison of analytically or empirically derived curves by national studies. The exercise highlighted the difficulty in correlating perceived damage percentage of stock to a specific intensity scale, to which not all experts were familiar with. The definition of collapse was also put into question. Given the large standard deviation of some of the results obtained, Bayesian updating by means of empirical single event recorded data was used to improve the experts' forecast. Results of this work are reported in D'Ayala et al. (2010) and Jaiswal et al. (2011). The Bayesian procedure directly helps to calibrate the prior seismic collapse fragility functions (defined using beta distribution) to the statistical field data at any or all levels of shaking intensity while preserving the capability to account for statistical uncertainty associated with collapse potential through posterior distributions. Several improvements to this approach were identified by the authors of the study. These included incorporation of the uncertainty in the shaking intensity at which collapse probability estimates are assigned, improvement of the process of elicitation, quantification of uncertainties associated with expert opinion, the careful consideration of variability in construction practices and level of building codes adoptions worldwide when comparing expert judgments for the same building types.

3.3 Factors Affecting the Reliability of Fragility Curves

A wealth of fragility curves for various buildings classes constructed using the aforementioned methodologies have been published over the past 40 years. The SYNER-G project (Kaynia 2013) produced a compendium of 415 sets of fragility curves for European, mainly masonry and reinforced concrete, buildings and numerous fragility functions for European infrastructure systems, including water, power, oil, gas and transportation systems and critical infrastructure. A new global compendium of existing fragility curves for masonry, reinforced concrete, steel and wooden buildings has also recently been compiled for the needs of the Global Earthquake Model (GEM). This compendium contains over 119 empirical and over 150 analytical sets of fragility curves for buildings worldwide (D'Ayala and Meslem 2013; Rossetto et al. 2013a).

Within the SYNER-G project (Kaynia 2013) a procedure for combining existing fragility curves, whose characteristics are close to the characteristics of the building class required by the future application, has been developed. The aim of this

procedure is to estimate the parameters of the mean fragility curves as well as to quantify their uncertainty for use in seismic risk assessments. This approach, however, does not account for the fact that some curves are more reliable than others (Rossetto et al. 2013a; D'Ayala and Meslem 2013). Therefore, it is deemed essential to move towards a more robust selection and, if necessary, combination procedure, which accounts not only for how relevant existing curves are to the needs of future seismic risk assessment projects but also how reliable they are. In order to do this, it is important to first understand what factors affect the reliability of the different types of fragility function. These are discussed in the following sections. The proposed fragility curve selection procedure is then presented in Sect. 3.4.

3.3.1 Factors Affecting the Reliability of Empirical Fragility Functions

In the fragility assessment of structures aleatory uncertainty is introduced by the natural variation in earthquakes and their resulting ground shaking, or the variation of the seismic response of the buildings of a given class. Epistemic uncertainty is introduced by small databases of often poor quality. Poor quality is associated with large errors introduced by missing data, biased sampling techniques, misclassification errors or data aggregated over large areas. Epistemic uncertainty is also introduced by the inability to account for the complete characteristics of the ground shaking in the selection of measures of the ground motion intensity (Rossetto et al. 2013a) as well as the measurement error in the intensity measure levels at the required locations. In theory, reliable Fragity function can be obtained by high quality large datasets of damage observations from multiple earthquake events. The main categories of factors affecting the reliability of empirical fragility functions are summarised in Table 3.2 and briefly summarised here. The reader is referred to Rossetto et al. (2013a) for a more detailed discussion.

The quality of the damage data is the most important determinant of the empirical fragility function reliability. Poor data quality often poses severe challenges to the reliable statistical analysis of the data. The typical survey methods used to assemble post-earthquake damage data are introduced in Table 3.1, where it is shown that most survey methods result in damage databases that are large in size but contain errors or are large in size but are associated with a low degree of refinement in the definitions of damage scales and building classes.

The damage scale used to collect the damage data from the field is important in determining the potential for misclassification errors and the usefulness of the developed fragility functions. In general terms, a damage scale that describes unambiguously a number of damage states in terms of structural and non-structural component damages will result in a more reliable and useful

Table 3.2 Categories of factors determining the reliability of empirical fragility functions

Factors:	Description:
Intensity measure:	Hazard parameters (e.g.: PGA, $S_a(T)$, $S_d(T)$)
	Isoseismic unit over which the damage data is aggregated (e.g. zip-code area, town etc.)
	IM estimation method (e.g. GMPE or recorded)
Damage characterisation:	Damage scale; consideration of non-structural damage
	Number of damage states (DS)
Class definition and sample size:	Sample size (size of database and completeness)
	Single or multiple building classes
Data quality:	Post-earthquake survey method
	Coverage, response and measurement errors in surveys
	Quantity of data in each isoseismic unit (e.g. number of buildings or loss observations)
	Number of seismic events, range of IM and DS covered by data
Derivation method:	Data manipulation or combination
	Relationship model
	Statistical modelling and optimisation method
	Treatment of uncertainty (sources of uncertainty, quantification)

empirical fragility function. The combination of several datasets from the same or different earthquakes are combined in the construction of empirical fragility curves can often be hampered by the use of different damage scales by each database. In this case, it is best practice to map the damage states of each damage scale onto those of the damage scale with the least number of damage states (e.g. as in Braga et al. 1982).

Due to the nature of earthquakes, the empirical data is typically seen to be clustered in the low-damage and low IM range. This means that extrapolations of fragility curves to the high IM range can be unreliable and that collapse fragility functions for many structure types are difficult to obtain empirically. As a matter of good practice, empirical fragility curves should not be used to estimate fragilities outside the range of IMs of the data that has been used in their derivation.

As mentioned in Sect. 3.2.1, PGA and PGV are the most commonly used ground motion intensity parameters in existing empirical fragility functions, with PGV being the preferred IM in Japanese studies. Only very few studies have adopted PGD. Both Rossetto (2004) and Sarabandi et al. (2004) observe a generally poor correlation of PGA, PGV and PGD with their databases of reinforced concrete building damage statistics. However, both note a slightly better correlation of PGD than PGV and PGA with their data. Peak ground motion parameters are unable to capture many of the characteristics of the strong ground motion that can affect the development of damage in structures. Hence, several recent empirical fragility studies have favoured the use of response spectrum based parameters as measures of ground motion intensity, in particular Spectral Acceleration (S_a) and Spectral Displacement (S_d) evaluated at the fundamental period of the assessed structures.

Spence et al. (1992), Singhal and Kiremidjian (1997) and Rossetto (2004) note that Sa provided a better correlation with their empirical damage data than PGA. Furthermore, Rossetto (2004) and Sarabandi et al. (2004) both observe a better correlation of Sd than Sa and PGA with their damage databases. The use of a spectral value for empirical fragility functions is, however, complicated by the need to characterise a building class by a single structural period of vibration. The issue of which elastic period of vibration should be used to characterise a given building class, which will be composed of structures with a range of geometrical and material characteristics, is simply not addressed in the literature, nor is the influence of this choice on the resulting fragility functions investigated.

Post-earthquake damage data at a building by building level is almost never available. Instead, the damage data is presented in aggregated form, as a damage histogram for different levels of ground motion intensities, or over geographical areas of varied size (e.g. a zip-code, village, district or town). In the latter case, the geographical area is assumed to have a constant ground motion intensity value, which is typically evaluated at its centroid. However, if the geographical unit is large there is likely to be a variation in the IM values across the unit (due to differing fault distances and soil conditions) which is not typically accounted for. The variation of ground motion over a geographical unit, variation in fundamental period of vibration of structures within a building class and uncertainty in the estimation of the ground motion at a site that arises from the use of a GMPE contribute to their actually being a level of uncertainty associated with the IM determination at a site of damage evaluation. No existing fragility study has yet taken this into account and all adopt statistical models that assume that the IM is known with certainty. However, an approach to the incorporation of this uncertainty is proposed in Rossetto et al. (2013b).

Three main statistical modelling approaches (nonlinear, linear and generalised linear) have been used by existing studies to fit parametric functions to their empirical data. The choice of statistical model is seen to have a potentially strong influence on the reliability and validity of existing empirical fragility functions.

Nonlinear statistical models have been used by Rota et al. (2008) and Rossetto and Elnashai (2003) amongst others. Nonlinear models assume that the mean response variable (damage state exceedance probability) is a nonlinear function of the ground motion intensity, and that the variance in response is constant and normally distributed at each intensity value. However, as the response can only have values in the range between [0,1] the normality assumption is violated near these value extremes. Furthermore, the assumption of constant variance is unrealistic in view of the fact that observational data indicates that uncertainty in seismic performance for large or small ground motion intensities is considered lower than for the intermediate intensity measure values. These issues raise questions on the reliability of past fragility relationships derived from nonlinear statistical models.

Linear models are the predominant statistical model used in the empirical fragility literature and are used for example by Liel and Linch (2012). Within linear models, the non-linear fragility function (e.g. cumulative lognormal distribution function) is transformed into a linear form. This results in the response variable

being expressed in terms of the inverse cumulative standard normal distribution of the probability that a damage state is being reached or exceeded. The positive implication of this transformation is that the assumption that the variance in response is constant and normally distributed at each intensity value (which it shares with the nonlinear method) is not violated, (see Rossetto et al. 2013b for further explanation). However, the negative implication of the transformation of the of the damage data, necessary for the estimation of the parameters of the linear model, is that it is seen to introduce bias into the mean fragility functions, which are not appropriately dealt with by existing empirical fragility approaches (Baker 2011) and raise questions as to the reliability of fragility curves derived with this statistical model.

Generalised linear models are an extension of the linear models, which allow the distribution of the response at any intensity value to be expressed in terms of any distribution of the exponential family except for the normal distribution. They present an advantage over the linear and nonlinear models as they do not require transformation of the damage data and do not assume constant variance of the response variable. They have been used to derive empirical fragility curves for buildings by Ioannou et al. (2012), bridges by Shinozuka et al. (2000) and Basöz et al. (1999) and for steel tanks by O' Roorke and So (2000). It is noted that Rossetto et al. (2013b) have suggested the use of Generalised additive models and non-parametric models for the generation of empirical functions, and shown their application for a small number of empirical building damage datasets.

3.3.2 Factors Affecting the Reliability of Analytical Fragility Functions

Different relationships and methodologies for the derivation of analytical fragility functions are available in the literature, covering different structure typologies and locations worldwide. As seen in Sect. 3.2.2 the fundamental elements of a fragility function are a suitable representation of the expected ground-motion, a suitable analytical or numerical model able to represent the response of the asset to the expected ground motion and a coherent means of relating the response to a damage state or threshold. For a fragility function obtained in this way to be considered reliable it is essential that there is internal coherence in the approach taken, i.e. the level of sophistication used in the modelling of each of the three fundamental elements above should be commensurate.

In the literature analytical fragility curves are derived using a variety of approaches that employ diverse structural modelling and analysis techniques, damage models, damage scales and numbers of damage states. Furthermore, in their attempts to account for uncertainties and intrinsic differences observable in the building stock and its response to seismic loading, a range of sampling approaches have also been used to select the parameter values to vary in the structural models

Table 3.3 Categories of factors determining the reliability of analytical fragility functions

Factors:	Description:
Intensity measure:	Hazard parameters (e.g.: PGA, $S_a(T)$, $S_d(T)$)
Damage characterisation:	Damage model: damage index
	Damage indicators
	Number of damage states (DS)
Class definition and sample size:	Sample size (multiple buildings; randomisation of parameters; single building)
	Sampling method (e.g. Monte Carlo, Latin hypercube, random)
Data quality:	Analysis type (e.g. Nonlinear Dynamic (NDA) or Static (NSA), Simplified Method (SM))
	Mathematical model (completeness of model, definition of material properties, con-figuration and geometry)
	Seismic demand (real ground motion records, code based spectra)
Derivation method:	Treatment of uncertainty (sources of uncertainty, quantification)
	Fitting methods for fragility curves

and seismic demand. Again, these sampling methods should be evaluated in the context of the structural and demand modelling. For instance structural modelling can be pursued using simple nonlinear single degree of freedom oscillators, nonlinear multi-degree of freedoms with lumped characteristics oscillators, more realistic 2D or 3D frame models where each structural element is accounted for in geometry and material properties. In this context, for instance, if a simplistic representation of the structural behaviour is adopted, which perhaps ignores the contribution of infill or the variability of stiffness across structural elements, it might be misleading in terms of perceived accuracy to carry out an extensive Monte Carlo simulation to generate a large number of capacity curves; the latter will provide an apparently good stochastic model but will be fundamentally flawed as they ignore a critical behaviour.

Given the variety of methods available to derive fragility functions it might appear difficult to compare and appraise existing analytical relationships, even when derived for the same structural class. Nevertheless, some fundamental factors that account for the quality, robustness and reliability of the analytical function independently of its derivation process can be identified and rated. These factors relate directly to the steps of the fragility curves construction process, as shown in Table 3.3. These factors are considered essential to the development of a robust analytical model that will simulate the seismic performance of a structural typology, and hence to lead to an accurate assessment of its fragility. A detailed review of their treatment and their most common applications in existing literature is presented in D'Ayala and Meslem (2013). In Sect. 3.4 these factors are considered in the development of a quality rating system that can aid users to select a fragility function appropriate for their application scope.

When reducing reality to a model, substantial simplifications are always required. It is hence paramount for the reliability of the outcome to keep a record of the consequences in terms or representativeness and in term of the epistemic uncertainty generated by introducing specific modelling strategies.

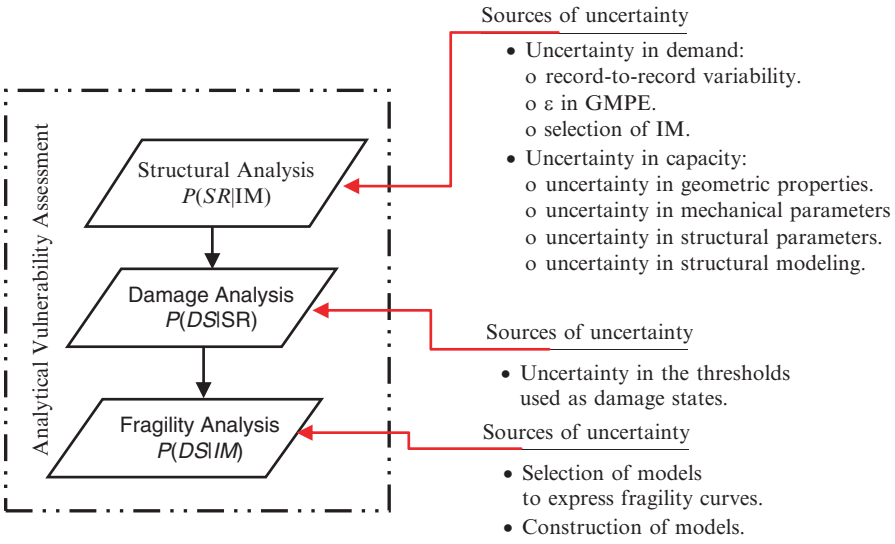

Fig. 3.2 Sources of uncertainty associated with analytical fragility assessment (D'Ayala and Meslem 2013)

The identification of sources of uncertainty in the capacity, demand and damage state thresholds, their quantification and their representation in the fragility function are considered fundamental steps in the derivation of a reliable fragility functions. A comprehensive list of possible source of uncertainties is compiled in Fig. 3.2.

With regard to the structural analysis, uncertainties are associated with both the capacity of the examined building/asset and the demand represented by an intensity measure. The uncertainty in the demand is caused by the natural variability among records, which encompasses the variability in mechanism of the seismic source, path attenuation and site effects of the seismic event. This uncertainty is typically taken into account either through the selection (and scaling) of natural ground motion records or by generating artificial records. This is often considered the main source of variability in response and in some studies is treated as aleatory (Ellingwood 2009). With regard to the selection of intensity measure (IM), PGA is the most widely used in past methodologies (D'Ayala and Meslem 2013), despite the fact that it produces structural response with considerable dispersion. An improvement on PGA is the use of elastic spectral acceleration, which characterizes the intensity measures of many recent analytical fragility functions (Molina et al. 2009). Research towards more efficient measures for characterizing the strong ground motion intensity had led to a few studies adopting elastic spectral displacement or the vector spectral acceleration (Bojórquez et al. 2009). However, as few ground motion prediction equations and hazard maps exist for these intensity measures, fragility functions that adopt these can be of very limited use in practical seismic risk assessments.

Uncertainty in the capacity is introduced through geometrical, mechanical, structural and modelling parameters. With reference to the geometrical properties, most studies consider one existing building or a fictitious "index" building to represent a class of buildings. Most commonly uncertainty in the capacity is accounted for by randomising the mechanical parameters of the construction materials, such as material properties, mass and damping in order to create a number of building models for the analysis (variants of the index building). Uncertainty in response, caused by variability in structural and geometric characteristics, can be accounted for by direct survey of a large number of real buildings and the definition of a median and standard deviation of the sample (e.g. D'Ayala 2005; Vacareanu et al. 2007). Also where possible, probabilistic distribution of parameters should represent actual exposures as not always certain characteristics are normally or lognormally distributed within a given region or building typology or sub-typology. It is noted, however, that the selected index building is typically simulated in terms of a 2D symmetrical model with deterministic geometrical properties, reducing the ability of the model to capture the variability in a building class.

When a single index building geometry is adopted for the representation of a building class, uncertainty in the structural response across the building class is often modeled by randomizing parameters of the construction material hysteretic models. For instance, the fragility curves of Jiang et al. (2012), Rajeev and Tesfamariam (2011), Bakhshi and Karimi (2006), and Rossetto and Elnashai (2005) are generated considering the variability associated with mechanical parameters, such as, compressive strength and elasticity modulus of concrete, tensile strength and elasticity modulus of steel reinforcement, hardening ratio of steel, and compressive strength of masonry infill, as random variables, to account for the uncertainty in capacity. The uncertainty in demand is also taken into account by selecting a certain number of ground motion records. However, in a recent study by D'Ayala and Meslem (2013) it is observed that modeling the uncertainty in the response of structures in this way has only a modest effect on the resulting slight and moderate damage state fragility curves. Instead, high variations, comparable in size to those resulting from the record-to-record uncertainties, result for the collapse state. The impact of these conclusions is that deterministic structural characteristics can be used for the construction of fragility curves for slight and moderate damage levels.

With regard to the damage analysis, damage threshold uncertainty is often neglected in a number of procedures found in the literature. However, in a few cases a probability distribution is assigned to the threshold of the damage state (in most cases a lognormal distribution) and treated as aleatory, (e.g. Shahzada et al. 2011; Uma et al. 2011; Kappos et al. 2006). Aslani and Miranda (2004), also consider the epistemic uncertainty in the mean parameter of this distribution.

As previously mentioned, the vast majority of analytical fragility functions are represented as lognormal cumulative distribution functions. In such representations, the lognormal standard deviation of the fragility function is used to represent the overall uncertainty due to the compounded uncertainty in the demand, capacity and damage state thresholds. In terms of total uncertainty, ATC-58 (ATC 2012) has suggested a default value of 0.6. Instead, both FEMA-NIBS (2003) and Kappos and

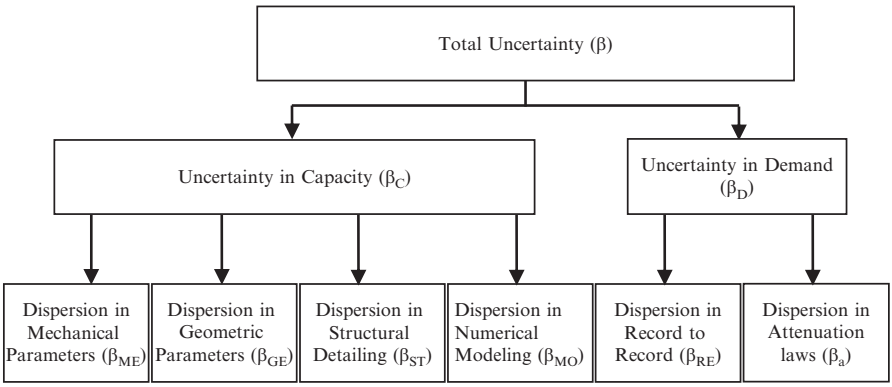

Fig. 3.3 Classification of different sources of uncertainty for fragility curve derivation (Modified from D'Ayala and Meslem 2013)

Panagopoulos (2010) suggest values of 0.75, 0.70, and 0.65 for buildings designed to old, moderate, and modern codes, respectively. Studies that adopt this procedure often numerically estimate one component only of the overall uncertainty, i.e. the record to record variability. A common assumption in the analytical fragility literature is that the different components of uncertainty within the adopted analytical approach can be considered independently. Hence, the total uncertainty (β) can be introduced in the fragility curves as the summation of the lognormal variances deriving from each component (β_i), as:

$$\beta = \sqrt{\sum_i \beta_i^2} \tag{3.4}$$

The number of the components used in Eq. (3.4), their description and their values varies according to the needs of the study. An overall view of the component included in several studies is presented in Fig. 3.3. Rarely are all components accounted for in a single study. Dispersion in attenuation law, might need to be removed when considering risk analysis, as this is usually explicitly accounted for in the hazard component.

For example, Wen et al. (2004) consider four lognormal variances representing the uncertainty associated with capacity curve, structure modeling, limit state values, and earthquake demand. By contrast, ATC-58 (ATC 2012) has recently recommended consideration of three contributors to the overall uncertainty accounting for record-to-record uncertainty, building definition, (as material strength, section dimensions, and rebar locations may be different than those detailed in documentation) and quality assurance, (quality and completeness of the nonlinear analysis model) accounting for the fact that hysteretic models may not accurately capture the behavior of these elements, even if their construction is precisely known.

As seen in Table 3.3, this set of parameters is considered in the present study as being highly influential on the reliability of fragility curves. In Sect. 3.4 a qualitative rating is associated to the strategy adopted for the choice of each of these parameters and their uncertainty treatment, in order to produce a value judgment of the suitability and reliability of the fragility functions available in literature.

3.3.3 Factors Affecting the Reliability of Expert Elicitation and Hybrid Fragility Functions

As discussed in Sect. 3.2.3, all expert elicitation procedures are strongly dependent on the selection of an appropriate panel of experts and adoption of an appropriate process to account for differing levels of expertise and confidence, and for combining the expert elicitation responses. Particularly in behavioural approaches, char-acter traits may not be sufficiently accounted for in the expert elicitation and response consensus. Hence, the final result may be influenced by the composition of the panel, say in terms of sexes and personalities. Mathematical approaches such as the Cooke (1991) classical method explicitly account for different levels of confidence and calibrate the expert responses with respect to the same benchmark (i.e. the seed questions). Hence, they do not tend to have this susceptibility. Mathematical expert elicitation approaches are in general regarded as more reliable than behavioural approaches (Ouchi 2004). Nevertheless, the mathematical procedure adopted in the aggregation of expert opinions once gathered, is seen to influence the final result. Using data (Klügel 2005) from a study of a design basis shutdown earthquake for a nuclear plant, Klügel shows a significant difference in the cumulative distribution functions of the seismic hazard resulting from the use of three different aggregation methods (Klügel 2011): direct Bayesian aggregation, equal weighting of expert responses or geometrical averaging. However, the study of different aggregation methods has largely been unexplored in the expert elicitation fragility literature, which in any case is very limited in quantity.

Few studies have explored the development of hybrid fragility functions, and as stated in Sect. 3.2.4, most of these have combined an analytical curve with empirical data. Hence, these curves typically are associated with all the sources of uncertainty of analytical fragility curves and are influenced by the factors described in Sect. 3.3.2. The degree of influence on the hybrid fragility function of the empirical data is highly dependent on the quantity and intensity range covered by the data. When single event data is adopted, damage observations often concern a limited range of values of the intensity measure, and the influence on the analytical curve is often seen to be very small, (e.g. in Singhal and Kiremidjian 1997). The combination of analytical fragility curves or indeed analytical and empirical fragility curves is not typically carried out. However, these topics are further explored in Sect. 3.5.

3.4 Proposed Framework for Choosing Amongst Fragility Curves

The relative wealth of existing fragility curves for various building classes provides a pool of potentially suitable expressions of fragility for future applications. Given the lack of established procedures for identifying appropriate fragility curves for future projects, a new framework for selecting suitable fragility curves for a particular application is proposed, and illustrated in Fig. 3.4. Central to the framework is a rating scheme for assessing the relevance and overall quality of the fragility curves (see Table 3.4). Only empirical and analytical fragility curves are considered in this section due to the scarcity of expert elicitation and hybrid fragility curves. However, the latter two types of fragility curves will be considered in future developments of the procedure.

The proposed framework for curve selection and underlying rating scheme were developed within the framework of the Global Earthquake Model project. The framework arises from a need to provide users of the GEM risk assessment tool, called OpenQuake platform (under development), with robust advice on selecting suitable fragility functions from the large repository collected, but also from the need to operate a critical selection in building up the repository to be adopted within the tool. The framework is loosely based on the generic scheme for vulnerability curve assessment proposed by Porter (2011). The same four fundamental attributes of vulnerability curves identified by Porter (2011) are also adopted for the assessment of fragility curves here. These are the curve *representativeness* of the characteristics of the assets and seismicity in the location being assessed, the *quality of the input* used to generate the fragility function, the *rationality* of the procedures followed to construct the curves and the *documentation quality*. Within the here proposed framework, these attributes are grouped into two "components": ***Relevance*** and ***Overall Quality***. These components are assumed to contribute equally to the determination of the usefulness and reliability of a fragility curve for a particular seismic risk assessment. The four attributes are also subdivided into sets of criteria for the attribute evaluation, which are different for empirical and analytical fragility curves (see Fig. 3.4). These criteria are described in greater detail in Tables A.1 and A.2 (Appendix to this Chapter) and include the factors identified in Sect. 3.3 as affecting the reliability of the curves. To aid the assessment and comparison of fragility curves, each criterion is assigned a rating of high (H), medium (M) or low (L). The description of the criteria ratings differs according to the component to which the criteria belong, as per Table 3.4. An overview of the components, attributes and criteria is provided below.

The ***Relevance*** component of the framework looks to assess the relevance of a fragility curve to the needs of a particular seismic risk application. It is essentially a first screening of available fragility curves to identify a pool of potentially useful fragility curves. The attribute of representativeness is assigned to the relevance component and is subdivided into three criteria:

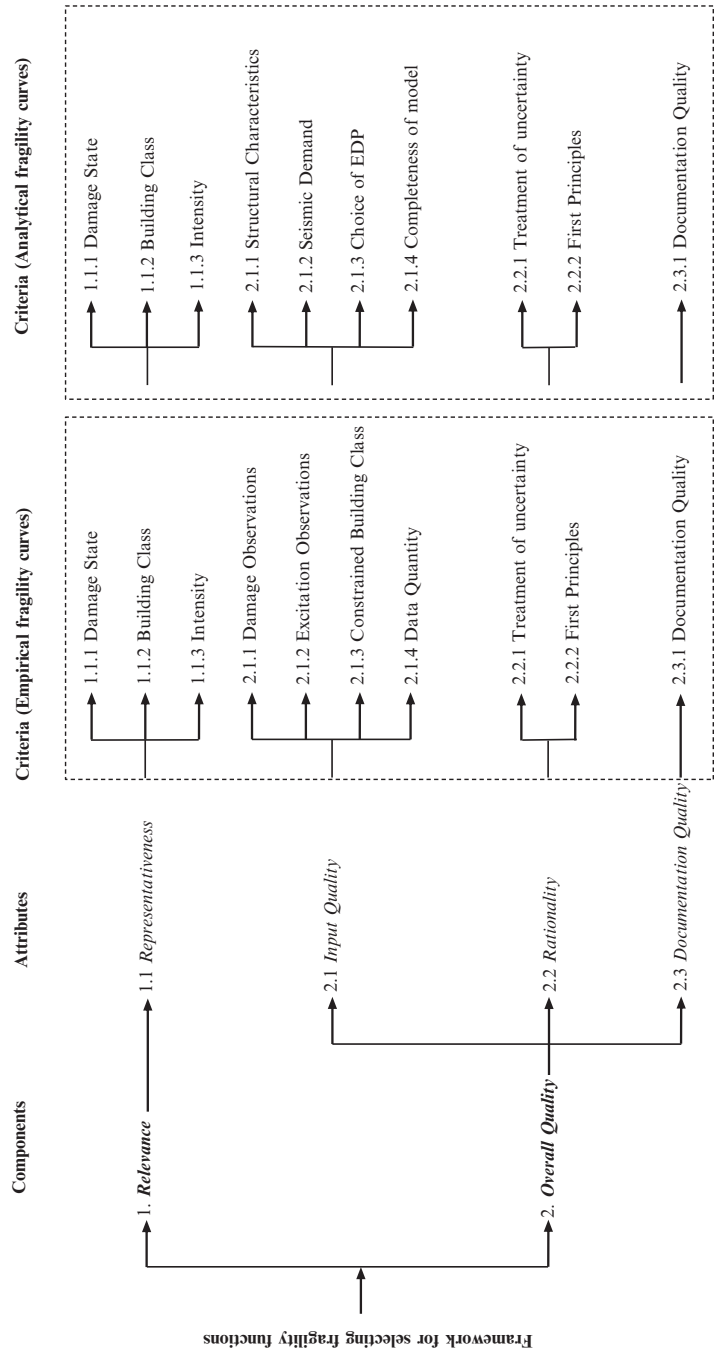

Fig. 3.4 Components, attributes and criteria for selecting among empirical and analytical fragility curves

Table 3.4 Description of the criteria ratings applied within each component

Rating	Component	Description
H	Overall quality	The work is of excellent quality and little if anything could have been done better
	Relevance	The fragility curve is highly relevant for the needs of the future application
M	Overall quality	The work is of acceptable quality, though there are areas for improvement or further research
	Relevance	Existing functions are moderately relevant to the needs of the future applications
L	Overall quality	The work is acceptable for use but only if there are no practical alternatives; and much improvement or further research is needed
	Relevance	Existing functions are not relevant for the application
NA	Overall quality	The rating cannot be applied
	Relevance	The rating cannot be applied

- *The damage state*. The relevance of a fragility curve corresponding to a damage state is characterized by how close the qualitative description of this damage states are to the required damage states.
- *The structural characteristics* of the buildings which include the geometric and material properties of the examined class as well as the dominant structural system and its design. The relevance of the fragility curve with regard to the structural characteristics is assessed according to how close the description of the building class of a fragility curve is to the required class, as well as how representative the location of these buildings is to the required location.
- *The ground motion intensity*. The relevance of a fragility curve according to the ground motion intensity is assessed according to three conditions, namely: the selected intensity measure type, the range of its levels. In addition in the case of analytical fragility functions, whether the ground motions used to construct the fragility curve derive from the same region and tectonic environment as that assessed.

It should be noted that for the empirical fragility assessment, the range of failure modes included in the description of a damage state, the variability of structural characteristics included in the required building class and the record-to-record variability are adequately represented in the post-earthquake data. This, however, is not the case for the analytical fragility assessment where the variability in all three characteristics needs to be explicitly modeled. For this reason, the relevance of the analytical fragility curves to the aforementioned characteristics also depends on whether the variability in the three characteristics has been taken into account (for the detailed conditions see Table A.1).

In the ***Relevance*** assessment, fragility curves with one or more criteria that have been assigned an 'L' rating are considered irrelevant to the needs of the application and are disregarded. The remaining moderately or highly relevant fragility curves form a pool of candidate curves, whose usefulness to the future application are determined by their

assessment under the ***Overall Quality*** component. This is assessed differently for empirical and analytical fragility functions, as described here.

The ***Overall Quality*** of candidate empirical fragility curves is assessed on the basis of three attributes: the *input quality*, as referred to the post-earthquake damage and excitation databases, the *rationality* of the procedures used for the construction of fragility curves and the *documentation quality* (See Fig. 3.4). The four criteria used to rate the *input quality* attribute for empirical fragility curves are:

- *Damage observations*: The quality of damage observations which are rated according to the clarity of the adopted damage scale definition and the size of errors in the design and execution of the survey, which can lead to significant bias to the fragility curves (e.g. Ioannou and Rossetto 2013).
- *Excitation observations*. The quality of the excitation observations is rated according to whether the observations represent the characteristics of the seismic event and whether the study attempts to identify and model important sources of uncertainty.
- *Constrained Building Classes*. The level of constraint in the definition of the building classes that the empirical data represents defines the level of variability in structural response expected across the sample. In theory, the more detailed the structural characteristics used to define a building class, the smaller the uncertainty.
- *Data quantity*. The quantity of the data affects the level of confidence around the fragility curves. This criterion is rated according to the total number of buildings in a given class used for the construction of fragility curves as well as the number of bins in which they are aggregated.

It should be noted that in the Porter (2011) rating scheme the rating of the attribute of rationality for a given curve also includes the assessment of its ability to predict independent data ('hindcasting') and to cross-validate with existing functions. However it is found that almost all existing empirical studies do not assess the predictive capacity of their fragility curves. Some studies do attempt cross-validation. However, the authors consider this to be a weak indicator of the overall quality of a curve; i.e. just because a developed fragility function looks like one from a different study does not mean that either are of high quality. For these reasons, both of these criteria are disregarded in the proposed framework.

The *documentation quality* attribute appraises whether sufficiently detailed and complete information is provided by the authors of the fragility function for an independent researcher to be able to reproduce the study.

This is at the basis of good research and science. It is however noted that poor documentation may result in other criteria also being scored low, e.g. if the assessor is unsure of the derivation procedure followed (*rationality*) or data used (*input quality*).

The ***Overall Quality*** component of analytical fragility curves is subdivided into the same three main attributes as for the empirical curves. The *input quality* attribute for the analytical fragility curves adopts the following criteria:

- Structural Characteristics, which refer to whether the selected material and geometrical characteristics correspond to the typical range of the characteristics of the considered building class.
- Seismic demand. This criterion assesses whether the real ground motions have been considered or the spectra or the more generic design code spectra have been adopted instead.
- The completeness of the mathematical model used to simulate the building class.
- Choice of EDP. This criterion refers to whether the adopted measure of engineering demand is capable of accurately representing the seismic behavior of the examined building class, and hence their consequent levels of damage.

In the case of the *rationality* attribute the same two criteria as for empirical fragility curves are used but the description of these criteria differs in order to account more specifically for the characteristics of analytical fragility curves:

- *First Principles*: This criterion assesses whether the study violates first principles. The assessment considers the type of analyses and damage models and whether the study is consistent to the strengths and limitations of the adopted analyses. For instance, it violates first principles to use a damage model based on hysteretic behavior if the structural analysis used is nonlinear static without adaptive material constitutive laws.
- *Treatment of uncertainty:* This criterion examines the quantification of the uncertainty in the ground motion, the structure capacity and damage model, as well as the sampling techniques adopted in order to model them, as discussed in Sect. 3.3.2.

The *documentation quality* is rated in exactly the same way as for the empirical functions.

Having rated the individual criteria, these ratings can be used to select the most relevant and high quality fragility functions for the site and asset class assessed. Porter (2011) advocates for an overall score to be assigned to each fragility function. However, this is not very informative and requires a subjective interpretation of which attributes (in the case of Porter 2011) are the most important, as it is unlikely that fragility functions score in a uniform manner across all attributes. Also, if multiple candidate curves exist that all score highly, which should be used?

The here proposed framework suggests different overall scores for the two components, i.e. ***Relevance*** and ***Overall Quality***. A procedure for determining the overall scores is not prescribed here, as it is recognized that the choice depends on individual risk assessments. It is however, obvious that high to medium relevance is a pre-requisite for selection, and that low scores in data quality and quantity for empirical functions, or structural details and seismic demand for analytical functions are strong reasons for eliminating fragility functions from the selection.

In cases where multiple curves have good scores in the overall quality component and are of high-to-medium relevance, then the selection of suitable fragility

curves is not a straightforward procedure. Instead it is here proposed that either a subset or all of these candidate fragility functions are combined for the fragility assessment. A logic tree procedure for combining curves is suggested in Sect. 3.4.1 and three different weighting schemes for combining fragility curves are illustrated and discussed in the context of an example application in Sect. 3.4.2.

3.4.1 Logic-Tree Procedure for Combining Multiple Fragility Curves

The proposed rating scheme aims to provide criteria for pre-selection of potentially suitable fragility curves for a given application. Given that multiple fragility curves exist for some countries and assets, it is possible that for some future applications more than one curve might be found to be moderately or highly relevant to the needs of these applications (here referred to as "candidate fragility curves"). In this case, the user may want to adopt a mean fragility function for the examined building/asset class that derives from the combination of a number of fragility curves (here referred to as the "combined mean fragility curve"). To date, there are no well-established procedures for combining the fragility curves with the exception of SYNER-G (2011) which attempts to estimate the mean fragility curve as well as quantify the uncertainty due to the presence of different models to express the fragility of a given asset class. For this reason, a logic tree approach with three weighting schemes is presented here focused on the estimation of the mean fragility curve. It should be noted that the quantification of uncertainty around the mean curve will be addressed in a latter study.

According to the suggested approach, the existing empirical fragility curves, found to be moderately or highly relevant to the needs of a future application, can be combined through the construction of a decision tree, as depicted in Fig. 3.5.

Then, the mean probability of exceedance for each level of intensity is estimated from the sum of the weighted candidate curves for the corresponding intensity measure level:

$$E\left[P\left(DS \geq ds_i \middle| IM = x\right)\right] = \sum_{j=1}^{n_{fragilitycurves}} w_j P\left(DS \geq ds_i \middle| IM = x, j\right) \qquad (3.5)$$

The resulting combined mean fragility curve is essentially a piecewise curve. A key component of this combination procedure is the determination of the weights $\mathbf{w} = [w_1, w_2, \ldots, w_j, \ldots, w_{nfragilitycurve}]$ assigned to each branch. The weights represent the confidence of the analyst in the relative quality of each candidate fragility curve. The determination of their values is not a straightforward procedure. For this reason, three weighting schemes are described below.

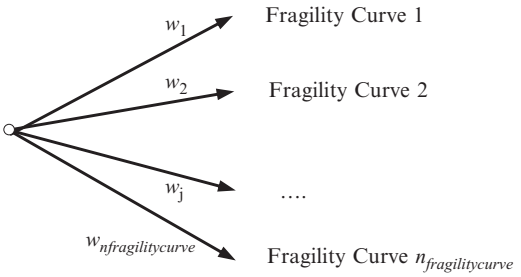

Fig. 3.5 Decision tree for candidate fragility curves corresponding to a single damage state for an examined building class

The first weighting scheme (WS1) assigns equal weights to the candidate fragility curves:

$$w_j = \frac{1}{n_{fragilitycurves}} \tag{3.6}$$

This scheme is closer to the first approach for combining fragility curves proposed by SYNER-G (2011). According to the SYNER-G approach, however, a beta distribution is fit to the values of the candidate fragility curves for each intensity level in order to quantify the epistemic uncertainty in a fragility curve due to the presence of different models. It should also be noted that the here proposed approach is more generic than the second approach for combining fragility curves favored by SYNER-G (2011) as it does not require that the candidate fragility curves are expressed in terms of the same parametric function, e.g. the lognormal cumulative distribution function. The main disadvantage of this approach is that all candidate fragility curves are considered to be equally reliable.

According to the second weighting scheme (WS2), the seven criteria corresponding to the three attributes of the ***Overall Quality*** are considered of equal importance. The weights are determined by quantifying the rating score of each criterion of the overall quality using Table 3.5. The sum of the values for the 7 criteria is then normalized such that the total sum of the weights for all candidate fragility curves adds up to 1. However, Scherbaum and Kuehn (2011) showed that this method tends to yield a mean fragility curve that is similar to that obtained from use of the above unweighted scheme (WS1).

The third weighting scheme (WS3) follows the procedure outlined by Scherbaum and Kuehn (2011). According to their approach, the user considers their confidence in the reliability as well as the representativeness of each candidate curve to the needs of the application, and accordingly assigns a weight $w_j \in [0,1]$. The sum of the weights across all candidate curves must equal 1. This procedure aims to provide a robust probabilistic framework for determining the weights that account for the fact that some criteria are more important than others. For example, the low rating of data quality is more important than the statistical model fitting procedure adopted for the construction of fragility curves.

Table 3.5 Quantification of the rating scores

Rating score	Value
H	3
M	2
L	1

3.4.2 Example Application of Different Selection and Combination Methods

An example application of the fragility curve selection and combination framework is provided here by considering the following hypothetical but realistic question:

> "What is the probability of heavy damage or collapse in ordinary Italian unreinforced mid-rise masonry buildings with regular layout for a peak ground acceleration of 0.25 g?"

It should be noted that a simple scenario based application is examined here. A future application of the proposed procedure will involve the use of fragility curves over a wide range of intensity measure levels.

The selection procedure proposed in Sect. 3.4 is applied to identify, from the GEM compendia of empirical and analytical fragility curves, one or more suitable curves to represent the fragility of the buildings being assessed. Firstly, ***Relevance*** of the fragility curves is determined for the criteria of building class, damage state and ground motion intensity (see Table A.1 for detailed criteria descriptions). With regard to the criterion of building class, a search in the GEM compendia is carried out considering the structural system, horizontal regularity and height of the masonry buildings being assessed. Only curves that are highly or moderately relevant to are retained. This yields a pool of 9 empirical and 13 analytical candidate fragility curves, which are found in 5 and 2 published sources, respectively. Their main characteristics as well as their rating scores are summarized in Tables 3.6 and 3.7. In examining the fragility functions in more detail, it is found that despite the fact that the curve developed by Colombi et al. (2008) appears to be moderately relevant to the needs of the application, the study does not provide the parametric function used to express the fragility curve or its parameters. It should be noted that a search in the Fragility Function Manager (see Chap. 13) developed by SYNER-G to accommodate this issue failed to yield any results. Therefore, this curve is ignored. With regard to the remaining candidate curves, Rota et al. (2008) as well as Borzi et al. (2008) have constructed fragility curves for subclasses of the examined building class. In the former study, the subclasses include additional characteristics on the type of floor system. In the latter study, the subclasses include more specific details on structural materials, (i.e. natural stone or brick masonry), and specific building heights. Other studies such as Coburn and Spence (2002) and Ioannou et al. (2012) also provide specific details on the construction material of the bearing walls, and their curves are also considered subsets of the assessed building class. However, Orsini (1999) develops fragility curves for a more generic building typology than is being assessed here, as they are defined for vulnerability classes of buildings as defined by EMS-98. These curves can still be considered moderately

Table 3.6 Potentially suitable empirical fragility curves for Italian mid-rise masonry buildings from GEM databases of existing fragility curves with their ratings

					2. Overall quality									
					1. Relevance			2.1. Input quality				2.2. Rationality		2.3. Doc. quality
GEM Taxonomy (Brzev et al. 2012)	Buildings class	DS	IM	References	.1.1	.1.2	.1.3	.1	.2	.3	.4	.1	.2	.1
MUR-CL99/LWAL-D99/R99/ F99/ H99/Y99/IR99/OC99	**Rubble stone masonry**	**EMS-98**	**PSI**	**Coburn and Spence** (2002)	**H**	**M**	**M**	**M**	**L**	**L**	**H**	**L**	**H**	**H**
M99-STDRE/LWAL-D99/R99/ F99/H99/Y99/IR99/OC99	**Unreinforced brick masonry**	**EMS-98**	**PSI**	**Coburn and Spence** (2002)	**H**	**M**	**M**	**M**	**L**	**L**	**H**	**L**	**H**	**H**
M99-MUN99 /LWAL-ND/R99/ F99/H99/Y99/IR99/OC99	Masonry-mid rise	4DS	S_d	Colombi et al. (2008)	H	M	M	L	L	M	H	L	L	L
M99-STRUB/LWAL-D99/R99/ F99/H99/Y99/IR99/OC99	Field stone masonry	MSK-76	PGA	Ioannou et al. (2012)	H	M	L							
M99-MUN99/LWAL-D99/R99/ F99/ H99/Y99/IR99/OC99	Vulnerability class A	8DS	PSI	Orsini (1999)	H	M	L							
M99-MUN99 /LWAL-D99/R99/ F99/H99/Y99/IR99/OC99	Vulnerability class B	8DS	PSI	Orsini (1999)	H	M	L							
M99-MUN99/LWAL-D99/R99/ F99/H99/Y99/IR99/OC99	Vulnerability class C	8DS	PSI	Orsini (1999)	H	M	L							
MUR-MUN99/LWAL-ND/ R99/ F99/H99/Y99/IR99/ OC99	**Regular-flexible floors-URM-mid rise**	**EMS-98**	**PGA**	**Rota et al.** (2008)	**H**	**M**	**H**	**H**	**M**	**H**	**H**	**L**	**H**	**M**
MUR-MUN99 /LWAL-ND/ R99/ F99/H99/Y99/IR99/ OC99	**Regular-Rigid floors-URM-mid rise**	**EMS-98**	**PGA**	**Rota et al.** (2008)	**H**	**M**	**H**	**H**	**M**	**H**	**H**	**L**	**H**	**M**

Table 3.7 Potentially suitable analytical fragility curves for Italian mid-rise masonry buildings from GEM databases of existing fragility curves with their ratings

					1. Relevance			2. Overall quality						
								2.1. Input quality				2.2. Rationality		2.3. Doc. quality
GEM Taxonomy (Brzev et al. 2012)	Buildings class	DS	IM	References	.1.1	.1.2	.1.3	.1	.2	.3	.4	.1	.2	.1
MUR-CLBRH/LWAL-ND/ R99/ F99/H:3/Y99/IRN/ OC99	**Regular-brick-high percentages of voids-3 storeys-URM**	**4DS (in-, out-of-plane)**	**PGA**	**Borzi et al.** (2008)	**H**	**M**	**M**	**H**	**M**	**H**	**M**	**M**	**L**	**M**
MUR-CLBRH/LWAL-ND/ R99/ F99/H:3/Y99/IRN/ OC99	**Regular-brick-low percentages of voids-3 storeys-URM**	**4DS (in-, out-of-plane)**	**PGA**	**Borzi et al.** (2008)	**H**	**M**	**M**	**H**	**M**	**H**	**M**	**M**	**L**	**M**
MUR-CLBRH/LWAL-ND/ R99/ F99/H:4/Y99/IRN/ OC99	**Regular-brick-low percentages of voids-4 storeys-URM**	**4DS (in-, out-of-plane)**	**PGA**	**Borzi et al.** (2008)	**H**	**M**	**M**	**H**	**M**	**H**	**M**	**M**	**L**	**M**
MUR-CLBRH/LWAL-ND/ R99/ F99/H:5/Y99/IRN/ OC99	**Regular-brick-low percentages of voids-5 storeys-URM**	**4DS (in-, out-of-plane)**	**PGA**	**Borzi et al.** (2008)	**H**	**M**	**M**	**H**	**M**	**H**	**M**	**M**	**L**	**M**
MUR-STRUB/LWAL-ND/ R99/ F99/H:4/Y99/IRN/ OC99	**Regular-natural stone-high quality-4 storeys-unreinforced**	**4DS (in-, out-of-plane)**	**PGA**	**Borzi et al.** (2008)	**H**	**M**	**M**	**H**	**M**	**H**	**M**	**M**	**L**	**M**
MUR-STDRE/LWAL-ND/ R99/ F99/H:4/Y99/IRN/ OC99	**Regular-natural stone-low quality-4 storeys-URM**	**4DS (in-, out-of-plane)**	**PGA**	**Borzi et al.** (2008)	**H**	**M**	**M**	**H**	**M**	**H**	**M**	**M**	**L**	**M**
MUR-MUN99 /LWAL-D99/ R99/ F99/H:4/Y99/IR99/ OC99	Masonry- 4 storeys	HAZUS-99 (in-plane)	S_d	Pagnini et al. (2008)	H	M	L							

relevant if it is assumed that the examined building class is a subset of vulnerability classes A, B and C as proposed by EMS-98. Finally, Pagnini et al. (2008) propose fragility curves for masonry 4-storey buildings accounting for the variability in the material as well as geometrical properties of their examined class.

With regard to the *damage state* criterion of ***Relevance***, the required state of heavy damage can be matched directly to a damage state within each of the candidate fragility curves. Therefore, all curves presented in Table 3.6 are considered highly relevant with regard to the damage state criterion. It is noted that if a particular damage scale had been stated in the hypothetical question, then only those curves adopting that particular damage state would have been rated as highly relevant, the others moderately so. It is here assumed that heavy damage corresponds to the DS4 state of the EMS-98 scale used for the construction of empirical fragility curves by Rota et al. (2008) and Coburn and Spence (2002), by the DS4 state of the MSK-76 damage scales adopted by Ioannou et al. (2012), and the level of 'very serious damage' (DS6) of the damage scale used by Orsini (1999). In the case of Borzi et al. (2008) heavy damage is attributed to the limit state where 80 % of the maximum shear resistance is attained. Finally, the state of heavy damage is equivalent to the synonymous HAZUS limit state for Pagnini et al. (2008), which is attained in the analysis when an equivalent single degree of freedom reaches the ultimate displacement.

The rating scores of the criterion of *ground motion intensity* appear to vary from high to low, given that the three conditions outlined in Table A.1 for this criterion are met by varying degrees by the examined studies. In particular, the fragility curves constructed by Rota et al. (2008) are considered highly relevant due to the use of PGA to express the ground motion intensity, the fact that the record-to-record variability is implicitly considered by the use of damage data from multiple events, the fact that the required 0.25 g is included in the range for which these two curves are valid and the sensitivity analysis which showed that the contribution of the measurement error in the intensity measure levels is small. The Borzi et al. (2008) curves are considered of moderate relevance given that their adopted response spectrum accounts for the variability in demand but it does not correspond to the requested location. Finally, the failure of Pagnini et al. (2008) to account for the variability in the demand by adopting a single response spectrum resulted in an 'L' rating score. For this reason, this study is removed from the candidate set of curves. The fragility curves constructed by Ioannou et al. (2012) and Orsini (1999) are considered irrelevant for the given application due to the fact that the required level of intensity lies outside the range of PGA values for which these curves are valid as presented in Fig. 3.6. These sets of fragility curves are therefore removed from the candidate pool.

The final revised pool of candidate curves contains 16 fragility functions. They are found to be moderately relevant to the three criteria of the application, as highlighted in Table 3.6. Twelve of these curves have been developed analytically by Borzi et al. (2008) curves and the remaining four are empirical curves constructed by Coburn and Spence (2002) and Rota et al. (2008). The ***Overall Quality*** of the fragility curves for each study is determined next.

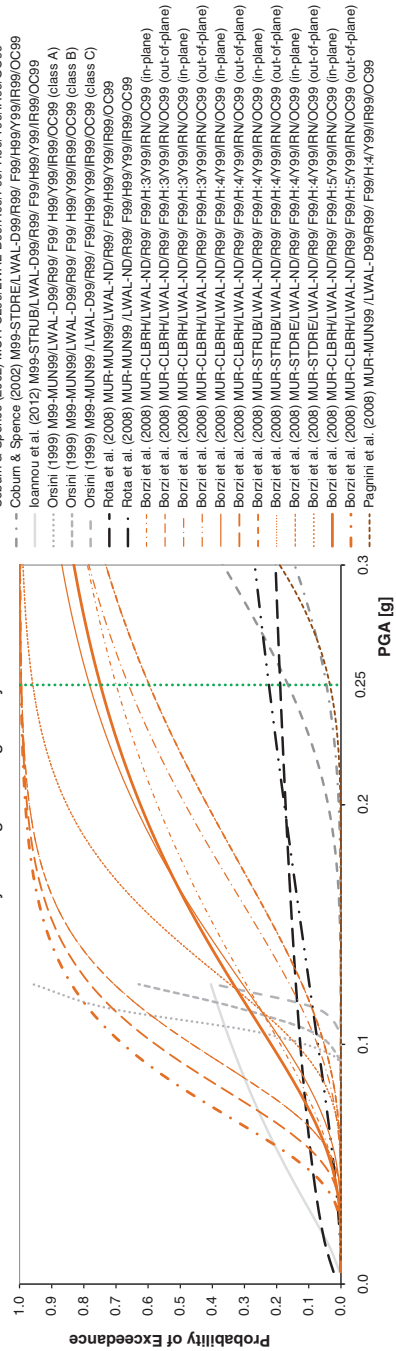

Fig. 3.6 Empirical and analytical fragility curves, which are moderately relevant to the building class of the presented application

With regard to the empirical fragility studies, that by Rota et al. (2008) is considered of moderate documentation quality and includes a thorough discussion on the input quality and the procedures followed for the construction of the fragility curves, although the confidence around the constructed curves is not provided. The sample size is considered of high quality because both building classes contain over 4,000 buildings. With regard to the input quality, the post-earthquake damage observations on which the functions are based suffered from no-coverage error, given that the total number of buildings has not been surveyed in many municipalities, and non-response error. The former error was addressed by comparing the number of buildings surveyed in each municipality with the total number of buildings in the 2001 census. A sensitivity analysis showed that for large databases (which is the case here) a no-coverage error as high as 40 % does not considerably affect the results. In addition, the non-response error, introduced by missing data on the survey forms, has been found to be small (~6 %). For these reasons, the quality of the observations is considered high. The quality of the excitation observations is also considered high given that the measurement error in the intensity measure levels has been shown to be small and a sensitivity of the ground motion measure to the fit is also examined. In addition, the well-constrained building classes used are also considered of high quality.

The study of Coburn and Spence (2002) is considered of moderate documentation quality due to the lack of a thorough discussion on the quality of the damage databases used. This reason, also leads to a moderate rating score being assigned to the damage observations criterion. The excitation observations are considered of low quality given that their values are estimated in terms of PSI, which is effectively determined from the damage observations. The data quantity criterion is assigned a high score given that a large sample size aggregated in at least 20 data points is adopted. The building classes are considered poorly constrained, and assigned a low rating, given that only very few structural characteristics have been used to describe the building classes.

With regard to the rationality attribute, it is noted that the treatment of uncertainty is generally poor across both Rota et al. (2008) and Coburn and Spence (2002). In both cases, data from multiple earthquakes are used without a sensitivity analysis being carried out to prove that the uncertainty in the damage data between events is trivial compared to the uncertainty in response across a building class. In addition, Rota et al. (2008) uses a questionable statistical model fitting method, which although accounts for the fact that some points have larger uncertainty than others, does not account for the number of buildings.

The overall quality of the analytical fragility curves developed by Borzi et al. (2008) is assessed next. With regard to the input quality criterion, a medium quality mathematical model is used by the study, which accounts for in-plane as well as out-of-plane failure modes. Their model is simplified in order to fit the mechanical method adopted for the simulation of its seismic performance. The seismic demand criterion is also assigned a moderate rating score due to the adopted code response spectrum, which accounts for uncertainty in the demand. The criterion of the structural characteristics of the building class is assigned an ‘H’

Table 3.8 Estimates of $P(DS \geq$ Heavy Damage or Collapse$|\ PGA = 0.25$ g) for four approaches proposed for combining the candidate fragility curves

Study	WS1 (16 curves)	WS1 (3 mean curves)	WS2 Overall rating per curve	w_j	WS31 w_j	**WS32** $\boldsymbol{w_j}$
Coburn and Spence (2002)	–	–	14	0.31	0.10	0.10
Rota et al. (2008)	–	–	16	0.36	0.70	0.45
Borzi et al. (2008)	–	–	15	0.32	0.20	0.45
***P*(*DS* ≥ Heavy damage or collapse| *PGA* = 0.25 g)**	**69 %**	**38 %**	**38 %**		**32 %**	**48 %**

rating as the uncertainty in material and geometrical parameters as well as the quality of the construction material are taken into account. The treatment of uncertainty is considered moderate given that the uncertainty in two out of the three components, namely: the demand and capacity is modeled through the use of Latin hypercube. The EDP is measured in terms of inter-storey drift so it can be considered of high quality. Finally, despite the fact that damage state thresholds are obtained from experimental data found in the literature and the fragility curves appear not to cross, the first principles criterion is considered 'L' due to the use of a simplified mechanical analysis method.

In what follows, the probability of the examined building class sustaining heavy damage or collapse for $PGA = 0.25$ g is estimated by combining these candidate curves using the procedures outlines in Sect. 3.4.1.

Firstly, the unweighted average approach is used to combine all 16 moderately relevant fragility curves by assuming that they are equally reliable (WS1). The probability of heavy damage or collapse for the examined building class is then estimated as the mean of the corresponding values from the 16 unweighted fragility curves, according to Eqs. (3.5) and (3.6). The probability is found to be equal to 69 % (see Table 3.8) and appears to be heavily influenced by the 12 fragility curves developed by Borzi et al. (2008). Nonetheless, the curves obtained from a single study are conditioned by the same limitations as indicated by the aforementioned discussion on the selection of the same ratings for the curves of each study, depicted in Tables 3.6 and 3.7. Therefore, the dominant influence of a single study, in this case of the study of Borzi et al. (2008), over the examined probability of exceedance could be reduced by combining the mean fragility curves for each study. The examined probability of exceedance is then estimated in terms of the average of the corresponding values from the three unweighted mean fragility curves (see Table 3.8). The examined probability of exceedance estimated by the latter approach is reduced by 45 %, indicating a considerably better seismic performance of the examined building class for the examined level of intensity.

Neither of the unweighted average approaches used accounts for the ***Overall Quality*** ratings assigned to each candidate fragility function. This can however be taken into account by assigning a different weighting scheme. According to WS2, the rating score for each criterion characterizing the fragility curves for each study

is quantified according to Table 3.5 and the overall quality is considered equal to the sum of these values. Given that all the candidate fragility curves in a single study are rated the same, the overall score for a curve per study is provided in Table 3.8. It is observed that this scoring approach suggests the curves constructed by Rota et al. (2008) are the most reliable, followed by Borzi et al. (2008) and Coburn and Spence (2002). The normalization of these scores results in very similar weights for the mean fragility curves for each study. This appears to confirm the observations made by Scherbaum and Kuehn (2011) that such a weighting scheme does not provide a reliable basis for selecting one curve over the other. In fact, for this weighting scheme, the combined mean probability of the examined building class suffering heavy damage or collapse for $PGA = 0.25$ g, presented in Table 3.8, is identical to the mean estimate using the WS1 scheme on the mean fragility curves for the three studies.

The limitations of the aforementioned weighting scheme are addressed by adopting WS3, which is based on the user's degree of belief in the overall usefulness of the candidate curves. Given the subjectivity involved in the determination of the weights according to this scheme two variations are provided for illustrative purposes.

According to WS31, the users (i.e. the authors in this case), based on the exercise of curve selection and the ratings in Table 3.6, are 70 % confident that the curves constructed by Rota et al. (2008) are the most representative of the seismic fragility of the examined building class given that they correspond to the examined building class and using high quality input data. The authors are 20 % confident that the mean fragility curves constructed by Borzi et al. (2008) for only two construction materials are suitable for the present application given that they are analytically obtained by a moderate quality model using simplified structural analyses. The curves constructed by Coburn and Spence (2002) are weighted by the remaining 10 % given that worldwide damage data, with perhaps very different seismic performance, have been used for the construction of these curves. Eq. (3.5) is adopted in order to estimate the expected probability of exceedance for $PGA = 0.25$ g. The estimate (see Table 3.8) based on this weighting scheme appears to be approximately 15 % lower than the unweighted estimate based on the three mean fragility curves. In this case, the difference appears to be notable but it is not significant.

According to WS32, the authors note that the curves proposed by Rota et al. (2008) appear to be rather flat and if extrapolated for PGA $= 3$ g the probability of heavy damage or collapse is only 57 %. This could be caused by the assumption that a coverage-error of 40 % is acceptable or by the fact that the non-homogenous damage data from different earthquakes have been aggregated together or the statistical model fitting technique adopted. For these reasons, the authors remain unconvinced that the curves proposed by Rota et al. (2008) are superior to the curves proposed by Borzi et al. (2008). For this reason, the same weight (45 %) is assigned to the curves of both studies. Similar to WS31, the curves constructed by Coburn and Spence (2002) are weighted by the remaining 10 %. Eq. (3.5) is adopted in order to estimate the expected probability of exceedance for $PGA = 0.25$ g. The estimate (see Table 3.8 and Fig. 3.7) based on this weighting scheme appears to be appear to be

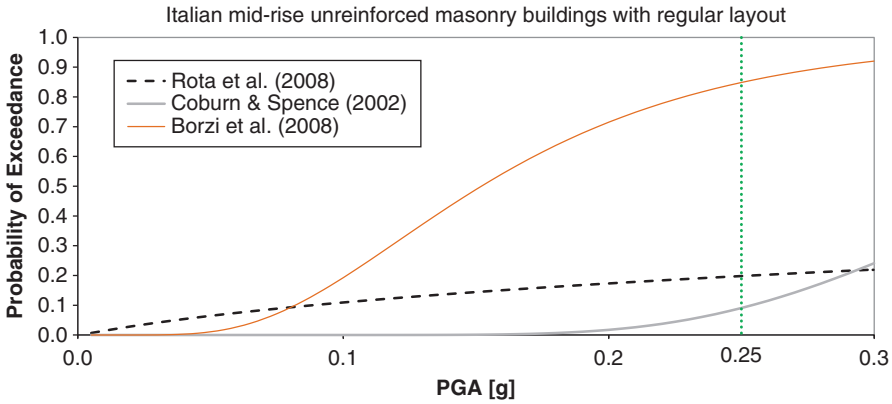

Fig. 3.7 Mean empirical and analytical candidate fragility curves based on three studies

approximately 52 % higher than the estimate based on the WS31 scheme highlighting the sensitivity of the weighting scheme to judgment and the need for a deep understanding of the advantages and the limitations of each procedure adopted for the construction of fragility curves.

3.5 Concluding Remarks

This chapter presents an overview of existing fragility curve construction approaches and discussed the factors seen in the literature to influence the reliability of analytical, empirical, expert-opinion based and hybrid fragility curves. These factors are taken into account in the proposal of a new framework for the selection of fragility functions for a particular seismic risk assessment application. The framework is discussed in detail and provides a rational approach for the selection and comparison of fragility curves of different type. The framework for selection is applied in an example application where different methods for combining fragility functions, in cases where multiple fragility functions exist for a particular application, are explored. The main observations from this exercise can be summarized as follows:

- The proposed fragility curve selection procedure provides a logical framework for the selection of fragility functions for a particular application from a compendium of such curves
- The framework of criteria and rating system provides an effective means of evaluating the factors regarded to impact the reliability of different types of fragility functions
- The combination of fragility functions through a weighting scheme based on quantifying the qualitative rating scores and their normalization appears to yield results very close to the unweighted mean. This is attributed to the fact that the

normalization is an act of convenience and results in fragility curves with being assigned non-informative overall scores.

- The process of criteria qualitative rating and user interpretation of the separate attributes can significantly aid and help to justify a more robust weighting scheme based on the user's degree of belief in the candidate fragility curves. In this example application the difference in damage state exceedance probability prediction compared to an unweighted scheme appears to be notable (~15 %).
- Finally, the exercise shows a significant reduction in the probability if the mean fragility curves for each study are combined instead of the individual fragility curves, which reduces the influence of the limitations of a single study with a large number of moderately or highly relevant curves.

It is highlighted here that these observations are based on a single application of the proposed fragility curve combination approaches and will need to be further investigated to be generalized. In particular, the quantification of uncertainty when combining fragility curves has not been considered here and remains an important area for further research. However, the observations regarding the usefulness of the proposed framework for fragility curve selection can be assumed to be more generally applicable.

Acknowledgments The Global Earthquake Model is acknowledged for its support of Dr. Ioanna Ioannou and Dr. Abdelghani Meslem in the research work that underpins this Chapter.

Appendix

Table A.1 Rating system of the **Relevance** of existing fragility curves

Attribute	Criterion	Conditions		Rate
1.	.2.1	Damage states:	Correspond to the requirements of the study	H
			Do not correspond to the requirements of the study, but their harmonisation to the needs of the study is possible	M
			Do not correspond to the requirements of the study and no harmonisation is feasible	L
		Variability in the thresholds[a]:	Considered	H
			Not considered	L
	.2.2	Building class and region:	The qualitative description of the building class and region for which the curve has been obtained is exactly the same as with the required class	H
			The building class of the curve is a subset or includes the required class. The same applied to region	M

(continued)

Table A.1 (continued)

Attribute	Criterion	Conditions		Rate
			The qualitative description of the building class and region for which the curve has been obtained is substantially different than the same as with the required class	L
		Variability in building characteristics[a]	Multiple buildings or Randomisation of geometrical or material parameters	H
			Limited number of buildings	M
			Single building	L
1.	.2.3	Intensity measure type:	Identical to the requirement of the application	H
			Appropriate conversion equation present	M
			No conversion equation present	L
		Intensity measure levels:	Includes the required IM levels	H
			The level is 20 % higher or lower than the min or max value of IM range	M
			Does not include the required IM levels	L
		Ground motion[b]:	Ground motion – Database at location of building and the variability in the ground motion is taken into account	H
			Spectra Regional Level – Spectrum from existing record from the required area and the variability in the ground motion is taken into account	
			Ground motion – Spectrum compatible synthetic record and the variability in the ground motion is taken into account	M
			Spectra National Level – Uniform hazard model and the variability in the ground motion is taken into account	
			Ground motion – Database unrelated to required location.	L
			Spectra Regional/National Level – Standard spectra	
			Variability in ground motion is not taken into account	
		Ground motion**:	The measurement error in the intensity measure levels is taken into account in the fragility assessment if the fragility for a given scenario is required. This is not necessary if the fragility curves are coupled with the hazard and this error is accounted for in the hazard assessment	H
			The measurement error in the intensity measure levels is NOT taken into account in the fragility assessment, although the vulnerability for a given scenario is required	L

[a]Only for analytical fragility curves
[b]Only for empirical fragility curves

Table A.2 Rating scheme of the **Overall Quality** of existing analytical fragility curves

Attribute	Criterion	Conditions		Rate
2.1.	.1	Material and geometric characteristics:	Representative of the characteristics of the assessed building class	H
			Not representative of the characteristics of the assessed building class	L
	.2	Representation of ground motion:	Real ground motion records	H
			Code based spectra	L
	.3	Selection of EDP:	Inter-story drift	H
			Top drift	M
	.4	Mathematic model	Structural modelling-3D element-by-element	H
			Structural modelling-2D element-by-element	M+
			Structural modelling-2D storey-by-storey	M-
			Structural modelling-1D global model	L
			Performance criteria-shear failure in members – Considered	H
			Performance criteria-shear failure in members – **NOT** considered	L
			Infill RC building – Modelled as infill frames	H
			Infill RC building – Modelled as bare frames	L
			Masonry buildings: performance criteria – Out of Plane failure mechanism – Considered	H
			Masonry buildings: performance criteria – Out of Plane failure mechanism – **NOT** considered	L
2.2.	.1	Parameters accounted for uncertainties:	Uncertainty in capacity + demand + damage thresholds is considered	H
			2/3 parameters are considered	M+
			1/3 parameters is considered	M-
			Not considered	L
		Modelling of record-to-record variability:	Large database of ground motions	H
			Lack of database of ground motions	L
		Used values of β:	Calculated	H
			Default	L
		Sampling method:	Monte Carlo or Latin hypercube sampling	H
			Full partitioning.	M
			Reduced partitioning.	L
			Simplified methods/direct capacity curve definition (Non-numerically-based).	L
2.2.	.2	Analysis type:	Nonlinear dynamic analysis methods	H
			Nonlinear static analysis methods	M
			Simplified methods/direct capacity curve definition (Non-numerically-based)	L
		Fragility curves:	The curves corresponding to different damage states for a given building class do not cross. The curves follow expected trends	H
			Not applicable	M

(continued)

Table A.2 (continued)

Attribute	Criterion	Conditions		Rate
			Obtained curves violate the first principles, e.g. fragility curves corresponding to different damage states for a given building class cross	L
		Definition of damage states:	Obtained from analysis of progress of local damage at elements level	H
			Use of damage model (to be consistent with analysis type)	M
			Use of simplified formula (based on simplified bilinear capacity curve)	L
			Default values	
2.3.	.1	Documentation quality	Reproducible study	H
			Only some parameters of the fragility functions are clearly defined	M
			Insufficient information is provided to the fragility function or the methodology	L

Table A.3 Rating scheme of the **Overall Quality** of existing empirical fragility curves

Attribute	Criterion	Conditions	Rate
2.1.	.1	Damage scales or loss measures are clearly defined. Negligible non-sampling errors. Significant non-sampling errors have been acknowledged and reduced using appropriate methods	H
		Damage scales or loss measures are clearly defined but some significant non-sampling errors have been treated by relying on assumptions which are not checked	M
		Damage scales or loss measures are defined with ambiguity. Significant non-sampling errors have not been reduced or reduced with questionable procedures	L
	.2	The IMLs have been determined from ground motion recording stations or GMPEs, and more than one intensity measure has been used in order to identify the one that fits the data best. The influence of the uncertainty in the ground motion in the fragility or vulnerability functions has been investigated	H
		The uncertainty in IM has been partially investigated or if more than one IMs has been used for the vulnerability or fragility assessment	M
2.1.	.2	IMLs are interdependent with the observed damage data. If they used a single intensity measure and did not explore any other sources of uncertainty	L
	.3	Building classes are defined in terms of building material, lateral-load resisting system, height and seismic code (age)	H
		Building classes are defined in terms of building material, lateral-load resisting system or in terms of vulnerability class, e.g. EMS98	M
		Crude building classes are defined, e.g. RC buildings, RC frames, abode buildings from worldwide databases	L
	.4	For continuous functions: Sample sizes $\geq$200 damage or loss observations. For aggregated damage data, a minimum of 20 observations per bin of IM is used for a minimum of 10 bins	H

(continued)

Table A.3 (continued)

Attribute	Criterion	Conditions	Rate
		For continuous functions: sample sizes between 20 and 200. For aggregated damage data, number of bins of IM between 5 and 10 are used with a minimum of 20 observations per bin	M
		For continuous functions: Sample sizes <20 units or units aggregated in <5 bins of IM	L
2.2.	.1	Data manipulations follow sensible procedures. Appropriate statistical models are selected and diagnostic tools demonstrate their goodness of fit	H
		Appropriate statistical models are selected, but diagnostic tools fail to demonstrate their goodness of fit	M
		Inappropriate statistical models are selected or data manipulations follow questionable procedures	L
	.2	The curves corresponding to different damage states for a given building class do not cross. The curves follow expected trends	H
		Not applicable	M
		Obtained curves violate the first principles, e.g. fragility curves corresponding to different damage states for a given building class cross	L
2.3	.1	All the necessary inputs, outputs, and analytical steps are clearly documented and the work is reproducible	H
		Only partial information regarding the aforementioned issues has been addressed in the work	M
		Insufficient information is provided to the fragility or vulnerability function or the methodology	L

References

ALA (2001) Seismic fragility formulations for water systems: Part 1 – Guidelines. American Lifelines Alliance, ASCE-FEMA

Amiri GG, Jalalian M, Amrei SAR (2007) Derivation of vulnerability functions based on observational data for Iran. In: Proceedings of international symposium on innovation and sustainability of structures in civil engineering, Tongji University, China

Anagnos T (1999) Development of an electrical substation equipment performance database for evaluation of equipment fragilities. PG&E/PEER report, Department of Civil and Environmental Engineering, San Jose State University, San Jose, CA, USA

Antoniou S, Pinho R (2004) Development and verification of a displacement-based adaptive pushover procedure. J Earthq Eng 8(5):643–661

Applied Technology Council (1985) ATC-13, Earthquake damage evaluation data for California. Redwood City, CA, 492 pp

Applied Technology Council (ATC) (2007) Recommended methodology for quantification of building system performance and response parameters. ATC-63 90% Draft, Redwood City, CA

Applied Technology Council (ATC) (2012) Seismic performance assessment of buildings, vol 1 – Methodology. ATC-58, Redwood City, CA

Argyroudis S, Pitilakis K (2012) Seismic fragility curves of shallow tunnels in alluvial deposits. Soil Dyn Earthq Eng 35:1–12

Aslani H, Miranda E (2004) Component-level and system-level sensitivity study for earthquake loss estimation. In: Proceedings of the thirteenth world conference on earthquake engineering structure, Vancouver, BC, Canada

Aspinall W, Cooke RM (1998) Expert judgement and the Montserrat volcano eruption. In: Mosleh A, Bari RA (eds) Proceedings of the 4th international conference on Probabilistic Safety Assessment and Management PSAM4, New York, USA, 13–18 Sept 1998

Baker J (2011) Fitting fragility functions to structural analysis data using maximum likelihood estimation, Working paper –PEER

Baker JW, Cornell CA (2003) Uncertainty specification and propagation for loss estimation using FOSM methods. In: Proceeding of the ninth International Conference on Applications of Statistics and Probability in Civil Engineering (ICASP9), 6–9 July 2003, San Francisco. Civil Engineering Risk and Reliability Association (CERRA), San Francisco

Baker JW, Cornell CA (2008) Uncertainty propagation in probabilistic seismic loss estimation. Struct Saf 30(3):236–252

Bakhshi A, Karimi K (2006) Method of developing fragility curves a case study for seismic assessment of masonry buildings in Iran. In: 7th international Congress in civil engineering, Tehran, Iran

Basoz NI, Kiremidjian AS, King SA, Law KH (1999) Statistical analysis of bridge damage data from the 1994 Northridge, CA, earthquake. Earthq Spectra 15(1):25–54

Bensi M, Der Kiureghian A, Straub D (2011) A Bayesian network methodology for infrastructure seismic risk assessment and decision support, PEER report 2011/2, March 2011

Bhuiyan AR, Alamb MS (2012) Seismic vulnerability assessment of a multi-span continuous highway bridge fitted with shape memory alloy bars and laminated rubber bearings. Earthq Spectra 28(4):1379–1404

Bojórquez E, Iervolino I, Reyes-Salazar A, Ruiz SE (2009) Comparing vector-valued intensity measures for fragility analysis of steel frames in the case of narrow-band ground motions. Eng Struct 45:472–480

Borzi B, Crowley H, Pinho R (2008) Simplified pushover-based earthquake loss assessment (SP-BELA) method for masonry buildings. Int J Archit Herit 2(4):353–376

Braga F, Dolce M, Liberatore D (1982) Southern Italy November 23, 1980 earthquake: a statistical study of damaged buildings and an ensuing review of the M.S.K.-76 scale, Report, Rome, Italy

Brzev S, Scawthorn C, Charleson A, Jaiswal K (2012) GEM basic building taxonomy, version 1.0, GEM ontology and taxonomy global component project. Available from http://www.nexus.globalquakemodel.org/gem-ontology-taxonomy/posts/updated-gem-basic-building-taxonomy-v1.0

Clemen RT, Winkler RL (1999) Combining probability distributions from experts in risk analysis. Risk Anal 19(2):187–203

Coburn AW, Spence RJS (2002) Earthquake protection. Wiley, Chichester

Colombi M, Borzi B, Crowley H, Onida M, Meroni F, Pinho R (2008) Deriving vulnerability curves using Italian earthquake damage data. Bull Earthq Eng 6(3):485–504

Cooke M (1991) Experts in uncertainty: opinion and subjective probability in science. Oxford University Press, Oxford

Cooke RM (2001) EXCALIBUR-Windows version of EXCALIBUR: software for performance based combination of expert judgements. Department of Mathematics, Delft University of Technology. Website: http://delta.am.eqi.tudelft.nl/risk/

Corigliano M, Scandella L, Lai CG, Paolucci R (2011) Seismic analysis of deep tunnels in near fault conditions: a case study in southern Italy. Bull Earthq Eng 9(4):975–995

Cornell CA, Krawinkler H (2000) Progress and challenges in seismic performance assessment. PEER Center News 3(2): Spring

D'Ayala D (2005) Force and displacement based vulnerability assessment for traditional buildings. Bull Earthq Eng 3(3):235–265

D'Ayala D (2013) Assessing the seismic vulnerability of masonry buildings. In: Tesfamariam S, Goda K (eds) Handbook of seismic risk analysis and management of civil infrastructure systems. Woodhead Publishing, Cambridge, pp 334–365

D'Ayala D, Meslem A (2013) Guide for Selection of existing analytical fragility curves and compilation of the database. GEM technical report 2013-X, GEM Foundation, Pavia, Italy
D'Ayala D, Jaiswal K, Wald DJ, Porter K, Greene M (2010) Collaborative effort to estimate collapse fragility for buildings worldwide: the WHE-PAGER project. In: Proceedings of the 9th US National and 10th Canadian conference on earthquake engineering structure: reaching beyond borders
Dalkey N (1969) The Delphi method: an experimental study of group opinion. A report prepared for United States Air Force Project Rand RM-5888-PR, 79 pp
Demircioglu MB, Erdik M, Hancilar U, Sesetyan K, Tuzun C, Yenidogan C, Zulfikar AC (2010) Technical manual– earthquake loss estimation routine ELER-v3.0, Department of Earthquake Engineering Structure, Bogazici University, Istanbul, 133 pp
Ellingwood B (2009) Quantifying and communicating uncertainty in seismic risk assessment. Struct Saf 31(2):179–187
Elnashai AS, Borzi B, Vlachos S (2004) Deformation-based vulnerability functions for RC bridges. Struct Eng 17(2):215–244
European Committee of Standardization (CEN) (2005) Eurocode 8: design of structures for earthquake resistance Part 3: Assessment and retrofitting of buildings, ENV 1998-3, Brussels, Belgium
Fajfar P (2000) A nonlinear analysis method for performance-based seismic design. Earthq Spectra 16(3):573–591
FEMA (2003) HAZUS-MH technical manual. Federal Emergency Management Agency, Washington, DC
FEMA 356 (2000) Pre-standard and commentary for the seismic rehabilitation of buildings. Report no 356, Federal Emergency Management Agency, American Society of Civil Engineers, Reston Virginia, USA
Giovinazzi S, King A (2009) Estimating seismic impacts on lifelines: an international review for RiskScape. In: Proceedings of the 2009 NZSEE conference, Christchurch, New Zealand
Grünthal G (ed) (1998) European Macroseismic Scale 1998. Cahiers du Centre Europèen de Gèodynamique et de Seismologie, vol 15. Conseil de l'Europe
Gűlkan P, Sucuoğlu H, Ergűnay O (1992) Earthquake vulnerability, loss and risk assessment in Turkey. In: Proceedings of 11th world conference on earthquake engineering structure, Madrid, Spain
Hancilar U, Taucer F, Corbane C (2011) Empirical fragility assessment after the January 12, 2010 Haiti earthquake, risk analysis VIII, B. C.A. WIT Press, Southampton
Hwang H, Liu JB, Chiu Y-H (2001) Seismic fragility analysis of highway bridges, MAEC report: project MAEC RR-4. Mid-America Earthquake Center, Urbana-Champaign
Ioannou I, Rossetto T (2013) Sensitivity of empirical fragility assessment of buildings to the misclassification error of damage. In: Proceedings of the 11th international conference on structural safety and Reliability (ICOSSAR 2013), Columbia University, New York, USA, 16–20 June 2013
Ioannou I, Rossetto T, Damian GN (2012) Use of regression analysis for the construction of empirical fragility curves. In: Proceedings of 15th world conference on earthquake engineering structure, Lisbon, Portugal, 24–28 September
Jaiswal K, Wald DJ (2010) Development of a semi-empirical loss model within the USGS Prompt Assessment of Global Earthquake for Response (PAGER) system. In: Proceedings of the 9th U.S. and 10th Canadian conference on earthquake engineering: reaching beyond borders, 25–29 July 2010, Toronto, ON, Canada, Paper No. 1095
Jaiswal K, Wald D, D'Ayala D (2011) Developing empirical collapse fragility functions for global building types. Earthq Spectra 27(3):775–795
Jaiswal KS, Aspinall WP, Perkins D, Wald D, Porter KA (2012) Use of expert judgement elicitation to estimate seismic vulnerability of selected building types. In: Proceedings of the 15th world conference on earthquake engineering structure, Lisbon, Portugal, 24–28 Sept 2012
Jiang H, Lu H, Chen L (2012) Seismic fragility assessment of RC moment-resisting frames designed according to the current Chinese seismic design code. J Asian Archit Build 11(1):153–160

Kappos AJ, Panagopoulos G (2010) Fragility curves for R/C buildings in Greece. Struct Infrastruct Eng 6(1):39–53

Kappos AJ, Panagopoulos G, Penelis G (2006) A hybrid method for the vulnerability assessment of R/C and URM buildings. Bull Earthq Eng 4(4):391–413

Karababa FS, Pomonis A (2010) Damage data analysis and vulnerability estimation following the August 14, 2003 Lefkada Island, Greece, earthquake. Bull Earthq Eng 9:1015–1046

Kaynia AM (ed) (2013) Guidelines for deriving seismic fragility functions of elements at risk: Buildings, lifelines, transportation networks and critical facilities. SYNER-G reference report 4. JRC scientific and policy report. Joint Research Centre, European Commission, pp 250. doi:10.2788/19605

Klügel J-U (2005) On the use of probabilistic seismic hazard analysis as an input for seismic PSA. In: Proceedings of the 18th international conference on structural mechanics in reactor technology (SMiRT18), Beijing, China, 7–12 Aug 2005. PaperKM02_2

Klügel J-U (2011) Uncertainty analysis and expert judgement in seismic hazard analysis. Pure Appl Geophys 168(1–2):27–53

Lagomarsino S, Cattari S (2013) Seismic vulnerability of existing buildings. In: Gueguen P (ed) Seismic vulnerability of structures. Wiley, Hoboken. doi:10.1002/9781118603925.ch1

Liel A, Linch K (2012) Vulnerability of reinforced-concrete-frame buildings and their occupants in the 2009 L'Aquila, Italy, earthquake. Nat Hazard Rev 13(1):11–23

Maruyama Y, Yamazaki F, Mizuno K, Tsuchiya Y, Yogai H (2010) Fragility curves for express-way embankments based on damage datasets after recent earthquakes in Japan. Soil Dyn Earthq Eng 30:1158–1167

Moehle J, Deierlein G (2004) A framework methodology for performance-based earthquake engineering structure. In: Proceedings of the 13th world conference on earthquake engineering structure, Vancouver, BC, Paper No. 679

Molina S, Lang DH, Lindholm CD (2009) User and technical manual, SELENA v4.0, NORSAR, Kjeller, Norway, 85 pp

Morris PA (1977) Combining expert judgements: a Bayesian approach. Manage Sci 23 (7):679–693

Nielson BG, DesRoches R (2007) Seismic fragility methodology for highway bridges using a component level approach. Earthq Eng Struct 36(6):823–839

O'Rourke MJ, So P (2000) Seismic fragility curves for on-grade steel tanks. Earthq Spectra 16 (4):801–815

Orsini G (1999) A model for buildings' vulnerability assessment using the parameterless scale of seismic intensity (PSI). Earthq Spectra 15(3):463–483

Ouchi F (2004) A literature review on the use of expert opinion in probabilistic risk analysis. World Bank policy research working paper 3201, February 2004

Pagnini L, Vicente R, Lagomarsimo S, Varum H (2008) A mechanical method for the vulnerability assessment of masonry buildings. In: Proceedings of 14th world conference on earthquake engineering structure, Beijing, China

Park YJ, Ang AHS (1985) Mechanistic seismic damage model for reinforced concrete. J Struct Eng 111(4):722–739

Porter K (2011) GEM vulnerability rating system, GEM global vulnerability estimation methods consortium. Available from www.nexus.globalquakemodel.org/gem-vulnerability/posts/

Rajeev P, Tesfamariam S (2011) Effect of construction quality variability on seismic fragility of reinforced concrete building. In: Proceedings of the ninth pacific conference on earthquake engineering structure building and Earthquake-Resilient Society, Auckland, New Zealand, 14–16 April

Rossetto T (2004) Vulnerability curves for the seismic assessment of reinforced concrete structure populations. Ph.D. thesis, Imperial College, London, UK

Rossetto T, Elnashai AS (2003) Derivation of vulnerability functions for European-type RC structures based on observational data. Eng Struct 25:1241–1263

Rossetto T, Elnashai AS (2005) A new analytical procedure for the derivation of displacement-based vulnerability curves for populations of RC structures. Eng Struct 27:397–409

Rossetto T, Ioannou I, Grant DN (2013a) Existing empirical fragility and vulnerability relationships: compendium and guide for selection. GEM technical report 2013-X, GEM Foundation, Pavia, Italy, April 2013, pp 62

Rossetto T, Ioannou I, Grant DN (2013b) Guidelines for the construction of empirical fragility and vulnerability relationships. GEM technical report 2013-X, GEM Foundation, Pavia, Italy

Rota M, Penna A, Strobbia CL (2008) Processing Italian damage data to derive typological fragility curves. Soil Dyn Earthq Eng 28(10):933–947

Sarabandi P, Pachakis D, King S, Kiremidjian A (2004) Empirical fragility functions from recent earthquakes In: Proceedings of 13th world conference on earthquake engineering structure, Vancouver, Canada

Scheibe M, Skutsch M, Schofer J (1975) Experiments in Delphi methodology. In: Linestone H, Turoff M (eds) The Delphi method: techniques and applications. Addison-Wesley, London

Scherbaum F, Kuehn NM (2011) Logic tree branch weights and probabilities: summing up to one is not enough. Earthq Spectra 27(4):1237–1251

Shahzada K, Gencturk B, Khan AN, Naseer A, Javed M, Fahad M (2011) Vulnerability assessment of typical buildings in Pakistan. Int J Earth Sci Eng 4:208–211

Shinozuka M, Feng MQ, Lee J, Naganuma T (2000) Statistical analysis of fragility curves. J Eng Mech-ASCE 126(12):1459–1467

Singhal A, Kiremidjian AS (1997) A method for earthquake motion damage relationships with application to reinforced concrete frames. State University of New York at Buffalo: National Center for Earthquake Engineering Structure Research Report NCEER-97-0008

Solberg KM, Dhakal RP, Mander JB, Bradley BA (2008) Computational and rapid expected annual loss estimation methodologies for structures. Earthq Eng Struct Dyn 37(1):81–101

Song J, Kang W (2009) System reliability and sensitivity under statistical dependence by matrix-based system reliability method. Struct Saf 31(2):148–156

Spence RJS, Coburn AW, Pomonis A (1992) Correlation of ground motion with building damage: The definition of a new damage-based seismic intensity scale. In: Proceedings of 10th world conference on earthquake engineering structure, Balkema, Rotterdam

Stafford PJ (2013) Uncertainties in ground motion prediction in probabilistic seismic hazard analysis (PSHA) of civil infrastructure. In: Tasfamarian S, Goda K (eds) Handbook of seismic risk analysis and management of civil infrastructure systems. Woodhead Publishing, Cambridge, pp 29–56

SYNER-G (2011) Fragility functions for common masonry building types in Europe. D3.2, University of Pavia, 177 pp

Uma SR, Ryu H, Luco N, Liel AB, Raghunandan M (2011) Comparison of main-shock and aftershock fragility curves developed for New Zealand and US buildings. In: Proceedings of the ninth pacific conference on earthquake engineering structure building and Earthquake-Resilient Society, Auckland, New Zealand, 14–16 April

Vacareanu R, Chesca AB, Georgescu B, Seki M (2007) Case study on the expected seismic losses of soft and weak ground floor buildings. International symposium on strong vrancea earthquake and risk mitigation, Bucharest, Romania, October

Vamvatsikos D, Cornell AC (2002) Incremental dynamic analysis. Earthq Eng Struct Dyn 31(3):491–514

Wen YK, Ellinwood BR, Bracci J (2004) Vulnerability function framework for consequence-based engineering, Mid-America Earthquake Center, CD Release 04-04

Yang TY (2013) Assessing seismic risks for new and existing buildings using performance-based earthquake engineering (PBEE) methodology. In: Tasfamarian S, Goda K (eds) Handbook of seismic risk analysis and management of civil infrastructure systems. Woodhead Publishing, London, pp 307–333

Chapter 4
Epistemic Uncertainty in Fragility Functions for European RC Buildings

Helen Crowley, Miriam Colombi, and Vitor Silva

Abstract This chapter briefly summarises the work carried out under the auspices of the SYNER-G project to collect, harmonize and compare fragility functions for European RC buildings. All of these functions have been stored in the Fragility Function Manager described in Chap. 13. Examples of a methodology for estimating the epistemic uncertainty across a collection of fragility functions is presented, which, as discussed herein, should first be carefully reviewed for reliability, for example following the methodology presented in Chap. 3.

4.1 Introduction

The identification of the seismic fragility functions for common buildings types is a fundamental component of a seismic risk loss assessment model and, for this reason, many research studies have addressed this topic in the recent past.

In the context of the SYNER-G Project, the main typologies of reinforced concrete buildings in Europe have been identified and the existing fragility functions have been reviewed with the objective of homogenizing the existing model building types (through a new taxonomy, called the SYNER-G taxonomy), and comparing these functions amongst themselves. The main output is method to identify a set of fragility functions (with associated uncertainties) for the main reinforced concrete typologies present in Europe. For further details, the reader is referred to Crowley et al. (2011a, b).

H. Crowley (✉) • M. Colombi • V. Silva
European Centre for Training and Research in Earthquake Engineering (EUCENTRE),
Via Ferrata 1, 27100 Pavia, Italy
e-mail: helen.crowley@eucentre.it; miriam.colombi@eucentre.it; vitor.silva@eucentre.it

K. Pitilakis et al. (eds.), *SYNER-G: Typology Definition and Fragility Functions for Physical Elements at Seismic Risk*, Geotechnical, Geological and Earthquake Engineering 27,
DOI 10.1007/978-94-007-7872-6_4,

4.2 Review of Fragility Functions for European Buildings

In the European continent, most of the buildings are constructed with masonry or reinforced concrete, and for this reason, the majority of the existing fragility functions in the academic literature treat these two types of structures. Fragility functions describe the probability of exceeding different limit states (such as damage levels) given a level of ground shaking. A "fragility function set", as referred to herein, represents a group of functions for a given building typology for a number of different limit states of damage. A large number of fragility function sets have been collected in the context of the SYNER-G project and they have been stored into a dynamic tool, the SYNER-G Fragility Function Manager, which is described in Chap. 13 of this book.

About 50 studies/publications have been reviewed as part of the project and for each study, usually more than one building typology is investigated and different fragility function sets are identified. For example, Polese et al. (2008) considered three different types of reinforced concrete buildings and developed three different fragility function sets. Therefore, in total, 415 fragility function sets for buildings have been collected in the project. The review of fragility functions is not claimed to be comprehensive, but it was carried out to develop the Fragility Function Manager, and additionally investigate the epistemic uncertainty of fragility functions, using the methodology described in Chap. 13.

As discussed in Chap. 1, different methodologies can be used for deriving fragility functions and it is possible to classify them into four generic groups: empirical (based on observed data), expert opinion-based, analytical (based on numerical models) and hybrid (typically a combination of empirical and analytical methods). An "unknown" class has been added in this study due to the fact that it could be unclear from the reference material which method has been used. In the pie charts below, the percentages of the different methodologies used in the 50 studies reviewed are shown for reinforced concrete buildings. Figure 4.1 shows the popularity of analytical methods for the derivation of fragility functions for European buildings, which is also an outcome of the fact that two recent European projects – RISK-UE (Mouroux and Le Brun 2006) and LESSLOSS (Calvi and Pinho 2004), both promoted the use of analytical methodologies for deriving fragility functions.

Another key element which is significant in the development of the fragility curves, is the Intensity Measure Type (IMT) that represents the reference ground motion parameter against which the probability of exceedance of a given limit state is plotted. The vulnerable conditions of a structure are defined for a certain level of ground shaking. An intensity measure describes the severity of earthquake shaking.

In the reviewed papers, different IMTs have been used to define the level of ground shaking. It is possible to group these IMTs into two main classes: observational intensity measure types and instrumental intensity measure types.

With regards to the observational IMTs, different macroseismic intensity scales could be used to identify the observed effects of ground shaking over a limited area.

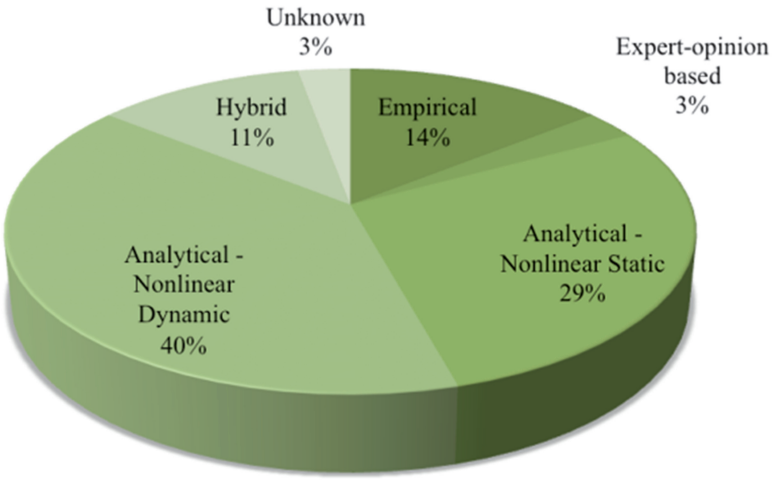

Fig. 4.1 Pie chart presenting the percentages of different methodologies used to develop fragility function for reinforced concrete buildings

In the reviewed papers, fragility functions have been estimated using the following different types of macroseismic intensity:

- MCS: Mercalli-Cancani-Sieberg Intensity Scale;
- MMI: Modified Mercalli Intensity Scale;
- MSK81: Medvedev-Sponheuer-Karnik Intensity Scale;
- EMS98: European Macroseismic Scale.

The instrumental IMTs (obtained from accelerograms), have the advantage that the severity of the earthquake is no longer subjective. In the reviewed papers, several instrumental IMTs are used to link the probability of exceeding different limit states to the ground shaking:

- PGA: peak ground acceleration;
- PGV: peak ground velocity;
- RMS: root mean square of the acceleration;
- $S_a(T_y)$: spectral acceleration at the elastic natural period T_y of the structure;
- $S_d(T_y)$ and $S_d(T_{LS})$: spectral displacement at the elastic natural period (T_y) of the structure or at the inelastic period (T_{LS}) corresponding to a specific limit state, respectively;
- Roof Drift Ratio: represents the ratio of the maximum displacement response at the roof and the height of the building.

The latter three intensity measures in the list above might be referred to as structure-dependent intensity measures as they are based on response parameters, and thus require structural information regarding the building typology in order to be used (Fig. 4.2).

In the pie charts above, the percentages concerning the different IMTs used in the studies are shown and as can be noted, peak ground acceleration has been the most commonly used intensity measure type in the studied literature.

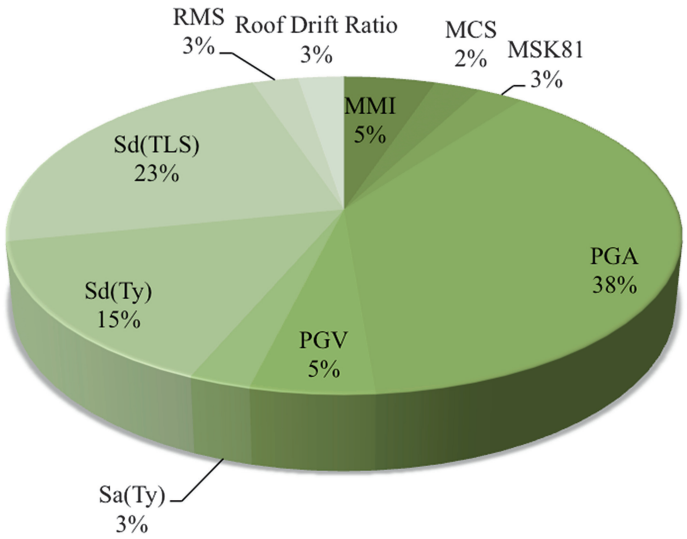

Fig. 4.2 Pie chart presenting the different percentages of intensity measure types used to develop fragility function for reinforced concrete buildings

4.3 Taxonomy of European Building Typologies

Fragility functions are developed for classes of buildings that have similar characteristics in terms of the attributes that affect seismic vulnerability. The classification of buildings based on their structural characteristics can be carried out with a "taxonomy".

A number of building taxonomies have been proposed over the past 30 years although many actually provide a list of building typologies rather than a scheme with which the main attributes of buildings can be classified. From the extensive study of fragility functions carried out in this work it became clear that existing taxonomies could leave out a large number of characteristics that could be used to distinguish the seismic performance of buildings, and in many cases it was not clear how these taxonomies should be simply expanded to include such information. Hence, a classification scheme for buildings was developed within the SYNER-G project. The main categories of this classification scheme proposed for buildings within SYNER-G are: force resisting mechanism (FRM), force resisting mechanism material (FRMM), plan regularity (P), elevation regularity (E), cladding (C), detailing (D), floor system (FS), roof system (RS), height level (H), and code level (CL). The attributes of the taxonomy that are most relevant for RC buildings are presented in Table 4.1. Readers are referred to Chap. 5 for a discussion of the attributes of the SYNER-G taxonomy used to describe masonry buildings.

Table 4.1 SYNER-G building taxonomy: attributes of importance for RC buildings

	Category	Sub-category
FRM	Moment resisting frame (MRF)	Embedded beams (EB);
	Structural wall (W)	Emergent beams (EGB)
	Flat slab (FS)	
	Precast (P)	
FRMM	Concrete (C)	Reinforced concrete (RC);
		High strength concrete (>50 MPa) (HSC); Average strength concrete (20–50 MPa) (ASC); Low strength concrete (<20 MPa) (LSC)
		High yield strength reinforcing bars (>300 MPa) (HY); Low yield strength reinforcing bars (<300 MPa) (LY);
		Classification of reinforcing bars based on EC2 (A,B,C);
		Smooth rebars (SB);
		Non-smooth rebars (NSB)
P	Regular (R)	
	Irregular (IR)	
E	Regular geometry (R)	
	Irregular geometry (IR)	
C	Regular infill vertically (RI)	Fired brick masonry (FB);
	Irregular infill vertically (IRI)	High % voids (H%); Low % voids (L%);
	Bare (B)	Autoclaved Aerated Concrete (AAC); Precast concrete (PC);
		Glazing (G);
		Single layer of cladding (SL); Double layer of cladding (DL);
		Open first floor (Pilotis) (P); Open upper floor (U).
D	Ductile (D)	
	Non-ductile (ND)	
FS	Rigid (R)	Reinforced concrete (RC); Steel (S); Timber (T).
	Flexible (F)	
HL	Low-rise (1–3) (L)	Number of stories (indicate the number)
	Mid-rise (4–7) (M)	
	High-rise (8–19) (H)	
	Tall (20+) (Ta)	
CL	None (NC)	
	Low (<0.1 g) (LC)	
	Moderate (0.1–0.3 g) (MC)	
	High (>0.3 g) (HC)	

FRM force resisting mechanism, *FRMM* force resisting mechanism material, *P* plan, *E* elevation, *C* cladding, *D* detailing, *FS* floor system, *HL* height level, *CL* code level

The building typology is defined using the label put in the brackets for each parameter within a given category. For example:

FRM1-FRM2/FRMM1-FRMM2/P/E/C-CM/D/FS-FSM/RS-RSM/HL-NS/CL

More than one label can be used per category separated by a dash. For example, a building with moment resisting frames and walls (dual system) would be MRF-W, a building with mixed construction of reinforced concrete and masonry would be RC-M. Not all categories need to be defined due to the fact that there might be lack of information about the structure. In this case, where information is unknown, it can be left by an X. In the following, two examples are shown:

- MRF/C-RC/X/X/RI-FB-H%/ND/R-RC/X/L-2/NC: moment resisting frame, in reinforced concrete with regular external infill panels in brick with a high percentages of voids, with non-ductile design details, with rigid reinforced concrete floor, low-rise, two storeys, not designed to a seismic code;
- BW/M/X/X/X/X/X/X/L/X: low-rise masonry bearing wall structure.

The proposed taxonomy is constructed with a modular structure. In this way, other categories and sub-categories can easily be added and all the different kind of European buildings can be taken into account. Subsequently, additional categories for describing the non-structural elements might be added.

This modular structure represents a new and a different approach in categorizing and classifying buildings. It has a flexible structure and it can be used to describe a considerable amount of different buildings. It can be updated at any time with new categories being added and different features can be added to existing categories. The SYNER-G taxonomy was defined by Charleson (2011) as having the most potential amongst all taxonomies reviewed and subsequently formed the basis of the Global Earthquake Model (GEM) Building Taxonomy (Brzev et al. 2012). It is proposed that in future European studies the GEM Building Taxonomy is used, as it has built upon and further improved the SYNER-G taxonomy.

4.4 Fragility Functions for RC Buildings

Following the review of fragility functions in Europe, and their classification using the SYNER-G building taxonomy, a tool was developed to store all of the functions, and allow users to harmonize and compare the functions. This tool is the Fragility Function Manager, described further in Chap. 13 of this book.

As described in Sect. 4.3, a taxonomy for European buildings has been derived in this project. This taxonomy has been assigned to all of the fragility functions collected (which can be found in Crowley et al. 2011a). The fragility functions for a given taxonomical description can then be filtered using the SYNER-G Fragility Function Manager.

One main class of reinforced concrete structures has been selected herein for the comparison of fragility functions: reinforced concrete buildings with moment

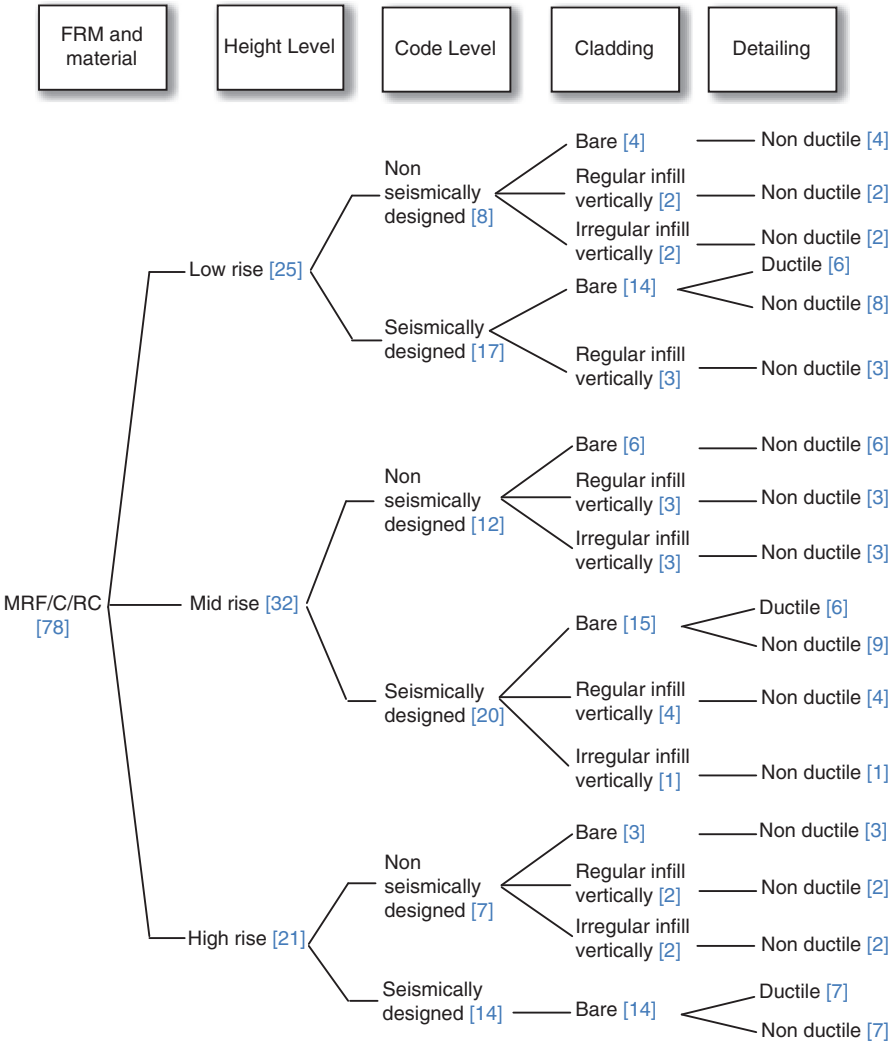

Fig. 4.3 Flow chart for a reinforced concrete with moment resisting frame building class. The number in *blue brackets* reports the available number of fragility function sets

resisting frames. A project has been created with the aforementioned tool to consider this main class and sub-projects have been developed to group the structures taking into account the height level, the code level, the cladding and the detailing (Fig. 4.3). Each column represents a different level of detail. In this way, the user can choose to compare fragility functions taking into account different levels of information. For instance, it should be possible to compare all the available fragility functions sets concerning reinforced concrete with moment resisting frame building that are low rise or all the available fragility functions

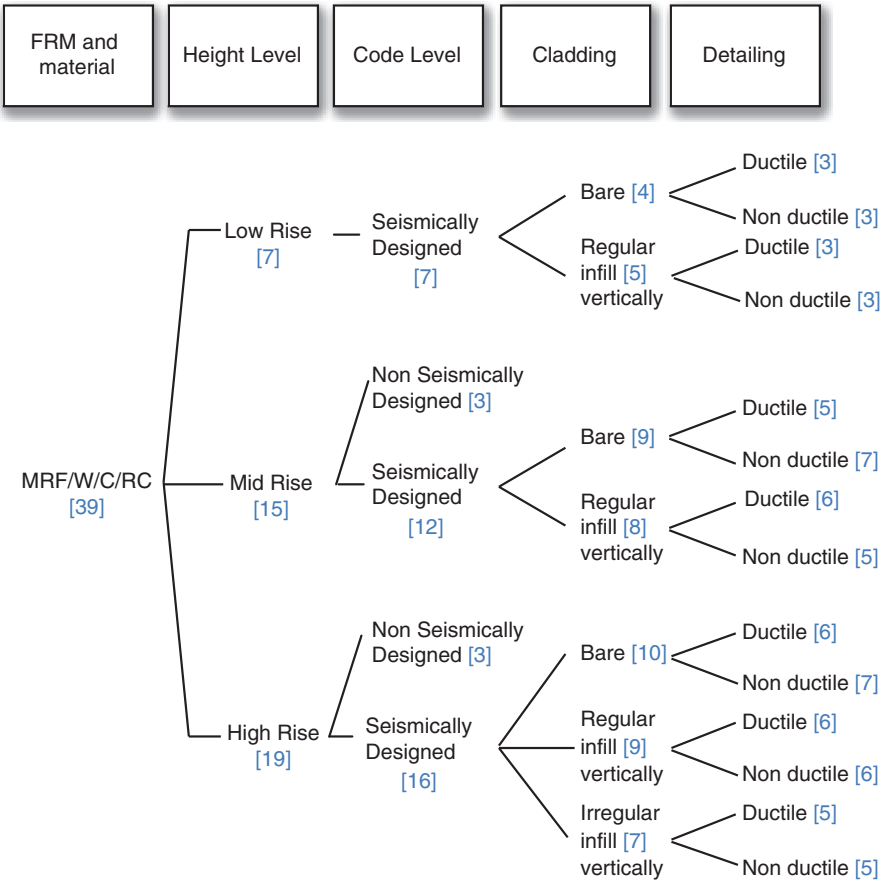

Fig. 4.4 Flow chart for a reinforced concrete with dual system building class. The number in *blue brackets* reports the available number of fragility function sets

sets concerning reinforced concrete with moment resisting frame building that are low rise, seismically designed, bare and ductile. In Fig. 4.4, the chart produced using the same exercise for reinforced concrete buildings with dual systems is also provided.

By observing Figs. 4.3 and 4.4 it is apparent which building types need to be analysed in future research developments. In fact, there are some classes that are represented by very few fragility curves (sometimes just one fragility function) and for this reason it is not possible to conduct a critical review and an exhaustive study of the epistemic uncertainties across the fragility functions of this typology.

A collection of fragility functions for a given RC building type has been produced, and then harmonized (in terms of the intensity measure type and limit

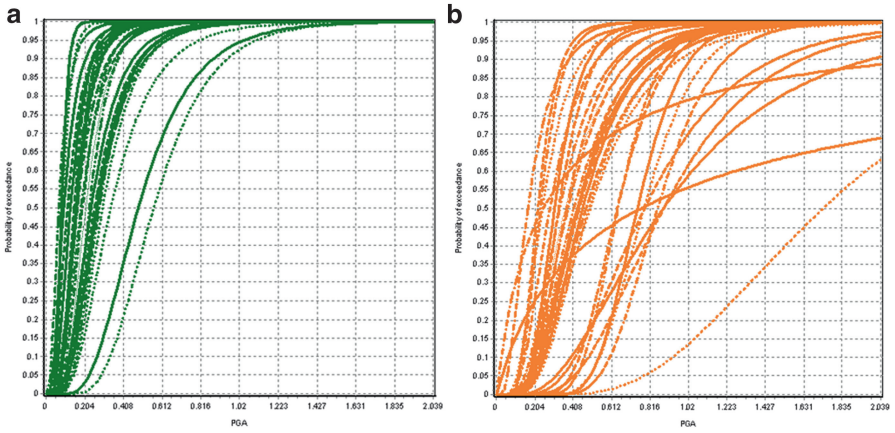

Fig. 4.5 Yield limit state (**a**) and collapse limit state (**b**) harmonised fragility functions for a reinforced concrete mid-rise building with moment resisting frame: MRF/C/RC/X/X/X/X/X/X/MR/X

states) and compared. In the following, four examples are described to show in detail the capability of the tool and the comparison between different literature studies. Readers that are interested in more guidance regarding the selection of fragility functions from a wide range of choices are referred to Chap. 3, where a methodology for selecting reliable fragility functions is presented. Such a method has not been applied herein, which is one reason for the very large epistemic uncertainty that can be seen across the fragility functions. The main reason for presenting the functions herein has been to demonstrate one possible methodology for estimating epistemic uncertainty, which has been implemented in the SYNER-G systemic vulnerability framework, which is described further in the companion Book (Systemic Seismic Vulnerability and Risk Assessment of Complex Urban, Lifeline Systems and Infrastructures: The SYNER-G Methodology and Applications).

The selected examples in Figs. 4.5, 4.6, 4.7 and 4.8 go from a lower level of detail (reinforced concrete building, mid rise, moment resisting frame) to a higher level of detail (reinforced concrete building, mid rise, moment resisting frame, seismically designed, bare and non ductile). Somewhat surprisingly, increasing the level of detail of the taxonomic description of the building typology does not necessarily reduce the epistemic uncertainty in the fragility functions. There are a wide range of reasons for the variability in the curves which include the methodology used to derive the functions (and the treatment of uncertainties within that method), the region of applicability, the limit state criteria applied, the intensity measure type employed (and the uncertainties associated with converting to a common intensity measure type). As discussed in Chap. 3, and as highlighted by the following results, an evaluation of these criteria should first be made, before fragility functions can be selected and compared.

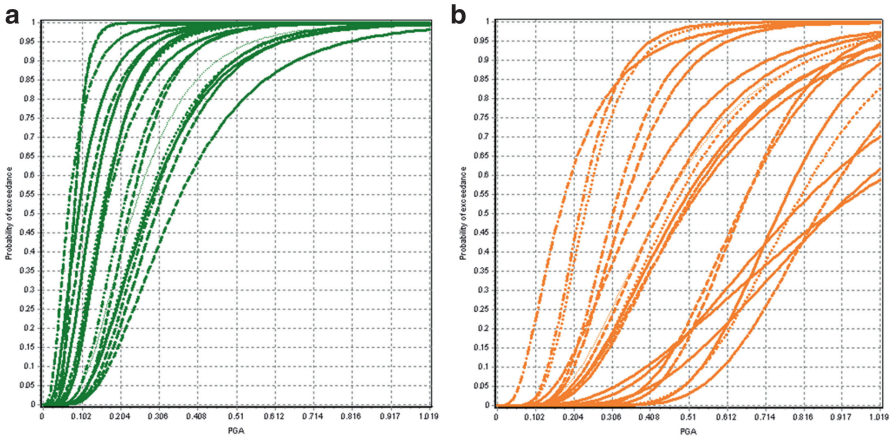

Fig. 4.6 Yield limit state (**a**) and collapse limit state (**b**) harmonised fragility functions for a reinforced concrete mid-rise building with moment resisting frame with lateral load design: MRF/C/RC/X/X/X/X/X/X/MR/C

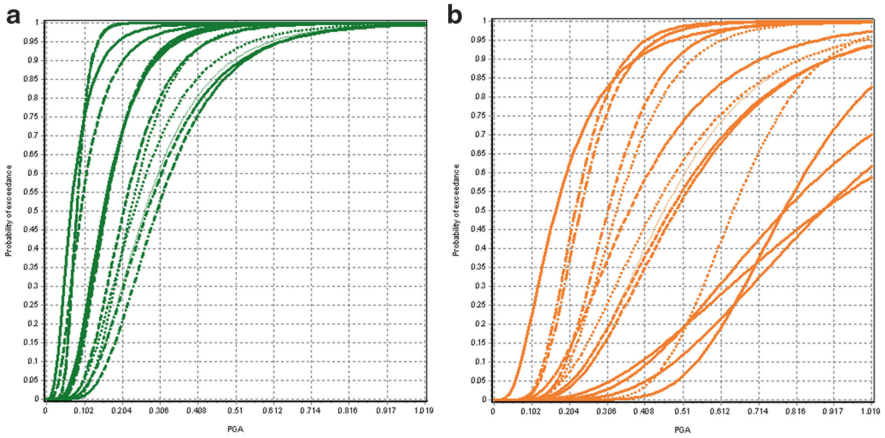

Fig. 4.7 Yield limit state (**a**) and collapse limit state (**b**) harmonised fragility functions for a reinforced concrete mid-rise building with bare moment resisting frame with lateral load design: MRF/C/RC/X/X/B/X/X/X/MR/C

For each reinforced concrete buildings class, in the Figs. 4.9, 4.10, 4.11 and 4.12 below are shown the mean curve and the individual fragility functions, whilst in the following Tables 4.2, 4.3, 4.3, 4.4, 4.5, 4.6, 4.7 and 4.8 are reported the mean and coefficient of variation (cv) of the lognormal parameters of the fragility functions (i.e. logarithmic mean and logarithmic standard deviation), as well as the corresponding correlation coefficient matrix. The methodology for estimating these parameters is presented in Chap. 13.

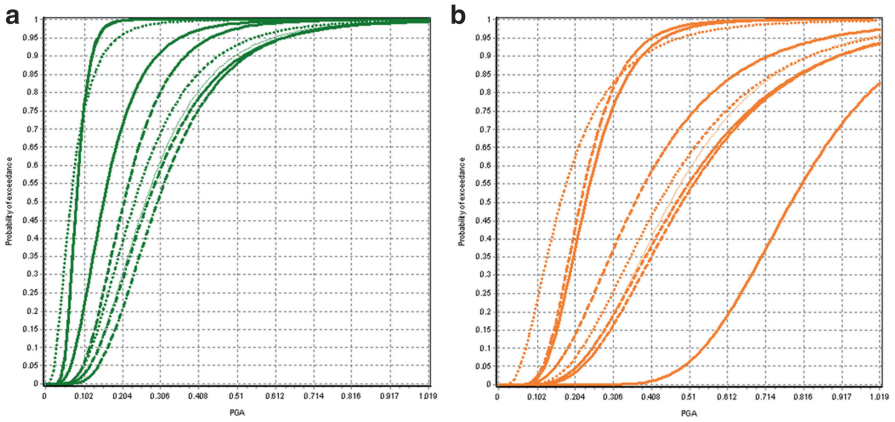

Fig. 4.8 Yield limit state (**a**) and collapse limit state (**b**) harmonised fragility functions for a reinforced concrete mid-rise building with bare moment resisting frame with lateral load design: MRF/C/RC/X/X/B/ND/X/X/MR/C

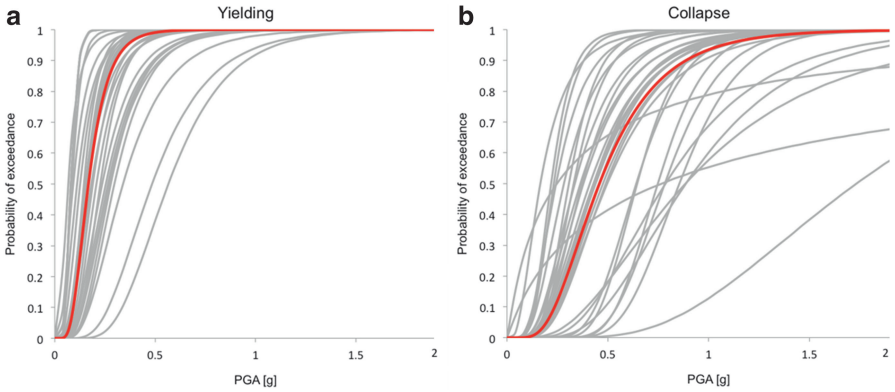

Fig. 4.9 Mean curve for yielding limit state (**a**) and collapse limit state (**b**) for a reinforced concrete mid-rise building with moment resisting frame

4.5 Concluding Remarks

As part of the study on existing fragility functions in Europe carried out within the SYNER-G project, a number of issues have been tackled from which the following recommendations can be extracted:

- A classification scheme (taxonomy) for European buildings has been proposed. The SYNER-G taxonomy has formed the basis of the GEM building taxonomy (Brzev et al. 2012), which if used in future research and risk assessment applications, will simplify the comparison of fragility functions across various studies.

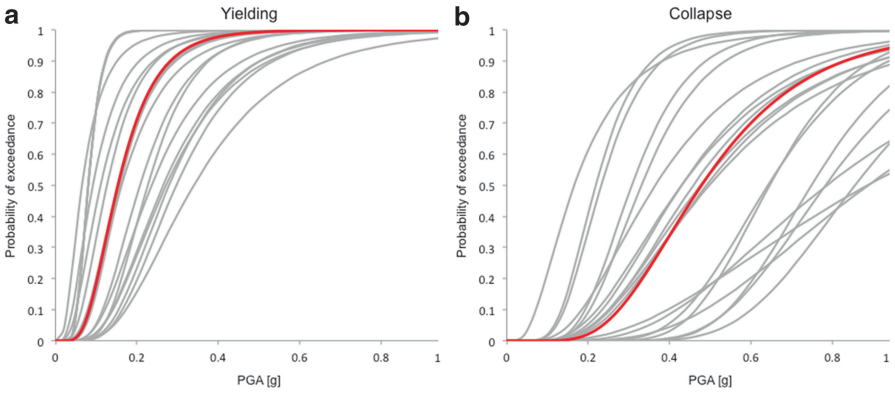

Fig. 4.10 Mean curve for yielding limit state (**a**) and collapse limit state (**b**) for reinforced concrete mid-rise building with bare moment resisting frame with lateral load design

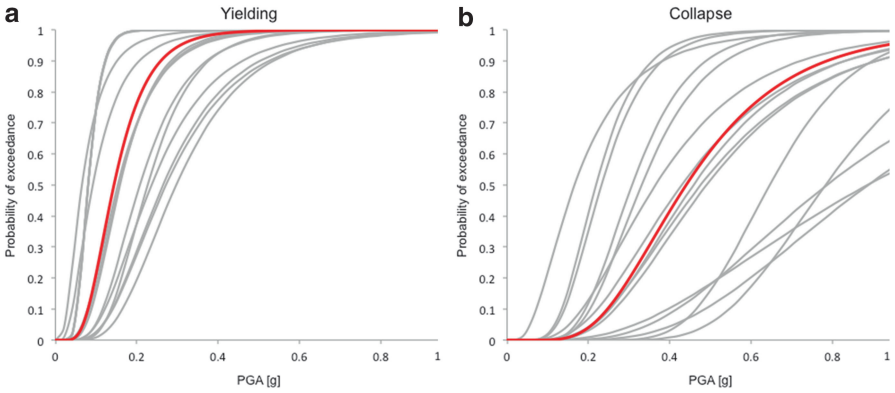

Fig. 4.11 Mean curve for yielding limit state (**a**) and collapse limit state (**b**) for a reinforced concrete mid-rise building with bare moment resisting frame with lateral load design

- A tool for those working on seismic risk assessment has been developed which allows fragility functions, that have until now been confined to the pages of academic literature, to be shared and compared. A recommendation for the future development of the Fragility Function Manager will be for the fragility functions to first be quality rated before a methodology to estimate the epistemic uncertainty is applied. Chapter 3 proposes that the reliability of a fragility function can be described in terms of a number of factors including the data quality, class definition and sampling method/size and derivation method. Such evaluations of fragility functions will aid users in selecting functions for risk assessment.
- It is recommended that future research into fragility functions in Europe takes into account the gaps that have been identified through the review carried out in this project. In particular, fragility functions for high rise moment resisting

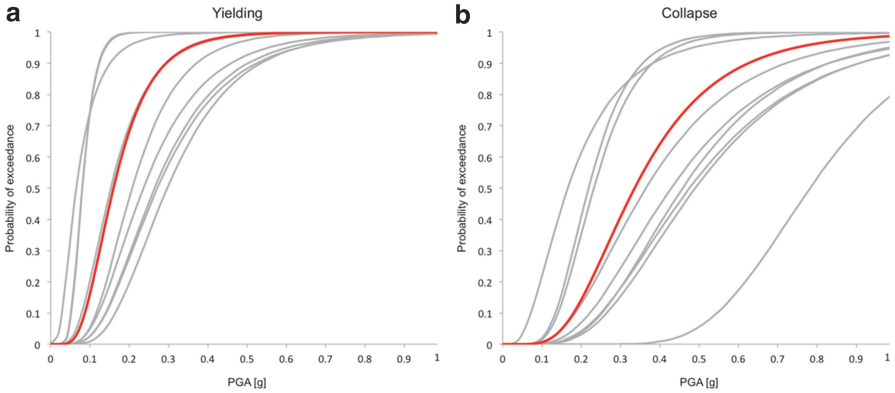

Fig. 4.12 Mean curve for yielding limit state (**a**) and collapse limit state (**b**) for a reinforced concrete mid-rise building with bare non-ductile moment resisting frame with lateral load design

Table 4.2 Mean and c_v of the lognormal fragility parameters for a reinforced concrete mid-rise building with moment resisting frame

	Yielding		Collapse	
	Logarithmic mean	Logarithmic standard deviation	Logarithmic mean	Logarithmic standard deviation
Mean	−1.853	0.481	−0.879	0.452
c_v (%)	26	19	48	23

Table 4.3 Correlation coefficient matrix for a reinforced concrete mid-rise building with moment resisting frame

	Median (yield)	Dispersion (yield)	Median (collapse)	Dispersion (collapse)
Median (yield)	1	0.116	0.537	0.272
Dispersion (yield)		1	0.278	0.008
Median (collapse)	Symmetric		1	−0.109
Dispersion (collapse)				1

Table 4.4 Mean and c_v of the lognormal fragility parameters for a reinforced concrete mid-rise building with moment resisting frame with lateral load design

	Yielding		Collapse	
	Logarithmic mean	Logarithmic standard deviation	Logarithmic mean	Logarithmic standard deviation
Mean	−1.876	0.476	−0.738	0.430
c_v (%)	28	21	67	28

Table 4.5 Correlation coefficient matrix for a reinforced concrete mid-rise building with bare moment resisting frame with lateral load design

	Median (yield)	Dispersion (yield)	Median (collapse)	Dispersion (collapse)
Median (yield)	1	0.152	0.386	0.094
Dispersion (yield)		1	0.371	0.354
Median (collapse)	Symmetric		1	−0.279
Dispersion (collapse)				1

Table 4.6 Mean and c_v of the lognormal fragility parameters for a reinforced concrete mid-rise building with bare moment resisting frame with lateral load design

	Yielding		Collapse	
	Logarithmic mean	Logarithmic standard Deviation	Logarithmic mean	Logarithmic standard deviation
Mean	−1.939	0.458	−0.821	0.452
c_v (%)	28	23	64	25

Table 4.7 Correlation coefficient matrix for a reinforced concrete mid-rise building with bare moment resisting frame with lateral load design

	Median (yield)	Dispersion (yield)	Median (collapse)	Dispersion (collapse)
Median (yield)	1	0.189	0.504	−0.041
Dispersion (yield)		1	0.276	0.723
Median (collapse)	Symmetric		1	−0.089
Dispersion (collapse)				1

Table 4.8 Mean and c_v of the lognormal fragility parameters for a reinforced concrete mid-rise building with bare non-ductile moment resisting frame with lateral load design

	Yielding		Collapse	
	Logarithmic mean	Logarithmic standard deviation	Logarithmic mean	Logarithmic standard deviation
Mean	−1.832	0.474	−1.091	0.485
c_v (%)	33	21	48	24

frames with seismic design and infills panels were not identified in the review, and frame-wall structures without seismic design were much less common than their seismically designed counterparts. The reason for the reduced number of studies is likely to be related to the lower frequency of these building typologies in Europe, but it is nevertheless suggested that the research herein could provide some guidance on where to focus fragility function efforts for RC buildings in

Table 4.9 Correlation coefficient matrix for a reinforced concrete mid-rise building with bare non-ductile moment resisting frame with lateral load design

	Median (yield)	Dispersion (yield)	Median (collapse)	Dispersion (collapse)
Median (yield)	1	0.158	0.783	0.033
Dispersion (yield)		1	0.118	0.614
Median (collapse)	Symmetric		1	−0.453
Dispersion (collapse)				1

the future. In the meantime, as mentioned previously, users of existing fragility functions are recommended to apply methodologies such as those described in Chap. 3 for evaluating and selecting robust fragility functions, and a methodology such as the one described in Chap. 13 for parameterizing the uncertainty across a number of functions.

References

Brzev S, Scawthorn C, Charleson AW, Jaiswal K (2012) Interim overview of GEM building taxonomy V2.0, GEM Foundation, December 2012. Available from URL: http://www.nexus.globalquakemodel.org/gem-building-taxonomy/posts/testing-and-evaluation-of-the-gem-building-taxonomy-v-2.0/at_download/attachment

Calvi GM, Pinho R (2004) LESSLOSS, a European integrated project on risk mitigation for earthquakes and landslides. Research report ROSE 2004/02. IUSS Press, 178 pp. ISBN: 88-7358-020-3

Charleson A (2011) Review of existing structural taxonomies. Available from URL: http://www.nexus.globalquakemodel.org/gem-building-taxonomy/posts/review-of-existing-structural-taxonomies

Crowley H, Colombi M, Silva V, Ahmad N, Fardis M, Tsionis G, Papailia A, Taucer F, Hancilar U, Yakut A, Erberik MA (2011a) D3.1 Fragility functions for common RC building types in Europe, SYNER-G Deliverable 3.1. Available from URL: http://www.vce.at/SYNER-G/files/dissemination/deliverables.html

Crowley H, Colombi M, Silva V, Ahmad N, Fardis M, Tsionis G, Karatoni T, Lyrantazaki F, Taucer F, Hancilar U, Yakut A, Erberik MA (2011b) D3.2 Fragility functions for common masonry building types in Europe, SYNER-G Deliverable 3.2. Available from URL: http://www.vce.at/SYNER-G/files/dissemination/deliverables.html

Mouroux P, Le Brun B (2006) Presentation of RISK-UE project. Bull Earthq Eng 4:323–339

Polese M, Verderame GM, Mariniello C, Iervolino I, Manfredi G (2008) Vulnerability analysis for gravity load designed RC buildings in Naples – Italy. J Earthq Eng 12(S2):234–245

Chapter 5
Fragility Functions of Masonry Buildings

Sergio Lagomarsino and Serena Cattari

Abstract This chapter proposes a method for the vulnerability assessment of ordinary masonry buildings at territorial scale, to be used in the framework of a probabilistic seismic risk analysis. The classification of the built environment is based on the SYNER-G taxonomy and is dependent on the available data in the study area; it consists in the aggregation of buildings characterized by a homogeneous seismic behavior, which is known from empirical damage on similar structures, proper analytical models or expert judgment. The general definition of fragility functions is recalled, through the use of static non linear analysis for the evaluation of the capacity spectrum and the calculation of the maximum displacement by the demand spectrum. The selection of proper intensity measures for masonry buildings is treated, as well as the definition of damage and performance limit states. A detailed procedure for the propagation of uncertainties is proposed, which is able to single out each independent contribution. Then, some recommendations for deriving fragility functions with different approaches are given. In particular, it is shown how the *macroseismic vulnerability method*, derived from EMS98, can be used by expert elicitation or if empirical data are available. Moreover, the DBV-*masonry* (Displacement Based Vulnerability) method is proposed as a powerful tool for the derivation of fragility function by an analytical approach. Finally, fragility functions are derived for ten different classes of masonry buildings, defined by a list of tags from the taxonomy, in order to show the capabilities of the proposed methods and their cross-validation.

S. Lagomarsino (✉) • S. Cattari
Department of Civil, Chemical and Environmental Engineering, University of Genoa,
Via Montallegro 1, 16145 Genova, Italy
e-mail: sergio.lagomarsino@unige.it; serena.cattari@unige.it

K. Pitilakis et al. (eds.), *SYNER-G: Typology Definition and Fragility Functions for Physical Elements at Seismic Risk*, Geotechnical, Geological and Earthquake Engineering 27,
DOI 10.1007/978-94-007-7872-6_5,

5.1 Typologies

The definition of fragility functions for masonry buildings is a hard task because we refer to a wide variety of constructions, which are characterized by very different types of masonry and structural systems, moving through historical periods and geographical areas.

As regards the first point, masonry is a composite material and the mechanical properties are related not only to those of the constituents, blocks (stone, solid clay bricks, adobe, etc.) and mortar (mud, lime, hydraulic lime, cement), but also to the dimensions and shape of the blocks, the interlocking in the external leaves and the transversal connection through thickness.

With reference to the structural systems, ancient constructions, but also recent vernacular ones, are very different from engineered masonry buildings, such as confined or reinforced masonry. The former were built by an empirical approach and are usually vulnerable, first of all to local mechanisms (out-of-plane behavior); however, in high seismic areas specific details were adopted to prevent from damage (metallic tie rods, timber belts, buttresses, connections of horizontal diaphragms to masonry walls, etc.). The latter have been specifically conceived to withstand the earthquake, after a detailed damage observation, as in the case of confined masonry (widely adopted in South American countries), or on the base of modeling and capacity design criteria, as in the case of unreinforced masonry building (with reinforced concrete – RC – ring beams at floor level) or reinforced masonry.

Among the masonry building may also be considered the mixed structures, such as the traditional mixed masonry-timber buildings or the rather modern mixed masonry-RC buildings. The formers may have different configurations: (a) timber reinforced masonry buildings, with horizontal timber ties at various levels and connected through thickness (e.g. in the Balkan, Greek and Turkish area); (b) timber-framed masonry buildings (e.g. frontal walls of pombaline buildings in Portugal, or smaller building with main bearing walls confined and braced with timber elements, all over the world); (c) buildings with masonry walls at the lower stories and timber frames at the upper ones. Besides confined masonry, the spread of RC technology in the first half of twentieth century has caused the birth of different types of mixed masonry-RC buildings, results of functional choices and often quite vulnerable: (a) masonry perimeter walls and RC interior frames; (b) raising of masonry buildings with RC framed structures.

Another important distinction is between ordinary and monumental masonry buildings. The latter category collects special type of assets, from the morphological point of view, such as: churches, mosques, towers, minarets, fortresses, etc.; they have a specific seismic behavior and, usually, a higher vulnerability, as testified by the last seismic events. Models and fragility functions defined for ordinary masonry buildings can be also used for monumental palaces, but in addition it is required an additional vulnerability assessment of some specific elements, if present (loggias, cloisters, colonnades, wide halls with double height, etc.).

This chapter is mainly focused on ordinary masonry buildings. In particular mechanical models and fragility functions are proposed for ordinary unreinforced masonry buildings. However, the general framework of the procedure outlined in the next section (Sect. 5.3), in terms of key assumptions, treatment of uncertainties and modeling issues, can be adopted also for the derivation of fragility functions of other masonry buildings typologies.

In Table 5.1 the main features that are useful for the taxonomy of masonry buildings are listed, according to the general approach proposed in SYNER-G project. Each building is described by a string of codes, separated by slashes and hyphens. Slashes mark the main categories of the taxonomy: FRM – Force Resisting Mechanism; FRMM – Force Resisting Mechanism Material; P – Plan; E – Elevation; CO – Cladding & Openings; DM – Detailing & Maintenance; FS – Floor System; RS – Roof System; HL – Height Level; CL – Code Level. Within each category, the list of possible options is defined by proper acronyms; a more detailed classification and sub-classification (in square brackets in Table 5.1) is related to some of the category options and can be indicated in the taxonomy by separating the list of codes by hyphens.

In the case of masonry buildings the FRM is always the Bearing Walls system (BW), which can present very different seismic behavior depending on geometry and constructive details. Usually reference is made to Out-of-Plane (OP) and In-Plane (IP) mechanism, depending on the connections and distance between masonry walls, as well as on the stiffness of horizontal diaphragms. If a global seismic (box-type) behavior can be assumed, a sub-classification is possible: each single wall may be analyzed by an equivalent frame model (EF) or by simplified models that assume the hypotheses of strong (SSWP) or weak (WSSP) spandrels. The choice of the most reliable model depends on available as-built information.

The category FRMM considers different structural material: Unreinforced Masonry (URM); Reinforced Masonry (RM); Confined Masonry (CM); Timber-framed Masonry (TM); mixed Masonry-RC (MRC). In particular, in the URM case, a detailed classification is important, with reference to blocks and mortar characteristics, because the mechanical properties vary in a wide range.

The configuration of the building Plan (P) is very important for the seismic vulnerability, both with reference to the regularity (R, IR) and to the possible interaction with other buildings (Isolated – I – or Aggregated in urban blocks – A). This information is useful to address the most probable collapse mechanisms (BW classification).

Information on the regularity in Elevation (E) may help in the definition of the behavior factor and the ductility, due to the possible different localization of the weak story.

The role of non-structural elements is almost negligible in masonry buildings, but it is important to know the regular distribution and percentage of openings (CO). A regular distribution (RO) may promote the WSSP behavior, which is characterized by a higher displacement capacity but a lower strength than the SSWP case. Moreover, a High percentage of openings (H %) at the base story, typical in the case of shops, may produce a weak story mechanism, which has a low displacement capacity.

Table 5.1 SYNER-G taxonomy for masonry buildings

	Category	Classification
FRM	Bearing Walls (BW)	Out of plane (OP); In plane (IP) [Equivalent Frame (EF), Weak Spandrels Strong Piers (WSSP), Strong Spandrels Weak Piers (SSWP)]
FRMM	Unreinforced Masonry (URM) Reinforced Masonry (RM) Confined Masonry (CM)	*Blocks*: Adobe (A); Fired brick (FB); Soft Stone (SS); Hard Stone (HS) [Regular Cut (RC), Uncut (UC), Rubble (RU)]; Hollow clay tile (HC) [High % of voids (H%), Low % of voids (L%), Concrete Masonry Unit (CMU), Autoclaved Aerated Concrete (AAC)]
	Timber-framed Masonry (TM)	*Mortar*: Lime mortar (LM); Cement mortar (CM); Mud mortar (MM); Hydraulic mortar (HM) *Strengthening*: Strengthened masonry (Sm) *Timber*: Confined and braced masonry panels (TC); Horizontal timber tie (TT) *Concrete and reinforcement*: [Average Strength (20-50 MPa)(ASC), Low Strength (<20 MPa) (LSC)]; [Vertical Reinforcement Bars (RBV), Vertical and Horizontal Reinforcement Bars (RBVH)]
P	Regular (R) Irregular (IR)	Isolated (I), Aggregate (A)
E	Regular geometry (R) Irregular geometry (IR)	
CO	Regular openings (RO) Irregular openings (IRO)	High % voids (H%), Low % voids (L%)
DM	*Details*: High quality details (HQD), Low quality details (LQD) *Maintenance*: Good Maintenance (HM), Low Maintenance (LM)	*Tie rods*: Without tie rods (WoT); With tie rods (WT) *Ring beams*: Without ring beams (WoRB); With ring beams (WRB)
FS	Rigid (R) Flexible (F)	Reinforced concrete (RC); Steel (S); Timber (T); Vault (V)
RS	Peaked (P)	*Material*: Timber (Ti); Corrugated Metal Sheet (CMS); Reinforced Concrete (RC); Thatch (Th)
	Flat (F)	Thrusting roof (Tr); Unthrusting roof (UTr)
	Gable End Walls (G)	
HL	Low-rise (1–2) (L) Mid-rise (3–5) (M) High-rise (6–7) (H) Tall (8+) (Ta)	Number of stories (indicate the number)
CL	Pre-Code (PC) None (NC) Low (<0.1 g) (LC) Moderate (0.1–0.3 g) (MC) High (>0.3 g) (HC)	*Pre-code Aseismic Construction*: Low Level (LAC); Moderate Level (MAC); High Level (HAC)

FRM force resisting mechanism, *FRMM* force resisting mechanism material, *P* plan, *E* elevation, *CO* cladding & openings, *DM* detailing & maintenance, *FS* floor system, *RS* roof system, *HL* height level, *CL* code level

Another important category, in particular in the case of URM buildings, is the quality of constructive details and the state of maintenance, which is an essential prerequisite in order to exploit the former aspect (DM). The attribution of High Quality Details (HQD) must consider the adherence to the rules of the art, which altogether define a local code of practice referred to different scales of the construction: the masonry (way to assure interlocking and transversal connection), the wall (distribution of openings, lintels, etc.) and the global construction (wall-wall and wall-horizontal diaphragms connections). The systematic presence of effective tie rods (WT) or ring beams (WRB) may prevent from out-of-plane mechanisms and increase the strength and ductility of spandrels, for the in-plane behavior; it is worth noting that RC ring beams drive the seismic response to weak story mechanism (SSWP behavior), while tie rods increase the ductility of uniform mechanisms (WSSP behavior).

The Floor System (FS) influences the seismic behavior, with reference both to its mass (which increases the horizontal seismic actions) and its stiffness (which allows a certain degree of redistribution of the horizontal seismic actions between the vertical walls). A rough categorization is obtained by distinguishing between Rigid (R) and Flexible (F); the attribution has to consider not only the stiffness but also the effectiveness of the connection with vertical walls. A more detailed classification can consider also the material and configuration (i.e. the presence of masonry vaults can also induce horizontal thrusts).

Similar information are required on the Roof System (RS), which is an important parameter for the vulnerability assessment, because of its mass (dynamically amplified due to its position at the top of the building) and the possible presence of a horizontal thrust (Tr), which can induce local collapse mechanisms.

The Height Level (HL) is very important because it influences very much the seismic vulnerability and is always available or very easily detectable. The possible categories (L, M, H and Ta) must be redefined, in terms of number of stories, for masonry buildings, because they are on average lower than RC or steel buildings.

Finally, the Code Level (CL) category is very important and must be properly defined in the case of masonry buildings, which are usually old and not seismically designed (PC); in this case, it is useful to estimate the local seismic culture, which is high (HAC) in areas frequently affected by earthquakes. For modern buildings, designed by considering a seismic code (LC, MC and HC), the categories should mainly consider the seismic hazard used for the design, taking also into account the accuracy of the code provisions.

The vulnerability assessment at territorial scale requires to group the buildings that have a similar seismic behavior in order to evaluate the damage and losses of the built environment due to a given hazard assessment. To this aim, the proposed taxonomy cannot be directly used, because available information is always incomplete and, anyway, a too very detailed subdivision of the building stock considered in the risk analysis might be useless and difficult to be managed.

Depending on the available data and after a preliminary study of the characteristics of the built environment in the urban area under investigation, the first step of the vulnerability assessment is to proceed to a proper classification of buildings. To this

aim, among the available information, the parameters that mostly affect the seismic behavior must be singled out. Each vulnerability class, which can be synthetically named by a number or a short acronym, is clearly identified by a precise taxonomy, that is a list of category and related classification information. Missing information in the taxonomy means that no data are available to better describe the buildings, so fragility functions must represent the average vulnerability of a large set of configurations. On the contrary, if some parameter is excluded, all other options should be listed in the taxonomy.

Fragility functions must be defined, according to suggestion of Sect. 5.4, for each building class. It is worth noting that the dispersion is higher when few building classes are used, each one including constructions characterized by quite different behavior; on the contrary, a too much detailed classification may lead to the definition of classes with quite similar fragility functions, but with a lower dispersion.

As an example, in the case of a risk analysis at regional scale, when little information is available, the following tags of the taxonomy could describe a possible classification:

– Class 1:/BW/URM-FB-HM/R/R/RO/HM/R/P/M/PC-MAC/
– Class 2:/BW/URM-HS-UC-LM/R-A/R/IRO/LM/F/G-Ti/M/PC-LAC/
– . . ..

If the analysis is focused on a urban district, with a small number of buildings, it is possible to limit the possible options, after a quick sample check survey, and split the classes proposed above, on the base of: quality of seismic design and construction details, materials of floor and roof system, etc.

5.2 Review of Existing Functions and Gaps

Many fragility functions have been developed and can be taken from the literature for the risk analysis of masonry buildings (Benedetti et al. 1988, 1990; HAZUS 1999; Kappos et al. 2008; D'Ayala and Ansal 2009; Barbat et al. 2010; Cattari et al. 2010, 2013; D'Ayala and Paganoni 2010; Ferreira et al. 2013). They have been derived according to different approaches, which can be traced back to the classification introduced in Chap. 2 (Sect. 3.2.) by Rossetto et al. (1) empirical (e.g. Nuti et al. 1998; Colombi et al. 2008; Rota et al. 2008); (2) expert elicitation based (e.g. Lagomarsino and Giovinazzi 2006); (3) analytical, based on nonlinear static approaches through simplified (e.g. Bernardini et al. 1990; D'Ayala et al. 1997; Calvi 1999; Glaister and Pinho 2003; Restrepo and Magenes 2004; D'Ayala 2005; Borzi et al. 2008; Molina et al. 2009; Oropeza et al. 2010; Pagnini et al. 2011; Lagomarsino and Cattari 2013) and detailed models (e.g. Rota et al. 2010) or based on linear dynamic approaches (e.g. Erberik 2008; Gehl et al. 2013); (4) hybrid methods (e.g. Jaiswal et al. 2011).

Many fragility functions have been obtained from observed damage after the occurrence of an earthquake; these data are valuable, because they are directly

correlated to the actual seismic behavior of buildings and can be very useful for validation of analytical methods and calibration of hybrid fragility functions. However, empirical fragility functions are strongly influenced by the reliability of the damage assessment, which is often made by a quick survey aimed to other scopes, as the building tagging for use and occupancy.

Once in the study area masonry building typologies have been analyzed and building classes defined, it is necessary to derive the appropriate fragility functions. To this end, for each class, fragility functions taken from different authors may be used and properly combined, but attention must be paid because these functions could be biased due to some parameters or aspects.

First of all, a crucial factor is the choice of the seismic intensity measure. Empirical data are usually referred to macroseismic intensity, which is not an instrumental measure but is based on a subjective evaluation. This approach is suitable when the aim of the risk analysis is to draw a comparative scenario, probably useful to plan mitigation strategies; for an accurate loss estimation, however, it is necessary to convert macroseismic intensity into an instrumental intensity measure, and this step introduces important approximation and normally huge uncertainties. On the contrary, if empirical fragility functions are given in terms of Peak Ground Acceleration (PGA), it is worth noting that this parameter is directly related to the spectral characteristics of the input motion of the specific seismic event. In these cases, the correlation between intensity and damage should present a low dispersion, which has to be increased before using those functions.

Another difficult task is the definition of consequences that are evaluated by the fragility functions. Usually Damage States (DS) are considered, which are referred to physical damage to structural and non-structural elements, but fragility functions can be also drawn in terms of a Damage Index (DI), related to the cost of repair, or of some Performance Indicators (PIs), which are related to the conditions of use (operational, occupancy, life safety). All the above mentioned effects (except DI) are discrete states and are defined by a qualitative judgment (in case of observational functions) or by a correlation with some structural parameter, as the interstory drift (in case of analytical based functions).

Finally, it is worth noting that the characteristics of masonry buildings are dependent from the local seismic culture and the available materials in the area; as an example, the apparently detailed description “irregular stone masonry with lime mortar” may correspond to very different seismic capacities, if it is assigned to buildings in different countries. Thus, the extrapolation of empirical fragility functions for traditional masonry buildings to other geographic areas is questionable.

In conclusion, the use of existing fragility functions has to be made carefully. In order to increase the reliability of the results, it is suggested to combine a significant number of fragility functions, obtained from different authors and with different methods, assigning to each one a proper subjective probability, related to the reliability of the source and the fitting with the characteristics of the building class under investigation, in order to obtain a weighted fragility function. Depending on the availability and reliability of fragility functions, the building classification should be more or less detailed. An excessive splitting of the built

environment into detailed classes, with associated low dispersed fragility functions, turns out to be specious if their reliability is not robust; in these cases it is better to reduce the number of buildings classes and ascribe to each one a more reliable fragility function, even if defined by a bigger dispersion.

In the context of analytical based on nonlinear static approaches, this chapter proposes a procedure to derive fragility functions for masonry buildings, once a building class is defined by tagging the various categories of the taxonomy (Table 5.1). The general framework of the method, the probabilistic key assumptions and the modeling bases are treated in Sect. 5.3, while some operative recommendations for the different possible approaches are given in Sect. 5.4. The development of tailored fragility functions is the suggested way to improve the reliability of the vulnerability and risk analysis.

5.3 Key Assumptions, Uncertainties and Modeling Issues

The fragility function gives the probability that a generic Limit State (LS) is reached given a value *im* of the Intensity Measure IM:

$$p_{LS}(im) = P\left(d > D_{LS} \middle| im\right) = P(im_{LS} < im) = \Phi\left(\frac{log\left(\frac{im}{IM_{LS}}\right)}{\beta_{LS}}\right) \tag{5.1}$$

where: d is a displacement representative of the building seismic behavior, D_{LS} is its Limit State threshold, IM_{LS} is the median value of the lognormal distribution of the intensity measure im_{LS} that produces the LS threshold and β_{LS} is the dispersion.

A fragility function is thus defined by two parameters: IM_{LS} and β_{LS}. The median intensity IM_{LS} can be obtained from the statistical analysis of data from damage observation after earthquakes (empirical methods) or by a mechanical model (analytical methods), which is considered representative of the average seismic behavior of buildings of that particular class.

The dispersion β_{LS} depends on different contributions, related to: (a) the uncertainties in the seismic demand (epistemic β_H, for the derivation of the hazard curve, and intrinsic β_D, in the variability of the seismic input described only by the value of IM); (b) the uncertain definition of the Limit State threshold (β_T); (c) the variability of the capacity (β_C) of buildings that belong to the considered vulnerability class (which collects buildings of different behavior, even if characterized by the same taxonomy tags). As all the above contributions can be assumed statistically independent, the dispersion is given by:

$$\beta_{LS} = \sqrt{\beta_H^2 + \beta_D^2 + \beta_T^2 + \beta_C^2} \tag{5.2}$$

In case of analytical methods each contribution can be computed, while for empirical methods β_{LS} is directly evaluated from the damage distribution of observed data, which includes all of them; however, in this case, it is necessary to verify if the dispersion has to be increased, because empirical data are not fully representative, in terms of masonry typology (β_C) or characteristics of the input motion (β_D).

The following sub-sections describe the main aspects related to the derivation of fragility functions for masonry buildings from analytical methods, based on nonlinear static approaches.

5.3.1 Seismic Capacity and Demand by Nonlinear Static Analysis

The seismic vulnerability of the building is described by its capacity curve, which gives the acceleration A of an equivalent nonlinear single-degree-of-freedom system, as a function of its displacement D. The capacity curve can be obtained by a proper conversion of the pushover curve, obtained by a nonlinear static analysis of a multi-degrees-of-freedom model of the structure, or through simplified analytical models. In the latter case the capacity is usually described by a bilinear curve, without hardening for masonry buildings.

The seismic demand is expressed by an Acceleration-Displacement Response Spectrum (ADRS), which gives the spectral acceleration S_a as a function of the spectral displacement S_d, for a damping coefficient $\xi_0 = 5\ \%$, considered valid in the initial elastic range. Usually in hazard analysis the spectral shape is assumed constant with the annual rate of exceeding, which is given by the hazard curve as a function of a proper IM of the ground motions.

The evaluation of the displacement demand for a given value *im* of the IM can be obtained through various methods, like the N2-Method originally proposed by Fajfar (1999), the Capacity Spectrum Method (Freeman 1998), the Displacement-Based Method (Calvi 1999), the Coefficient Method (FEMA 356 2000; ASCE/SEI 41/06 2007), the MADRS Method (FEMA 440 2005). They all consider, under different approaches, the reduction of the seismic demand in the nonlinear phase of the building response. These methods look for the intersection of the capacity with the properly reduced demand, by using either acceleration/displacement or displacement/period as coordinates ($S_d = S_a T^2/4\pi^2$).

For the evaluation of fragility functions it is necessary to get the value IM_{LS} of the IM that produces any LS threshold. To this end the use of over-damped spectra (Freeman 1998) is very effective, once these thresholds D_{LS} have been fixed on the capacity curve (Sect. 5.3.3) and the corresponding equivalent viscous damping ξ_{LS} is evaluated, which also takes into account the hysteretic contribution. It results:

$$IM_{LS} = \frac{D_{LS}}{S_{d1}(T_{LS})\eta(\xi_{LS})} \tag{5.3}$$

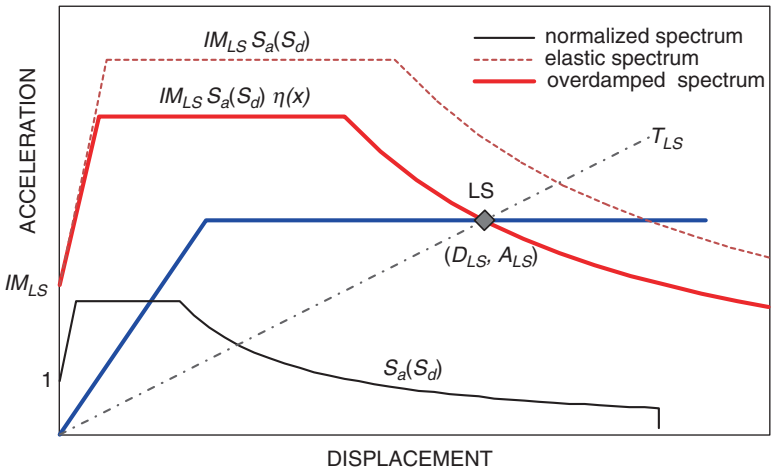

Fig. 5.1 Application of overdamped spectra for the evaluation of IM_{LS}

where: S_{dI} is the displacement response spectrum, normalized to IM, T_{LS} is the linear equivalent period corresponding to LS:

$$T_{LS} = 2\pi\sqrt{\frac{D_{LS}}{A(D_{LS})}} \tag{5.4}$$

and $\eta(\xi_{LS})$ is the damping correction factor (CEN 2004):

$$\eta(\xi_{LS}) = \sqrt{\frac{10}{5+\xi_{LS}}} \tag{5.5}$$

It is worth noting that over-damped spectrum is obtained simply multiplying by $\eta(\xi_{LS})$ in the range of typical periods for buildings, while for very low and high periods the effect of damping tends to vanish.

Figure 5.1 shows the procedure, considering generic LS on the capacity curve and the identification of IM_{LS}, using PGA as IM and a typical response spectrum shape.

5.3.2 *Identification of Proper Intensity Measures*

The vulnerability assessment, embodied by the application of fragility functions, is one of the steps of the seismic risk analysis. The identification of the proper

Intensity Measure (IM) comes out from different constraints, which are first of all related to the adopted hazard model, to the typology of the exposed asset but also to the availability of data and fragility functions for all different exposed assets.

Empirical fragility functions are usually expressed in terms of the macroseismic intensity I (defined according to the different Macroseismic Scales: EMS, MCS, MM), which can be regarded as an empirical IM. The macroseismic intensity already contains implicitly the vulnerability, because it is defined on the basis of the damage observation; in order to overcome this gap, modern macroseismic scales, such as EMS, assign the intensity taking into account a detailed building types classification. The accuracy of the risk analysis results is then linked to the reliability of the hazard assessment, if an empirical IM is used.

Analytical based or hybrid fragility functions are, on the contrary, related to instrumental IMs, which are related to parameters of the ground motion (PGA, PGV, PGD) or of the structural response of an elastic SDOF system (spectral acceleration S_a or spectral displacement S_d, for a given value of the period of vibration T). Sometimes, integral IMs can be useful, which consider a specific integration of a motion parameter (Arias Intensity I_A) or of a spectral value (Housner Intensity I_H) (Douglas et al. 2013).

Correlation is necessary when hazard and vulnerability assessments are made by using different IMs or one wants to calibrate analytical fragility functions (related to a detailed building classification) by available empirical fragility functions (referred to wider classes of buildings). Anyhow, the use of correlation always increases the uncertainties of the results (dispersion β_{LS} of the fragility function).

Similarly to what has been said about different types of fragility functions (empirical, expert elicitation, analytical based and hybrid), for the identification of proper IMs it is worth noting that empirical ones give results coarse but correct on average, while instrumental IMs allow to better take into account a detailed taxonomy, in the definition of building classes, and the local site effects, but, when these fragility functions are used, it is necessary to pay attention to the characteristics of the input motion that was considered for their derivation.

The seismic performance of a masonry building cannot be described by only one IM but, at least, the response spectra shape should be known. If a vector-valued hazard assessment is available (Bazzurro and Cornell 2002), more than one IM could be used and vector-valued fragility functions derived (e.g. Gehl et al. 2013). If already available fragility functions are used, it is better to refer to the spectral value for the period compatible with the specific Limit State threshold (acceleration $S_a(T)$ and displacement $S_d(T)$ response spectra are linked by the period of vibration T, so the two IMs are equivalent). In this case the dispersion β_{LS} of the fragility function is mainly due to the variability of the capacity of buildings in the class.

Most of available fragility functions are in terms of PGA; in this case, if the difference between the spectral shapes of the input motion obtained by the hazard assessment and that used for deriving the fragility function is known, it is possible to properly tune the last one. Otherwise, the use of PGA as IM implies a wider dispersion β_{LS} of the fragility function, due to the uncertainty in the spectral shape.

As masonry buildings are usually not flexible, PGD or spectral values for long periods ($T > 1$ s) are not significant, except for some types of monumental structures (churches, slender towers) or for the verification of local mechanisms.

With reference to local site amplification, spectral values are better correlated with vulnerability, because they take into account the modification of the seismic input for the significant periods. If PGA is used, fragility functions should be tuned by considering a mean ratio between the spectral values on local site and stiff soil conditions, for the relevant periods of the buildings, or a greater value of the dispersion should be used, in order to consider the increased uncertainty due to the spectral demand (β_D).

In case of using empirical IM (macroseismic intensity), it is not correct to include local site amplification in the hazard curve, because this phenomena affects buildings depending on their dynamic properties; a possible solution is to modify the empirical fragility function, so considering it as representative of the vulnerability of a particular class of buildings on a specific soil type (Lagomarsino and Giovinazzi 2006).

5.3.3 Definition of Damage States and Performance Levels

In seismic risk analysis the scenario of the built environment is expressed in terms of Damage States (DS), which are a discrete qualitative description of the overall damage in structural and non-structural elements of the building. Usually five damage states are considered: DS1 slight, DS2 moderate, DS3 extensive, DS4 near collapse and DS5 collapse.

Empirical methods describe the DS through a qualitative damage observation, on the basis of distribution and severity of cracks, according to specific forms and sketches; to this end, modern macroseismic scales can be a good reference (e.g. EMS98, Grunthal 1998).

In the case of analytical methods, if a detailed numerical model of the building is available, the damage in each structural element is obtained through static or dynamic nonlinear analysis and a sort of virtual damage state attribution could be made. However, it is worth noting that numerical models give continuum damage variables and identification of discrete DS is not an easy task. As an example, Cattari and Lagomarsino (2012) have proposed a multi-scale approach for masonry buildings that defines Limit States (LS) on the capacity curve by checking (i) the spread of damage in masonry elements (piers and spandrels), (ii) the interstory drift in masonry walls and (iii) the global behavior of the building (described by its capacity curve). LSs are the thresholds that separate various DSs (Fig. 5.2).

Damage States can be related to specific performances of the building: the use and occupancy, the safety of people and the reparability (in terms of economic convenience). Usually Performance Limit States (PLS) can be defined as coincident to related Damage Limit States (LS); this means the fulfillment of a certain

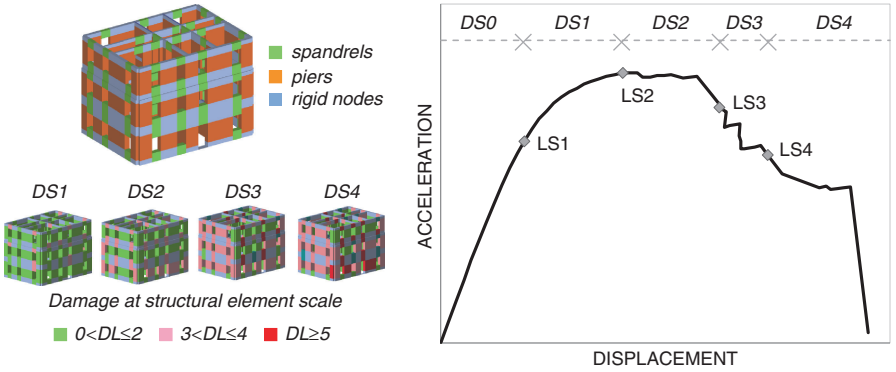

Fig. 5.2 Example of capacity curve of a masonry building, obtained by pushover analysis on a detailed model, with the definition of LS thresholds and DS ranges

performance is guaranteed if the seismic displacement demand is not beyond the corresponding LS threshold.

The above mentioned detailed mechanical based methods are used in hybrid approaches, while analytical methods adopt simplified models, which give directly the capacity curve without a detailed description of damage in the building. In these cases, LSs may be defined: (a) by considering limit values of macro-parameters of the building response, on which the simplified model is based (as, for example, the interstory drift); (b) by a heuristic approach, which considers that the transition from a DS to the following one usually occurs in certain positions of the capacity curve. An example of the former case is presented in Sect. 5.4.2.1. In the latter, a possible positioning of LSs is obtained as follows (Fig. 5.3a): LS1: $D_1 = 0.7D_y$; LS2: $D_2 = c_2 D_y$; LS3: $D_3 = c_3 D_2 + (1 - c_3)D_4$; LS4: $D_4 = D_u$. The position of LS2 depends on the complexity and irregularity of the building; the coefficient c_2 may vary between 1.2 and 2, being lower for simple and regular buildings. LS3 is usually closer to LS4, in particular for simple and regular buildings ($0.3 < c_3 < 0.5$).

Equivalent viscous damping may be defined for each LS as a function of the displacement (Fig. 5.3b), by a simple relation (Calvi 1999; Priestley et al. 2007; Blandon and Priestley 2005):

$$\xi_{LS} = \xi_0 + \xi_H \left[1 - \left(\frac{D_y}{D_{LS}} \right)^{\zeta} \right] \tag{5.6}$$

where: ξ_0 is the initial damping (usually assumed equal to 5 %), ξ_H is the maximum hysteretic damping and ζ is a free parameter (ranging between 0.5 and 1).

Once the seismic demand is defined (Sect. 5.3.2), by the spectral shape and the selection of a proper Intensity Measure to scale it, the values IM_{LSk} and the dispersions β_{LSk} (k = 1,. . .,4) can be evaluated by (5.3) and by the procedure described in Sect. 5.3.4. Fragility curves are then given by (5.1) and shown in Fig. 5.4a.

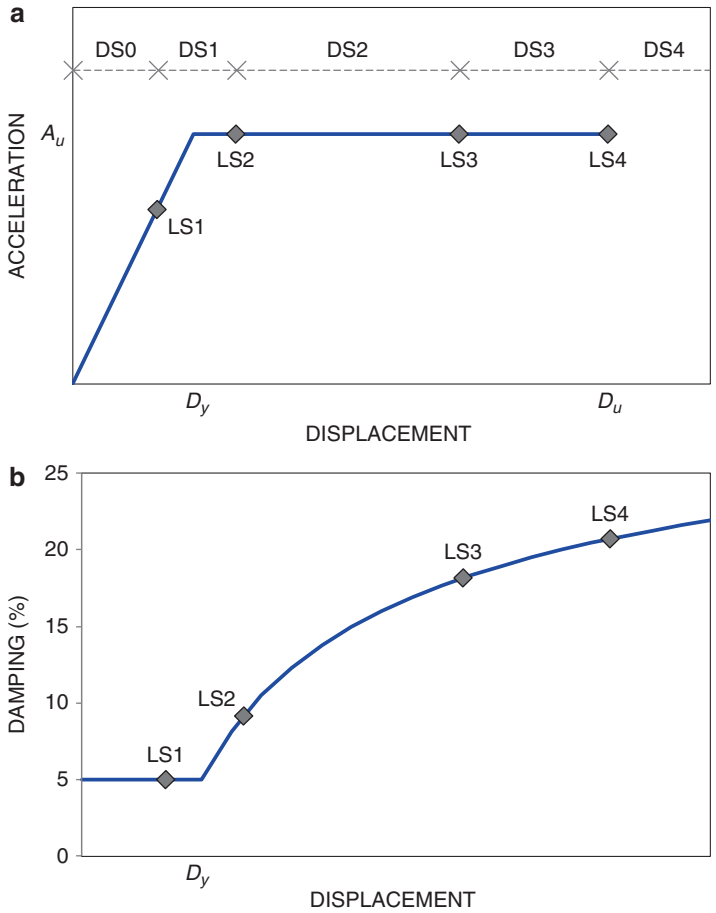

Fig. 5.3 (**a**) Example of capacity curve of a class of masonry buildings, with heuristic definition of LS thresholds ($c_2 = 1.35$, $c_3 = 0.4$) and (**b**) typical equivalent viscous damping relation

The DS probability distribution, for a given value of the IM, can be thus obtained from fragility functions; for k = 1, 2 and 3, the discrete probabilities are given by:

$$p_{DSk}(im) = p_{LSk}(im) - p_{LSk+1}(im) = \Phi\left(\frac{log\left(\frac{im}{IM_{LSk}}\right)}{\beta_{LSk}}\right) - \Phi\left(\frac{log\left(\frac{im}{IM_{LSk+1}}\right)}{\beta_{LSk+1}}\right) \quad (5.7)$$

With regards to DS4, it is worth noting that analytical methods usually are not able to define LS5, and thus p_{LS5}; this LS occurs after important local collapse mechanisms that make the mechanical model meaningless. If it is considered that DS4 is generically named "complete" damage, including both "near collapse" and "collapse" DSs, it results that $p_{DS4} = p_{LS4}$. However, by assuming that the

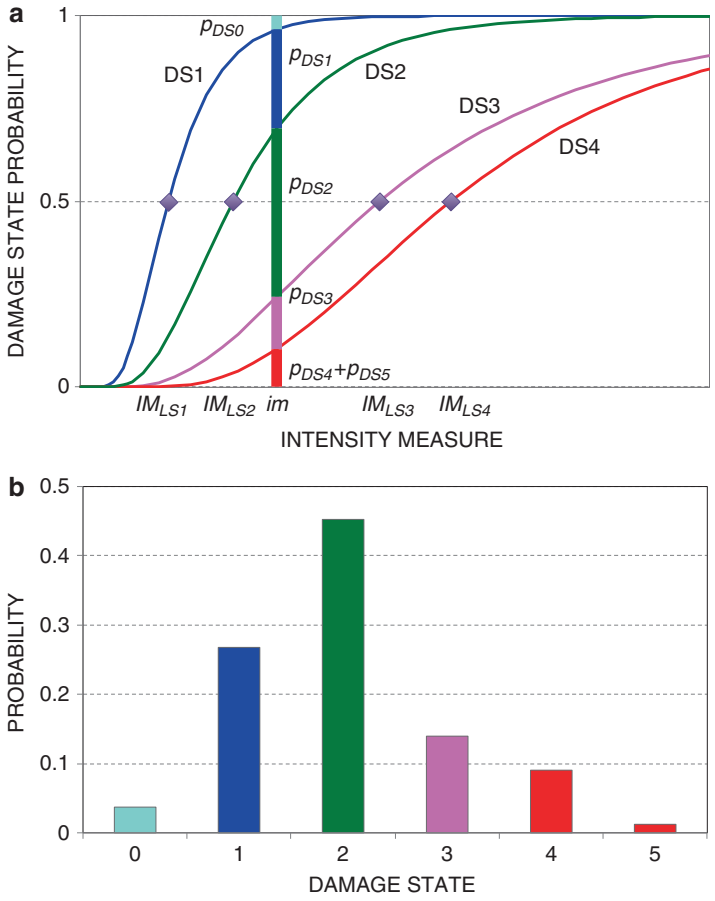

Fig. 5.4 (**a**) Fragility curves and (**b**) damage States probability distribution

probability distribution of DSs is well represented by the binomial distribution, it is possible to share p_{LS4} according to the following formulas ($\mu_{DS} = \sum {}_1^4 p_{LSk}$):

$$p_{DS5}(im) = 0.8\left[1 - \left(1 - 0.14\mu_{DS}^{1.4}\right)^{0.35}\right] p_{LS4}(im) \tag{5.8}$$

$$p_{DS4}(im) = p_{LS4}(im) - p_{DS5}(im) \tag{5.9}$$

In order to complete the DS distribution it is necessary to evaluate the probability that the building has "no damage" (DS0):

$$p_{DS0}(im) = 1 - p_{LS1}(im) = 1 - \Phi\left(\frac{log\left(\frac{im}{IM_{LS1}}\right)}{\beta_{LS1}}\right) \tag{5.10}$$

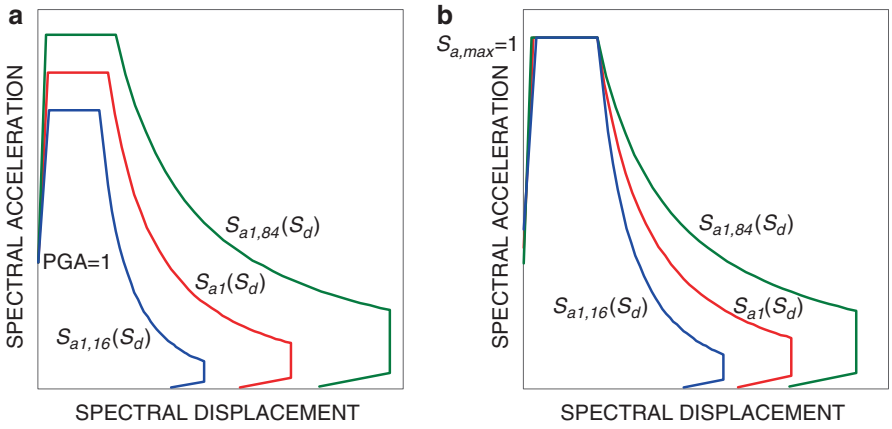

Fig. 5.5 Influence of the selection of the IM on the propagation due to the uncertainty on the spectral shape of the seismic demand: (**a**) IM = PGA; (**b**) IM = $_{Sa,max}$

Figure 5.4b shows a typical discrete damage distribution of damage states, directly obtained from fragility functions of Fig. 5.4a for a given value IM = *im*.

5.3.4 Sources of Uncertainties and Propagation

In a probabilistic seismic risk analysis many uncertainties have to be taken into account; Pinto gives a general overview in Chap. 2 (Sect. 2.2). Their propagation is considered in fragility functions through the dispersion β_{LS}, which can be evaluated by Eq. (5.2). The estimation of different contributions is discussed in the following.

5.3.4.1 β_D – Uncertainty on the Spectral Shape of the Seismic Demand

The Probabilistic Seismic Hazard Analysis (PSHA) gives the occurrence of earthquakes with a proper IM through the hazard curve $\lambda(im)$. Usually a fixed shape of Acceleration-Displacement Response Spectrum is associated, except the case of a complex Vector-Valued PSHA (Bazzurro and Cornell 2002). The normalized response spectrum $S_{a1}(S_d)$, scaled to the value $im = 1$, can be defined as a stepwise function or through some analytical formulas in fixed ranges of the period T (as it is made in seismic codes).

In order to take into account the uncertainty on the spectral shape, which plays a significant role due to the large variability of possible records, it is necessary to define the response spectra $S_{a1,16}(S_d)$ and $S_{a1,84}(S_d)$, for the confidence levels 16 and 84 %. They can be obtained by the selection of a large number of real digital records, compatible with the characteristics of earthquakes that give the maximum contribution to the hazard and of soil conditions; in particular, from the disaggregation of the PSHA, it is important to consider: magnitude, epicentral distance, focal depth, source mechanism. Figure 5.5a shows a typical example of a median response

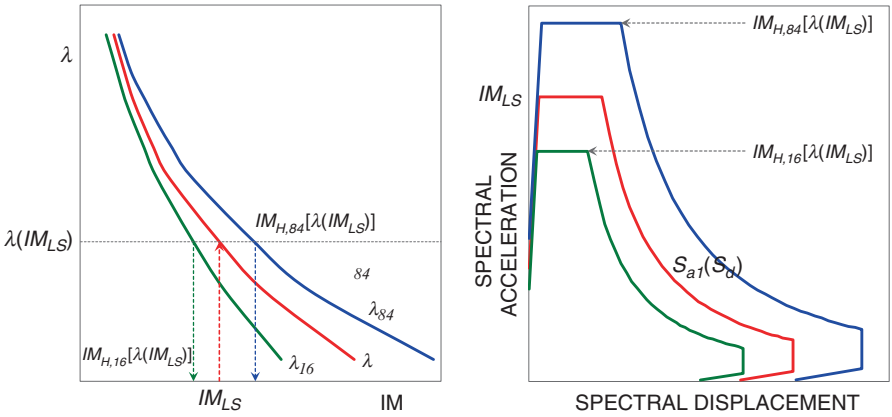

Fig. 5.6 Influence on the spectral demand of the epistemic uncertainty on the hazard curve

spectrum and the corresponding confidence intervals, if the Peak Ground Acceleration *PGA* is used ad IM; Fig. 5.5b shows the same response spectra in the case where the maximum spectral acceleration $S_{a,max}$ is assumed as IM.

For each LS, the estimation of β_D requires the evaluation of the intensity measures $IM_{D,16}$ and $IM_{D,84}$ that correspond to a displacement demand equal to D_{LS}, on the median capacity curve of the considered class of buildings, by using the confidence levels response spectra $S_{a1,16}(S_d)$ and $S_{a1,84}(S_d)$ respectively. It results:

$$\beta_D = 0.5|log(IM_{D,84}) - log(IM_{D,16})| \tag{5.11}$$

This contribution to the dispersion is lower if a good IM is used. It is quite evident from Fig. 5.5 that, at least for LS1 and LS2, $S_{a,max}$ is better than *PGA*.

5.3.4.2 β_H – Epistemic Uncertainty on the Hazard Curve

Epistemic uncertainties in the seismic sources and the attenuation laws give rise to confidence intervals, which can be summarized by the hazard curves $\lambda_{16}(im)$ and $\lambda_{84}(im)$, representative of the confidence levels 16 and 84 %.

For each LS, it is necessary to valuate IM_{LS} that corresponds to the displacement demand D_{LS} on the median capacity curve of the considered building class, by using the median response spectrum $S_{a1}(S_d)$. The dispersion β_H is given by:

$$\beta_H = 0.5[log(IM_{H,84}[\lambda(IM_{LS})]) - log(IM_{H,16}[\lambda(IM_{LS})])] \tag{5.12}$$

where $IM_{H,16}$ and $IM_{H,84}$ are the inverse functions of $\lambda_{16}(im)$ and $\lambda_{84}(im)$, respectively, and $\lambda(im)$ is the median hazard curve.

Figure 5.6 shows an example of hazard curves, median and confidence intervals, and the corresponding response spectra; in this case for the evaluation of β_H only the median response spectrum is used.

5.3.4.3 β_C – Uncertainty on the Capacity Curve

The dispersion on the capacity curve of a masonry building is related to random variables, such as the material parameters (strength and stiffness on masonry), the geometry (effective thickness of masonry walls and vaults), the drift capacity of masonry panels or the in-plane stiffness of horizontal diaphragms, but also to epistemic model uncertainties, related for example to the assumptions in the definition of the equivalent frame or in modeling the connection between walls. Usually, if accurate as-built information is available, these uncertainties can be reduced.

This is not the case in seismic vulnerability analysis at territorial scale, when an "equivalent capacity curve" must be evaluated representative of a wide class of buildings, defined by the taxonomy through a proper list of tags. Then the above parameters have to be considered as random variables, with a dispersion compatible with the variability of the characteristics of buildings in the class.

The uncertainty propagation can be evaluated by Monte Carlo simulations or by using the response surface method (Pagnini et al. 2011; Liel et al. 2009). The latter approach is very effective and is based on the approximation of the surface of $log(IM_{LS})$, in the hyperspace of the significant random variables, by a hyper-plane, whose coefficients are determined by a least square regression on a set of numerical experiments. If N is the number of random variables, $M = 2^N$ models are defined by a complete factorial combination at two levels, in which each variable assumes values correspondent to the confidence levels of 16 or 84 %. The matrix $\mathbf{Z}$ (M rows $\times$ N columns) collects in each row the combination of values assumed by each standard normalized random variable (-1 for confidence level 16 %, +1 for confidence level 84 %).

For the i-th model, the capacity curve $A_i(D)$ is obtained and the Limit States are fixed ($D_{LSk,i}$, k = 1,. . .,4). By considering a generic LS, the value $IM_{LS,i}$ is evaluated by the median seismic demand $S_{a1}(S_d)$, using (5.3). The vector $\mathbf{Y}$ (M rows) collects the values $log(IM_{LS,i})$, $i = 1,\ldots,M$. The angular coefficients of the hyper-plane are obtained as:

$$\boldsymbol{\alpha} = \left(\mathbf{Z}^T\mathbf{Z}\right)^{-1}\mathbf{Z}^T\mathbf{Y} \tag{5.13}$$

By assuming the parameters as statistically independent, The dispersion β_C is given by:

$$\beta_C = \sqrt{\boldsymbol{\alpha}^T\boldsymbol{\alpha}} \tag{5.14}$$

5.3.4.4 β_T – Uncertainty on the Limit State Thresholds

The definition of the LS thresholds is also subjected to dispersion, because models adopted for the evaluation of the capacity curve are simplified and the displacements D_{LS} usually derives from a heuristic approach.

Considering the median capacity curve, obtained by using the mean values of the N random variables, D_{LSk} (k = 1,. . .,4), usually distributed as in Fig. 5.3a, can be assumed as median values. Proper distributions should be defined for these random

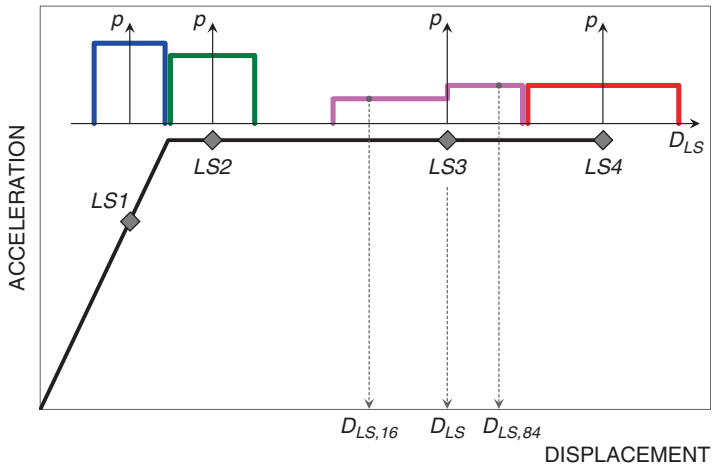

Fig. 5.7 Uncertain definition of the LS thresholds

variables, which take into account that in a single building the k-th DS could be reached a little bit before or after the median value D_{LSk}. It is reasonable to assume the four distributions do not intersect. LS1 is always in the "elastic" branch of the capacity curve. LS2 is in the first part of the "plastic" branch and it is not reasonable to assume it moves too much further the median value D_{LS2}. The position of LS3 is very variable and sometimes it occurs even for a low value of the displacement, but the possible intervals of LS2 and LS3 can be separated.

The use of a Beta distribution seems to be the best option, but for the sake of simplicity, due to the large number of uncertainties involved in a seismic risk analysis, very simple uniform distributions are suggested, which probably lead to a slight overestimation of β_T. Figure 5.7 shows a proposal, with the indication, for a generic LS, of the 16 and 84 % confidence levels of D_{LS}, named $D_{LS,16}$ and $D_{LS,84}$; they are simply obtained by moving from the median value, on the left and right side, of 2/3 of the semi-wide of the uniform distribution.

For each LS, it is then necessary to evaluate $IM_{T,16}$ and $IM_{T,84}$ that corresponds to a displacement demand equal to $D_{LS,16}$ and $D_{LS,84}$ on the median capacity curve of the considered class of buildings, by using the median response spectrum $S_{a1}(S_d)$. The dispersion β_T is given by:

$$\beta_T = 0.5[log(IM_{T,84}) - log(IM_{T,16})] \tag{5.15}$$

5.4 Recommendations for Deriving Fragility Functions

After a proper building classification, tailored to data already available or that can be acquired through the survey, fragility functions can be defined by using existing ones or developing new customized curves.

In the first case, for each building class, the available functions have to be collected and examined. After the assignment of a subjective probability to each one (logic tree approach), related to its reliability and coherence with the considered building class, the fragility function can be obtained by a simple weighted summation. The use of existing fragility functions must consider several critical aspects. When a fragility function refers to a broader class of buildings, the dispersion β_{LS} should be reduced and it is worth considering if the mean value IM_{LS} has to be modified (if the behavior of the subclass is better or worse than the average). When a fragility function refers to a subclass of buildings, within the class of interest, it would be necessary to have fragility functions for the other subclasses (in the other branches of the logic tree), otherwise the obtained final fragility function would result biased; as an alternative, the dispersion β_{LS} should be increased and the mean value IM_{LS} properly modified, on the base of expert judgment.

Next sections give some hints for the development of new fragility functions. This can be done either by empirical data, if a robust database of damage observations is available in the area or in other regions where built environment has similar characteristics, or by analytical data, by the definition of mechanical models representative of each building class and able to assess the dispersion due to the variability of seismic behavior in the class.

5.4.1 From Empirical/Macroseismic Data

In this ambit, Lagomarsino and Giovinazzi (2006) have proposed a macroseismic vulnerability model, which can be considered an expert elicitation method. It is directly derived from the European Macroseismic Scale (Grunthal 1998), which defines six vulnerability classes (named from A to F) and various building types (seven of them related to masonry buildings).

It is worth noting that macroseismic scales are not instrumental based and they implicitly contain a vulnerability model. If a building class is considered, the linguistic definitions of EMS98 may be translated in quantitative terms, by the fuzzy set theory, and an incomplete Damage states Probability Matrix (DPM) is obtained. The completion is made by using the binomial probability distribution. The vulnerability is synthetically expressed by a vulnerability curve (Bernardini et al. 2011), which gives the mean damage $\mu_D(=\sum kp_{DSk})$ as a function of the macroseismic intensity I:

$$\mu_D = 2.5 + 3tanh\left(\frac{I + 6.25V - 12.7}{Q}\right) \quad (0 \leq \mu_D \leq 5) \tag{5.16}$$

where: the vulnerability index V and the ductility index Q are parameters representative of the seismic behavior of a group of homogeneous buildings.

The vulnerability index has been defined to vary between 0 and 1 for the six vulnerability classes of EMS98. To each building class a plausible range of values

Table 5.2 Ranges of maximum plausibility for vulnerability index of the six EMS98 classes

Building class	A	B	C	D	E	F
V	0.84 ÷ 0.92	0.68 ÷ 0.76	0.52 ÷ 0.60	0.36 ÷ 0.44	0.20 ÷ 0.28	0.04 ÷ 0.12

of V is associated, defined by a proper membership function, according to the fuzzy set theory (Klir and Yuan 1995); Table 5.2 shows intervals for each class of maximum plausibility. The ductility index is equal to 3, in order to obtain the best fit.

Fragility functions, in terms of macroseismic intensity I, can be evaluated by the binomial distribution:

$$p_{LSk} = \sum_{i=k}^{5} p_{DSi} \quad (k = 1, \ldots 5) \tag{5.17}$$

$$p_{DSk} = \frac{5!}{k!(5-k)!} \left(\frac{\mu_D(I)}{5}\right)^k \left(1 - \frac{\mu_D(I)}{5}\right)^{5-k} \quad (k = 0, \ldots 5) \tag{5.18}$$

Limit States can be identified on the vulnerability curve as points for which $p_{LSk} = 0.5$ ($k = 1$,. . .,5). The vulnerability curve is, for the macroseismic method, analogous of the capacity curve for the analytical ones. Figure 5.8a shows the vulnerability curves, with LS thresholds, for the central (white expected) values for the six EMS98 vulnerability classes. Figure 5.8b shows the correspondent fragility functions of DSs for Class B ($V = 0.72$).

If a proper correlation law between intensity and PGA is assumed, the fragility functions in terms of PGA are obtained; it is worth noting that, given the high number of uncertainties involved in the process, all macroseismic intensity scales may be assumed equivalent to this end. Many correlations may be found in literature, which have been calibrated in different areas and are usually in the form:

$$I = a_1 + a_2 Log(PGA) \tag{5.19}$$

Figure 5.8c shows the fragility functions in terms of PGA, having assumed two different correlation laws: (a) Faccioli and Cauzzi (2006), described by Eq. (5.16) with $a_1 = 6.54$, $a_2 = 4.51$ (PGA in m/s^2); (b) Murphy and O'Brien (1977) for Europe ($a_1 = 7$, $a_2 = 4$), which gives higher values of PGA for I > 8, if compared to the former one. It is worth noting that fragility functions looks very similar to a lognormal cumulative distribution; the dashed lines represent the best fit, which is obtained for all LSs by the following values of the dispersion: (a) $\beta_{LS} = 0.54$; (b) $\beta_{LS} = 0.61$.

It is worth noting that fragility functions in Fig. 5.8 refer to the central value of V for Class B and can be considered representative of a subset of buildings in the class. In order to consider the whole class, the range of plausible values of the

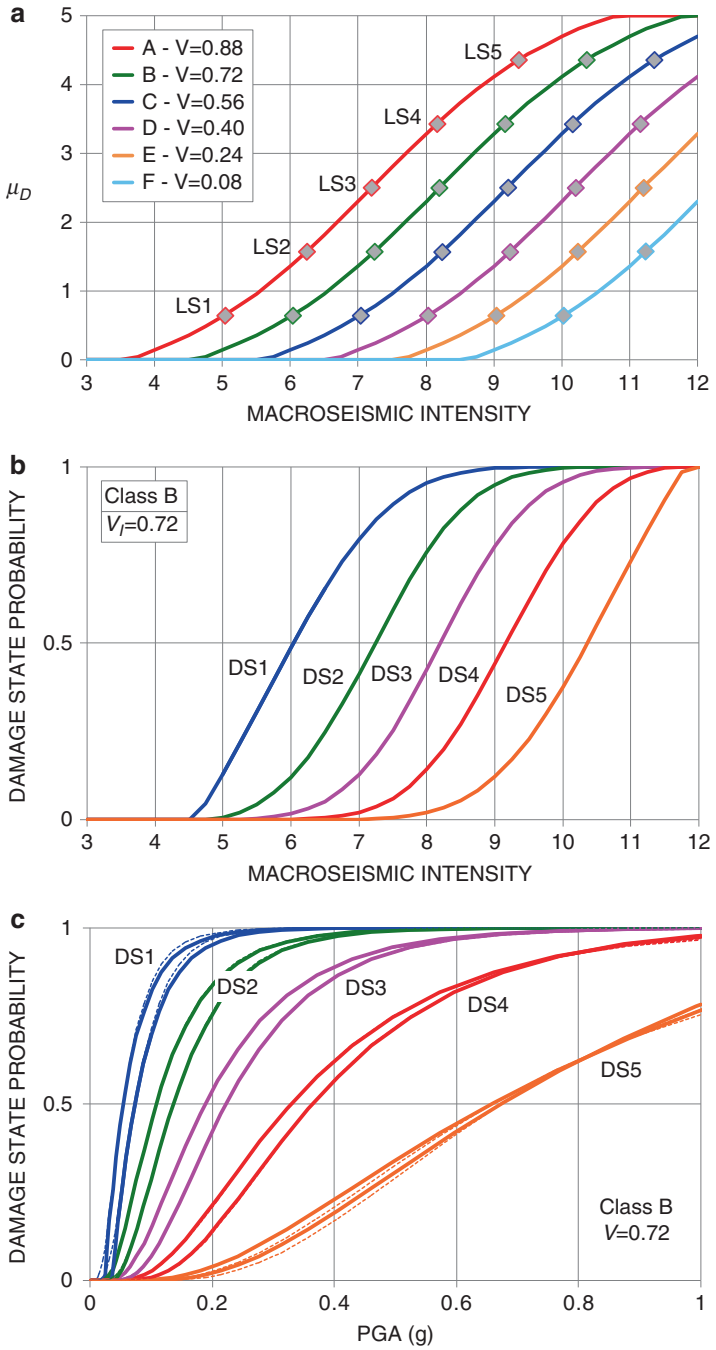

Fig. 5.8 Central values of V: (**a**) vulnerability curves for the EMS98 vulnerability classes, with indication of LS; fragility functions of Class B in intensity (**b**) and PGA (**c**)

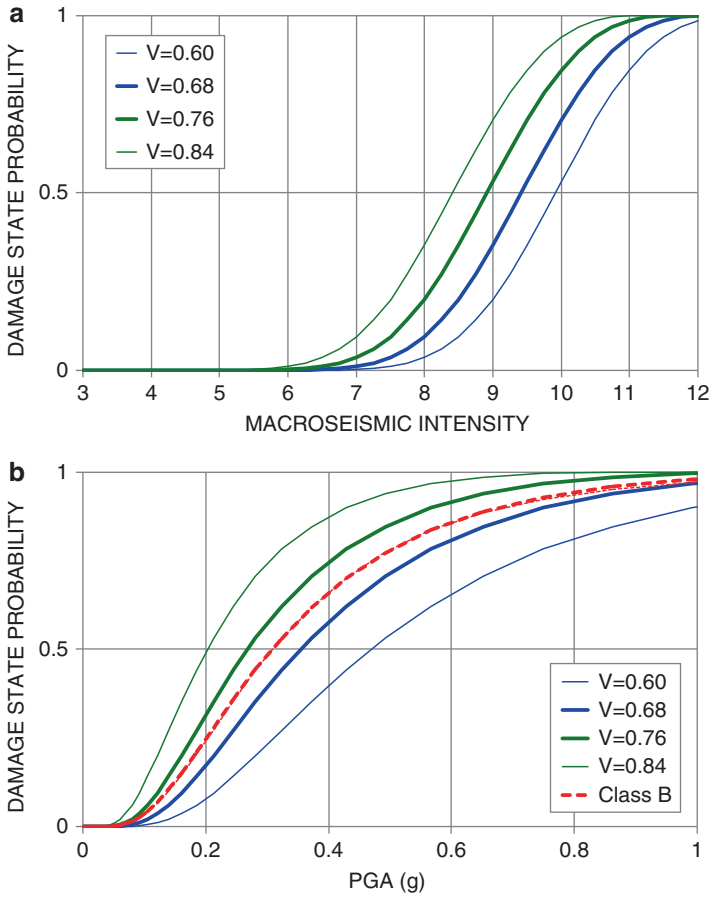

Fig. 5.9 (**a**) Fragility curves of DS4 for Class B, in terms of macroseismic intensity, considering all plausible values of *V*; (**b**) corresponding fragility curves in terms of PGA, with derivation of the overall behavior of Class B (*dashed lines*)

vulnerability index *V* must be considered. As an example, Fig. 5.9a shows fragility functions of LS4 in terms of macroseismic intensity, for the extreme plausible values of the vulnerability index *V* and for the two values that define the interval of maximum plausibility (Table 5.2). Figure 5.9b shows the fragility functions in terms of PGA (considering Murphy and O'Brien correlation law). The fragility function of the whole vulnerability class is obtained by a convolution of all plausible fragility functions; the result is the dashed line in Fig. 5.9b, which is well fitted by a lognormal cumulative distribution with dispersion $\beta_{LS4} = 0.64$ (0.57 in case of Faccioli and Cauzzi correlation law). The dispersion is increased a little because in this case the fragility function represents the behavior of all different building of the class, instead of a small sub-set of these.

EMS98 proposes a classification of buildings into various types, according to masonry and horizontal diaphragms characteristics. The seismic behavior of these macro-typologies can include two or even more vulnerability classes, each one with a different subjective probability (see Fig. 5 in Lagomarsino and Giovinazzi 2006). The corresponding vulnerability functions for each DS can be obtained with the procedure described above and showed in Fig. 5.9b. As an example, if the building class involves two EMS98 vulnerability classes, the value of β_{LS}, for the two considered correlation laws, increases to: (a) 0.62; (b) 0.7.

Within the ambit of SYNER-G seismic risk procedure, once the building classes have been defined by a proper list of tags from the taxonomy, fragility functions may be derived through the macroseismic method by defining a proper membership function for the vulnerability index (range of plausible values). The range can be very wide, if the building class is generic, while can be very narrow, smaller than that of a single EMS98 vulnerability class, if much information is available.

The general format of the macroseismic vulnerability method can also be used when empirical data are available. In this case, for a specific building class (defined by data acquired and by the constructive characteristic of the built environment in the area where damage survey was made), the DSs distribution (and thus the mean damage μ_D) is supposed to be known for one or more values of the macroseismic intensity. If only one point of the vulnerability curve is available, the vulnerability index V can be fitted and, for each LS, the corresponding IM_{LS} can be evaluated and a proper value of β_{LS} can be assumed, by considering the variability of behavior in the class. If damage data are available for more values of the intensity, both V and Q can be fitted. After the conversion into fragility functions, the values of β_{LS} may be directly fitted.

5.4.2 From Analytical Methods

5.4.2.1 Use of Simplified Mechanical Models

The use of simplified mechanical models presents the following main advantages: (a) fully employ all results of PSHA (instrumental IMs, seismic input in the spectral form); (b) keep explicitly into account the various parameters that determine the structural response (and evaluate accurately the uncertainty propagation). However, the reliability of the vulnerability assessment is affected by the capability of the model to simulate the actual seismic response of the examined class; to this end simplified models must be validated and calibrated with observed damage or results from more sophisticated models.

Making reference to the taxonomy in Table 5.1, this section deals with Unreinforced Masonry (URM), among the FRMM. The first Force Resisting Mechanism to be considered is the Out-of-Plane response (OP), which occurs in ancient masonry buildings without good connections. Buildings vulnerable to these mechanisms suffer moderate damage (DS2) even for low levels of seismic intensity. The problem of assessing OP mechanisms is crucial in aggregates of buildings in ancient historical

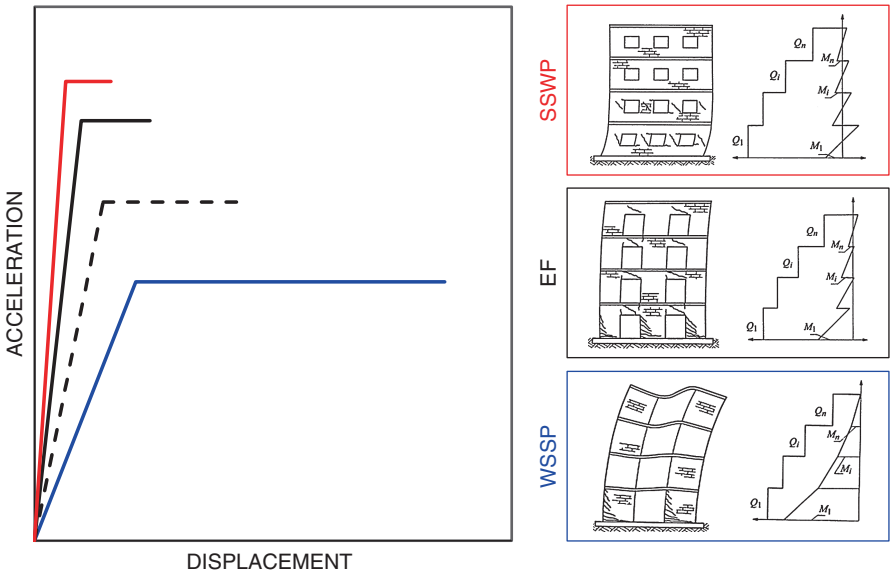

Fig. 5.10 Influence of the stiffness and strength of masonry piers and spandrels on the capacity curve: generalized internal forces (V, M) in masonry piers and damage patterns according to the EF model and the two limit conditions of SSWP and WSSP (Adapted from Tomaževič 1999)

centers, formed all along the centuries through progressive additions and continuous transformations (such as unstable raising), which produced a large sample of vulnerabilities: unconnected portions of the main façade, irregularities in elevation, staggered floors, thrusting roofs. Simplified mechanical-based models are available to derive fragility functions of masonry buildings with regard to these mechanisms (e.g. Bernardini et al. 1990; D'Ayala and Speranza 2003; D'Ayala 2005).

As far as global response of existing masonry buildings is concerned, in-plane behavior of masonry walls can be modeled by an Equivalent Frame (EF), made by vertical piers (the columns) and horizontal spandrels (the beams), connected by rigid nodes of non-zero size. The generalized actions in masonry elements, all along the pushover analysis, depend on the relative stiffness and strength of piers and spandrels. The solution can be obtained only numerically, while analytical simplified models can make reference to two limit conditions: (1) Strong Spandrels Weak Piers (SSWP), which corresponds to the shear-type frame model and is associated to the occurrence of a soft-story failure; (2) Weak Spandrels Strong Piers (WSSP), in which full height piers (from the base to the top) work like fixed-end cantilevers and fail at the base due to axial and bending failure (rocking with crushing at the toe). Figure 5.10 summarizes the effects of the coupling effectiveness of masonry piers, both in terms of deformed shape at collapse and distribution of the generalized forces (shear V and bending moment M), in a masonry building subjected to seismic loads, passing from the case of very weak spandrels (WSSP) to the shear-type idealization (SSWP). The effects on the capacity curve, in terms of overall strength, stiffness and displacement capacities, are also shown.

It is evident, in particular for medium and high-rise buildings, the range of variation of the seismic response is significant; thus, it is necessary to be able to catch these different behaviors for a reliable assessment. Usually, the presence of specific constructive details plays a crucial role in addressing the choice of the correct intermediate behavior between the two limit idealizations (WSSP and SSWP). In general, the SSWP hypothesis is consistent with new masonry buildings, in which masonry spandrels are always connected to lintels, tie beams and floor slabs, made of steel or reinforced concrete. On the contrary, in ancient buildings spandrels are in many cases quite weak elements, as lintels are in timber or made by masonry arches, tie beams are very rare and horizontal diaphragms are flexible (e.g. due to the presence of vaults or wooden floors). In these cases the behavior is closer to WSSP.

Among the different mechanical models proposed in literature (as mentioned in Sect. 5.2), in this section the DBV-*masonry* (Displacement Based Vulnerability) method is suggested. It was originally proposed by (Cattari et al. 2005) with some further modifications (Pagnini et al. 2011; Lagomarsino and Cattari 2013). The analytical formulation makes reference to the SSWP model, under the simplified hypothesis, in the evaluation of the total base shear, that all masonry piers fail at the same time, which is true if they are more or less of the same size and the building is regular in plan. The vulnerability of actual buildings, which do not meet these hypotheses, is estimated applying proper corrective factors. Similarly it is possible to evaluate the capacity curve of buildings characterized by EF or WSSP behavior.

This model can be used to derive fragility functions for masonry buildings, both isolated or in aggregate, making reference to the global behavior. Thus, in case of possible activation also of out-of-plane mechanisms, in particular for aggregated buildings in historical centers, in addition another model should be used in a complementary way. Fragility curves representative of OP (Out-of-Plane) and IP (In-Plane) seismic response have to be combined by the logic tree approach.

DBV-*masonry* model defines the capacity curve by three variables: the pseudo-elastic period of the structure T_y; the spectral acceleration at yielding A_y (equal to the ultimate one A_u, because no hardening is assumed); the ultimate displacement capacity D_u (corresponding to LS4). In the case of masonry buildings the evaluation by a proper model of A_y instead of the yield displacement D_y seems to be more reliable. The evaluation of these variables requires the definition of limited number of mechanical and geometrical parameters, the assumption of a fundamental modal shape and the attribution of specific correction factors, aimed to take into account the effects related to the comprehensive set of constructive and morphological details (categories P, E, CO, DM, FS and CL of Table 5.1).

In order to evaluate a fragility function representative of a wide class of buildings, proper ranges of values should be defined for all parameters. However, only those whose variability significantly affects the response have to be assumed as random variables, with a proper probability distribution and related parameters (mean value and confidence levels at 16 and 84 %), for the evaluation of the contribution β_C to the total dispersion of the fragility function, for each LS.

The reference prototype of the building class could present different characteristics along the two principal directions (X and Y); this is particularly

important for buildings in urban aggregates (due to the different percentage of openings in two directions and the usual disposition of timber floors), but also in isolated buildings the prototype could be asymmetric. Thus, two capacity curves are obtained, defined by $T_{y,X}$, $A_{u,X}$, $D_{u,X}$ and $T_{y,Y}$, $A_{u,Y}$, $D_{u,Y}$ for the X and Y directions, respectively, and the related fragility functions are evaluated. For the risk analysis, the worse direction has to be assumed, which could not be the same for all LS and in the all range of values of the IM.

Figure 5.11 summarizes the basic steps of the application of such simplified mechanical model, which are summarized as follows: (1) analysis of available data from on site survey in order to aggregate the built environment in classes of homogeneous behavior; (2) definition of all necessary parameters and factors in two directions (X and Y); (3) evaluation of the capacity curves; (4) derivation of the related analytical fragility functions.

The parameters and factors that are necessary to define the capacity curve according to the DBV-*masonry* model are:

- N: number of stories ($i = 1,\ldots,N$ is the level counter);
- $\phi_{X,i}$ and $\phi_{Y,i}$: i-th component of the assumed normalized modal shape in X ($\boldsymbol{\phi_X}$) and Y ($\boldsymbol{\phi_Y}$) directions, respectively ($\phi_{X,N} = \phi_{Y,N} = 1$);
- h_i: interstory height of i-th level;
- q_i: total seismic floor load at i-th level (dead load and a fraction of live loads);
- $\zeta_{X,i}$: fraction of floor load supported by walls in X direction at i-th level (variable from 0 to 1); then, in Y direction, $\zeta_{Y,i} = 1 - \zeta_{X,i}$;
- γ_i: masonry specific weight at i-th level;
- $\kappa_{X,i}$ and $\kappa_{Y,i}$: spandrels contribution fraction to the mass of i-th level; it is defined as the ratio of the total volume of the walls (spandrels and piers) over that of the piers only, computed separately in X and Y direction;
- $\tau_{k,X}$ and $\tau_{k,Y}$: shear strength of masonry at ground level in X and Y direction, respectively;
- $G_{X,i}$ and $G_{Y,i}$: shear modulus of masonry at i-th level in X and Y direction;
- $\alpha_{X,i}$ and $\alpha_{Y,i}$: resistant area ratio at i-th level, in X and Y direction, computed with respect the gross area;
- $K_{1,X}$, $K_{2,X}$, $K_{3,X}$, $K_{4,X}$ and $K_{1,Y}$, $K_{2,Y}$, $K_{3,Y}$, $K_{4,Y}$: correction factors of the base shear strength at ground floor in X and Y direction, respectively; they affect the computation of $A_{u,X}$ and $A_{u,Y}$;
- $K_{5,X}$, $K_{6,X}$ and $K_{5,Y}$, $K_{6,Y}$: correction factors of the initial stiffness in X and Y direction, respectively; they affect the computation of $T_{y,X}$ and $T_{y,Y}$;
- $\Delta_{S,LS4}$, $\Delta_{F,LS4}$: interstory drift limit values assumed for the shear (S) and flexural (F) response of masonry piers, corresponding to LS4;
- ε_X and ε_Y: weight assigned to the in-plane SSWP mechanism in X and Y direction, respectively.

By way of example, in the following the expressions presented only refer to X direction; moreover, all the summations, where not differently specified, are intended as extended from 1 to N.

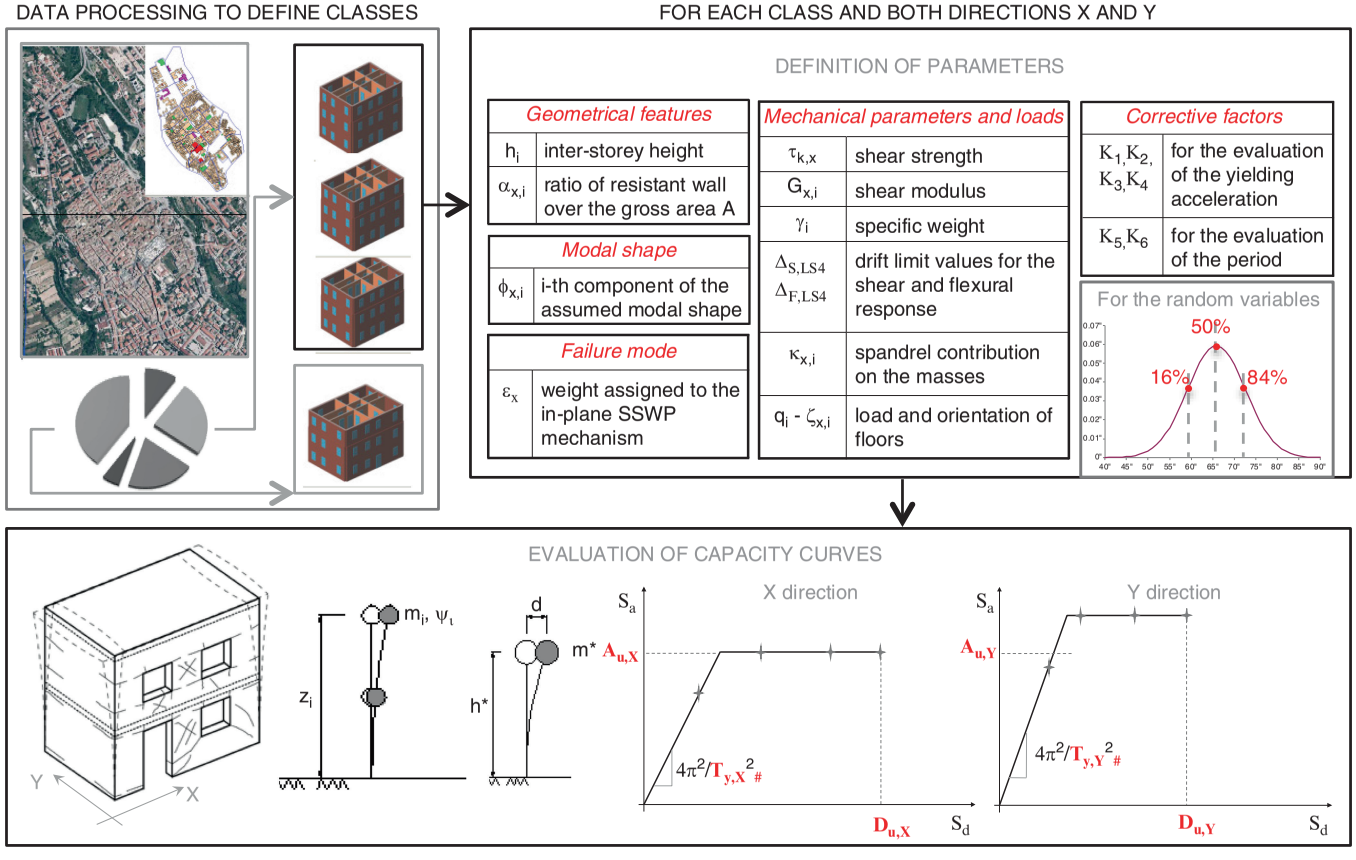

Fig. 5.11 Basic steps of the procedure: classification of the built environment and use of DBV-*masonry* model for defining the capacity curves

The spectral acceleration at yielding and ultimate $A_{u,X}$ is provided by:

$$A_{u,X} = \frac{f_X}{m_X^* \Gamma_X} g \tag{5.20}$$

where: f_X is the base shear at ground floor for unity gross area; Γ_X and m_X^* are the participation factor and the equivalent mass of the equivalent SDOF system; g is the gravity acceleration (equal to 9.81 m/s^2). According to Fajfar (1999), Γ_X and m_X^* are computed on basis of the assumed modal shape $\boldsymbol{\phi_X}$ as follows:

$$\Gamma_X = \frac{\sum m_i \phi_{X,i}}{\sum m_i \phi_{X,i}^2} = \frac{m_X^*}{\sum m_i \phi_{X,i}^2} \tag{5.21}$$

where, by using the common lumped masses distribution (Fig. 5.11), m_i is the mass of the i-th story defined as:

$$m_i = q_i + 0.5 \sum_{i}^{i+1} h_k \gamma_k (\alpha_{X,k} \kappa_{X,k} + \alpha_{Y,k} \kappa_{Y,k}) \tag{5.22}$$

where it is formally defined $\alpha_{X,N+1}$ (and $\alpha_{Y,N+1}$) equal to 0.

The base shear f_X is basically related to the shear strength offered by the resistant walls area at the first floor level; only the contribution of walls that are parallel to the examined direction is considered. The analytical formulation starts from the hypothesis that masonry piers fail at the same time, with a fixed rotation constraint at both ends (shear type model – SSWP), according to a diagonal shear failure mode; then correction factors are introduced in order to consider also WSSP and intermediate seismic behaviors (EF). The derivation of correction factors is discussed later and proper values are provided in Table 5.4. It is worth noting that also the WSSP model could be analytically formulated in a simple way, on the basis of a cantilever model for full-height piers subjected to a prevailing flexural failure mode. However, in that way it would lead to results too conservative, since even for small but non-zero strength of spandrels, the contribution to the total shear strength is not negligible.

In particular f_X may be computed as follows:

$$f_X = \alpha_{X,1} \tau_X \prod_{1}^{4} K_{i,X} \tag{5.23}$$

where:

- τ_X is the masonry shear strength at the ground level, according to the criterion proposed by Turnsek and Cacovic (1970) as:

$$\tau_X = \tau_{k,X} \sqrt{1 + \frac{\sigma_X}{1.5 \tau_{k,X}}} \tag{5.24}$$

where σ_X is the average vertical compressive stress at the middle height of the first level masonry piers:

$$\sigma_X = \frac{\sum \zeta_{X,i} q_i + \sum \gamma_i h_i \alpha_{X,i} \kappa_{X,i} - 0.5 \gamma_1 h_1 \alpha_{X,1} \kappa_{X,1}}{\alpha_{X,1}} \tag{5.25}$$

- $K_{1,X}$ modifies the strength as a function of the main prevailing failure mode expected at scale of masonry piers; it varies from 0.8 (in case of a prevailing flexural behaviour, with very slender panels) to 1.5;
- $K_{2,X}$ accounts for the influence of the non homogeneous size of the masonry piers (related to CO category tags);
- $K_{3,X}$ accounts for the influence of geometric and shape irregularities in the plan configuration (related to E category tags);
- $K_{4,X}$ accounts for the effectiveness of spandrels, which influence the global failure mechanism of the building (EF, WSSP and SSWP).

The definition of the elastic period $T_{y,X}$ is based on the proposal of Pagnini et al. (2011), which originally referred only to the contribution of the shear stiffness, with the introduction of some additional correction factors. From the general definition of the period of a SDOF system, it follows:

$$T_{y,X} = 2\pi \sqrt{\frac{m^*}{g k_X^*}} = 2\pi H \sqrt{\frac{\sum m_i \phi_{X,i}}{g \prod_5^6 K_{i,X} \sum G_{X,i} h_i \alpha_{X,i}}} \tag{5.26}$$

where H is the total height (equal to $\Sigma\, h_i$) and k_X^* is the stiffness of the SDOF system, being defined as:

$$k_X^* = \frac{\prod_5^6 K_{i,X} \sum G_{X,i} h_i \alpha_{X,i}}{H^2} \tag{5.27}$$

The introduction of $K_{i,X}$ ($i = 5,6$) correction factors aims to consider the flexural contribution in piers ($K_{5,X}$) and the effects on the stiffness related to the spandrel influence on the boundary conditions on piers ($K_{6,X}$). It is worth noting that, since the bilinear behavior assumed for the capacity curve is an approximation of the actual response, this period has to be considered as representative of a partially cracked state; as a consequence, mechanical parameters representative of cracked conditions have to be assumed.

Finally, the ultimate displacement capacity $D_{u,X}$ may be calculated as a function of a proper combination of two basic collapse modes (WSSP and SSWP).

In case of WSSP mode, by assuming a linear deformed shape at collapse, $D_{u,WSSP}$ is computed as:

$$D_{u,SSWP} = \Delta_{LS4} \frac{H}{\Gamma_X} \tag{5.28}$$

where Δ_{LS4} is alternatively assumed equal to $\Delta_{S,LS4}$ or $\Delta_{F,LS4}$ as a function of the prevailing failure mode in masonry piers for the examined direction (if shear or flexural one).

In case of SSWP mode, by assuming a soft storey mechanism located at ground floor, $D_{u,SSWP}$ is given by:

$$D_{u,SSWP} = \Delta_{LS4} h_1 + D_{y,X}\left(1 - \frac{\Gamma_X}{N}\right) \tag{5.29}$$

where $D_{y,X} = A_{u,X}(T_{y,X}/2\pi)^2$ is the yielding displacement; the latter term accounts for the elastic deformed shape, assumed as linear, that involves the whole building.

Finally, $D_{u,X}$ is computed as a combination of the afore introduced values, related to the possible failure modes, as:

$$D_{u,X} = \varepsilon_X D_{u,SSWP} + (1 - \varepsilon_X) D_{u,WSSP} \tag{5.30}$$

A proper assignment of ε_X allows considering intermediate failure modes, which occur in Equivalent Frame (EF) behavior.

The proposed expressions allow to consider building prototypes characterized by an irregular configuration at the various levels, as often is observed in actual cases, in particular in historical centers where porticos and shops are present at the ground level. However, it is sometimes possible to define more regular configurations, for which the above proposed formulas may be simplified. In particular it could be considered a constant or linear variation with height of $\alpha_{X,i}$, or a constant mass at each floor ($m_i = M/N$, where M is the total mass per unit gross area of the building), or even constant values with height of parameters q_i, $\zeta_{X,i}$, $\kappa_{X,i}$, $\kappa_{Y,i}$, γ_i, $G_{X,i}$. A common assumption for the modal shape $\boldsymbol{\phi}$ is the linear one. Table 5.3 summarizes how some of the previous expressions are modified in the case these assumptions are adopted. They are useful for application at large scale, in order to reduce the effort in achieving all necessary data.

Table 5.4 illustrates the ranges for correction factors for $K_{i,X}$ and $K_{i,Y}$ ($i = 2,\ldots,5$) as a function of two basic failure modes (WSSP, SSWP); they have been calibrated on the basis of comparison with results carried out by detailed numerical non linear static analyses using Tremuri software (Lagomarsino et al. 2012, 2013). Indeed, for some of them (such as $K_{2,X}$, $K_{3,X}$ and $K_{6,X}$) analytical formulations may be found in Lagomarsino and Cattari (2013) and in an Italian document of Guidelines for cultural heritage buildings (Recommendations P.C.M. 2011). However, since these latter formulations imply a degree of accuracy of data incompatible in most of cases with aims of vulnerability analyses at large scale, their evaluation on expert judgment basis seems to be more realistic.

Table 5.3 Expressions for m_i, σ_X, $T_{y,X}$, m_X^* and Γ_X for calculation of capacity curve in X direction, in case of adoption of some simplified assumptions

Simplified assumption	Resulting simplified expressions
Linear variation for $\alpha_{X(Y),i}$ $\alpha_{X,i} = \alpha_{X,1}\,(1-\beta_X - i\beta_X)$ $\alpha_{Y,i} = \alpha_{Y,1}\,(1-\beta_Y - i\beta_Y)$	$m_i = q + h\gamma\{\alpha_{X,1}\kappa_X[1+\beta_X - \beta_X(i+0.5)] + \alpha_{Y,1}\kappa_Y[1+\beta_Y - \beta_Y(i+0.5)]\} \quad i = 1, N-1$ $m_N = q + 0.5h\gamma[\alpha_{X,1}\kappa_X(1+\beta_X - N\beta_X) + \alpha_{Y,1}\kappa_Y(1+\beta_Y - N\beta_Y)]$ $\sigma_X = \frac{N\zeta_X q}{\alpha_{X,1}} + h\gamma\kappa_X\left[N(1+\beta_X) - 0.5 - \beta_X\sum i\right]$
$\alpha_{X,i} = \alpha_{X,1}$ $\alpha_{Y,i} = \alpha_{Y,1}$	$m_i = q + h\gamma(\alpha_{X,1}\kappa_X + \alpha_{Y,1}\kappa_Y) \quad i = 1, N-1$ $m_N = q + 0.5h\gamma(\alpha_{X,1}\kappa_X + \alpha_{Y,1}\kappa_Y)$ $\sigma_X = \frac{N\zeta_X q}{\alpha_{X,1}} + h\gamma\kappa_X(N-0.5)$ $T_{y,X} = 2\pi\frac{H}{N}\sqrt{\frac{Nm_i\sum\phi_{X,i}}{gGh\alpha_{X,1}\prod_5^6 K_{i,X}}}$
$\alpha_{X,i} = \alpha_{X,1}$ $\alpha_{Y,i} = \alpha_{Y,1}$ $m_i = M/N$ Linear mode shape $\boldsymbol{\phi}$	$m_X^* = \frac{M}{N^2}\sum i; \quad \Gamma_X = \frac{3N}{2N+1}$ $T_{y,X} = 2\pi\sqrt{\frac{Mh\sum i}{gGN\alpha_{X,1}\prod_5^6 K_{i,X}}}$ *where* $M = Nq + H\gamma(\alpha_{X,1}\kappa_X + \alpha_{Y,1}\kappa_Y)$

Table 5.4 Ranges proposed for the correction factors K_i ($i = 1,...6$)

Correction factor	EF	WSSP	SSWP
K_1	0.8 ÷ 1.5	0.8 ÷ 1	1 ÷ 1.5
K_2	0.8 ÷ 1	1	1
K_3	0.75 ÷ 1	0.75 ÷ 1	0.75 ÷ 1
K_4	0.6 ÷ 1	0.5 ÷ 0.8	1
K_5	0.4 ÷ 0.8	0.4 ÷ 0.8	0.6 ÷ 0.8
K_6	0.6 ÷ 1	0.3 ÷ 0.7	1

Table 5.5 Proposed ranges for the interstory drift limits

	Δ_S (shear)	Δ_F (flexural)
LS3	0.0025–0.004	0.004–0.008
LS4	0.004–0.006	0.008–0.012

Once the capacity curves in X and Y directions have been evaluated, the displacement values related to the different LS have to be defined.

In particular, the values of the displacement thresholds D_{LS1} and D_{LS2} are proposed as a function of the yielding displacement $D_{y,X}$ (or $D_{y,Y}$); as a consequence, they may be expressed as analytical functions of the mechanical and geometrical parameters on which the model is based on. Considering that the period is associated to a cracked state, it seems coherent to define the slight damage (D_{LS1}) before $D_{y,X}$. In particular the following relationships (based on expert judgment) are proposed:

$$\begin{aligned} D_{LS1} &= 0.7 D_{y,X} \\ D_{LS2} &= c_2 D_{y,X} \end{aligned} \tag{5.31}$$

where c_2 is a coefficient that varies as a function of the prevailing global failure mode. It is proposed to assume a value for c_2 from 1.2 to 2 (Lagomarsino and Cattari 2013), varying from the SSWP to the WSSP failure mode, as introduced also in Sect. 5.3.3. This differentiation is based on the different global behavior that occurs for these two failure modes. In particular, it is observed that, in case of WSSP mode, damage spreads progressively with a first localization of the damage on spandrels and with a subsequent collapse of piers only in the final phase. Thus the pushover curve is from the beginning strongly non linear. On the contrary, in case of SSWP, collapse damage in piers occurs suddenly and this justifies the definition of LS2 closer to $D_{y,X}$ than in the case of WSSP mode. Moreover, in case of the SSWP failure mode, since damage in piers strongly compromises both the operational requirements and reparability of buildings, it seems justifiable the distance of the slight damage state (DS1) from the moderate one (DS2) is smaller than in the WSSP case.

Finally, with reference to D_{LS3}, it seems reasonable to define it by assuming a formulation analogous to that of $D_{LS4} = D_{u,X}$ that is from Eq. (5.30) by properly defining interstory drift limit for masonry: $\Delta_{S,LS3}$, $\Delta_{F,LS3}$.

Table 5.5 proposes some possible ranges of interstory drift limits for LS3 and LS4. Reference values are also proposed in both national and international codes, e.g. in Eurocode 8-Part 3 (CEN 2005) and in ASCE/SEI 41/06 (2007), as well in literature (Calvi 1999). Limit values proposed in codes seem much more

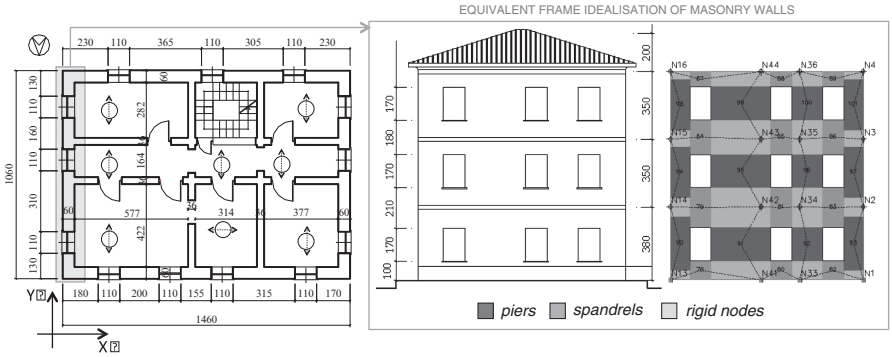

Fig. 5.12 Plan configuration of the URM building analyzed and equivalent frame idealization of a wall oriented in Y direction (see Fig. 5.2 for a 3D view of the model)

representative of LS3, being on the safe side because they are used for the design, while in this case they have to be used for the vulnerability assessment, so they must be correct on average. According to this, it seems reasonable to assume higher drift limits as proposed in Table 5.5.

5.4.2.2 Use of Static or Dynamic Analyses on Prototype Buildings

An alternative to the use of simplified analytical models is to assume, for each building class, one or more then one completely defined prototype buildings, and to perform static pushover or incremental dynamic analyses with detailed MDOF nonlinear models. The variability of seismic response can be evaluated by analyzing the uncertainties propagation of model parameters and/or by considering a proper number of different prototypes, representative of the class.

This approach can be more detailed than the one presented in Sect. 5.4.2.1, because specific constructive details of buildings in the region under investigation may be taken into account explicitly. However, it is strongly dependent from the choice of prototypes and it is necessary to be sure they are really representative of all the building stock.

5.4.2.3 Validation

In order to validate the simplified mechanical model illustrated in section Sect. 5.4.2.1, a three storey URM building is considered and a comparison has been made with the capacity curves obtained by pushover analyses with a detailed equivalent frame modelling; to this end, Tremuri program has been used (Lagomarsino et al. 2012, 2013; Cattari and Lagomarsino 2013a). Figure 5.12 shows the plan configuration of the examined building and the equivalent frame idealization of a wall. In particular, masonry panels have been modelled by non linear beams characterized by multi-linear constitutive laws, recently implemented in the program (Cattari and Lagomarsino 2013b).

Table 5.6 Parameters adopted for the URM prototype building examined

	Level				FRM			
	1	2	3		EF-a	EF-b	WWSP	SSWP
E		750		K_1	1	0.9	0.8	1.1
$G_{X,i} - G_{Y,i}$		250		K_2	0.9	0.9	1	1
$\tau_{k,X} - \tau_{k,Y}$		0.076		K_3	1	1	1	1
$\mathbf{f_m}$		3.2		K_4	0.9	0.75	0.6	1
γ_i		18		K_5	0.7	0.7	0.7	0.7
$\zeta_{X,i}$		0.75		K_6	0.9	0.8	0.3	1
q_i	3.95	3.95	6.68[a]	ε_Y	0.8	0.5	0	1
$\mathbf{t_{ext}}$	0.6	0.6	0.4	ε_X	0.8	0.5	0	1
$\mathbf{t_{int}}$	0.36	0.36	0.24	$\Delta_{S,LS4}$	0.005			
h_i	3.8	3.5	3.5	$\Delta_{F,LS4}$	0.008			
$\alpha_{X,i}$	0.130	0.130	0.087	$\phi_X - \phi_Y$	Linear			
$\alpha_{Y,i}$	0.101	0.101	0.066					
$\kappa_{X,i} - \kappa_{Y,i}$	1.13	1.15	1.15					

E (Young modulus) – $G_{X,i} - \tau_{k,X} - f_m$ (masonry compressive strength) in MPa
γ_i in kN/m^3 – q_i in kN/m^2
t_{ext} (thickness of external walls) and t_{int} (thickness of internal wall) in meters
[a]On the top level an additional load (equal to 2.37 kN/m^2) was added in order to consider the mass contribution of the wooden roof

This building is considered to be made of fired bricks with hydraulic mortar (FB-HM) and is representative of an existing URM structure in which IP mechanism prevails, according to the EF behavior; in particular two situations are considered: (EF-a) with ring beams (HQD-WRB); (EF-b) without ring beams and tie-rods but with spandrels efficiently connected and supported by architraves (HQD-WoT-WoRB). Floors are rigid, being made by a mixed masonry-r.c. typology. According to the taxonomy discussed in Sect. 5.1, the two examined prototype buildings are defined by the following tags:

- EF-a:/BW-EF/URM-FB-HM/R-I/R/RO/HQD-WRB/R-RC/P-Ti/M-3/PC-HAC
- EF-b:/BW-EF/URM-FB-HM/R-I/R/RO/HQD-WoT-WoRB/R-RC/P-Ti/M-3/PC-HAC

Two additional configurations have been analyzed to be representative of the limit conditions of WSSP and SSWP behaviors.

The simulation of the four prototype buildings by Tremuri has been made by considering for spandrels the following assumptions:

- EF-a: non linear r.c. beams have been coupled to spandrels;
- EF-b: the flexural spandrel behavior has been described by the strength criterion proposed in Cattari and Lagomarsino (2008), which considers an equivalent horizontal tensile strength of masonry, due to the interlocking between blocks;
- WSSP: only horizontal displacements have been coupled for piers;
- SSWP: fixed-end rotation condition has been considered for piers at each floor.

Table 5.6 summarizes the parameters adopted for both the detailed and simplified models, for the four considered cases (those employed only in the equivalent frame one are in bold).

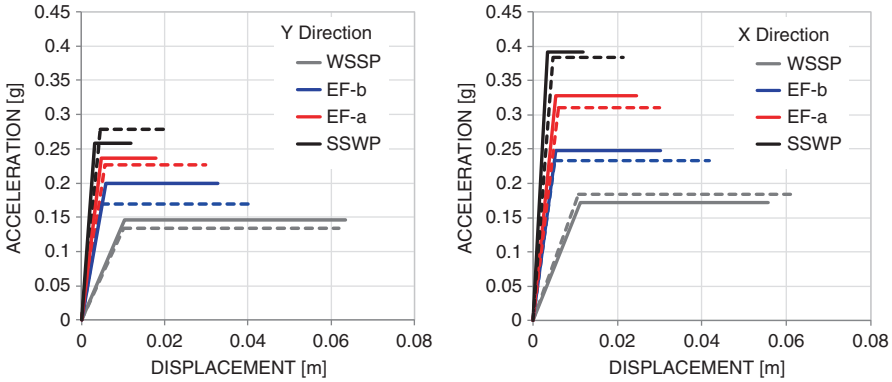

Fig. 5.13 Comparison between the capacity curves obtained from the simplified mechanical model and the detailed one in Y and X direction, respectively

Figure 5.13 illustrates the comparison between the capacity curves obtained from the simplified mechanical model (dotted lines) and the detailed one (continuous lines), for the X and Y direction, respectively. Despite some unavoidable differences, the simplified model provides results in a good agreement with the detailed one, being able, through the assignment of the correction factors K_i, to consider the different behavior of four examined cases. It is worth noting that, for sake of simplicity, the same correction factors have been assumed in X and Y direction. However, in Y direction the number of openings is lower than in the X one, and the distribution is less regular; this justifies the better agreement obtained in the X direction for the EF-a and EF-b configurations.

The overestimation of the ultimate displacement provided by the simplified model could be ascribed to the fact that the drift is computed, in this case, on the overall height, while, in the case of the detailed one, on the height of each single panel (in general lower due to the equivalent frame idealization).

Finally, by way of example, Fig. 5.14 shows some output results at scale of each single pier in the case of detailed model, compared with the average values considered as an approximation in the case of the simplified model.

In Fig. 5.14a the compressive stress obtained from Tremuri program in each pier at the ground level, after the application of the vertical loads, is compared with the average stress state computed from Eq. (5.25) and used in the simplified model; it emerges a certain degree of variability but a general good agreement. Figure 5.14b illustrates the slenderness and the contribution of the flexural stiffness at scale of each pier in case of the detailed model: this latter effect is taken into account in an approximate way through the K_5 factor in the simplified model.

Another validation of the proposed analytical method, based on damage observation data after L'Aquila earthquake (2009), is presented in Cattari et al. (2013).

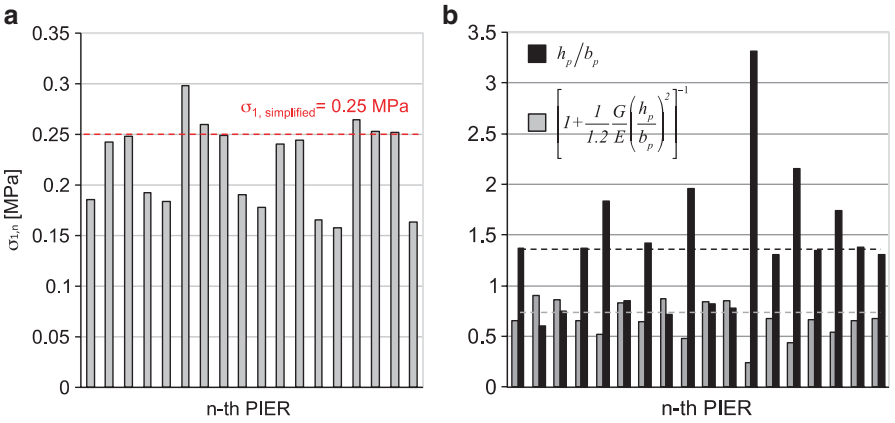

Fig. 5.14 Results of piers in X direction (ground level) from the detailed model: (**a**) compressive stress state; (**b**) slenderness and influence of flexural stiffness

5.4.3 From Hybrid Approaches

Hybrid approaches are based on a combination of the methods described in Sects. 5.4.1 and 5.4.2.

In particular, empirical data in terms of macroseismic intensity can be interpreted by means of the macroseismic vulnerability method (Lagomarsino and Giovinazzi 2006, Bernardini et al. 2011), by fitting, for each defined building class, the two free parameters: the vulnerability index V and the ductility index Q. Then, fragility functions can be obtained through a proper I-PGA correlation. Simplified or detailed mechanical models provide fragility functions by a complementary approach.

The comparison provides a cross-validation of the two methods and helps in the definition of more reliable function for the seismic risk analysis. Depending on the specific case, a different degree of reliability can be ascribed to the two approaches.

5.5 Proposal of Fragility Functions for Masonry Buildings

In this section fragility functions for some widespread typologies masonry buildings are proposed. They have been derived from the analytical simplified model proposed in Sect. 5.4.2.1; the results are compared with fragility curves derived by the macroseismic vulnerability model (described in Sect. 5.4.1).

Four classes of URM building are considered, related to different types of Blocks (see Table 5.1 for the meaning of the taxonomy tags): rubble (HS-RU), uncut (HS-UC), fired bricks (FB), hollow clay tile (HC); lime mortar (LM) is

Table 5.7 Nominal value of parameters assumed as deterministic variables

Parameter	URM1	URM2	URM3	URM4	URM5
γ_i	19	20	18	18	15
ε_X	0.7	0.5	0.5	0.7	0.7
$\zeta_{X,i}$	0.5	0.5	0.5	0.5	0.5
$\kappa_{X,i} - \kappa_{Y,i}$	1.05	1.05	1.05	1.05	1.05
q_i (q_N)	2 (1.5)	2.5 (1.5)	3.5 (3)	3.5 (3)	3.5 (3)
$\phi_{X,i}$	Linear	Linear	Linear	Linear	Linear
$K_{1,X}$	1	1	1	1	1
$K_{2,X}$	0.8	0.8	0.9	0.9	0.9
$K_{3,X}$	1	1	1[a]	1	1
$K_{4,X}$	0.6	0.7	0.7	0.8	0.9
$K_{5,X}$	0.7	0.7	0.7	0.7	0.7
$K_{6,X}$	0.55	0.8	0.8	0.85	0.9

q_i in kN/m^2

[a]In case of plan irregularity, the value of 0.8 has been assumed

considered for the first three block types, while cement mortar (CM) is assumed for the latter. Different classes of height have been considered, in order to show what a mechanical based model is able to distinguish in the seismic behavior, with reference to the four DSs. Finally, in case of FB, both the alterative cases of presence of tie rods (WT) or r.c. ring beams (WRB) are considered, as well as, in the former case, the influence of plan irregularity. Summing up, ten different classes have been investigated, defined by the following lists of tags of the taxonomy:

- URM1-L: BW-IP/URM-HS-RU-LM/R/R/x/LQD-WoT-WoRB/F-T/P-T/L/PC
- URM2-L: BW-IP/URM-HS-UC-LM/R/R/x/LQD-WT/F-T/P-T/L/PC
- URM2-M: BW-IP/URM-HS-UC-LM/R/R/x/LQD-WT/F-T/P-T/M/PC
- URM3-M: BW-IP/URM-FB-LM/R/R/x/LQD-WT/R-S/P-RC/M/PC
- URM3-H: BW-IP/URM-FB-LM/R/R/x/LQD-WT/R-S/P-RC/H/PC
- URM3-M-IR: BW-IP/URM-FB-LM/IR/R/x/LQD-WT/R-S/P-RC/M/PC
- URM3-H-IR: BW-IP/URM-FB-LM/IR/R/x/LQD-WT/R-S/P-RC/H/PC
- URM4-M: BW-IP/URM-FB-LM/R/R/x/HQD-WRB/R-RC/P-RC/M/PC
- URM4-H: BW-IP/URM-FB-LM/R/R/x/HQD-WRB/R-RC/P-RC/H/PC
- URM5-M: BW-IP/URM-HC-CM/R/R/x/HQD-WRB/R-RC/P-RC/M/MC

Table 5.7 shows the parameters for which a nominal representative value is assumed for each different classes, considering their influence on the dispersion is limited. Table 5.8 presents the range of values for the four set of parameters assumed as random: the masonry mechanical properties ($G_{X,i}$ and $\tau_{k,X}$); the interstory height (h_i); the resistant area ratio ($\alpha_{X,i}$); the interstory drift limits ($\Delta_{S,LS4}$, $\Delta_{F,LS4}$, $\Delta_{S,LS3}$, $\Delta_{F,LS3}$). Parameters of the same set are assumed fully correlated (16 and 84 % confidence levels are shown and a lognormal distribution is assumed).

PGA is assumed as IM and the median response spectrum shape is that of soil B – type 1, according to EC8 (CEN 2004). The epistemic uncertainty on the hazard

Table 5.8 16 and 84 % confidence levels of parameter assumed as random variables

	URM1		URM2		URM3		URM4		URM5	
Parameter	16 %	84 %	16 %	84 %	16 %	84 %	16 %	84 %	16 %	84 %
$G_{X,i}$	230	350	340	480	400	600	400	600	875	1,400
$\tau_{k,X}$	0.020	0.032	0.035	0.051	0.060	0.092	0.060	0.092	0.240	0.320
h_i	2.80	3.20	2.80	3.30	2.70	3.30	2.70	3.30	2.70	3.00
$\alpha_{X,1}$ [a]	0.14	0.16	0.13	0.15	0.08	0.12	0.08	0.12	0.05	0.07
$\Delta_{S,LS4}$	0.002	0.004	0.002	0.004	0.004	0.006	0.004	0.006	0.004	0.006
$\Delta_{F,LS4}$	0.004	0.006	0.004	0.006	0.007	0.009	0.007	0.009	0.007	0.009
$\Delta_{S,LS3}$	0.001	0.003	0.001	0.003	0.002	0.004	0.002	0.004	0.002	0.004
$\Delta_{F,LS3}$	0.002	0.004	0.002	0.004	0.004	0.006	0.004	0.006	0.004	0.006

$G_{X,i}$ and $\tau_{k,X}$ in MPa; h_i in m

[a]In case of M and H height levels a linear variation is assumed, starting from the 3rd level

curve was assumed $\beta_H = 0.2$, while the uncertainty due to the response spectrum shape (β_D) was obtained, on the basis of the procedure described in Sect. 5.3.4, by considering the following ranges of characteristic values for the normalized acceleration response spectrum (where υ is the exponent of T in branch for $T > T_C$):

- $S_{a1,16}(T_C) = 2.0 - \upsilon_{16} = 1.1$
- $S_{a1,84}(T_C) = 3.2 - \upsilon_{16} = 0.9$

The LS thresholds have been obtained by using $c_2 = 1.5$ (see Sect. 5.3.3) and from proper drift limits (see Table 5.8). The uncertainty in their definition was defined in accordance to the assumptions in Fig. 5.7.

Fragility functions are obtained by the analytical model for each building class and for each number of stories; as in this case classes of height are considered (Low-rise, Medium-rise, and High-rise), fragility curves are obtained by a weighted average of the fragility curves for each number of stories. To this end, for Low-rise sub-class, it is assumed that 80 % have two stories and only 20 % are one-story buildings; for Medium-rise and High-rise buildings, a uniform distribution of height was considered.

Figure 5.15 shows, as an example, fragility curves of DS2 (a) and DS3 (b) for classes URM2-L and URM2-M. It is worth noting that the fragility curve obtained from the weighted average is not a lognormal cumulative function, but the parameters of a lognormal can be evaluated by least squares regression. At least for this class, it is worth noting that the building height has a bigger influence on DS2 than on DS3.

In Table 5.9 the two parameters of the fragility functions (PGA_{LS} and β_{LS}) for each damage state and the ten building classes considered in this section are listed. It is worth noting that the dispersion β_{LS} is, on average, equal to 0.51; only in very few cases it is lower than 0.42 or greater than 0.6. These value are similar but a little bit lower than those obtained in Sect. 5.4.1 from the macroseismic vulnerability method; this is correct, because greater uncertainties are implicitly included in the

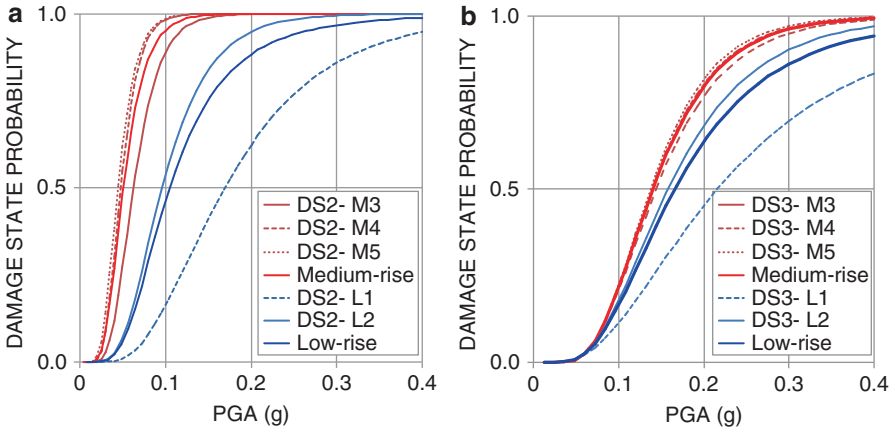

Fig. 5.15 Fragility curves of DS2 and DS3 for URM2-L and URM2-M classes: both the curves for single number of stories and the weighted average for height classes are shown

Table 5.9 Values of PGA_{LS} and β_{LS} of the fragility functions for the building classes examined

	DS1		DS2		DS3		DS4	
Class	PGA_{LS}	β_{LS}	PGA_{LS}	β_{LS}	PGA_{LS}	β_{LS}	PGA_{LS}	β_{LS}
URM1-L	0.041	0.65	0.074	0.61	0.131	0.53	0.160	0.47
URM2-L	0.057	0.52	0.105	0.53	0.166	0.54	0.203	0.505
URM2-M	0.026	0.475	0.051	0.40	0.140	0.43	0.178	0.41
URM3-M	0.057	0.50	0.104	0.49	0.253	0.56	0.325	0.61
URM3-H	0.043	0.43	0.096	0.38	0.253	0.54	0.323	0.60
URM3-M-IR	0.043	0.48	0.079	0.44	0.220	0.50	0.282	0.54
URM3-H-IR	0.032	0.42	0.072	0.37	0.221	0.49	0.281	0.53
URM4-M	0.065	0.51	0.118	0.52	0.231	0.55	0.302	0.59
URM4-H	0.048	0.43	0.107	0.39	0.226	0.51	0.292	0.56
URM5-M	0.189	0.54	0.343	0.58	0.399	0.79	0.492	0.68

latter approach, which has been derived by expert elicitation (derivation from the EMS98) and requires the establishment of a correlation between Intensity and PGA.

In order to validate the reliability of the obtained fragility functions, a comparison with those obtained by the macroseismic vulnerability method is presented. To this end, Fig. 5.16 compares, for all the examined building classes, the values of PGA_{LS} obtained by the analytical model with plausible ranges estimated by the macroseismic vulnerability model (considering the corresponding wider building class of EMS98, taking into account only of the building height category).

Finally, Figures from 5.17, 5.18, 5.19 and 5.20 show the fragility curves obtained for the ten buildings classes considered in this section. These fragility

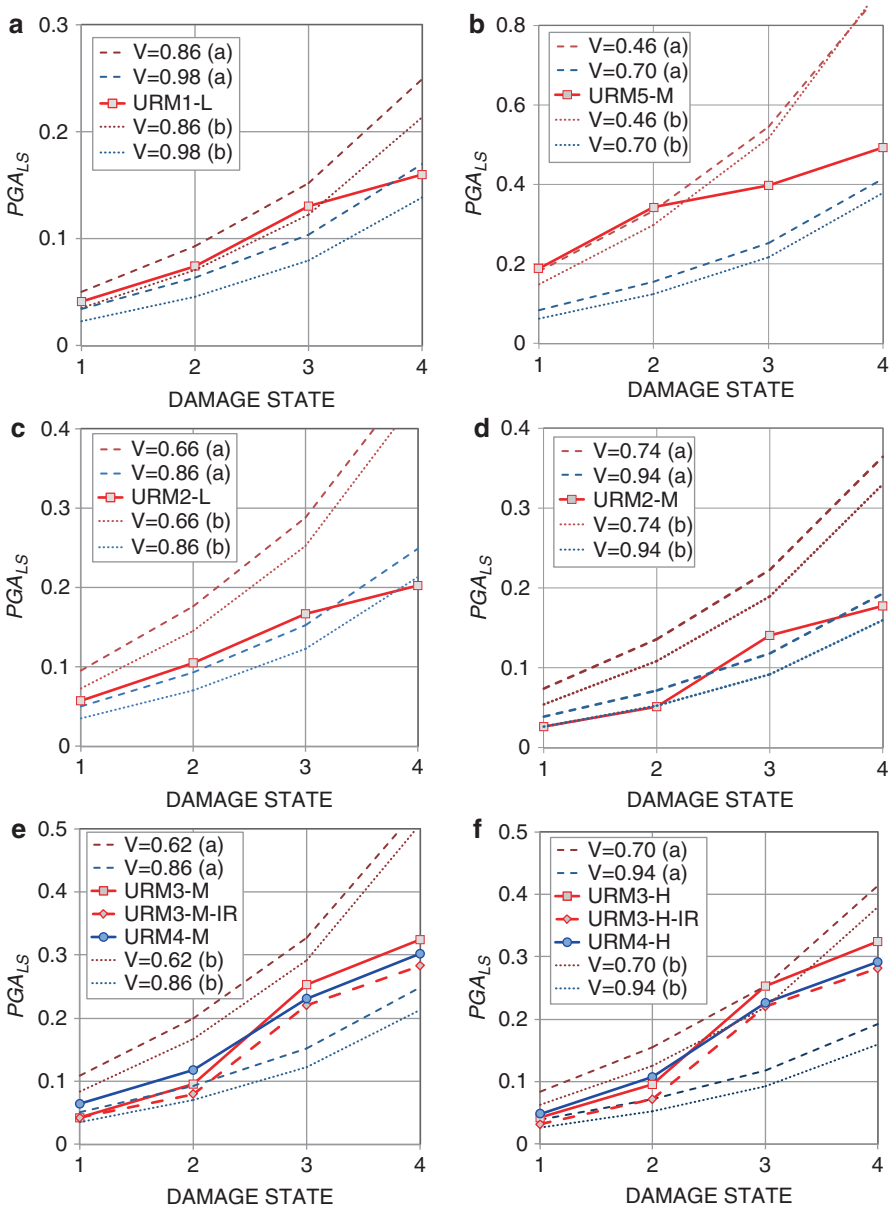

Fig. 5.16 Comparison between PGA_{LS} values obtained from the simplified mechanical model and the macroseismic method for the ten building classes considered

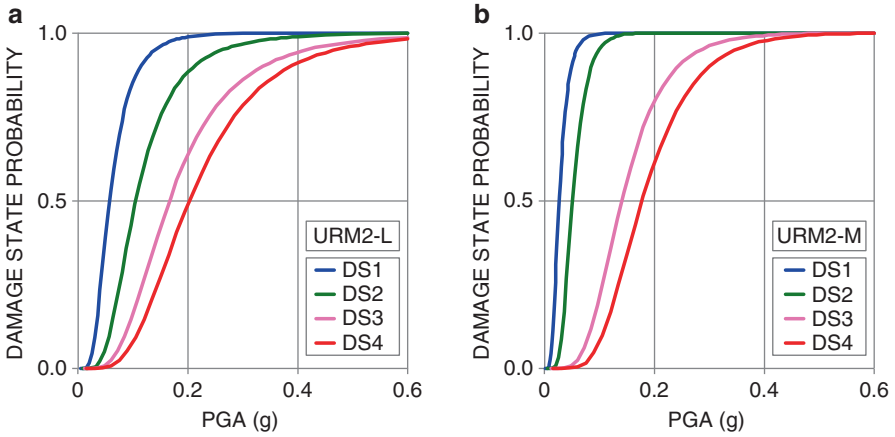

Fig. 5.17 Fragility curves obtained for URM2-L (**a**) and URM2-M (**b**) classes

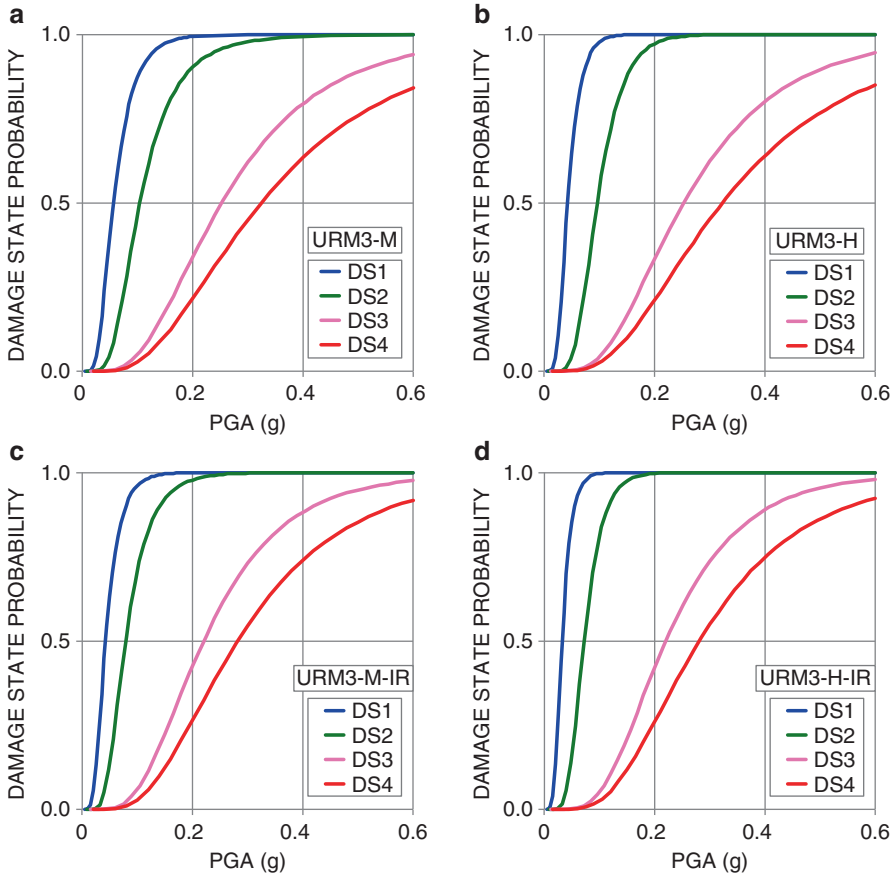

Fig. 5.18 Fragility curves for URM3-M and URM3-H classes in case of regular (**a**, **b**) and irregular (**c**, **d**) plan configuration

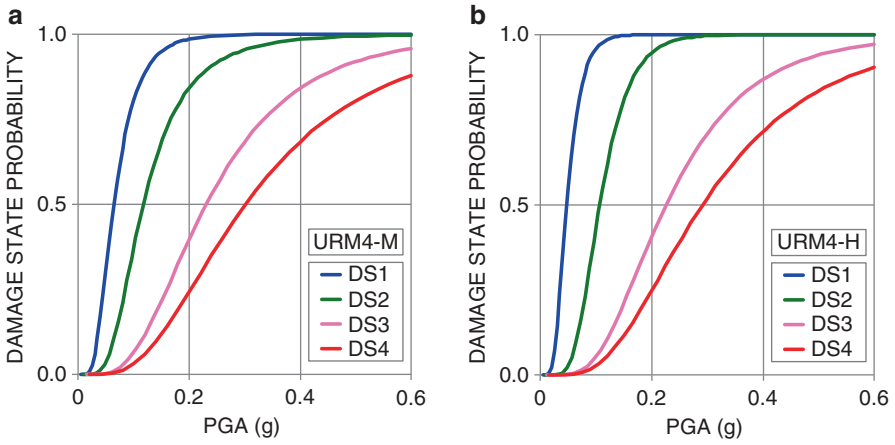

Fig. 5.19 Fragility curves obtained for URM4-M and URM4-H classes

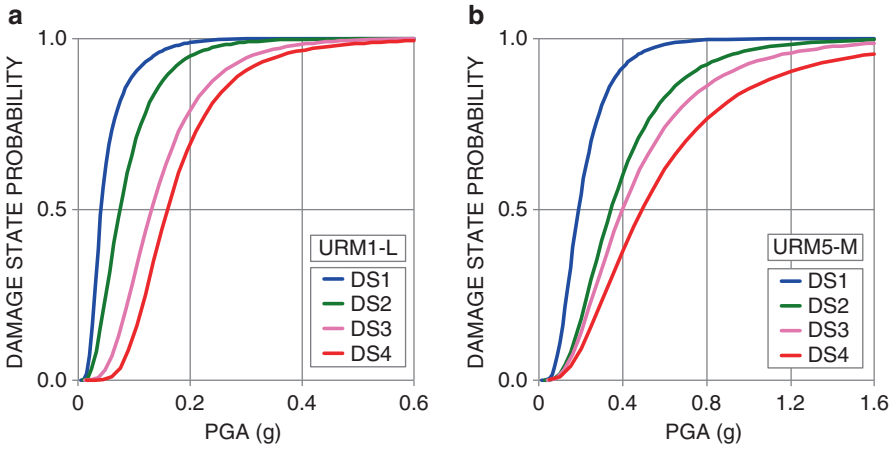

Fig. 5.20 Fragility functions obtained for URM1-L (**a**) and URM5-M (**b**) classes

functions could be implemented in the Fragility Manager Tool of SYNER-G (see Chap. 13) or other to be developed in the future.

References

ASCE/SEI 41/06 (2007) Seismic rehabilitation of existing buildings. American Society of Civil Engineers, Reston

Barbat AH, Carreño ML, Pujades LG, Lantada N, Cardona OD, Murulanda MC (2010) Seismic vulnerability and risk evaluation methods for urban areas. A review with application to a pilot area. Struct Infrastruct Eng 6(1–2):17–38

Bazzurro P, Cornell CA (2002) Vector-valued probabilistic seismic hazard analysis (VPSHA). In: Proceedings of 7th U.S. National conference on earthquake engineering, Boston, MA, 21–25 July, Paper No. 61

Benedetti D, Benzoni G, Parisi MA (1988) Seismic vulnerability and risk evaluation for old urban nuclei. Earthq Eng Struct Dyn 16:183–201. doi:10.1002/eqe.4290160203

Bernardini A, Gori R, Modena C (1990) An application of coupled analytical models and experiential knowledge for seismic vulnerability analyses of masonry buildings. In: Koridze A (ed) Engineering aspects of earthquake phenomena, vol 3. Omega Scientific, Oxon, pp 161–180

Bernardini A, Lagomarsino S, Mannella A, Martinelli A, Milano L, Parodi S (2011) Forecasting seismic damage scenarios of residential buildings from rough inventories: a case-study in the Abruzzo Region (Italy). Proc IMechE Part O J Risk Reliab 224:279–296

Blandon CA, Priestley MJN (2005) Equivalent viscous damping equations for direct displacement based design. J Earthq Eng 9(SI 2):257–278

Borzi B, Crowley H, Pinho R (2008) Simplified pushover-based earthquake loss assessment (SP-BELA) method for masonry buildings. Int J Archit Herit 2(4):353–376

Calvi GM (1999) A displacement-based approach for vulnerability evaluation of classes of buildings. J Earthq Eng 3(3):411–438

Cattari S, Lagomarsino S (2008) A strength criterion for the flexural behaviour of spandrel in un-reinforced masonry walls. In: Proceedings of 14th WCEE, Beijing, China

Cattari S, Lagomarsino S (2012) Performance-based approach to earthquake protection of masonry cultural heritage. In: Jasieńko J (ed) Proceedings of structural analysis of historical constructions, © 2012 DWE, Wrocław, Poland. ISSN 0860-2395, ISBN 978-83-7125-216-7, pp 2914–2922

Cattari S, Lagomarsino S (2013a) Seismic assessment of mixed masonry-reinforced concrete buildings by nonlinear static analyses. Earthq Struct 4(3):241–264

Cattari S, Lagomarsino S (2013b) Analisi non lineari per la simulazione del danno di un fabbricato in San Felice sul Panaro (Emilia, 2012). In: Proceedings of XV Italian conference on earthquake engineering (ANIDIS "L'Ingegneria Sismica in Italia"), Padua, 1–4 July 2013 (In Italian)

Cattari S, Curti E, Giovinazzi S, Lagomarsino S, Parodi S, Penna A (2005) Un modello meccanico per l'analisi di vulnerabilità del costruito in muratura a scala urbana. In: Proceedings of 11th Italian conference on earthquake engineering, Genoa, Italy (in Italian)

Cattari S, Lagomarsino S, Pagnini C, Parodi S (2010) Probabilistic seismic damage scenario by mechanical models: the case study of Sulmona (Italy). In: Proceedings of 14th ECEE, Ohrid, Macedonia, CD-ROM

Cattari S, Lagomarsino S, Pagnini LC, Parodi S (2013) Validazione di scenari di danno ottenuti con modelli meccanici: il caso studio di Pettino (L'Aquila, 2009). In: Proceedings of 15th Italian conference on earthquake engineering. Padua, Italy (in Italian)

CEN (2004) Eurocode 8: design of structures for earthquake resistance – Part 1: General rules, seismic actions and rules for buildings. EN1998-1:2004, Comité Européen de Normalisation, Brussels

CEN (2005) Eurocode 8: design of structures for earthquake resistance – Part 3: Assessment and retrofitting of buildings. EN1998-3:2005, Comité Européen de Normalisation, Brussels

Colombi M, Borzi B, Crowley H, Onida M, Meroni F, Pinho R (2008) Deriving vulnerability curves using Italian earthquake damage data. Bull Earthq Eng 6(3):485–504

D'Ayala D (2005) Force and displacement based vulnerability assessment for traditional buildings. Bull Earthq Eng 3:235–265

D'Ayala D, Ansal A (2009) Non linear push over assessment of historic buildings in Istanbul to define vulnerability functions. In: Proceedings of earthquake and tsunami, international conference, Istanbul, Turkey

D'Ayala D, Paganoni S (2010) Assessment and analysis of damage in L'Aquila historic city centre after 6th April 2009. Bull Earthq Eng 9:479–509

D'Ayala D, Speranza E (2003) Definition of collapse mechanisms and seismic vulnerability of historic masonry buildings. Earthquake Spectra 19:479–509

D'Ayala D, Spence R, Oliveira C, Pomonis A (1997) Earthquake loss estimation for Europe's historic town centres. Earthq Spectra 13(4):773–793

Douglas J, Seyedi D, Ulrich T, Modaressi H, Foerster E, Pitilakis K, Pitilakis D, Karatzetzou A, Gazetas G, Garini G, Loli M (2013) Evaluation of seismic hazard for the assessment of historical elements at risk: description of input and selection of intensity measures. Bull Earthq Eng SI (in print)

Erberik MA (2008) Generation of fragility curves for Turkish masonry buildings considering in-plane failure modes. Earthq Eng Struct Dyn 37:387–405

Faccioli E, Cauzzi C (2006) Macroseismic intensities for seismic scenarios estimated from instrumentally based correlations. In: Proceedings of the first European conference on earthquake engineering and seismology, Ginevra, 3–8 Sept 2006. CD-ROM

Fajfar P (1999) Capacity spectrum method based on inelastic spectra. Earthq Eng Struct Dyn 28(9):979–993

FEMA 356 (2000) Pre-standard and commentary for the seismic rehabilitation of buildings. Applied Technology Council (ATC), Washington, DC

FEMA 440 (2005) Improvement of nonlinear static seismic analysis procedures. Applied Technology Council (ATC), Washington, DC

Ferreira TM, Vicente R, Mendes da Silva JAR, Varum H, Costa A (2013) Seismic vulnerability assessment of historical urban centres: case study of the old city centre in Seixal. Port Bull Earthq Eng. doi:10.1007/s10518-013-9447-2

Freeman SA (1998) The capacity spectrum method as a tool for seismic design. In: Proceedings of 11th European conference of earthquake engineering, Paris, France

Gehl P, Seyedi D, Douglas J (2013) Vector-valued fragility functions for seismic risk evaluation. Bull Earthq Eng 11:365–384. doi:10.1007/s10518 012-9402-7

Glaister S, Pinho R (2003) Development of a simplified deformation-based method for seismic vulnerability assessment. J Earthq Eng 7(SI 1):107–140

Grunthal G (1998) European macroseismic scale, vol 15. Chaiers du Centre Européen de Géodynamique et de Séismologie, Luxembourg

HAZUS (1999) Earthquake loss estimation methodology. Technical and user manuals, vol 1–3. Federal Emergency Management Agency (FEMA), National Institute of Building Sciences, Washington, DC

Jaiswal K, Wald D, D'Ayala D (2011) Developing empirical collapse fragility functions for global building types. Earthq Spectra 27(3):775–795

Kappos AJ, Panagopoulos G, Penelis GG (2008) Development of a seismic damage and loss scenario for contemporary and historical buildings in Thessaloniki, Greece. Soil Dyn Earthq Eng 28(10–11):836–850

Klir GJ, Yuan B (1995) Fuzzy sets and fuzzy logic. Theory and applications. Prentice Hall, Upper Saddle River

Lagomarsino S, Cattari S (2013) Chapter 1: Seismic vulnerability of existing buildings: observational and mechanical approaches for application in urban areas. In: Gueguen P (ed) Seismic vulnerability of structures. ISTE Ltd./Wiley, London, pp 1–62. ISBN 978-1-84821-524-5

Lagomarsino S, Giovinazzi S (2006) Macroseismic and mechanical models for the vulnerability assessment of current buildings. Bull Earthq Eng 4(4):445–463

Lagomarsino S, Penna A, Galasco A, Cattari S (2012) TREMURI program: seismic analysis of 3D masonry buildings. Release 2.0, University of Genoa, Italy (mailto: tremuri@gmail.com)

Lagomarsino S, Penna A, Galasco A, Cattari S (2013) TREMURI program: an equivalent frame model for the nonlinear seismic analysis of masonry buildings, Engineering Structures, 56, pp. 1787–1799, http://dx.doi.org /10.1016/j.engstruct.2013.08.002

Liel AB, Haselton CB, Deierlein GG, Baker JW (2009) Incorporating modeling uncertainties in the assessment of seismic collapse risk of buildings. Struct Saf 31:197–211. doi:10.1016/j.strusafe.2008.06.002

Molina S, Lang DH, Lindholm D (2009) SELENA: an open-source tool for seismic risk and loss assessment using a logic tree computation procedure. Comput Geosci 36(3):257–269

Murphy JR, O'Brien LJ (1977) The correlation of peak ground acceleration amplitude with seismic intensity and other physical parameters. Bull Seismol Soc Am 67:877–915

Nuti C, Santini S, Vanzi I (1998) Seismic risks of the Italian hospitals. In: Proceedings of 11th European conference on earthquake engineering, Paris, France

Oropeza M, Michel C, Lestuzzi P (2010) A simplified analytical methodology for fragility curves estimation in existing buildings. In: Proceedings 14th European conference on earthquake engineering, Ohrid, Macedonia

Pagnini LC, Vicente RS, Lagomarsino S, Varum H (2011) A mechanical model for the seismic vulnerability assessment of old masonry buildings. Earthq Struct 2(1):25–42

Priestley MJN, Calvi GM, Kowalsky MJ (2007) Displacement-based seismic design of structures. IUSS Press, Pavia, 721 pp

Recommendations P.C.M. 9/2/2011 (2011) Seismic assessment and risk mitigation of cultural heritage according to Italian Technical Code for Constructions (NTC 2008). G.U. n 47 of 26-2-2011, Suppl Ord n. 54 (in Italian)

Restrepo-Vélez LF, Magenes G (2004) Simplified procedure for the seismic risk assessment of unreinforced masonry buildings. In: Proceedings of 13th world conference on earthquake engineering, Vancouver, Canada

Rota M, Penna A, Strobbia CL (2008) Processing Italian damage data to derive typological fragility curves. Soil Dyn Earthq Eng 28(10–11):933–947

Rota M, Penna A, Magenes G (2010) A methodology for deriving analytical fragility curves for masonry buildings based on stochastic nonlinear analyses. Eng Struct 32:1312–1323

Tomaževič M (1999) Earthquake resistant design of masonry buildings, vol 1, Series on innovation in structures and construction. Imperial College Press, London. ISBN 1-86094-006-8

Turnšek V, Čačovič F (1970) Some experimental results on the strength of brick masonry walls. In: Proceedings of the 2nd international brick masonry conference, Stoke-on-Trent, pp 149–156

Chapter 6
Fragility Functions of Electric Power Stations

Francesco Cavalieri, Paolo Franchin, and Paolo Emilio Pinto

Abstract This chapter presents a state-of-the-art on fragility models for the components of Electric Power Networks (EPNs) available in the technical literature. First, the main characteristics of an electric power network and its taxonomy are introduced. Then, the main recent works on fragility functions of electric components are listed, and details are provided for a few selected ones. In the last section, the fragility curves which are most suited for use in the European context are selected, with the indication of parameters and relevant information. The selection has been based both on the data supporting the models and on the adopted systemic approach to the simulation of EPN within the SYNER-G general methodology for infrastructural systems' vulnerability assessment. The latter adopts a capacitive, detailed flow-based modelling with short-circuits propagation over the network and requires the modelling of the substation internal logic.

6.1 Taxonomy of Electric Power Networks

6.1.1 Description of an Electric Power Network

A modern Electric Power Network (EPN) is a complex interconnected system that can be subdivided into four major parts:

- Generation
- Transformation
- Transmission and Distribution
- Loads

F. Cavalieri (✉) • P. Franchin • P.E. Pinto
Department of Structural Engineering and Geotechnics, University of Rome 'La Sapienza', Via Gramsci 53, 00197 Rome, Italy
e-mail: francesco.cavalieri@uniroma1.it; paolo.franchin@uniroma1.it; pinto@uniroma1.it

K. Pitilakis et al. (eds.), *SYNER-G: Typology Definition and Fragility Functions for Physical Elements at Seismic Risk*, Geotechnical, Geological and Earthquake Engineering 27,
DOI 10.1007/978-94-007-7872-6_6,

These are briefly described in the following. The interested reader can see Saadat (2002) for details.

Generation of electric power is carried out in power plants (Fig. 6.1, left), composed of several three-phase AC (Alternate Current) generators known as synchronous generators or alternators. Synchronous generators have two synchronously rotating fields, one of which is produced by the rotor driven at synchronous speed and excited by DC (Direct Current), while the second one is produced in the stator windings by the three-phase armature currents. The DC current for the rotor windings is provided by the excitation systems, which maintain generator voltage and control the reactive power flow. Because of the absence of the commutator, AC generators can generate high power (typically real power produced can vary from 50 to 1,500 MW) at high voltage, typically 30 kV.

At the time when the first EPNs were established in the world, individual electric companies were operating at different frequencies anywhere, in US ranging from 25 to 133 Hz. As the need for interconnection and parallel operation became evident, a standard frequency of 60 Hz was adopted throughout the US and Canada, while most European countries selected the 50 Hz system. These two AC frequencies are still in use at the present time.

One of the major components of a power network is the transformer (Fig. 6.1, right), which transfers power with very high efficiency from one level of voltage to another level. The power transferred to the secondary winding is almost the same as the primary, except for losses in the transformer. Therefore, using a *step-up* transformer of voltage ratio a will reduce the secondary current of a ratio $1/a$, reducing losses in the line, which are inversely proportional to voltage and directly proportional to distance. This makes the transmission of power over long distances possible. At the receiving end of the transmission lines *step-down* transformers are used to reduce the voltage to suitable values for distribution or utilization.

The purpose of a *power delivery system* (Fig. 6.2), also known as *transmission and distribution* (*T&D*) *system*, is to transfer electric energy from generating units at various locations to the customers demanding the loads.

A T&D system is divided into two general tiers: a *transmission system* that spans long distances at high voltages on the order of hundreds of kilovolts (kV), usually between 60 and 750 kV, and a more local *distribution system* at intermediate voltages. The latter is further divided into a medium voltage distribution system, at voltages in the low tens of kV, and a low voltage distribution system, which consists of the wires that directly connect most domestic and small commercial customers, at voltages in the 220–240 volts (V) range for Europe. The distribution system can be both overhead and underground.

The T&D systems are generally characterized by two different topological structures: the transmission system is an interconnected redundant grid, composed of stations as nodes and transmission lines as edges, while the distribution system is a tree-like network, following the main streets in a city and reaching the end users. Figure 6.3 shows the two topological structures.

The European high voltage transmission grid, composed of lines with a voltage greater or equal to 220 kV, is displayed in Fig. 6.4. The image has been taken from Poljanšek et al. (2010).

Fig. 6.1 Power-plant (*left*) and high voltage transformer (*right*)

The lines at different voltages are terminated in *substations*. In general, an electric substation is a facility that serves as a source of energy supply for the local distribution area in which it is located or changes the current voltage.

Depending on their functions, substations can be grouped into two typologies, in particular:

1. Distribution substations.
2. Transformation/distribution substations.

Substations layouts are extremely variable. They can be entirely enclosed in buildings, with all the equipment assembled into one metal clad unit, or with step-down transformers, high voltage switches, oil circuit breakers, and lightning arresters located outside the building. Figure 6.5 shows typical Italian (European) layouts for the station types above (Vanzi 1996).

The most important component inside a substation is the (load) bus (see Fig. 6.5a), made up of two bar systems (BS), connected by one bars-connecting line (BCL), as shown in Fig. 6.6. Each one of these so-called macro-components is made up of several micro-components (all of them are listed in Fig. 6.5). In particular, a BS is made up of three bars and three voltage transformers, while the BCL is composed of three current transformers, three circuit breakers and six vertical sectionalizing switches. Given the three-phase nature of the system, all micro-components are present in groups of three pieces, one per phase, and correspondingly all lines linked to the load bus have three cables. The power supply to the protection system provides power to boxes, which in turn feed the circuit breakers and make them active against propagation of short-circuits. In Fig. 6.6, only one box is shown, serving the three circuit breakers of the BCL; however, one box each is also present for all lines, which are composed of a number of micro-components (as shown in Fig. 6.5). The bar system collects

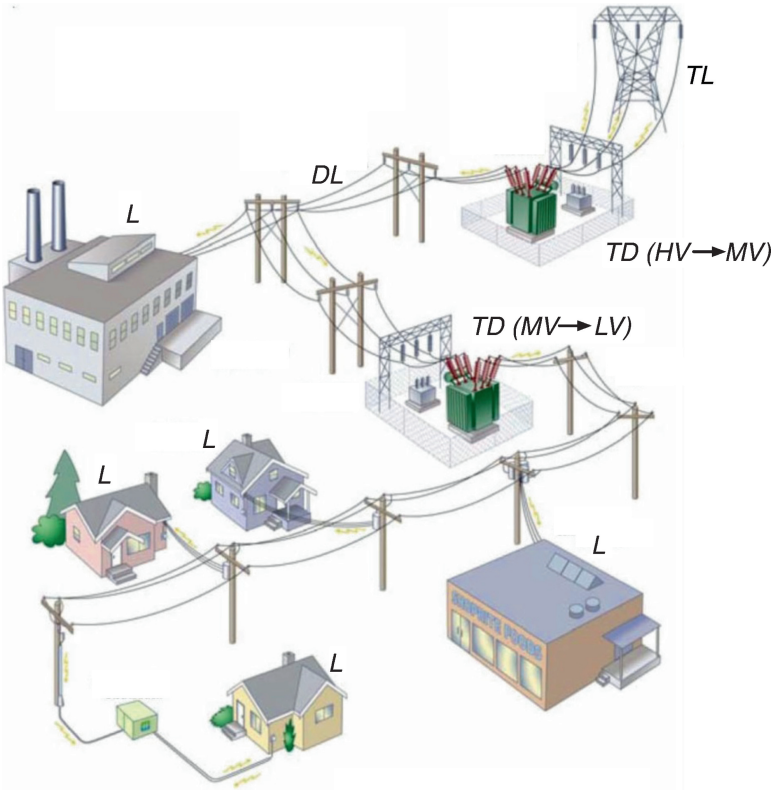

Fig. 6.2 Sketch of a T&D system for an EPN (*TL* = Transmission lines, *DL* = Distribution lines, *TD* (*HV* → *MV*) = Transformation (from high to medium voltage) and Distribution station, *TD* (*MV* → *LV*) = Transformation (from medium to low voltage) and Distribution station, *L* = Load)

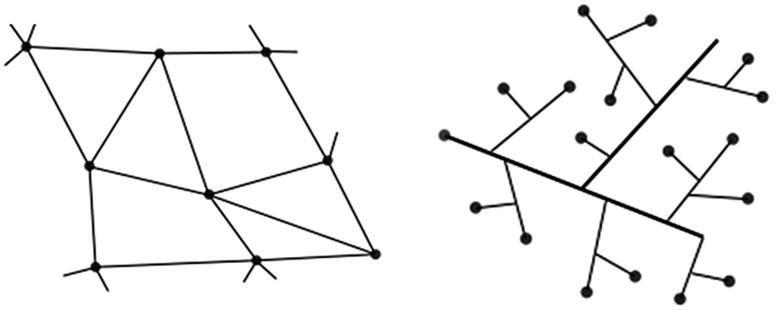

Fig. 6.3 Typical topological structures, grid-like (*on the left*) and tree-like (*on the right*), respectively for transmission and distribution systems

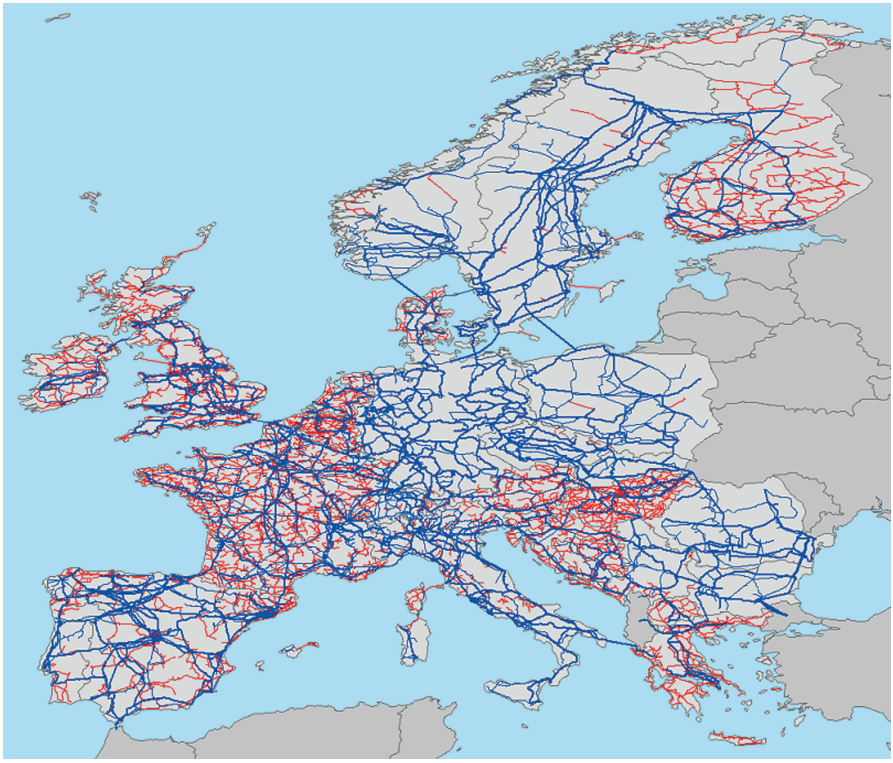

Fig. 6.4 European high voltage (220 kV and above) transmission grid. Higher voltage lines in *blue*, lower voltage lines in *red*. Line thickness is proportional to voltage

incoming currents and spreads them into the outgoing lines. To achieve this aim, the ingoing and outgoing lines could be attached to the same BS, and hence the need for a second BS is only to provide redundancy for maintenance purposes. Thus the BCL function is to connect the two BS's in ordinary operating conditions, when the currents flow through BS1, the BCL and leave the station through BS2.

When the transformation function is required (type 2 above), two buses at two different voltages are present (Fig. 6.5b). Since also power delivery is required, one or both buses are load buses. Given this modelling of substations' internal logic, in the SYNER-G model of an electric power network, buses, rather than stations, are the network nodes.

Finally the electric power is delivered to the single customers through distribution circuits, which include poles, wires, in-line equipment and utility-owned equipment at customer sites and lines. The latter are typically above ground in States such as US or Japan, and underground overall in Europe. Distribution circuits either consist of anchored or unanchored components.

Loads of power systems are divided into *industrial*, *commercial* and *residential*.

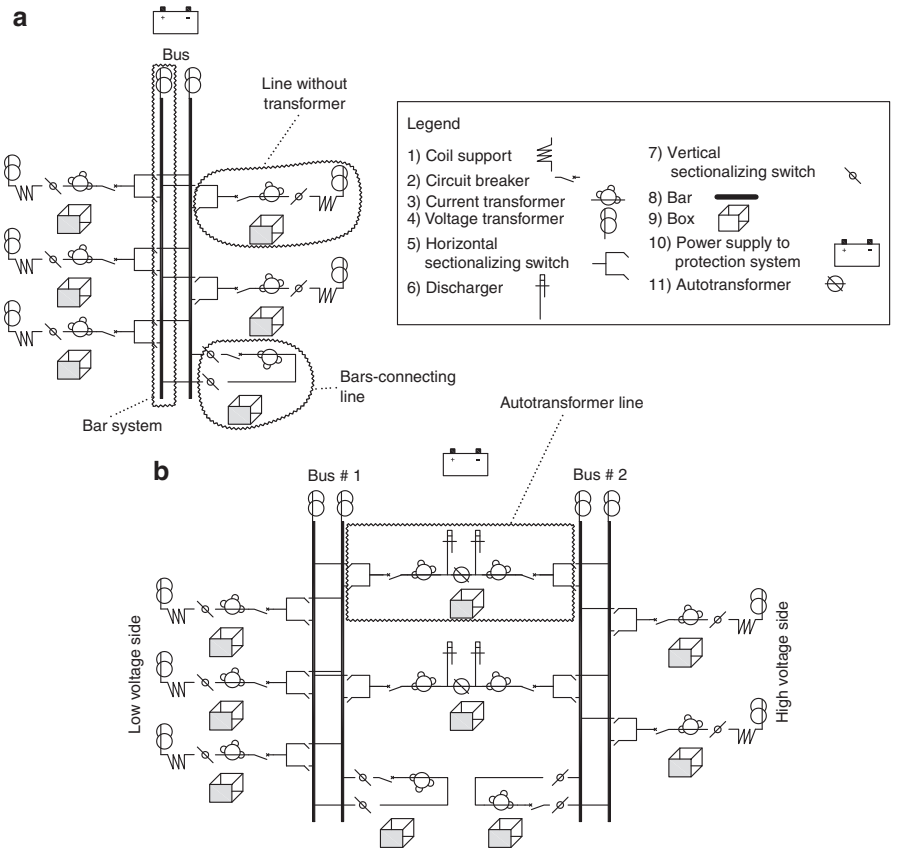

Fig. 6.5 Layouts of: (**a**) distribution substations; (**b**) transformation/distribution substations

Industrial loads are served directly from the high voltage transmission system or medium voltage distribution system. Commercial and residential loads consist largely of lighting, heating and cooling.

Loads are independent of frequency and consume negligibly small reactive power. The real power of loads is expressed in terms of kilowatts (kW) or megawatts (MW).

The magnitude of load varies throughout the day and power must be available to consumers on demand. The greatest value of load during a 24-h period is called *peak demand*. Smaller peaking generators may be commissioned to meet the peak load that occurs for only a few hours. In order to assess the usefulness of the generating plant the load factor is defined, which is the ratio of average load over a designated period of time to the peak load occurring in that period. Load factors may be given for a day, a month or a year.

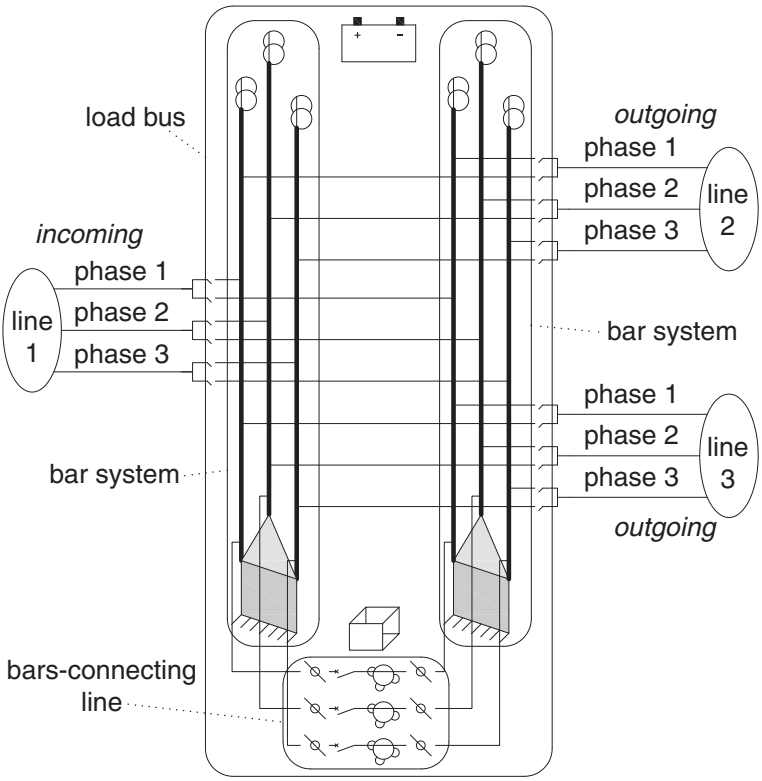

Fig. 6.6 Layout of a typical load bus with redundant bar systems

6.1.2 Identification of the Main Typologies for Electric Power Network Components in Europe

Electric power networks components, with particular reference to the European context, are listed in Table 6.1. The electric power system is a network. As such, at the highest level, components are either nodes or edges. In most studies fragility curves are specified at this level and no further decomposition is carried out. In reality, however, each component is a system in itself and can be analyzed in terms of its constituents. Table 6.1 is non homogeneous in this respect because it lists some components, such as power generation plants or lines, without breaking them up into parts, while it presents a detailed decomposition of substations into macro-components and micro-components. This reflects the work carried out within SYNER-G, where particular attention was devoted to the modelling of the internal logic of substations (see Figs. 6.5 and 6.6), while models from the literature were adopted for power plants and lines (e.g. HAZUS, FEMA 2003).

Table 6.1 Main typologies of EPN components in Europe

Group	Sub-group	Component	Description
Generation plant	–	–	Industrial facility for the generation of electric power
Line	Buried	–	Overhead conductor for power transmission, using high-voltage three-phase alternating current (AC)
	Overhead	–	Underground cables for power transmission, using high-voltage three-phase alternating current (AC)
Substation	Macro-components	Autotransformer line (Fig. 6.5b)	Line within a transformation/distribution substation, made up of: autotransformer + dischargers + current transformers + circuit breakers + hor. sect. switches + box
		Line without transformer (Fig. 6.5)	End of line, contained in substations, made up of: voltage transformer + coil support + hor. and vert. sect. switches + current transformer + circuit breaker + box
		Bars-connecting line (Fig. 6.6)	Line connecting two bar systems, made up of: vert. sect. switches + current transformer + circuit breaker + box
		Bar system (Fig. 6.6)	System made up of: voltage transformer + bar
		Cluster	System made up of: pothead + 6 lightning arresters + bus
	Micro-components	Circuit breaker	Automatically operated electrical switch designed to protect an electrical circuit or station from damage caused by overload or short-circuit
		Lightning arrester or Discharger	Device used to protect an electrical circuit or station from the damaging effects of lightning
		Horizontal disconnect/ sectionalizing switch	Horizontal switch for disconnecting a section of a power line from the source of energy
		Vertical disconnect/ sectionalizing switch	Vertical switch for disconnecting a section of a power line from the source of energy
		Transformer or Autotransformer	Electrical device to step up or step down voltage
		Current transformer	Device used for measurement of alternating electric currents
		Voltage transformer	Device used for measurement of voltage
		Box or Control house	Booth for allocation of equipment for feeding circuit breakers with power
		Power supply to protection system	Battery providing power to boxes
		Coil support	Support for a coil, i.e. a set of windings creating an inductor or electromagnet

(continued)

Table 6.1 (continued)

Group	Sub-group	Component	Description
		Bar	Horizontal elevated bar (and support to bar) to attach lines within a station
		Pothead	Support structure to bars
		Regulator	Device designed to automatically maintain a constant voltage level
		Bus	Ensemble of bar systems to attach lines within stations
		Capacitor bank	Condenser used to store energy electrostatically and to supply huge pulses of current

Actually overhead lines are generally not considered as vulnerable elements. On the contrary, underground lines, which are scarcely diffused in Europe, can be vulnerable to ground deformations, depending on some technological features of their laying.

It has to be remarked that most authors do not explicitly distinguish between micro- and macro-components and also that authors often assign different names to the same micro-component. This distinction is made here where the internal logic of substations is modelled, i.e., partial functioning (continued service with reduced power flow) is accounted for. The corresponding modelling effort is higher than when a substation is considered as a single component with a binary state (fail/safe), but can be reduced by assembling sub-sets of micro-components that are serially arranged within the substation in order to reduce them to a single element: the macro-component. The substation layout is then composed of general (non-serial) arrangement of macro-components which can lead to partial functioning states, depending on the distribution of damage. The review in the next section will make clear how most fragility studies stick to the model of substation as a node, instead of adopting a finer internal discretization and, most importantly, using buses as nodes.

6.2 Review of Existing Fragility Functions for Electric Power System Components

Table 6.2 reports the main recent works on fragility functions of electric power system components, with the indication of the methodology used to evaluate the curves, the components considered and the damage states and indices. The fragilities are expressed in terms of PGA in all but one case (420 kV circuit breaker, Vanzi et al. 2004), in which they are function of spectral acceleration.

Deliverable Report D3.3 (Pinto et al. 2010), contains tables with the details about the fragility functions from all the works listed in Table 6.2. Here below further details are given to a selected few either because they are widely employed (HAZUS 2003) or because they present a markedly different approach in the

Table 6.2 Reviewed works on fragility curves for EPN components

Reference	Methodology	Element	Damage states and indices
Anagnos (1999)	Empirical, with two normal functions	6 electric micro-components	Failure with different failure modes depending on the considered component
Anagnos and Ostrom (2000)	Empirical, with two normal functions	500 kV circuit breaker and 230 kV horizontal disconnect switch	Failure with different failure modes depending on the considered component
Ang et al. (1996)	Empirical, with lognormal function	6 electric micro-components and 500 kV–230 kV substations	Failure based on power imbalance, abnormal voltage, unstable condition and operational power interruption
Bettinali et al. (2004)	Numerical	11 electric micro-components	Failure
Dueñas-Osorio et al. (2007)	Empirical, with lognormal function	The whole electric power grid	Failure based on substation functionality; $CL = 20$, 50 and 80 %
FEMA – HAZUS^{MH} Technical Manual (2003)	Numerical, Boolean approach	Substation, distribution circuits, generation plant and 4 micro-components	Slight/minor; Moderate; Extensive; Complete
Giovinazzi and King (2009)	Empirical (log-normal function)/ Numerical	Medium voltage substation	Slight/minor; Moderate; Extensive; Complete
Hwang and Huo (1998)	Empirical (lognormal function)/ Numerical	9 electric micro-components, pothead structure and 115/12 kV transformer	Failure
Hwang and Chou (1998)	Numerical, dynamic analyses, event tree/ fault tree	6 electric micro-components, 1 macro-component and substation	Failure
Liu et al. (2003)	Empirical, with two normal functions	500kV- 230 kV three-phase transformers	Failure
Rasulo et al. (2004)	Numerical	11 electric micro-components and substation	Failure
Shinozuka et al. (2007)	Empirical, with lognormal function	Transformer, circuit breaker, disconnect switch and bus	Failure based on imbalance of power and abnormal voltage
Straub and Der Kiureghian (2008)	Empirical (log-normal function)/ Bayesian analysis	1-phase 230 kV transformer, 230 kV live tank circuit breaker and systems of these components	Failure

(continued)

Table 6.2 (continued)

Reference	Methodology	Element	Damage states and indices
Vanzi (1996)	Numerical, FORM/SORM methods	11 electric micro-components and 4 macro-components	Failure
Vanzi (2000)	Numerical, optimization problem	Distribution substation	Failure
Vanzi et al. (2004)	Numerical, Cornell method	420 kV circuit breaker	Failure

derivation (e.g. Straub and Der Kiureghian 2008; Hwang and Chou 1998), or finally because of the unusual attempt of providing a fragility for the entire system (Dueñas-Osorio et al. 2007). Together with the fragility functions, the corresponding damage scales are presented, when significant, i.e. when more than two damage states are considered for the component at hand and its damage state directly affects the network serviceability in terms of power output. These scales do not quantify the reduction of power flow corresponding to each damage state, i.e. the functional consequence of physical damage. Actually, however, the performance of the network and even of a single station cannot be predicted without a power flow analysis, continued serviceability resulting from the interaction between various components, both inside the individual station and within the neighbouring ones, as well as from the spread of short circuits to other parts of the station and to the remaining parts of the network.

All the fragility curves presented in this chapter are in the form of lognormal cumulative distribution functions, defined in terms of the logarithmic mean λ and the logarithmic standard deviation β.

Several of the surveyed works do not report numerical parameters for the fragility curves. Given the importance of having the parameters for using these models in an infrastructure simulation analysis, such parameters have been approximately determined from percentiles graphically retrieved from the curves. This operation has been done in different ways. Where possible, i.e. for those curves reaching values from 0 to more the 0.75 in the selected *intensity measure* (IM) range, the 25th, 50th (corresponding to the median m) and 75th percentiles have been graphically retrieved from the curves. Given these three values, λ and β were determined from Eqs. (6.1) and (6.2),

$$\lambda = \ln(m) \tag{6.1}$$

$$\beta = 0.74^{*}\left[\ln\left(75^{\text{th}}\ \text{percentile}\right) - \ln\left(25^{\text{th}}\ \text{percentile}\right)\right] = 0.74^{*}IQR \tag{6.2}$$

where IQR is the interquartile range of the associated normal distribution.

For the few remaining curves, β was computed with different expressions depending on the case. These are all similar to Eq. (6.2), in which the 25th and 75th percentiles were replaced by two available percentile values, while the coefficient 0.74 was replaced by a coefficient numerically obtained from normal random sampling. The λ parameter was determined as in Eq. (6.1), with the m value read from the curve if possible, otherwise assumed in a way that the approximate curve, with a fixed value of the β parameter, results as close as possible to the original one.

The "Method" entry in the tables indicates the method employed to derive the fragility curves:

- Empirical: statistical regression on data from damage surveys in actual events, or test from laboratory;
- Numerical: uses response data from numerical simulations of the component under earthquake input.

The HAZUS methodology considers both generation plants and transmission substations as nodes of the electric power network, characterized by a set of fragility functions (one per limit state), instead of modelling their internal logic. The classification of these facilities is done based on power output for generation plants and voltage for substations. Different sets of curves are also provided for facilities with *anchored* or *unanchored* components, meaning designed with special seismic tiedowns or tiebacks, and designed with manufacturer's normal requirements, respectively. The probability of the generic facility reaching or exceeding different damage states, as defined by the damage level of its subcomponents, has been evaluated using Boolean combinations of subcomponents' damage functions. In general, such combinations do not produce a lognormal distribution, so a lognormal curve has been fitted to the resulting probability distribution.

Tables 6.3, 6.4, 6.5, 6.6, 6.7, 6.8, 6.9, 6.10, 6.11, 6.12, 6.13, 6.14, and 6.15 report the main characteristics and parameters of the fragility curves of the different types of generation plants and substations, as well as their damage scales. The curves are visualized in Figs. 6.7, 6.8, 6.9, 6.10, and 6.11.

Straub and Der Kiureghian (2008) presented an improved empirical model for the derivation of fragility curves, addressing the statistical dependence among observations of seismic performances (arising from common but unknown factors influencing the observations), as well as the statistical uncertainty associated with the resulting fragility estimates. The authors demonstrated that the improved formulation could lead to significantly different fragility estimates than those obtained with the conventional assumptions. The work deals with two electrical components, i.e. the 1-phase 230 kV transformer and the 230 kV live tank circuit breaker. Both of them are considered either as standing alone or grouped in two different ways within the substation, i.e. forming a parallel system with five components and several K-out-of-N systems (with $N = 5$ and PGA $= 0.2$ g). A K-out-of-N system consists of N components and functions if at least K of them survive, so that the extremes $K = 1$ and $K = N$ represent parallel and series systems, respectively; other equipment in the substation is assumed not to fail.

A further novelty of this work is the use of Bayesian statistics to estimate the parameters $\boldsymbol{\theta}$ of the fragility model from the set of observations $\boldsymbol{z}$, the latter

Table 6.3 Characteristics of fragility functions for generation plants and substations

Field	Value
Elements at risk	Small (less than 200 MW) and medium/large (more than 200 MW) generation plants Low voltage (34.5–150 kV), medium voltage (150–350 kV) and high voltage (350 kV and above) substations
Reference	FEMA – HAZUS^{MH} Technical Manual (2003)
Method	Numerical
Function	Lognormal, LN(λ, β)
Typology	Two typologies: (1) Anchored/seismic components (2) Unanchored/standard components
Damage states	Slight/minor, moderate, extensive, complete
Seismic intensity parameter	PGA (g)

Table 6.4 Fragility function parameters for small generation plants with anchored components

Damage state	Median (g)	λ	β
Slight/minor	0.10	−2.30	0.55
Moderate	0.21	−1.56	0.55
Extensive	0.48	−0.73	0.50
Complete	0.78	−0.25	0.50

Table 6.5 Fragility function parameters for small generation plants with unanchored components

Damage state	Median (g)	λ	β
Slight/minor	0.10	−2.30	0.50
Moderate	0.17	−1.77	0.50
Extensive	0.42	−0.87	0.50
Complete	0.58	−0.54	0.55

Table 6.6 Fragility function parameters for medium/large generation plants with anchored components

Damage state	Median (g)	λ	β
Slight/minor	0.10	−2.30	0.60
Moderate	0.25	−1.39	0.60
Extensive	0.52	−0.65	0.55
Complete	0.92	−0.08	0.55

Table 6.7 Fragility function parameters for medium/large generation plants with unanchored components

Damage state	Median (g)	λ	β
Slight/minor	0.10	−2.30	0.60
Moderate	0.22	−1.51	0.55
Extensive	0.49	−0.71	0.50
Complete	0.79	−0.24	0.50

containing data on failures and survivals of equipment items in different electrical substations during past earthquake events. In this method, the posterior distribution of $\boldsymbol{\theta}$ given the observations, f($\boldsymbol{\theta}$|z), is obtained by combining the prior distribution of $\boldsymbol{\theta}$, f($\boldsymbol{\theta}$), and the likelihood of $\boldsymbol{\theta}$, L($\boldsymbol{\theta}$|z).

Table 6.8 Damage scale for generation plants

Damage state	description	Serviceability	Power availability
Complete	Extensive damage to large horizontal vessels beyond repair, extensive damage to large motor operated valves, or the building being in complete damage state	Not repairable	No power available
Extensive	Considerable damage to motor driven pumps, or considerable damage to large vertical pumps, or the building being in extensive damage state	Operational after repairs	
Moderate	Chattering of instrument panels and racks, considerable damage to boilers and pressure vessels, or the building being in moderate damage state	Operational without repair	Reduced power flow
Slight/ minor	Turbine tripping, or light damage to diesel generator, or the building being in minor damage state		
None	None		Nominal power flow

Table 6.9 Fragility function parameters for low voltage substations with anchored components

Damage state	Median (g)	λ	β
Slight/minor	0.15	−1.90	0.70
Moderate	0.29	−1.24	0.55
Extensive	0.45	−0.80	0.45
Complete	0.90	−0.10	0.45

Table 6.10 Fragility function parameters for low voltage substations with unanchored components

Damage state	Median (g)	λ	β
Slight/minor	0.13	−2.04	0.65
Moderate	0.26	−1.35	0.50
Extensive	0.34	−1.08	0.40
Complete	0.74	−0.30	0.40

Table 6.11 Fragility function parameters for medium voltage substations with anchored components

Damage state	Median (g)	λ	β
Slight/minor	0.15	−1.9	0.6
Moderate	0.25	−1.39	0.5
Extensive	0.35	−1.05	0.4
Complete	0.7	−0.36	0.4

Table 6.12 Fragility function parameters for medium voltage substations with unanchored components

Damage state	Median (g)	λ	β
Slight/minor	0.1	−2.30	0.6
Moderate	0.2	−1.61	0.5
Extensive	0.3	−1.20	0.4
Complete	0.5	−0.69	0.4

Table 6.13 Fragility function parameters for high voltage substations with anchored components

Damage state	Median (g)	λ	β
Slight/minor	0.11	−2.21	0.50
Moderate	0.15	−1.90	0.45
Extensive	0.20	−1.61	0.35
Complete	0.47	−0.76	0.40

Table 6.14 Fragility function parameters for high voltage substations with unanchored components

Damage state	Median (g)	λ	β
Slight/minor	0.09	−2.41	0.50
Moderate	0.13	−2.04	0.40
Extensive	0.17	−1.77	0.35
Complete	0.38	−0.97	0.35

Table 6.15 Damage scale for substations

Damage state	description	Serviceability	Power availability
Complete	Failure of all disconnect switches, all circuit breakers, all transformers, or all current transformers, or the building being in complete damage state	Not repairable	No power available
Extensive	Failure of 70 % of disconnect switches (e.g., misalignment), 70 % of circuit breakers, 70 % of current transformers (e.g., oil leaking from transformers, porcelain cracked), or failure of 70 % of transformers (e.g., leakage of transformer radiators), or the building being in extensive damage state	Operational after repairs	
Moderate	Failure of 40 % of disconnect switches (e.g., misalignment), or 40 % of circuit breakers (e.g., circuit breaker phase sliding off its pad, circuit breaker tipping over, or interrupter-head falling to the ground), or failure of 40 % of current transformers (e.g., oil leaking from transformers, porcelain cracked), or the building being in moderate damage state	Operational without repair	Reduced power flow
Slight/minor	Failure of 5 % of the disconnect switches (i.e., misalignment), or failure of 5 % of the circuit breakers (i.e., circuit breaker phase sliding off its pad, circuit breaker tipping over, or interrupter-head falling to the ground), or the building being in minor damage state		
None	None		Nominal power flow

Tables 6.16, 6.17 and 6.18 report the main characteristics and parameters of the fragility curves (shown in Fig. 6.12) of the two components taken as standing alone, while Tables 6.19, 6.20, 6.21, 6.22, and 6.23 are referred to the fragility curves (shown in Figs. 6.13 and 6.14) for the two groupings of components.

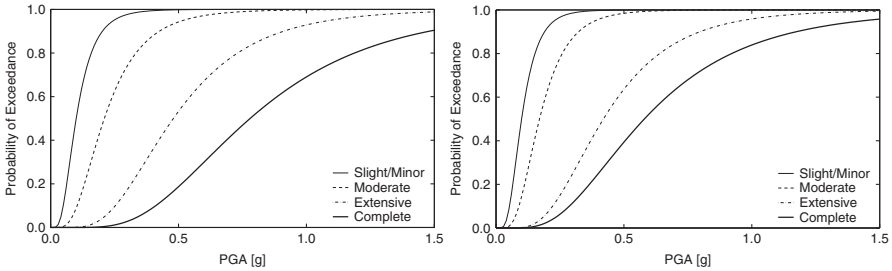

Fig. 6.7 Fragility curves for small generation plants, with anchored (*left*) and unanchored (*right components*)

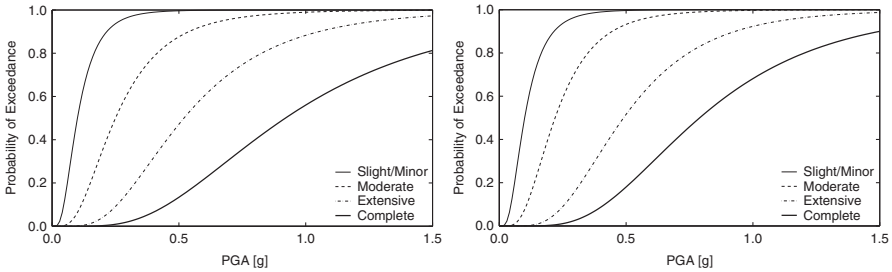

Fig. 6.8 Fragility curves for medium/large generation plants, with anchored (*left*) and unanchored (*right components*)

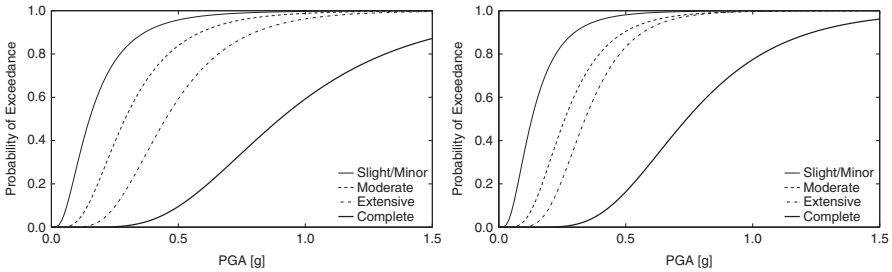

Fig. 6.9 Fragility curves for low voltage substations, with anchored (*left*) and unanchored (*right components*)

Hwang and Chou (1998) used the event tree/fault tree technique to evaluate the performance of an electric substation in the event of an earthquake. For the construction of event trees and fault trees, the substation's internal logic must be modelled. Substation 21, an important power supplier to several major hospitals in downtown Memphis, has been taken as reference. According to its internal layout, the substation is modelled consisting of many pieces of equipment, such as pothead structures, lightning arresters, switches, a control house, oil circuit breakers (OCB), transformers and regulators. Several micro-components are grouped to form

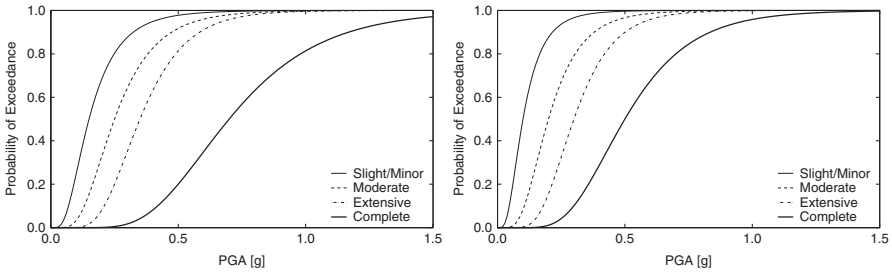

Fig. 6.10 Fragility curves for medium voltage substations, with anchored (*left*) and unanchored (*right components*)

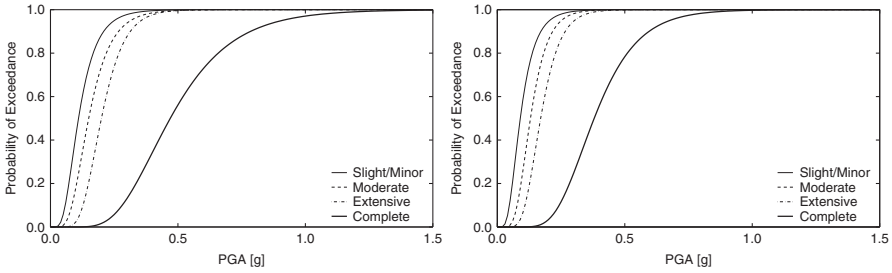

Fig. 6.11 Fragility curves for high voltage substations, with anchored (*left*) and unanchored (*right components*)

Table 6.16 Characteristics of fragility functions for 1-phase 230 kV transformers and 230 kV live tank circuit breakers

Field	Value
Elements at risk	1-phase 230 kV transformer and 230 kV live tank circuit breaker
Reference	Straub and Der Kiureghian (2008)
Method	Empirical
Function	Lognormal, LN(λ, β)
Damage states	Failure (Collapse)
Seismic intensity parameter	PGA (g)
Background	Data-set on the performance of electrical substation equipment in past earthquakes, compiled by Anagnos; Bayesian analysis

Table 6.17 Fragility function parameters for 1-phase 230 kV transformer (in this and subsequent figures, the abbreviation 'perc.' stands for percentile)

Typology of model	25th perc. (g)	Median (g)	λ	β
Traditional	0.35	0.62	−0.48	0.85
Improved	0.36	0.93	−0.07	1.41
Predictive	0.35	0.78	−0.25	1.19

Table 6.18 Fragility function parameters for 230 kV live tank circuit breaker

Typology of model	25th perc. (g)	Median (g)	75th perc. (g)	λ	β
Traditional	0.140	0.200	0.270	−1.610	0.490
Improved	0.007	0.200	–	−1.610	4.970
Predictive	0.025	0.200	–	−1.610	3.080

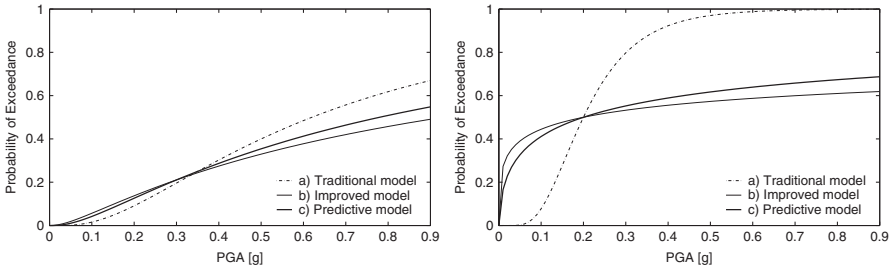

Fig. 6.12 Fragility curves for 1-phase 230 kV transformer (*left*) and 230 kV live tank circuit breaker (*right*). (**a**) statistical dependence and statistical uncertainty are both neglected (traditional model); (**b**) only statistical dependence is considered (improved model); (**c**) both effects are included (predictive model)

Table 6.19 Characteristics of fragility functions for two different groupings of 1-phase 230 kV transformers and 230 kV live tank circuit breakers

Field	Value
Elements at risk	1-phase 230 kV transformer and 230 kV live tank circuit breakers
Reference	Straub and Der Kiureghian 2008
Method	Empirical
Function	Lognormal, LN(λ, β)
Typology	Two typologies: (1) parallel systems with five components (2) K-out-of-N systems, with $N = 5$ (PGA = 0.2 g)
Damage states	Failure (Collapse)
Seismic intensity parameter	PGA (g)
Background	Data-set on the performance of electrical substation equipment in past earthquakes, compiled by Anagnos; Bayesian analysis

Table 6.20 Fragility function parameters for parallel systems with five 1-phase 230 kV transformers

Typology of model	1st perc. (g)	Median (g)	5th perc. (g)	λ	β
Traditional	0.23	2.10	0.46	0.74	1.02
Improved	0.48	1.90	0.72	0.64	0.60
Predictive	0.58	2.65	0.90	0.97	0.65

Table 6.21 Fragility function parameters for *K*-out-of-*N* systems, with $N = 5$ (PGA $= 0.2$ g), of 1-phase 230 kV transformers

Typology of model	5th perc. (g)	Median (g)	10th perc. (g)	λ	β
Traditional	2.7	5.5	3.5	1.70	0.68
Improved	–	5.5	3.8	1.61	0.43
Predictive	–	5.5	4.0	1.61	0.40

Table 6.22 Fragility function parameters for parallel systems with five 230 kV live tank circuit breakers

Typology of model	5th perc. (g)	Median (g)	10th perc. (g)	λ	β
Traditional	–	0.90	–	−0.10	2.61
Improved	0.20	2.50	0.35	0.92	1.54
Predictive	0.25	4.50	0.47	1.50	1.74

Table 6.23 Fragility function parameters for *K*-out-of-*N* systems, with $N = 5$ (PGA $= 0.2$ g), of 230 kV live tank circuit breakers

Typology of model	6th perc. (g)	Median (g)	λ	β
Traditional	–	3.00	1.10	1.75
Improved	1.10	3.00	1.10	0.65
Predictive	1.20	3.00	1.10	0.59

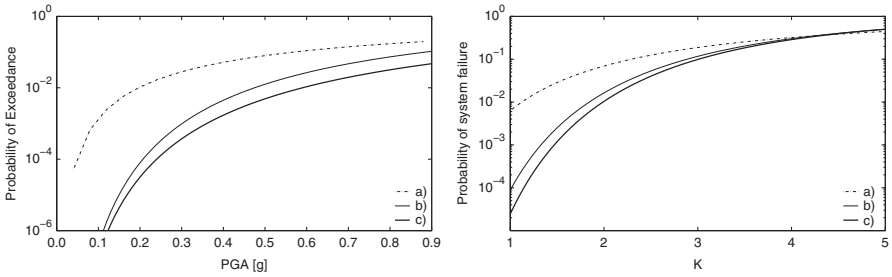

Fig. 6.13 Fragility curves for 1-phase 230 kV transformer: parallel systems with five components (*left*) and *K*-out-of-*N* systems, with $N = 5$ (PGA $= 0.2$ g) (*right*)

macro-components. The fragility curve of a macro-component is determined using the fault tree and the fragility data of micro-components appearing in the tree. In this case, the only macro-component considered is the cluster, made up of a pothead structure, six lightning arresters and a bus. Moreover, an OCB, if remotely controlled, may fail due to its own failure or damage to the control house.

Given the fragility data of macro- and micro-components, it is possible to create event trees, in order to determine the probabilities that the substation as a whole fails at various levels of ground shaking.

Tables 6.24 and 6.25 report the main characteristics and parameters of the fragility curves, which are shown in Fig. 6.15.

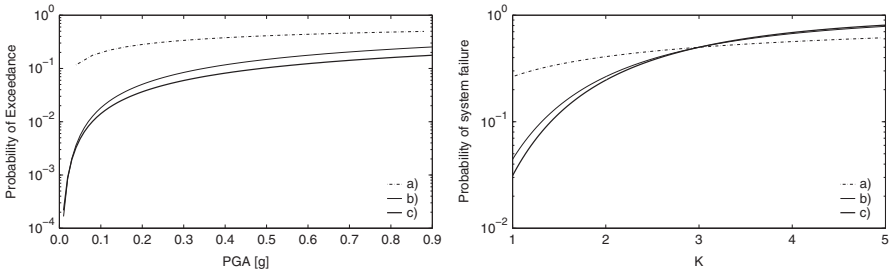

Fig. 6.14 Fragility curves for 230 kV live tank circuit breaker: parallel systems with five components (*left*) and *K*-out-of-*N* systems, with $N = 5$ (PGA $= 0.2$ g) (*right*)

Table 6.24 Characteristics of fragility functions for substations with existing and retrofitted transformers

Field	Value
Elements at risk	Substation
Reference	Hwang and Chou (1998)
Method	Numerical
Function	Lognormal, LN(λ, β)
Typology	Two typologies: (1) Substation with existing transformers (2) Substation with retrofitted transformers
Damage states	Failure (Collapse)
Seismic intensity parameter	PGA (g)
Background	Fragility data of individual components in substation 21 in Memphis

Table 6.25 Fragility function parameters for substations with existing and retrofitted transformers

Typology of substation	25th perc. (g)	Median (g)	75th perc. (g)	λ	β
With existing transf.	0.13	0.17	0.20	−1.77	0.32
With retrofitted transf.	0.55	0.67	–	−0.40	0.29

The paper by Dueñas-Osorio et al. (2007) presents fragility curves related to the whole electric power grid.

Tables 6.26 and 6.27 report the characteristics and parameters of fragility functions of power grids composed of substations having all the same voltage level. These fragilities express the probability of the system to exceed an *extensive damage* limit state. This limit state implies damage beyond short-term repair, leaving the network systems under consideration as completely non-functional. The curves are displayed in Fig. 6.16.

On the other hand, Tables 6.28 and 6.29 report the characteristics and parameters of fragility functions (displayed in Fig. 6.17) of power grids for three different damage states, corresponding to three values of Connectivity Loss (CL). In this case

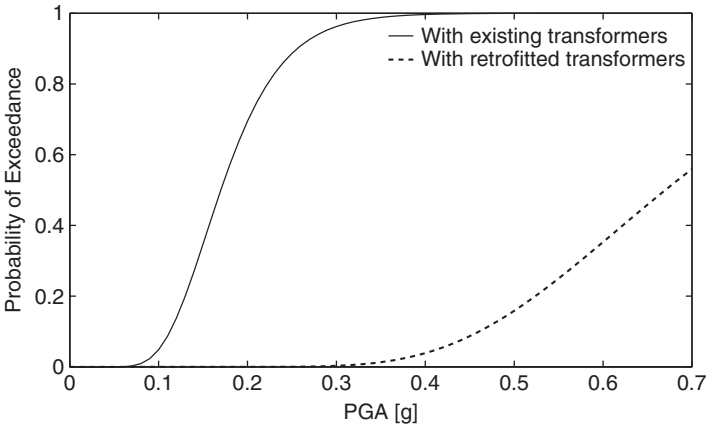

Fig. 6.15 Fragility curves for substations with existing and retrofitted transformers

Table 6.26 Characteristics of fragility functions for power grids made up of substations of different voltages

Field	Value
Element at risk	Electric power grid
Reference	Dueñas-Osorio et al. (2007)
Method	Empirical
Function	Lognormal, LN(λ, β)
Typology	Three typologies: (1) High voltage substation (more than 350 kV) (2) Medium voltage substation (150–350 kV) (3) Low voltage substation (less than 150 kV)
Damage states	Failure (Collapse)
Seismic intensity parameter	PGA (g)
Background	Empirical data from US west coast earthquakes

Table 6.27 Fragility function parameters for power grids made up of substations of different voltages

Substation voltage	25th perc. (g)	Median (g)	75th perc. (g)	λ	β
Low	0.33	0.45	0.60	−0.80	0.44
Medium	0.26	0.35	0.46	−1.05	0.42
High	0.16	0.20	0.25	−1.61	0.35

a damage scale has been derived (Table 6.30), linking the damage state to the power grid serviceability.

It has to be noted that a fragility function of the whole power grid can be considered a final result of an *ad hoc* study for a network, rather than a "portable" function which can be used for other systems. It has been reported here to give the reader a wider state of the art.

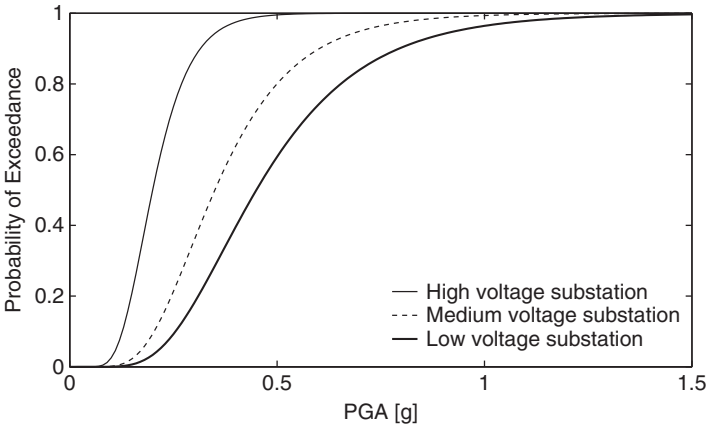

Fig. 6.16 Fragility curves for power grids made up of substations of different voltages

Table 6.28 Characteristics of fragility functions for power grids for different connectivity loss values

Field	Value
Element at risk	Electric power grid
Reference	Dueñas-Osorio et al. (2007)
Method	Empirical
Function	Lognormal, LN(λ, β)
Damage states	20 % *CL*, 50 % *CL*, 80 % *CL*
Seismic intensity parameter	PGA (g)
Background	Empirical data from US west coast earthquakes

Table 6.29 Fragility function parameters for power grids for different connectivity loss values

Connectivity loss level (%)	25th perc. (g)	Median (g)	75th perc. (g)	λ	β
20	0.08	0.10	0.11	−2.34	0.22
50	0.20	0.22	0.23	−1.54	0.10
80	0.24	0.25	0.27	−1.37	0.11

6.3 Selected Fragility Functions of Electric Power System Components for Use in SYNER-G Systemic Vulnerability Analysis

In this section an appropriate fragility function is chosen, among the available ones, for the EPN macro- and micro-components that are of interest within SYNER-G (i.e. are employed within the systemic vulnerability analysis). Such components, rather than the substation as a whole, are considered since the internal logic of substations has been modelled, according to the layouts shown in Figs. 6.5 and 6.6.

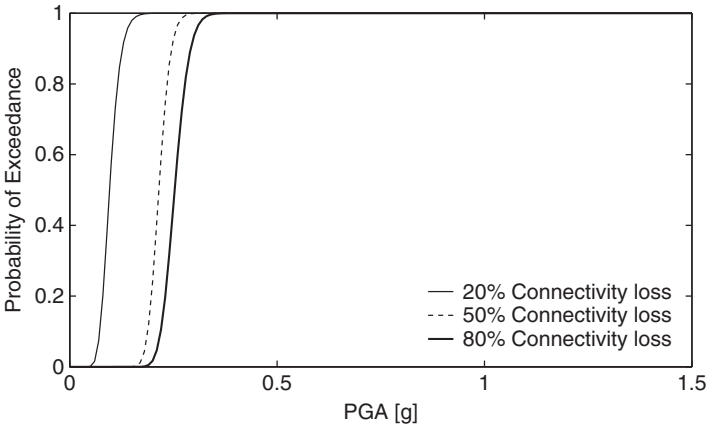

Fig. 6.17 Fragility curves for power grids for different connectivity loss values

Table 6.30 Damage scale for power grids for different connectivity loss values

Damage state	description	Serviceability	Power availability
CL = 80 %	Connectivity loss levels of CL = 20, 50 and 80 % represent three limiting states to measure the ability of the network to function properly. More precisely, they quantify the likelihood of the distribution nodes to decrease their capacity to be connected to generation nodes as function of seismic intensity	Operational after repairs	No power available
CL = 50 %		Operational without repair	Reduced power flow
CL = 20 %			
None	None		Nominal power flow

The considered macro-components are those defined by Vanzi (1996), for which only the curves retrieved by Vanzi exist.

Concerning the micro-components, the curves proposed by Vanzi (1996) have been obtained using data from shaking table tests on components installed in Italian substations. For this reason, compared with the other available curves, they appear to be the most appropriate in the European context and, hence, have been chosen within SYNER-G. The curves refer to components produced during the 80s and 90s, installed in substation of the Italian high voltage EPN (voltages ranging from 220 to 380 kV).

The macro-component cluster and the last four micro-components in Table 6.1 have not been considered, since they are installed only in US substations.

The fragility functions of generation plants proposed by HAZUS are not included in this section, meaning that such plants are considered not vulnerable in the current SYNER-G model. In fact, these stations are critical facilities and, as such, they need a detailed case by case study on their internal logic, rather than being studied as single components.

Table 6.31 Characteristics of fragility functions for macro-components

Field	Value
Element at risk	4 electric macro-components
Reference	Vanzi 1996
Method	Numerical, FORM/SORM methods
Function	Lognormal, LN(λ, β)
Damage states	Failure (Collapse)
Seismic intensity parameter	PGA (m/s^2)
Background	Fragilities of micro-components considered by the same author
Comments	The failures of interconnected vulnerable microelements are assumed as independent events

Table 6.32 Fragility function parameters for macro-components

Component	25th perc. (m/s^2)	Median (m/s^2)	75th perc. (m/s^2)	λ	β
Line without transformer	1.8	2.2	2.4	0.79	0.21
Bars-connecting line	2.0	2.4	2.6	0.88	0.19
Bars	1.2	1.5	2.0	0.41	0.38
Autotransformer line	1.5	1.8	2.3	0.59	0.32

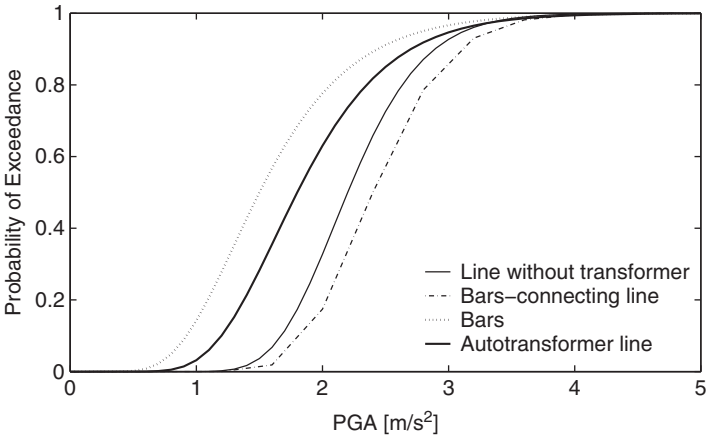

Fig. 6.18 Fragility curves for macro-components

6.3.1 Fragility Functions of Macro-Components

Tables 6.31 and 6.32 report the characteristics and parameters of fragility functions of the electric macro-components defined by Vanzi (1996), listed here for reference. Such functions are displayed in Fig. 6.18.

1. Autotransformer line (autotransformer + dischargers + current transformers + circuit breakers + horizontal sectionalizing switches + box)

2. Line without transformer (voltage transformer + coil support + horizontal and vertical sectionalizing switches + current transformer + circuit breaker + box)
3. Bars-connecting line (vertical sectionalizing switches + current transformer + circuit breaker + box)
4. Bars (voltage transformer + bar)

6.3.2 *Fragility Functions of Micro-components*

Tables 6.33 and 6.34 report the characteristics and parameters of fragility functions for the electric micro-components defined by Vanzi (1996), listed here for reference. Such functions are displayed in Fig. 6.19.

1. Coil support
2. Circuit breaker
3. Current transformer
4. Voltage transformer
5. Horizontal sectionalizing switch
6. Discharger
7. Vertical sectionalizing switch
8. Bar
9. Box
10. Power supply to protection system
11. Autotransformer

Table 6.33 Characteristics of fragility functions for micro-components

Field	Value
Element at risk	11 electric micro-components
References	Vanzi 1996
Method	Numerical
Function	Lognormal, LN(λ, β)
Damage states	Failure (Collapse)
Seismic intensity parameter	PGA (m/s^2)
Background	Cornell method
Comments	The retrieved fragility curves take into account the uncertainties about both the mechanical properties and the dynamic input

Table 6.34 Fragility function parameters for micro-components

Component	λ	β
Coil support	1.36	0.34
Circuit breaker	1.66	0.33
Current transformer	1.43	0.27
Voltage transformer	1.79	0.27
Horizontal sectionalizing switch	1.75	0.22
Discharger	2.27	0.32
Vertical sectionalizing switch	1.69	0.34
Bar	1.48	0.44
Box	2.93	0.52
Power supply to protection system	1.40	0.16
Autotransformer	3.16	0.29

Taken from Vanzi (2000)

6.3.3 Substation Fragilities Consistent with the Selected Micro-components and Layouts

The EPN model adopted in SYNER-G involves the substation's internal logic modelling, which allows for taking into account partial functionings and the short-circuit propagation. However, if a connectivity or capacitive analysis is required at a simpler level, i.e. considering substations as single components characterized by one fragility curve (e.g. as in the HAZUS approach), it is possible to obtain a curve consistent with the employed components and layouts. In particular, the fragility function for the generic load bus (Fig. 6.20) is derived from those of the micro-components, considering the bus as a series of the BS's and the BCL (macro-components), which in turn are series systems of their micro-components.

A distribution substation contains only one bus, hence its fragility is that shown in Fig. 6.20. On the other hand, a transformation/distribution substation contains two buses linked by two autotransformer lines. Including the latter in the series system introduced above allows for obtaining the substation fragility.

An analogous procedure should be applied to generation plants, in order to derive the fragility curve from those of their components. This has not been done yet at the current stage, given the lack of data about the generators' typical layouts and fragility models for their components. In place of more refined curves, the ones proposed by HAZUS can be used.

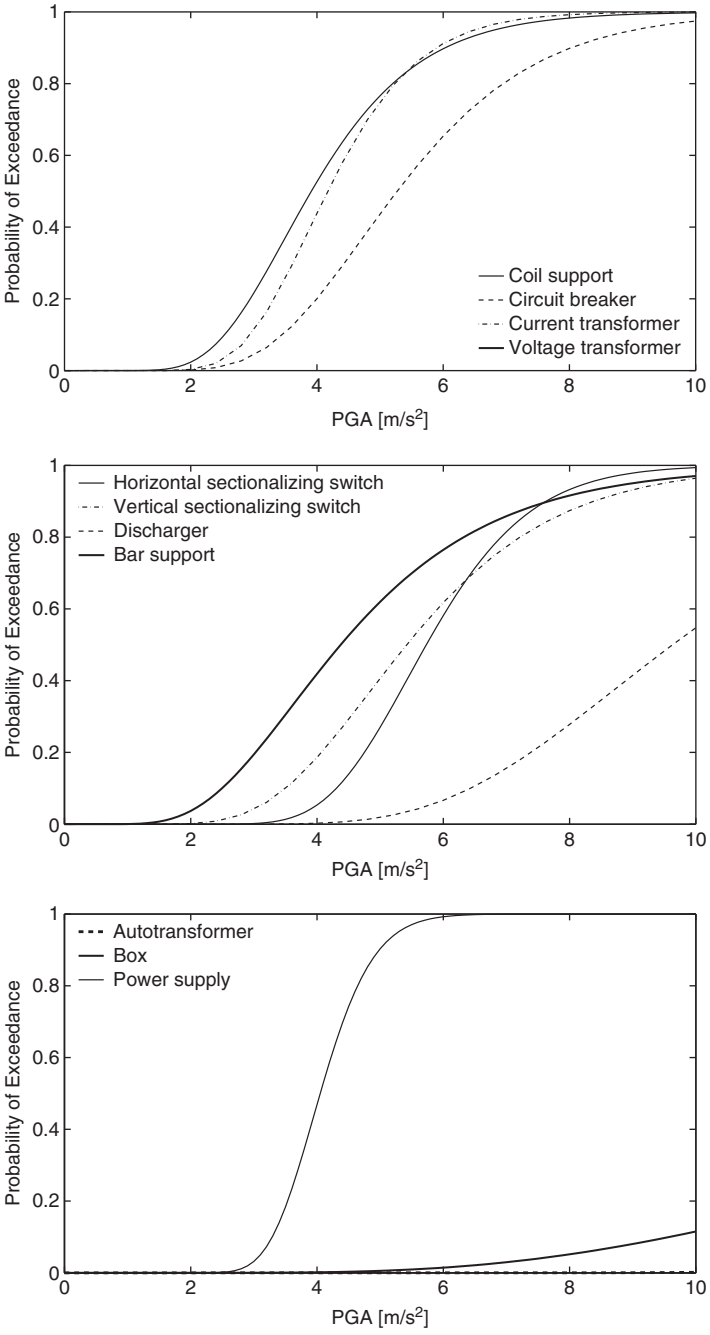

Fig. 6.19 Fragility curves for micro-components

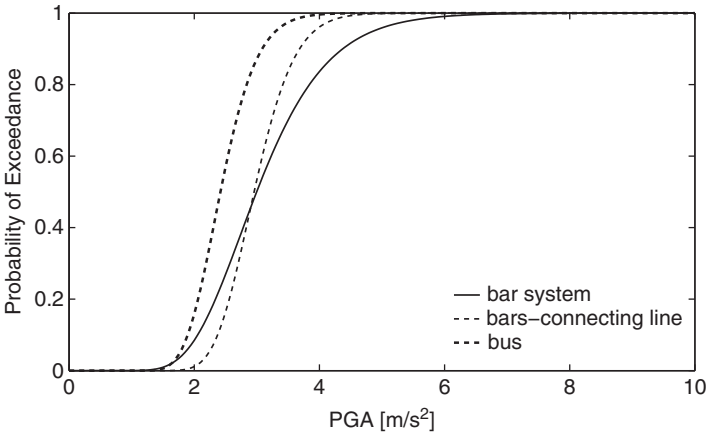

Fig. 6.20 Fragility curve for the generic load bus

References

Anagnos T (1999) Development of an electrical substation equipment performance database for evaluation of equipment fragilities. Report Department of Civil and Environmental Engineering, San Jose State University, San Jose, CA, USA, for PG&E/PEER

Anagnos T, Ostrom DK (2000). Electrical substation equipment damage database for updating fragility estimates. In Proceedings of 12th world conference on earthquake engineering, Auckland, New Zealand

Ang AH-S, Pires JA, Villaverde R (1996) A model for the seismic reliability assessment of electric power transmission systems. Reliab Eng Syst Saf 51(1):7–22

Bettinali, F, Rasulo A, Vanzi I, Imperatore S, Evangelista S (2004) Influenza dei parametri di sismicità sull'analisi affidabilistica della rete di trasmissione elettrica: applicazione ad un caso studio. In 23° Convegno Nazionale of GNGTS, Rome, Italy

Dueñas-Osorio L, Craig JI, Goodno BJ (2007) Seismic response of critical interdependent networks. Earthq Eng Struct Dyn 36(2):285–306

FEMA (2003) HAZUS^{MH} MR4 multi-hazard loss estimation methodology – earthquake model – technical manual

Giovinazzi S, King A (2009) Estimating seismic impacts on lifelines: an international review for RiskScape. In Proceedings of 2009 NZSEE conference, Christchurch

Hwang HHM, Chou T (1998) Evaluation of seismic performance of an electric substation using event tree/fault tree technique. Probab Eng Mech 13(2):117–124

Hwang HHM, Huo JR (1998) Seismic fragility analysis of electric substation equipment and structures. Probab Eng Mech 13(2):107–116

Liu G-Y, Liu C-W, Wang YJ (2003). Montecarlo simulation for the seismic response analysis of electric power system in Taiwan. In Proceedings of NCREE/JRC joint workshop, Taipei, Taiwan

Pinto PE, Cavalieri F, Franchin P, Vanzi I (2010) Fragility functions for electric power system elements. SYNER-G Deliverable Report D3.3

Poljanšek K, Bono F, Gutiérrez E (2010) GIS-based method to assess seismic vulnerability of interconnected infrastructure. A case of EU gas and electricity networks. JRC Scientific and technical reports

Rasulo A, Goretti A, Nuti C (2004) Performance of lifelines during the 2002 Molise, Italy, earthquake. Earthq Spectra 20(S1):S301–S314

Saadat H (2002) Power system analysis, 2nd edn. McGraw-Hill Primis Custom Publishing, Boston
Shinozuka M, Dong X, Chen TC, Jin X (2007) Seismic performance of electric transmission network under component failures. Earthq Eng Struct Dyn 36(2):227–244
Straub D, Der Kiureghian A (2008) Improved seismic fragility modeling from empirical data. Struct Saf 30(4):320–336
Vanzi I (1996) Seismic reliability of electric power networks: methodology and application. Struct Saf 18(4):311–327
Vanzi I (2000) Structural upgrading strategy for electric power networks under seismic action. Earthq Eng Struct Dyn 29(7):1053–1073
Vanzi I, Rasulo A, Sigismondo S (2004) Valutazione della sicurezza al sisma del sistema reti elettriche e procedura di adeguamento: fase B, fragilità dei componenti. Report Dipartimento di Progettazione, Riabilitazione e Controllo delle Strutture, University G. D'Annunzio of Chieti and Pescara, Italy, for Pricos–Cesi S.p.A., contract U0950, (in Italian)

Chapter 7
Fragility Functions of Gas and Oil Networks

Pierre Gehl, Nicolas Desramaut, Arnaud Réveillère, and Hormoz Modaressi

Abstract The present chapter aims to present and review fragility curves for components of gas and oil system networks. These fragility functions need to be applicable to the specific European context and they should be available for a variety of network components such as buried pipelines, storage tanks and processing facilities (i.e. compression and reduction stations). Based on a literature review, it is found that the available fragility functions are mostly empirical and should be applied to the European context, given the current lack of data needed to validate potential analytical methods of vulnerability assessment. For buried pipelines, fragility relations are reviewed with respect to both wave propagation and ground failure. Existing fragility curves for storage tanks and processing facilities are also critically appraised, according to the modelling assumptions and the derivation techniques (e.g. fault-tree analysis, numerical simulation or empirical relation).

7.1 Introduction

Like other utility systems, gas and oil networks are prone to sustain major physical damages, as proven by past earthquakes. However, besides the lifeline disruption, other consequences often include the pollution of waterways or the onset of fires and explosions. Therefore the accurate vulnerability assessment of gas and oil network components is of critical importance and it is to be focused on the elements

P. Gehl (✉) • N. Desramaut • A. Réveillère
BRGM, 3 avenue Claude-Guillemin, BP 36009, 45060 Orléans Cedex 2, France
e-mail: P.Gehl@brgm.fr; n.desramaut@brgm.fr; a.reveillere@brgm.fr

H. Modaressi
Formerly at BRGM, 3 avenue Claude-Guillemin, BP 36009, 45060 Orléans Cedex 2, France
e-mail: hormoz.modaressi@gmail.com

K. Pitilakis et al. (eds.), *SYNER-G: Typology Definition and Fragility Functions for Physical Elements at Seismic Risk*, Geotechnical, Geological and Earthquake Engineering 27,
DOI 10.1007/978-94-007-7872-6_7,

that are vital to the network operation, namely the piping system, and the storage and processing facilities. In the SYNER-G project (SYNER-G 2009–2013), the identification of specific typologies that may be representative of the European context has been especially carried out through three gas networks (Thessaloniki in Greece, Vienna in Austria and the L'Aquila area in Central Italy).

In the light of post-earthquake damage observations, it is possible to identify the damaging mechanisms for each of the components, depending on the type of seismic action (i.e. transient ground motion or permanent ground deformation) or the component typology (e.g. ductile or brittle pipelines). Relevant intensity measures (IM) and damage scales have also to be selected in order to ensure a proper integration of the fragility functions with the SYNER-G general methodology. However, the physical damage states that can be sampled from fragility curves may also present some shortcomings, since it appears that there is not straightforward correlation between the damage level (i.e. usually based on monetary consideration, like the cost to replace or repair the component) and its immediate consequences on the network operations.

Based on these considerations, a critical review of existing fragility functions for pipelines, storage tanks and processing facilities is then made. Some recommendations are given on which functions can be applied to European typologies, according to a series of criteria: intensity measure, derivation technique (e.g. empirical, numerical, Bayesian, fault-tree analysis), quality of the data used and modelling assumptions. Finally, some limitations and gaps with respect to the identified typologies are discussed.

7.2 Identification of the Main Typologies

The various elements composing the gas and oil transportation and distribution networks can be roughly classified into three categories, i.e. the actual edges of the network (pipelines), the storage tanks and finally the different facilities that perform specific operations such as pressure control or pumping.

7.2.1 Pipelines

The first typological distinction that can be made for pipelines is whether they are buried or elevated above ground, usually on a steel or concrete support. Since buried pipelines are the most typical means of transportation for hydrocarbon products – especially around inhabited areas –, the present chapter will mostly emphasize on this typology.

Table 7.1 Most common types of materials and connections used in the design of buried pipelines

Material type	Connection type
Asbestos-cement (AC)	Arc welded
Cast iron (CI)	Bell and spigot
Ductile iron (DI)	Cemented
Concrete (C)	Riveted
Polyvinyl chloride (PVC)	Rubber gasket
Welded steel (WS)	Gas welded
Medium density polyethylene (MDPE)	
High density polyethylene (HDPE)	

Natural gas networks are operating at various pressures, depending on their scale:

- supra-regional transmission pipelines: these pipelines operate at very high pressure (~100 bar) and present large diameters (up to 1.40 m). Such pipelines can cover large areas (e.g. from West Siberia to Europe, from Norway to France);
- regional transmission/distribution pipelines: these pipes still operate at high pressure (from 1 to 70 bar) and are used to connect local distribution systems;
- local distribution pipelines: these smaller pipelines usually operate in the medium (0.1–4 bar) or low-pressure (<0.1 bar) range.

Therefore the design pressure of the different pipeline types will influence a set of typological features and mechanical standards, namely:

- material type,
- material strength,
- diameter,
- wall thickness,
- smoothness of coating,
- type of connection,
- design flow.

Among the criteria listed above, the material and the connection types are of crucial importance, since they govern the behaviour and the potential failure modes of buried pipelines in the case of an earthquake. Reports from American Lifeline Alliance (ALA 2001) and HAZUS (NIBS 2004) have detailed some of the most common types of materials and connections used for buried pipelines (see Table 7.1). Finally, another relevant criterion to classify pipelines might be the age or the corrosion state, as shown by the poor performance of ancient pipelines in past earthquake events (ALA 2001).

While Table 7.1 details a series of materials that are mostly suitable for water or waste-water transport, pipelines specifically designed for oil and gas are more likely to be made of ductile materials such as steel or PVC. Also, another specific material type is polyethylene (medium or high density, i.e. MDPE or HDPE), which is used in more recent networks due to its high ductility.

For instance, in the case-study areas considered in the SYNER-G project, some specific typologies have been identified, as shown in Table 7.2.

Table 7.2 Main features of some pipeline networks identified in the SYNER-G project

Area	Network	Pressure (bar)	Material	Diameter (mm)
Greece (Thessaloniki)	Transmission	19	WS	100–250
	Distribution	4	PVC	125–160
Austria (Vienna)	Supra-regional	84	WS	200–1,400
	Transmission	16	PVC	–
	Distribution	1	PVC	–
Italy (L'Aquila)	Transmission	64	WS	104
	Distribution	2.5–3	WS/HDPE	25–300/32–400
	Distribution (local)	0.025–0.035		

7.2.2 Storage Facilities

A first distinction can be made between underground and surface storage facilities. Sub-surface facilities for natural gas storage are usually used to balance seasonal variations in demand (i.e. between the heating and non-heating periods). These facilities are located 100 m below the surface and they are usually natural geological reservoirs, such as depleted oil or gas fields or salt caverns.

Aside from underground storage facilities, natural gas is usually stored while in its liquefied state (LNG) in specific LNG tanks: they can represent huge facilities, making them too specific objects for a statistical fragility analysis.

On the other hand, oil storage tanks are atmospheric reservoirs (i.e. vertical cylindrical tanks), which are often categorized by the following features:

- material: steel or reinforced concrete,
- construction type: at grade or elevated,
- anchored or unanchored,
- roof type,
- capacity,
- shape factor: height-on-diameter ratio,
- amount of content in the tank: full, half-full, empty.

The most common typologies are usually based on the material type, the construction type and the anchorage of components. Finally, it should be noted that tanks are just a part of the storages facilities, which include also components like inlet/outlet pipelines or mechanical equipment.

7.2.3 Processing Plants/Stations

In the case of the gas network, processing stations can be first classified according to their function within the system, i.e. compression, metering or pressure reduction.

Compressor stations are used to supply the gas with a given amount of pressure or energy to keep it flowing. They are located along the transmission lines to ensure the transport over long distances and around the storage facilities in order to inject the gas into the distribution network.

Fig. 7.1 Pictures of the outside (*left*) and inside (*right*) of a RE.MI cabin (Esposito et al. 2013)

This type of station usually includes one or more compressor units, auxiliary equipment for secondary functions (i.e. power generation or cooling of discharge gas) and a SCADA (Supervisory Control And Data Acquisition) system. Most of these stations are housed in low-rise buildings and the following features are often used to identify the typologies:

- with anchored or unanchored components,
- within low-rise buildings, made of masonry or reinforced concrete.

For instance, in some European countries like Greece, compressor stations are usually housed in low-rise RC buildings with anchored components.

Metering/Pressure reduction stations (M/R stations) are used to control the amount and quality of the gas flowing through the lines. They usually include a pressure reduction facility in order to set the gas pressure at the required level for industrial or commercial use. Usually such stations include the following features:

- gas pre-heating,
- gas-pressure reduction and regulation,
- gas odorizing,
- gas-pressure measure,
- control through a SCADA system.

These stations have very strong specificities depending on the area where they are located. For instance, in central Italy (i.e. the L'Aquila area), these M/R stations are referred to as RE.MI cabins (i.e. "REgolazione e MIsura" in Italian, see Fig. 7.1) and they are housed in one-storey RC buildings with steel roofs, without any SCADA system (Esposito 2011; Esposito et al. 2013).

These large disparities and the specificities of the operations performed within M/R stations prevent them from being included in the same typology as the compressor stations.

Reduction groups are very local stations that reduce the gas pressure to the level of the distribution network for individual houses. They are the last step of the transmission-distribution chain. They consist in small equipment that can be buried, sheltered in a kiosk or housed within a building. Again, in central Italy, these reduction groups are referred to as GR stations (i.e. "Gruppi di Riduzione" in Italian)

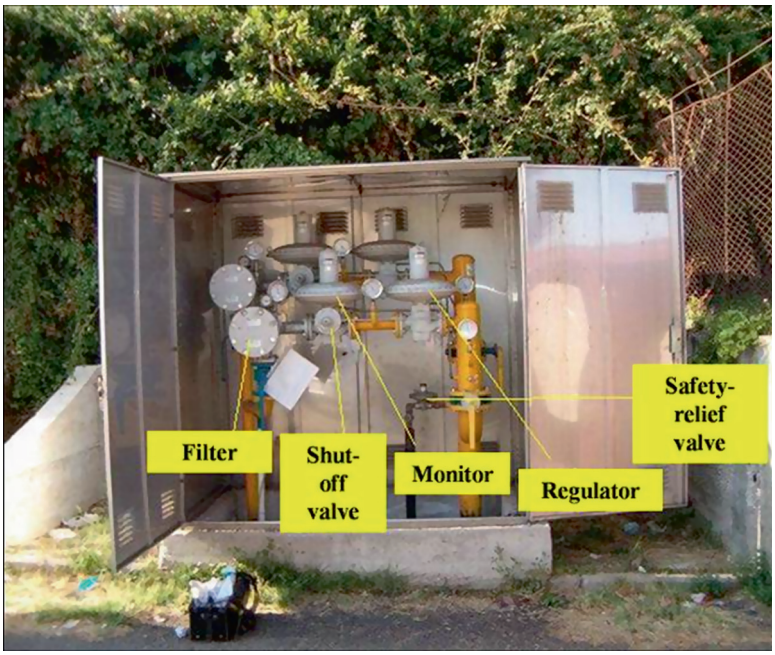

Fig. 7.2 Picture of a GRF station (Esposito et al. 2013)

(Esposito 2011; Esposito et al. 2013). Depending on the amount of gas and level of service pressure required by the end user, and depending on whether or not a final node is included in the system, three types of RG exists in L'Aquila gas network:

- (1) Reduction and measure groups (i.e. GRM), located along the medium-pressure network and directly connected to large-pressure users;
- (b) Reduction groups that are smaller than GRM (i.e. GRU), for medium-pressure users connected to the final node of a medium-pressure system;
- (c) Final reduction groups (i.e. GRF), connected to the low-pressure network (see example in Fig. 7.2).

Pumping stations along oil pipelines can be assimilated to the same typology as gas compression stations, pumps and compressors possessing very similar characteristics and functionalities.

7.3 Description of Damage Mechanisms and Failures Modes

The various elements composing gas and oil networks are sensitive to very different seismic intensity measures (e.g. acceleration or displacement), depending on their very nature (e.g. buried or at-grade elements, ductile or fragile materials...). Therefore the following section is devoted to the description of the various damage mechanisms that can impact the network components.

Table 7.3 Overview of the two main types of damage mechanisms affecting buried pipelines

	Ground failure	Transient ground deformation
Hazard	Surface faulting, liquefaction, landslides	R-waves, S-waves
Intensity measure	PGD (permanent ground deformation)	PGA, PGV, strain
Spatial impact	Local and very site-specific	Large and distributed

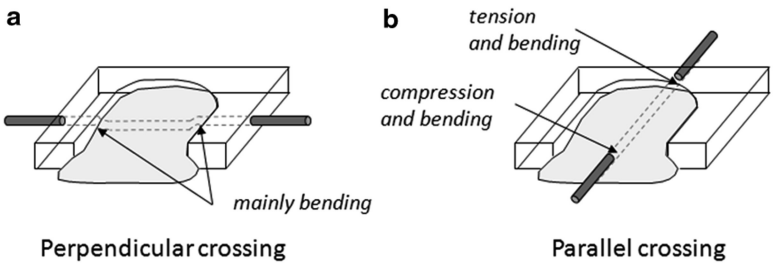

Fig. 7.3 Pipeline damage in (**a**) perpendicular and (**b**) parallel crossings of a lateral spread (Adapted from Rauch 1997)

7.3.1 Damage Mechanisms of Buried Pipelines

Like many other underground components, buried pipelines are very sensitive to permanent ground deformation (resulting from various types of ground failures), in addition to transient ground deformation due to seismic wave propagation: the characteristics of these physical phenomena are summed up in Table 7.3. Indeed, according to Eguchi (1987), past earthquakes have caused significant damages to underground pipelines throughout the world, mainly due to faulting, landslides or liquefaction (Hall 1987).

7.3.1.1 Damage from Permanent Ground Deformation

The first sign of damage to buried pipelines is the 1906 San Francisco earthquake, which resulted in significant fires through the city, due to the rupture of water lines needed by fire-hydrants. Regarding the causes of damage, according to O'Rourke and Liu (1999), only around 5 % of the area that was affected by strong ground shaking was subjected to lateral spreading, yet approximately 50 % of all pipeline failures occurred within one city of these zones, thus showing the high impact of ground failure on pipeline damage.

Damage to buried pipelines induced by permanent ground deformation is usually the main source of failure, as shown by numerous examples of past earthquakes: 1952 Kern County, 1964 Niigata, 1964 Alaska, 2007 Niigata and 2011 Christchurch earthquakes. During the 1971 San Fernando earthquake, the steel pipeline system withstood significant ground shaking, yet it was damaged by abrupt vertical or lateral dislocations or ground ruptures: lateral spreading (Fig. 7.3) induced severe

damages during that earthquake (EERI 1986; O'Rourke and Trautmann 1981; O'Rourke 1988). Regarding liquefaction, a good example is the 1964 Niigata earthquake, where the average failure ratio for one of the pipeline systems was as high as 0.97 per km, with all kinds of failure types (e.g. pipe body breaks, weld breaks, joint separations).

7.3.1.2 Damage from Transient Ground Motion

O'Rourke and Ayala (1990) report that a few earthquakes have induced damages to pipelines only by the effect of seismic wave propagation, such as the 1985 Michoacan earthquake, which damaged a large corrosion-free modern continuous steel pipeline, or the 1989 Loma Prieta earthquake. Yet, in most cases, it appears that seismic wave propagation damaged mainly pipelines that were previously weakened either by corrosion or welds of poor quality (EERI 1986). Other events, like the 1994 Northridge, 1995 Kobe, 1999 Kocaeli or 1999 Chi-Chi earthquakes, confirmed the relative vulnerability of piping systems to strong ground motions and the somewhat good performance of recent welded-steel pipes with respect to seismic wave propagation.

As a result, the emphasis is put on the ductility of pipes and the quality of weld when building earthquake resistant piping systems: still, pipe welds or joints seem to be the most vulnerable parts of this component.

7.3.1.3 Identification of Failure Modes for Buried Pipelines

Continuous pipelines like welded-steel pipes usually fail due to compressive strains that induce buckling of the pipe body, or warping and wrinkling of the pipe wall (ALA 2001). This deformation may not generate leakage, yet the modification of the pipe cross-section may produce disruption of the gas/oil flow. A crucial factor for the resistance of continuous pipelines is the quality of the welds, as past studies have shown that pipes constructed before the 1930s with poor quality welds experienced damages mostly at the joint locations.

Segmented or jointed pipelines usually consist of rigid pipe segments (e.g. cast-iron or concrete, which are not used in gas networks) connected through loose or flexible joints. Three main failure modes have been identified for this typology (ALA 2001): tensile and bending deformations of the pipe barrel, excessive rotation of a joint, and pull-out of the joint (Singhal 1984). This pipeline type is however much less frequent in oil/gas piping networks.

Aside from these usual failure modes, a piping system is more vulnerable at discontinuities like pipe elbows, tees, in-lines valves or connections to adjacent structures (storage tanks, racks, facilities, etc.): high stresses are especially concentrating at these anchor points and rigid locations (ALA 2001). Also, corrosion has the effect of decreasing the wall thickness and creating heterogeneous zones that may lead to stress concentrations.

7.3.2 Damage Mechanisms of Storage Tanks

Damage to atmospheric storage tanks (i.e. vertical cylinders) has also been quite extensively documented in past earthquakes (EERI 1986). Damage reports from past earthquakes indicate that unanchored tanks seemed to be the most vulnerable ones, together with vertical cylinders tanks with a large height-to-diameter ratio (EERI 1990). The inherent vulnerability of most storage tanks is also aggravated by the amount of liquid stored, as full tanks are subject to larger lateral forces and overturning moments due to liquid sloshing, which can also damage the tank roof. As a result, failure modes of storage tanks are usually characterized using the following classification (NZNSEE 1986; Kennedy and Kassawara 1989; ALA 2001):

- *shell buckling*: it is one of the most common forms of damage in steel tanks. It is expressed via an outward buckling of the bottom shell courses ("elephant foot") that can sometimes occur over the full circumference of the tank. This phenomenon may lead to the loss of the content due to rupture of the welds, and less frequently to the total collapse of the tank.
- *roof damage*: ground shaking may induce oil sloshing inside the tank. When tanks are full or nearly full, this sloshing motion generates an upward pressure distribution against the tank roof. This may cause a rupture of the joints between the wail and the roof, leading to a spillage of tank contents over the tank walls. Observations from past earthquakes show that floating roofs have generally endured more severe damage than fixed steel roofs.
- *anchorage failure*: many tanks are anchored with steel braces or bolts, but it is still possible that these anchors may be pulled out or stretched by the seismic load. However, the failure of anchoring components does not necessary imply the loss of the tank contents.
- *tank support system failure*: this failure mode is specific for above-grade tanks, elevated by steel columns or frames. Even if the failure of the supporting system often leads to complete loss of contents, this issue is of less concern to large oil storage tanks, which are usually built at grade.
- *foundation failure*: this phenomenon can be common in the case of poor foundation conditions prone to liquefaction, resulting in base rotation and important settlements. In the case of unanchored tanks, tensile stress can also generate uplift displacement of the tank base, separating it from the baseplate.
- *hydrodynamic pressure failure*: ground shaking generates pressures between the fluid and the tank walls, thus resulting in tensile hoop stresses. The induced loads may then lead to splitting of the wall and leakage, especially in the case of steel tanks with riveted joints.
- *connecting pipe failure*: this is one of the most common failure modes that can induce a total loss of the tank contents. The fracture of the pipes at the connections to the tank results from differential displacement between the piping and the tank (uplift displacements, foundation failure).
- *manhole failure*: because of significant stresses against the manhole cover, the latter can fail which results in loss of content through the opening (Fig. 7.4).

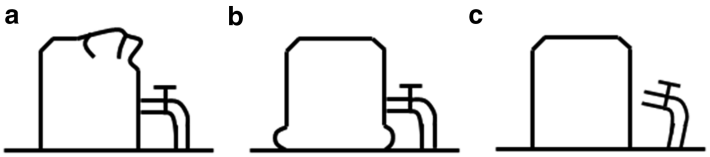

Fig. 7.4 Schematic view of some of the most common failure modes of storage tanks: (**a**) roof damage due to sloshing, (**b**) elephant's foot buckling and (**c**) disconnection of inlet/outlet piping

7.3.3 Damage Mechanisms of Processing Plants/Stations

Reports from previous earthquakes mention limited examples of damaged support facilities (EERI 1986), since it is usually found that modern facilities (compression stations, pumping stations, control stations, etc.) that are built according to seismic codes with anchored equipment exhibit good resistance to ground shaking. The anchorage of subcomponents is especially a crucial point, as unanchored equipment can lead to the rupture of electrical connections or the tipping and sliding of mechanical parts. As a result, support facilities are less documented with respect to their damages and the associated failures modes. However, failure of the various components of these facilities may be used to identify the global damage mechanism:

- *building*: the collapse of the structure sheltering the facility may damage the equipment with falling debris;
- *pump/compressor*: this key element is connected to the piping system and its failure, due to sliding or rocking if unanchored, can generate leakage or breakage of the pipe;
- *electrical/mechanical components*: these miscellaneous components, which are essential for the compressor to operate, can also be damaged if not anchored;
- *electric power supply*: external power can be shut down because of the electric power network disruption, or the connection failure between the power lines and the facility building. However, most facilities are equipped with backup power generators.

Regarding in-line valves, many types are found along the piping network (gate valves, butterfly valves, check valves, ball valves, etc.) and they can be either buried with the pipeline or located in underground concrete vaults. Finally, SCADA equipment includes many components (instrumentation, power supply, communication components, vaults, etc.). For hardware located in metal cabinets, the main observed damages comprise batteries falling over, circuit boards dislodging and gross movement of the cabinet enclosure (ALA 2001). Regarding pressure/flow measuring instruments, ground shaking is likely to induce air bubbles that can provoke false reading.

Table 7.4 Solutions for longitudinal ground strain as a function of incidence angle θ, particle velocity v_p and apparent wave propagation velocity c (St John and Zahrah 1987; Hashash et al. 2001)

Wave type	Longitudinal strain	Maximum longitudinal strain
P wave	$\varepsilon_P = \frac{v_{pP}}{c_P} . \cos^2\theta$	$\varepsilon_P = \frac{v_{pP}}{c_P}$ for $\theta = 0°$
S wave	$\varepsilon_S = \frac{v_{pS}}{c_S} . \sin\theta . \cos\theta$	$\varepsilon_S = \frac{v_{pS}}{2c_S}$ for $\theta = 45°$
R wave	$\varepsilon_R = \frac{v_{pR}}{c_R} . \cos^2\theta$	$\varepsilon_R = \frac{v_{pR}}{c_R}$ for $\theta = 0°$

7.3.4 Key Modelling Issues

This section details some of the specific characteristics that must be accounted for when modelling the different network components in the frame of a numerical analysis.

7.3.4.1 Buried Pipelines

Analytical modelling of the behaviour of buried pipelines submitted to ground motion requires taking the whole [pipeline-soil] system into account. Since inertia forces are not relevant in the case of buried components, the seismic action has to be represented in terms of ground strain: the longitudinal strain is usually acknowledged to have the most impact on the failure of pipelines. While assuming a constant shape for a single surface wave, the peak horizontal ground strain ε_p can be expressed as the following (Newmark 1967; Newmark and Rosenblueth 1971), where v_p is the peak horizontal particle velocity and c the apparent wave propagation velocity with respect to the surface:

$$\varepsilon = \frac{v_p}{c} \tag{7.1}$$

Using this formulation, St John and Zahrah (1987) proposed solution to estimate longitudinal ground strain with respect to incidence angle θ, for different types of waves (see Table 7.4). It can be observed that the longitudinal strain is maximal when the wave incidence is parallel for P- and R- waves, and oblique (i.e. $\theta = 45°$) for S-waves.

The particle velocity can then be assimilated to the PGV, thus providing a relation between the seismic ground motion and the resulting ground strain, allowing for instance back-analysis of past earthquakes to get an estimate of the maximum ground strain. Moreover, it is also possible to obtain a relation between the permanent ground deformation (PGD) and the ground strain, using for instance pre- and post-earthquake photogrammetric analyses: therefore this enables to use a single measure to characterise both phenomena (i.e. transient deformation and ground failure) and to propose a consistent fragility relationship for all types of event (O'Rourke and Deyoe 2004).

Finally, the analysis of the connections between the pipe segments and the influence of the wave incidence angle with respect to the pipe alignment should also be given special care in the fragility analysis.

7.3.4.2 Storage Tanks

In the case of vertical cylinder tanks, one key issue consists in the fluid–structure interaction that may influence the global behaviour of the tank under dynamic excitation (i.e. sloshing of fluid may modify the response of the tank walls and even induce damage). For instance, empirical observations and structural analyses have shown that tanks whose filling level is greater than 50 % are more vulnerable to earthquakes (Salzano et al. 2003), while the height-over-radius ration constitutes also an important factor for the seismic response of tanks.

The presence or not of anchorage of the tank to its base will also greatly condition the outcome of the analysis, since an unanchored tank may be subject to sliding and rotating on its base, making it unusable while the tank structure itself may still be intact. The same comment can also be made regarding the equipment servicing the storage tank (i.e. inlet/outlet pipes): these subcomponents should be considered in the analysis, since they could easily get torn apart from the main structure, rendering it once again unusable.

7.3.4.3 Processing Plants/Stations

Support facilities are usually sheltered in a small building and a first level of analysis consists of only considering the fragility of the building (i.e. if there is extensive damage to the building, the facility is considered non-functional). However, it is the damage to the mechanical or electrical components within the building that should be considered, as they have a fair chance to rupture or get disconnected, especially if they are unanchored. A distinction between the acceleration- or displacement-sensitive components should first be made and the various building response parameters should be estimated at each story (e.g. both floor and roof accelerations or displacements in the case of drift-sensitive equipment). The different configurations of equipment that may exist within a given station would make this type of analysis very case-specific however.

7.4 Review of Existing Fragility Functions and Gaps

This section is devoted to a description of the most common fragility functions that are available in the literature, along with their associated intensity measures and damage scales.

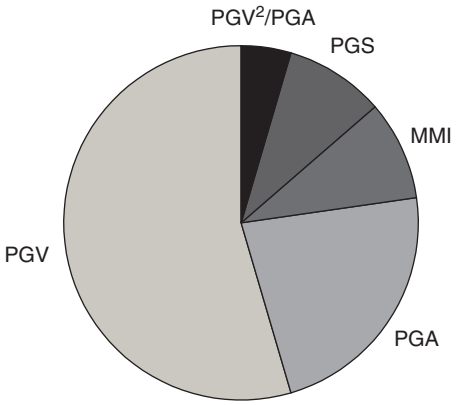

Fig. 7.5 Relative proportions of the IM types used in common fragility functions

7.4.1 Definition of Adequate Intensity Measures

A short review of some commonly used intensity measures is proposed for the different components of oil and gas networks.

7.4.1.1 Buried Pipelines

Existing fragility relations considering the effect of wave propagation consider a variety of intensity measures such as PGA, PGV, PGV^2/PGA, PGS (peak ground strain) or MMI (macroseismic intensity). The proportions of the IMs used in the reviewed fragility functions are summed up in Fig. 7.5.

It is observed that a wide majority of the fragility relations use the PGV as an intensity measure: this choice is in line with the conclusions of Sect. 7.3.4.1, in the sense that there is a direct link between the longitudinal ground strain and the PGV. Recent studies have even started to propose the peak ground strain (PGS) as a more adequate intensity measure. However, the use of PGV still seems to remain popular, due to its straightforward computation, using for instance a recorded signal or a ground-motion prediction equation, as opposed to the ground strain.

It can be also noticed that most fragility relations do not consider the direction of the pipe whereas it is acknowledged that the longitudinal strain is responsible for the failures. This is justified because once used on the distribution network of a study case, these relations are applied to a large number of pipelines that can be assumed to be randomly oriented.

In the case of damage due to ground failure, all existing fragility relations use the permanent ground deformation (PGD) as the intensity measure. However, it is worth noticing that the study by O'Rourke and Deyoe (2004) has established a good correlation between ground strain and repair rate for both transient and permanent deformations, thus also allowing the use of ground strain as an intensity measure in the case of permanent ground failure.

7.4.1.2 Storage Tanks

Past studies on the vulnerability of storage tanks usually propose PGA as the earthquake descriptor used to define the fragility curves. This seems to be a reasonable choice as this acceleration-driven parameter is appropriate to account for the inertia forces inherent to these large and usually tall structures and the liquid contents within the tanks.

7.4.1.3 Processing Plants/Stations

As most facilities are sheltered in a building, a commonly-used parameter is the PGA, since it is widely used to describe the fragility of RC or masonry buildings. Also, the behavior of anchored or unanchored components within the facility seems acceleration-driven and their fragility are indeed expressed with respect to PGA in HAZUS (NIBS 2004).

7.4.2 Definition of Damage Scales

Damage scales are defined for each of the components considered here, in order to identify the possible damage states that have to be included in the analysis.

7.4.2.1 Pipelines

Damage to pipelines is commonly expressed in repair rate (*RR*), i.e. number of repairs per unit of length (usually in km). For a give pipeline tract of length *L* with a given *RR*, the probability to get a total number of *n* repairs over the pipeline length is then estimated through a Poisson distribution:

$$P(N = n) = \frac{(RR.L)^n}{n!}.e^{-RR.L} \tag{7.2}$$

The repair rate does not make any distinction on the type of repair or their severity: this is due to the fact that most of the fragility relations for pipelines rely on empirical data that do not usually include the nature of the repairs. However, according to HAZUS (NIBS 2004), the type of repair or damage depends on the type of hazard: a damaged pipe due to ground failure is more likely to present a break (it is assumed 80 % breaks and 20 % leaks), whereas ground shaking may induce more leak-related damages (e.g. 20 % breaks and 80 % leaks). Finally, using the HAZUS assumption and considering the type of hazard, it is possible to assess the probability to have a pipe break or a pipe leak along the length of the segment (see Table 7.5).

Table 7.5 Proposed damage states for pipeline components

Damage state		Damage description
DS0	No damage	No leak or break
DS1	Leakage	At least one leak along the pipe length
DS2	Failure	At least one break along the pipe length

Table 7.6 Damage states proposed by HAZUS (NIBS 2004) and O'Rourke and So (2000)

Damage state		Damage description
DS1	None	No damage to tank or inlet/outlet pipes
DS2	Slight/minor	Damage to roof other than buckling, minor loss of contents, minor damage to piping, but no elephant's foot buckling
DS3	Moderate	Elephant's foot buckling with minor loss of content, buckling in the upper course
DS4	Extensive	Elephant's foot buckling with major loss of content, severe damage, broken inlet/outlet pipes
DS5	Complete/collapse	Total failure, tank collapse

Table 7.7 Comparison of failure modes and resulting loss of contents (ALA 2001)

Most common damage modes	Repair cost (% of tank value)	Content loss (%)
Rupture of drain pipe	1–2	50–100
Rupture of overflow pipe	1–2	0–2
Rupture of inlet/outlet pipe	1–5	100
Rupture of bottom plate from bottom course	2–20	100
Roof system partial damage	2–20	0–10
Roof system collapse	5–30	0–20
Upper shell buckling	10–40	0–20
Elephant's foot buckling with no leak	30–80	0
Elephant's foot buckling with leak	40–100	100

7.4.2.2 Storage Tanks

Fragility curves from the literature, whether they are empirical or analytical, usually propose the same number of damage states (i.e. five, including "no damage") and very similar definitions (O'Rourke and So 2000; ALA 2001; NIBS 2004; Berahman and Behnamfar 2007). The detailed damage states used by HAZUS (NIBS 2004) and O'Rourke and So (2000) are presented in Table 7.6.

The damage states definition by ALA (2001) is very similar, apart from the inclusion of upper course buckling in DS3 and of inlet/outlet pipes damage in DS4.

However, the damage states presented above are based on direct economic losses (i.e. percentage of the tank replacement cost), whereas Table 7.7 shows that there is no obvious correlation between this criterion and the functionality of the tank.

Thus, a rupture of an inlet/outlet pipe would only generate repair costs of 1–5 % of the total tank value, but this would put the tank completely out of service. Therefore we can assume that, as soon as damage state DS2 (e.g. damage to piping) is reached, the functionality of the tank may be totally lost, at least for a short amount of time.

Table 7.8 Damage states definitions for tank farms, according to HAZUS methodology (NIBS 2004)

Damage state		Damage description
DS1	None	Fully functional
DS2	Slight/minor	Malfunction of tank farm for a short time (less than 3 days) due to loss of backup power or light damage to tanks
DS3	Moderate	Malfunction of tank farm for a week or so due to loss of backup power, extensive damage to various equipment, or considerable damage to tanks
DS4	Extensive	Extensive damage to tanks or elevated pipes
DS5	Complete	Complete failure of all elevated pipes, or collapse of tanks

As an alternative, the HAZUS methodology proposes to consider not only the physical tank body (NIBS 2004), but the whole system needed to deliver the contents to the pipeline network: tank body, elevated pipes, commercial power, backup generators, electrical/mechanical equipment... Accounting for the role of each component, a damage scale that can be somewhat linked to functionality/serviceability indicators is presented in Table 7.8.

7.4.2.3 Processing Plants/Stations

If the damage to support facilities is simply addressed by considering the vulnerability of the building that shelter them, then the associated damage scale is just the same as the one of the corresponding building (e.g. see Ghobarah 2004; Rossetto and Elnashai 2003; NIBS 2004).

On the other hand, if the emphasis is put on the mechanical or electrical components within the facility, then a global damage scale has to be derived for the local damage and functionality loss of the components, using a fault-tree analysis for instance. For example, a slight/minor damage (e.g. short-time malfunction of the plant) to the station may be induced by the loss of electrical power and backup generators, or a slight damage to the building. Such an approach was used in the LESSLOSS (2007) and SRMLIFE (2003–2007) projects, which resulted in the damage scale presented in Table 7.9.

It is to be noticed that the damage states described in Table 7.6 are not solely linked to the physical damage and that they were also defined so that they match the corresponding functionality loss.

Finally, regarding in-line valves or SCADA equipment, as it was explained before, no quantitative study of their vulnerability is available and therefore no relevant damage states can be defined for these components.

7.4.3 Description of Existing Functions

A critical review of existing fragility functions is proposed, based on the derivation method, the data used and the typologies covered.

Table 7.9 Damage scale proposed in LESSLOSS (2007) and SRMLIFE (2003–2007) for pumping/compression stations

Damage state		Damage description	Functionality loss	
DS1	None	No damage	Normal function	Full function
DS2	Slight/minor	Slight damage to building or full loss of commercial power and backup power for few days (<3 days)	Several stops and reduced flow of gas in the transmission gas pipelines	
DS3	Moderate	Considerable damage to mechanical and electrical equipment or considerable damage to building or loss of electric power and of backup for 7 days	Disability of boosting gas in compression station	Malfunction (full function after repairs)
DS4	Extensive	Building being extensively damaged, or the pumps badly damaged beyond repair		Full loss of function (unrepairable damage)
DS5	Complete	Building collapsed		

7.4.3.1 Pipelines

In the case of fragility functions for transient ground motion, a literature review has led to a non-exhaustive list of around 20 empirical relations, which are summed up in Table 7.10, along with the typologies they cover, the amount of data they rely on and the intensity measure they use. Some of these empirical relations are on a standard functional form (i.e. "backbone curve") and the differences in terms of diameter size, material and connection type are accounted for by the use of a multiplicative factor K that alters the final repair rate. Therefore the backbone curve of the fragility relation represents the repair rate under usual conditions (i.e. $K = 1$), while a smaller or greater K factor represents configurations where the resulting damage is reduced or amplified, respectively.

The relations described in Table 7.9 are all based on empirical data collected from post-earthquake observations. Usually, some adjustments to the raw data are performed: for instance, in the ALA (2001) methodology, only the damage to the main pipe is used to assess the relative vulnerability of different pipe materials. Also, data points assumed to contain permanent ground displacement effects can be eliminated when studying only the effects of ground shaking. Then, based on the data points, a correlation procedure is performed in order to fit a predefined functional form with the empirical data. For example, ALA (2001) explored a linear model ($RR = a.IM$) and a power model ($RR = b.IM^c$). Depending on the consistency of the available data, it is possible to build specific models based on various factors such as pipe material, pipe diameter or pipe connections.

Regarding the effects of ground failure, some specific fragility functions have also been empirically derived and they are detailed in Table 7.11.

Table 7.10 Summary of the existing pipeline fragility relations for transient ground motion

Reference	Typology	IM	No of earthquakes studied
Katayama et al. (1975)	Mainly cast-iron pipes Poor, average or good conditions	PGA	6
Isoyama and Katayama (1982)	Mainly cast-iron pipes	PGA	1
Eguchi (1983)	WSGWJ (welded-steel gas-welded joints), WSAWJ (welded-steel arc-welded joints), AC (asbestos cement), WSCJ (welded-steel caulked joints), CI (cast iron)	MMI	4
Barenberg (1988)	Mainly cast-iron pipes	PGV	3
Eguchi (1991)	WSGWJ (welded-steel gas-welded joints), WSAWJ (welded-steel arc-welded joints), AC (asbestos cement), WSCJ (welded-steel caulked joints), CI (cast iron), DI (ductile iron), PVC, PE (polyethylene)	MMI	4
O'Rourke et al. (1991)	–	MMI	7
Hamada (1991)	–	PGA	2
O'Rourke and Ayala (1993) HAZUS (NIBS 2004)	Brittle or flexible pipes	PGV	6
Eidinger et al. (1995) Eidinger (1998)	Material type Joint type Diameter Soil type	PGV	7
O'Rourke et al. (1998)	Mainly cast-iron pipes	PGV, PGA, MMI	4
Isoyama et al. (1998)	Material type Diameter	PGV	1
Toprak (1998)	No distinction	PGV	1
O'Rourke and Jeon (1999)	Mainly cast-iron pipes Diameter	PGV	1
Eidinger and Avila (1999)	Material type Joint type Diameter Soil type	PGV	–
Isoyama et al. (2000)	Material type: CI, DI, PVC, steel, AC Diameter Soil type	PGA, PGV	1
ALA (2001)	Material type Joint type Diameter Soil type	PGV	18

(continued)

Table 7.10 (continued)

Reference	Typology	IM	No of earthquakes studied
Chen et al. (2002)	Diameter Material type	PGA, PGV, MMI	1
Pineda and Ordaz (2003)	Mainly brittle pipes (CI, AC)	PGV	1
O'Rourke and Deyoe (2004)	Mainly cast-iron pipes	PGV, PGS	5
Pineda and Ordaz (2007)	Mainly brittle pipes (CI, AC)	PGV^2/PGA	1
Maruyama and Yamazaki (2010)	Material type (CI, DI, PVC)	PGV	4
O'Rourke et al. (2012)	Mainly brittle pipes (CI, AC)	GMPGV (geometric mean of PGV)	4 (1 earthquake sequence)

Table 7.11 Summary of the existing pipeline fragility relations for ground failure

Reference	Typology	IM
Eguchi et al. (1983)	Material type: WS, AC, CI Joint type: gas-welded joints, arc-welded joints, caulked joints	PGD
Honegger and Eguchi (1992) HAZUS (NIBS 2004)	Ductile (DI, steel, PVC) or brittle (AC, concrete, CI) pipes	PGD
Heubach (1995)	Material type Joint type	PGD
Ballantyne et al. (1996)	Material type:	PGD
Eidinger and Avila (1999)	Ductile or brittle pipes	PGD
ALA (2001)	Material type Joint type	PGD
O'Rourke et al. (2012)	Material type: AC, CI, PVC	Angular distortion (β) and lateral strain (ε_{HP})

Comparatively, there are fewer examples of analytical fragility functions for buried pipelines. For instance, Terzi et al. (2007) developed fragility curves for the case of segmented pipelines subjected to permanent ground deformation, using a FEM model and accounting for pipe-soil interaction. The results were confronted with the case of a PVC pipeline that suffered damage from the 2003 Lefkas earthquake.

7.4.3.2 Storage Tanks

O'Rourke and So (2000) proposed empirical fragility curves for on-grade steel tanks based on more than 400 tank damages from 9 earthquake events in the United States (California and Alaska). The size of the available data allowed the authors to investigate the effects of two parameters, i.e. the tank's height-to-diameter ratio and the relative amount of stored contents. However, no distinction was made between anchored and unanchored tanks. A logistic regression enabled to fit the empirical data and to express the fragility parameters using a lognormal cumulative distribution.

The fragility curves proposed by ALA (2001) are also based on empirical data from 532 tanks, which experienced strong ground motions of 0.1 g or higher. A typology distinction is made depending on the percentage of stored contents and the anchorage of the tank to the baseplate. Like O'Rourke and So (2000), the ALA study concludes that the tanks that are less than half-full did not experience enough damage to compute fragility curves for DS4 and DS5. Thus, only the tanks with a fill percentage higher than 50 % were considered to estimate additional curves, based on the anchorage of tanks.

Based on the field observations previously reported by ALA (2001), Berahman and Behnamfar (2007) used a Bayesian approach to improve the empirical procedure. They accounted for both aleatory and epistemic (model bias, small data sample, measurement errors...) uncertainties. Fragility models are developed using a probabilistic limit state function and a reliability integral, solved with Monte-Carlo simulation. It was found that the fragility curves were less conservative than purely empirical models from ALA (2001), suggesting a better tank performance than expected. Also, one important result is that commonly-used lognormal distributions do not seem to be the best fit to the available empirical data. However, this study was only conducted for a specific typology of tanks (unanchored at-grade steel tanks) and other sets of fragility curves should be built to cover all typologies. Finally, the proposed fragility curves are based on an integral formulation and are not associated with an analytical form (like the lognormal distribution, which can be easily described with two parameters).

On the other hand, Iervolino et al. (2004) introduced an analytical approach to build fragility curves for unanchored steel tanks. Only one damage state is accounted for, i.e. failure by elephant's foot buckling. The final fragility curve is expressed as a cumulative lognormal distribution, which median and standard deviation parameters are evaluated through a response surface based on two variables (i.e. the fluid height-over-radius ratio and friction coefficient between the tank and the baseplate).

The study by Salzano et al. (2003) focuses also on the role of the fill level (i.e. near full or >50 %) for atmospheric tanks, with anchored or unanchored components. The results are based on empirical data from mostly north-American earthquakes.

Finally, the HAZUS methodology (NIBS 2004) proposes fragility curves for "tanks farms", accounting also for the fragility of the equipment that is needed for a proper operation of the tank (i.e. electric power, tank body, elevated pipes and various electrical/mechanical components). A fault-tree analysis is then used to assess the global functionality of the "tank farm" based on the specific damage state of each of its components.

7.4.3.3 Processing Plants/Stations

Various past research projects have tackled the issue of gas compression stations. For instance, a study from the European LESSLOSS project (LESSLOSS 2007) has proposed a hybrid approach, by considering both the fragility of the building and the logic tree relation between the components of the stations. A cumulative lognormal distribution of the damage probability was estimated, by using fragility curves by Kappos et al. (2006) for RC low-rise buildings with anchored components, designed with a low-level or advanced seismic code.

The SRMLIFE Greek project (SRMLIFE 2003–2007) also used this hybrid approach for pumping/compression stations, based on fragility curves for buildings by Kappos et al. (2006). The SRMLIFE study focused on specific fragility curves for Greek typologies (i.e. RC low-rise buildings with anchored components), while the fragility of the sub-components has been taken from the HAZUS methodology.

Finally, fragility curves have been also proposed in the HAZUS methodology (NIBS 2004), where the fragility curves of all components are used into a fault-tree analysis to obtain the global fragility function of pumping plants. A typological distinction is made between plants with anchored or unanchored components.

7.4.4 Comparative Analysis and Limitations

Based on the available fragility functions in the literature, a critical review is performed, with the aim of identifying the most adequate functions and the existing gaps.

7.4.4.1 Pipelines

According to the available typologies for gas & oil pipelines in Europe (mostly welded-steel, PVC and HDPE continuous ductile pipes), it is necessary to focus on fragility relations that are most adequate for ductile pipelines. Moreover, if we assume the use of PGV and PGD as respective intensity indexes for ground shaking

and ground failures, it could be concluded that the following relations constitute good candidates:

- For wave propagation:
  - O'Rourke and Ayala (1993), which is used in HAZUS;
  - Eidinger et al. (1995) and Eidinger (1998);
  - Isoyama et al. (2000);
  - ALA (2001);
- For ground failure:
  - Eguchi et al. (1983);
  - Honegger and Eguchi (1992), which is used in HAZUS;
  - Eidinger and Avila (1999);
  - ALA (2001);

Some of these relations have been tested and confronted to a European case study (2003 Lefkas earthquake, Pitilakis et al. 2006), however only for water distribution pipelines (mainly brittle pipes): therefore these results may not apply to the specific case of gas and oil pipelines. More recently, Esposito et al. (2013) have compared available fragility curves in the literature with actual damage observations on the L'Aquila gas system.

Regarding the effects of transient ground motion, it is noted that the ALA (2001) study is the most recent one, as the HAZUS curves are still based on the O'Rourke and Ayala (1993) study. The ALA (2001) relations are based on the largest set of empirical data, including the 1994 Northridge earthquake: 18 events are used, as opposed to 6 in the study by O'Rourke and Ayala (1993). Moreover, the data from ALA (2001) is based on the study from O'Rourke and Ayala (1993) enriched with other datasets. In the ALA (2001) study, a balanced sample of U.S., Central American and Japanese earthquake is used, accounting for the variability of pipeline codes among various countries. Also, the consequent amount of data points (81, as opposed to 11 in O'Rourke and Ayala 1993) allows for a more balanced distribution of pipeline typologies.

Moreover, the review by Tromans (2004) compares some of the existing empirical relations: these curves are plotted on Fig. 7.6, assuming a corrective factor $K = 1$ (i.e. the "backbone curve", see Sect. 7.4.3.1).

As stated by O'Rourke (1999), the fragility relation by O'Rourke and Ayala (1993) seems to be over-conservative, with pipeline repair rates being unduly affected by the long durations of ground shaking experienced during the 1985 Michoacan earthquake (Tromans 2004). The relations by ALA (2001) and Isoyama et al. (2000) offer the longest applicability range, as opposed to the O'Rourke and Ayala (1993) and Eidinger et al. (1995) relations, which should not be extrapolated to large values of PGV. The use of the relations by O'Rourke and Ayala (1993) is also advocated by some validation studies carried out on the 1999 Düzce and 2003 Lefkas earthquakes, in the case of ductile pipelines (Alexoudi 2005). Finally, it may be useful to quote some of the conclusions drawn by Tromans (2004) in his review:

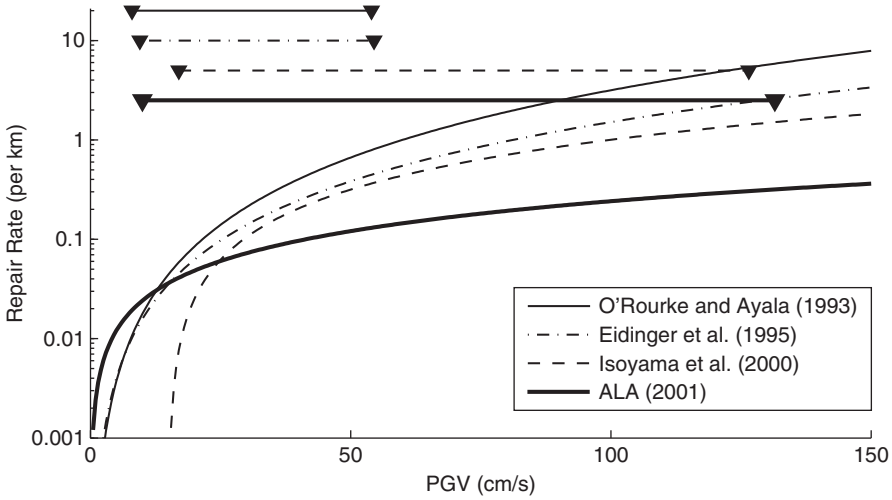

Fig. 7.6 Comparison of the pipeline fragility relations for PGV. *Straight lines* refer to the range of applicability of a given relation, approximated from knowledge of the dataset from which it was derived (Tromans 2004)

- The relation by O'Rourke et al. (1998) is to be used specifically in the U.S., as data from other locations have not been included: moreover, this relation should only be applied to cast-iron pipes.
- The relation by Isoyama et al. (2000) is suggested for Japan. Application to other locations is difficult, due to the specific topographic classification scheme, which is not normally used outside of Japan;
- For general applications, the relation by ALA (2001) is recommended, as it is derived from a global database.

The ALA (2001) relation may then represent an adequate solution to assess the vulnerability of buried ductile pipelines. It yields the repair rate (*RR* in repairs per km) as a function of PGV (in cm/s) via the following equation:

$$RR = K_1 0.002416 PGV \tag{7.3}$$

The parameter K_1 is used to adjust the fragility with respect to the backbone curve, based on the material, the connection type, the soil type and the pipe diameter (see Table 7.12).

The repair rate relation presented above allows assessing most of the specific typologies identified in the gas systems studied within the SYNER-G project (see Sect. 7.2.1):

- Greek transmission lines (WS, small diameter): $K_1 = 0.6$
- Greek distribution lines, Austrian transmission and distribution lines (PVC, small diameter): $K_1 = 0.5$
- Austrian supra-regional lines (WS, large diameter): $K_1 = 0.15$

Table 7.12 Some values of the K_1 parameter in the ALA (2001) relation for transient ground motion, for welded steel and PVC pipes

Material	Joint type	Soil type	Diameter	K_1
WS	Arc welded	Unknown	Small	0.6
	Arc welded	Corrosive	Small	0.9
	Arc welded	Non corrosive	Small	0.3
	Arc welded	All	Large	0.15
	Rubber gasket	Unknown	Small	0.7
	Screwed	All	Small	1.3
	Riveted	All	Small	1.3
PVC	Rubber gasket	All	Small	0.5

A *small* diameter is considered to be comprised between 10.16 and 30.48 cm and a *large* one is greater than 40.64 cm

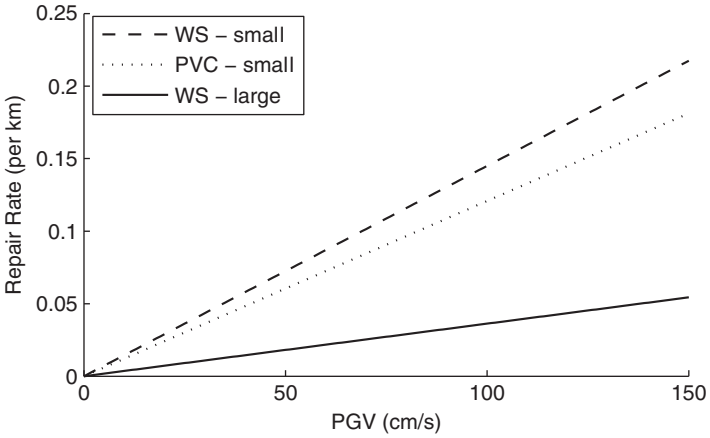

Fig. 7.7 Proposed repair rate for the most common gas pipeline typologies, due to wave propagation (ALA 2001)

The repair rate of these different configurations is plotted in Fig. 7.7 as a function of PGV.

However, existing relations fail to address the case of polyethylene pipelines (MDPE and HDPE), which are more and more commonly used in the gas distribution networks (e.g. the L'Aquila gas network). Still, the absence of observed damages on these pipes (O'Rourke et al. 2012, on the Canterbury earthquake sequence) leads to assume a very good response of these pipelines to seismic action.

Regarding the effects of ground failure, the relation by ALA (2001) is also the most recent one, as the one proposed by the HAZUS methodology is taken from Honegger and Eguchi (1992). The dataset from ALA (2001) comprises 41 data points from 4 earthquakes (one Japanese and three U.S.), with liquefaction as the main failure mechanism. Thus, the ALA (2001) curve is based on the most complete empirical data. A comparison of some fragility curves (use of the "backbone curve", without any corrective factors) is given in Fig. 7.8.

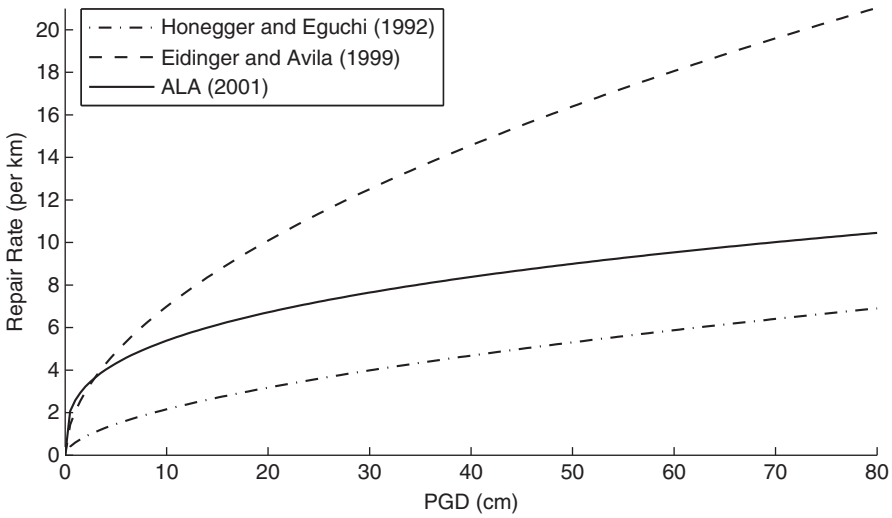

Fig. 7.8 Comparison of three repair rate relations for ground failure, with respect to PGD

Table 7.13 Some values of the K_2 parameter in the ALA (2001) relation for ground failure, for welded steel and PVC pipes

Material	Joint type	K_1
Unknown	Unknown	1.0
WS	Arc welded, lap welds	0.15
	Rubber gasket	0.7
PVC	Rubber gasket	0.8

Figure 7.8 shows important discrepancies between the different studies: the curve by (ALA 2001) lies in between the relations from Honegger and Eguchi (1992) and Eidinger and Avila (1999). Based on this discussion and in order to be coherent with the fragility curve selected for transient ground motion, we finally propose to adopt the relation from ALA (2001), as a function of PGD in cm:

$$RR = K_2 2.5829 PGD^{0.319} \tag{7.4}$$

The corrective factor K_2 depends on the pipe material and the connection type (see Table 7.13) and the following values are proposed in ALA (2001) for the most common pipelines typologies that are encountered in a European context (see Fig. 7.9):

- Greek transmission lines (WS, small diameter): $K_2 = 0.7$
- Greek distribution lines, Austrian transmission and distribution lines (PVC, small diameter): $K_2 = 0.8$
- Austrian supra-regional lines (WS, large diameter): $K_2 = 0.15$

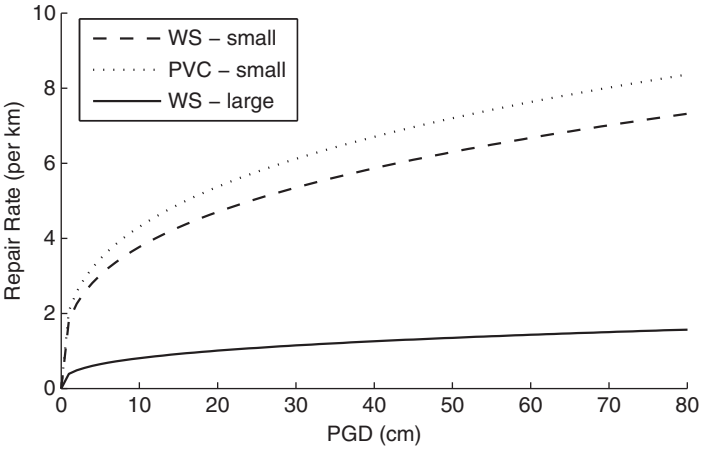

Fig. 7.9 Proposed repair rate for the most common gas pipeline typologies, due to ground failure (ALA 2001)

Again, the existing empirical relations fail to address the case of MDPE or HDPE pipelines. However, a recent experiment performed by O'Rourke et al. (2012) on a HDPE pipeline segment has revealed that the maximum strain (i.e. 8 %) induced by a strike-slip displacement of 1.2 m was far below the strain levels causing pipe wall rupture. However, the squeeze-off of the pipe and the associated loss of cross-sectional area were found to be a potential failure mechanism for polyethylene pipelines.

7.4.4.2 Storage Tanks

The studies by O'Rourke and So (2000) and ALA (2001) are the most thorough, as they allow for distinction between many characteristics such as the percentage of content stored, anchorage of components and height-over-radius ratio. However, some of the proposed fragility curves are based on really scarce empirical data, and this may raise issues on the reliability of the regression. Also, the damage states proposed by these two studies are mostly defined by physical damage mechanisms that prove to be difficult to link to any loss of functionality. Besides, oil storage tanks are located in very complex facilities (e.g. refineries, storage facilities. . .) and considering only the damage to the tank body seems to be a quite simplistic and rather non conservative approach: indeed, the whole "tank farm" system should be accounted for, including elevated pipes, power sources, mechanical equipment, etc.

It is then proposed to adopt the fragility curves for "tank farms" developed in the HAZUS methodology (NIBS 2004). These curves can be applied to on-grade steel tanks, with a distinction on whether components are anchored or not (see Table 7.14 and Fig. 7.10).

Table 7.14 Fragility parameters (median α and standard-deviation β) for tank farms proposed by HAZUS (NIBS 2004)

Typology	Damage state	α (g)	β
Tank farm with anchored components	Slight/minor	0.29	0.55
	Moderate	0.50	0.55
	Extensive		
	Complete	0.87	0.50
Tank farm with unanchored components	Slight/minor	0.12	0.55
	Moderate	0.23	0.55
	Extensive	0.41	0.55
	Complete	0.68	0.55

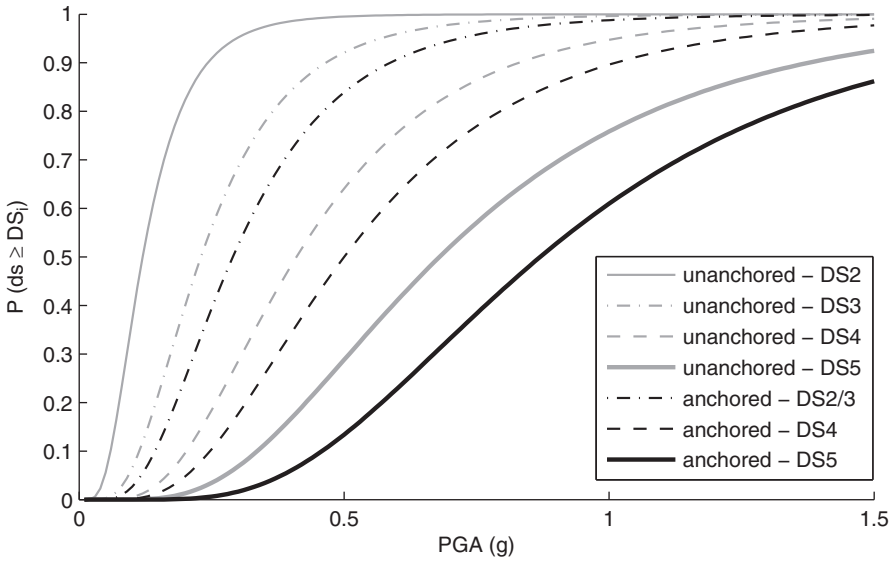

Fig. 7.10 Fragility curves for steel tank farms, proposed by HAZUS (NIBS 2004)

7.4.4.3 Processing Plants/Stations

The case of the Greek gas compression stations can be covered by the specific fragility functions that have been developed within the SRMLIFE Greek project. These fragility curves (see Table 7.15 and Fig. 7.11) are applicable to gas stations that are housed in low-rise RC buildings with anchored components.

Apart from the Greek context, the typology of generic European gas stations is not well known, and one solution could be to use the generic fragility curves of the HAZUS methodology (NIBS 2004), which are based only on the distinction between anchored and unanchored components (see Table 7.16 and Fig. 7.12).

In the case of the specific components identified in central Italy, there are no ready-to-use fragility functions. However, a fault-tree decomposition of the

Table 7.15 Fragility parameters (median α and standard-deviation β) for Greek compression plants, according to SRM-LIFE (2003–2007)

Typology	Damage state	α (g)	β
Anchored components, low-rise RC building (advanced code)	Minor	0.30	0.70
	Moderate	0.55	0.45
	Extensive	0.80	0.50
	Complete	2.20	0.70

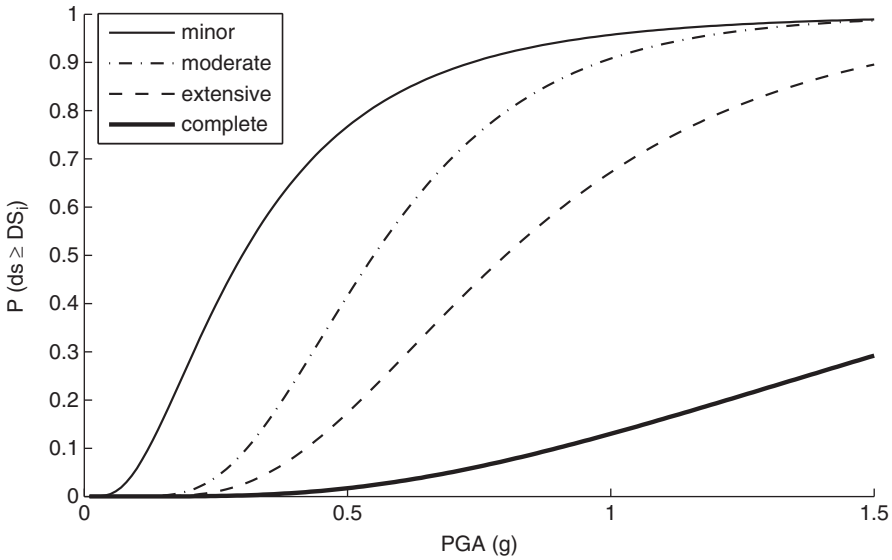

Fig. 7.11 Fragility curves for Greek compression stations, proposed by SRM-LIFE (2003–2007)

Table 7.16 Fragility parameters (median α and standard-deviation β) for pumping plants, according to HAZUS (NIBS 2004)

Typology	Damage state	α (g)	β
Anchored components	Minor	0.15	0.75
	Moderate	0.34	0.65
	Extensive	0.77	0.65
	Complete	1.50	0.80
Unanchored components	Minor	0.12	0.60
	Moderate	0.24	0.60
	Extensive	0.77	0.65
	Complete	1.55	0.80

sub-components may be helpful to assess the relative vulnerability of these stations. Regarding RE.MI cabins, all subcomponents are assumed to be unanchored and simply supported on the ground (with the exception of bowls that are located in a separated area and ceiling-mounted). These cabins may be decomposed in structural component (i.e. buildings), regulators and mechanical equipment (heat exchangers, boilers and bowls) and a fault-tree analysis is presented in Fig. 7.13.

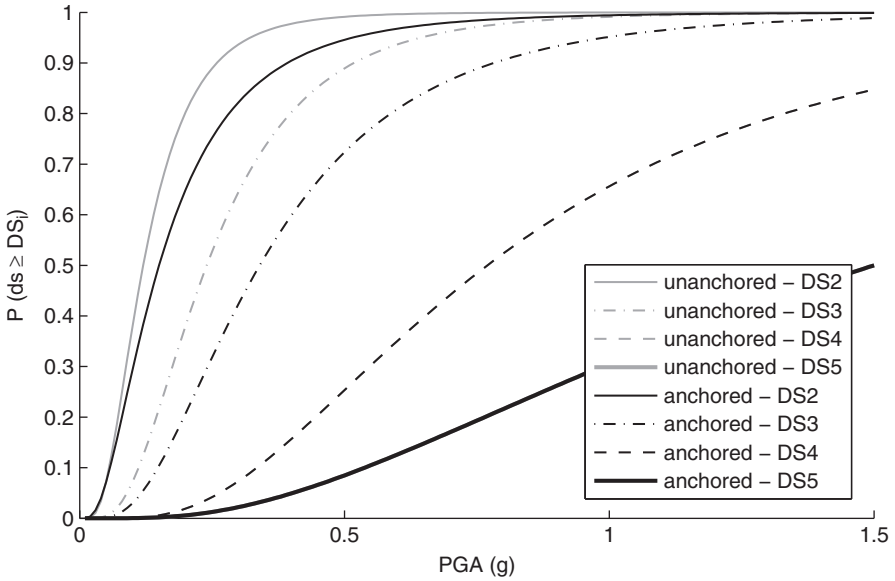

Fig. 7.12 Fragility curves for pumping plants, proposed by HAZUS (NIBS 2004)

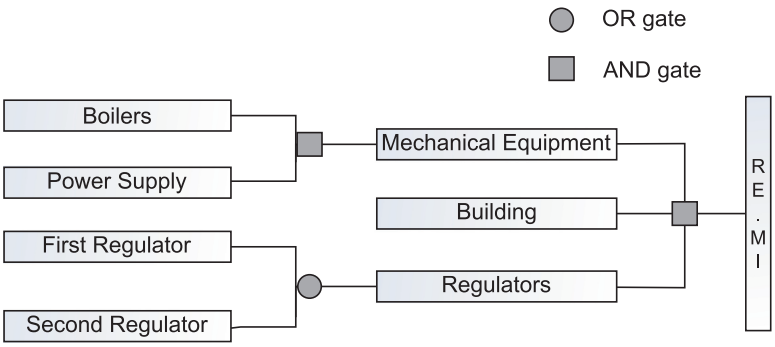

Fig. 7.13 Fault-tree decomposition of a RE.MI cabin (Esposito 2011)

Since gas supply has to be maintained at all times, two installations are mounted in parallel where each installation is characterized by a regulator and a monitor. The monitor is a safety device that has to be able to prevent the outlet pressure from exceeding safe thresholds in the case of complete failure of the regulator, taking over the function of the primary, normally active regulator. Besides, when boilers break down the gas flow is not ensured, since the freezing stops the system.

On the other hand, reduction groups (i.e. GR) can be broken down in regulators and masonry housing (when it is present, otherwise the group is sheltered within a kiosk) and the corresponding fault-tree is detailed in Fig. 7.14.

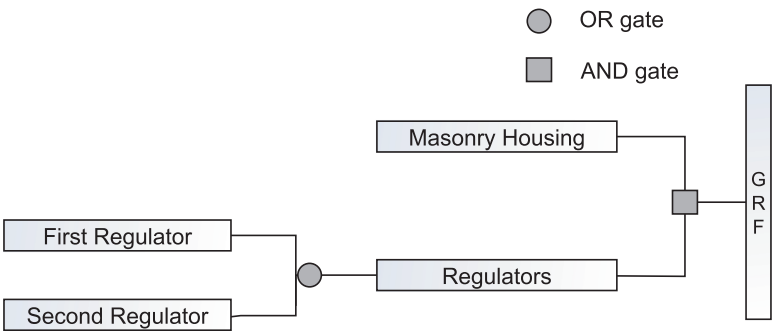

Fig. 7.14 Fault-tree decomposition of a reduction group (Esposito 2011)

In most cases the safety device is ensured by the presence of shut-off valves that are able to block the gas flow. When the pressure exceeds a maximum value, the valves close. However, some reduction groups do not include a second regulator and this characteristic implies a higher vulnerability.

7.5 Conclusions

The present review of available fragility functions for components of gas and oil networks has yielded some valuable lessons for future work on this topic. First, on a more general note, it appears that the case of the vulnerability of gas and oil networks should be more investigated regarding the dramatic consequences that can potentially result from component failures: most of the fragility functions presented here (especially for pipelines) have been developed for water supply networks and their adaptation to the case of gas and oil networks should be taken with extreme care. For instance, the impact of the different constitutive properties (especially the viscosity) of liquefied gas or oil should be investigated, thus introducing even more complex fluid–solid interactions in the analyses. The difficulty to properly tackle most of the modelling issues presented here may also be one of the reasons why most of the fragility functions are derived from empirical data and not from numerical computations or experimentations. The direct consequence is that these empirical relations, which are usually based on data from American or Japanese earthquakes, may not be suitable to European typologies.

In the case of buried pipelines, the emphasis has been put on ductile pipes, which are most common for gas and oil networks as opposed to brittle pipes (e.g. cast-iron, concrete) that are usually found in water supply systems. Whether damage is induced by transient wave propagation or by permanent ground deformation, it has been found that the use of the empirical relations by ALA (2001) might be reasonable for European pipeline typologies, which are essentially composed of welded-steel and PVC materials. For the networks where polyethylene pipelines are

present, there is currently no fragility function available; however O'Rourke et al. (2012) confirm the excellent behaviour of this material under seismic action, since almost no damage has been recorded for MDPE or HDPE pipes in recent earthquakes.

A series of empirical fragility functions have also been reviewed, especially for at-grade steel tanks, which are common features of the vertical cylinders that are used to store hydrocarbons in oil refineries. The complexity of the mechanical and electrical equipment that is supporting the storage operations is accounted for by the HAZUS (NIBS 2004) fragility curves for 'tank farms'. However, the case of gas storage is less straightforward and the very specific features of the different storage facilities (e.g. LNG tanks for liquefied natural gas, underground cavities for seasonal storage, air-tight spherical or cylindrical tanks for special gases) prevent the use of generic fragility curves.

Finally, regarding processing facilities (i.e. compression or reduction stations), different levels of analysis are available, the most basic one consisting of the sole fragility analysis of the building housing the station. An alternative resides in the use of a fault-tree analysis to derive the global station fragility from the particular fragility of each of its subcomponents. Specific fragility curves are available for Greek gas compression stations and other compression/pumping stations could be assessed with generic fragility curves from HAZUS (NIBS 2004). More specific typologies have also been identified (i.e. RE.MI cabins and GRF groups in Central Italy) and, unfortunately, they could not be satisfyingly associated with any fragility functions. However, these stations could be decomposed into a fault-tree, revealing precious information on the criticality of some subcomponents and the relative vulnerability of stations that comprise redundant equipment or not.

Acknowledgments The authors are grateful to Simona Esposito and Iunio Iervolino from AMRA and to Kyriazis Pitilakis, Kalliopi Kakderi and Sotiris Argyroudis from the Aristotle University of Thessaloniki for having shared their knowledge concerning the existing component typologies of the L'Aquila and Thessaloniki gas networks.

References

ALA (2001) Seismic fragility formulations for water systems. American Lifeline Alliance, ASCE, Washington, DC

Alexoudi M (2005) Contribution to seismic assessment of lifelines in urban areas. Development of a holistic methodology for seismic risk. Ph.D. thesis, Civil Engineering Department, Aristotle University of Thessaloniki, Greece

Ballantyne D, Heubach W, Archibald P (1996) Earthquake vulnerability of the Greater Vancouver Water District's p*ipeline s*ystem. In: Proceedings of the Pan Pacific Hazards'96 conference, Vancouver, BC, Canada

Barenberg ME (1988) Correlation of pipe damage with ground motion. J Geotech Eng 114(6):706–711

Berahman F, Behnamfar F (2007) Seismic fragility curves for unanchored on-grade steel storage tanks: Bayesian approach. J Earthq Eng 11(2):1–31

Chen WW, Shih B, Chen YC, Hung JH, Hwang HH (2002) Seismic response of natural gas and water pipelines in the Ji-Ji earthquake. Soil Dyn Earthq Eng 22:1209–1214

EERI (1986) Reducing earthquake hazards: lessons learned from earthquakes. Earthquake Engineering Research Institute, El Cerrito, Publication n°86-02

EERI (1990) Loma Prieta earthquake reconnaissance report. Supplement to vol. 6. Earthquake Engineering Research Institute, El Cerrito, CA

Eguchi RT (1987) Seismic risk to natural gas and oil systems. FEMA 139. Earthq Hazard Reduct Ser 30:15–33

Eguchi RT (1991) Early post-earthquake damage detection for underground lifelines. Final report to the National Science Foundation, Dames and Moore PC, Los Angeles, CA

Eguchi RT, Legg MR, Taylor CE, Philipson LL, Wiggins JH (1983) Earthquake performance of water and natural gas supply system. J. H. Wiggins Company, NSF Grant PFR-8005083, Report 83-1396-5

Eidinger J (1998) Lifelines, water distribution system in the Loma Prieta, California, Earthquake of October 17, 1989. In: Schiff A (ed) Performance of the built environment – lifelines. US Geological Survey Professional Paper 1552-A, A63–A80

Eidinger J, Avila E (1999) Guidelines for the seismic upgrade of water transmission facilities. ASCE, TCLEE, Monograph 15

Eidinger J, Maison B, Lee D, Lau BB (1995) East Bay municipality utility district water distribution damage in 1989 Loma Prieta earthquake. In: Proceedings of the fourth US conference on lifeline earthquake engineering, Monograph 6. ASCE, New York, pp 240–247

Esposito S (2011) Systemic seismic risk analysis of gas distribution networks. Ph.D. thesis, University of Naples Federico II, Italy, Advisor: I. Iervolino. Available at: wpage.unina.it/iuniervo

Esposito S, Giovinazzi S, Elefante L, Iervolino I (2013) Performance of the L'Aquila (central Italy) gas distribution network in the 2009 (Mw 6.3) earthquake. Bull Earthq Eng (Nov 2013)

Ghobarah A (2004) On drift limits with different damage levels. In: Proceedings of international workshop on performance-based seismic design concepts and implementation, Bled, Slovenia

Hall WJ (1987) Earthquake engineering research needs concerning gas and liquid fuel lifelines. FEMA 139. Earthq Hazard Reduct Ser 30:35–49

Hamada M (1991) Estimation of earthquake damage to lifeline systems in Japan. In: Proceedings of the third Japan-US workshop on earthquake resistant design of lifeline facilities and countermeasures for soil liquefaction, San Francisco, CA

Hashash YMA, Hook JJ, Schmidt B, Yao JIC (2001) Seismic design and analysis of underground structures. Tunn Undergr Space Technol 16:247–293

Heubach W (1995) Seismic damage estimation for buried pipeline systems. In: O'Rourke M (ed) Proceedings of the 4th US conference on lifeline earthquake engineering, Monograph No. 6, TCLEE/ASCE, pp 312–319

Honegger DG, Eguchi RT (1992) Determination of the relative vulnerabilities to seismic damage for San Diego County Water Authority (SDCWA) water transmission pipelines, October. Cited in NIBS (2004)

Iervolino I, Fabbrocino G, Manfredi G (2004) Fragility of standard industrial structures by a response surface based method. J Earthq Eng 8(6):927–945

Isoyama R, Katayama T (1982) Reliability evaluation of water supply systems during earthquake, vol 30(1). Report of the Institute of Industrial Science, University of Tokyo, Tokyo

Isoyama R, Ishida E, Yune K, Shirozu T (1998) Study on seismic damage estimation procedure for water pipes. J Jpn Water Works Assoc 67(2):25–40

Isoyama R, Ishida E, Yune K, Shirozu T (2000) Seismic damage estimation procedure for water supply pipelines. In: Proceedings of the twelfth world conference on earthquake engineering, Paper n°1762, Auckland

Kappos A, Panagopoulos G, Panagiotopoulos C, Penelis G (2006) A hybrid method for the vulnerability assessment of R/C and URM buildings. Bull Earthq Eng 44:391–413

Katayama T, Kubo K, Sato N (1975) Earthquake damage to water and gas distribution systems. In: Proceedings of the US national conference on earthquake engineering, EERI, Oakland, CA, pp 396–405

Kennedy RP, Kassawara RP (1989) Seismic evaluation of large flat-bottomed tanks. In: Proceedings of the second symposium on current issues related to nuclear power plant structures, equipment, and piping with emphasis on resolution of seismic issues in low-seismicity regions, EPRI NP-6437-D

LESSLOSS (2007) Damage scenarios for selected urban areas (for water and gas systems, sewage mains, tunnels and waterfront structures: Thessaloniki, Istanbul (European side), Düzce. LESSLOSS Project Deliverable n°117

Maruyama Y, Yamazaki F (2010) Construction of fragility curve for water distribution pipes based on damage datasets from recent earthquakes in Japan. In: Proceedings of the 9th U.S. National and 10th Canadian conference on earthquake engineering, Toronto, ON, Canada, 25–29 July 2010

Newmark NM (1967) Problems in wave propagation in soil and rocks. In: Proceedings of the international symposium on wave propagation and dynamic properties of earth materials, University of New Mexico Press, pp 7–26

Newmark NM, Rosenblueth E (1971) Fundamentals of earthquake engineering. Prentice-Hall, Englewood Cliffs

NIBS (2004) Earthquake loss estimation methodology HAZUS. National Institute of Building Sciences, FEMA, Washington, DC

NZNSEE (1986) Seismic design of storage tanks. Recommendations of a Study Group of the New Zealand National Society for Earthquake Engineering

O'Rourke MJ (1988) Mitigation of seismic effects on water systems. In: Proceedings of the TCLEE/ASCE symposium on the seismic design and construction of complex civil engineering systems, St Louis, MO, pp 65–78

O'Rourke MJ (1999) Estimation of post-earthquake water system serviceability. In: Proceedings of the 7th Japan-US workshop on earthquake resistant design of lifeline facilities and countermeasures for soil liquefaction, MCEER, State University of New York at Buffalo, Buffalo, NY, pp 391–403

O'Rourke MJ, Ayala G (1990) Seismic damage to pipeline: case study. J Transp Eng 116 (2):123–134

O'Rourke MJ, Ayala G (1993) Pipeline damage due to wave propagation. J Geotech Eng 119 (9):1490–1498

O'Rourke MJ, Deyoe E (2004) Seismic damage to segment buried pipe. Earthq Spectra 20 (4):1167–1183

O'Rourke TD, Jeon SS (1999) Factors affecting water supply damage caused by the Northridge earthquake. In: Proceedings of the fifth US conference of lifeline earthquake engineering, Seattle, WA

O'Rourke MJ, Liu X (1999) Response of buried pipelines subject to earthquake effects. MCEER Monograph No. 3RI. 1986. Reducing earthquake hazards: lessons learned from earthquakes. Publication n°86-02. Earthquake Engineering Research Institute, El Cerrito, CA

O'Rourke MJ, So P (2000) Seismic fragility curves for on-grade steel tanks. Earthq Spectra 16(4)

O'Rourke TD, Trautmann CH (1981) Earthquake ground rupture effects on jointed pipe. In: Smith DJ (ed) Proceedings of the second specialty conference of the technical council on lifeline earthquake engineering, pp 65–80

O'Rourke TD, Gowdy TE, Stewart HE, Pease JW (1991) Lifeline and geotechnical aspects of the 1989 Loma Prieta earthquake. In: Proceedings of the second international conference on recent advances in geotechnical earthquake engineering and soil dynamics, St Louis, MO

O'Rourke TD, Toprak S, Sano Y (1998) Factors affecting water supply damage caused by the Northridge earthquake. In: Proceedings of the sixth US national conference on earthquake engineering, Seattle, USA

O'Rourke TD, Jeon SS, Toprak S, Cubrinovski M, Jung JK (2012) Underground lifeline system performance during the Canterbury earthquake sequence. In: Proceedings of the 15th world conference on earthquake engineering, Lisbon, Portugal

Pineda O, Ordaz M (2003) Seismic vulnerability function for high diameter buried pipelines: Mexico City's primary water system case. Proc Int Conf Pipeline Eng Constr 2:1145–1154

Pineda O, Ordaz M (2007) A new seismic parameter to estimate damage in buried pipelines due to seismic wave propagation. J Earthq Eng 11(5):773–786

Pitilakis K, Alexoudi M, Argyroudis S, Monge O, Martin C (2006) Earthquake risk assessment of lifelines. Bull Earthq Eng 4:365–390

Rauch AF (1997) EPOLLS: an empirical method for predicting surface displacements due to liquefaction-induced lateral spreading in earthquakes. Ph.D. thesis, Virginia Polytechnic Institute and State University, Blacksburg, VA

Rossetto T, Elnashai A (2003) Derivation of vulnerability functions for European-type RC structures based on observational data. Eng Struct 25:1241–1263

Salzano E, Iervolino I, Fabbrocino G (2003) Seismic risk of atmospheric storage tanks in the framework of quantitative risk analysis. J Loss Prev Process Ind 16:403–409

Singhal AC (1984) Nonlinear behavior of ductile iron pipeline joints. J Tech Topics Civil Eng 110(1):29–47

SRMLIFE (2003–2007) Development of a global methodology for the vulnerability assessment and risk management of lifelines, infrastructures and critical facilities. Application to the metropolitan area of Thessaloniki. Research Project, General Secretariat for Research and Technology, Greece

St John CM, Zahrah TF (1987) Aseismic design of underground structures. Tunn Undergr Space Technol 2(2):165–197

SYNER-G (2009–2013) Systemic seismic vulnerability and risk analysis for buildings, lifeline networks and infrastructures safety gain. Research Project, European Commission, 7th Framework Programme, Contract Number: 244061

Terzi VG, Alexoudi MN, Hatzigogos TN (2007) Numerical assessment of damage state of segmented pipelines due to permanent ground deformation. In: Proceedings of the tenth international conference on applications of statistics and probability in civil engineering, Tokyo, Japan, p 202

Toprak S (1998) Earthquake effects on buried lifeline systems. Ph.D. thesis, Cornell University, Ithaca, NY

Tromans I (2004) Behaviour of buried water supply pipelines in earthquake zones. Ph.D. thesis, Imperial College of Science, Technology and Medicine, University of London

Chapter 8
Fragility Functions of Water and Waste-Water Systems

Kalliopi Kakderi and Sotiris Argyroudis

Abstract This chapter presents the state-of-the-art on the fragility models for the vulnerability assessment of the water and waste-water networks' components. First, the main characteristics and typologies of the two networks' components such as water sources, treatment plants, pumping and lift stations, tanks and conduits are introduced. Then, the main damage mechanisms and failure modes are summarized for each component based on the experiences from past earthquakes. A literature review of existing fragility models is performed including damage scales, seismic intensity measures and fragility functions. Finally, the fragility functions which are most suited for use in the European context are proposed, together with their parameters and relevant information.

8.1 Introduction

Water and waste-water systems are prone to damage from earthquakes, not only under severe levels of shaking but under moderate levels as well. The experience from past earthquakes shows that seismic damage to water system elements can cause extended direct and indirect economic losses with serious environmental and societal impact.

The seismic response of water and waste-water systems to transient (ground shaking) and permanent ground deformations (induced phenomena like liquefaction, fault crossing and landslides) concerns both the pipeline networks and the other structures composing the systems. One of the main characteristics of these systems is the spatial extent over large geographic areas with different geotechnical and geo-morphological conditions. Pipeline response is addressed for permanent ground deformation (PGD) triggered primarily by liquefaction, landslides, and

K. Kakderi (✉) • S. Argyroudis
Department of Civil Engineering, Aristotle University of Thessaloniki,
Thessaloniki 54124, Greece
e-mail: kkakderi@gmail.com; sarg@civil.auth.gr

K. Pitilakis et al. (eds.), *SYNER-G: Typology Definition and Fragility Functions for Physical Elements at Seismic Risk*, Geotechnical, Geological and Earthquake Engineering 27,
DOI 10.1007/978-94-007-7872-6_8,

surface fault movement, and transient ground deformation (TGD) associated with wave propagation effects that are principally recoverable, but may involve relatively small amounts of residual deformation on the order of few cm or less (O'Rourke et al. 2012).

Damage data collected after earthquakes is commonly used to develop empirical fragility functions for pipelines. These functions relate the repair rates (RR) expressed as repairs/km with the peak ground velocity (PGV) or permanent ground deformation (PGD) for different pipe types. In recent years, the increased density of strong motion records, in combination with new technologies such as geographical information systems (GIS) and remote sensing technologies (e.g. LiDAR) for measurement of ground movements contributed to the development and verification of such relationships. The vulnerability of other components (e.g. tanks, pumping stations etc.) is expressed through fragility curves that were derived based on empirical, numerical or expert judgement methods. Fault-tree analysis is also applied for complex components, such as water treatment plants.

In the following, the main typologies of water and waste-water system components are first identified. A short review of past earthquake damages on water and waste-water system elements is provided and the corresponding failure modes are classified. The general description of existing methodologies and damage states definitions is followed by a review of existing fragility functions and the proposal of vulnerability functions for the individual components of each network.

8.2 Identification of Main Typologies

In this section, the main typologies of water and waste-water systems' components are identified and their main features are briefly described.

8.2.1 Water System

A potable water supply is necessary for drinking, food preparation, sanitation, irrigation etc. Water (which may be non-potable) is also required for cooling equipment and fire-extinguishing. A water supply system consists of transmission and distribution systems:

- The transmission system stores "raw" water and conveys it to treatment plants. Such a system is made up of canals, tunnels, elevated aqueducts and buried pipelines, pumping stations and reservoirs.
- The distribution system delivers treated water to customers.

Depending on the topography and local conditions the water may be conveyed through free-flow conduits, closed conduits or a combination of both. Therefore,

water may be conveyed by gravity flow or by pumping under pressure. Various components comprise water supply systems, as listed below:

- Water source.
- Treatment plant.
- Pumping station.
- Storage.
- Conduits (pipes, tunnel, canals).
- Supervisory Control and Data Acquisition (SCADA).

Typical water sources are springs, shallow or deep wells, rivers, natural lakes and impounding reservoirs. Wells are used in many cities both as primary and supplementary source of water. They include a pump to bring the water up to the surface, which is housed in a building together with associated electromechanical equipment.

Water treatment plants are complex facilities that are generally composed of a number of connected physical and chemical unit processes whose role is to improve the water quality. Common components include pre-sedimentation basins, aerators, detention tanks, flocculators, clarifiers, backwash tanks, conduit and channels, coal sand or sand filters, mixing tanks, settling tanks, clear wells, and chemical tanks.

A pumping station is a facility that boosts water pressure in both transmission and distribution systems. They typically comprise buildings, importation structures, pumps and motor units, pipes, valves and associated electrical and control equipment. Main typology parameters include size, anchorage of sub-components, equipment and backup power.

Water conduits can be free-flow or pressurized. Free-flow conduits have a limited application in water supply due to the danger of contamination of treated water. However, they are used for transmission of raw water.

The typology of pipes mainly depends on the following features: location (buried, elevated or underwater), material (type, strength), geometry (diameter, wall thickness), type of joints, continuity (segmented or continuous elements) and corrosiveness (age and soil conditions). The most common types of materials and connections used for buried pipelines are also given in Chap. 7 (see Table 7.1).

Canals and tunnels are free-flowing conduits. Canals are usually open to the atmosphere and follow the slope of the terrain, usually having trapezoidal or rectangular cross-section. Tunnels are constructed with a circular or horseshoe cross-section shape. To reduce water losses they are usually lined, however, when constructed in stable impermeable rock they can be without lining.

Storage tanks can be located at the start, along the length or at the end of a water transmission/distribution system. Their function is to store water, provide surge relief volumes, provide detention times for disinfection, and other uses. The main typological features include the material (concrete, steel, wood), size, anchorage, position (at-grade or elevated), type of roof, seismic design, foundation type and construction technique.

The typological features and classification considered in SYNER-G for the water supply network are summarized in Table 8.1.

8.2.2 Waste-Water System

Waste-water systems can alternatively be called sewer networks. They are comprised of components that work together to collect, transmit, treat and dispose sewage.

The waste-water system is composed of various components, including:

- Treatment plant.
- Lift station.
- Conduits (pipes, tunnels).
- Supervisory Control and Data Acquisition (SCADA).

Waste-water is usually conveyed by gravity flow through pipelines and tunnels mostly made of brittle materials. Their typology is similar to the water system conduits.

Waste-water treatment plants are complex facilities which include a number of buildings and underground or on-ground reinforced concrete tanks and basins. Common components include trickling filters, clarifiers, chlorine tanks, recirculation and waste-water pumping stations, chlorine storage and handling, tanks and pipelines. Concrete channels are used to convey the waste-water from one location to another within the network. The mechanical, electrical and control equipment, as well as piping and valves, are housed within buildings.

Lift or pumping stations serve to raise sewage over topographical rises or to boost the disposals. They are usually composed of a building, one or more pumps, electrical equipment, and, in some cases, backup power systems.

The typological features and classification considered in SYNER-G for the waste-water network are summarized in Table 8.2.

8.3 Description of Damage Mechanisms and Failures Modes

Most of damages in past earthquakes have been observed in pipes, both for water and waste-water systems and secondarily in pumping stations, tanks, lift stations and water/waste-water treatment plants. The pipeline damages can mainly be attributed to permanent ground deformation due to liquefaction, landsliding and surface fault rupture. However, damages due to transient ground motion are quite frequent. Rigidity of the pipe body, connection type, age and corrosion are some of the factors that influence the seismic response of water and waste-water system elements.

Table 8.1 SYNER-G taxonomy for water supply network

Category	Classification/sub-component
Sources Springs Rivers Natural lakes Impounding reservoirs Wells (shallow/deep) (anchored/unanchored sub-components)	Electric power, electric equipment, well pump, building
Treatment plants Small Medium Large (anchored/unanchored sub-components)	Electric power, electric equipment, chlorination equipment, sediment flocculation, basins, baffles, paddles, scrapers, chemical tanks, elevated pipe, filter gallery
Pumping stations Small Medium Large (anchored/unanchored sub-components)	Electric power, equipment, vertical/horizontal pump, building
Storage tanks Closed tanks Open cut reservoirs	Material type (wood, steel, concrete, masonry), capacity (small, medium, large), anchorage (yes/no), position (at grade, elevated by columns or frames), type of roof (R/C, steel, wood), seismic design (yes/no), construction type (elevated by columns, built "at-grade" to rest directly on the ground, build "at-grade" to rest on a foundation, concrete pile foundation), presence of side-located inlet–outlet pipes, volume (height, diameter), thicknesses, operational function (full, nearly full, less than full)
Pipes	Location (buried/elevated), type (continuous/segmented), material/type, strength (ductile iron, steel, PVC (acrylonitrile-butadienestyrene/ABS), polyethylene/PE, reinforced plastic mortar/RPM, resin transfer molding/RTM- asbestos-cement pipes, cast iron, concrete, clay), type of joints (rigid/flexible), capacity (diameter), geometry (wall thickness), type of coating and lining, depth, history of failure, appurtenances and branches, corrosiveness of soil conditions, age, pressure
Tunnels	Construction technique, liner system, geologic conditions
Canals Open cut or built up using levees Reinforced, unreinforced liners or unlined embankments	Material (wood, steel, concrete), appurtenances and branches location, age of construction, geometrical characteristics (width, depth, capacity), section (orthogonal, trapezoid, etc.), inclination
SCADA system	

Table 8.2 SYNER-G taxonomy for waste-water network

Category	Classification/sub-component
Treatment plants	Electric power, electric equipment, chlorination equipment, sediment flocculation, chemical tanks, elevated pipe, building
Small	
Medium	
Large	
(anchored/unanchored sub-components)	
Pumping (lift) stations	
As in water supply network pumping stations	
Pipes	
As in water supply network pipes	
Tunnels	
As in water supply tunnels	
SCADA system	

8.3.1 Water System

There are numerous references of water system damages during earthquakes in USA (EERI 1990; NRC 1994; Lew et al. 1994; EERI 1995; Schiff 1995), Japan (Shinozuka 1995; Chung et al. 1996; Shrestha 2001), and more recently in New Zealand (Cubrinovski et al. 2010). On the other hand, limited records have been recorded after earthquakes in Europe as for example in 1999 Kocaeli and Düzce earthquakes in Turkey (O'Rourke et al. 2000; Tang 2000; Tromans 2004; Alexoudi 2005), 2003 Lefkas earthquake in Greece (Alexoudi 2005; Alexoudi et al. 2006), and 2009 L'Aquila earthquake (Stewart et al. 2009).

The level of perturbation due to water supply systems' failures is closely connected with restoration time and the number of customers. Important factors for the restoration time is the extent and distribution of damages, the organization of the water network company including the availability of personnel and spare parts of water elements as well as the interactions between different systems after the earthquake (e.g. pipelines from different utility systems lying in the same ditch or the coordination of repairing crews of different utility networks). As an example, after the 1995 Hyogo-ken Nanbu (Kobe) earthquake, restoration lasted 14 days and 450 people were involved. About 1,757 failures of main water system were fixed; in the secondary network the fixed repairs were about 62,300 (Shinozuka 1995; Chung et al. 1996). The restoration time after the 1994 Northridge earthquake was about 7 days (Lew et al. 1994; Todd et al. 1994; O'Rourke and Palmer 1994), while the water system was functional almost immediately after the 1989 Loma Prieta earthquake (EERI 1990).

In general, water system failures can include disability of the network:

- To supply the available water and pressure for fire-fighting purposes in the end-point node.
- To serve customers' needs in summer with maximum daily consumption.
- To supply water to all customers independent of the region and the elevation.

Based on empirical observations and structural analysis, tanks whose filling level is greater than 50 % seem to be vulnerable to earthquakes (Salzano et al. 2003). An important factor for the seismic response of tanks is the height over radius ratio. According to ASCE (1987) the main failure modes for tanks are: shell buckling mode, roof and miscellaneous steel damage, anchorage failure, foundation failure, support system failure, hydrodynamic pressure failure, connecting pipe failure and manhole failure.

The main failure modes of water treatment plants and its elements are described by ASCE (1987) and include damage/malfunction in diversion structure, inlet control building, screen house, grit collection-aeration of water, chemical building, mixing-coagulation and sedimentation basins, filter building, post-chlorination, outlet building.

Canal failure is often closely related to the increased friction between the water and the liner, as the result of debris residue that is lowering hydraulic capacity. Debris may have entered into the canal causing higher sediment transport, which could cause scour of the liner or earthen embankments. Damage to overcrossings may also occur. Overcrossing damage could include the collapse of highway bridges and leakage of non-potable material pipelines running over the deck such as oil, gas, etc. Damage to bridge abutments can cause constriction of the canal's cross-section to such an extent leading to significant flow restriction which warrants immediate shutdown and repair (ALA 2001a).

Ground shaking induces stresses in the liner system of tunnels. If the level of shaking is high, the liner can crack, which can result in tunnel collapse. For water tunnels, the impact of liner failure may or may not be immediate. Generally, small cracks in liners do not directly impact the flow of water through the tunnel, although minor increases in head loss are possible. Over time, small cracks allow water to enter the native materials behind the liner, which can cause erosion and ultimately can extend damage to the liner. The factors that lead to major damage are fault offset through the tunnel itself or landslide at the tunnel portals.

Pumping stations are complex systems with several components, therefore damages are closely related with the failure modes of their sub-components.

Direct damage to pipelines is breakage and leakage; the percentage of leakages and breakages is relevant to the pipe diameter (Eidinger 1998). It depends also on the type of hazard, transient wave propagation or ground failure. Damage to segmented pipes (e.g., cast iron pipe having caulked bell-and-spigot joints) will be heavy when crossing surface ruptured faults according to ALA (2001a, b). Moreover, pipe breaks occur due to relative vertical (differential) settlements at transition zones from fill to better soil, and in areas of alluvial soils prone to localized liquefaction. Breaks can also occur where pipes enter tanks or buildings. Landslides may also produce localized, severe damage to buried pipes. Experience has also shown that welded pipelines with bends, elbows and local eccentricities will concentrate deformation at these features especially if permanent ground deformations develop compression strains. Segmented pipes with rigid caulking cannot tolerate much movement before leakage occurs. Pipeline damage tends to concentrate at discontinuities such as pipe elbows, tees, in-line valves, reaction

Table 8.3 Possible failure modes for pipes as a result of wave propagation

Typology	Failure mode	Reference(s)
Continuous pipes	Tensile failure, wrinkling, beam buckling, welded slip joint	O'Rourke and Liu (1999)
Segmented pipes	Axial pull-out, crushing of bell and spigot joints, joint rotation, round flexural cracks	Singhal (1984), O'Rourke and Liu (1999)
Segmented pipes	Axial pull-out, joint rotation, tensile and bending deformations of the pipe barrel	ALA (2001a)

Table 8.4 Possible failure modes for pipes as a result of ground failure

Cause	Failure modes	Reference(s)
Liquefaction	Settlement, transverse movement, axial deformation	O'Rourke and Palmer (1996)
Landslide, fault crossing	Perpendicular crossing: pipelines subject mainly to bending	O'Rourke et al. (1998)
	Oblique crossing: pipelines subject to compression and bending	
	Parallel crossing: pipelines subject to tension and bending	

blocks and service connections. Such features create anchor points or rigid locations that promote force/stress concentrations. Locally high stresses can also occur at pipeline connections to adjacent structures (e.g., tanks, buildings and bridges). Age and corrosion will accentuate damage, especially in segmented steel, threaded steel and cast iron pipes. Age effects are possibly strongly correlated with corrosion effects. Corrosion weakens pipes by decreasing the material's thickness and by creating stress concentrations. Damage mechanisms of buried pipelines are also described in Chap. 7 (Sect. 7.3.1) for gas pipelines.

The basic failure modes of pipes for the case of wave propagation are given in Table 8.3.

The main failure modes of water pipes due to liquefaction, landslides and fault crossing are given in Table 8.4.

8.3.2 Waste-Water System

As in water systems, the main damages in waste-water networks were observed in pipes; secondarily in lift stations and waste-water treatment plants. The pipeline damages can be attributed mainly to permanent ground deformation and less to wave propagation. Rigid pipe body, connections, age and corrosion are some of the factors that influence the seismic response of waste-water networks. Direct damage

to waste-water networks is often followed by indirect seismic effects like pavement collapse, road blockage, disrupted traffic flow, water pollution, soil pollution and potential public health problems.

There are several references of waste-water system damages during earthquakes in USA (EERI 1990; NRC 1994; Lew et al. 1994; EERI 1995; Schiff 1995) and Japan (Shinozuka 1995; Chung et al. 1996; Shrestha 2001; Scawthorn et al. 2006) and more recently in New Zealand (Cubrinovski et al. 2010) and Chile (EERI 2010). On the other hand, in Europe, very limited data are available as for example in 1999 Düzce earthquake in Turkey (Erdik 2000; Uçkan et al. 2005) and 2003 Lefkas earthquake in Greece (Alexoudi 2005).

The main failures of waste-water systems' components are similar to the water systems' components. However, waste-water pipes sometimes do not fail immediately after an earthquake, as the induced cracks and leakages may cause pipe failure after several days, weeks or even months.

8.4 Review of Existing Fragility Functions

This section provides a description of the most common fragility functions that are available in the literature, along with their associated intensity measures and damage scales.

8.4.1 Definition of Adequate Intensity Measures

A main issue in the fragility assessment is to define the appropriate ground-motion intensity measure (IM) that best captures the response of the exposed element and minimizes the dispersion of that response. The IM is also related to the approach that is followed for the derivation of fragility functions. As a general remark, the empirical fragility curves relate the observed damages with the seismic intensity. In this case, the more suitable intensity measures are PGA and PGV, which can be estimated from strong ground motion records at close distance and similar soil conditions. In general, this correlation of reported damages to instrumental recordings estimated from the available data, which in turn are rather limited, is among the main sources of uncertainties regarding the reliability of the proposed fragility curves.

For linear lifeline systems like pipelines it has been proved that peak ground velocity is better correlated to the observed damages. An alternative approach may be the use of ground strains (longitudinal and transversal) or/and differential ground displacements, which are directly correlated to the ground velocity. For other components it may be peak ground acceleration or spectral acceleration (i.e. buildings, tanks, water treatment plants). Permanent ground deformation (PGD) is a widely used parameter for ground failure (e.g. liquefaction). A short review of the most commonly used intensity measures is given for the different components of water and waste-water systems.

8.4.1.1 Water System

Existing fragility relations for pipelines for wave propagation are based on a variety of intensity measures such as PGA, PGV, PGS (peak ground strain) or MMI (macroseismic intensity). The majority of the fragility relations use PGV in the sense that there is a direct link between the longitudinal ground strain and PGV (e.g. Toprak 1998; O'Rourke et al. 2012). When ground failure is considered, permanent ground deformation (PGD) is the most commonly used factor for the description of induced damage. In some recent studies, PGV^2/PGA and GMPGV (geometric mean of PGV) are also used. A review of intensity measures for buried pipelines is also given in Chap. 7 (Sect. 7.4.1.1).

For canals, PGV and PGD are equally used as for the derivation of the fragility, while for storage tanks, PGA is the most commonly used parameter. This acceleration-driven parameter is appropriate to account for the inertia forces inherent to these large and usually tall structures.

For all other elements (water sources, water treatment plants, pumping stations) PGA is almost exclusively used, since most facilities are sheltered in a building and PGA is widely used to describe the fragility of R/C or masonry structures.

8.4.1.2 Waste-Water System

For waste-water pipelines the same IMs are applied as in water supply system. Also for sewage tunnels the reader should see Chap. 10 where the fragility functions for roadway and railway tunnels are described. For all other elements (waste-water treatment plants, lift stations) again PGA is almost exclusively used, since most facilities are sheltered in a building and PGA is widely used to describe the fragility of R/C or masonry structures.

8.4.2 Definition of Damage Scales

This section summarizes the parameters used in the literature for defining damage scales in different water and waste-water systems' elements.

8.4.2.1 Water System

Table 8.5 summarizes the parameters for the definition of damage states for the various water systems' components based on the literature. Regarding SCADA equipment, no quantitative study of their vulnerability is available and therefore no relevant damage states can be defined for these components.

Table 8.5 Damage states definition parameters for water systems' components

Component	Damage parameters	Reference(s)
Water source	Type and extent (level) of structural damage	NIBS (2004)
	Serviceability state	NIBS (2004)
Water treatment plant	Type and extent (level) of structural damage	NIBS (2004), SRM-LIFE (2007)
	Serviceability state	NIBS (2004), SRM-LIFE (2007)
	Functionality level	Ballantyne et al. (2009)
	Restoration cost (% of replacement cost)	Ballantyne et al. (2009)
Pumping station	Type and extent (level) of structural damage	NIBS (2004), SRM-LIFE (2007)
	Serviceability state	NIBS (2004), SRM-LIFE (SRMLIFE 2007)
	Reliability index	Scawthorn (1996)
Storage tank	Description of the type and extent (level) of structural damage	O'Rourke and So (2000), NIBS (2004), SRM-LIFE (2007)
	Loss of content	O'Rourke and So (2000), ALA (2001a, b), NIBS (2004), SRM-LIFE (2007), Berahman and Behnamfar (2007)
Canal	Hydraulic performance of a canal	
Pipe	Repair rate (repairs per km)	Katayama et al. (1975), Isoyama and Katayama (1982), ATC-13 (1985), O'Rourke et al. (1991), Honegger and Eguchi (1992), O' Rourke and Ayala (1993), Eidinger et al. (1995), Heubach (1995), Eidinger (1998), O'Rourke et al. (1998), Toprak (1998), O'Rourke and Jeon (1999), Eidinger and Avila (1999), Isoyama et al. (2000), ALA (2001a, b), Chen et al. (2002), Pineda and Ordaz (2003), Yeh et al. (2006), Pineda and Ordaz (2007), O'Rourke et al. (2012)
	Breaks per pipe length	Eguchi et al. (1983), Barenberg (1988), Wang et al. (1991), O'Rourke and Deyoe (2004)
	Vulnerability class	Ballantyne and Heubach (1996)
Tunnel	See Chap. 10	
SCADA	–	

8.4.2.2 Waste-Water System

Table 8.6 summarizes the parameters for the definition of damage states for the various waste-water systems' components based on a literature review. For SCADA equipment, no quantitative vulnerability study is available and therefore no relevant damage states can be defined for these components.

Table 8.6 Damage states definition parameters for waste-water systems' components

Component	Damage parameters	Reference(s)
Waste-water treatment plants	Type and extent (level) of structural damage	NIBS (2004), SRM-LIFE (2007)
	Serviceability state	NIBS (2004), SRM-LIFE (2007)
Pipes, Tunnels	As in water system	
Lift stations	Type and extent (level) of structural damage	NIBS (2004), SRM-LIFE (2007)
	Serviceability state	NIBS (2004), SRM-LIFE (2007)
SCADA	–	

8.4.3 Description of Existing Fragility Functions

This section describes the most common fragility functions that are available in the literature for water and waste-water systems' components, along with their associated intensity measures and damage scales, the methodology used for their derivation and the adopted classification schemes.

8.4.3.1 Water System

As already mentioned before, empirical relations have been proposed for the estimation of pipe damage, which relate intensity measures (IM) (mainly PGV and PGD) with repair rate/km (RR/km). Recently, more advanced approaches have been proposed, which consider ground strains and/or other parameters as appropriate earthquake intensity measures. A detailed review of the available functions for pipelines has already been given in Chap. 7 (Sect. 7.4.3.1).

For storage tanks various empirical functions have been proposed (O'Rourke and So 2000; ALA 2001a, b; NIBS 2004). Recently, empirical functions have been improved using Bayesian approach by Berahman and Behnamfar (2007), while Iervolino et al. (2004) introduced an analytical approach to build fragility curves for unanchored steel tanks. An analytical review of available fragility functions for storage tanks is given in Chap. 7 (Sect. 7.4.3.2).

Water sources, water treatment plants and pumping stations are complex elements consisting of various sub-components. Their seismic response depends on the response of the simple components (NIBS 2004; Ballantyne et al. 2009).

Table 8.7 presents a brief review of existing fragility functions for water sources, water treatment plants, pumping stations, storage tanks, pipes, tunnels, canals and conduits.

Table 8.7 Review of existing fragility functions for water supply system elements

Component	Reference	Methodology	Classification	IM
Water sources	NIBS (2004)	HAZUS – empirical fragility functions	Anchorage of sub-components	PGA
	SRMLIFE (2007)	Empirical fragility functions	Building seismic design level	PGA
Water treatment plants	NIBS (2004)	HAZUS – empirical fragility functions	Anchorage of sub-components, size	PGA
	SRM-LIFE (2007)	HAZUS – empirical fragility functions	Anchorage of sub-components	PGA
Pumping stations	Scawthorn (1996)	No fragility functions. Pumping station fault-tree diagram	There are no fragility curves given for sub-components	–
	NIBS (2004)	HAZUS – empirical fragility functions	Anchorage of sub-components	PGA
	SRM-LIFE (2007)	Empirical fragility functions	Building seismic design level	PGA
Storage tanks	O'Rourke and So (2000)	Empirical fragility functions	On-grade steel tanks Height to diameter ratio, amount of stored content	PGA
	ALA (2001a, b)	Empirical fragility functions	Anchorage, material, size, seismic design, roof	PGA, PGD
	NIBS (2004)	HAZUS – empirical fragility functions	Above ground R/C tanks	PGA
	Berahman and Behnamfar (2007)	Bayesian approach	Unanchored on-grade steel tanks	PGA
Pipes	See Tables 7.10 and 7.11 in Chap. 7 (Sect. 7.4.3.1)			
Tunnels	As in roadway system (see Chap. 10)			
Canals	ALA (2001a, b)	Empirical	–	PGV, PGD

8.4.3.2 Waste-Water System

Table 8.8 presents a brief review of existing fragility functions for waste landfills, waste-water treatment plants, lift stations, pipes, tunnels and conduits.

8.5 Recommendations

On the basis of a critical review of available fragility functions in the literature, the most adequate functions are identified and described in this section for different elements of water and waste-water systems.

Table 8.8 Review of existing fragility functions for waste-water system elements

Component	Reference	Methodology	Classification	IM
Solid waste landfills	Matasovic et al. (1998)	According to the real damage observations	–	–
Waste- water treatment plants	NIBS (2004)	HAZUS – empirical fragility functions	Anchorage of sub-components, size	PGA
	SRM-LIFE (2007)	SRM-LIFE based on HAZUS empirical fragility functions	Complex component with anchored sub-components independently from the size but according to the building type	PGA
Lift stations	As in water supply system			
Pipes	As in water supply system			
Tunnels	As in roadway system (see Chap. 10)			

Table 8.9 Parameters of fragility curves for water sources (wells), SRM-LIFE (2007)

		Peak ground acceleration (PGA)	
Description	Damage state	Median (g)	β (log-standard deviation)
Anchored components (low-rise R/C building with low level seismic design)	Minor	0.16	0.70
	Moderate	0.18	0.65
	Extensive	0.30	0.65
	Complete	0.40	0.75
Anchored components (low-rise R/C building with high level seismic design)	Minor	0.25	0.55
	Moderate	0.45	0.50
	Extensive	0.85	0.55
	Complete	2.10	0.70

8.5.1 Water System

The most adequate fragility functions and in some cases alternative relationships are presented in the followings for the water system components, along with their damage states' definitions.

8.5.1.1 Water Sources

The fragility curves proposed in the Greek project SRM-LIFE (2007) could be used for the vulnerability assessment of water sources (wells) (Table 8.9 and Fig. 8.1). They were derived through fault-tree analysis, using the fault-tree and the fragility

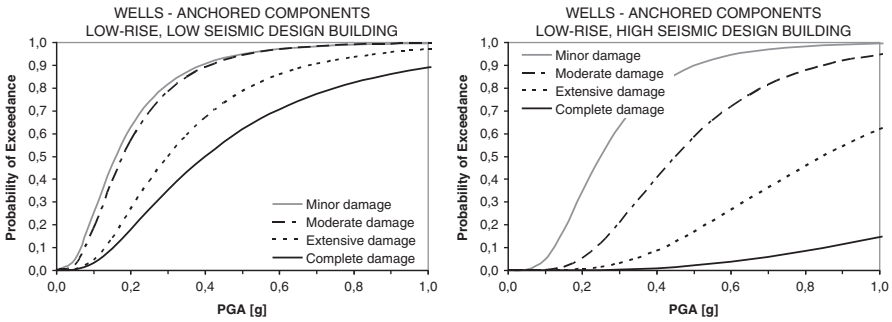

Fig. 8.1 Fragility curves for water sources (wells) with anchored components, low – rise R/C building with low (*left*) and high (*right*) level of seismic design, SRM-LIFE (2007)

Table 8.10 Description of damage states for water sources (wells), SRM-LIFE (2007)

Damage state	Description	Restoration cost (%)	Serviceability	
Minor	Malfunction of well pump and motor for a short time (less than 3 days) due to loss of electric power and backup power, if any, or light damage to buildings	10–30	Normal flow and water pressure	Operational after limited repairs
Moderate	Malfunction of well pump and motor for about a week due to loss of electric power and backup power, if any, considerable damage to mechanical and electrical equipment, or moderate damage to buildings	30–50	Reduce flow and water pressure	Operational after repairs
Extensive	Extensive building damage or extensive distortion of the well pump and vertical shaft	50–75		Partially operational after extensive repairs
Complete	Building collapse	75–100	No water available	Not repairable

curves of sub-components proposed in HAZUS (NIBS 2004). A semi-anchorage of sub-components is considered (i.e. anchorage of sub-components without following specific guidelines resulting in uncertainty on its final response), while for the buildings' sub-components, the typology and fragility curves proposed in SRM-LIFE were used. These curves are applicable to water sources housed in low-rise R/C buildings, according to Greek buildings' typology.

The description of damage states, restoration cost (as a percentage of the replacement cost) and serviceability levels are provided in Table 8.10.

Table 8.11 Parameters of fragility curves for water sources (wells), HAZUS (NIBS 2004)

		Peak ground acceleration (PGA)	
Description	Damage state	Median (g)	β (log-standard deviation)
Wells	Minor	0.15	0.75
	Moderate	0.36	0.65
	Extensive	0.72	0.65
	Complete	1.50	0.80

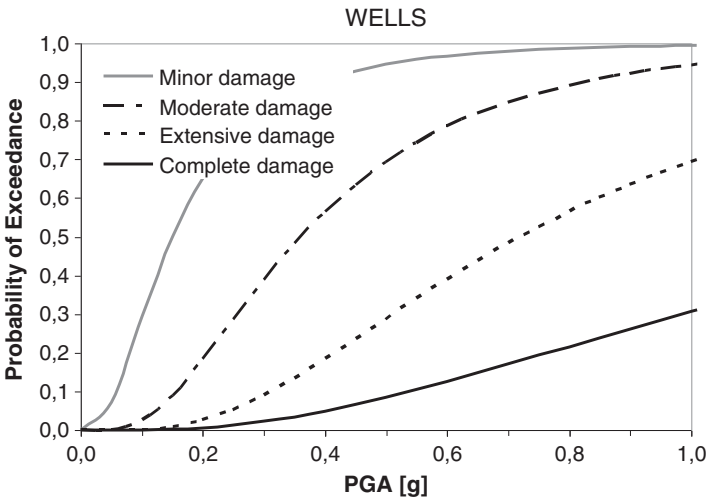

Fig. 8.2 Fragility curves for water sources (wells), HAZUS (NIBS 2004)

Alternatively, the generic fragility functions from HAZUS methodology (NIBS 2004) for water sources (wells) could be used (Table 8.11 and Fig. 8.2). Damage states definitions are the same as in Table 8.10.

8.5.1.2 Water Treatment Plants

The fragility curves from SRM-LIFE (2007) are suggested for the vulnerability assessment of water treatment plants. They were derived through fault-tree analysis, using the fault-tree and the fragility curves of sub-components proposed in HAZUS (NIBS 2004). These curves are applicable to water treatment plants with anchored components with no backup power.

The description of damage states for water treatment plants is provided in Table 8.12 while the corresponding fragility curves are given in Table 8.13 and illustrated in Fig. 8.3.

Alternatively, the generic fragility functions from HAZUS methodology (NIBS 2004) for water treatment plants could be used (Table 8.14 and Fig. 8.4). The definition of damage states is the same as in Table 8.12.

Table 8.12 Description of damage states for water treatment plants, SRM-LIFE (2007)

Damage state	Description	Restoration cost (%)	Serviceability	
Minor	Malfunction of plant for a short time (<3 days) due to loss of electric power, considerable damage to various equipment, light damage to sedimentation basins, light damage to chlorination tanks, or light damage to chemical tanks. Loss of water quality may occur	10–30	Normal flow and water pressure	Operational after limited repairs
Moderate	Malfunction of plant for about a week due to loss of electric power and backup power, if any, extensive damage to various equipments, considerable damage to sedimentation basins, considerable damage to chlorination tanks with no loss of contents, or considerable damage to chemical tanks. Loss of water quality is imminent	30–50	Reduce flow and water pressure	Operational after repairs
Extensive	Extensive damage to the pipes connecting different basins and chemical units. Shutdown of the plant is likely	50–75		Partially operational after extensive repairs
Complete	Complete failure of all pipings or extensive damage to the filter gallery	75–100	Not water available	Not repairable

Table 8.13 Parameters of fragility curves for water treatment plants, SRM-LIFE (2007)

Description	Damage state	Peak ground acceleration (PGA)	
		Median (g)	β (log-standard deviation)
Water treatment plants with anchored components	Minor	0.15	0.30
	Moderate	0.30	0.25
	Extensive	0.55	0.60
	Complete	0.90	0.55

8.5.1.3 Pumping Stations

The fragility curves proposed in SRM-LIFE (2007) could be used for the vulnerability assessment of pumping stations (Table 8.15 and Fig. 8.5). They were derived using the same methodology as in water sources. These curves are applicable to pumping stations, without backup power, housed in low-rise R/C buildings, according to Greek buildings' typology.

The description of damage states for pumping stations is provided in Table 8.16.

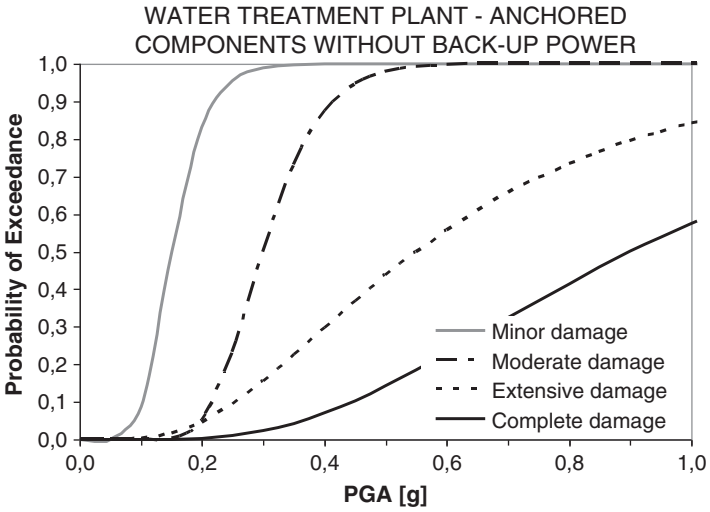

Fig. 8.3 Fragility curves for water treatment plants (anchored components), SRM-LIFE (2007)

Table 8.14 Parameters of fragility curves for water treatment plants, HAZUS (NIBS 2004)

			Peak ground acceleration (PGA)	
Description		Damage state	Median (g)	β (log-standard deviation)
Small water treatment plants [10–50 million gallons per day (mgd)]	Anchored sub-components	Minor	0.25	0.50
		Moderate	0.38	0.50
		Extensive	0.53	0.60
		Complete	0.83	0.60
	Unanchored sub-components	Minor	0.16	0.40
		Moderate	0.27	0.40
		Extensive	0.53	0.60
		Complete	0.83	0.60
Medium water treatment plants (50–200 mgd)	Anchored sub-components	Minor	0.37	0.40
		Moderate	0.52	0.40
		Extensive	0.73	0.50
		Complete	1.28	0.50
	Unanchored sub-components	Minor	0.20	0.40
		Moderate	0.35	0.40
		Extensive	0.75	0.50
		Complete	1.28	0.50
Large water treatment plants (>200 mgd)	Anchored sub-components	Minor	0.44	0.40
		Moderate	0.58	0.40
		Extensive	0.87	0.45
		Complete	1.57	0.45
	Unanchored sub-components	Minor	0.22	0.40
		Moderate	0.35	0.40
		Extensive	0.87	0.45
		Complete	1.57	0.45

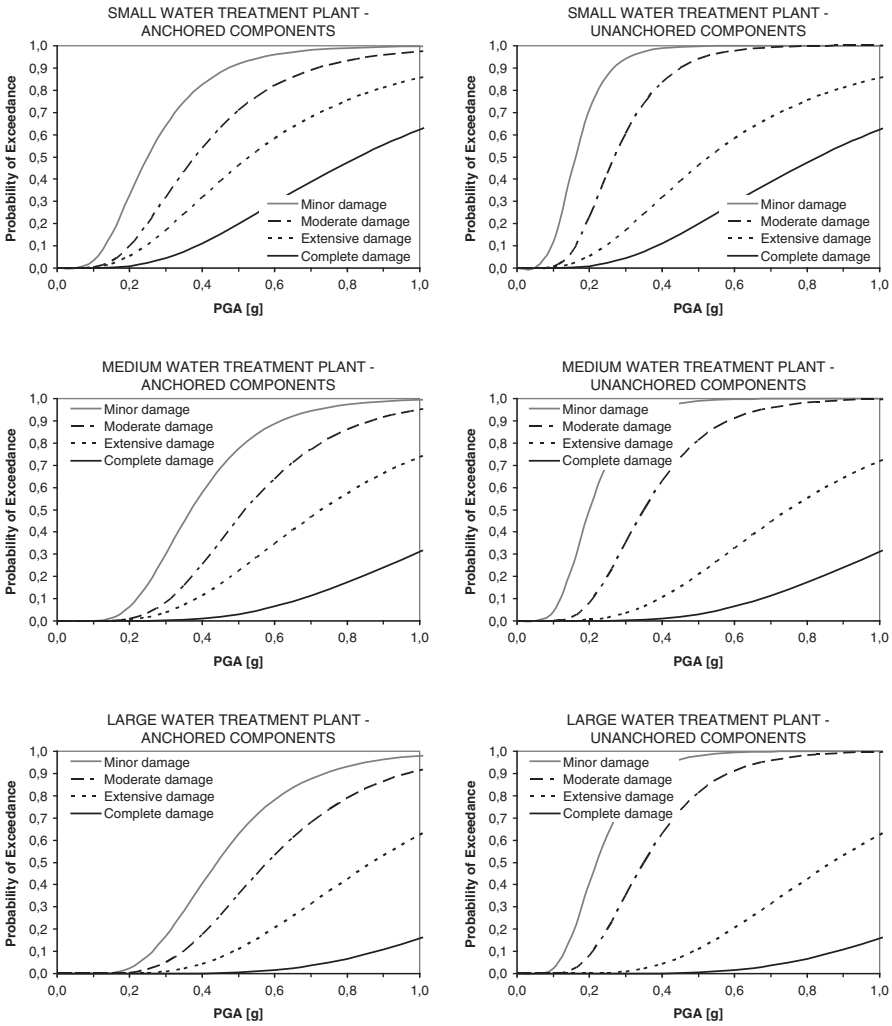

Fig. 8.4 Fragility curves for water treatment plants, HAZUS (NIBS 2004)

Alternatively, the generic fragility functions from HAZUS methodology (NIBS 2004) for pumping stations could be used (Table 8.17 and Fig. 8.6). The definition of damage states is the same as in Table 8.16.

8.5.1.4 Storage Tanks

In Europe, the most common typology is R/C tanks without anchorage; however there are not available studies for the evaluation of their fragility. The empirical fragility curves by ALA are suggested for the vulnerability assessment of R/C tanks

Table 8.15 Parameters of fragility curves for pumping stations, SRM-LIFE (2007)

		Peak ground acceleration (PGA)	
Description	Damage state	Median (g)	β (log-standard deviation)
Anchored components (low-rise R/C building with low level seismic design)	Minor	0.10	0.55
	Moderate	0.15	0.55
	Extensive	0.30	0.70
	Complete	0.40	0.75
Anchored components (low-rise R/C building with high level seismic design)	Minor	0.15	0.30
	Moderate	0.30	0.35
	Extensive	1.1	0.55
	Complete	2.1	0.70

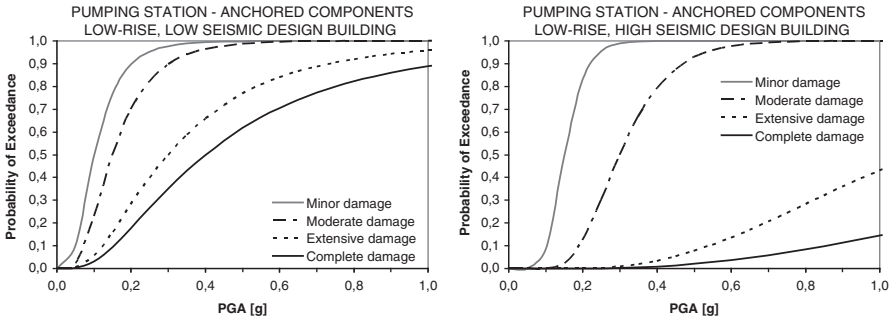

Fig. 8.5 Fragility curves for pumping stations, with anchored components and low-rise R/C building with low (*left*) and high (*right*) level of seismic design, SRM-LIFE (2007)

Table 8.16 Description of damage states for pumping stations, SRM-LIFE (2007)

Damage state	Description	Restoration cost (%)	Serviceability	
Minor	Malfunction of plant for a short time (<3 days) due to electric power loss or slight building damage	10–30	Normal flow and water pressure	Operational after limited repairs
Moderate	Loss of electric power for about a week, considerable damage to mechanical and electrical equipment, or moderate building damage	30–50	Reduced flow and water pressure	Operational after repairs
Extensive	Extensive building damage or extensive, beyond repair, pumps' damage	50–75		Partially operational after extensive repairs
Complete	Building collapse	75–100	Not water available	Not repairable

Table 8.17 Parameters of fragility curves for pumping stations, HAZUS (NIBS 2004)

		Peak ground acceleration (PGA)		
Description	Damage state	Median (g)	β (log-standard deviation)	
Small pumping stations (<10 mgd)	Anchored components	Minor	0.15	0.70
		Moderate	0.36	0.65
		Extensive	0.66	0.65
		Complete	1.50	0.80
	Unanchored components	Minor	0.13	0.60
		Moderate	0.28	0.50
		Extensive	0.66	0.65
		Complete	1.50	0.80
Medium/large pumping stations (>10 mgd)	Anchored components	Minor	0.15	0.75
		Moderate	0.36	0.65
		Extensive	0.77	0.65
		Complete	1.50	0.80
	Unanchored components	Minor	0.13	0.70
		Moderate	0.28	0.50
		Extensive	0.77	0.65
		Complete	1.50	0.80

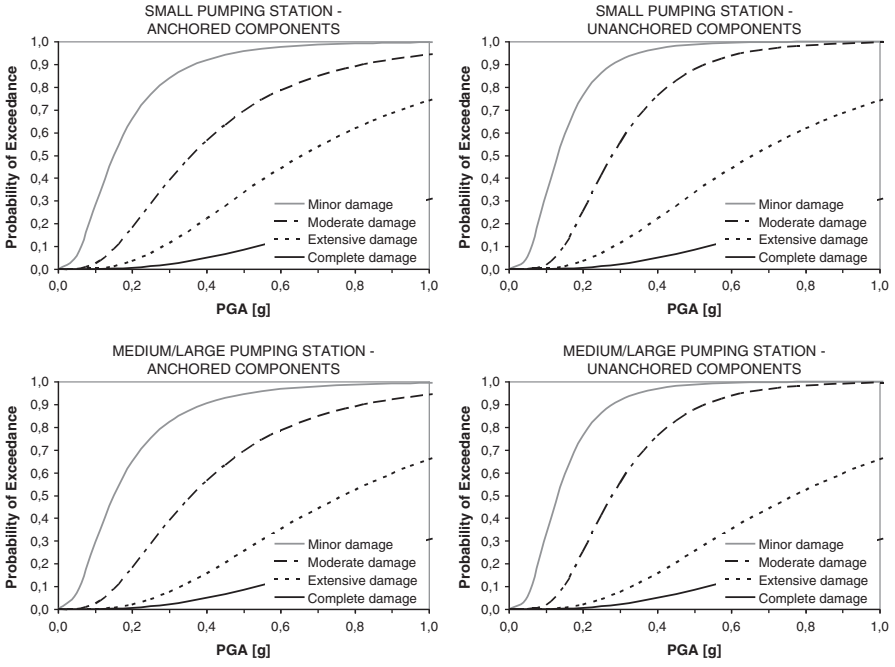

Fig. 8.6 Fragility curves for pumping stations, HAZUS (NIBS 2004)

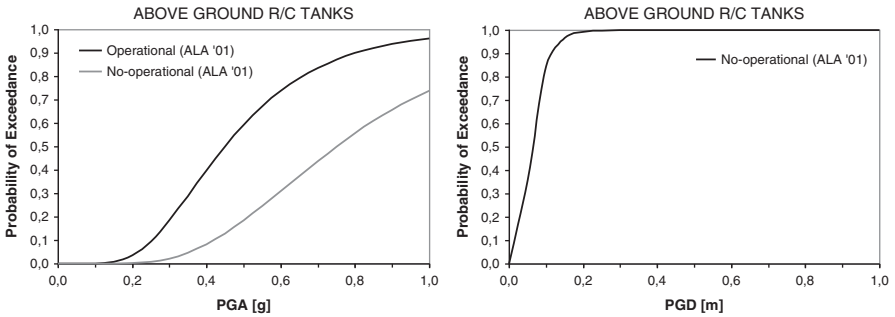

Fig. 8.7 Fragility curves for above ground R/C tanks subject to wave propagation (*left*) and permanent ground deformations (*right*) (ALA 2001a, b)

Table 8.18 Fragility curves for anchored R/C at grade tanks (wave propagation), ALA (2001a, b)

		Peak ground acceleration (PGA)	
Failure type	Serviceability	Median (g)	β (log-standard deviation)
Uplift of wall– crush concrete	No operational	1.30	0.50
Cracking or shearing of tank wall		1.60	0.50
Sliding		1.10	0.50
Hoop overstress	Operational	4.10	0.50

Table 8.19 Fragility curves for unanchored R/C at grade tanks (wave propagation), ALA (2001a, b)

		Peak ground acceleration (PGA)		
Failure type	Serviceability	Median (g)	β (log-standard deviation)	
Cracking or shearing of tank wall	Loss of context	No operational	1.05	0.45
Roof damage	No loss of context	Operational	2.60	0.45
Uplift of wall– crush concrete	Small leak		2.00	0.45
Sliding	Small leak		0.25	0.45
Hoop overstress	Loss of context	No operational	0.75	0.45
	Small leak	Operational	0.45	0.45

subject to ground shaking or ground failure (Fig. 8.7, Table 8.18, 8.19, 8.20, and 8.21). These functions are based on a large set of empirical data, considered as the most recent and complete ones. Due to lack of other studies, the fragility curves provided by HAZUS for steel and wood tanks are recommended (Fig. 8.8, Table 8.22). They are based on combination of empirical data and engineering judgment and appear as a reasonable compromise for common applications. It is also noted that the HAZUS curves are applicable for water tanks which are at least 80 % full at the time of the earthquake.

Table 8.20 Fragility curves for open reservoirs with or without seismic design (wave propagation), ALA (2001a, b)

			Peak ground acceleration (PGA)	
Failure type		Serviceability	Median (g)	β (log-standard deviation)
Roof damage	Extensive	Operational	1.00	0.55
	Minor		0.60	0.55

Table 8.21 Fragility curves for unanchored R/C at grade tanks (permanent ground deformations), ALA (2001a, b)

			Permanent ground deformation (PGD)	
Typology		Serviceability	Median (m)	β (log-standard deviation)
R/C	Anchored	No operational	0.06	0.50
	Unanchored			
Steel	At columns		0.06	0.50
	At grade		0.09	0.50
Wooden		No operational	0.09	0.50
Without roof		Operational	0.20	0.50

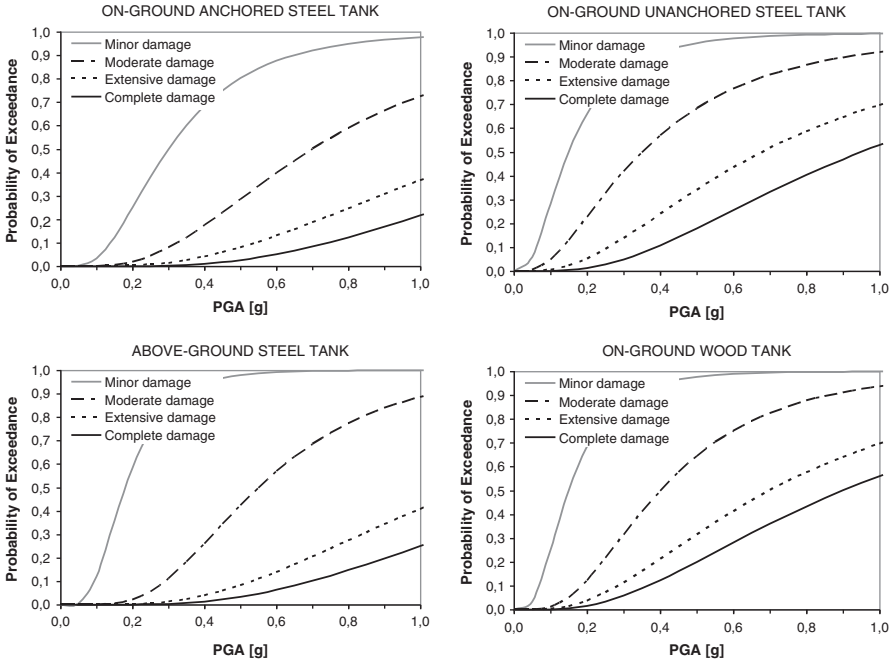

Fig. 8.8 Fragility curves for steel and wood tanks (HAZUS, NIBS 2004)

Table 8.22 Fragility curves for steel and wood tanks (wave propagation), HAZUS, NIBS (2004)

		Peak ground acceleration (PGA)	
Typology	Damage states	Median (g)	β (log-standard deviation)
On-ground anchored steel tanks	Minor	0.30	0.60
	Moderate	0.7	0.60
	Extensive	1.25	0.65
	Complete	1.62	0.60
On-ground unanchored steel tanks	Minor	0.15	0.70
	Moderate	0.35	0.75
	Extensive	0.68	0.75
	Complete	0.95	0.70
Above-ground steel tanks	Minor	0.18	0.50
	Moderate	0.55	0.50
	Extensive	1.15	0.60
	Complete	1.50	0.60
On-ground wood tanks	Minor	0.15	0.60
	Moderate	0.40	0.60
	Extensive	0.70	0.70
	Complete	0.90	0.70

8.5.1.5 Canals

The only available study for the vulnerability assessment of canals is provided by ALA (2001a, b) where different damage states are defined and related with levels of permanent ground deformation. Tables 8.23, 8.24, and 8.25 provide the description of damage states, and the vulnerability of canals due to wave propagation and ground failure.

8.5.1.6 Pipes

The main factor controlling pipe vulnerability to earthquake shaking or ground deformation is the pipe material. Old distribution networks are mainly brittle (e.g. asbestos-cement or concrete) with low flexibility. In modern or upgraded networks, ductile pipes (e.g. ductile iron, steel or PVC) are mostly used. These pipes are more flexible and therefore more earthquake resistant (Isoyama et al. 2000). However, fragility functions based only on pipe material cannot accurately estimate seismic damage. Factors such as pipe diameter, joint type, soil conditions may also affect seismic vulnerability.

A review of the existing empirical relations by Tromans (2004) provides a comparative illustration of the most commonly used functions, assuming a corrective factor $K = 1$ (i.e. the "backbone curve" without considering the effect of the pipe material and/or other factors) (see Chap. 7, Fig. 7.6). It is obvious that available functions have important discrepancies in terms of the predictive repair rates as well as their applicability range. Regarding the effects of ground failure, the

Table 8.23 Description of damage states for canals (ALA 2001a, b)

Damage state	Description	Damage rate
No damage	The canal has the same hydraulic performance after the earthquake	
Minor damage	Some increase in the leak rate of the canal is occurred. Damage to the canal liner may occur, causing increased friction between the water and the liner and lowering hydraulic capacity. The liner damage may be due to PGDs in the form of settlements or lateral spreads due to liquefaction, movement due to landslide, offset movement due to fault offset, or excessive ground shaking. Landslide debris may have entered into the canal causing higher sediment transport, which could cause scour of the liner or earthen embankments. Overall, the canal can be operated at up to 90 % of capacity without having to be shut down for repairs	Minor damage to unreinforced liners or unlined embankments may be expected at Repair Rate/km 0.1 for ground shaking velocities of PGV = 0.50 to 0.90 m/s. The minor damage rate drops to 0.01 repairs per kilometer for ground shaking velocities of PGV = 0.15 to 0.40 m/s and 0 below that. Damage to reinforced liners is one quarter of these rates. Bounds on the damage estimate can be estimated assuming plus 100 % to minus 50 % at the plus or minus one standard deviation level, respectively
Moderate damage	Some increase in the leak rate of the canal is occurred. Damage to the canal liner is occurred, causing increased friction between water and the liner, lowering hydraulic capacity. The liner damage may be due to PGDs in the form of settlements or lateral spreads due to liquefaction, movement due to landslide, offset movement due to fault offset, or excessive ground shaking. Landslide debris may enter into the canal causing higher sediment transport, which could cause scour of the liner or earthen embankments. Overall, the canal can be operated in the short term at up to 50–90 % of capacity; however, a shutdown of the canal soon after the earthquake is required to make repairs. Damage to canal overcrossings may occur, and temporary shutdown of the canal is needed to make repairs. Damage to bridge abutments could cause constriction of the canal's cross-section to such an extent that it causes a significant flow restriction	Moderate damage is expected if lateral or vertical movements of the embankments due to liquefaction or landslide are in the range of 2.5–13 cm. Moderate damage occurs due to fault offset across the canal of 2.5–13 cm. Moderate damage is expected if small debris flows into the canal from adjacent landslides

(continued)

Table 8.23 (continued)

Damage state	Description	Damage rate
Major damage	The canal is damaged to such an extent that immediate shutdown is required. The damage may be due to PGDs in the form of settlements or lateral spreads due to liquefaction, movement due to landslide, offset movement due to fault offset, or excessive ground shaking. Landslide debris may enter the canal and cause excessive sediment transport, or may block the canal's cross-section to such a degree that the flow of water is disrupted, overflowing over the canal's banks and causing subsequent flooding. Damage to overcrossings may occur, requiring immediate shutdown of the canal. Overcrossing damage could include the collapse of highway bridges and leakage of non-potable material pipelines such as oil, gas, etc. Damage to bridge abutments could cause constriction of the canal's cross-section to such an extent that a significant flow restriction which warrants immediate shutdown and repair	Major damage is expected if PGDs of the embankments are predicted to be 15 cm or greater. Major damage occurs due to fault offset across the canal of 15 cm or more. Major damage is expected if a significant amount of debris is predicted to flow into the canal from adjacent landslides. The differentiation of moderate or major damage states for debris flows into the canal should factor in hydraulic constraints caused by the size of the debris flow, the potential for scour due to the type of debris and water quality requirement

Table 8.24 Vulnerability of canals for wave propagation (ALA 2001a, b)

Typology	PGV < 0.5 m/s	PGV > 0.5 m/s (RR $= 0.1$ repair/km)
Unreinforced liners or unlined	No	Minor
Reinforced liners	No	No

Table 8.25 Vulnerability of canals for permanent deformations (ALA 2001a, b)

Typology	PGD < 0.025 m	PGD ≥ 0.025 m	PGD ≥ 0.15 m
Unreinforced liners or unlined	No/minor	Moderate	Major damages
Reinforced liners			

comparison of some fragility curves (using the "backbone curve", without any corrective factors), is also given in Chap. 7 (Fig. 7.8).

Empirical functions for pipelines have been validated based on damage data from earthquakes in Turkey (Kocaeli, Ms = 7.8, 17-08-1999 and Düzce, Ms = 7.3, 12-11-1999) and Greece (Lefkas, Ms = 6.4, 14/8/2003). In particular relevant studies in Düzce case (Alexoudi 2005; Pitilakis et al. 2005; Alexoudi et al. 2007, 2008, 2010) for water and waste-water systems compared the observed damages with several empirical curves proposed in the literature (O'Rourke and

Ayala 1993; Isoyama et al. 1998; Eidinger and Avila 1999; ALA 2001a, b). Considering that the water distribution network in Düzce is mainly made up of brittle pipes, a good agreement was achieved between the observed and estimated damages for ground shaking, especially when the O' Rourke and Ayala (1993) fragility relation, that is also proposed in HAZUS methodology, was applied. Moreover, the spatial distribution of damages using the O'Rourke and Ayala (1993) relation was generally well correlated with the Tromans (2004) and Alexoudi (2005) recorded data from Kocaeli earthquake, given the inherent uncertainties in the recorded damages and in the individual characteristics of the pipes.

In case of Lefkas earthquake, empirical relations for ground shaking (O'Rourke and Ayala 1993; Eidinger and Avila 1999; Isoyama et al. 1998; ALA 2001a, b) and ground failure (Honegger and Eguchi 1992; Eidinger and Avila 1999; Heubach 1995; ALA 2001a, b) have been compared with recorded damages of the water supply system (Alexoudi 2005; Pitilakis et al. 2005). The water distribution network of Lefkas is composed mainly by PVC (ductile) pipes with special couplings in the joints, while some brittle (asbestos-cement) pipelines also exist. The damages observed along the coastline, resulted from permanent ground deformation due to soil liquefaction. The rest were attributed to wave propagation and material failures. In general, the fragility functions proposed in NIBS (2004) for both ground shaking (O'Rourke and Ayala 1993) and ground failure (Honegger and Eguchi 1992) seem to better capture the behavior of the system in terms of total number of failures.

Based on these validation studies in the European context, the HAZUS (NIBS 2004) fragility functions for water pipes are deemed to adequately estimate the total number of repairs both due to wave propagation and ground failure, especially in case of brittle pipelines. In particular, for wave propagation, the O'Rourke and Ayala (1993) relation (Eq. 8.1), which yields the repair rate (*RR* in repairs per km) as a function of PGV (in cm/s), seems to provide good estimates.

$$\mathrm{RR} = \mathrm{K} \cdot \left(0.0001 \cdot \mathrm{PGV}^{2.25}\right) \tag{8.1}$$

For ground failure, it is the Honegger and Eguchi (1992) relation in respect to the permanent ground deformation (PGD) in m.

$$\mathrm{RR} = \mathrm{K} \cdot \left(7.821 \cdot \mathrm{PGD}^{0.56}\right) \tag{8.2}$$

The corrective factor K for both relationships is equal to 1 for brittle pipes (CI, AC, RCC) and 0.3 for ductile pipes (DI, S, PVC). It is assumed that damage due to wave propagation will consist of 80 % leaks and 20 % breaks, while damage due to ground failure will consist of 20 % leaks and 80 % breaks.

However, according to some studies (Tromans 2004; O'Rourke 1999) the fragility relation by O'Rourke and Ayala (1993) seems to be over-conservative. It is seldomly based on data from the U.S., while the more recent relations of ALA (2001a, b) are based on a largest set of empirical data and offer a quite long applicability range. Alternatively, the ALA (2001a, b) relations are recommended

Table 8.26 K_1 parameter in ALA (2001a, b) relation for transient ground motion, for pipes

Pipe material	Joint type	Soils	Diameter	K_1
Unknown	Unknown	Unknown	Unknown	1.00
Cast iron	Cement	All	Small	1.00
			Large	0.50
		Corrosive	Small	1.40
			Large	0.70
		Non corrosive	Small	0.70
			Large	0.35
	Rubber gasket	All	Small	0.80
			Large	0.40
Welded steel	Lap – Arc welded	All	Small	0.60
		Corrosive		0.90
		Non corrosive		0.30
		All	Large	0.15
	Screwed	All	Small	0.70
	Rubber gasket			1.30
	Riveted			1.30
Asbestos cement	Rubber gasket	All	Small	0.50
	Cement			1.00
Concrete w/Stl Cyl.	Lap – Arc welded	All	Large	0.70
	Cement			1.00
	Rubber gasket			0.80
PVC	Rubber gasket	All	Small	0.50
Ductile iron	Rubber gasket	All	Small	0.50
			Large	0.25

for general applications. They yield the repair rate (*RR* in repairs per km) as a function of PGV (in cm/s) for ground shaking and PGD (cm) for ground failure via the following equations:

$$\mathrm{RR} = \mathrm{K}_1 \cdot 0.002416 \cdot \mathrm{PGV} \tag{8.3}$$

where K_1 is the parameter used to adjust the fragility with respect to the backbone curve, based on the material, the connection type, the soil type and the pipe diameter (Table 8.26).

$$RR = K_2\ 2.5829 PGD^{0.319} \tag{8.4}$$

The corrective factor K_2 depends on the pipe material and the connection type (Table 8.27).

8.5.1.7 Tunnels

As in roadway system (see Chap. 10).

Table 8.27 K_2 parameter in ALA (2001a, b) relation for ground failure, for pipes

Pipe material	Joint type	K_2
Unknown	Unknown	1.00
Cast iron	Cement	1.00
	Rubber gasket	0.80
	Mechanical restrained	0.70
Welded steel	Arc welded, lap welds (large diameter, non corrosive)	0.15
	Rubber gasket	0.70
Asbestos cement	Rubber gasket	0.80
	Cement	1.00
Concrete w/Stl Cyl.	Welded	0.60
	Cement	1.00
	Rubber gasket	0.70
PVC	Rubber gasket	0.80
Ductile iron	Rubber gasket	0.50

Table 8.28 Parameters of fragility curves for waste-water treatment plants, SRM-LIFE (2007)

		Peak ground acceleration (PGA)	
Description	Damage state	Median (g)	β (log-standard deviation)
Waste-water treatment plants with anchored components (low-rise R/C building with low level seismic design)	Minor	0.15	0.35
	Moderate	0.30	0.20
	Extensive	0.45	0.50
	Complete	0.50	0.50
Waste-water treatment plants with anchored components (low-rise R/C building with high level seismic design)	Minor	0.15	0.35
	Moderate	0.30	0.20
	Extensive	0.45	0.50
	Complete	1.00	0.50

8.5.2 Waste-Water System

The most adequate fragility functions and in some cases alternative relationships are presented in the followings for the waste-water system components, along their damage states' definitions.

8.5.2.1 Waste-Water Treatment Plants

The fragility curves from SRM-LIFE (2007) are suggested for the vulnerability assessment of waste-water treatment plants (Table 8.28 and Fig. 8.9). Again fault-tree analysis is used, based on the fault-tree and the fragility curves of sub-components proposed in HAZUS (NIBS 2004). A semi-anchorage of

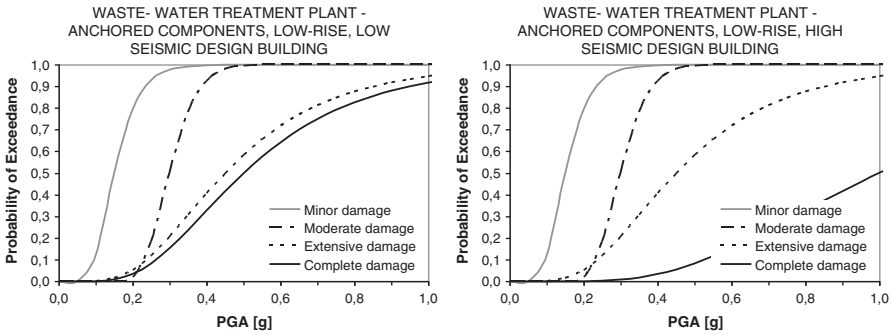

Fig. 8.9 Fragility curves for waste-water treatment plants with anchored components, low-rise R/C building with low (*left*) and high (*right*) level of seismic design, SRM-LIFE (2007)

sub-components is considered (i.e. anchorage of sub-components without following specific guidelines resulting in uncertainty on its final response), while for the building housing different sub-components, the typology and fragility curves proposed in SRM-LIFE were used. These curves are applicable to treatment plants, without backup power, housed in low-rise R/C buildings, according to Greek buildings' typology.

The description of damage states, restoration cost (as percentage of replacement cost) and serviceability levels for waste-water treatment plants is provided in Table 8.29.

Alternatively, the generic fragility functions provided in HAZUS methodology (NIBS 2004) for waste-water treatment plants could be used. They are based on the distinction between anchored and unanchored sub-components for small, medium and large waste-water treatment plants (Table 8.30 and Fig. 8.10). The damage states definitions are the same as in Table 8.29.

8.5.2.2 Lift Stations

The fragility curves proposed in SRM-LIFE (2007) are proposed for the vulnerability assessment of lift stations, following the same approach as in waste-water treatment plants. These curves are applicable to lift stations, without backup power, housed in low-rise R/C buildings, according to Greek buildings' typology.

The description of damage states for lift stations is provided in Table 8.31 while the corresponding vulnerability curves are given in Table 8.32 and illustrated in Fig. 8.11.

Alternatively, the generic fragility functions from HAZUS methodology (NIBS 2004) for lift stations could also be used. Damage functions for lift stations are similar to those of pumping plants in water supply systems.

Table 8.29 Description of damage states for waste-water treatment plants, SRM-LIFE (2007)

Damage state	Description	Restoration cost (%)	Serviceability	
Minor	Malfunction of plant for a short time (<3 days) due to loss of electric power, considerable damage to various equipment, light damage to sedimentation basins, light damage to chlorination tanks, or light damage to chemical tanks	10–30	Normal flow and pressure	Operational after limited repairs
Moderate	Malfunction of plant for about a week due to loss of electric power, extensive damage to various equipment, considerable damage to sedimentation basins, considerable damage to chlorination tanks with no loss of contents, or considerable damage to chemical tanks	30–50	Reduced flow and pressure	Operational after repairs
Extensive	Extensive damage to the pipes connecting different basins and chemical units	50–75		Partially operational after extensive repairs
Complete	Complete failure of all pipings or extensive damages to buildings equipment	75–100	No available	Not repairable

Table 8.30 Parameters of fragility curves for waste-water treatment plants, HAZUS (NIBS 2004)

		Peak ground acceleration (PGA)		
Description	Damage state	Median (g)	β (log-standard deviation)	
Small waste-water treatment plants [<50 million gallons per day (mgd)]	Anchored sub-components	Minor	0.23	0.40
		Moderate	0.35	0.40
		Extensive	0.48	0.50
		Complete	0.80	0.55
	Unanchored sub-components	Minor	0.16	0.40
		Moderate	0.26	0.40
		Extensive	0.48	0.50
		Complete	0.80	0.55
Medium waste-water treatment plants (50–200 mgd)	Anchored sub-components	Minor	0.33	0.40
		Moderate	0.49	0.40
		Extensive	0.70	0.45
		Complete	1.23	0.55
	Unanchored sub-components	Minor	0.20	0.40
		Moderate	0.33	0.40
		Extensive	0.70	0.45
		Complete	1.23	0.55

(continued)

Table 8.30 (continued)

Description	Damage state	Peak ground acceleration (PGA)		
		Median (g)	β (log-standard deviation)	
Large waste-water treatment plants (>200 mgd)	Anchored sub-components	Minor	0.40	0.40
		Moderate	0.56	0.40
		Extensive	0.84	0.40
		Complete	1.50	0.40
	Unanchored sub-components	Minor	0.22	0.40
		Moderate	0.35	0.40
		Extensive	0.84	0.40
		Complete	1.50	0.40

8.5.2.3 Conduits

For **tunnels** as in roadway system (see Chap. 10).

For **pipes** as proposed for water supply system (Sect. 8.5.1.6).

8.6 Conclusions

The main characteristics and typologies of water and waste-water networks' components were summarized along with the main damage mechanisms and failure modes. Some components such as water sources, treatment plants and pumping or lift stations are actually complex sub-systems consisting of different sub-components. Therefore their vulnerability assessment is based on the fragilities of the sub-components and is usually estimated through a fault-tree approach. An important feature of the water and waste-water networks' components is the existence of anchorage of the sub-components as well as the seismic design level of structural elements.

Available fragility functions have been collected and reviewed for all main components of the two systems. The existing fragility functions are based on empirical data, while the use of analytical or expert judgment approaches is rather limited. An important issue in the vulnerability assessment is the use of seismic intensity measures (IM) that best capture the response of the exposed element. As a general remark, the empirical relations use PGA and PGV to describe the seismic intensity for ground shaking and PGD for ground failure. For all structures except pipes the most often used IM is the PGA. For pipeline and canal elements, PGV is the main descriptor of ground motion severity level.

For water sources, water treatment plants, pumping stations, waste-water treatment plants and lift stations the fragility curves that have been derived in SRM-LIFE (2007) are suggested, referring to specific typologies common in

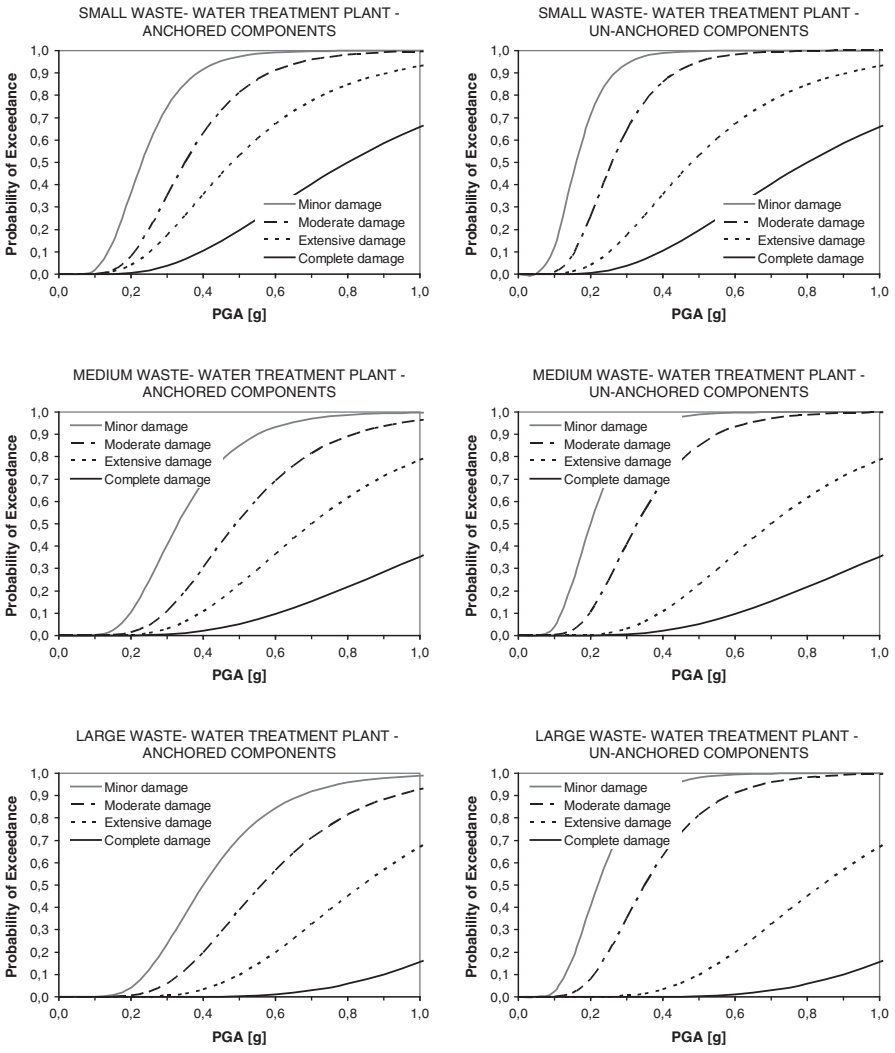

Fig. 8.10 Fragility curves for waste-water treatment plants, HAZUS (NIBS 2004)

Greece and probably in the whole European context. Alternatively, the generic fragility functions that are included in HAZUS (NIBS 2004) methodology can also be used.

For R/C storage tanks subject to ground shaking or ground failure, the fragility curves by ALA (2001a, b) are suggested. They are based on a large set of empirical data and are considered as the most recent and complete ones. For steel and wood tanks the fragility curves provided in HAZUS (NIBS 2004) methodology are recommended.

The vulnerability of canals due to wave propagation and ground failure can be estimated based on the ALA (2001a, b) procedure, which is actually the only available.

Table 8.31 Description of damage states for lift stations, SRM-LIFE (2007)

Damage state	Description	Restoration cost (%)	Serviceability	
Minor	Malfunction of lift station for a short time (<3 days) due to loss of electric power or slight damage to buildings	10–30	Normal flow	Operational after limited repairs
Moderate	Loss of electric power for about a week, considerable damage to mechanical and electrical equipment, or moderate damage to buildings	30–50	Reduce flow	Operational after repairs
Extensive	Extensive building damage or extensive, beyond repair pumps' damage	50–75		Partially operational after extensive repairs
Complete	Building collapse	75–100	Not water	Not repairable

Table 8.32 Parameters of fragility curves for lift stations, SRM-LIFE (2007)

		Peak ground acceleration (PGA)	
Description	Damage state	Median (g)	β (log-standard deviation)
Anchored components (low-rise R/C building with low level seismic design)	Minor	0.10	0.55
	Moderate	0.15	0.55
	Extensive	0.30	0.70
	Complete	0.40	0.75
Anchored components (low-rise R/C building with high level seismic design)	Minor	0.15	0.30
	Moderate	0.30	0.35
	Extensive	1.1	0.55
	Complete	2.1	0.70

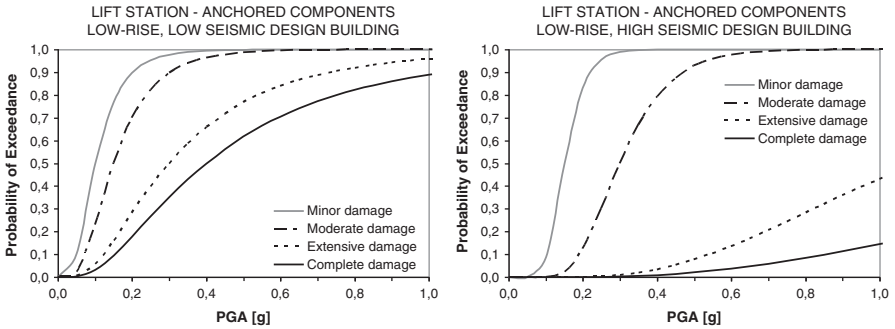

Fig. 8.11 Fragility curves for lift stations, with anchored components, low-rise R/C building with low (*left*) and high (*right*) level of seismic design, SRM-LIFE (2007)

The vulnerability of pipes is essentially performed using empirical fragility relationships that correlate the repair ratio with seismic intensity. Corrective factors are also applied to account for discrete pipe features such as the material, diameter or joint type. Based on the relatively few well-reported damages in water systems in Europe it seems that the empirical relations by HAZUS (NIBS 2004) provide an overall good estimation of the expected damages. Alternatively, the ALA (2001a, b) relations can be applied for water and waste-water pipes.

For tunnels, the reader is referred to the recommendations of Chap. 10 for roadway/railway systems.

Finally, the proposed damage states for each component are related with the restoration cost (as percentage of the replacement cost) and the serviceability level which can be applied for estimation of the total losses of the networks (economic and functional). These thresholds are qualitative and are given here as a general outline, while the user could modify accordingly.

Acknowledgments The authors are grateful to Dr Maria Alexoudi for sharing her knowledge on water and waste-water networks' components typologies, functionality and fragility assessment methods.

References

Alexoudi M (2005) Contribution to seismic assessment of lifelines in urban areas. Development of holistic methodology for seismic risk. Dissertation, Department of Civil Engineering, Aristotle University of Thessaloniki, Greece (in Greek)

Alexoudi M, Kakderi K, Pitilakis K (2006) The role of site effects in the vulnerability assessment of water systems. Application to Lefkas. In: Proceedings of 5th national conference of geotechnical and environmental engineering, Xanthi, Greece, 31 May–2 June 2006 (in Greek)

Alexoudi M, Manou D, Hatzigogos Th (2007) The influence of probabilistic loading and site-effects in the earthquake risk assessment of water system. The case of Düzce. In: Proceedings of 10th international conference on applications of statistics and probability in civil engineering, Tokyo, Japan, 31 July–3 Aug 2007

Alexoudi M, Manou D, Pitilakis K (2008) Seismic vulnerability analysis of waste-water system. Methodology and application for Düzce and Kocaeli earthquakes. In: Proceedings of 14th WCEE, Beijing, China, 12–17 Oct 2008

Alexoudi M, Manou D, Pitilakis K (2010) Influence of local site conditions in the seismic risk assessment of the water system in Düzce (Turkey). In: Proceedings of 6th national conference of geotechnical and environmental engineering, Volos, Greece, 29 Sept–1 Oct 2010 (in Greek)

American Lifelines Alliance (2001a) Seismic fragility formulations for water systems. Part 1 – Guideline, ASCE-FEMA, p 104

American Lifelines Alliance (2001b) Seismic fragility formulations for water systems. Part 2 – Appendices, ASCE-FEMA, p 239

Applied Technology Council (ATC) (1985) ATC-13-Earthquake damage evaluation data for California. Applied Technology Council (ATC), Redwood City

ASCE (1987) Planning, operation, rehabilitation and automation of irrigation water delivery systems. In: Zimbelman D (ed) Proceedings of a symposium sponsored by the irrigation and drainage division, Portland, Oregon, 28–30 July, p 391

Ballantyne D, Heubach W (1996) Use of GIS to evaluate earthquake hazard effects and mitigation on pipeline systems – case studies. In: Proceedings of the 6th Japan- U.S. workshop on

earthquake resistant design of lifeline facilities and countermeasures against soil liquefaction, Technical Report NCEER-96-0012

Ballantyne D, Perimon T, Martins P (2009) Water treatment plant seismic risk assessment for the joint water commission, Hillsboro, Oregon. TCLEE 2009, pp 1–10. doi:10.1061/41050(357) 120

Barenberg ME (1988) Correlation of pipe damage with ground motion. J Geotech Eng 114 (6):706–711

Berahman F, Behnamfar F (2007) Seismic fragility curves for unanchored on-grade steel storage tanks: Bayesian approach. J Earthq Eng 11(2):166–192

Chen WW, Shih B, Chen YC, Hung JH, Hwang HH (2002) Seismic response of natural gas and water pipelines in the Ji-Ji earthquake. Soil Dyn Earthq Eng 22:1209–1214

Chung RM, Ballantyne DB, Comeau E et al (1996) January 17, 1995 Hyogoken-Nanbu (Kobe) earthquake: performance of structures, lifelines and fire protection system. NIST Special Publication 901 (ICSSC TR18), National Institute of Standards and Technology, Gaithersburg, Maryland, p 573

Cubrinovski M, Green R, Allen J et al (2010) Geotechnical reconnaissance of the 2010 Darfield (New Zealand) earthquake. University of Canterbury, p 173

EERI (1990) Loma Prieta earthquake of October 17, 1989: reconnaissance report. Earthquake Spectra, Supplement to vol. 6, Earthquake Engineering Research Institute, Oakland, CA

EERI (1995) Northridge earthquake of January 17, 1994: reconnaissance report. Earthquake Spectra, Supplement C to vol. 11, Earthquake Engineering Research Institute, Oakland, CA

EERI (2010) The Mw 8.8 Chile earthquake of February 27, 2010. EERI special earthquake report, Earthquake Engineering Research Institute, p 20

Eguchi RT, Legg MR, Taylor CE, Philipson LL, Wiggins JH (1983) Earthquake performance of water and natural gas supply system. J Wiggins Co, NSF Grant PFR-8005083, Technical Report 83-1396-5

Eidinger J (1998) Lifelines, water distribution system in the Loma Prieta, California, Earthquake of October 17, 1989, performance of the build environment-lifelines. In: Schiff A (ed) US Geological Survey professional paper 1552-A, pp A63–A80

Eidinger J, Avila E (1999) Guidelines for the seismic upgrade of water transmission facilities. Monograph No. 15, TCLEE/ASCE

Eidinger J, Maison B, Lee D, Lau B (1995) East bay municipality utility district water distribution damage in 1989 Loma Prieta Earthquake. In: O'Rourke M (ed) Proceedings of the 4th US conference on lifeline earthquake engineering, Monograph No. 6. TCLEE/ASCE, pp 240–247

Erdik M (2000) Report on 1999 Kocaeli and Duzce (Turkey) Earthquakes. In: Casciati F, Magonette G (eds) Proceedings of the 3rd international workshop on structural control, Paris, France, 6–8 July 2000. World Scientific Publishing Co. Pte Ltd, Singapore

Heubach W (1995) Seismic damage estimation for buried pipeline systems. In: O'Rourke M (ed) Proceedings of the 4th US conference on lifeline earthquake engineering, Monograph No. 6, TCLEE/ASCE, pp 312–319

Honegger DG, Eguchi RT (1992) Determination of the relative vulnerabilities to seismic damage for San Diego country water authority (SDCWA) water transmission pipelines, October

Iervolino I, Fabbrocino G, Manfredi G (2004) Fragility of standard industrial structures by a response surface based method. J Earthq Eng 8(6):927–945

Isoyama R, Katayama T (1982) Reliability evaluation of water supply systems during earthquakes. Report of the Institute of Industrial Science, University at Tokyo, February, vol 30, no.1

Isoyama R, Ishida E, Yune K, Shirozu T (1998) Seismic damage estimation procedure for water supply pipelines. In: Proceedings IWSA international workshop: anti-seismic measures on water supply (Water & Earthquake'98 Tokyo)

Isoyama R, Ishida E, Yune K, Shirozu T (2000) Seismic damage estimation procedure for water supply pipelines. In: Proceedings of the 12th world conference on earthquake engineering, CD-ROM, Paper No. 1762

Katayama T, Kubo K, Sato N (1975) Earthquake damage to water and gas distribution systems. In: Proceedings of the U.S. national conference on earthquake engineering, EERI, Oakland, CA, pp 396–405

Lew HS, Cooper J, Hacopian S, Hays W, Mahokey M (1994) The January 17, 1994, Northridge earthquake (California). In: Ranfaste NJ (ed), NIST special publication 871. National Institute of Standards and Technology, Gaithersburg, Maryland

Matasovic N, Kavazanjian E, Anderson R (1998) Performance of solid waste landfills in earthquakes. Earthq Spectra 14(2):319–334

National Institute of Building Sciences (NIBS) (2004) Earthquake loss estimation methodology. HAZUS'04, technical manual, vol 1. Federal Emergency Management Agency (FEMA), Washington, DC

NRC (1994) Practical lessons learned from Loma Prieta earthquake. National Research Council, National Academy Press, Washington, DC

O'Rourke MJ (1999) Estimation of post-earthquake water system serviceability. In: Proceedings of the 7th Japan-US workshop on earthquake resistant design of lifeline facilities and countermeasures for soil liquefaction, MCEER, State University of New York at Buffalo, Buffalo, NY, pp 391–403

O'Rourke MJ, Ayala G (1993) Pipeline damage due to wave propagation. J Geotech Eng, ASCE 119(9):1490–1498

O'Rourke MJ, Deyoe E (2004) Seismic damage to segmented buried pipe. Earthq Spectra 20 (4):1167–1183

O'Rourke TD, Jeon SS (1999) Factors affecting the earthquake damage of water distribution systems. In: Elliot M, McDonough P (eds) Proceedings of the 5th US conference on lifeline earthquake engineering, Seattle WA, 12–14 Aug 1999. Monograph No. 16, TCLEE/ASCE, pp 379–388

O'Rourke MJ, Liu X (1999) Response of buried pipelines subject to earthquake effects. MCEER Monograph No. 3, Multidisciplinary Center for Earthquake Engineering Research, University of Buffalo, Buffalo, New York, p 249

O'Rourke TD, Palmer MC (eds) (1994) The Northridge, California earthquake of January 17, 1994, performance of gas transmission pipelines. Technical report NCEER-94-0011, National Center for Earthquake Engineering Research, Buffalo, NY

O'Rourke TD, Palmer MC (1996) Earthquake performance of gas transmission pipelines. Earthq Spectra 12(3):493–527

O'Rourke MJ, So P (2000) Seismic fragility curves for on-grade steel tanks. Earthq Spectra 16 (4):801–815

O'Rourke TD, Gowdy TE, Stewart HE, Pease JW (1991) Lifeline and geotechnical aspects of the 1989 Loma Prieta earthquake. In: Proceedings of the 2nd international conference on recent advances in geotechnical earthquake engineering and soil dynamics, St Luis, MO

O'Rourke TD, Toprak S, Sano Y (1998) Factors affecting water supply damage caused by the Northridge earthquake. In: Proceedings of the 6th US national conference on earthquake engineering, Seattle, Washington, 31 May–4 June 1998

O'Rourke TD, Erdogan FH, Savage WL, Lund LV, Tang A, Basoz N, Edwards C, Tezel G, Wong F (2000) Water, gas, electric power and telecommunications performance, Kocaeli, Turkey, Earthquake of August 17, 1999: reconnaissance report, Earthquake Spectra, Supplement A to vol. 16

O'Rourke TD, Jeon SS, Toprak S, Cubrinovski M, Jung JK (2012) Underground lifeline system performance during the Canterbury earthquake sequence. In: Proceedings of the 15th world conference on earthquake engineering, Lisbon, Portugal

Pineda O, Ordaz M (2003) Seismic vulnerability function for high diameter buried pipelines: Mexico City's primary water system case. Proc Int Conf Pipeline Eng Constr 2:1145–1154

Pineda O, Ordaz M (2007) A new seismic parameter to estimate damage in buried pipelines due to seismic wave propagation. J Earthq Eng 11(5):773–786

Pitilakis K, Alexoudi M, Kakderi K, Manou D, Batum E, Raptakis D (2005) Vulnerability analysis of water systems in strong earthquakes. The case of Lefkas (Greece) and Düzce (Turkey). In: Proceedings of international symposium on the geodynamics of eastern Mediterranean: active Tectonics of the Aegean, Istanbul, Turkey, 15–18 June 2005

Salzano E, Iervolino I, Fabbrocino G (2003) Seismic risk of atmospheric storage tanks in the framework of quantitative risk analysis. J Loss Prev Process Ind 16:403–409

Scawthorn Ch (1996) Reliability-based design of water supply systems. In: Proceedings of the 6th Japan-US workshop on earthquake resistant design of lifeline facilities and countermeasures against soil liquefaction, technical report NCEER −96-0012

Scawthorn C, Miyajima M, Ono Y, Kiyono J, Hamada M (2006). Lifeline aspects of the 2004 Niigata Ken Chuetsu, Japan, earthquake. Earthquake Spectra, Supplement 1 to Vol. 22, S89–S110

Schiff AJ (ed) (1995) Northridge earthquake lifeline performance and post-earthquake response. Monograph No.8. TCLEE/ASCE, New York, p 339

Shinozuka M (ed) (1995) The Hanshin-Awaji earthquake of January 17, 1995, performance of lifelines. Technical report NCEER-95-0015, National Center for Earthquake Engineering Research, Buffalo, NY

Shrestha BK (2001) Disaster reduction and response preparedness in Japan: A Hyogo approach. In: Proceedings of the 2nd conference on disaster communications (CDC 2001), Tampere, Finland, 28–30 May 2001

Singhal AC (1984) Nonlinear behavior of ductile iron pipeline joints. J Tech Topics Civil Eng, ASCE 110(1):29–37

SRMLIFE (2007) Development of a global methodology for the vulnerability assessment and risk management of lifelines, infrastructures and critical facilities. Application to the metropolitan area of Thessaloniki. Research project, General Secretariat for Research and Technology, Greece

Stewart JP, Di Capua G et al (2009) Preliminary report on the seismological and geotechnical aspects of the April 6 2009 L'Aquila earthquake in central Italy (Version 2.0). Report of the National Science Foundation-Sponsored GeoEngineering Extreme Events Reconnaissance (GEER) Team

Tang A (ed) (2000) Izmit Kocaeli, Turkey earthquake of August 17, 1999 including Duzce earthquake of November 12, 1999: lifeline performance. Monograph No 17, TCLEE/ASCE, March 2000

Todd D, Carino N, Chung R, Lew HS, Taylor AW, Walton WD (1994) 1994 Northridge earthquake: performance of structures, lifelines and fire protection systems, NISTIR Publication 5396. National Institute of Standards and Technology, Gaithersburg, Maryland, p 171

Toprak S (1998) Earthquake effects on buried lifeline systems. Dissertation, Cornell University

Tromans I (2004) Behaviour of buried water supply pipelines in earthquake zones. Dissertation, Imperial College of Science, Technology and Medicine, University of London

Uçkan E, Durukal E, Demircioğlu M, Siyahi B, Erdik M (2005) Observed damage at buried pipelines during the 1999 Kocaeli (Izmit) Turkey Earthquake. European Geosciences Union (EGU) General Assembly, EGU 05-A-10583, Vienna, 24–29 April 2005, p 295

Wang LRL, Wang JCC, Ishibashi I (1991) GIS applications in seismic loss estimation model for Portland, Oregon water and sewer systems. US Geological Survey, Open file report

Yeh CH, Shih BJ, Chang CH, Chen WYW, Liu GY, Hung HY (2006) Seismic damage assessment of potable water pipelines. In: Proceedings of the 4th international conference earthquake engineering, Paper No. 247, Taipei, Taiwan, 12–13 Oct 2006

Chapter 9
Fragility Functions of Road and Railway Bridges

Georgios Tsionis and Michael N. Fardis

Abstract This Chapter presents a literature review of seismic fragility functions for reinforced concrete road and railway bridges. It first covers the main issues in fragility analysis, such as the systems for classification of bridges, methods for deriving fragility functions, intensity measures, damage states and damage measures. A section is dedicated to the way the uncertainties regarding the seismic action, geometry, material properties and modelling are treated in existing studies. The Chapter deals also with the recent developments that examine special issues which were not addressed in the first generation of fragility curves. They refer to damaged and retrofitted bridges, the effects of corrosion, skew, spatial variability of the seismic action and liquefaction. Finally, a method for fast fragility analysis of regular bridges is presented. The method applies to bridges with continuous deck monolithically connected to the piers or supported on elastomeric bearings and with free or constrained transverse translation at the abutments.

9.1 Introduction

Damage to bridges incurs economic loss in the form of repair or replacement costs and disruption of traffic. Furthermore, bridges are critical in the post-earthquake emergency phase for the transportation of victims, rescue teams, first-aid supplies and equipment between the affected and neighbouring areas. For these reasons, they are included in vulnerability studies that aim to predict the seismic risk in a region in terms of the expected damage suffered by individual structures, or populations thereof, and complex systems.

The European collaborative research project SYNER-G (www.syner-g.eu) focused on systemic seismic vulnerability and risk analysis of buildings, lifelines

G. Tsionis • M.N. Fardis (✉)
Department of Civil Engineering, University of Patras, Patras, 26504, Greece
e-mail: tsionis@upatras.gr; fardis@upatras.gr

K. Pitilakis et al. (eds.), *SYNER-G: Typology Definition and Fragility Functions for Physical Elements at Seismic Risk*, Geotechnical, Geological and Earthquake Engineering 27,
DOI 10.1007/978-94-007-7872-6_9,

and infrastructures. The work presented herein was motivated by the project objectives to encompass all past and ongoing knowledge at international level in the field of assessment of the physical vulnerability of assets and to develop, where necessary, new fragility curves that consider the distinctive typological features of European construction and practice.

Risk analysis may be performed for a specific bridge or for the inventory in a region, in which case a taxonomy is necessary. Another elementary issue is the methodology for the production of fragility curves. Empirical and opinion-based curves are limited in number, while most previous studies make use of numerical analysis. As regards intensity measures, the criteria for the selection of the most appropriate one are mainly the correlation with damage and the effort required for its computation. The typologies examined in the reviewed studies are listed in Table 9.1 together with the adopted methodologies and intensity measures. Fragility curves are developed for several damage states, each one defined by threshold values of component damage measures and possibly associated to the functionality of the bridge. Finally, there is a concern about the uncertainty related to the modelling, to the seismic action, the geometry and the material properties.

Recent studies examine aspects that were not addressed in the first generation of fragility curves. For example, fragility curves are used to compare the effectiveness of retrofit measures; then the improvement of fragility is quantified. Refinements in vulnerability analysis of bridges refer also to the effects of skew and cumulative seismic damage after the main shock. As regards the seismic action, the effect of spatial variability is included in the analysis and the hazard is related not only to ground shaking but also to ground failure such as liquefaction. Also, fragility curves are developed for the whole lifetime of a bridge in order to account for corrosion and flood scour.

The last section of the Chapter presents a procedure for fast fragility analysis of regular bridges together with example applications for typical European construction. Further to road bridges, the analysis covers railway bridges, that were not studied in the past. This is achieved by considering operational limits for the horizontal deck deformations and the constrained transverse translation of the deck at the abutments. This structural solution is frequently adopted to protect the tracks from deformations due to relative motion of the deck and the access slab. The methodology is implemented in a numerical tool that uses as input the span length and number, cross-section type, pier height and number of columns per pier to design bridges according to Eurocode 2 (CEN 2005c) and, where applicable, Eurocode 8 (CEN 2005d) and to produce their fragility curves. The minimal computational demand renders this tool very efficient for the fragility analysis of a large population of bridges for which only basic information about the geometry is available.

The scope of the Chapter is limited to the most common structural type of reinforced concrete multi-span bridges with simply-supported or continuous deck connected to the piers monolithically or through bearings. There are few studies on the seismic fragility of bridges made of other materials. For instance, Shama and Mander (2003) exploited test results to propose fragility curves for timber bridges. Special typologies such as truss, arch, cable-stayed (e.g. Khan et al. 2004; Casciati et al. 2008) and suspension bridges require ad-hoc fragility analysis.

Table 9.1 Typologies, methodology and intensity measures used in existing fragility functions for bridges

Reference	Typology (deck type; connection to piers; seismic design)[a]	Methodology	Intensity measure
ATC (1985)	Continuous, simply-supported; monolithic, bearings; –	Expert opinion	Mercalli Intensity
Avşar et al. (2011)	Continuous; elastomeric bearings; new code	MDOF nonlinear dynamic	PGA, PGV, ASI
Aygün et al. (2011)	Continuous; fixed bearings; –	MDOF nonlinear dynamic	PGA
Azevedo et al. (2010)	–; –; old, new code	Adapted from FEMA (2010)	$S_a(T = 1\ s)$
Banerjee and Shinozuka (2008)	Continuous w/joint(s); monolithic; –	MDOF nonlinear dynamic	PGA
Basöz et al. (1999)	Continuous, simply-sup.; –; new code, retrofitted; Northridge	Empirical	PGA
Cardone et al. (2011)	Simply-sup.; fixed, sliding, elastomeric bearings; old code	Nonlinear static (adaptive)	PGA
Ceresa et al. (2012a)	Continuous, simply-sup.; elastomeric bearings; old code	MDOF nonlinear dynamic	PGA
Choe et al. (2009)	Continuous; monolithic; new code	Nonlinear static	$S_a(T_1)$
Choi et al. (2004)	Cont., simply-sup.; fixed, sliding, elast. bearings; new code	MDOF nonlinear dynamic	PGA
De Felice and Giannini (2010)	Simply-supported; bearings; old code	SDOF nonlinear dynamic	$S_a(T_1)$
Elnashai et al. (2004)	–; –; –; Northridge; Kobe	Empirical	PGA
Elnashai et al. (2004)	Continuous; monolithic; new code	MDOF nonlinear dynamic	PGA
FEMA (2010)	Cont., simply-sup.; fixed, sliding, elast. bearings; old, new code	Nonlinear static	$S_a(T = 1\ s)$
Franchin et al. (2006)	Simply-supported; –; new code	MDOF nonlinear dynamic	$S_a(T_1)$
Gardoni et al. (2003)	Continuous w/ joint(s); –; new code	Nonlinear static	$S_a(T_1)$
Gardoni and Rosowsky (2009)	Continuous; monolithic; new code	Nonlinear static	$S_a(T_1)$
Jeong and Elnashai (2007)	Continuous w/ or w/o joints, simply-supported; –; –	MDOF/SDOF nonlinear dynamic	PGA
Karim and Yamazaki (2001)	Bridge piers; –; old, new code	SDOF nonlinear dynamic	PGA, PGV
Karim and Yamazaki (2003)	Continuous; monolithic, elastomeric bearings; –; 4 code levels	SDOF nonlinear dynamic	PGA, PGV, SI
Karim and Yamazaki (2003)	Continuous; monolithic; new code	SDOF nonlinear dynamic	PGA, PGV, SI
Kibboua et al. (2011)	Bridge piers; –; new code	SDOF nonlinear dynamic	PGA
Kim and Shinozuka (2004)	Continuous w/or w/o joints; monolithic; old code, retrofitted	MDOF nonlinear dynamic	PGA
Kurian et al. (2006)	Simply-supported; bearings; –	MDOF/SDOF nonlinear dynamic	PGA
Kwon and Elnashai (2009)	Continuous; fixed and expansion bearings; –	MDOF nonlinear dynamic	PGA
Kwon et al. (2009)	Continuous; monolithic; old code	MDOF nonlinear dynamic	PGA
Li et al. (2012)	Continuous; monolithic, old code	MDOF nonlinear dynamic	PGA

(continued)

Table 9.1 (continued)

Reference	Typology (deck type; connection to piers; seismic design)[a]	Methodology	Intensity measure
Lupoi et al. (2004)	Continuous; –; new code	MDOF nonlinear dynamic	PGA
Lupoi et al. (2005)	Continuous; –; new code	MDOF nonlinear dynamic	PGA
Mackie and Stojadinović (2004a)	Continuous; –; new code	SDOF nonlinear dynamic	$S_a(T_1)$
Mackie and Stojadinović (2007)	Continuous; monolithic; –	Nonlinear dynamic	$S_a(T_1)$, CAD
Marano et al. (2006)	Continuous; –; old code	SDOF nonlinear dynamic	PGA
Monti and Nisticò (2002)	Simply-supported; –; old code	Nonlinear static	PGA
Moschonas et al. (2009)	Continuous; monolithic, elastomeric bearings; new code	Nonlinear static	PGA
Nateghi and Shahsavar (2004)	Continuous; elastomeric bearings; –	MDOF nonlinear dynamic	PGA, PGV
Nielson and DesRoches (2007)	Simply-sup.; elastomeric bearings and steel dowels; old code	MDOF nonlinear dynamic	PGA
Padgett and DesRoches (2009)	Simply sup.; fixed, movable, elastomeric bearings; retrofitted	MDOF nonlinear dynamic	PGA
Park and Choi (2011)	Simply-supported; fixed, expansion bearings; no seismic design	MDOF nonlinear dynamic	PGA, $S_a(T_1)$
Prasad and Banerjee (2013)	Continuous; monolithic; new code	MDOF nonlinear dynamic	PGA
Qi'ang et al. (2012)	Continuous; monolithic; –	MDOF nonlinear dynamic	PGA
Saxena et al. (2000)	Continuous; –; –	MDOF nonlinear dynamic	PGA
Shinozuka et al. (2000a)	– ; –; –; Hanshin Expressway	Empirical	PGA
Shinozuka et al. (2000a)	Continuous; –; new code	Nonlinear dynamic	PGA
Shinozuka et al. (2000b)	Continuous; –; new code	Nonlinear static	PGA
Shirazian et al. (2011)	Simply-supported; fixed bearings; –	SDOF nonlinear dynamic	PGA
Sullivan (2010)	Simply-supported; fixed, movable bearings; old code	MDOF nonlinear dynamic	PGA
Tanaka et al. (2000)	–; –; –; Hanshin Expressway bridges	Empirical	PGA
Yamazaki et al. (2000)	–; –; –; Kobe highway bridges	Empirical	PGA, PGV, JMAI
Yi et al. (2007)	Continuous; –; –	Nonlinear dynamic	Return period
Zhang et al. (2008)	Cont., simply-sup., joint; monolithic, elast. bearings; old code	Static analysis (for liquefaction)	PGD
Zhang et al. (2008)	Cont., simply-sup., joint; monolithic, elast. bearings; old code	MDOF nonlinear dynamic	PGA
Zhong et al. (2012)	Continuous; monolithic; new code	Nonlinear static	$S_a(T_1)$

[a]For empirical fragility curves the seismic event is also reported

9.2 Bridge Classification Systems

Bridge classification systems for the purpose of vulnerability assessment were first proposed in the USA. ATC (1985) grouped bridges in three classes, based on the span length, deck continuity and deck-pier connection. RMS (1995) proposed 12 classes, defined by the structural type and level of seismic design. Basöz and Kiremidjian (1996) developed a more detailed classification system where the material and the structural system are used to describe ten basic classes, while the number of spans, deck continuity, type of abutment and number of columns per pier describe the sub-categories within each class. The taxonomy for bridges in HAZUS (FEMA 2010) comprises 28 classes, based on the level of seismic design, number of spans, span continuity, structural system and type of piers, abutments and bearings.

In the framework of the European research project RISK-UE (Argyroudis et al. 2003) bridges were classified in 15 categories, according to material, bent type, span continuity and seismic design. Moschonas et al. (2009) developed a classification scheme where the type of pier, deck and their connection were taken as the most significant factors for the seismic response of bridges; the possible combinations summed up to 36 classes. Ordinary modern highway bridges in Turkey were classified by Avşar et al. (2011) on the basis of the number of spans, number of columns per pier and skew angle, leading to four major classes. The span length, pier height, superstructure and substructure type were used as secondary attributes.

Within SYNER-G a modular taxonomy for bridges was proposed (Hancilar and Taucer 2013). The main features used to describe a bridge comprise the material, type and structural system of the deck, type of piers and their connection to the deck, number of spans, type of connection to the abutments, skew, regularity, type of foundation and level of seismic design. Where additional information may be available, sub-categories are introduced in the classification system, e.g. type of bearings (fixed, sliding, elastomeric, etc.) for the case of deck connected to the piers through bearings. This structure allows to describe a wide range of bridges and may be expanded to include new categories.

9.3 Methods for Construction of Fragility Curves

9.3.1 Empirical Methods

Empirical fragility curves for bridges are scarce in comparison to those for buildings. Basöz et al. (1999) used damage data from the 1994 Northridge earthquake to produce damage probability matrices and fragility curves for as-built (with seismic design) or retrofitted bridges with continuous or simply-supported deck. Following the 1995 Kobe earthquake, fragility curves were proposed based on the damage observed on the bridges of the Hanshin Expressway (Shinozuka et al. 2000a; Tanaka

et al. 2000) and those managed by the Japan Highway Public Corporation (Yamazaki et al. 2000). Elnashai et al. (2004) derived fragility curves using damage data from both events and demonstrated how the curves resulting from the combination of databases with significantly different amounts of data may not be representative of the event related to the smaller database.

9.3.2 Expert Opinion

Fragility assessment based on expert judgment was developed for bridges and other facilities in California (ATC 1985). Earthquake engineering experts were asked to provide estimates of the probability of a bridge being in one of seven damage states and of the expected restoration time. To reduce the uncertainty due to the subjective nature of the estimates, experts were also asked to rate their experience. The results were presented in the form of damage probability matrices, later converted to vulnerability functions and restoration curves. Vulnerability functions describe the expected damage of bridges as a function of a seismic intensity measure, in the present case the Modified Mercalli Intensity, while restoration curves define the fraction of pre-earthquake capacity or usability as function of time after the earthquake. These functions and curves are applicable to standard construction, i.e. with seismic design, in California. It was proposed to move the curves one or two intensity units up or down so as to cover non-standard or special structures respectively. The original data were later revised to reflect seismic design and construction practices in other regions.

9.3.3 Numerical Methods

9.3.3.1 Nonlinear Static Analysis

The capacity spectrum method makes use of an equivalent single-degree-of-freedom (SDOF) system which is characterised by the capacity curve of the full multi-degree-of-freedom (MDOF) structure obtained by nonlinear static (pushover) analysis. The force-displacement capacity curve is converted to the acceleration-displacement format, e.g. according to the N2 method (Fajfar and Gašperšič 1996). Damage states are defined on the capacity curve and the corresponding median value of the intensity measure is either read directly, if it is the spectral displacement, or it is taken from the damped acceleration-displacement response spectrum that intersects the capacity curve at that point, if it is the spectral or peak ground acceleration. The damping ratio of the spectrum should match the displacement of the SDOF system at each performance level.

The earliest application of the capacity spectrum method for the development of bridge fragility curves was in HAZUS and its updates (FEMA 2010), where a

uniform value of standard deviation $\beta = 0.6$ was adopted on the basis of observed data. HAZUS provides the median values of fragility curves for reference bridges together with modification factors that account for the skew, period and arch action of the deck of specific bridges. The fragility curves of HAZUS were adapted by Azevedo et al. (2010) for the bridges in the greater Lisbon area, based on the requirements of the applicable seismic design code for the performance objectives and the material properties.

Moschonas et al. (2009) applied the capacity spectrum method for the development of fragility curves for modern highway bridges in Greece. The analysis was performed for the earthquake acting separately in the longitudinal and the transverse direction of the bridge and considering the closure of the gap between the deck and the abutments. The pushover curve of each bridge was estimated by means of nonlinear static analysis, following the fundamental mode shape, and was then converted to an equivalent bilinear curve, or a quadrilinear one when deck-abutment gaps were included in the model. A default value for the lognormal standard deviation $\beta = 0.6$ was used throughout.

For the estimation of fragility curves for existing multi-span simply-supported highway bridges in Italy, Cardone et al. (2011) performed adaptive pushover analysis, where the modal properties at each step were used to estimate the shape of the displacement increment vector, as well as for the conversion of the capacity curve to the acceleration-displacement response spectrum format. Again, a uniform value, $\beta = 0.6$, was used for the standard deviation.

9.3.3.2 Nonlinear Dynamic Analysis

Nonlinear time-history analysis is more time-consuming than the capacity spectrum method, but makes it possible to account for the variability of the ground motion by running analyses for a set of recorded or artificial accelerograms. It is also appropriate when modes higher than the fundamental one, considered in the standard pushover analysis, are significant for the structural response. In the context of Monte-Carlo simulation, the analysis is performed on a bin of structures of the same basic configuration but different values of selected parameters, e.g. geometry, material properties, etc. These are apparently the reasons why most of the studies listed in Table 9.1 used nonlinear time-history analysis.

There are two main options for time-history analysis performed with the intention to produce fragility curves. “Multi-stripe” analysis is performed for a set of scaled accelerograms that cover a range of values of the intensity measure. “Cloud” analysis employs a suite of unscaled records and requires fewer computations. Each record may be further used with a different realisation of the basic structure, when the variability of other parameters is included in the study.

Analysis is normally performed for a complete three-dimensional model of the bridge that properly accounts for the nonlinear behaviour of all key components such as the piers, bearings, joints, soil, etc. When the bridge is analysed in the longitudinal direction only, e.g. Karim and Yamazaki (2003), or it is approximated

by single piers, an SDOF model may be employed. To reduce the computation time, Marano et al. (2006) performed pushover analysis of the complete bridge in order to define the properties of an equivalent SDOF system that was subsequently used in the time-history analyses.

Shinozuka et al. (2000b) compared fragility curves for a four-span regular bridge obtained with either the capacity spectrum method or with nonlinear dynamic analysis. The fragility curves were in excellent agreement for the state of minor damage. For the high values of peak ground acceleration, the capacity spectrum method underestimated the response parameters by as much as 50 % and the agreement between the fragility curves was not as good for the major damage state. Also Moschonas et al. (2009) obtained similar fragility curves for a three-span regular bridge with monolithic deck-pier connection that were produced based on nonlinear dynamic analysis or on the capacity spectrum method. However, this conclusion cannot be extended to cases where higher modes have a significant contribution to the seismic response.

Banerjee and Shinozuka (2008) compared empirical fragility curves and numerical ones that were based on nonlinear dynamic analyses of three RC bridges with different geometry, using a set of 60 artificial accelerograms. The analytical curves were more conservative than the empirical ones. An iterative optimisation procedure was then developed so that the limit values of damage measures were calibrated and a better agreement was obtained between empirical and numerical fragility curves.

9.3.4 Parameterised Fragility Curves

It is verified (e.g. Zhang et al. 2008), that bridges with different structural configuration will have different fragility curves. Besides, bridges belonging to the same class may have different fragilities because of their specific geometric characteristics (e.g. Moschonas et al. 2009). To avoid time-consuming calculations for individual bridges, parameterised fragility curves were proposed in literature.

Karim and Yamazaki (2003) developed fragility curves for idealised bridges with fixed or sliding bearings based on nonlinear dynamic analyses of 30 bridge models for a suite of 250 accelerograms and found a strong correlation between the mean and standard deviation of the fragility curves and the ratio of the base shear capacity to the design base shear. Likewise, Mackie and Stojadinović (2007) produced fragility curves based on time-history analysis of 22 two-span bridges with monolithic deck-pier connection, considering different values of the span length, pier height, material properties, amount of longitudinal and transverse reinforcement and soil stiffness. The medians and dispersions of the fragility curves were expressed as functions of the force-reduction factor of the bridge. When the 5 %-damped spectral acceleration at the fundamental period, $S_a(T_1)$, was used as intensity measure, the dispersions were practically independent of this factor.

Jeong and Elnashai (2007) developed a method where nonlinear dynamic analysis of equivalent SDOF models is performed for several bridges and for a range of earthquake intensities in order to create a database of demand values for the damage measure. The database is used to estimate the mean value and standard deviation of the demand on a structure, characterised by its stiffness and strength, as a function of the earthquake intensity. The fragility curves are then produced by comparing demand to capacity and incorporate the uncertainty due to earthquake records, the limit states and modelling simplifications. Similarly, response surfaces express a relation, usually polynomial, between a set of random variables including an intensity measure, and the response parameter. Response surfaces were used by De Felice and Giannini (2010) to produce fragility curves for simply-supported viaducts, based on a reduced number of simulations.

9.4 Intensity Measures

Peak ground acceleration (PGA) is the most common seismic intensity measure because it has been demonstrated to have high correlation with damage. Other intensity measures used in existing fragility studies for bridges are the peak ground velocity (PGV) and the acceleration or velocity spectrum intensity (SI). Multivariate measures have also been proposed but not widely adopted, either because they are difficult to estimate, or because they do not show improved correlation to damage.

Yamazaki et al. (2000) produced empirical fragility curves using PGA, PGV and the Japan Meteorological Agency (JMA) Intensity. They were in slightly better agreement with the numerical curves developed by Karim and Yamazaki (2001) when PGA was used as intensity measure instead of PGV. Further to PGA and PGV, Karim and Yamazaki (2003) examined the velocity SI, defined as the average amplitude of the 20 %-damped velocity response spectrum between $T_i = 0.1$ s and $T_f = 2.5$ s. An exponential relationship was established between each intensity measure and the Park and Ang (1985) Damage Index of bridges, by means of nonlinear dynamic analyses. SI was found to be better correlated to damage than PGA, while an even higher coefficient of determination (R^2) was obtained for the combination of SI and PGA.

A comprehensive study by Mackie and Stojadinović (2004b) examined the efficiency of hundreds of intensity measures. Efficiency is based on the dispersion of the demand measure. PGV was found to be the most efficient among intensity measures that are calculated directly from the time-history. The efficiency of such measures depends on the period range. To overcome this weakness, spectral quantities may be employed. Within this group, spectral displacement at the fundamental period was the most efficient. At the expense of increased computational effort, improved efficiency was obtained if spectral intensity measures were averaged over a range of periods or if the spectral measures for the first two periods of vibration were combined.

Padgett et al. (2008) examined several intensity measures in terms of efficiency, practicality and proficiency. Practicality refers to the correlation between the intensity measure and the demand; proficiency reflects the composite effect of efficiency and practicality. The statistical dependency of the intensity measures on the characteristics of the ground motion, termed sufficiency, and the effort required to assess the hazard, termed computability, were also examined. PGA was judged to be the optimal intensity measure considering all criteria, independently of the use of recorded or artificial accelerograms. Spectral acceleration for the geometric mean of the fundamental periods in the longitudinal and the transverse directions also performed well, but ranked lower as to computability.

In a dedicated study, Avşar and Yakut (2010) investigated the correlation between different intensity measures and damage of highway bridges in Turkey. Nonlinear dynamic analysis was performed for 52 prototype bridges and the damage, in terms of deck displacement and column curvature, was correlated to PGA, PGV, the ratio PGA/PGV and also to acceleration spectrum intensity (ASI). ASI was defined as the area under the 5 %-damped elastic response spectrum within the periods T_i and T_f. The values $T_i = 0.40$ s and $T_f = 1.10$ s were selected, so as to reflect the period range for the ordinary highway bridges in Turkey. Both damage measures had higher coefficients of determination with ASI and PGV than with PGA and PGA/PGV.

9.5 Damage States and Damage Measures

Fragility assessment of bridges involves several damage states. More than half of the works reviewed in Table 9.1 make use of five damage states, namely: no damage, slight, moderate, extensive or complete damage. Although different wording is used, the definitions seem to originate from the first version of HAZUS. Intermediate, i.e. moderate or extensive, damage states are not examined in some of the studies available in literature. Moreover, a couple of studies consider only collapse or loss of load-bearing capacity.

Damage measures refer to specific components of the bridge, in particular piers, cap beams, bearings, abutments, deck and gaps. Drift ratio, curvature, rotation and displacement are the pier response quantities normally used as damage measures. Indicative threshold values adopted by different authors are compared in Table 9.2, where the subscripts –y and –u refer to yielding and ultimate capacity. Drift limits are taken from literature or from experimental data (Li et al. 2012). As regards curvature ductility, similar values are adopted. Note that the higher values used by Nielson and DesRoches (2007) relate to steel-jacketed columns. Divergence in the threshold values for the rotation of the pier end is due to the fact that they originate from experimental data in Qi'ang et al. (2012) and Saxena et al. (2000), while they have been calculated for a specific bridge by Yi et al. (2007).

Bearings are often the critical elements in bridges and are therefore included in the model used for the development of fragility curves. There is no consensus on the limit

Table 9.2 Definition of damage states for bridge piers

		Damage state			
Damage measure	Reference	Slight	Moderate	Extensive	Complete
Drift ratio, δ/h	Banerjee and Shinozuka (2008)	1.0 %	2.5 %	5.0 %	7.5 %
	Kim and Shinozuka (2004)	0.7 %	1.5 %	2.5 %	5.0 %
	Li et al. (2012)	1.45 %	2.6 %	4.3 %	6.9 %
	Yi et al. (2007)	0.7 %	1.5 %	2.5 %	5.0 %
Curvature, φ	Avşar et al. (2011)	φ_y			φ_u
	Cardone et al. (2011)	φ_y	$0.5\varphi_u$		φ_u
	Choi et al. (2004)	φ_y	$2.0\varphi_y$	$4.0\varphi_y$	$7.0\varphi_y$
	Jeong and Elnashai (2007)	φ_y			φ_u
	Nielson and DesRoches (2007)	$1.3\varphi_y$	$2.1\varphi_y$	$3.5\varphi_y$	$5.2\varphi_y$
	Padgett and DesRoches (2009)	$9.4\varphi_y$	$17.7\varphi_y$	$26.1\varphi_y$	$30.2\varphi_y$
	Zhang et al. (2008)	φ_y	$2.0\varphi_y$	$4.0\varphi_y$	$7.0\varphi_y$
Rotation, θ	Qi'ang et al. (2012)	θ_y	$2.0\theta_y$	$6.0\theta_y$	$11.0\theta_y$
	Saxena et al. (2000)	θ_y	$2.0\theta_y$	$6.0\theta_y$	$11.0\theta_y$
	Shinozuka et al. (2000b)	θ_y		$2.0\theta_y$	
	Yi et al. (2007)	θ_y	$1.3\theta_y$	$2.6\theta_y$	
Displacement, δ	Monti and Nisticò (2002)	$0.5\delta_u$		$0.7\delta_u$	δ_u

Table 9.3 Definition of damage states for bearings

		Damage state			
Damage measure	Reference	Slight	Moderate	Extensive	Complete
Shear deformation of elastomeric bearings, γ	Moschonas et al. (2009)	0.2	1.5	2.0	5.0
	Zhang et al. (2008)	1.0	1.5	2.0	2.5
Displacement in longitudinal direction, δ (mm)	Choi et al. (2004)[a]	1/-	6/50	20/100	40/150
	Ghosh and Padgett (2010)[a]	6/37	20/104	40/136	187/187

[a]Fixed bearings/expansion bearings

states; the choice depends on the available data from manufacturers, guidance from design codes and engineering judgement, resulting in different values as, for example, the shear deformation of elastomeric bearings and the two extreme damage states in Table 9.3. Divergence is also observed for fixed and expansion bearings when the limit values are based on experimental data only (Choi et al. 2004) or a combination with expert opinion (Ghosh and Padgett 2010). The friction force, horizontal strength and the displacement that lead to unseating of the deck have also been used as damage measures for the bearings.

Other damage measures used in previous studies include concrete and steel strain at the component level, as well as the Park and Ang (1985) Damage Index and the bridge displacement ductility, calculated from the capacity curve.

9.6 Aggregation of Damage from Component to System

As discussed in Sect. 9.5, damage measures refer to specific components, such as piers, bearings, gaps, etc. These need to be combined in order to specify the damage state of the complete bridge. In most existing studies, bridges are treated as series systems and their damage states are defined by the most vulnerable components.

Choi et al. (2004) estimated the fragilities of several bridge systems assuming that the components are either statistically independent, or totally dependent. The two approaches gave similar results for the lower damage states, but diverged for the higher ones. The resulting fragility curves were close for those systems where a component was markedly more fragile than the others and were further apart for systems with components of similar fragilities.

Lupoi et al. (2004) developed fragility curves for a regular bridge by considering the correlation between failure modes and the dependence of both demand and capacity on the material properties. Accounting for the correlation led to higher fragilities compared to the case of independent failure modes.

A more detailed probabilistic approach was adopted by Nielson and DesRoches (2007) who estimated the probability of the bridge being in a damage state as the union of the probabilities of its components being in that damage state. The correlation coefficients between the component damage measures were estimated from nonlinear dynamic analysis of eight prototype bridges. The error between the bridge fragility calculated in this way and the upper and lower bound was in the order of 10 % and 40 %, respectively. The bridge fragility was closer to the upper-bound, particularly for the higher damage states, in which case few components contributed to the system fragility. The importance of including all the components was highlighted by the fact that, at the different damage states, the median of the system fragility curve was 40–160 % smaller than the one of the pier alone.

Zhang et al. (2008) suggested to estimate the damage state of the bridge as the weighted sum of the damage states of the piers and the bearings. The proposed weight factors for piers and bearings were respectively 0.75 and 0.25, reflecting their relative importance for the load-carrying capacity and the repair cost. The bridge system was considered to attain the highest damage state when any component reached it.

Qi'ang et al. (2012) adopted a bi-dimensional performance limit state definition for the bridge system that combined the rotation at the column end and the transverse translation at the abutment. The fragility was higher when the two damage measures were considered independent, and it decreased with increasing interdependency.

9.7 Bridge Functionality

Damage states may be further associated to the functionality of the bridge. Monti and Nisticò (2002) proposed three levels of functionality: full for light damage, emergency traffic for high damage, and closure for (near) collapse. Lehman

Table 9.4 Definition of bridge functionality levels by Lehman et al. (2004)

Performance level	Functionality	Damage	Repair
Fully operational	Full service	Minimal damage: hairline cracks	Limited epoxy injection
Delayed operational	Limited service (emergency traffic)	Moderate: open cracks, spalling	Epoxy injection, concrete patching
Stability	Closed	Severe: buckling, bar fracture, concrete crushing	Replacement of damaged section

Table 9.5 Definition of bridge functionality levels by Mackie and Stojadinović (2006)

Functionality level	Remaining traffic capacity (%)	Loss of lateral load-carrying capacity (%)	Loss of vertical load-carrying capacity (%)
Immediate access	100	<2	<5
Weight restriction	75	<5	<20
One lane open only	50	<15	<35
Emergency access only	25	<25	<50
Closed	0	>25	>50

et al. (2004) also defined three service levels, each associated to a description of physical damage and the required repair, as in Table 9.4.

Mackie and Stojadinović (2006) identified five levels of traffic capacity, ranging from immediate access to closure, related to the remaining traffic capacity of the bridge. Functionality levels were defined by the loss of vertical and lateral load-capacity as shown in Table 9.5. Among the approaches examined for relating the vertical load-carrying capacity and the intensity measure, detailed analysis of the bridge to establish a relation between the residual horizontal capacity and the maximum horizontal displacement showed the lowest model error.

Padgett and DesRoches (2007a) used data collected from experts to relate damage states and bridge functionality. Results were presented as functionality probability matrices that provide the probability that the bridge functionality will be 0, 50 or 100 % in a number of days after an earthquake that causes a certain level of damage on abutments, bearings, columns and footings.

Based on observed data from California, HAZUS (FEMA 2010) provided restoration curves for highway bridges, as shown in Fig. 9.1. They give the percentage of functionality of a bridge that suffered a given damage level as a function of time following the seismic event. For example, a bridge with moderate damage is expected to be fully functional after approximately 10 days, whereas more than 3 months will be needed to fully restore the functionality of bridge with extensive damage.

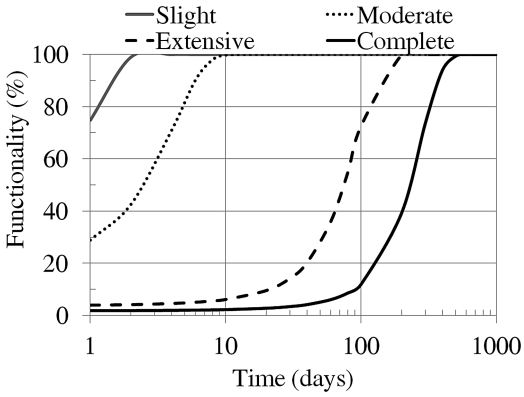

Fig. 9.1 Restoration curves for highway bridges, after HAZUS (FEMA 2010)

9.8 Treatment of Uncertainties

Modelling and propagation of uncertainties is extensively discussed in Chap. 2. The present section focuses on the way aleatory and, to a lesser extent, epistemic uncertainties are treated in previous studies and how they affect the fragility curves for bridges. Uncertainty exists in the seismic hazard, demand and capacity of elements.

9.8.1 Variability of the Seismic Action

The type and number of ground motion time-histories are key issues in dynamic analyses. In the studies reported in Table 9.1 recorded and artificial accelerograms are equally used, while a few among them use a combination thereof. Karim and Yamazaki (2001) obtained different fragility curves for each set of records from the Kobe, Northridge, Kushiro-Oki and Chibaken-Toho-Oki earthquakes. The work of Moschonas et al. (2009) resulted in much higher probabilities of exceeding all damage states when using the code design spectrum, instead of the average spectrum of recorded earthquakes.

The effect of artificial and recorded accelerograms on the fragility curves of multi-span simply-supported bridges was studied in detail by Ceresa et al. (2012b). Artificial accelerograms were generated, and real earthquake records which matched a target response spectrum were selected from the European Strong Motion Database. The two sets gave similar results regarding the damage ratio, but the mean value of the standard deviation for the analyses with the recorded accelerograms was in the mean 1.5 times higher than for the artificial ones. Because of the higher energy content, the artificial accelerograms resulted in slightly higher probabilities of failure, but overall, and despite the higher variability of the recorded accelerograms, the fragility curves obtained from the two sets were similar, particularly for the low damage state.

The number of time-histories used in previous works on the fragility of bridges ranged from seven to as much as 250, with the majority of the studies employing less than 100 records. To obtain a reasonable variation in the mean and standard deviation, Nielson and Pang (2011) recommended the use of at least 80 ground motion records, whereas Lupoi et al. (2005) found that approximately 10 records were sufficient to give a reasonably stable estimate of the probability of failure.

9.8.2 Variability of Geometric and Material Properties

Padgett and DesRoches (2007b) performed an analysis of sensitivity to identify the parameters that affect the fragility of the bridge. Parameters that affected the response in terms of pier ductility and deformation of the deck and bearings, and the fragility of several components or of the most vulnerable one were ranked as more important. Among the examined parameters, bearing and foundation stiffness, incidence angle of the earthquake and the basic geometry, i.e. span length, column height and deck width, were found to be the most important. On the other hand, Padgett et al. (2013) concluded that, for damage due to liquefaction, the fragility curves were influenced by a different set of parameters, mainly those related to the soil properties. The effect of parameters was consistent for all damage states and far more pronounced on the median than the dispersion of fragility curves. The latter was more affected by the variability of the seismic motion characteristics.

With a view to study the uncertainty in the demand and capacity models, Padgett et al. (2013) further calculated the confidence bounds of the component fragility curves, considering only the variability of the most significant parameters. Among the elements, expansion bearings showed the widest bounds and piers displayed the narrowest bounds. The extent of bounds for any component was similar at all damage states.

Regarding in particular the variability of the material properties, Padgett and DesRoches (2007b) reported that the variability of concrete and steel strength did not have a noticeable effect on the response, as was previously observed for buildings by Kwon and Elnashai (2006). However, De Felice and Giannini (2010) found out that the effect of the uncertainty of concrete strength was similar or even more important than that of the earthquake input when shear failure modes were activated.

9.8.3 Uncertainty Due to Modelling

The results and the required computation time depend on the model refinement. Therefore it is interesting to examine the uncertainty related to simplifications in the numerical models used to estimate the demand. Kunnath et al. (2006) investigated

the effect of using linear or nonlinear models. The nonlinear model comprised the elastic deck and cap beams and nonlinear elements for the piers, shear keys, longitudinal and vertical restrainers and bearings; the elastic model used the effective stiffness of piers and cap beams. Although the two models gave different peak demands for certain records and values of the intensity measure, the median demands were quite similar, as were the probabilities of closure of the bridge.

Jeong and Elnashai (2007) compared the maximum ductility demand in regular bridges obtained from time-history analysis of an MDOF and an equivalent SDOF model and estimated that the mean value for the MDOF system was 1.07 times the mean value of the SDOF, while the standard error was 0.1 or 0.17 for different structural systems. Kurian et al. (2006) studied a three-span simply-supported bridge using either the full MDOF model with distributed mass along the deck or an SDOF system with tributary deck mass. The fragility curves obtained using the SDOF model predicted higher probability of damage than those based on the MDOF system, particularly for the higher damage states.

Kunnath et al. (2006) found that accounting for the soil compliance in the numerical model increased the probability of closure, in comparison to the case of fixed support. Models with different levels of discretisation were used by Kwon and Elnashai (2009) to study the effect of soil-structure interaction on the fragility of a three-span bridge with the deck supported on fixed and expansion bearings. The various modelling approaches did not affect the component fragilities in the longitudinal direction, but resulted in notable differences in the fragility of components in the transverse direction and consequently in the system fragility.

Li et al. (2012) used experimental data and measured earthquake response to calibrate the numerical models employed for the deck, piers and soil to produce fragility curves for a two-span overpass. The initial numerical model was found to largely underestimate the probability of damage compared to the improved one. Bayesian updating of the fragility curves, using the results of a small number of hybrid tests, resulted in fragility curves similar to those based on the calibrated model. Furthermore, the fragility curves based on the calibrated model or Bayesian updating showed lower uncertainty with respect to those for the initial model.

When additional information is available, Bayesian updating may be used at several stages of the development of fragility curves. Applications for bridges include the combination of physics-based definition of limit states with the judgemental assessment by bridge inspectors (Nielson and DesRoches 2007), the use of experimental data to derive probabilistic models for deformation and shear demand (Gardoni et al. 2003) or to improve probabilistic models for capacity (Choe et al. 2007) and the estimation of model parameters using predictions of the model itself (Gardoni and Rosowsky 2009).

The studies reviewed in this section suggest that it might not be worthwhile to build a highly refined model of the structure or to perform analyses with several tens of accelerograms. It is more meaningful to direct the additional effort to modelling the soil, as this will improve the accuracy of the results. Regarding the other sources

Table 9.6 Coefficients of variation of fragility curve parameters, after Crowley (2011)

	Minor damage		Collapse	
Bridge class	Mean	St. deviation	Mean	St. deviation
Deck-pier connection through bearings, regular	0.27	0.33	12.67	0.31
Deck-pier connection through bearings, irregular	0.32	0.54	3.58	0.27
Monolithic deck-pier connection, regular	0.50	0.56	6.73	0.40
Monolithic deck-pier connection, irregular	0.32	0.37	2.51	0.42

of uncertainty, the variability of material properties is not as important as that of the characteristics of the seismic action, except for shear-deficient members and for the properties of soil susceptible to liquefaction (see Sect. 9.9.6).

9.8.4 Variability of Fragility Curve Parameters

Having reviewed each source of uncertainty separately, reference is made to the variability of parameters in about 90 fragility curves from literature (Crowley 2011). Different intensity measures were converted to PGA; the limit states were harmonised by taking the first one in each study as "minor damage" and the last one as "collapse". Histograms of the mean value and standard deviation were then produced and used to calculate the corresponding coefficients of variation. The results in Table 9.6 show that for the minor damage state the variability of the mean of the fragility curves was similar to that of the standard deviation. At the collapse damage state, the variability of the standard deviation remained essentially unchanged, but that of the mean value was largely increased, reflecting the range of bridge typologies and the different definitions of collapse adopted in each study.

The variability of the parameters of fragility curves from literature is illustrated in Fig. 9.2, which shows curves developed by different authors for the same bridge typology. The continuous lines are for three-span highway bridges with the deck monolithically connected to three-column piers. The dashed lines are for multi-span bridges where the deck is made up of girders with concrete topping and is supported through elastomeric bearings on two-column piers. All bridges are designed according to modern seismic codes. Elnashai et al. (2004) and Avşar et al. (2011) performed nonlinear dynamic analyses with recorded accelerograms and accounted for the variability of geometry and material parameters, while Moschonas et al. (2009) employed pushover analysis of individual bridges. Large differences are observed on the mean values for all damage states. Also, the curves based on time-history analysis have much smaller standard deviation than the default value $\beta = 0.6$ used with the nonlinear static analysis. In view of the different predictions of damage, the end-user will have to carefully select the fragility curves that are most appropriate for the population of bridges or the specific structure of interest in practical applications. An alternative approach is to make use of "mean" fragility curves and properly account for the large variability of their parameters, as shown in Table 9.6.

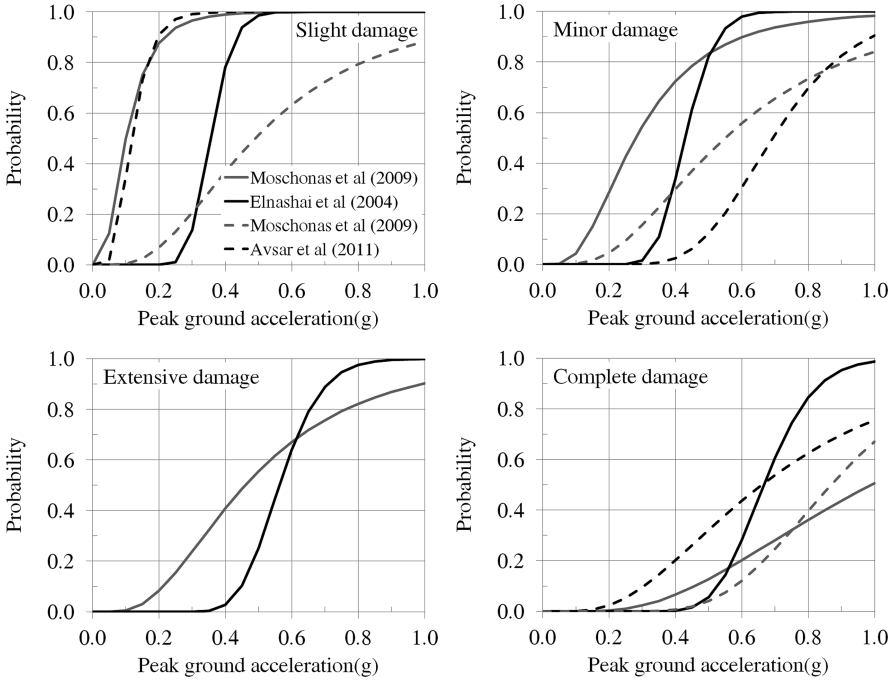

Fig. 9.2 Fragility curves for multi-span continuous bridges with monolithic deck-pier connection (*continuous lines*) or deck supported on bearings (*dashed lines*)

9.9 Special Issues

9.9.1 Ageing Bridges

The effect of corrosion on the seismic fragility of reinforced concrete bridges was investigated by Choe et al. (2009) using probabilistic demand and capacity models. They employed the reduced area of steel and accounted for the uncertainty in the structural properties and in the time of corrosion initiation. An application to a two-span overpass produced an increase in the probability of failure in the order of five percentage points in 100 years. Sensitivity analysis showed that, as regards the fragility curves, corrosion of the transverse reinforcement of piers was more important than of the longitudinal reinforcing bars.

Zhong et al. (2012) produced fragility curves for bridges subject to corrosion, employing a detailed probabilistic model not only for the loss of steel but also for the stiffness degradation of the concrete cover. The results highlighted the varying in time effect of corrosion on flexural and shear failure modes of bridge piers.

Gardoni and Rosowsky (2009) used probabilistic models for demand and capacity to compute the ratio of the fragility of a bridge subject to corrosion to

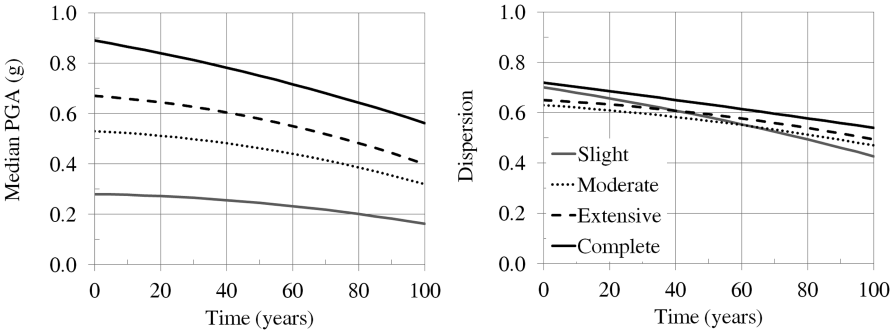

Fig. 9.3 Effect of ageing on the median (*left*) and dispersion (*right*) of fragility curves for a multi-span continuous bridge (From data in Ghosh and Padgett 2010)

that of the pristine bridge. The models accounted for flexural and shear failure modes, for the increase in demand and the decrease in capacity due to the reduction of the reinforcing bar diameter, and for the increased uncertainty over time. A methodology was also developed for improving the fragility estimates using field data for the dynamic properties of the bridge and the extent of corrosion.

Ghosh and Padgett (2010) developed analytical functions that relate the parameters of the fragility curves to the life of the structure. Probabilistic estimates of loss of steel area were obtained accounting for the variability in the corrosion initiation time, corrosion rate and penetration. Corrosion was found to increase the fragility of bridges, although it decreased the fragility of certain elements. For example, corrosion of the steel expansion bearings over the abutments and accumulation of debris resulted in higher friction coefficient and smaller deformation of the bearings in the longitudinal direction, leading to reduced pounding of the deck against the abutments. Some results are shown here in Fig. 9.3, referring to a three-span bridge with a continuous deck supported on bearings. Figure 9.3 indicates that corrosion reduces the median values for all damage states by around 40 % in 100 years. A slight reduction of the dispersion is also observed with time. This procedure was later supplemented with the uncertainty in repair strategies in order to estimate the expected loss of ageing bridges (Ghosh and Padgett 2011).

Further to steel corrosion and concrete spalling, Dong et al. (2013) investigated the effect of flood scour on the fragility of bridges. The numerical model used to perform time-history analysis was updated with reduced steel area for corroded rebars and by removing the concrete cover after spalling. To account for scouring, the spring elements between the soil and the foundation piles were removed. Similar to other studies, it was concluded that, as the effects of corrosion accumulate with time, the increase in fragility becomes higher near the end of the bridge lifetime. Flood-induced scour was also found to significantly increase the fragility.

Prasad and Banerjee (2013) studied the effect of scour on the seismic fragility of multi-span bridges with monolithic deck-pier connection. The soil-pile springs within the scour depth were removed from the model in order to simulate the loss

of lateral support. Scour was found to increase the probability of damage, but there was no further change after a certain scour depth. It was also shown that the effect of scour weakened for higher stiffness of the piles.

9.9.2 Damaged Bridges

Franchin and Pinto (2009) proposed a criterion for the usability of damaged bridges accounting for aftershocks. Assuming a model for the probability of occurrence of an aftershock within a period of time after the main shock, the criterion states that a bridge should remain closed for as long as the risk of collapse of the damaged structure due to an aftershock is higher than the risk of collapse of the intact bridge owing to a main shock. The probability of collapse of the damaged structure may be calculated by time-history analyses with a sufficient number of pairs of ground motion records applied consecutively. The limited ability of models to estimate the residual capacity and the lack of an appropriate physical measure of it were identified as the major difficulties for practical application.

Kumar et al. (2009) confirmed the unfavourable effect of cumulative seismic damage on the fragility of bridge piers. Monte-Carlo simulation of the seismic action during the life cycle of a bridge was performed considering the magnitude, distance from source, etc as random variables and a Poisson process for the occurrence of earthquakes. Accounting for the reduction in stiffness and the increase in yield displacement, low-cycle fatigue resulted in a significant increase in fragility with time. For a specific application, cumulative damage was found to have a stronger influence on the fragility than corrosion did.

9.9.3 Retrofitted Bridges

Fragility curves are normally used to identify those bridges or classes of bridges in a region that are more vulnerable and should be given priority in retrofitting. They may be further used to compare alternative retrofit measures as illustrated by Kim and Shinozuka (2004) for the case of two multi-span bridges typical in California, before and after adding steel jackets to the columns. The results indicated a decrease in fragility with jacketing, which was more evident at the higher damage states. The ratio of the median values of the fragility curves after and before the retrofit is used to produce the “enhancement curve” in Fig. 9.4. This curve may be used to estimate the improvement in fragility of a similar bridges due to retrofit.

Fragility curves were also used by Padgett and DesRoches (2009) to study the effect of alternative retrofit solutions for multi-span bridges with continuous or simply-supported deck composed of steel or concrete girders, typical of the Central

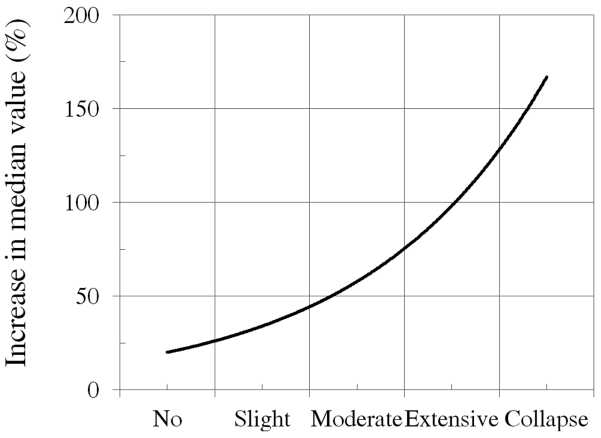

Fig. 9.4 Increase in median values of fragility curves following retrofit of columns (From data in Kim and Shinozuka 2004)

and South-eastern United States. Fragility curves were produced at both component and system level. It was demonstrated that the effect of each intervention depends on the bridge structural type and damage state considered. Modification factors were proposed for the median values of fragility curves for each retrofit solution, while a limited influence was observed on the dispersion.

9.9.4 Skewed Bridges

Most previous studies deal with straight bridges, although skew is known to increase the seismic fragility. On the basis of nonlinear dynamic analyses, Sullivan (2010) concluded that skew angles less than 30° did not significantly alter the parameters of fragility curves of multi-span simply-supported bridges designed with pre-1990 design codes. For higher skew values, the mean values decreased and the standard deviations remained practically unchanged. Skew angle was found to have a beneficial effect on the fragility of components for longitudinal earthquake and a negative effect for transverse earthquake, which was the critical direction for the system fragility.

Avşar et al. (2011) confirmed the increased mean value and the negligible influence on the dispersion of fragility curves for new highway bridges with the deck supported on bearings and a skew angle higher than 30°. Skew did not alter the fragility curves for the lower damage grade, corresponding to yielding.

Zakeri et al. (2013) investigated the effect of skew on a wide range of bridge types. It was found that older bridges in which damage was concentrated on the columns and bridges with integral abutments were not affected by skew. On the other hand, skew angle was found to influence the fragility of bridges with the deck supported on bearings at the abutments.

9.9.5 Railway Bridges

There is very limited research on fragility curves specific to railway bridges. Nateghi and Shahsavar (2004) produced fragility curves for a 215 m-long railway bridge. Park and Choi (2011) studied a special type of railway bridge consisting of a steel girder deck supported through steel bearings on massive concrete piers without reinforcement. Fragility curves were produced by means of MDOF nonlinear dynamic analysis with 20 artificial accelerograms, accounting for the variability of concrete strength, damping ratio and angle of incidence of the earthquake with respect to the bridge axis. At component level, bearings in the longitudinal direction were critical, whereas piers suffered practically no damage. Although the bridge was not designed for earthquake loading, the 50 % probability of exceeding light damage approximately corresponded to PGA = 0.85 g.

In Sect. 9.10 railway bridges are differentiated from road bridges by considering the appropriate traffic and permanent loads, constrained transverse translation of the deck at the abutments, and by examining the deck horizontal deformation as an additional damage measure.

9.9.6 Liquefaction

Most existing fragility curves for bridges consider only the seismic hazard due to ground shaking. Dedicated studies have shown that soil liquefaction may have a positive or negative effect on the individual components, depending on the type of deck-pier connection and on the soil stratigraphy at each support. Zhang et al. (2008) produced fragility curves for typical bridges in California considering liquefaction by performing equivalent static analysis, where lateral spreading of the soil was simulated by imposing displacements on the free edges of springs connected to the foundation elements of the model. The variability of the soil properties and the soil layer depth was included in the analysis. Bridges with monolithic deck-pier connection were found to be significantly more vulnerable to lateral spreading resulting from liquefaction than those on bearings. The bridge damage state was calculated as a weighted sum of the damage of piers and bearings, the weights being respectively 0.75 and 0.25.

Kwon et al. (2009) studied a two-span bridge with monolithic deck-pier connection. The effect of liquefaction was to reduce the seismic forces on the bridge and consequently the fragility, particularly for the higher damage grades. The probability of damage was further reduced when liquefaction was considered at all supports instead of at the base of the central column only.

Aygün et al. (2011) performed time-history analysis of the bridge-soil system, where a 3D model of a continuous bridge with the deck connected to the piers through fixed bearings was combined with 2D soil elements and 1D springs for soil-pile interaction. Accounting for the variability of the geometry, material and soil

properties, component fragility curves were produced for a suite of synthetic accelerograms. Liquefaction resulted in higher dispersion of the seismic demand. It affected mostly the fragility of piers and piles and to a lesser extent that of bearings and abutments. Because of larger displacements, bearings showed higher probability of damage due to liquefaction. On the other hand, the effect on piers and piles depended on the local soil conditions.

9.9.7 Spatial Variability of the Seismic Motion

In the presence of geological discontinuities, or marked topographical features and for long bridges, the spatial variability of the seismic motion is expected to affect the response of bridges (e.g. Sextos et al. 2003a, b). The subject was studied by Saxena et al. (2000) who generated earthquake time-histories that accounted for wave propagation and loss of coherence, and used them as input in nonlinear dynamic analyses of a 12-span regular bridge, considering either the same or different soil properties at the supports. It was concluded that spatial variability increased the fragility for all damage states, particularly in the case of soft soil at all supports or different soil properties along the bridge.

Lupoi et al. (2005) adopted a statistical approach to study the effects of loss of coherence, wave-passage and local site conditions on the fragility curves of four-span bridges with monolithic deck-pier connection. Piers of different height were considered in order to generate regular and irregular configurations. It was observed that asynchronous input consistently increased the probabilities of failure, particularly for irregular bridges. The highest fragility was calculated for the least uniform soil pattern; it was found that the impact of local soil conditions on fragility was more important than that of the wave-passage and the loss of coherency.

9.10 A Method for Fast Fragility Analysis of Regular Bridges

9.10.1 Scope

A method for fast fragility analysis of regular bridges is presented in this section. The objective is to construct fragility curves for specific bridges as a function of a few basic parameters such as the type of deck-pier connection (monolithic or through elastomeric bearings, as shown schematically in Fig. 9.5), transverse translation at the abutments (free or constrained), bridge length l, type of pier cross-section (hollow rectangular, wall-type rectangular or solid circular, as shown in Fig. 9.6), number of columns per pier, pier height h and level of seismic design.

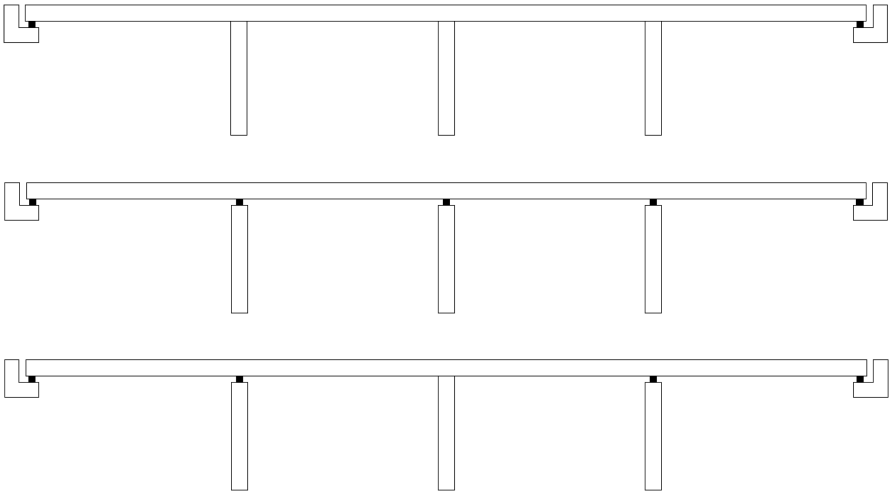

Fig. 9.5 Type of deck-pier connection: monolithic (*top*), through bearings (*middle*), combination of fixed connection at central pier and bearings (*bottom*)

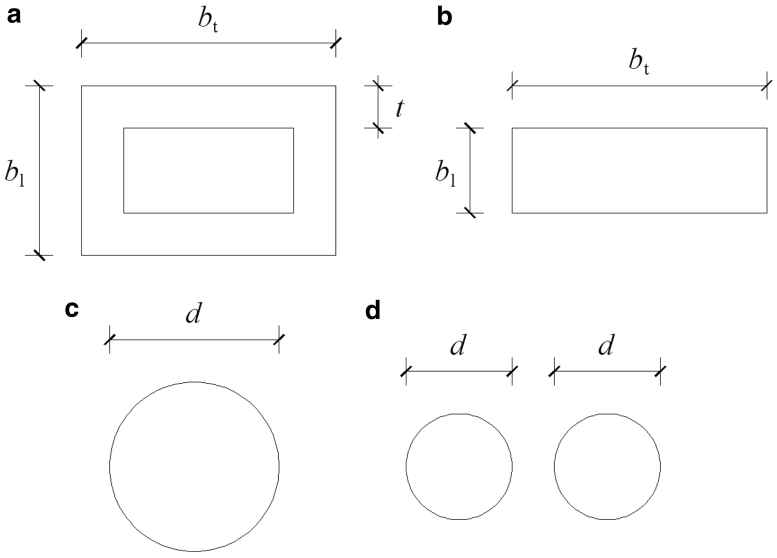

Fig. 9.6 Pier cross-sections: rectangular hollow (**a**), wall-type (**b**), circular (**c**) and two-column circular (**d**)

Starting from the base geometry, the method follows the design procedure of Eurocode 2 (EC2) and, for bridges with seismic design, Eurocode 8 (EC8). The relevant detailing requirements are satisfied and iterations are performed where necessary. At the end of this step, the capacity quantities are established. The demand quantities are estimated next, according to the assessment procedure and rules given in Part 3 of Eurocode 8 (CEN 2005e). Fragility curves are then calculated at component level from the conditional probability that demand exceeds capacity. The dispersion accounts for model uncertainties, the variability of materials and geometry and that of the seismic action for given peak ground acceleration.

The method applies also to railway bridges, characterised by the constrained transverse translation of the deck at the abutments, and examines the relevant operational limits for the horizontal deformation of the deck. The method requires input data that is available for any bridge and performs the calculations in real time.

9.10.2 Design of the Deck, Piers and Bearings

The deck is free to translate longitudinally at the abutments. For railway bridges, it is taken as transversely constrained there and for road bridges it is transversely free. The permanent loads on the deck comprise the self-weight of the deck including side-walks, ballast and sleepers in railway bridges and surfacing of road bridges. Load models from CEN (2003) are adopted for the traffic loads.

The piers are considered fixed at the base. Their cross-sectional dimensions are chosen to meet the slenderness limit of Eurocode 2 (CEN 2004a) so that 2nd-order effects may be neglected under the persistent-and-transient combination of actions per Eqs. 6.10a, 6.10b in EN 1990 (CEN 2002). Their longitudinal and transverse reinforcement is initially dimensioned for the ultimate limit state (ULS) in bending with axial load and shear for the persistent-and-transient combination of actions including the effects of geometric imperfections per Eurocode 2 (CEN 2004a).

The elastomeric bearings are dimensioned according to EN 1337 (CEN 2005a). For the persistent-and-transient design situation – including the effects of creep, shrinkage and design thermal actions – it is verified that the design shear strain due to translational movements is $\varepsilon_{q,d} \leq 1.0$ and that the total nominal design strain in the elastomer is $\varepsilon_{t,d} \leq 7.0/\gamma_m$, where γ_m is a partial safety factor for the resistance. The verifications are repeated for the seismic design situation, i.e. for the design seismic action combined with creep, shrinkage and half the design thermal actions; the bearing dimensions are updated as necessary. The seismic displacements are iteratively estimated from the elastic displacement spectrum and the stiffness of the bearings, as controlled by their size. The design of the bearings for the persistent-and-transient design situation, including creep, shrinkage and thermal actions, takes place for the combination of these actions per EN 1991-2 (CEN 2003), considering the longitudinal displacement of the underside of the deck over the bearing due to the rotation of the deck section owing to the traffic and other vertical loads in the said combination which are not balanced by prestressing.

Seismic analysis of the bridge is performed for the design spectrum of Eurocode 8 (CEN 2004b). The behaviour factor is $q = 1.5$ for bridges with deck on bearings (limited ductile behaviour) and $q = 3.5\lambda(\alpha_s)$ for those with monolithic deck-pier connection (design for ductile behaviour), with $\lambda(\alpha_s) = \sqrt{(\alpha_s/3)}$ if the pier has shear span ratio, α_s, in the range $1 \leq \alpha_s < 3$, or $\lambda(\alpha_s) = 1$ if $3 \leq \alpha_s$. There is no reduction of the q-value for axial load, as the slenderness limit of Eurocode 2 produces normalised axial force $\eta_k < 0.3$.

The "rigid deck model" of Eurocode 8 (CEN 2005d) is used in the longitudinal direction of all the bridges and in the transverse direction of those with free transverse translation at the abutments. The model consists of an SDOF system of the deck with: (a) the total mass of the deck added to the masses in the upper half of all piers which are rigidly connected to the deck, and (b) the total stiffness of the individual supports. The composite pier-bearing stiffness is used for the piers that support the deck via bearings; the deck displacement is attributed to the pier and the bearing in proportion to their flexibilities. In the transverse direction of bridges with the deck monolithically connected to single-column piers, the rotational degree-of-freedom at the pier top is slaved to the horizontal translation there, so as to consider the effect of the rotational mass moment of inertia of the deck about its axis.

In the transverse direction of bridges with constrained transverse translation at the abutments, modal response spectrum analysis is performed. The mass of the deck is distributed along its length and half of the mass of each pier is lumped at its top. In bridges with up to three intermediate supports, the piers are considered discretely. If the piers are more than three, their transverse stiffness is smeared along the deck which is then considered as a beam on a continuous elastic lateral support. The modal properties of symmetric bridges are calculated with closed-form solutions (Fardis and Tsionis 2013).

In bridges designed for seismic action, the vertical reinforcement of piers is dimensioned for the ULS in bending with axial load from the action effects obtained from the analysis for the seismic design situation. Following Part 2 of Eurocode 8 (CEN 2005e), if the pier supports the deck via bearings, the effective stiffness of piers for use in the seismic analysis is taken equal to the stiffness of the uncracked gross section. If the pier is monolithically connected to the deck, its secant stiffness at the yield point is used as calculated from the design ultimate moment and the section's yield curvature per Annex C of EC8-2 (CEN 2005e). Iterations are necessary, starting from the initial reinforcement from the ULS due to geometric imperfections and the minimum detailing requirements for the number, spacing and ratio of vertical bars in the section. The transverse reinforcement of piers is dimensioned to meet the confinement requirements of Eurocode 8 and the ULS in shear. In bridges with monolithic deck-pier connection, the capacity design shears are determined from the plastic mechanism. The design shear resistance of the piers is calculated after applying the Eurocode 8 reduction factors for bridges with limited ductile or ductile behaviour, as appropriate.

In the specific case of piers with two columns, the transverse seismic forces acting at the centroid of the deck section produce an overturning moment that induces a tensile axial load in one column and a compressive one in the other. The dimensioning for the ULS in bending and shear and the calculation of confinement reinforcement are performed for the most adverse case, i.e. low axial load for bending and shear and high axial load for confinement.

After the design procedure is completed, the expected values of the yield and ultimate chord rotation and the shear resistance of the piers are established. They are calculated from the expressions developed by Biskinis and Fardis (2010a, b, 2013) and Biskinis at al. (2004), which have been adopted in Part 3 of Eurocode 8 (CEN 2005e) and the ***fib*** Model Code 2010 (***fib*** 2012).

9.10.3 Fragility Analysis

Peak ground acceleration is selected as the seismic intensity measure. Fragility curves are constructed for two damage states: yielding of piers and ultimate state of piers and bearings. The damage measures for piers are the peak chord rotation at the ends where rotation is constrained and the peak shear force. For bearings, the relative displacement between the deck and the top of the pier is checked against the eccentricity of vertical load that leads to rollover and the shear deformation of the bearings. Lastly, the maximum angle of rotation of the ends of the deck and the peak seismic curvature of the deck in railway bridges are compared to the operational limits of Annex A1 of EN 1990 (CEN 2005b).

Displacement and deformation demands are estimated from analysis with the 5 %-damped elastic spectrum and the "equal displacement rule" (Bardakis and Fardis 2011; CEN 2005d). Elastic analysis with the "rigid deck model" or modal response spectrum analysis is performed using the secant-to-yield-point stiffness of the piers (Biskinis and Fardis 2010a, 2013; CEN 2005d; ***fib*** 2012) computed with mean material strengths: $f_{cm} = f_{ck} + 8$ MPa for concrete, $f_{ym} = 1.15\, f_{yk}$ for steel. After the formation of plastic hinges at pier ends, the shear forces are determined from the mean values of the moment resistances. The seismic analyses give the median values of the damage measures as a function of the intensity measure.

As the analysis is deterministic, the demand is computed on the basis of the deterministic state of the system at that value of peak ground acceleration. For example, the shear force of a pier is calculated from the moment resistance if the conditional probability that a plastic hinge is formed is higher than 50 %.

The last step is the computation of the (conditional on peak ground acceleration) probability of exceedance of each damage state from the probability distributions of the damage measure demands and of the corresponding capacities. Fragility curves are constructed for piers and bearings separately in the transverse (T) and the longitudinal (L) directions.

Table 9.7 Coefficients of variation

Demand	CoV	Capacity	CoV
Spectral value for given PGA and fundamental period	0.25	Shear resistance in diagonal tension, circular pier	0.16
Shear force demand for given spectral value at fundamental period	0.15	Shear resistance in diagonal tension, rectangular or hollow pier	0.14
Displacement demand for given spectral value at fundamental period	0.20	Shear resistance in web compression, rectangular or hollow pier	0.18
Daily temperature	0.67	Yield chord rotation, circular pier	0.32
Creep and shrinkage strains	0.60	Yield chord rotation, rectangular or hollow pier	0.29
		Ultimate chord rotation, circular pier	0.30
		Ultimate chord rotation, rectangular pier	0.36
		Ultimate chord rotation, hollow pier	0.29
		Deformation capacity of bearings	0.30

9.10.4 Uncertainty in Demand and Capacity

The dispersions of demand and capacity measures are calculated from the coefficients of variation (CoV) listed in Table 9.7. The CoV-values for the pier deformation demands for given excitation spectrum are based on the numerical analyses reported by Bardakis and Fardis (2011). Those for creep and shrinkage are based on the scatter associated with the relevant models (CEN 2004a) and the natural dispersion of the variables they use. The coefficient of variation of daily temperature derives from the presumed standard deviation and yearly mean, e.g. 10 and 15 °C, respectively, for the applications presented in 9.10.5.

The coefficients of variation of the pier capacities reflect the uncertainty in the models, including the scatter in material and geometric properties, as have been quantified by Biskinis and Fardis (2010a, b, 2013) and Biskinis et al. (2004). The coefficients of variation for the deformation capacity of bearings come from the literature, alongside cyclic tests on elastomeric or Lead Rubber bearings tested at the Structures Lab of the University of Patras. The same sources give the mean shear modulus and shear deformation capacity used in the example applications, respectively $G = 900$ kPa and 165 %.

9.10.5 Example Applications

The methodology has been implemented in a numerical tool that uses as input the basic geometry of the bridge, performs design iterations according to Eurocode 2 and, if desired, Eurocode 8, and produces as output the component fragility curves. While the coefficients of variation reported in Table 9.7 are used for the

applications, the user may input different ones in case such information exists for the bridges of interest.

For the applications presented in the following, the deck is a single-box prestressed concrete girder of constant cross-section. All spans are equal and have a length of 40 m. The top slab is 14 m wide and 0.45 m thick; the bottom slab is 7 m wide and 0.35 m thick. The web thickness is 0.7 m in railway bridges and 0.5 m in road bridges. The deck has two 1.25 m-wide side-walks, weighing 10 kN/m each. Ballast and sleepers weigh 16 kN/m^2 and surfacing of road bridge decks weighs 2 kN/m^2. Normal traffic according to Load Model 71 is considered for the railway bridges and Load Model 1 for the road ones (CEN 2003). Concrete is C30/37 and steel is of grade 500 and Class C.

The bearings are designed for creep and shrinkage of the deck estimated for rapid hardening cement; age at prestressing 3 days; curing for 4 days; span completion in 15 days; mean relative humidity and temperature during the lifetime 70 % and 15 °C; and long-term prestress balancing the permanent loads. The design uniform temperature difference from construction is ±50 °C.

Seismic analysis of the bridge is performed for the EC8 design spectrum, with a design peak ground acceleration on rock equal to 0.25 g and the recommended Type 1 spectrum for Ground C (firm soil).

Perfect correlation of failure modes is considered at the component level and the fragility curves at the ultimate state are taken at the worse of the possible conditions, i.e. flexural or shear failure for piers and rollover or shear deformation for bearings.

Example applications for typical European structures are discussed first for bridges with monolithic deck-pier connection. Figure 9.7 presents the fragility curves for the piers of a bridge with free transverse translation of the deck at the abutments. Different curves in each plot refer to the longitudinal (L) and the transverse (T) directions. It is shown that piers with rectangular hollow cross section designed without seismic provisions are likely to fail in shear, possibly before flexural yielding (Fig. 9.7 left), but design to EC8 reduces considerably this possibility (Fig. 9.7 right). Pre-emptive shear failure is avoided also in taller bridges where piers are less vulnerable at both damage states.

Further parametric analyses, not illustrated here for brevity, show that piers in longer bridges are slightly less vulnerable for the ultimate damage state, but might have higher probability of exceeding the yielding damage state. As regards seismic design, bridges designed according to Eurocode 8 are expected to fail only at very high levels of peak ground acceleration, whereas even those designed per Eurocode 2 possess some seismic resistance. In bridges designed for gravity loads alone, circular piers are the least vulnerable for the ultimate damage state and hollow ones the most; the inverse holds for the yielding damage state. On the other hand, the fragility of piers designed for seismic resistance does not depend on the type of cross-section.

Figure 9.8 presents the fragility curves related to the angle and curvature of the deck in railway bridges, based on the traffic velocity and the operational limits in

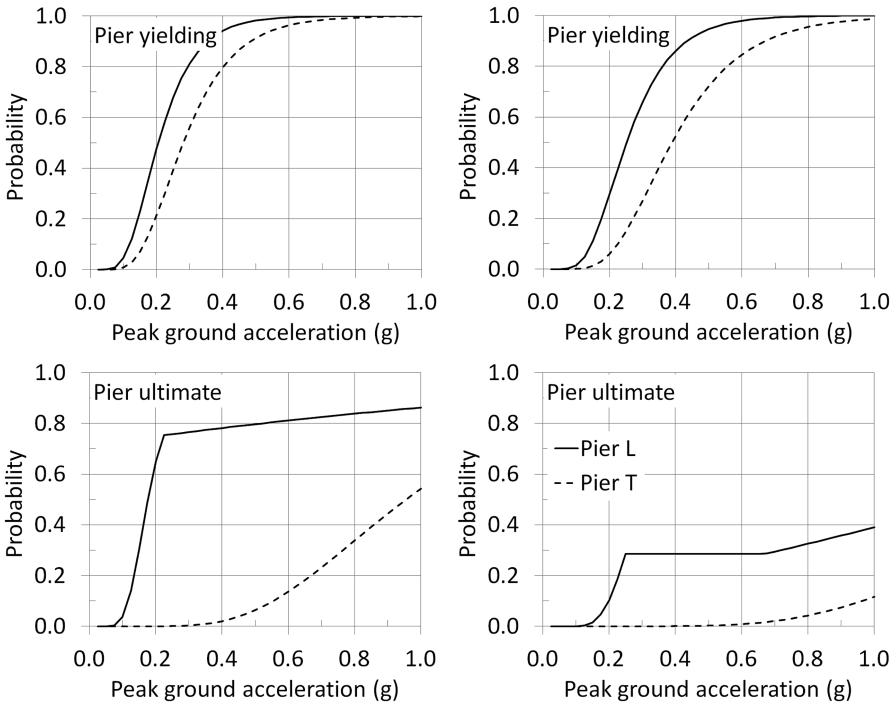

Fig. 9.7 Fragility curves of road bridges with monolithic deck-pier connection, $l = 80$ m and hollow piers with $h = 10$ m, designed to EC2 (*left*) or EC8 (*right*)

Annex A1 of EN 1990 (CEN 2005c). Although Eurocode 8 does not provide specific rules for the transverse deformation of the deck, the results in Fig. 9.8 show that seismic design reduces the probability of exceeding the limit values. The results demonstrate also that longer bridges have higher probabilities of exceeding these deformation limits and that the deformation angle is more critical than the deck curvature.

Figures 9.9 and 9.10 show results for bridges with the deck supported on bearings. Different curves in each plot are for the longitudinal (L) and the transverse (T) direction, and in Fig. 9.9 for the different piers, numbered symmetrically with respect to deck mid-length. These and similar results demonstrate that the ultimate damage state is reached because of failure of the bearings, due to rollover or shearing and that the vulnerability of this typology is not influenced by the type of pier cross-section. The plots in the third rows of Figs. 9.9 and 9.10 show that seismic design reduces significantly the probability of failure of bearings in bridges with constrained transverse translation at the abutments, but not for those with free translation. Seismic design improves also the performance of piers at both damage states, but may slightly increase the vulnerability in terms of the deck horizontal deformation, as shown in the last row of Fig. 9.9.

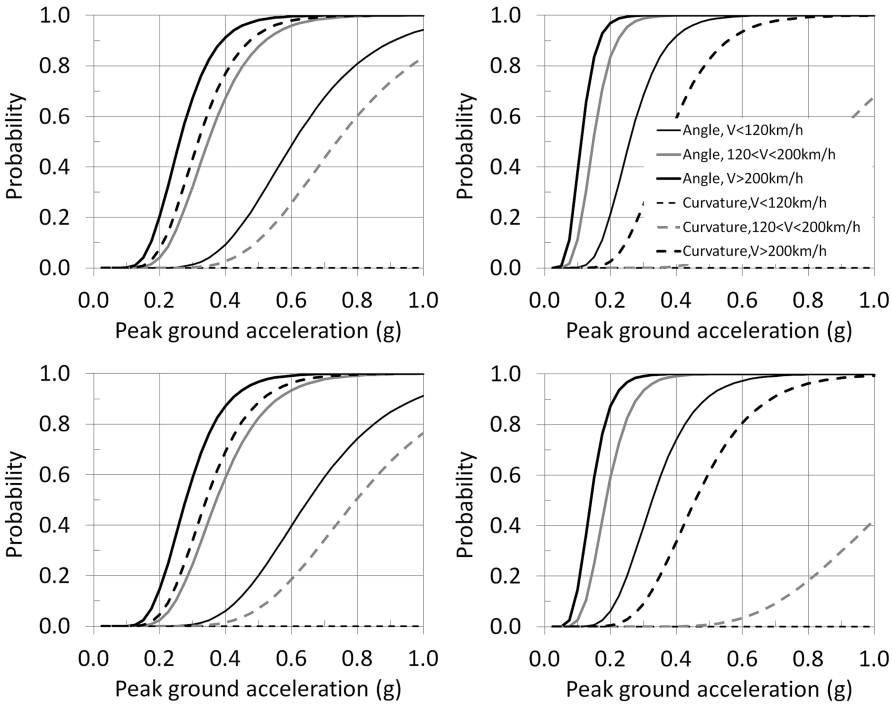

Fig. 9.8 Fragility curves for the deck horizontal deformation of railway bridges with monolithic deck-pier connection, $l = 80$ m (*left*) or $l = 240$ m (*right*), designed to EC2 (*top*) or EC8 (*bottom*) and circular piers with $h = 10$ m

Additional parametric analyses support the conclusion that longer and taller bridges with the deck supported on bearings are less vulnerable as regards all damage states and damage measures and that the longitudinal direction is generally the most critical.

For bridges that are not located in seismic regions, the designer may select the structural solution with a fixed point at the central pier (e.g. with articulation) and the deck supported on bearings at the top of the remaining piers. The fragility curves for a bridge with constrained transverse displacement at the abutments and design for gravity alone are shown in Fig. 9.11. As for the other bridge typologies, hollow piers are vulnerable in shear, but taller ones are protected against this failure mode. Comparison of the second and third rows indicates that bearings appear likely to exceed the ultimate limit state before the central pier does. Piers and bearings in taller bridges are less vulnerable as regards all damage states and both directions. On the contrary, the horizontal deck deformations are more critical for taller bridges.

Overall and despite the different geometric and dynamic characteristics, bridges with monolithic deck-pier connection or fixed connection at the central pier and the

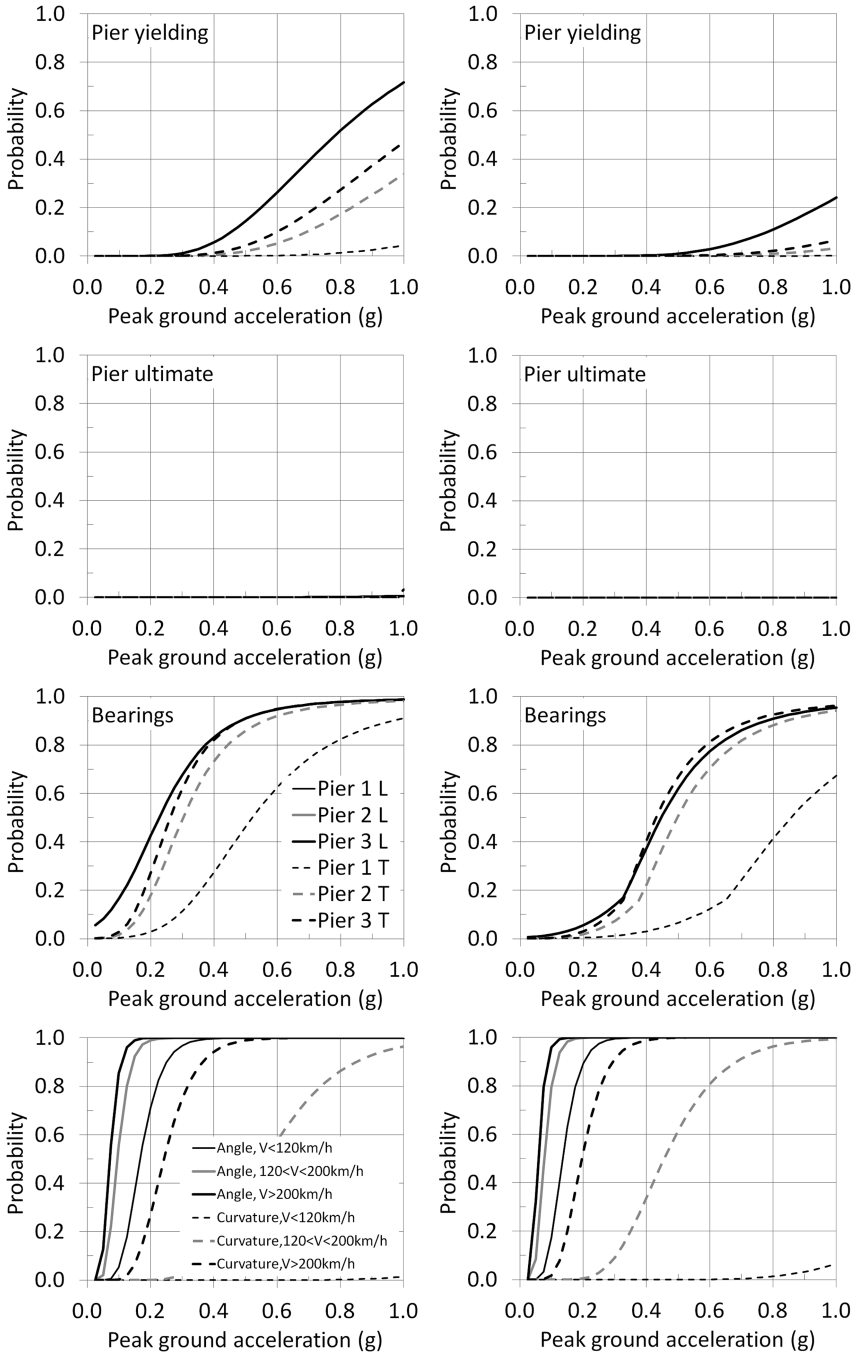

Fig. 9.9 Fragility curves of railway bridges with deck supported on bearings, $l = 240$ m and rectangular piers with $h = 10$ m, designed to EC2 (*left*) or EC8 (*right*)

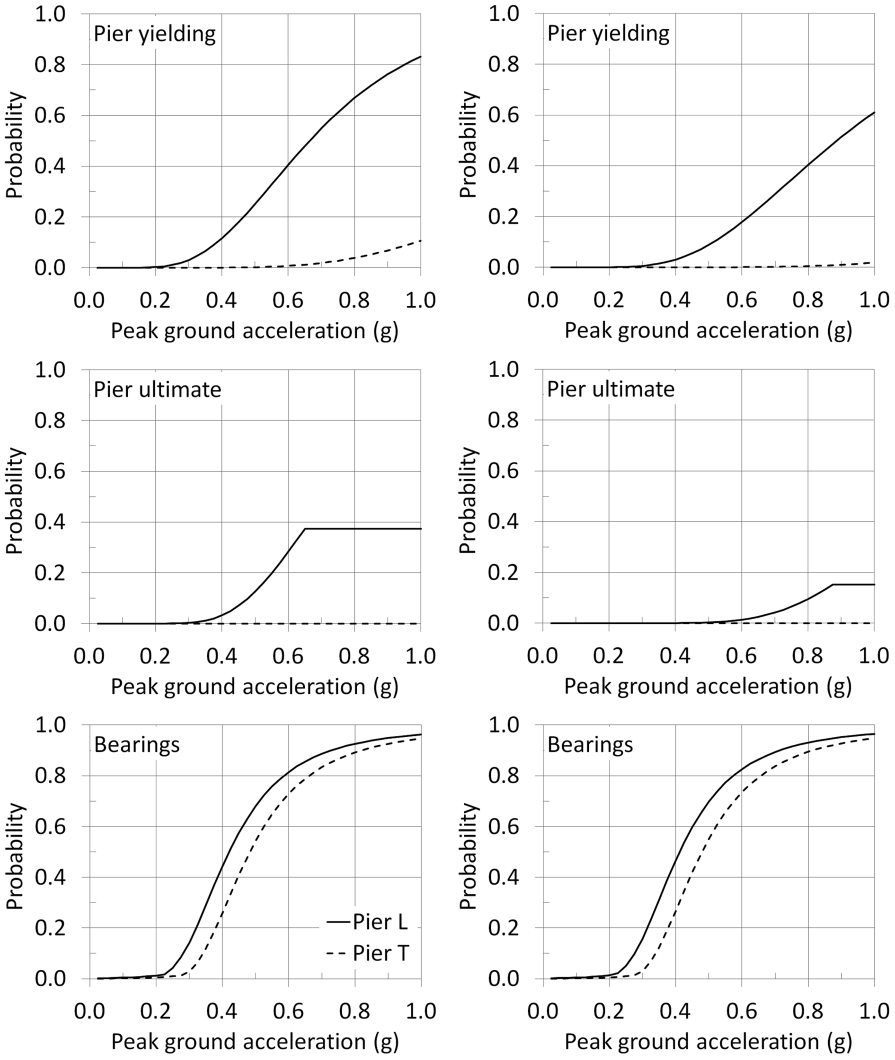

Fig. 9.10 Fragility curves of road bridges with deck supported on bearings, $l = 120$ m and hollow piers with $h = 10$ m, designed to EC2 (*left*) or EC8 (*right*)

same level of seismic design have rather similar fragilities for all components and damage states, no matter whether the transverse translation at the abutments is free or constrained. However, the piers and particularly the bearings in railway bridges with the deck supported on bearings are significantly more vulnerable than those in road bridges. It is thus necessary to account for the fixity conditions of the deck at the abutments in bridges with bearings at all supports.

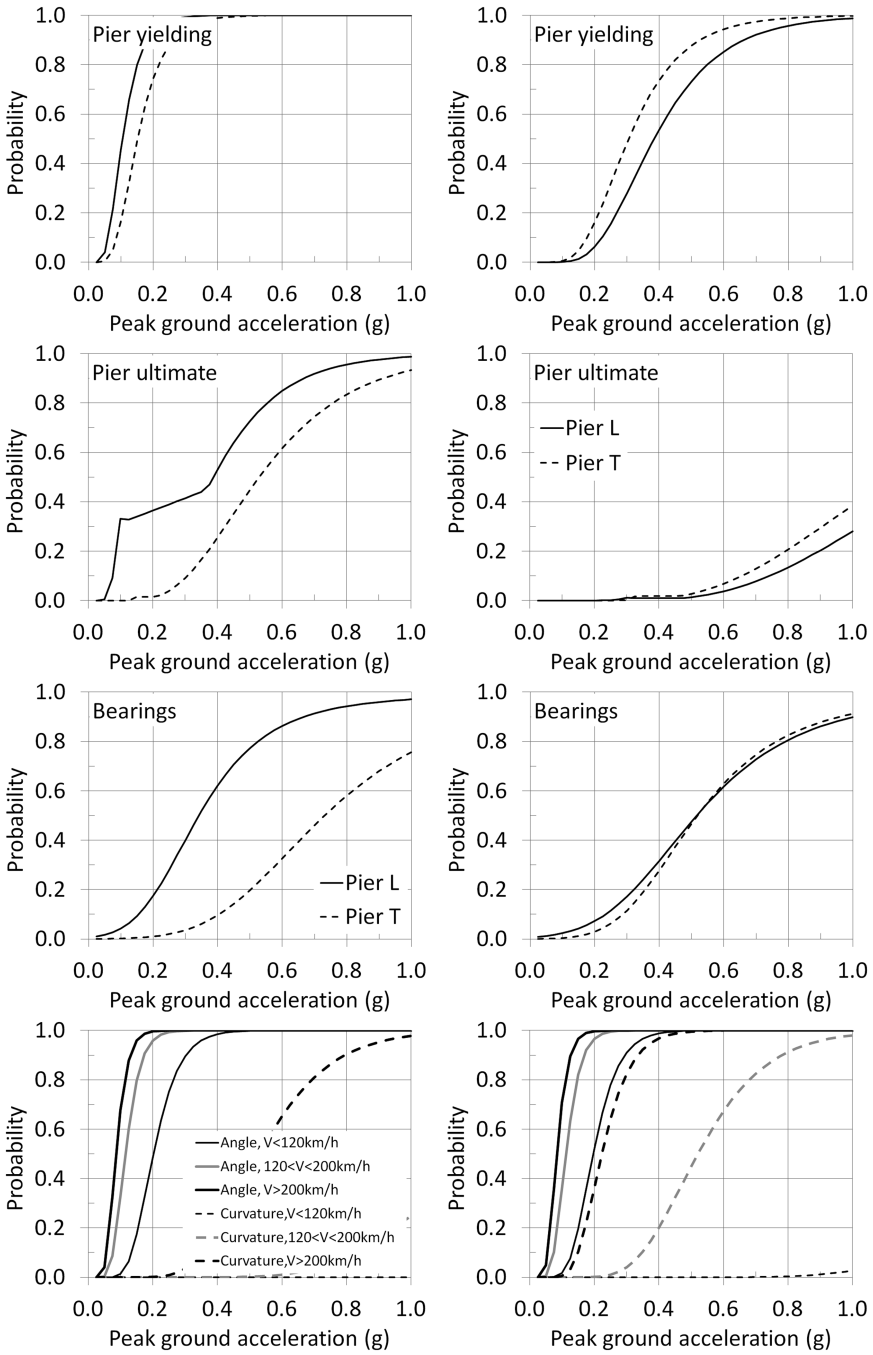

Fig. 9.11 Fragility curves of railway bridges with deck supported on bearings with fixed connection to the central pier, $l = 160$ m and hollow piers with $h = 10$ m (*left*) or $h = 25$ m (*right*)

9.11 Concluding Remarks

The approaches available for risk assessment of bridges have been reviewed. One option is to employ fragility curves from literature. Existing curves depend on the structural type and very often also on the individual characteristics of bridges belonging to the same typological class. This requires careful selection of the most appropriate set of curves for practical applications. Mean fragility curves have also been explored, but the large dispersion of their parameters is difficult to accommodate.

The other choice is to develop new fragility curves for bridge classes or single structures. Previous studies show that different methods produce diverging curves, particularly for the most severe damage states. The reviewed sensitivity studies offer guidance for making informed choices regarding several aspects of fragility analysis. In case supplementary information and resources are available, or where the importance of the structure justifies it, detailed studies may be performed to account for the adverse effects of corrosion and cumulative seismic damage during the lifetime of the bridge. These topics, together with asynchronous excitation and the case-dependent consequences of retrofitting and liquefaction, have been the object of recent research activity.

Finally, an intermediate approach is to develop parameterised fragility curves, whose mean and standard deviation are expressed as functions of the strength and stiffness of a specific structure. The proposed methodology for fast fragility analysis also avoids time-consuming calculations and produces fragility curves for individual bridges using as input only their base geometry. It may be further extended to the fragility analysis of real bridges, provided that data on their geometry and reinforcement are available.

Acknowledgments The research leading to these results received funding from the European Community's 7th Framework Programme (FP7/2007-2013) under grant agreement n° 244061.

References

Argyroudis S, Monge O, Finazzi D, Pessina V (2003) Vulnerability assessment of lifelines and essential facilities: methodological handbook, Appendix 1: roadway transportation system. Report n°GTR-RSK 0101-152av7

ATC (1985) Earthquake damage evaluation data for California. Applied Technology Council, Redwood

Avşar Ö, Yakut A (2010) Evaluation of ground motion intensity measures for the fragility curves of ordinary highway bridges in Turkey. In: Proceedings of the 9th US national & 10th Canadian conference on earthquake engineering, Toronto

Avşar Ö, Yakut A, Caner A (2011) Analytical fragility curves for ordinary highway bridges in Turkey. Earthq Spectra 27(4):971–996

Aygün B, Dueñas-Osorio L, Padgett JE, DesRoches R (2011) Efficient longitudinal seismic fragility assessment of a multispan continuous steel bridge on liquefiable soils. ASCE J Bridge Eng 16(1):93–107

Azevedo J, Guerreiro L, Bento R, Lopes M, Proença J (2010) Seismic vulnerability of lifelines in the greater Lisbon area. Bull Earthq Eng 8(1):157–180

Banerjee S, Shinozuka M (2008) Mechanistic quantification of RC bridge damage states under earthquake through fragility analysis. Probab Eng Mech 23(1):12–22

Bardakis VG, Fardis MN (2011) Nonlinear dynamic v elastic analysis for seismic deformation demands in concrete bridges having deck integral with the piers. Bull Earthq Eng 9(2):519–536

Basöz N, Kiremidjian AS (1996) Risk assessment for highway transportation systems. The John A. Blume Earthquake Engineering Center, Stanford

Basöz NI, Kiremidjian AS, King SA, Law KH (1999) Statistical analysis of bridge damage data from the 1994 Northridge, CA, earthquake. Earthq Spectra 15(1):25–54

Biskinis DE, Fardis MN (2010a) Deformations at flexural yielding of members with continuous or lapspliced bars. Struct Concr 11(3):127–138

Biskinis DE, Fardis MN (2010b) Flexure-controlled ultimate deformations of members with continuous or lap-spliced bars. Struct Concr 11(2):93–108

Biskinis DE, Fardis MN (2013) Stiffness and cyclic deformation capacity of circular RC columns with or without lap-splices and FRP-wrapping. Bull Earthq Eng 11(5):1447–1466. doi:10.1007/s10518-013-9442-7

Biskinis DE, Roupakias G, Fardis MN (2004) Degradation of shear strength of RC members with inelastic cyclic displacements. ACI Struct J 101(6):773–783

Cardone D, Perrone G, Sofia S (2011) A performance-based adaptive methodology for the seismic evaluation of multi-span simply supported deck bridges. Bull Earthq Eng 9(5):1463–1498

Casciati F, Cimellaro GP, Domaneschi M (2008) Seismic reliability of a cable-stayed bridge retrofitted with hysteretic devices. Comput Struct 86(17–18):1769–1781

CEN (2002) EN 1990 Eurocode: basis of structural design. European Committee for Standardization, Brussels

CEN (2003) EN 1991-2 Eurocode 1: actions on structures – Part 2: Traffic loads on bridges. European Committee for Standardization, Brussels

CEN (2004a) EN 1992-1-1 Eurocode 2: design of concrete structures – Part 1-1: General rules and rules for buildings. European Committee for Standardization, Brussels

CEN (2004b) EN 1998-1 Eurocode 8: design of structures for earthquake resistance – Part 1: General rules, seismic actions and rules for buildings. European Committee for Standardization, Brussels

CEN (2005a) EN 1337-3 structural bearings – Part 3: Elastomeric bearings. European Committee for Standardization, Brussels

CEN (2005b) EN 1990 Eurocode: basis of structural design – Annex A2: application for bridges. European Committee for Standardization, Brussels

CEN (2005c) EN 1992-2 Eurocode 2: design of concrete structures – concrete bridges – design and detailing rules. European Committee for Standardization, Brussels

CEN (2005d) EN 1998-2 Eurocode 8: design of structures for earthquake resistance – Part 2: Bridges. European Committee for Standardization, Brussels

CEN (2005e) EN 1998-3 Eurocode 8: design of structures for earthquake resistance – Part 3: Assessment and retrofitting of buildings. European Committee of Standardization, Brussels

Ceresa P, Borzi B, Noto F, Onida M (2012a) Application of a probabilistic mechanics-based methodology for the seismic risk assessment of the Italian RC bridges. In: 15th world conference on earthquake engineering, Lisbon

Ceresa P, Fiorini E, Borzi B (2012b) Effects of the seismic input variability on the seismic risk assessment of RC bridges. In: 15th world conference on earthquake engineering, Lisbon

Choe D-E, Gardoni P, Rosowsky D (2007) Closed-form fragility estimates, parameter sensitivity, and Bayesian updating for RC columns. ASCE J Eng Mech 133(7):833–843

Choe D-E, Gardoni P, Rosowsky D, Haukaas T (2009) Seismic fragility estimates for reinforced concrete bridges subject to corrosion. Struct Saf 31:275–283
Choi E, DesRoches R, Nielson B (2004) Seismic fragility of typical bridges in moderate seismic zones. Eng Struct 26(2):187–199
Crowley H (ed) (2011) Fragility functions for roadway bridges. SYNER-G Deliverable D3.6
De Felice G, Giannini R (2010) An efficient approach for seismic fragility assessment with application to old reinforced concrete bridges. J Earthq Eng 14(2):231–251
Dong Y, Frangopol DM, Saydam D (2013) Time-variant sustainability assessment of seismically vulnerable bridges subjected to multiple hazards. Earthq Eng Struct Dyn 42(10):1451–1467
Elnashai AS, Borzi B, Vlachos S (2004) Deformation-based vulnerability functions for RC bridges. Struct Eng Mech 17(2):215–244
Fajfar P, Gašperšič P (1996) The N2 method for the seismic damage analysis of RC buildings. Earthq Eng Struct Dyn 25(1):31–46
Fardis MN, Tsionis G (2013) Eigenvalues and modes of distributed-mass symmetric multispan bridges with restrained ends for seismic response analysis. Eng Struct 51:141–149
FEMA (2010) Hazus MH MR5 technical manual. Federal Emergency Management Agency, Washington, DC
fib (2012) Model code 2010 – final draft. Bulletins 65/66, Federation Internationale du Beton, Lausanne
Franchin P, Pinto PE (2009) Allowing traffic over mainshock-damaged bridges. J Earthq Eng 13(5):585–599
Franchin P, Lupoi A, Pinto PE (2006) On the role of road networks in reducing human losses after earthquakes. J Earthq Eng 10(2):195–206
Gardoni P, Rosowsky D (2009) Seismic fragility increment functions for deteriorating reinforced concrete bridges. Struct Infrastruct Eng 7(11):869–879
Gardoni P, Mosalam KM, Der Kiureghian A (2003) Probabilistic seismic models and fragility estimates for RC bridges. J Earthq Eng 7(1):79–106
Ghosh J, Padgett JE (2010) Aging considerations in the development of time-dependent seismic fragility curves. ASCE J Struct Eng 136(12):1497–1511
Ghosh J, Padgett JE (2011) Probabilistic seismic loss assessment of aging bridges using a component-level cost estimation approach. Earthq Eng Struct Dyn 40(15):1743–1761
Hancilar U, Taucer F (eds) (2013) Guidelines for typology definition of European physical assets for earthquake risk assessment. Publications Office of the European Union, Luxembourg
Jeong SH, Elnashai AS (2007) Probabilistic fragility analysis parameterized by fundamental response quantities. Eng Struct 29(6):1238–1251
Karim KR, Yamazaki F (2001) Effect of earthquake ground motions on fragility curves of highway bridge piers based on numerical simulation. Earthq Eng Struct Dyn 30(12):1839–1856
Karim KR, Yamazaki F (2003) A simplified method of constructing fragility curves for highway bridges. Earthq Eng Struct Dyn 32(10):1603–1626
Khan RA, Datta TK, Ahmad S (2004) Seismic risk analysis of cable stayed bridges with support flexibility. In: 13th world conference on earthquake engineering, Vancouver
Kibboua A, Naili M, Benouar D, Kehila F (2011) Analytical fragility curves for typical Algerian reinforced concrete bridge piers. Struct Eng Mech 39(3):411–442
Kim S-H, Shinozuka M (2004) Development of fragility curves of bridges retrofitted by column jacketing. Probab Eng Mech 19(1–2):105–112
Kumar R, Gardoni P, Sanchez-Silva M (2009) Effect of cumulative seismic damage and corrosion on the life-cycle cost of reinforced concrete bridges. Earthq Eng Struct Dyn 38(7):887–905
Kunnath SK, Larson L, Miranda E (2006) Modeling considerations in probabilistic performance-based seismic evaluation: case study of the I-880 viaduct. Earthq Eng Struct Dyn 35(1):57–75
Kurian SA, Deb SK, Dutta A (2006) Seismic vulnerability assessment of a railway overbridge using fragility curves. In: 4th international conference on earthquake engineering, Taipei
Kwon O-S, Elnashai A (2006) The effect of material and ground motion uncertainty on the seismic vulnerability curves of RC structure. Eng Struct 28(2):289–303

Kwon O-S, Elnashai AS (2009) Fragility analysis of a highway over-crossing bridge with consideration of soil–structure interactions. Struct Infrastruct Eng 6(1–2):159–178
Kwon O, Sextos AG, Elnashai, AS (2009) Seismic fragility of a bridge on liquefaction susceptible soil. In: 10th international conference on structure safety and reliability, Osaka
Lehman D, Moehle J, Mahin S, Calderone A, Henry L (2004) Experimental evaluation of the seismic performance of reinforced concrete bridge columns. ASCE J Struct Eng 130 (6):869–879
Li J, Spencer BF, Elnashai AS (2012) Bayesian updating of fragility functions using hybrid simulation. ASCE J Struct Eng 139(7):1160–1171
Lupoi G, Franchin P, Lupoi A, Pinto PE (2004) Seismic fragility analysis of structural systems. In: 13th world conference on earthquake engineering, Vancouver
Lupoi A, Franchin P, Pinto PE, Monti G (2005) Seismic design of bridges accounting for spatial variability of ground motion. Earthq Eng Struct Dyn 34(4–5):327–348
Mackie K, Stojadinović B (2004a) Fragility curves for reinforced concrete highway overpass bridges. In: 13th world conference on earthquake engineering, Vancouver
Mackie K, Stojadinović B (2004b) Improving probabilistic seismic demand models through refined intensity measures. In: 13th world conference on earthquake engineering, Vancouver
Mackie KR, Stojadinović B (2006) Post-earthquake functionality of highway overpass bridges. Earthq Eng Struct Dyn 35(1):77–93
Mackie K, Stojadinović B (2007) R -factor parameterized bridge damage fragility curves. ASCE J Bridge Eng 12(4):500–510
Marano GC, Greco R, Mezzina M (2006) Analytical evaluation of fragility curves by using stochastic approach. In: 2nd fib international congress, Naples
Monti G, Nisticò N (2002) Simple probability-based assessment of bridges under scenario earthquakes. ASCE J Bridge Eng 7(2):104–114
Moschonas IF, Kappos AJ, Panetsos P, Papadopoulos V, Makarios T, Thanopoulos P (2009) Seismic fragility curves for Greek bridges: methodology and case studies. Bull Earthq Eng 7(2):439–468
Nateghi F, Shahsavar VL (2004) Development of fragility and reliability curves for seismic evaluation of a major prestressed concrete bridge. In: 13th world conference on earthquake engineering, Vancouver
Nielson BG, DesRoches R (2007) Seismic fragility methodology for highway bridges using a component level approach. Earthq Eng Struct Dyn 36(6):823–839
Nielson BG, Pang WC (2011) Effect of ground motion suite size on uncertainty estimation in seismic bridge fragility modeling. In: 2011 structures congress, Las Vegas
Padgett JE, DesRoches R (2007a) Bridge functionality relationships for improved seismic risk assessment of transportation networks. Earthq Spectra 23(1):115–130
Padgett JE, DesRoches R (2007b) Sensitivity of seismic response and fragility to parameter uncertainty. ASCE J Struct Eng 133(12):1710–1718
Padgett JE, DesRoches R (2009) Retrofitted bridge fragility analysis for typical classes of multispan bridges. Earthq Spectra 25(1):117–141
Padgett JE, Nielson BG, DesRoches R (2008) Selection of optimal intensity measures in probabilistic seismic demand models of highway bridge portfolios. Earthq Eng Struct Dyn 37(5):711–725
Padgett JE, Ghosh J, Dueñas-Osorio L (2013) Effects of liquefiable soil and bridge modelling parameters on the seismic reliability of critical structural components. Struct Infrastruct Eng 9(1):59–77
Park YJ, Ang AHS (1985) Seismic damage analysis of reinforced concrete buildings. ASCE J Struct Eng 111(4):740–757
Park J, Choi E (2011) Fragility analysis of track-on steel-plate-girder railway bridges in Korea. Eng Struct 33(3):696–705
Prasad GG, Banerjee S (2013) The impact of flood-induced scour on seismic fragility characteristics of bridges. J Earthq Eng 17(6):803–828

Qi'ang W, Ziyan W, Shukui L (2012) Seismic fragility analysis of highway bridges considering multi-dimensional performance limit state. Earthq Eng Eng Vib 11(2):185–193

RMS (1995) Development of a standardized earthquake loss estimation methodology. Risk Management Solutions, Menlo Park

Saxena V, Deodatis G, Shinozuka M, Feng MQ (2000) Development of fragility curves for multi-span reinforced concrete bridges. In: International conference on Monte-Carlo simulation, Monaco

Sextos A, Pitilakis K, Kappos A (2003a) Inelastic dynamic analysis of RC bridges accounting for spatial variability of ground motion, site effects and soil-structure interaction phenomena. Part 1: Methodology and analytical tools. Earthq Eng Struct Dyn 32(4):607–627

Sextos A, Pitilakis K, Kappos A (2003b) Inelastic dynamic analysis of RC bridges accounting for spatial variability of ground motion, site effects and soil-structure interaction phenomena. Part 2: Parametric analysis. Earthq Eng Struct Dyn 32(4):629–652

Shama AA, Mander JB (2003) The seismic performance of braced timber pile bents. Earthq Eng Struct Dyn 32(3):463–482

Shinozuka M, Feng MQ, Lee J, Naganuma T (2000a) Statistical analysis of fragility curves. ASCE J Eng Mech 126(12):1224–1231

Shinozuka M, Feng MQ, Kim HK, Kim SH (2000b) Nonlinear static procedure for fragility curve development. ASCE J Eng Mech 126(12):1287–1295

Shirazian S, Ghayamghamian MR, Nouri GR (2011) Developing of fragility curve for two-span simply supported concrete bridge in near-fault area. World Acad Sci Eng Technol 51:571–575

Sullivan IT (2010) Analytical seismic fragility curves for skewed multi-span steel girder bridges. M.Sc. dissertation, Clemson University

Tanaka S, Kameda H, Nojima N, Ohnishi S (2000) Evaluation of seismic fragility for highway transportation systems. In: 12th world conference on earthquake engineering, Auckland

Yamazaki F, Motomura H, Hamada T (2000) Damage assessment of expressway networks in Japan based on seismic monitoring. In: 12th world conference on earthquake engineering, Auckland

Yi JH, Kim SH, Kushiyama S (2007) PDF interpolation technique for seismic fragility analysis of bridges. Eng Struct 29(7):1312–1322

Zakeri B, Padgett JE, Amiri GG (2013) Fragility analysis of skewed single frame concrete box girder bridges. ASCE J Perform Constr Facil. doi:10.1061/(ASCE)CF.1943-5509.0000435

Zhang J, Huo Y, Brandenberg SJ, Kashighandi P (2008) Effects of structural characterizations on fragility functions of bridges subject to seismic shaking and lateral spreading. Earthq Eng Eng Vib 7(4):369–382

Zhong J, Gardoni P, Rosowsky D (2012) Seismic fragility estimates for corroding reinforced concrete bridges. Struct Infrastruct Eng 8(1):55–69

Chapter 10
Fragility Functions of Highway and Railway Infrastructure

Sotiris Argyroudis and Amir M. Kaynia

Abstract The experience of past earthquakes has revealed that highway and railway elements are quite vulnerable to earthquake shaking and induced phenomena such as soil liquefaction or landslide; damages to these elements can seriously affect the transportation of products and people in both short-term (emergency actions) and long-term period. The objective of this chapter is to propose appropriate fragility functions for roadway and railway components other than bridges that are presented separately in Chap. 9. To this end, the main typological features are summarized and a short review of earthquake damages together with damage states definitions are provided for these elements. Fragility curves from literature are collected and reviewed. In some cases these functions are modified and adapted, while in other cases new fragility curves are developed. A general procedure for the derivation of analytical fragility curves that was followed in SYNER-G is described. This approach takes into account the effect of structure geometry, ground motion characteristics, soil conditions and associated uncertainties. New fragility curves are presented for tunnels in soil, embankments, cuttings and bridge abutments based on numerical analyses due to ground shaking. Finally, the proposed fragility functions are summarized and a general scheme to identify the functionality of roadway and railway elements due to different damage levels is outlined.

S. Argyroudis (✉)
Department of Civil Engineering, Aristotle University of Thessaloniki, 54124 Thessaloniki, Greece
e-mail: sarg@civil.auth.gr

A.M. Kaynia
Norwegian Geotechnical Institute (NGI), Ullevål Stadion, N-0806, P.O. Box. 3930 Oslo, Norway

Department of Structural Engineering, Norwegian University of Science and Technology (NTNU), 7491 Trondheim, Norway
e-mail: Amir.M.Kaynia@ngi.no

K. Pitilakis et al. (eds.), *SYNER-G: Typology Definition and Fragility Functions for Physical Elements at Seismic Risk*, Geotechnical, Geological and Earthquake Engineering 27, DOI 10.1007/978-94-007-7872-6_10,

10.1 Introduction

Roadway and railway systems are complex networks of various components like bridges, roads, tunnels, embankments, retaining walls, slopes, tracks and building facilities. Past earthquakes indicate that some of these elements are quite vulnerable, and in addition, involve lengthy repair time or rerouting difficulties. For example, the disruption to the road network can strongly affect the emergency efforts immediately after the earthquake and the rebuilding and other business activities in the following period. Typical paradigms of damage to highway and railway structures can be found in recent earthquakes such as the 2011 Christchurch, New Zealand; 2010 Chile; 2009 L'Aquila, Italy; 2007 Niigata-Chuetsu Oki and 2004 Niigata-ken Chuetsu, Japan and others. In these events the damages due to geotechnical hazards were particularly important.

The complexity of elements at risk, their construction variability, and until recently, the lack of well-documented damage and loss data from strong earthquakes have made the vulnerability assessment of each component or the network as a whole, quite a complicated problem. Consideration of the spatial extension of roadway/railway networks, the interactions with other systems and the inherent uncertainties in seismic hazard and vulnerability estimates, have made the risk assessment of transportation networks a complex and challenging issue.

In the following sections, the main typological features, damage classification and definitions are given for the roadway and railway elements that considered in the SYNER-G taxonomy. A brief review of available fragility curves and their evaluation methods are presented. The existing fragility curves are limited and generally inadequate, especially for the case of induced deformations by liquefaction, lateral spreading, landslide and fault rupture. The derivation of new analytical fragility curves due to seismic shaking is described for specific components and the parameters of the proposed fragility functions are presented. In case of ground failure, preliminary fragility curves are proposed based on expert judgment, while further research is needed on this topic.

10.2 Identification of Main Typologies

Most of the roadway and railway elements are categorized as earth structures; therefore, a main typological feature is the ground type, which characterizes either a construction or its foundation and surrounding material. Different soil classification systems are available based on various soil properties. A widely used scheme is the one provided by Eurocode 8 (2004), which is based on the soil's average shear wave velocity on the top 30 m, V_{s30}.

In case of roadways, the main element is the road itself, which is passing over bridges, embankments or through tunnels and other civil works. Therefore, the hierarchy of roads according to their functions and capacities is an important

parameter for the description of the typologies of the roadway elements. Different classification schemes exist based on speed limits, number of lanes and other criteria.

In case of railway infrastructure, the key part is the track, which consists of elements such as rails, sleepers and ballast that transfer the static and dynamic loads to the foundation soil. Different classification schemes exist which are based on speed limits, construction materials, usage of track and other parameters.

In addition to the above main attributes, other important typological features are given in the following for each element. It is noted that bridges are presented separately in Chap. 9.

- Tunnels: the basic parameters for the description of the typology are the construction method (bored or mined, cut-and-cover, immersed), the shape (circular, rectangular, horseshoe, etc.), the depth (surface, shallow, deep), the geological conditions (rock, alluvial), and supporting system (concrete, masonry, steel, etc.).
- Embankments, cuts and slopes: the main typological features are the geometrical parameters of the construction (i.e. slope angle, height).
- Road pavements: the basic parameter is the number of traffic lanes which is based on the functional hierarchy of the network.
- Bridge abutments: their typology is related to the structural type of bridge (e.g. stub, partial or full depth, integral abutment); other main typological features are the depth and the soil conditions of foundation and fill material behind the abutment. The depth is dependent on the surrounding topography and abutment geometry, while the backfill material behaviour depends on its compaction level.

The typological features and classification considered in SYNER-G are summarized in Table 10.1.

10.3 Damage Description

Earthquake effects on roadway and railway elements can be grouped into two categories, (1) ground shaking (expressed often in terms of peak ground acceleration, PGA); and (2) ground failure such as liquefaction, fault displacement, and slope instability (expressed in terms of permanent ground deformation, PGD). A brief summary is given below for each element:

- Tunnels: Three types of deformations express the response of underground structures to seismic motions, (1) axial compression and extension, (2) longitudinal bending, and (3) ovaling/racking. Typical damages include (Owen and Scholl 1981; ALA 2001; Corigliano 2007): slope instability leading to tunnel collapse, portal failure, roof or wall collapse, invert uplift spalling, cracking or crushing of the concrete lining, slabbing or spalling of the rock around the opening, bending and buckling of reinforcing bars, pavement cracks, wall deformation, local opening of joints and obstruction of the opening.

Table 10.1 SYNER-G taxonomy for roadway and railway network

Category	Sub-category
Bridges	See Chap. 9
Tunnels	Construction method: bored or mined, cut-and-cover, immersed
	Shape: circular, rectangular, horseshoe, etc.
	Depth: surface, shallow, deep
	Geological conditions: rock/alluvial
	Supporting system: concrete, masonry, steel, etc.
Embankments (road/track on)	Geometrical parameters of the construction, i.e. slope angle, height
	Soil conditions
	Water table
Cuts (road/track in)	Geometrical parameters of the construction, i.e. slope angle, height
	Soil conditions
	Water table
Slopes (road/track on or running along)	Geometrical parameters of the construction, i.e. slope angle, height
	Soil conditions
	Water table
Bridge abutments	Geometry of the abutment i.e. height, width
	Soil conditions of foundation
	Fill material behind the abutment
Road pavements (ground failure)	Number of traffic lanes
Railway tracks (ground failure)	Ballasted, slab tracks

- Embankments: When the foundation bearing capacity is lost due to static and dynamic loading, for example due to soil liquefaction, the embankment may spread laterally and settle at the same time. This could lead to lateral movement of embankment (from a few centimetres to several meters) resulting in opening of cracks in the road pavement or displacement of the railway tracks.
- Cuts and slopes: Earthquake induced landslides and rock falls can cause partial or complete blockage of the road/track as well as the structural damage to the road pavement or railway track. In addition, roads/tracks constructed in cuts and on slopes are subjected to failure or large movements of the slopes on the sides of the road/track.
- Bridge abutments/retaining walls: Approach backfills behind bridge abutments/retaining walls are vulnerable to earthquake-induced differential settlement. Approach-fill settlement has been the most commonly occurring type of highway system damage during recent earthquakes. In addition, pounding of the deck to the abutment can seriously affect the overall response of the bridge (Argyroudis et al. 2013a). This type of damage does not often result in extensive repair costs; however, it may have a serious impact on the functionality of the road network during the emergency period. In case of railway network, where the tolerance to ground deformation is lower, the impairment of functionality is more significant.

Table 10.2 Definition of damage states for roadway and railway elements (embankments, cuts, abutments, slopes, tracks) in SYNER-G

	Permanent ground deformation (m)					
	Roadway			Railway		
Damage state	Min	Max	Mean	Min	Max	Mean
DS1. Minor	0.02	0.08	0.05	0.01	0.05	0.003
DS2. Moderate	0.08	0.22	0.15	0.05	0.10	0.008
DS3. Extensive/complete	0.22	0.58	0.40	0.10	0.30	0.200

- Road pavement: Damage to road pavement can be direct (e.g. fault ruptures, settlement, lateral spreading) or indirect (e.g. collapsed buildings, landslide debris, damage to underlying pipelines).
- Railway track damage in past earthquakes have included displaced ballast, broken ties, pulled apart joints, broken rails, buckled rail, large lateral displacements and loss of vertical support for track over large distances. Signal systems have suffered limited damages in relatively low magnitude earthquakes due to broken batteries, overturned electrical relays and wrapped wires in pole lines. Such damage are often highly disruptive but can be quickly repaired. Moreover, losses might occur in larger earthquakes in terms of more extensive damage such as broken signal masts (Byers 2004).

Different damage criteria have been proposed for the fragility analysis of roadway and railway elements. The number of damage states is variable and is related with the functionality, traffic state, and/or the repair duration. In empirical and expert judgment methods, the extent of damage is described qualitatively (e.g. extent of cracks or settlements). In analytical methods the damage levels are defined based on the range of a specific damage index such as permanent ground deformation, capacity and factor of safety, which is also related to the serviceability level of the network.

The damage states in Table 10.2, in terms of permanent ground deformation (PGD), have been proposed in SYNER-G and have been used for roadway and railway components. In particular, a mean value of PGD was estimated for minor, moderate, and extensive/complete damage based on a range of values (min, max) from a review of the literature. In Table 10.3 and Table 10.4 the damage states for each component are defined and also correlated to the serviceability of the network.

10.4 Review of Existing Fragility Functions

The existing fragility functions are based on empirical, analytical or expert judgment methods. Most of the available fragility curves follow a lognormal cumulative distribution. The number of damage states and the type of intensity measure vary

Table 10.3 Description of damage states for roadway/railway components in SYNER-G

	Description	Serviceability
Tunnels		
DS1	Minor cracking and spalling and other minor distress to tunnel liners	Open to traffic, closed or partially closed during inspection, cleaning and possible repair works
DS2	Ranges from major cracking and spalling to rock falls	Closed during repair works for 2–3 days
DS3	Collapse of liner or surrounding soils to the extent that the tunnel is blocked either immediately or within a few days after the main shock	Closed for a long period of time
Metro/urban tunnels in soil		
DS1	Minor cracking and spalling and other minor distress to tunnel lining	Open to traffic, closed or partially closed during inspection and possible repair works
DS2	Major cracking and spalling of tunnel lining	Closed during repair works for 2–3 days
DS3	Extensive damage of liner or surrounding soils to the extent that the tunnel is blocked either immediately or within a few days after the main shock	Closed for a long period of time
Embankments (road/track on)		
DS1	Surface slide of embankment at the top of slope; minor cracks on road surface; minor track displacement	Open, reduced speed
DS2	Deep slide or slump of embankment; medium cracks on road surface and/or settlement; medium track displacement	Partially open during repairs (roadway). Closed during repairs (railway)
DS3	Extensive slump and slide of embankment; extensive cracks on road surface and/or settlement; extensive tracks displacement	Partially open during repair or closed during reconstruction works (roadway). Closed (railway)
Cuts (road/track in)		
DS1	Surface slide; minor cracks on road surface; minor displacement of the tracks	Open, reduced speed
DS2	Deep slide or slump; medium cracks on road surface and/or settlement; medium displacement of the tracks	Partially open during repairs (roadway). Closed during repairs (railway)
DS3	Extensive slump and slide; extensive cracks on road surface and/or settlement; extensive displacement of the tracks	Partially open or closed during repairs/ reconstruction (roadway). Closed (railway)

depending on the method and the element at risk. Most common intensity measure types (IMTs) are peak ground acceleration (PGA) when ground shaking is the cause of damage or permanent ground deformation (PGD) in case of ground failure. A brief review of existing fragility functions for roadway and railway elements is given in the following. The corresponding review of methods and IMTs for bridges is provided in Chap. 9.

Table 10.4 Description of damage states for roadway/railway components in SYNER-G (cont.)

	Description	Serviceability
Bridge abutments		
DS1	Minor settlement of approach fill (roadway: 2–8 m; railway: 1–5 cm)	Open. Reduced speeds or partially closed during repair
DS2	Moderate settlement of approach fill (roadway: 8–22 cm; railway: 5–10 cm)	Closed or partially closed during repair works (roadway). Closed (railway)
DS3	Extensive settlement of approach fill (roadway: >22 cm; railway: >10 cm)	Closed during repair/reconstruction works
Slopes (road/track on or running along)		
DS1	Surface slide at top of slope; minor cracks on road surface; minor track displacement	Open, reduced speed
DS2	Deep slide or slump; medium cracks on road surface and/or settlement; medium displacement of the track	Partially open or closed during repairs (roadway). Closed during repairs (railway)
DS3	Extensive slump and slide; extensive cracks on road surface; extensive displacement of the track	Closed during repairs/reconstruction
Road pavements		
DS1	Slight cracking/offset of pavement surface	Open. Reduced speeds or partially closed during repair works
DS2	Localized moderate cracking/offset of pavement	Closed during repairs (few days)
DS3	Major cracking/offset of pavement and subsurface soil	Closed during repairs (few days to weeks)
Tracks		
DS1	Minor (localized) derailment due to slight differential settlement of embankment or ground offset	Operational after inspection or short repairs
DS2	Considerable derailment due to differential settlement or ground offset	Closed to traffic. Local repairs or replacement of tracks is required
DS3	Major differential settlement of the ground resulting in potential derailment over extended length	Closed to traffic. Replacement of track's segments is required. Duration of closure depends on length of damaged lines

10.4.1 Tunnels

Until recently, the vulnerability assessment of tunnels has mainly been based on expert judgment (ATC13 1985; NIBS 2004) or empirical fragility curves (ALA 2001; Corigliano 2007) derived from actual damage in past earthquakes. In the study by Corigliano (2007) all deep tunnels are classified in one category and the proposed fragility curves are given as functions of peak ground velocity (PGV) for none/slight and moderate damage. The HAZUS approach (NIBS 2004) is based on judgment and limited empirical data set by Dowding and Rozen (1978) and Owen and Scholl (1981), providing fragility curves both for ground shaking (PGA) and ground failure (PGD). In ALA approach tunnels are distinguished based on

Table 10.5 Fragility function parameters for tunnels (ALA 2001)

Typology	Damage state	μ (g)	β
Rock tunnels with poor-to-average construction and conditions	Minor/slight	0.35	0.4
	Moderate	0.55	0.4
	Heavy	1.10	0.5
Rock tunnels with good construction and conditions	Minor/slight	0.61	0.4
	Moderate	0.82	0.4
	Heavy	NA	–
Alluvial (soil) and cut and cover tunnels with poor to average construction	Minor/slight	0.30	0.4
	Moderate	0.45	0.4
	Heavy	0.95	0.5
Alluvial (soil) and cut and cover tunnels with good construction	Minor/slight	0.50	0.4
	Moderate	0.70	0.4
	Heavy	NA	–

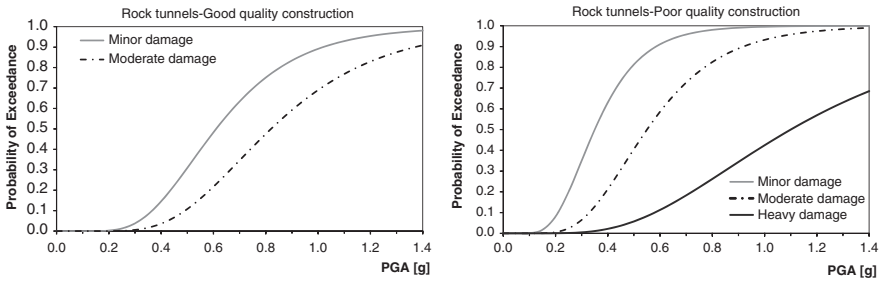

Fig. 10.1 Fragility curves for tunnels in rock (ALA 2001)

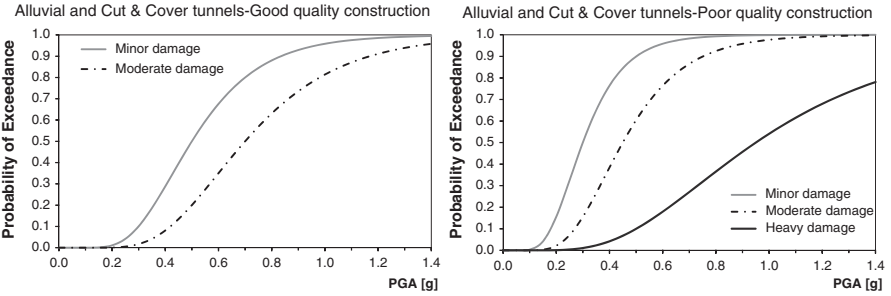

Fig. 10.2 Fragility curves for tunnels in alluvial and cut and cover (ALA 2001)

geology conditions and quality of construction. Fragility curves are given as functions of PGA for three damage states. The parameters of the lognormal distribution in terms of medians (μ) and standard deviations (β) are given in Table 10.5. The fragility curves are illustrated in Figs. 10.1 and 10.2.

A limited number of numerical approaches for the fragility analysis of tunnels are available. Salmon et al. (2003) presented analytical fragility curves for bored and cut and cover tunnels of the BART project as a function of PGA (ground shaking) and PGD (fault offset). These curves are site specific and their use is limited to the BART project. In the framework of LessLoss (2007) project, Argyroudis and Pitilakis (2007) proposed a preliminary set of analytical fragility curves for circular (bored) tunnels due to permanent ground deformation (PGD).

In the SYNER-G project new analytical fragility curves were proposed for shallow/metro tunnels in alluvial soil for different conditions (circular/bored and rectangular/cut and cover) due to ground shaking (see Sect. 10.5.2). In case of permanent ground deformations the generic fragility curves by HAZUS methodology can be applied as a first approximation, however further research is needed on this topic.

10.4.2 Embankments, Cuts and Slopes

Maruyama et al. (2010) proposed empirical curves for expressway embankments based on damage datasets from recent earthquakes in Japan. The fragility functions relate the number of damage incidents per km of expressway to PGV. Lagaros et al. (2009) proposed analytical fragility curves for embankments based on pseudostatic slope stability analyses, through Monte Carlo simulation method and neural network metamodels. The damage states are defined based on factor of safety, while the main purpose of the study is to highlight the computational effort of different approaches. The ATC-13 (1985) approach provided fragility curves for six slope classes, which are defined by the critical acceleration based on expert opinion as a function of earthquake intensity MMI. Finally, an expert judgment approach to determining the physical vulnerability of roads for a given debris flow volume is proposed by Winter et al. (2013). Damage probabilities were assessed based on a detailed questionnaire to experts.

In the framework of SYNER-G, new analytical fragility curves have been developed as functions of PGA, for embankments and cuts of different heights and soil conditions (see Sect. 10.5.4). In case of roads and tracks on slopes new fragility curves were proposed following the approach adopted by Pitilakis et al. (2010). In particular, the threshold PGD values of Table 10.2 were used for the estimation of the corresponding PGA medians based on the model by Bray and Travasarou (2007). The slopes were classified through the yield acceleration coefficient k_y (Table 10.6, Figs. 10.3 and 10.4).

10.4.3 Retaining Walls and Approach Fills

The ATC-13 (1985) approach provided damage probability matrices for retaining walls for different levels of MMI based on expert opinion. Salmon et al. (2003)

Table 10.6 Fragility function parameters for roads and tracks on slopes

		$k_y = 0.05$		$k_y = 0.1$		$k_y = 0.2$		$k_y = 0.3$	
Typology	Damage state	μ (g)	β	μ (g)	β	μ (g)	β	μ (g)	β
Road on or running along slope	Minor	0.14	0.40	0.25	0.35	0.45	0.35	0.64	0.30
	Moderate	0.22	0.40	0.40	0.35	0.71	0.35	1.00	0.30
	Extensive/ complete	0.37	0.40	0.64	0.35	1.11	0.35	1.55	0.30
Track on or running along slope	Minor	0.11	0.60	0.20	0.60	0.37	0.60	0.52	0.60
	Moderate	0.17	0.60	0.30	0.60	0.54	0.60	0.78	0.60
	Extensive/ complete	0.26	0.60	0.45	0.60	0.80	0.60	1.13	0.60

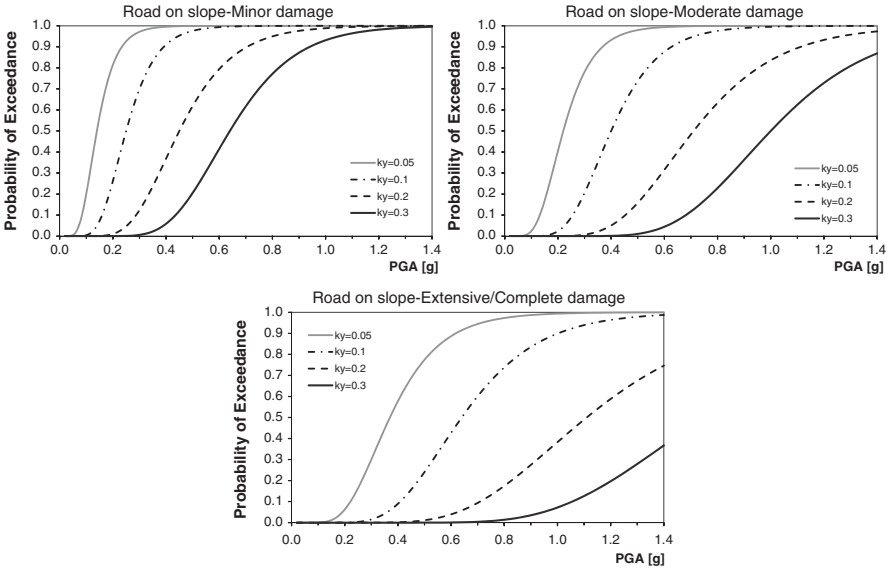

Fig. 10.3 Fragility curves at various damage states and different yield coefficients (k_y) for roads on slope (Kaynia 2013)

reported analytical fragility curves for retaining walls of the BART project as functions of PGA. However, the typological characteristics of the walls are not given; therefore, the fragility functions are considered as project specific. REDARS methodology (Werner et al. 2006) provides threshold values of PGD for different damage levels, related to the repair cost, duration and traffic states of bridge approach fills and road pavements for California highways. They are based on expert judgment and are not given in the form of fragility functions.

In the framework of SYNER-G, new analytical curves for bridge abutments on shallow foundations are proposed as functions of PGA for different soil conditions and abutment heights (see Sect. 10.5.3).

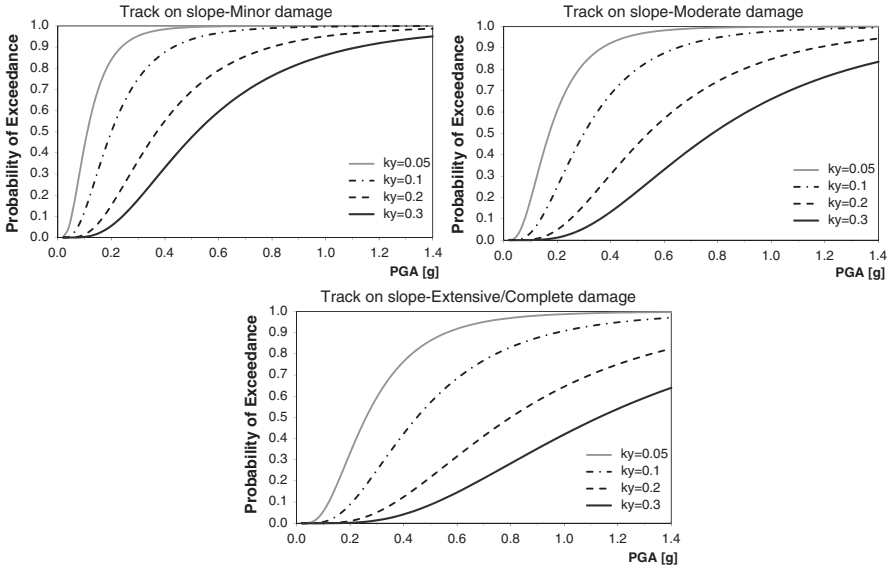

Fig. 10.4 Fragility curves at various damage states and different yield coefficients (k_y) for tracks on slope (Kaynia 2013)

Table 10.7 Fragility function parameters for road pavements

Typology	Damage state	μ (m)	β
2 traffic lanes (Urban roads)	Minor	0.15	0.7
	Moderate	0.30	0.7
	Extensive/complete	0.60	0.7
≥4 traffic lanes (Major roads)	Minor	0.30	0.7
	Moderate	0.60	0.7
	Extensive/complete	1.50	0.7

10.4.4 Road Pavements and Railway Tracks

HAZUS methodology (NIBS 2004) includes fragility curves for major and urban roads as functions of PGD (fault offset, liquefaction, landslide) (Table 10.7, Fig. 10.5). These curves have been validated in SYNER-G using observed damage in road pavements during past earthquakes in Greece. The results indicated a good agreement between the estimated and observed damages (Kaynia et al. 2011). The aforementioned functions, which are based on expert judgment, are also suggested for railway tracks in HAZUS methodology. However, the tolerance of railways to damage is lower and therefore these functions are generally considered unsatisfactory. In SYNER-G, new PGD thresholds to different damage states have been proposed for railway tracks. These values are applied for the derivation of fragility

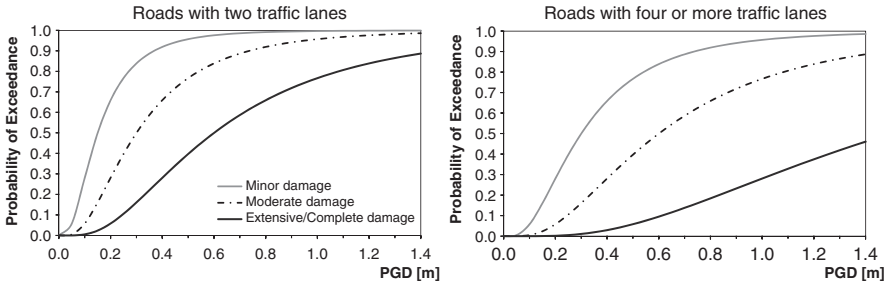

Fig. 10.5 Fragility curves for road pavements subjected to ground failure (NIBS 2004)

Table 10.8 Fragility function parameters for railway tracks

Damage state	μ (m)	β
Minor	0.03	0.70
Moderate	0.08	0.70
Extensive/complete	0.20	0.70

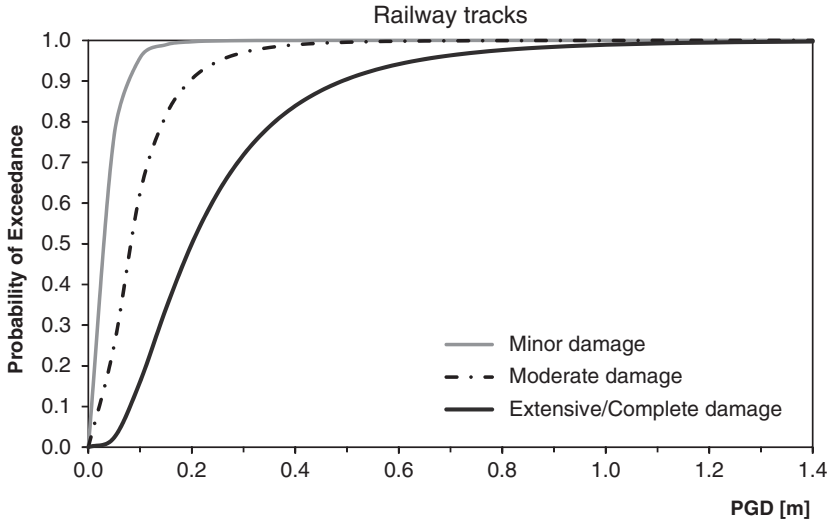

Fig. 10.6 Fragility curves for railway tracks subjected to ground failure (Kaynia 2013)

functions for railway tracks subjected to ground failure (Table 10.8 and Fig. 10.6). As a first approximation, these fragility curves can be applied for road pavements and railway tracks subjected to permanent ground deformations (e.g. by liquefaction, fault crossing, and landslide) independently of their location on embankment, cut, slope or flat ground. However, further investigation is needed on this subject to study the effects of soil and topography conditions as well as the peculiarities of each component.

10.5 New Analytical Fragility Curves for Ground Shaking

The existing fragility curves for roadway and railway components are mainly based on empirical or expert judgment approaches both for ground shaking and ground failure. In many cases they do not cover adequately the typologies, soil conditions and ground motion characteristics. In the framework of SYNER-G, new analytical fragility curves were developed for tunnels in alluvial soil and roadway/railway bridge abutments, embankments and cuts subjected to ground shaking. In the following, a brief description of the general procedure for the derivation of the analytical fragility curves is given. Next, the main modeling issues are described, and finally, the parameters of the new fragility curves are summarized for each component. The response of roadway and railway infrastructures due to earthquake-induced geohazards such as landslides and ground failure needs further research in order to develop adequate fragility curves for all elements.

10.5.1 Key Modeling Issues and Treatment of Uncertainties

The general procedure followed in SYNER-G for the derivation of analytical fragility curves for roadway and railway elements is described by Argyroudis et al. (2013b). The effects of soil conditions and ground motion characteristics on the element's response are taken into account by using different typical soil profiles and seismic input motions. The response of the free field soil profiles is calculated through 1D numerical analysis with increasing ground motion amplitude at the seismic basement ($V_s > 800$ m/s). 2D dynamic or quasi-static analysis is used for the non-linear seismic response of the soil-structure. This approach allows the evaluation of fragility curves considering the distinctive features of the element geometries, the input motion characteristics and the soil properties.

The level of damage is described by a damage index expressing the exceedance of certain limit states (Table 10.2), and the fragility curves are estimated based on the evolution of damage index with increasing earthquake acceleration, considering the associated uncertainties. An example is given in Fig. 10.7 where the different points indicate the results of the analyses in terms of damage index for different levels of earthquake shaking. The solid line is produced based on a regression analysis in which the median threshold value of the intensity measure to cause the i_{th} damage state is estimated based on the definition of damage index (mean values in Table 10.2). The fragility curve is described by a lognormal distribution function which is defined by two parameters, the median threshold value of the earthquake intensity measure type IMT (e.g. PGA) required to cause the i_{th} damage state and the total standard deviation, β_{tot}, which describes the total variability associated with each fragility curve. Three primary sources of uncertainty are usually considered (NIBS 2004), namely the definition of damage states, β_{DS}, the response and

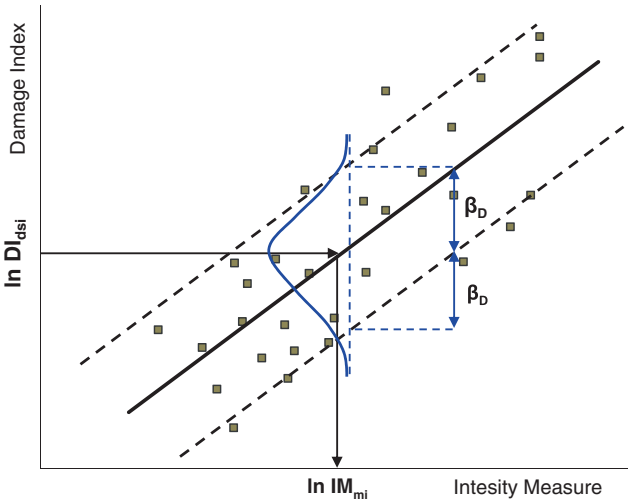

Fig. 10.7 Example of evolution of damage with earthquake intensity measure and definition of threshold median value for the damage state i, and definition of standard deviation (β_D) due to input motion (demand)

resistance (capacity) of the element, β_C, and the earthquake input motion (demand), β_D. The total uncertainty is estimated as the root of the sum of the squares of the component dispersions assuming that they are stochastically independent lognormal-distributed random variables.

In the absence of a more rigorous estimation, the uncertainty parameters can be obtained from the literature (e.g. NIBS 2004). However, the uncertainty associated with seismic demand (β_D), is described by the variability in response due to the variability of ground motion in numerical simulations.

10.5.2 Shallow Tunnels

Numerical fragility curves for shallow metro (urban) tunnels in alluvial deposits were developed by considering structural parameters, local soil conditions and – input ground motion characteristics. In particular, the transverse seismic response of the tunnel due to upward travelling shear waves was evaluated under quasi-static conditions by applying on the tunnel cross-section and the surrounding soil the free field seismic ground deformations, which were calculated independently though 1D equivalent linear analysis. Different tunnel cross-sections, input motions and soil profiles were employed. By defining the damage levels according to the exceedance of strength capacity of the most critical sections of the tunnel, the fragility curves were constructed as functions of the level and the type of seismic excitation. The comparison between the new fragility curves and the existing empirical ones has highlighted the important role of the local soil conditions (Argyroudis and Pitilakis 2012).

Table 10.9 Definition of damage states for tunnel lining

Damage state (DS)	Range of damage index (DI)	Central value of damage index
DS1. Minor/slight	$1.0 < M/M_{Rd} \leq 1.5$	1.25
DS2. Moderate	$1.5 < M/M_{Rd} \leq 2.5$	2.00
DS3. Extensive	$2.5 < M/M_{Rd} \leq 3.5$	3.00
DS4. Collapse	$M/M_{Rd} > 3.5$	–

10.5.2.1 Damage States

The damage states of existing empirical fragility curves are based on a qualitative damage description from past earthquakes. In the present study the damage index (DI) is defined as the ratio between the bending moment demand, M, and the capacity bending moment of the tunnel cross-section, M_{Rd}. This definition is compatible with the use of displacements, according to the equal displacement approximation. Based on previous experience of damages in shallow tunnels and applying engineering judgment, four damage states were considered due to ground shaking. They refer to minor, moderate, extensive and complete damage of the tunnel lining as described in Table 10.9.

10.5.2.2 Model Parameters

Two typical tunnel sections were considered, a circular (bored) tunnel with a 10 m diameter and a rectangular (cut and cover) one-barrel frame with dimensions 16 × 10 m. The lining of the circular tunnel is composed of 0.50 m thick precast concrete segments, while the rectangular tunnel has 0.9 m thick concrete walls, 1.2 m thick roof slab and 1.4 m thick base slab. The circular and rectangular tunnel was placed at 10 m and 3.5 m depths, respectively. Fourteen ideal soil deposits were considered corresponding to ground types B, C and D of Eurocode 8 (2004), ranged according to the shear wave velocity, V_{s30}, values. Three different soil thicknesses equal to 30, 60 and 120 m were assumed, and typical values of the different soil parameters were selected for each soil layer.

Records on rock sites from different earthquakes were selected such that their average response spectrum matched fairly well the response spectrum of Eurocode 8. These earthquake records were scaled from 0.1 to 0.7 g and used as input motion in 1D ground response analyses. The estimated seismic ground deformations were applied on the boundaries of the soil-tunnel model in order to calculate the induced stresses in the tunnel as a function of PGA and finally to estimate the fragilty curves (Argyroudis and Pitilakis 2012).

10.5.2.3 1D and 2D Numerical Analyses

The imposed quasi-static seismic ground displacements were computed using 1D equivalent linear approach with the code EERA (Bardet et al. 2000). The variations

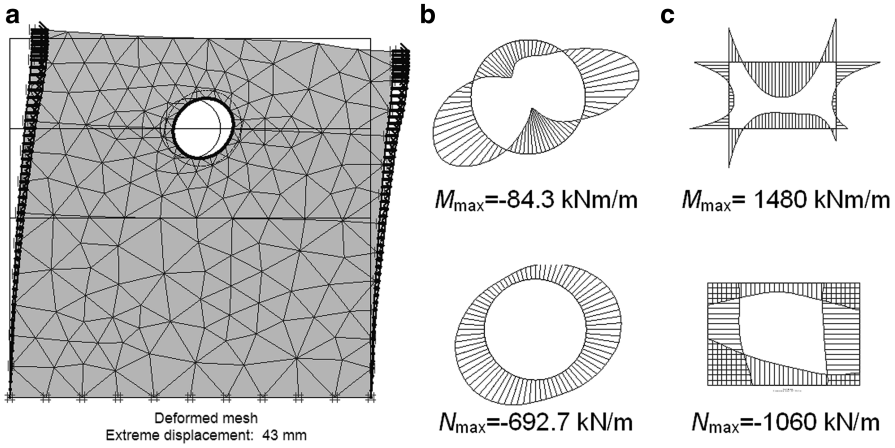

Fig. 10.8 Example of 2D analysis of tunnel: deformed mesh (**a**), total moment and axial forces of the circular (**b**) and rectangular (**c**) tunnel lining (soil profile: type B, depth: 60 m; input motion: Kypseli, 0.3 g)

of shear modulus G/G_o (where G_o is the initial shear modulus) and damping ratio with the shear strain level γ were defined according to the available data in the literature as a function of plasticity index and effective stress. The PGA value computed on the surface of each soil profile was selected as the representative IMT in the fragility curves.

A plane strain ground model with the tunnel cross-section was analysed using the finite element code PLAXIS 2D (Plaxis 1998). Prior to the application of the imposed displacement, a set of initial static analyses was performed to properly model the initial static conditions, the excavation of the tunnel and the construction of the lining. The behaviour of the tunnel lining is assumed to be linear elastic, while the soil was characterized by a Mohr-Coulomb yield criterion in all the stages of the analysis. Figure 10.8 shows a representative example of the tunnel response after imposing the shear ground displacements.

10.5.2.4 Derivation of Fragility Curves

For the derivation of fragility curves the general procedure described in Sect. 10.5.1 is followed. In particular, the median PGA value for each damage state is based on the relationship between the computed damage indices versus PGA on the free field and the definitions of damage states given in Table 10.9. A value equal to 0.4 was assigned for the uncertainty associated with the definition of damage states, β_{DS}, following the approach of HAZUS (NIBS 2004) for buildings; the uncertainty due to the capacity, β_C, is assigned equal to 0.3 according to analyses for bored tunnels of BART system (Salmon et al. 2003). The last source of uncertainty, associated with seismic demand, is described by the standard deviation of the damage indices

Table 10.10 Parameters of numerical fragility curves for urban tunnels in different ground types

		Ground type B		Ground type C		Ground type D	
Typology	Damage state	μ (g)	β	μ (g)	β	μ (g)	β
Circular urban tunnels	Minor	1.24	0.55	0.55	0.70	0.47	0.75
	Moderate	1.51	0.55	0.82	0.70	0.66	0.75
	Extensive	1.74	0.55	1.05	0.70	0.83	0.75
Rectangular urban tunnels	Minor	0.75	0.55	0.38	0.55	0.36	0.55
	Moderate	1.28	0.55	0.76	0.55	0.73	0.55
	Extensive	1.73	0.55	1.08	0.55	1.05	0.55

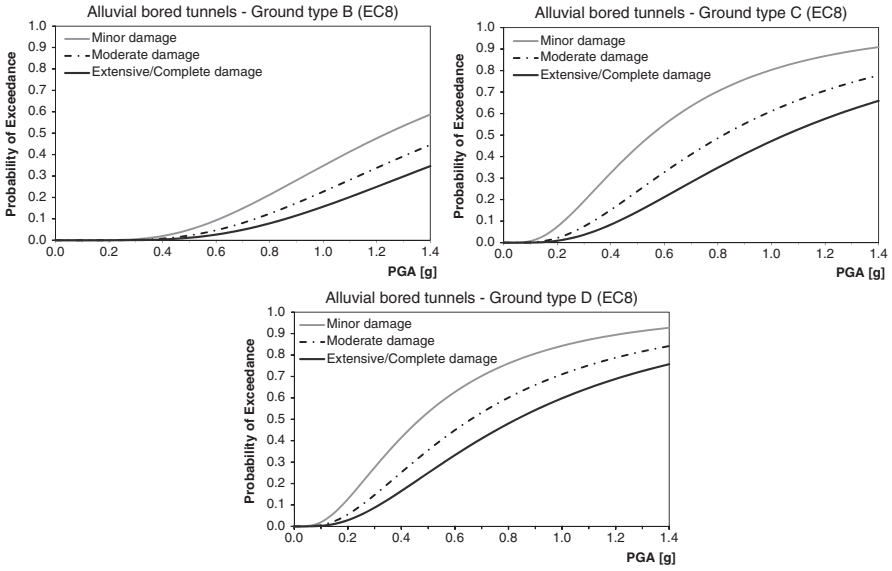

Fig. 10.9 Fragility curves for circular (bored) metro/urban tunnel section

that have been calculated for the different input motions at each level of PGA. The parameters of the lognormal distribution in terms of medians and standard deviations are given in Table 10.10 and the corresponding fragility curves are shown in Figs. 10.9 and 10.10.

10.5.3 Bridge Abutments

New analytical fragility curves for bridge abutment-approach fill system were developed in SYNER-G (Argyroudis et al. 2013b). The response of the abutment was evaluated from dynamic analyses with an increasing level of seismic shaking

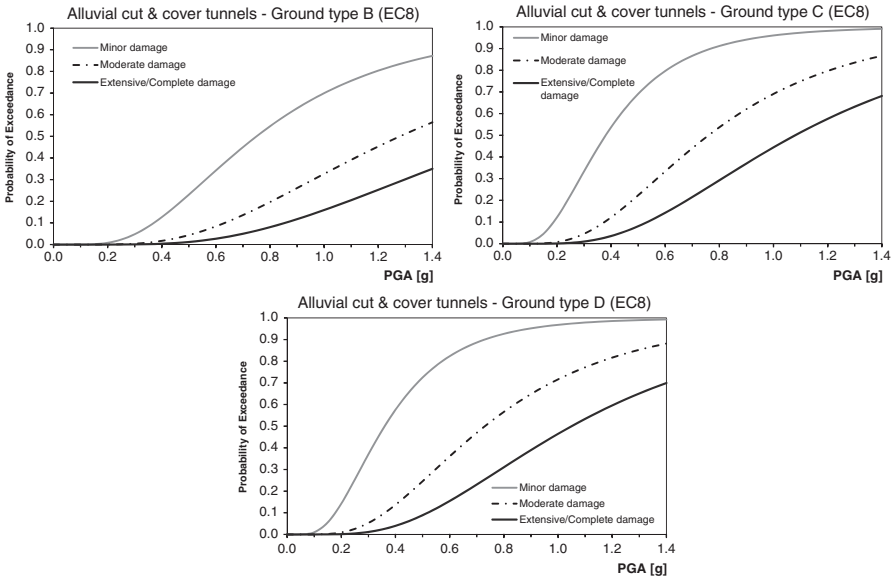

Fig. 10.10 Fragility curves for rectangular (cut and cover) metro/urban tunnel section

following the general procedure briefly described in Sect. 10.5.1. In particular, the soil behaviour was simulated through a 2D fully coupled FE model using an elasto-plastic criterion. A calibration procedure was followed in order to account for the dependency of both stiffness and damping on the ground strain level. The effect of soil conditions and ground motion characteristics in the global soil and structure response was taken into account by considering different typical soil profiles and seismic input motions. The performance of the wall, and thus the level of damage, was described by the settlement observed on the backfill.

10.5.3.1 Model Parameters

Representative and simplified bridge abutment geometries with two different heights equal to 6.0 and 7.5 m were modeled as cantilever retaining wall (Fig. 10.11). The bridge deck is supported by the abutment on bearings while its total load is simulated by a vertical load equal to 200 kN.

Five real earthquake records were selected such that their average response spectrum matched fairly well the response spectrum of Eurocode 8 on rock. The earthquake records were from: Kocaeli 1999, Gebze; Hector Mine 1999, Hector; Parnitha 1999, Kypseli; Loma Prieta 1989, Diamond Height; Umbria Marche 1998, Gubbio-Piana. The time histories of these records were scaled from 0.1 to 0.5 g and were applied at the base of the soil model in order to calculate the response of the backfill-abutment due to an increasing level of seismic intensity.

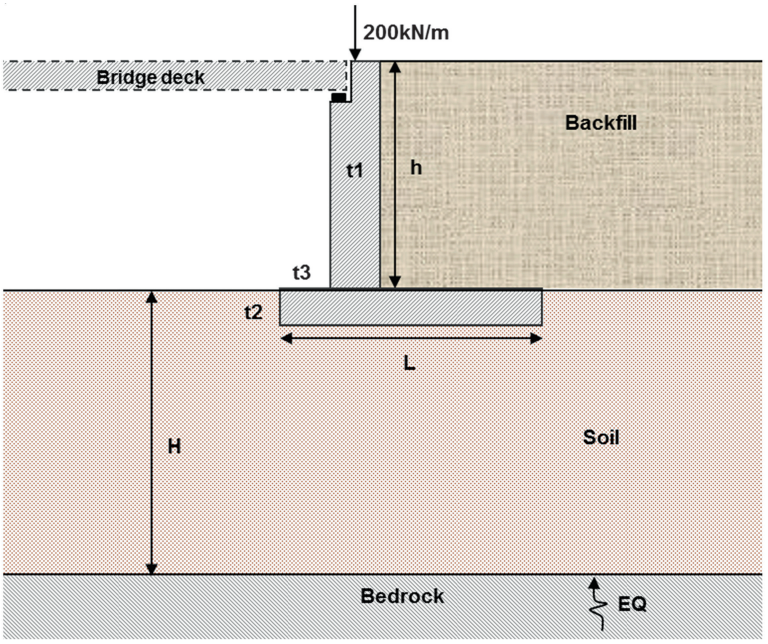

L (m)	h (m)	H (m)	t_1 (m)	t_2 (m)	t_3 (m)	γ_c^* (kN/m^3)	E_c (kN/m^2)
5.5	6.0	50.0	1.0	1.0	1.5	24.0	3.5E+07
6.5	7.5	50.0	1.0	1.0	2.5		

* γ_c: unit weight of concrete

Fig. 10.11 Properties of soil/backfill/abutment under study

Two ideal soil deposits of 50 m, corresponding to ground types C and D in Eurocode 8 were considered. Typical values of the soil parameters were selected for both the soil profile and the backfill. The 1D ground response analyses were performed using 1D equivalent linear approach with the code EERA (Bardet et al. 2000). A calibration procedure was followed in order to account for the dependency of both stiffness and damping on the strain level. Details for the model parameters are given in Argyroudis et al. (2013b).

The numerical simulations were performed using the finite element code PLAXIS 2D (Plaxis 2011). A close-up of the mesh employed in the study is shown in Fig. 10.12. All the analyses were carried out by performing a set of initial static stages to simulate the initial weight, the installation of the abutment and the backfill, followed by the dynamic analyses.

10.5.3.2 Derivation of Fragility Curves

The derivation of the fragility curves from the results of the numerical simulations was similar to that presented in Sect. 10.5.1. The threshold PGD values of Table 10.2

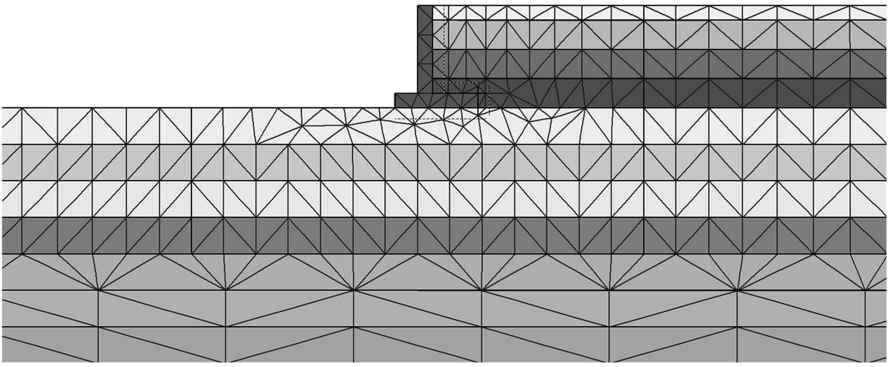

Fig. 10.12 Finite element mesh used in the analyses of bridge abutment

Table 10.11 Parameters of numerical fragility curves for roadway and railway abutments in different ground types

		Ground type C				Ground type D			
		h = 6 m		h = 7.5 m		h = 6 m		h = 7.5 m	
Typology	Damage state	μ (g)	β	μ (g)	β	μ (g)	β	μ (g)	β
Roadway	Minor	0.38	0.70	0.26	0.70	0.20	0.90	0.18	0.90
	Moderate	0.64	0.70	0.52	0.70	0.45	0.90	0.39	0.90
	Extensive/ complete	1.02	0.70	0.97	0.70	0.93	0.90	0.78	0.90
Railway	Minor	0.29	0.70	0.19	0.70	0.14	0.90	0.12	0.90
	Moderate	0.46	0.70	0.34	0.70	0.27	0.90	0.23	0.90
	Extensive/ complete	0.73	0.70	0.63	0.70	0.56	0.90	0.47	0.90

were used for the estimation of median PGA values for each damage state through the corresponding diagrams that describe the evolution of damage with PGA. The parameters of the fragility curves are presented in Table 10.11. The fragility curves for complete damage are derived based on extrapolation of the available computed results. Damage records from a recent earthquake in Japan were used to validate the proposed fragility curves (Argyroudis et al. 2013b) (Figs. 10.13 and 10.14).

10.5.4 Embankments and Cuts

New analytical fragility curves for embankments and cuts were developed in SYNER-G. The response of the system was evaluated based on dynamic analyses with increasing level of seismic intensity following the procedure described in Sect. 10.5.1. Further developments for the seismic performance and fragility assessment of roadway embankments are provided in Argyroudis and Kaynia (2013).

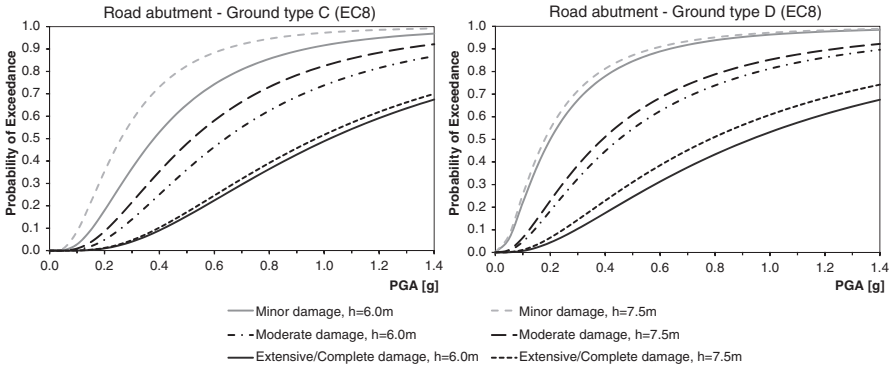

Fig. 10.13 Fragility curves for road abutments, ground type C (*left*) and D (*right*)

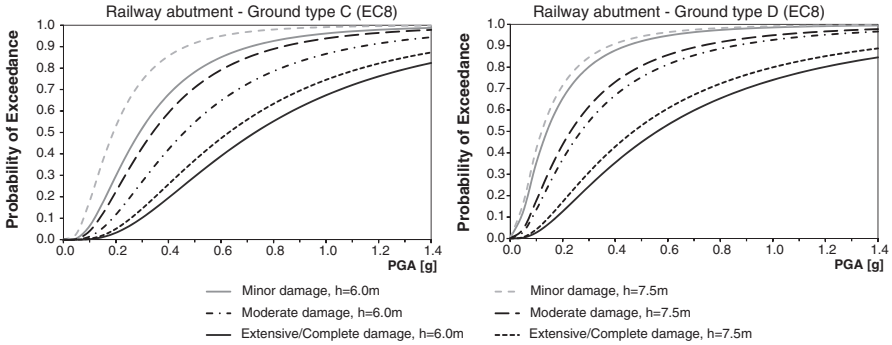

Fig. 10.14 Fragility curves for railway abutments, ground type C (*left*) and D (*right*)

10.5.4.1 Model Parameters

Representative geometries are considered with heights equal to 2.0 and 4.0 m for the embankment and 4.0 and 6.0 m for the cut; preliminary analyses indicated that typical engineered cuttings shallower than 4.0 m are practically not vulnerable to earthquake shaking. The top width of the embankment and the bottom width of the cut is 20 m. The same earthquake records used in the analysis of bridge abutments were applied in these analyses. The earthquake time histories were scaled from 0.1 to 0.7 g and the response of embankment/cut is calculated as a function of PGA on the ground surface.

Two ideal soil deposits of 50 m corresponding to ground types C and D with shear wave velocity (V_{s30}) in the range defined by Eurocode 8 were considered

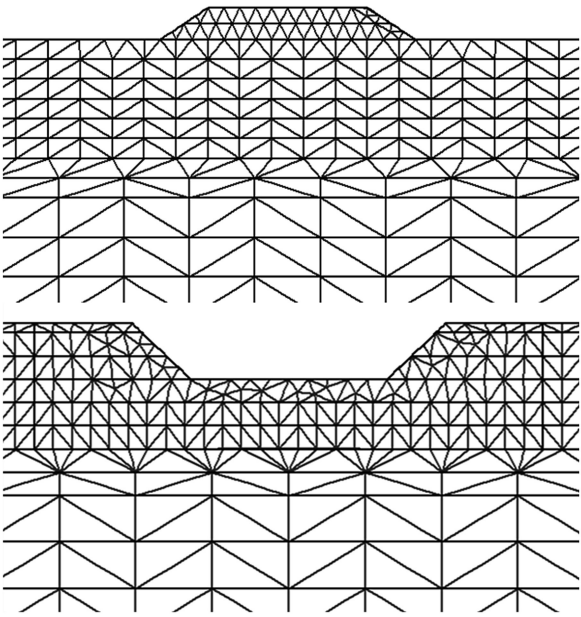

Fig. 10.15 Finite element mesh used in the analyses of embankment (*up*) and cut (*down*)

similar to those used in case of abutments. Typical values of soil properties are selected for the embankment. The numerical simulations are performed with the finite element code PLAXIS 2D (Plaxis 2011). A close-up of the models is shown in Fig. 10.15.

10.5.4.2 Derivation of Fragility Curves

The derivation of fragility curves was based on a diagram of the computed damage indices in terms of average total permanent ground deformation, PGD, on embankment or cut surface, versus PGA on the ground surface as illustrated in Fig. 10.8. A relationship was established by linear regression analysis relating PGD to PGA on the ground surface in the free field. The median threshold value of PGA was then obtained for each damage state based on the aforementioned relationship and the definitions given in Table 10.2. The lognormal standard deviation, β_{tot}, which describes the total variability associated with each fragility curve, was estimated as described in Sect. 10.5.1. The estimated parameters of the fragility curves are presented in Tables 10.12 and 10.13. The derived curves are plotted in Figs. 10.16, 10.17, 10.18, and 10.19 for roadway and railway elements. For simplicity and in order to avoid intersection of the different fragility curves in case of the embankments, the plots are given for an average lognormal standard deviation equal to 0.9 for ground type C and 0.8 for ground type D.

Table 10.12 Parameters of numerical fragility curves for roadway and railway embankments in different ground types

		Ground type C				Ground type D			
		h = 2 m		h = 4 m		h = 2 m		h = 4 m	
Typology	Damage state	μ (g)	β	μ (g)	β	μ (g)	β	μ (g)	β
Roadway	Minor	0.65	1.00	0.51	0.90	0.47	0.90	0.31	0.70
	Moderate	1.04	1.00	0.88	0.90	0.66	0.90	0.48	0.70
	Extensive/ complete	1.57	1.00	1.42	0.90	0.89	0.90	0.72	0.70
Railway	Minor	0.52	1.00	0.36	0.90	0.40	0.90	0.25	0.70
	Moderate	0.77	1.00	0.57	0.90	0.53	0.90	0.37	0.70
	Extensive/ complete	1.17	1.00	0.91	0.90	0.72	0.90	0.54	0.70

Table 10.13 Parameters of numerical fragility curves for roadway and railway cuts in different ground types

		Ground type C		Ground type D			
		h = 6 m		h = 4 m		h = 6 m	
Typology	Damage state	μ (g)	β	μ (g)	β	μ (g)	β
Roadway	Minor	0.59	1.00	0.44	1.00	0.38	1.00
	Moderate	1.09	1.00	0.92	1.00	0.77	1.00
	Extensive/complete	1.90	1.00	1.77	1.00	1.46	1.00
Railway	Minor	0.44	1.00	0.31	1.00	0.27	1.00
	Moderate	0.74	1.00	0.58	1.00	0.49	1.00
	Extensive/complete	1.29	1.00	1.11	1.00	0.93	1.00

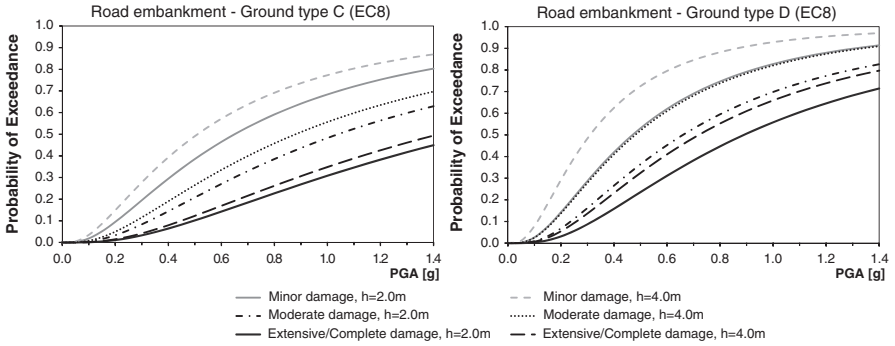

Fig. 10.16 Fragility curves for road embankments in ground type C (*left*) and D (*right*)

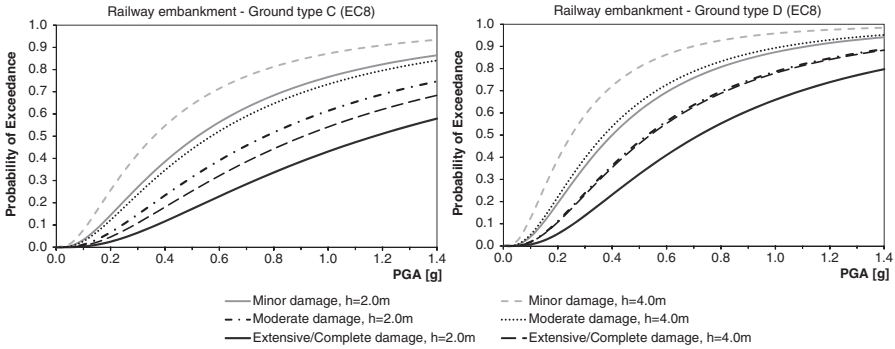

Fig. 10.17 Fragility curves for railway embankments in ground type C (*left*) and D (*right*)

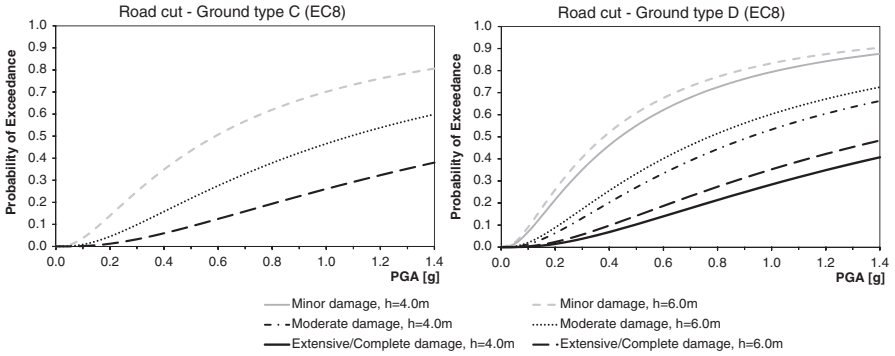

Fig. 10.18 Fragility curves for road cuts in ground type C (*left*) and D (*right*)

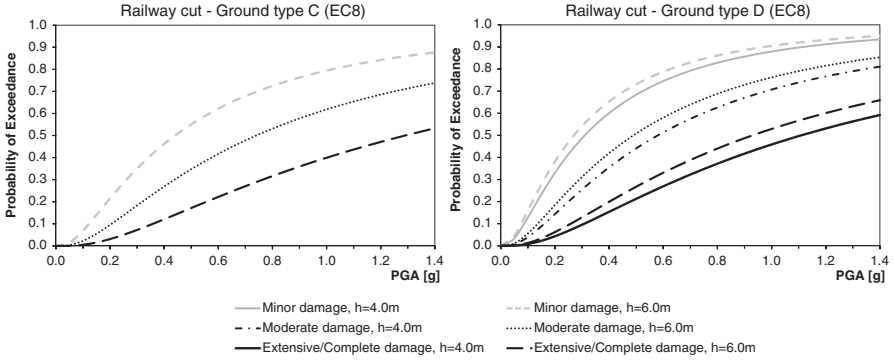

Fig. 10.19 Fragility curves for railway cuts in ground type C (*left*) and D (*right*)

10.6 Conclusions and Recommendations

A brief review of available fragility curves and their evaluation methods were presented for roadway and railway elements. The main typological features and damage states definitions were summarized. Tunnels, embankments, road pavements, slopes, cuts, railway tracks and bridge abutments are earth structures and are thus directly affected by the local soil conditions. In the framework of SYNER-G new analytical fragility curves are proposed for urban tunnels in alluvial soil, embankments and cuts, and bridge abutments for roadways and railways subjected to ground shaking. The effects of soil type and ground motion characteristics were taken into account by using typical soil profiles and seismic input motions. The response of the soil profiles was calculated through 1D equivalent linear analyses, while the non-linear response of the soil-structure system was calculated through 2D quasi-static or dynamic analyses. The available fragility curves for ground failure are limited; therefore, the case of the vulnerability of roadway and railway components due to liquefaction, landslide, rock-falls and fault rupture should further be investigated.

The proposed fragility functions for roadway and railway elements based on past and new developments presented herein are outlined in Table 10.14. Fragility functions for tunnels, embankments, cuts, slopes and bridge abutments correspond to ground shaking intensity in terms of PGA on the surface, while those for road

Table 10.14 Summary of proposed fragility functions for road/rail elements under ground shaking and ground failure

Element	Methodology	Classification	IMT
Urban tunnels in alluvial	SYNER-G	Ground type: B, C, D (EC8)	PGA
	Numerical analysis	Circular (bored)	
		Rectangular (cut and cover)	
Other tunnels	ALA (2001)	Rock or alluvial/cut and cover	PGA
	Empirical	Good or poor to average construction and conditions	
Embankment (road/track on)	SYNER-G	Ground type: C, D (EC8)	PGA
	Numerical analysis	Height: 2.0, 4.0 m	
Cuts (road/track in)	SYNER-G	Ground type: C, D (EC8)	PGA
	Numerical analysis	Height: 2.0, 4.0 m	
Slopes (road/track on or running along)	SAFELAND (Pitilakis et al. 2010)	Yield coefficient, k_y	PGA
	Expert judgment/ empirical	Earthquake magnitude	
Bridge abutments	SYNER-G	Ground type: C, D (EC8)	PGA
	Numerical analysis	Height: 6.0, 7.5 m	
Road pavements (ground failure)	HAZUS	2 traffic lanes (Urban roads)	PGD
	Expert judgment	>=4 traffic lanes (Major roads)	
Railway tracks (ground failure)	SYNER-G	All	PGD
	Expert judgment		

Table 10.15 General proposal for functionality of roadway elements

Damage state	Bridge	Tunnel	Embankment	Cut	Abutment	Slope	Road pavement
Minor	o	o	o	o	o	o	o
Moderate	p/o	c	p/o	p/o	p/o	p/o	p/o
Extensive/complete	c	c	c	c	c	c	

o open, *p*/*o* partially open (not applied when the roadway has one traffic lane), *c* closed

Table 10.16 Definition of functionality of roadway elements in relation to open traffic lanes before and after the earthquake

	Number of lanes each way open to traffic after EQ			
Damage state	Pre-EQ lanes = 1	Pre-EQ lanes = 2	Pre-EQ lanes = 3	Pre-EQ lanes = 4
Minor	1	2	3	4
Moderate	0	1	2	3
Extensive/complete	0	0	0	1

Table 10.17 General proposal for functionality of railway elements

Damage State	Bridge	Tunnel	Embankment	Cut	Abutment	Slope	Tracks
Minor	sr	sr	sr	sr	sr	sr	sr
Moderate	c	c	c	c	c	c	c
Extensive/complete	c	c	c	c	c	c	c

sr speed restriction, *c* closed

pavements and railway tracks are referred to ground failure in terms of permanent ground displacements.

The performance of a roadway system, at the component level, can be described through the reduction of functional traffic lanes due to damage, which is directly connected to the reduction of speed and capacity of the system. The general scheme in Table 10.15 can be used as a basis to estimate the functionality of roadway components due to different damage levels. Three levels of functionality are described, namely, open, partially open, and closed. The partially open state is defined based on the number of lanes of the undamaged road (Table 10.16), which is based on the REDARS approach (Werner et al. 2006). It is noted that the partially open state is not applied when the roadway has a single traffic lane. A general scheme for the functionality of railway elements is given in Table 10.17 where three levels of functionality are described (fully functional, functional but with speed restrictions, not functional/closed).

Acknowledgments The research leading to these results received funding from the European Community's 7th Framework Programme (FP7/2007-2013) under grant agreement n° 244061

References

American Lifelines Alliance (ALA) (2001) Seismic fragility formulations for water systems, Part 1– Guideline, ASCE-FEMA, Reston, VA2001, 104 p

Argyroudis S, Kaynia AM (2013) Analytical fragility functions for roadways and railways on embankments and in cuts due to seismic shaking, submitted to Bulletin of Earthquake Engineering

Argyroudis S, Pitilakis K (2007) Development of vulnerability curves for circular shallow tunnels due to ground shaking and ground failure. In: Crosta GB, Frattini P (eds) Landslides: from mapping to loss and risk estimation. LESSLOSS report no. 2007/01. IUSS Press, Pavia, ISBN: 978-88-6198-005-1:175–184

Argyroudis S, Pitilakis K (2012) Seismic fragility curves of shallow tunnels in alluvial deposits. Soil Dyn Earthq Eng 35:1–12

Argyroudis S, Mitoulis S, Pitilakis K (2013a) Seismic response of bridge abutments on surface foundation subjected to collision forces. In: Proceedings of 4th international conference on computational methods in structural dynamics and earthquake engineering (COMPDYN), Kos Island, Greece, 12–14 June 2013

Argyroudis S, Kaynia AM, Pitilakis K (2013b) Development of fragility functions for geotechnical constructions: application to cantilever retaining walls. Soil Dyn Earthq Eng 50:106–116

ATC-13 (1985) Earthquake damage evaluation data for California. Applied Technology Council, Redwood City

Bardet JP, Ichii K, Lin CH (2000) EERA: a computer program for equivalent-linear earthquake site response analyses of layered soil deposits. University of Southern California, Department of Civil Engineering, Los Angeles, 40 p

Bray J, Travasarou T (2007) Simplified procedure for estimating earthquake-induced deviatoric slope displacements. J Geotech Geoenviron Eng 133(4):381–392

Byers W (2004) Railroad lifeline damage in earthquakes. In: Proceedings of 13th world conference on earthquake engineering, Vancouver, BC, Canada, 1–6 Aug 2004, Paper No. 324

Corigliano M (2007) Seismic response of deep tunnels in near-fault conditions. Ph.D. dissertation, Politecnico di Torino, Italy, p 222

Dowding CH, Rozen A (1978) Damage to rock tunnels from earthquake shaking. J Geotech Eng Div 104:175–191

EC8. Eurocode 8 (2004) Design of structures for earthquake resistance. European Committee for Standardisation, Brussels. The European Standard EN 1998-1

Kaynia AM (ed) (2013) Guidelines for deriving seismic fragility functions of elements at risk: buildings, lifelines, transportation networks and critical facilities. SYNER-G reference report 4, Publications Office of the European Union, ISBN 978-92-79-28966-8, doi:10.2788/19605

Kaynia AM, Johansson J, Argyroudis S, Pitilakis K (2011) D3.8-Fragility functions for roadway system elements, Deliverable of SYNER-G EC Project

Lagaros N, Tsompanakis Y, Psarropoulos P, Georgopoulos E (2009) Computationally efficient seismic fragility analysis of geostructures. Comput Struct 87:1195–1203

LessLoss (2007) Risk mitigation for earthquakes and landslides, Research Project, European Commission, GOCE-CT-2003-505448

Maruyama Y, Yamazaki F, Mizuno K, Tsuchiya Y, Yogai H (2010) Fragility curves for expressway embankments based on damage datasets after recent earthquakes in Japan. Soil Dyn Earthq Eng 30:1158–1167

National Institute of Building Sciences (NIBS) (2004) HAZUS-MH: users's manual and technical manuals. Report prepared for the Federal Emergency Management Agency, Washington, DC

Owen GN, Scholl RE (1981) Earthquake engineering of large underground structures, in report no. FHWA/RD-80/195, Federal Highway Administration and National Science Foundation, 279 p

Pitilakis K et al (2010) Physical vulnerability of elements at risk to landslides: methodology for evaluation, fragility curves and damage states for buildings and lifelines. Deliverable 2.5 in EU FP7 research project no. 226479. SafeLand: living with landslide risk in Europe: assessment, effects of global change, and risk management strategies

Plaxis 2D (1998) Reference manual, version 7

Plaxis 2D (2011) Reference manual, version 9

Salmon M, Wang J, Jones D, Wu Ch (2003) Fragility formulations for the BART system. In: Proceedings of the 6th U.S. conference on lifeline earthquake engineering, TCLEE, Long Beach, 10–13 Aug 2003

Werner SD, Taylor CE, Cho S, Lavoie J-P, Huyck C, Eitzel C, Chung H, Eguchi RT (2006) REDARS 2: methodology and software for seismic risk analysis of highway systems, MCEER-06-SP08

Winter M, Smith JT, Fotopoulou S, Pitilakis K, Mavrouli O, Corominas J, Argyroudis S (2013) The physical vulnerability of roads to debris flow. In: Proceedings of the 18th international conference on soil mechanics and geotechnical engineering, Paris, 2–6 Sept 2013

Chapter 11
Fragility Functions of Harbor Elements

Kalliopi Kakderi and Kyriazis Pitilakis

Abstract Experience gained from recent strong seismic events has demonstrated the high vulnerability of waterfront structures and port facilities to strong ground shaking and associated phenomena resulting to severe physical damages and important economic losses. The objective of this Chapter is to review and propose fragility curves and methods to assess the seismic vulnerability for the most important components of a harbor system, namely waterfront structures, cargo handling and storage components and infrastructures within the European context in terms of construction practice and seismicity. After a short review, the observed during past earthquakes different failure modes are identified and classified and a detailed taxonomy is proposed with special emphasis to European specific features. Based on the taxonomy and the proposed classification of the different elements at risk, adequate fragility curves are provided.

11.1 Introduction

Port transportation systems are vital lifelines that contain a wide variety of facilities for passenger operations and transport, cargo handling and storage, rail and road transport of facility users and cargoes, communication, guidance, maintenance, administration, utilities, and various supporting operations. Ports offer wide-open areas that can be used for emergency or refuge activities after a damaging earthquake. Moreover, they can play an important role during the recovery period by providing transportation means.

The combination of hazard, importance, vulnerability and exposure of the port structures leads to a potentially high seismic risk. In fact, the consequences of earthquake-induced damage are not only related to life safety and repair costs of the

K. Kakderi (✉) • K. Pitilakis
Department of Civil Engineering, Aristotle University,
P.O.Box. 424, 54124 Thessaloniki, Greece
e-mail: kkakderi@gmail.com; kpitilak@civil.auth.gr

K. Pitilakis et al. (eds.), *SYNER-G: Typology Definition and Fragility Functions for Physical Elements at Seismic Risk*, Geotechnical, Geological and Earthquake Engineering 27,
DOI 10.1007/978-94-007-7872-6_11,

structures, but also to interruption of port serviceability in the immediate aftermath of an earthquake. Experience gained from past strong seismic events e.g. Loma Prieta in 1989, Hyogoken-Nanbu in 1995, Tokachi-Oki in 2003 just to name few of them has demonstrated the dramatic seismic vulnerability of port structures, the severe damages that can be caused by ground shaking, and the high economic losses and societal impact due to earthquake damage (Werner et al. 1999).

The aim of this Chapter is twofold: to propose adequate taxonomy and typology for all elements comprising a harbor facility, considering the European specific features, and then based on the taxonomy to review, discuss and propose fragility curves for the most important harbor elements namely waterfront structures, cargo handling and storage components and infrastructures.

11.2 Description of Damage Mechanisms and Failures Modes

Ports may be prone to damage from even moderate earthquakes. Different components exhibit different seismic performance depending on their characteristics and the type of seismic input. In this section physical damages during past earthquakes and main causes of damage for the various harbor elements are summarized and failure modes are classified.

11.2.1 Physical Damages/Main Causes of Damage

By far, the most significant source of earthquake-induced damage to port and harbor facilities is the increase of induced earth pressures caused by inertial forces to the retained ground mass and by hydrodynamic force and pore-water pressure build-up in the saturated cohesionless soils that prevail at these facilities. This pressure build-up can lead to excessive lateral pressures to quay walls. Liquefaction and massive submarine sliding are also very important causes for spectacular failures (ATC-25, ATC 1991). Other sources are local permanent ground deformations, ground failure and extensive settlement related to ground shaking (Pachakis and Kiremidjian 2004; Werner 1998). Yet, the liquefaction of loose, saturated, sandy soils that often prevail at coastal areas (especially reclaimed land and uncompacted fills) is the most widespread source of seismic damage to port structures. Past experience has demonstrated that even moderate levels of earthquake intensity can cause liquefaction resulting in reduced stiffness and loss of shear strength of the soils. This can in turn lead to induced soil settlements, increased lateral earth pressures against retaining structures and loss of passive resistance against walls and anchors (PIANC 2001). Finally, port structures are also subjected to damage due to tsunamis. Buildings in port areas are subjected to damage due to shaking as well as damage caused by loss of bearing capacity or lateral movement of the foundation soils.

There is a large number of references regarding seismic damage of port structures, mostly during earthquakes in the USA and Japan [e.g. Loma Prieta 1989, EERI (1990), Ferritto (1997); Hyogo-ken Nanbu (Kobe) 1995, Bardet et al. (1995), Ferritto (1997), PIANC (2001); Chi-Chi 1999, EERI (2001)]. In Europe similar observations are quite limited, while the majority of port structures in Europe are located in moderate to high hazard zones based on the national seismic codes (Borg and Lai 2007). The Kocaeli earthquake (Turkey, 17/8/1999, Ms = 7.4), caused extensive damage to the numerous waterfront piers and port facilities around Izmit Bay (EERI 2000). In Greece, earthquake damage to waterfront structures has been recorded during the Kalamata (13/9/1986, Ms = 6.2) and Lefkas (14/8/2003, Ms = 6.4) earthquakes. The Kalamata main harbor quay wall, in spite of being damaged, preserved its serviceability during and after the earthquake (Pitilakis and Moutsakis 1989). During the Lefkas earthquake, damage was observed to the quay walls of the city port and Marina waterfront structures, mostly consisting of lateral sliding and tilting of walls, settlement of backfills and apron pavement cracking (Kakderi et al. 2006). Liquefaction was most probably the primary source of seismic damage in most cases.

11.2.1.1 Waterfront Structures

Extensive seismic damage is usually attributed to the occurrence of liquefaction phenomena. Lateral ground displacements generated by liquefaction-induced lateral spread can cause substantial damage to port structures often even under moderate earthquakes (Werner 1998). Typical examples are the 1995 Hyogo-ken Nanbu (Kobe) and 2001 Nisqually earthquakes, while the occurrence of liquefaction in the backfill was the main reason for damage sustained to gravity quay walls, as for example during the 1993 earthquake at Kushiro-oki and the 1994 earthquake at Hokkaido Toho-oki (Na et al. 2009a).

The seismic behavior of port structures is largely governed by the local soil conditions and supporting soils' properties. During the 1995 Hyogo-ken Nanbu (Kobe) earthquake, the caisson type quay walls of identical configuration, located at the site in a close proximity with a similar average soil property, experienced significantly different degrees of damage (Inatomi et al. 1997). Relatively poor seismic performance of many ports is primarily due to the poor foundation and backfill soils that are common in waterfront environments.

11.2.1.2 Cargo Handling and Storage Components

Experience from past earthquakes shows that properly designed cranes perform well if the foundations and the supporting soils perform well. Damages to cranes after earthquake events could be not only due to ground shaking, but also due to movement of the rail foundation caused by ground failure or permanent ground deformation without predominant failure mechanism. While not in use, cranes are

restrained or anchored to foundation rails, preventing their relative movement or derailment. In this case, they are subjected to inertia forces like any other structure with fixed foundation connections. However, even in cases where relative movement or derailment is possible (for example when anchors have failed or while cranes are in use), cranes may overturn due to liquefaction of the underlying soil fills or/and the occurrence of important differential settlements, or they may be induced to bending type of failure due to ground detachment of a foundation member (PIANC 2001). Overturned cranes may induce damage to adjacent structures and other facilities. Finally, disruption of crane's functionality may be induced by settlement and/or horizontal movement of foundation rails due to permanent ground deformations and liquefaction of subjacent soil layers, as were the cases of the ports of Oakland, Derince and Kobe during the Loma Prieta, Kocaeli and Hyogo-ken Nanbu (Kobe) earthquakes. Rail de-alignment may cause damage to wheels and cranes immobility (ATC-25, ATC 1991). Downtime of cranes may vary from a few days (in cases of simple derailment) to several months due to severe earthquake damage.

Early container cranes are lighter and less stable than today's larger jumbo cranes. During an earthquake, the earlier cranes would lift from the rails before significant inertia forces could develop in the crane structure. Current large cranes, with 30 m or greater rail gages, are much heavier, which results in significantly larger seismic forces in the crane structure. Recent studies (Soderberg et al. 2009) indicate that many jumbo cranes will be extensively damaged in moderate earthquakes, and many of them will be severely damaged, or will collapse, in a major earthquake.

11.2.1.3 Port Infrastructures

Port infrastructure components include utility and transportation systems as well as buildings and liquid storage reservoirs like oil tanks. All utility systems may be present at ports. Both roadway and rail access links are commonly required to transfer waterborne cargo and people.

There are examples of both poor and good seismic performance of utility lifelines at ports during past earthquakes. The most common cause of seismic damage to roadway and railway systems is Permanent Ground Deformation (PGD).

11.2.2 Classification of Failure Modes

In general, damage to port facilities may be the following:

- Deformation and failure of dikes.
- Lateral sliding, rotation, settlement and deformation of waterfront retaining structures.

- Buckling, yielding and fracture of pile supports at piers and wharves (particularly battered piles).
- Displacement of crane rails with resulting disruption of crane operations.
- Extensive settlement and cracking of pavements within storage yards and along access roadways.
- Damage to buried or collocated pipelines.
- Potential for disruption of supporting lifelines that service port facilities.
- Serious damages of various warehouse and storage facilities.

In the following, failure modes of waterfront structures and cargo handing components (cranes) are described. Failure modes for buildings, storage components, lifelines and utility systems are similar to other assets of this type and described in the relevant chapters of this book.

11.2.2.1 Waterfront Structures

Most failures of waterfront structures are associated with outward sliding, deformation and tilting of quay walls and sheet-pile bulkheads. Residual tilting reduces the static factor of safety (FS) after the earthquake, while sliding is more a serviceability rather than a safety problem. Block-type quay walls are vulnerable to earthquake-induced sliding between layers of blocks. This damage has often been accompanied by extensive settlement and cracking of paved aprons. The principal failure mode of sheet-pile bulkheads has been insufficient anchor resistance, primarily because the anchors were installed at shallow depths, where backfill is most susceptible to loss of strength due to pore-water pressure build-up or liquefaction. Insufficient distance between the anchor and the bulkhead wall can also lead to failure. In case of waterfront structures supported on piles, possible failure modes are also related to seismic damage induced to piles themselves. Pile-supported docks typically perform well, unless soil failures such as major submarine landslides occur. In such cases, piers have undergone extensive sliding and buckling and yielding of pile supports. Batter piles have damaged pier piles caps and decking because of their large lateral stiffness (ATC-25, ATC 1991). Finally, increased damage probabilities due to differential ground settlement are attributed to structures supported by different types of foundations (surface foundations on landfills and pile foundations).

The characteristic damage patterns of caisson-type quay walls during the 1995 Hyogo-ken Nanbu (Kobe) earthquake were large lateral movements, tilting, and settlements of caissons and ground movements of the backfill in the form of lateral movements and settlements of the apron (Inatomi et al. 1997). In the case of caisson-type quay walls subjected to earthquake excitation, typical damage modes are seaward displacement, settlement and tilting.

For gravity-type quay walls, possible modes of seismic failure are classified as indicated in Table 11.1 (Kakderi et al. 2006).

Table 11.1 Earthquake induced failure modes of gravity-type quay walls

Component	Failure modes
Quay walls	Outward sliding
	Tilting
	Settlement
	Overturning and extensive tilting
	Collapse
	Apron pavement cracking
	Cracking with corresponding pavement settlement relative to wall
Backfill materials	Ground fracture and cracking of road surface
	Waterspouts from ground fissures and sand boils
	Settlement of backfill
	Differential ground settlement
	Lateral ground movement (lateral spreading)

11.2.2.2 Cargo Handling Components

Early cranes may be tipped and lifted from their rails without significant damage. Some cranes that tip may not land on their rails. Often, even though the wheels are off the rails, the portal frame response may still remain in the elastic range. Restoring the wheels to the rail is not difficult because after lifting the frame with jacks, the portal frame pulls the wheels back over the rail.

When crane supports fail significant damage may occur. If the crane rails spread, the crane legs also spread until plastic hinging develops in the portal frame and the whole crane may collapse in particular due to excessive spreading.

The jumbo cranes are more massive, have greater portal clearances, and are more stable, resulting in much larger lateral loads on them. The strength of the portal frame has not kept up with the increased lateral seismic loading demand. If modern jumbo cranes are designed to early criteria, they cannot tip elastically and permanent damage will occur. For these cranes, the following performance is predicted in seismic areas (Soderberg et al. 2009):

- In a design operating level earthquake (OLE) of 72 year mean return interval (MRI), the portal frame would suffer significant damage consisting of localized plate buckling at the leg to portal connection and possibly other areas of the portal frame.
- In a large 475 year MRI earthquake, the portal frame would be significantly damaged resulting in possible crane collapse. Performance in this level earthquake is highly dependent on the ability of the plastic hinges to maintain adequate strength over the many cycles of loading.
- Damage to the portal frame occurs due to lateral displacement in the trolley travel direction.

11.3 Identification of Main Typologies

In this section, the main typologies of harbor components are identified and their main features are briefly described.

11.3.1 Waterfront Structures

Port waterfront structures are quite broad and varied; they include a range of earthen embankments, retaining structures/dikes (e.g. at wharves, embankment, breakwaters, and dredged shipping lanes and waterway) and berthing structures. The embankments may be homogeneous or multi-lift earth fill, armored with rock rip rap or other materials, and may possibly be topped with a concrete structure. Berthing structures at ports may be composed of earth retaining walls, pile supported marginal wharves, pile-supported piers, or combinations of these.

Seven specific types of port waterfront structures are considered in the following:

- Embankments.
- Piles (common element for many types of waterfront and other types of port components).
- Marginal wharves.
- Gravity retaining structures.
- Steel sheet pile wharves.
- Mooring and breasting dolphins.
- Piers.

According to NIBS (2004) waterfront structures include:

- Wharves.
- Seawalls.
- Piers.

From an engineering point of view, waterfront structures are complex soil-structure systems that consist of various combinations of structural and foundation types. Typological descriptions of port waterfront structures are more or less detailed. Some port structures are “mixed” and cannot be characterized by a single structural or foundation type.

Wood, steel or concrete piles often support waterfront structures. Batter piles have been also used to resist lateral loads from wave action and small impact of vessels. Seawalls are caisson walls retaining earth fill material.

The basic typological parameters of waterfront structures are geometry, section type, construction material, foundation type, existence and type of anchorage. Types of backfill and foundation soil, along with the existence of rubble foundation are determinant factors of their seismic behavior (Ichii 2003).

A more exhaustive typology may be used as in the following (Werner 1998; PIANC 2001):

Gravity retaining structures along the waterfront (quay walls/piers): concrete block walls (block work), massive walls (monolithic structure), concrete caissons (monolithic structure), cantilever structures (monolithic structure), cellular sheet pile retaining structures, steel plate cylindrical caissons or cribwork quay walls. Founded on rubble and soil or rock.

Sheet pile wharves with auxiliary structures for anchoring or sheet pile with platform (horizontal pile-supported slab). Sheet pile, pile, fill-soil foundation. Often made of steel.

Marginal wharves are pile structures, often partly soil-retaining and with auxiliary structures for anchoring. Deck types are: cast-in-place concrete flat slabs, cast-in-place concrete beam and slab structures, long-span concrete box girder deck system, precast pre-stressed concrete panels, precast normally-reinforced concrete panels, ballasted deck pavement systems. Also, structures on columns with auxiliary structures for horizontal force absorption, being sometimes partly soil retaining.

Piers usually of deck slabs supported on pile caps and piles from wood, steel or concrete (with or without batter piles). Piers are typically perpendicular to the shore line and in that sense they are distinguished from wharves, which are parallel to the shore line and usually include an earth or rock dike structure.

Mooring and breasting dolphins: monolithic gravity structures, founded on rubble and soil or rock (sometimes pile foundation), or pile structures (floating dock wharves).

Embankments could be native soils, rock and sand dike with backland fills, bulkheads and sea walls and breakwaters (vertical face and rubble mound types). Breakwaters are further classified into: conventional caisson breakwater with vertical front (monolithic gravity structure, foundation on rubble bedding layer and soil or rock), "vertically composite" caisson breakwater (monolithic gravity structure, foundation on high rubble mound), "horizontally composite" caisson breakwater (monolithic gravity structure with mound of blocks on one side, foundation on bedding layer and soil or rock), "block work" breakwater (block work gravity structure, foundation on bedding layer, or rubble mound, and soil or rock), piled breakwater, multi layer rubble mound breakwater with superstructure (mound with or without monolithic crown wall super structure, mound on soil foundation), reshaped rubble mound (berm breakwater) (mound without superstructure, mound on soil foundation).

Pile types include: pre-stressed concrete piles, large-diameter pre-stressed concrete cylinder piles, cast-in-drilled-holes (CIDH) concrete piles, steel H-piles, steel pipe piles, large-diameter steel pipe piles, timber piles, vertical pile systems, batter pile systems.

11.3.2 Cargo Handling and Storage Components

Cargo handling and storage components include container storage areas, liquid storage tanks and material handling equipment. Cranes and cargo handling equipment are large equipment items used to load and unload freight from vessels.

Cranes and cargo handling equipment are described (NIBS 2004) with respect to whether the cranes are:

- Anchored/Unanchored.
- Stationary/Rail mounted.

They could also be classified according to the cargo capacity and cargo type.

The foundation type and the relative location of the cranes and the storage facilities with respect to the waterfront structures are also important parameters.

Other parameter, which is important when considering interactions between port components, is the power supply and backup type (electric or fuel). A more detailed typology may be used as follows (Werner 1998):

- Cranes include rail, tire and track mounted gantry and revolver cranes, mobile cranes and crane foundations and power supply systems.
- Tanks could be anchored and unanchored, above grade and partially buried, tank foundations and containment berms.
- Other cargo handling and storage components include port equipment (stationary or mounted on rails) and structural systems used for material handling and transport (cranes, conveyors, transfer towers and stacker/reclaimer equipment), tunnels and pipelines, and temporary transitional storage and containment components.

11.3.3 Port Infrastructures

Port infrastructure components include:

- Utility systems (electric power system, water and waste-water system, natural gas, liquid fuel, communications system, fire-fighting system).
- Transportation infrastructures (roadway, railway, bridges).
- Buildings (sheds and warehouses, office buildings, maintenance buildings, passenger terminals, traffic control buildings).

The reader is referred to the respective chapters of this book.

11.4 Review of Existing Fragility Functions

A review of existing fragility functions for port systems' components, covering waterfront structures, cargo handling and storage components, and port infrastructures, is presented in the following sections. For port infrastructures (building structures, utility and transportation systems), there are no specific fragility studies (except for fuel facilities), and their vulnerability assessment is performed using available fragility functions for buildings and the components of the lifeline systems referred to other relevant chapters of the book.

11.4.1 Waterfront Structures

The type and degree of seismic damages of the waterfront structures depend on the typology, local site conditions, intensity of the seismic loading and the occurrence of liquefaction. The design factors of safety also play a very important role in their seismic behavior. In current engineering practice the seismic design of earth retaining structures is usually carried out using empirical methods. According to most seismic codes worldwide, waterfront structures are designed using simplified, pseudo-static or simplified static, force-based equilibrium approaches and pseudo-dynamic techniques (Steedman and Zeng 1990). An alternative approach is the use of displacement-based methods. An estimate of earthquake-induced deformation may be obtained by performing simplified dynamic analyses (sliding block method; Newmark 1965; Richards and Elms 1979) or alternatively advanced non-linear time-history analyses using numerical finite difference or finite element simulations (full dynamic analysis; e.g. Whitman 1990; Finn et al. 1992; Iai and Kameoka 1993; Al-Homoud and Whitman 1999; Green and Ebeling 2002; Psarropoulos et al. 2005). For static conditions, the prediction of actual earth pressures and permanent deformations, which are necessary for the construction of fragility curves, constitutes a complicated soil-structure interaction problem. In the dynamic response the situation is even more complicated. The dynamic response of the simplest type of retaining wall depends on the mass and stiffness of the wall, the backfill and the underlying ground conditions, as well as the interaction among these components and the characteristics of the seismic input.

Empirical fragility curves describing earthquake induced damage in waterfront structures are proposed in HAZUS (NIBS 2004). They describe lognormal cumulative distributions which give the probability of reaching or exceeding certain damage states for a given level of permanent ground deformation (PGD). The damage index is based on the description of the type and extent (level) of structural damage and serviceability state. In this case, no distinction between the different wall typologies and no specification of the type and source of ground deformation (deformation due to ground shaking or ground failure) are made.

Analytical methods have also been used for the vulnerability assessment of quay walls. The standard structural-engineering approach for seismic design of retaining structures relies on soil-structure interaction models; alternatively, a full dynamic analysis can be performed (Pathmanathan et al. 2007; Pasquali et al. 2008; Li Destri Nicosia 2008; Green et al. 2008). This kind of analysis provides a useful insight into the seismic behavior of waterfront structures but cannot be easily applied to vulnerability assessment of different wall typologies and foundation conditions, under different levels of seismic excitation.

Ichii 2003 and 2004 proposed several analytical fragility curves for the assessment of direct earthquake-induced damage to gravity-type quay walls using simplified dynamic finite element analysis, considering also the occurrence of liquefaction phenomena. Different vulnerability curves are given in the form of log-normal probability distributions for different peak ground acceleration levels (PGA). Seismic performance of quay walls appears to be governed by the following parameters:

- Width-to-height ratio of the wall (W/H).
- Normalized thickness of sand deposit (D_1/H). Intermediate deposits to the stiff subsoil layers can be either natural or artificial.
- Equivalent N_{SPT} values (N_{65}) of sand deposits below and behind the wall.

The damage index used is the normalized seaward displacement and restoration cost. The proposed vulnerability curves are expressed in the form of two-parameter (median and log-standard deviation) lognormal distribution functions.

Kakderi and Pitilakis (2010) proposed fragility curves for waterfront/retaining structures for ground shaking without the occurrence of liquefaction, using available data from past earthquake damages in Europe and worldwide and numerical analysis of typical cases. Typical waterfront structures, with different geometry, foundation soil conditions and seismic excitations, were studied using appropriate numerical modeling. The corresponding damage levels were estimated with respect to the induced residual displacements and the seismic response of the soil-structure system. Analytical fragility curves were constructed for the different types of gravity waterfront structures and foundation conditions, which are given in terms of two parameters (median and standard deviation β) lognormal cumulative distributions for different levels of peak ground acceleration levels (PGA) at outcrop conditions. Four different classes were considered based on:

- Wall height H ($>$ and $\leq$10 m).
- Soil foundation conditions (V_s values) (soil types B and C according to EC8 2002).

Na et al. (2008) investigated the effect of liquefaction and lateral spreading on the seismic response of (gravity type) caisson quay walls, using nonlinear dynamic analyses of soil–structure system. A 2D numerical model, representing a specific berth located in Port Island, Kobe and damaged in the 1995 Kobe earthquake, was used to simulate the seismic behavior. Using the residual horizontal displacement of top seaside corner of the quay wall as a seismic demand, the authors proposed two sets of fragility curves representing an original and a retrofitted structure, to assess

the response of the specific berth typologies for different levels of PGA at stiff soil to rock site. Damage states are described with regards to the normalized residual horizontal seaward displacement. However, the parameters of the fragility relations are not provided. Na and Shinozuka (2009) further presented a methodology to estimate the effects of the earthquake on the performance of the operation system of a container terminal in seaports by integrating simulation models for terminal operation and fragility curves of port components in the context of seismic risk analysis. System fragility curves were developed based on fragility curves of independent wharf components.

Focusing on pile-supported wharves Na et al. (2009b) evaluated seismic behavior of port structures recognizing that most of the parameters controlling the properties of soil are of random nature. The response of such structures inherently presents a complex soil-structure interaction problem involving ground shaking, pile-failure mechanism, liquefaction and lateral spreading in backfill and sand layers. Using an effective stress analysis model of a representative model of a typical pile-supported wharf in the west coast of United States, two sets of fragility curves were proposed for different levels of peak ground acceleration (PGA); with or without consideration of uncertainty in soil parameters. The residual horizontal displacement of a dike and a deck was used to define the damage states. Parameters of the fragility relations are not provided and the results of this study can be utilized only to evaluate the seismic vulnerability of similar pile supported wharves.

In the study performed by Ko et al. (2010), the seismic fragility analysis for the sheet pile wharves of the Hualien Harbor in Taiwan was performed using 2D finite element nonlinear dynamic analysis; fragility curves were proposed in terms of two parameters (median and standard deviation β) lognormal cumulative distribution functions. The damage index used was the maximum residual displacement at the top of the sheet pile wall subjected to different levels of peak ground acceleration (PGA) in the free field. The proposed fragility curves refer to the specific sheet pile cross sections of wharves of the Hualien Harbor in Taiwan (anchors at the upper part and soil embedment at the lower part, with or without additional gravity retaining wall, heights 16–20 m and stiff, non-cohesive foundation soil).

Table 11.2 presents a summary of the existing fragility functions for quay walls.

Aiming at developing fragility curves for small quay walls based on Greek data (typology and construction practice), Kakderi et al. (2006) evaluated the reliability of the existing fragility curves (HAZUS, NIBS 2004 and Ichii 2003) based on the actual seismic performance of the quay walls in the city of Lefkas, which sustained significant deformations during the 2003 earthquake. The newly constructed quay walls in the Marina suffered minor to moderate damages with observed relative residual seaward displacements of the order of 12–15 cm. There is some evidence that, at least in few locations, a partial liquefaction of the foundation subsoil occurred (Margaris et al. 2003). The validation study was based on the results of a site-specific ground motion analysis performed for the specific scenario earthquake. The effect of liquefaction phenomena on ground motion characteristics was also considered and the assessment of liquefaction induced permanent ground deformations was carried out. The results of the study indicated that the

Table 11.2 Summary review of existing fragility functions for quay walls

Reference	Methodology	Classification	IM
NIBS (2004)	HAZUS – empirical fragility functions	No distinction between different wall typologies	PGD
Ichii (2003, 2004)	Analytical fragility curves using simplified dynamic finite element analysis, considering also the occurrence of liquefaction phenomena	Gravity-type (caisson) quay walls. 20 different classes based on: Equivalent N_{SPT} value below and behind wall (range: 5–25) Aspect ratio of the wall (W/H) (range:0.65–1.05) Normalized depth of sand deposit below wall (D_1/H) (range: 0–1)	PGA (outcrop conditions)
Kakderi and Pitilakis (2010)	Analytical fragility curves using 2D finite element analysis, only for ground shaking, without presence of liquefaction.	Gravity-type (monolithic) quay walls. Four different classes based on: Wall height H ($>$ and $\leq$ 10 m). Soil foundation conditions (V_s values) (soil types B and C according to EC8 2002)	PGA (outcrop conditions)
Ko et al. (2010)	Analytical fragility curves using 2D finite element nonlinear dynamic analysis	Two sheet pile cross sections of wharves of the Hualien Harbor in Taiwan (anchors at the upper part and soil embedment at the lower part, with or without additional gravity retaining wall) H = 16 and 20 m Stiff, non-cohesive foundation soil	PGA (free-field conditions)
Na et al. (2009b)[a]	Analytical approach (effective stress analysis method, nonlinear time history analysis). Liquefaction and lateral spreading in backfill and sand layers is taken into consideration	Pile-supported wharves Two sets of fragility curves: with or without consideration of uncertainty in soil parameters	PGA
Na and Shinozuka (2009), Na et al. (2008)[b]	Analytical approach using numerical model (Nonlinear time history analysis), considering also the occurrence of liquefaction phenomena (effective stress analysis)	Gravity-type (caisson) quay wall Two sets of fragility curves representing an original and a retrofitted structure	PGA (stiff soil to rock site)

[a]Parameters of the fragility relations are not provided

[b]Parameters of the fragility relations are not provided. A methodology is presented to develop system fragility curves for a container terminal based on fragility curves of independent wharf components

vulnerability assessment and damage state distribution using the HAZUS (NIBS 2004) relationships was well compared with the observed damage, while damages based on the vulnerability curves proposed from Ichii (2003) seemed to be slightly overestimated.

11.4.1.1 Cargo Handling and Storage Components

The performance of cranes during earthquakes is critical, since crane damage and subsequent downtime has a major impact on indirect losses and post-disaster recovery. Identifying the key parameters which negatively affect the seismic response of cranes is the first step in developing fragility relationships, and ultimately, performance-based design recommendations.

The only available fragility curves describing earthquake-induced damage to cargo handling and storage components are the ones proposed in HAZUS (NIBS 2004) based on expert judgment. They are described through lognormal cumulative distributions which give the probability of reaching or exceeding certain damage states for a given level of peak ground acceleration (PGA) and permanent ground deformation (PGD). Four damage states are used, while the damage index is based on the description of the type and extent (level) of structural damage and serviceability state. A distinction is made between stationary (anchored) and rail-mounted (unanchored) cranes.

11.4.1.2 Port Infrastructures

For the review of existing fragility functions of building facilities and port infrastructures except oil facilities, the reader is referred to the respective chapters of this book. In the following, a review of existing fragility relations for liquid fuel systems is provided.

11.4.1.2.1 Liquid Fuel Systems

Empirical fragility curves that describe earthquake-induced damage to fuel facilities due to ground shaking and ground failure are proposed in HAZUS (NIBS 2004). Five damage states are used and the damage index is based on the description of the type and extent (level) of structural damage and serviceability state. The classification of fuel facilities is based on the existence or not of anchorage of equipment and back up power.

In the framework of the Greek research project SRM-LIFE (2007) fragility curves for liquid fuel facilities were derived using a fault-tree analysis similar to HAZUS (NIBS 2004), modifying accordingly the fragility curves of the sub-components with respect to Greek typologies. For the building sub-component, the fragility curves proposed by Kappos et al. (2006) for European

Table 11.3 Review of existing fragility functions for fuel facilities

Reference	Methodology	Classification	IM
NIBS (2004)	HAZUS – empirical fragility functions	Five different classes based on: Anchorage of equipment[a] backup power	PGA, PGD
SRM-LIFE (2007)	Empirical fragility functions	Seven different classes based on: backup power Building's level of seismic design	PGA, PGD

[a]Anchored equipment in general refers to equipment designed with special seismic tiedowns or tiebacks, while unanchored equipment refers to equipment designed with no special considerations other than the manufacturer's normal requirements

building typologies were used (R/C dual system, regularly infilled, low-rise building). The derived fragility curves describe lognormal cumulative distributions which give the probability of reaching or exceeding certain damage states for a given peak ground acceleration (PGA) and permanent ground deformation (PGD). Five damage states were used, while the damage index is based on the description of the type and extent (level) of structural damage and serviceability state. Seven types of fuel facilities were considered with respect to the existence or not of back-up power and the building's level of seismic design.

Table 11.3 presents a summary review of the existing fragility functions for fuel facilities.

11.4.2 Intensity Indexes

An important issue is the question of what ground motion intensity parameter best captures the response of each element and minimizes the dispersion of that response. This is also related to the approach that is followed for the derivation of fragility curves (see Chap. 1). There is a wide range of intensity measures (IMs) used to assess vulnerability (and losses) through the development of adequate fragility curves. Table 11.4 is a comprehensive list of the different descriptors used for the components in harbor systems.

11.4.3 Performance Indicators

Consequences of damaging earthquakes (Table 11.5) may include reduction or disruption of transport capacity, requiring some repairs. It is also possible to describe impacts on system dysfunction (Werner 1995). For the individual components, the indicators listed in Table 11.6 could be used.

Table 11.4 Intensity measures for vulnerability assessment of harbor elements

Component	Reference	IM	Comments
Waterfront structures	NIBS (2004)	PGD	Empirical fragility curves for waterfront structures. No distinction between different typologies. No specification of type and source of ground deformation (deformation due to ground shaking or ground failure)
	Ichii (2003, 2004)	PGA	Analytical fragility curves for gravity type quay walls. Simplified dynamic finite element analysis, considering also occurrence of liquefaction phenomena
	Kakderi and Pitilakis (2010)	PGA	Analytical fragility curves for ordinary gravity quay walls/retaining structures' typologies commonly used in Europe, exclusively for ground shaking (no liquefaction and ground failure)
	Ko et al. (2010)	PGA	Analytical fragility curves for sheet pile wharves of Hualien Harbor in Taiwan
	Na et al. (2009b)	PGA	Analytical fragility curves for pile-supported wharves. Liquefaction and lateral spreading in backfill and sand layers is taken into consideration
	Na and Shinozuka (2009), Na et al. (2008)	PGA	Analytical fragility curves for gravity-type (caisson) quay wall, considering also occurrence of liquefaction phenomena (effective stress analysis)
Cranes and cargo handling equipment	NIBS (2004)	PGA, PGD	Expert judgment

11.4.4 Damage States

This section presents a list of the parameters used in the literature for defining damage states in different harbor elements.

11.4.4.1 Waterfront Structures

The parameters defining damage states of quay walls are as follows:

- Level of structural damage (HAZUS, NIBS 2004).
- Serviceability (HAZUS, NIBS 2004; OCDI 2002).
- Normalized seaward displacement/sliding (Ichii 2003; PIANC 2001).
- Residual tilting towards the sea (PIANC 2001).
- Level of apron damage (differential settlement, residual tilting) (PIANC 2001).
- Permanent/residual displacement at top of wall (Uwabe 1983).
- Horizontal displacement of quay wall (OCDI 2002).

Table 11.5 Possible consequences of earthquake on port transportation systems

Serviceability		Seismic performance (Werner 1995)	
No transportation available	Not repairable	Uncontrolled	Beyond collapse control
		Collapse control	Significant damage may occur that may not be repairable but will not be sufficient to endanger life safety of occupants or users of the component
Reduced transportation	Operational after repairs	Damage control	Requires that damage may occur but should be repairable, controllable and within acceptable limits
Nominal transportation	Operational without repairs	Collapse control	No loss of function and only minor or negligible damage

Table 11.6 Possible consequences of earthquake on port transportation systems

Components	Performance indicators
Waterfront structures (quaywalls)	Ratio of length functioning
	Available docking length per ship category
	Residual displacement and tilting
	Differential settlement on apron and between apron and non-apron areas
Cargo handling and storage components	Differential displacement of parallel track (derailment, misalignment or toppling)
	Peak response of structural members and equipment

Especially for caisson-type quay walls:

- Residual displacements of the caisson and apron (PIANC 2001).
- Peak response stresses/strains of cell and cell joint (PIANC 2001).

Parameters defining damage states of sheet-pile walls are:

- Normalized seaward displacement/sliding of sheet-pile wall and apron (PIANC 2001).
- Peak response stresses/strains of sheet-pile wall mad tie-rod (PIANC 2001).
- (Maximum) residual displacement at top of sheet pile (Uwabe 1983; Gazetas et al. 1990).
- Horizontal displacement (OCDI 2002).
- Serviceability (OCDI 2002).

The parameters defining damage states of pile-supported wharves are as follows:

- Residual displacements (differential settlement between deck and land behind, residual tilting towards the sea) (PIANC 2001).
- Peak response of piles (PIANC 2001).

It is noticed that according to EC8 – Part 5 (EC8 2002), possible failure modes of earth retaining structures are considered to be bending for flexible structures and sliding and/or rotation for gravity structures. The design of earth retaining structures should ensure the following requirements:

- Stability of foundation soil (overall stability, local soil failure by sliding and/or bearing capacity failure).
- Resistance of anchorage.
- Structural strength.

11.4.4.2 Cargo Handling and Storage Components

Damage states for cargo handling and storage components are based on the description of the type and the extent of structural damage and the serviceability state.

11.5 Recommended Fragility Curves

The following sections present the recommended fragility curves and the associated informative data for the various structures and components of harbors.

11.5.1 Waterfront Structures

Based on the evaluation of the reliability of existing fragility curves (see Sect. 11.4.1) and considering also the range of applicability of existing functions, the HAZUS (NIBS 2004) generic fragility curves are proposed for the vulnerability assessment of quay walls for the case of ground failure. The description of damage states for waterfront structures is provided in Table 11.7, while the corresponding vulnerability curves are given in Table 11.8 and Fig. 11.1.

For the case of ground shaking, without considering the occurrence of liquefaction, the analytically derived fragility curves of Kakderi and Pitilakis (2010) for gravity walls are proposed, since they are the only ones available for this case. The description of damage states for waterfront structures is provided in Table 11.9, while the corresponding vulnerability curves are given in Table 11.10 and Fig. 11.2.

11.5.2 Cargo Handling and Storage Components

The only available study for the vulnerability assessment of cargo handling and storage components is provided by HAZUS (NIBS 2004). The description of

Table 11.7 Description of damage states for waterfront structures subject to ground failure according to NIBS (2004)

Damage state	Description	Serviceability	
Minor	Minor ground settlement resulting in few piles (for piers/seawalls) getting broken and damaged. Cracks are formed on the surface of the wharf. Repair may be needed	Reduced use	Operational without repair
Moderate	Considerable ground settlement with several piles (for piers/seawalls) getting broken and damaged	Not usable	Operational after repairs
Extensive	Failure of many piles, extensive sliding of piers, and significant ground settlement causing extensive cracking of pavements		Not repairable
Complete	Failure of most piles due to significant ground settlement. Extensive damage is widespread at the port facility		

Table 11.8 Parameters of fragility curves for waterfront structures subject to ground failure according to NIBS (2004)

	Permanent ground deformation (PGD)	
Damage state	Median (m)	β (log-standard deviation)
Minor	0.13	0.50
Moderate	0.30	0.50
Extensive	0.43	0.50
Complete	1.09	0.50

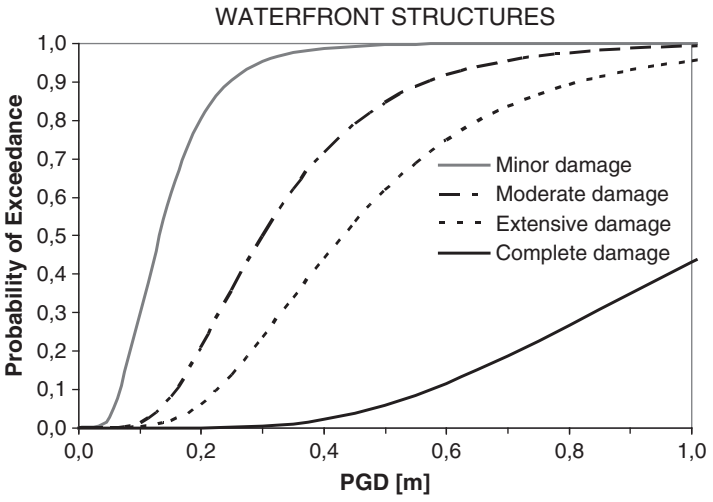

Fig. 11.1 Fragility curves for waterfront structures subject to ground failure according to NIBS (2004)

Table 11.9 Description of damage states for waterfront structures subject to ground shaking according to Kakderi and Pitilakis (2010)

Damage state	Normalized residual hor. displ. (u_x/H)
Minor	Less than 1.5 %
Moderate	1.5–5 %
Extensive	5–10 %
Complete	Larger than 10 %

Table 11.10 Parameters of fragility curves for waterfront structures subject to ground shaking according to Kakderi and Pitilakis (2010)

	Median PGA (g) (rock outcrop conditions)			
	Minor damages	Moderate damages	Extensive damages	β (log-standard deviation)
$H \leq 10$ m, $V_s = 250$ m/s	0.11	0.37	0.81	0.54
$H \leq 10$ m, $V_s = 500$ m/s	0.07	0.34	–	0.58
$H > 10$ m, $V_s = 250$ m/s	0.14	0.44	0.96	0.49
$H > 10$ m, $V_s = 500$ m/s	0.10	0.40	–	0.57

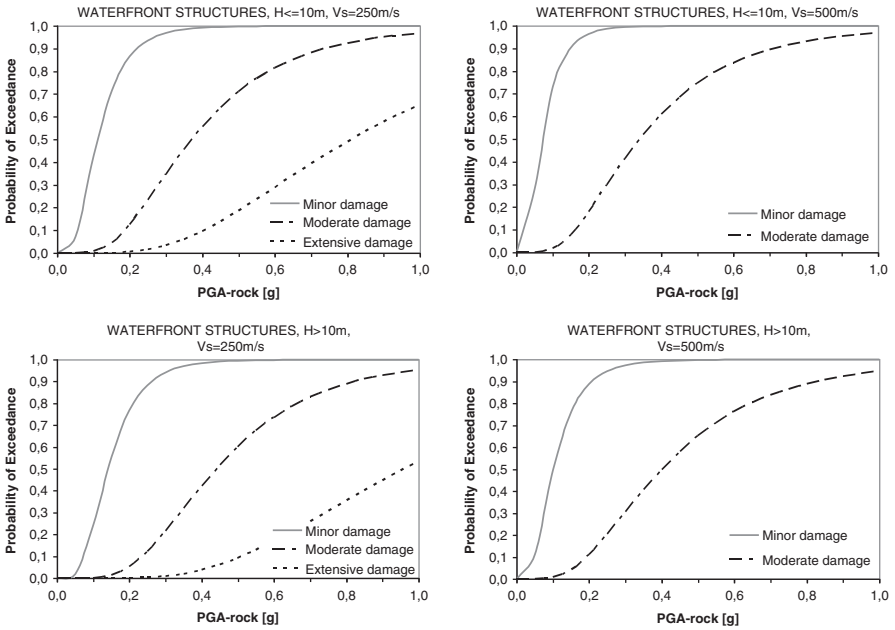

Fig. 11.2 Fragility curves for waterfront structures subject to ground shaking according to Kakderi and Pitilakis (2010)

Table 11.11 Description of damage states for cargo handling and storage components subject to ground shaking and ground failure according to NIBS (2004)

	Description			
Damage state	Stationary equipment	Unanchored or rail mounted equipment	Serviceability	
Minor	Slight damage to structural members with no loss of function	Minor derailment or misalignment without any major structural damage to the rail mount. Minor repair and adjustments may be required before the crane becomes operable	Reduced use	Operational without repair
Moderate	Derailment due to differential displacement of parallel track. Rail repair and some repair to structural members is required		Not usable	Operational after repairs
Extensive/ complete	Considerable damage to equipment. Toppled or totally derailed cranes are likely to occur. Replacement of structural members is required			Not repairable

Table 11.12 Parameters of fragility curves for cargo handling and storage components subject to ground shaking and ground failure according to NIBS (2004)

		Peak ground acceleration (PGA)		Permanent ground deformation (PGD)	
Description	Damage state	Median (g)	β (log-standard deviation)	Median (m)	β (log-standard deviation)
Stationary equipment	Minor	0.30	0.60	0.08	0.60
	Moderate	0.50	0.60	0.15	0.70
	Extensive/ complete	1.00	0.70	0.30	0.70
Unanchored or rail mounted equipment	Minor	0.15	0.60	0.05	0.60
	Moderate	0.35	0.60	0.10	0.60
	Extensive/ complete	0.80	0.70	0.25	0.70

damage states for cargo handling and storage components is provided in Table 11.11, while the corresponding vulnerability curves are given in Table 11.12 and Fig. 11.3.

11.5.3 Port Infrastructures

For buildings, utility systems and transportation infrastructures, the reader is referred to the respective chapters of this book.

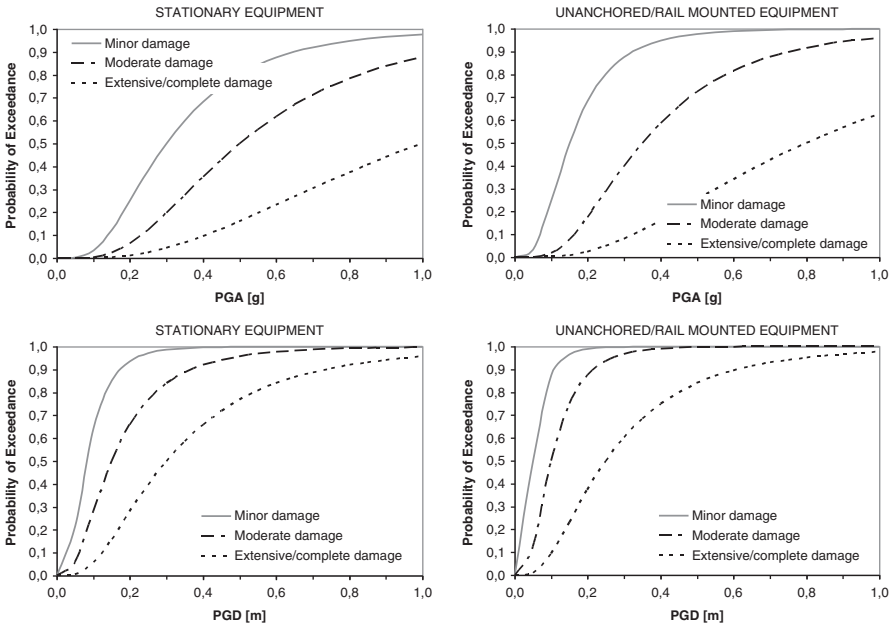

Fig. 11.3 Fragility curves for cargo handling and storage components subject to ground shaking (*up*) and ground failure (*down*) according to NIBS (2004)

For the vulnerability assessment of liquid fuel facilities, the fragility curves proposed in SRM-LIFE (2007) could be used (Tables 11.13 and 11.14, Figs. 11.4 and 11.5). These curves are applicable to fuel facilities with unanchored equipment, housed in low-rise R/C buildings, according to Greek buildings' typology. The description of damage states for fuel facilities is provided in Tables 11.15 and 11.16.

Alternatively, the generic fragility functions from HAZUS methodology (NIBS 2004) for fuel facilities could be used for ground shaking (Table 11.17 and Fig. 11.6). For ground failure (facilities with buried tanks) the same curves as in SMR-LIFE are applied. The definition of damage states is the same as in Tables 11.15 and 11.16.

11.6 Conclusions

Harbors are complex facilities comprising a variety of components like port structures and cargo handling equipment as well as building facilities and infrastructure networks. Experience gained from recent strong seismic events has demonstrated the high vulnerability of waterfront structures and port

Table 11.13 Parameters of fragility curves for fuel facilities subject to ground shaking according to SRM-LIFE (2007)

		Peak ground acceleration (PGA)	
Description	Damage state	Median (g)	β (log-standard deviation)
Unanchored equipment with backup power – building with low level seismic design	Minor	0.12	0.50
	Moderate	0.23	0.50
	Extensive	0.43	0.60
	Complete	0.62	0.60
Unanchored equipment without backup power– building with low level seismic design	Minor	0.10	0.50
	Moderate	0.19	0.45
	Extensive	0.43	0.60
	Complete	0.62	0.60
Unanchored equipment with backup power– building with medium level seismic design	Minor	0.13	0.50
	Moderate	0.26	0.50
	Extensive	0.56	0.60
	Complete	0.80	0.60
Unanchored equipment without backup power– building with medium level seismic design	Minor	0.11	0.50
	Moderate	0.20	0.45
	Extensive	0.56	0.60
	Complete	0.80	0.60
Unanchored equipment with backup power– building with high level seismic design	Minor	0.14	0.50
	Moderate	0.27	0.50
	Extensive	0.61	0.60
	Complete	0.90	0.60
Unanchored equipment without backup power– building with high level seismic design	Minor	0.12	0.50
	Moderate	0.21	0.45
	Extensive	0.61	0.60
	Complete	0.90	0.60

Table 11.14 Parameters of fragility curves for fuel facilities subject to ground failure according to SRM-LIFE (2007)

		Permanent ground deformation (PGD)	
Description	Damage state	Median (m)	β (log-standard deviation)
Facilities with buried tanks	Minor	0.10	0.50
	Moderate	0.20	0.50
	Extensive/complete	0.61	0.50

facilities to strong ground shaking and associated phenomena (permanent ground deformations) resulting to severe physical damages and important economic losses.

The characteristics and typologies of all important harbor components were summarized along with the main damage mechanisms and failure modes.

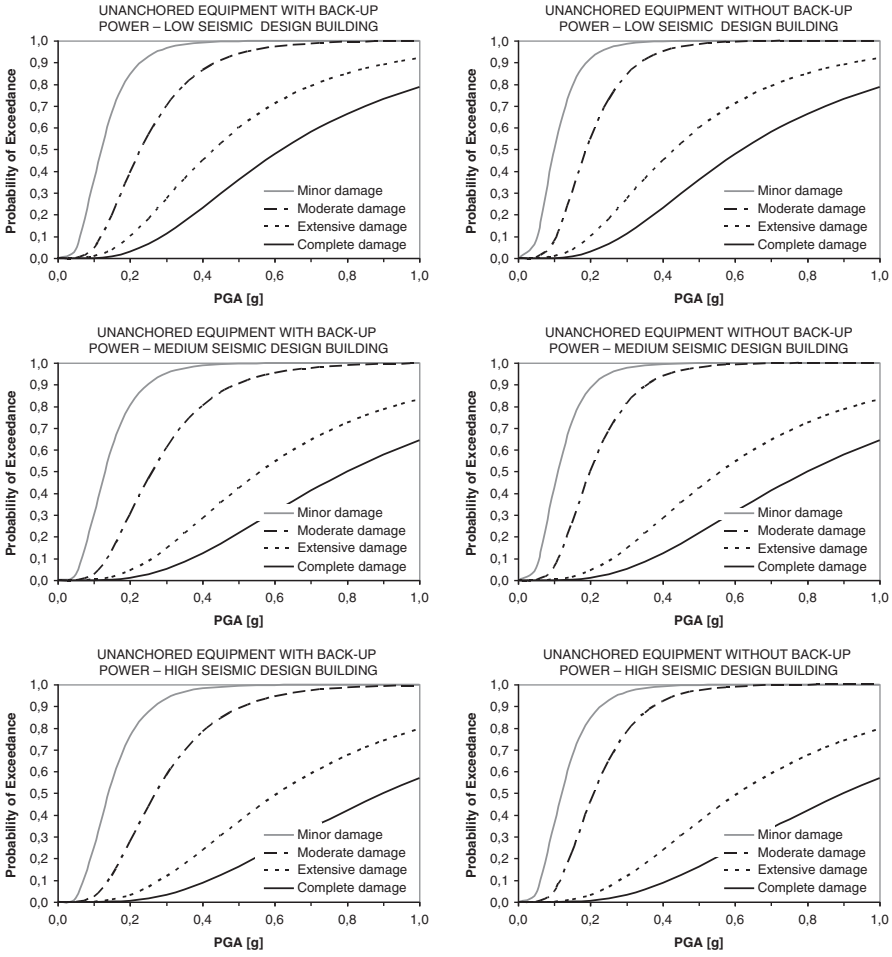

Fig. 11.4 Fragility curves for fuel facilities subject to ground shaking according to SRM-LIFE (2007)

Classification of the seismic intensity measures (IMs) used in the vulnerability assessment is also provided for all elements at risk. In most cases PGA and PGD are used. Available fragility functions have been collected and reviewed for all components of harbor facilities. The existing fragility functions are mainly based on empirical data and/or expert judgment. Especially, for waterfront structures several analytical approaches have also been developed in the recent years.

Based on the evaluation of existing fragility curves and considering also the range of applicability of existing functions, HAZUS (NIBS 2004) generic fragility curves are proposed for the vulnerability assessment of quay walls for the case of

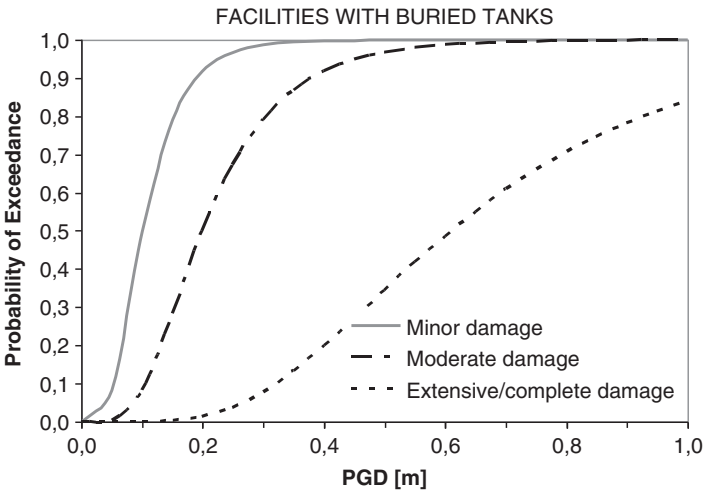

Fig. 11.5 Fragility curves for fuel facilities subject to ground failure according to SRM-LIFE (2007)

Table 11.15 Description of damage states for fuel facilities subject to ground shaking according to SRM-LIFE (2007)

Damage state	Description			
	Anchored equipment	Unanchored equipment	Serviceability	
Minor	Slight damage to pump building, minor damage to anchor of tanks, or loss of off-site power (check electric power systems for more on this) for a very short period and minor damage to backup power (i.e. to diesel generators, if available)	Elephant foot buckling of tanks with no leakage or loss of contents, slight damage to pump building, or loss of commercial power for a very short period and minor damage to backup power (i.e. to diesel generators, if available)	Reduced use	Operational without repair
Moderate	Elephant foot buckling of tanks with no leakage or loss of contents, considerable damage to equipment, moderate damage to pump building, or loss of commercial power for few days and malfunction of backup power (i.e., diesel generators, if available)	Elephant foot buckling of tanks with partial loss of contents, moderate damage to pump building, loss of commercial power for few days and malfunction of backup power (i.e., diesel generators, if available)	Not usable	Operational after repairs

(continued)

Table 11.15 (continued)

Damage state	Description		Serviceability
	Anchored equipment	Unanchored equipment	
Extensive	Elephant foot buckling of tanks with loss of contents, extensive damage to pumps (cracked/sheared shafts), or extensive damage to pump building	Weld failure at base of tank with loss of contents, extensive damage to pump building, or extensive damage to pumps (cracked/sheared shafts)	Not repairable
Complete	Weld failure at base of tank with loss of contents, or extensive to complete damage to pump building	Tearing of tank wall or implosion of tank (with total loss of content), or extensive/complete damage to pump building	

Table 11.16 Description of damage states for fuel facilities subject to ground failure according to SRM-LIFE (2007)

Damage state	Description	Serviceability	
	Buried tanks (PGD related damage)		
Minor	Minor uplift (few inches) of the buried tanks or minor cracking of concrete walls	Reduced use	Operational without repair
Moderate	Damage to roof supporting columns, and considerable cracking of walls	Not usable	Operational after repairs
Extensive/ complete	Considerable uplift (more than 30 cm) of the tanks and rupture of the attached piping		Not repairable

ground failure. For the case of gravity walls subjected to ground shaking, without considering the occurrence of liquefaction, the analytically derived fragility curves of Kakderi and Pitilakis (2010) for gravity walls are proposed, since they are the only ones available for this case.

The vulnerability of cargo handling equipment can be estimated based on the HAZUS (NIBS 2004) procedure, which is actually the only available.

Finally, for fuel facilities the fragility curves that have been derived in SRM-LIFE (2007) are suggested, referring to specific typologies common in Greece. Alternatively, the generic fragility functions that are included in HAZUS (NIBS 2004) methodology can also be used.

Table 11.17 Parameters of fragility curves for fuel facilities subject to ground shaking according to HAZUS (NIBS 2004)

		Peak ground acceleration (PGA)	
Description	Damage state	Median (g)	β (log-standard deviation)
Anchored components with backup power	Minor	0.23	0.50
	Moderate	0.43	0.45
	Extensive	0.64	0.60
	Complete	1.10	0.60
Anchored components without backup power	Minor	0.12	0.55
	Moderate	0.27	0.50
	Extensive	0.64	0.60
	Complete	1.10	0.60
Unanchored components with backup power	Minor	0.10	0.55
	Moderate	0.23	0.50
	Extensive	0.48	0.60
	Complete	0.80	0.60
Unanchored components without backup power	Minor	0.09	0.50
	Moderate	0.20	0.45
	Extensive	0.48	0.60
	Complete	0.80	0.60

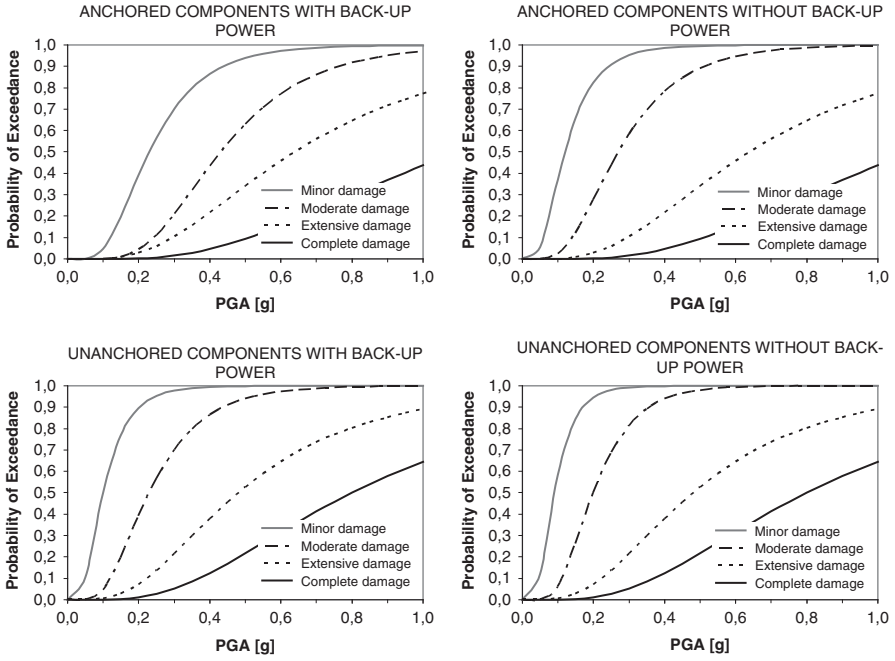

Fig. 11.6 Fragility curves for fuel facilities subject to ground shaking according to HAZUS (NIBS 2004)

References

Al-Homoud AS, Whitman RV (1999) Seismic analysis and design of rigid bridge abutments considering rotation and sliding incorporating non-linear soil behaviour. Soil Dyn Earthq Eng 18(4):247–277

Applied Technology Council (ATC) (1991) Seismic vulnerability and impact of disruption of lifelines in the Conterminous United States, ATC-25, Redwood City, CA

Bardet JP, Oka F, Sugito M, Yashima A (1995) The Great Hanshin earthquake disaster, the January 17, 1995 South Hyogo Prefecture Earthquake. Preliminary investigation report, Department of Civil Engineering, Gifu University

Borg RC, Lai CG (2007) Seismic performance, analysis and design of wharf structures: a comparison of worldwide typologies. In: 4th international conference on earthquake geotechnical engineering, p 1760

EC8 (2002) Euro code, Part 5. European Standard

EERI (1990) Loma Prieta earthquake reconnaissance report, chapter 8: lifelines. Earthq Spectra, Sup. to Vol. 6:239–338

EERI (2000) Izmit-Kocaeli earthquake reconnaissance report, chapter 13: performance of waterfront structures. Earthq Spectra, Sup. to Vol. 16:141–162

EERI (2001) Chi-Chi earthquake reconnaissance report, chapter 4: soil liquefaction. Earthq Spectra, Sup. to Vol. 17

Ferritto JM (1997) Seismic design criteria for lifelines. Naval Facilities Engineering Service Center, Technical report

Finn WDL, Wu G, Yoshida N (1992) Seismic response of sheet pile walls. In: 10th WCEE, vol 3, pp 1689–1694

Gazetas G, Dakoulas P, Dennehy K (1990) Empirical seismic design method for waterfront anchored sheet pile walls. In: ASCE specialty conference on design and perform of earth retaining structure, ASCE Geotechn. Special Publ. 25:232–250

Green RA, Ebeling RM (2002) Seismic analysis of cantilever retaining walls, phase I. ERDC/ITL TR-02-3, Information technology laboratory, US army corps of engineering, Engineering Research and Development Center, Vicksburg, MS

Green RA, Olgun CG, Cameron WI (2008) Response and modelling of cantilever retaining walls subjected to seismic motions. Comput Aided Civil Infrastruct Eng 23(4):309–322

Iai S, Kameoka T (1993) Finite element analysis of earthquake induced damage to anchored sheet pile quay walls. Soils Found 33(1):71–91

Ichii K (2003) Application of performance-based seismic design concept for caisson-type quay walls. Ph.D. dissertation, Kyoto University

Ichii K (2004) Fragility curves for gravity-type quay walls based on effective stress analyses. In: 13th WCEE, Vancouver, BC

Inatomi T, Zen K et al (1997) Damage to port and port-related facilities by the 1995 Hyogoken-Nanbu earthquake. Technical note of the Port and Harbour Research Institute, p 857

International Navigation Association (PIANC) – Chairman: Iai S (2001) Seismic design guidelines for port structures, Bakelma, 474 p

Kakderi K, Pitilakis K (2010) Seismic analysis and fragility curves of gravity waterfront structures. In: Fifth international conference on recent advances in geotechnical earthquake engineering and soil dynamics and symposium in Honour of Prof. I. M. Idriss, 6.04a

Kakderi K, Raptakis D, Argyroudis S, Alexoudi M, Pitilakis K (2006) Seismic response and vulnerability assessment of Quaywalls. The case of Lefkas. In: 5th national conference of geotechnical and environmental engineering (in Greek)

Kappos A, Panagopoulos G, Panagiotopoulos G, Penelis G (2006) A hybrid method for the vulnerability assessment of RC and URM buildings. Bull Earthq Eng 4(4):391–413

Ko Y-Y, Yang H-H, Chen C-H (2010) Seismic fragility analysis for sheet pile wharves – case study of the Hualien harbor in Taiwan. In: Fifth international conference on recent advances in

geotechnical earthquake engineering and soil dynamics and symposium in Honor of Prof. I.M. Idriss, 6.05a

Li Destri Nicosia G (2008) On seismic design and advanced numerical modelling of flexible cantilever walls under earthquake loading. Master thesis, Istituto Universitario di Studi Superiori di Pavia, Italy

Margaris B, Papaioannou Ch, Theodulidis N, Savaidis A, Anastasiadis A, Klimis N, Makra K, Demosthenous M, Karakostas Ch, Lekidis V, Makarios T, Salonikios T, Sous I, Carydis P, Lekkas E, Lozios S, Skourtsos E, Danamos G (2003) Preliminary observations on the August 14, 2003, Lefkada Island (Western Greece) Earthquake. EERI Special Earthquake Report: 1–12, Joint report by Institute of Engineering Seismology and Earthquake Engineering, National Technical University of Athens

Na UJ, Shinozuka M (2009) Simulation-based seismic loss estimation of seaport transportation system. Reliab Eng Syst Saf 94(3):722–731

Na UJ, Chaudhuri SR, Shinozuka M (2008) Probabilistic assessment for seismic performance of port structures. Soil Dyn Earthq Eng 28(2):147–158

Na UJ, Chaudhuri SR, Shinozuka M (2009a) Effects of spatial variation of soil properties on seismic performance of port structures. Soil Dyn Earthq Eng 29(3):537–545

Na UJ, Chaudhuri SR, Shinozuka M (2009b) Performance evaluation of pile supported Wharf under seismic loading. In: Tang A, Werner S (eds) 2009 TCLEE conference: lifeline earthquake engineering in a multihazard environment, ASCE, pp 1032–1041

National Institute of Building Sciences (NIBS) (2004) HAZUS-MH: users's manual and technical manuals. Report prepared for the FEMA

Newmark N (1965) Effects of earthquakes on dams and embankments. Geotechnique 15(2):139–160

OCDI (2002) Technical standards and commentaries for port and harbour facilities in Japan. The overseas coastal area devel. Institute of Japan, 600 p

Pachakis D, Kiremidjian AS (2004) Estimation of downtime-related revenue losses in seaports following scenario earthquakes. Earth Spectra 20(2):427–449

Pasquali R, Lai CG, Corigliano M (2008) Seismic analysis and design of Blockwork-Wharf structures. In: 14th WCEE, Beijing, China

Pathmanathan R, Franchin P, Lai C, Pinto P (2007) Numerical modelling of seismic response of cantilever earth-retaining structures. In: 4th international conference on earthquake geotechnical engineering, p 1269

Pitilakis K, Moutsakis A (1989) Seismic analysis and behaviour of gravity retaining walls – the case of Kalamata harbour quay wall. Soils Found 29(1):1–17

Psarropoulos PN, Klonaris G, Gazetas G (2005) Seismic earth pressures on rigid and flexible retaining walls. J Soil Dyn Earthq Eng 25(7–10):795–809

Richards RJ, Elms DG (1979) Seismic behavior of gravity retaining walls. J Geotechn Eng Div, Am Soc Civil Eng 105(GT4):449–464

Soderberg E, Hsieh J, Dix A (2009) Seismic guidelines for container cranes. In: 2009 TCLEE conference, lifeline earthquake engineering in a multihazard environment, Oakland, CA

SRM-LIFE (2007) Development of a global methodology for the vulnerability assessment and risk management of lifelines, infrastructures and critical facilities. Application to the metropolitan area of Thessaloniki. Research project, G. Secretariat for Research and Techniques, Greece

Steedman RS, Zeng X (1990) The influence of phase on the calculation of pseudo-static earth pressure on a retaining wall. Geotechnique 40(1):103–112

Uwabe T (1983) Estimation of earthquake damage deformation and cost of quaywalls based on earthquake damage records. Technical note of port and harbour Research Institute, 197 p

Werner SD (1995) Seismic performance and risk reduction for ports and air transportation systems. Critical issues and state-of-the-art in lifeline earthquake engineering. TCLEE monograph N°7. ASCE:57–69

Werner SD (1998) Seismic guidelines for ports. TCLEE Monograph N°12, ASCE, 366 p

Werner SD, Taylor CE, Ferritto JM (1999) Seismic risk reduction planning for ports lifelines. In: 5th U.S. conference on lifeline earthquake engineering, TCLEE, Monograph No. 16

Whitman RV (1990) Seismic design and behavior of gravity retaining walls. In: Special conference on design and construction of earth retaining structures, ASCE, New York. Design and construction of earth retaining structures, ASCE, pp 817–842

Chapter 12
Component Fragilities and System Performance of Health Care Facilities

Alessio Lupoi, Francesco Cavalieri, and Paolo Franchin

Abstract Hospitals belong to the so-called "complex-social" systems since they depend on several components of different nature to function properly and they provide a societal service to citizens. The basic components of a hospital are: the staff, the organization and the facility. They jointly "contribute" to provide medical care to patients. This chapter focus on the seismic assessment of the facility. A hospital has to be capable of providing medical after the occurrence of a major earthquake; hence the facility target performance is set as operational. Such a performance depends on the response of both structural and non-structural elements. Fragility curves for "typical" non-structural elements are provided. A probabilistic-based procedure for the evaluation of the fragility curve of the facility is then derived. Finally, an index adequate to measure the performance of the hospital under emergency condition is proposed.

12.1 Seismic Performance of Hospital Systems: A Summary

12.1.1 System Components

Hospitals play a fundamental *societal* function of assistance to citizens in everyday life but also to victims of natural disasters. In fact, hospitals have a lead role in facing an emergency condition due to a mass casualty event.

A. Lupoi (✉) • F. Cavalieri • P. Franchin
Department of Structural and Geotechnical Engineering, University of Rome 'La Sapienza', Via Gramsci 53, 00197 Rome, Italy
e-mail: alessio.lupoi@uniroma1.it; francesco.cavalieri@uniroma1.it; paolo.franchin@uniroma1.it

K. Pitilakis et al. (eds.), *SYNER-G: Typology Definition and Fragility Functions for Physical Elements at Seismic Risk*, Geotechnical, Geological and Earthquake Engineering 27, DOI 10.1007/978-94-007-7872-6_12,

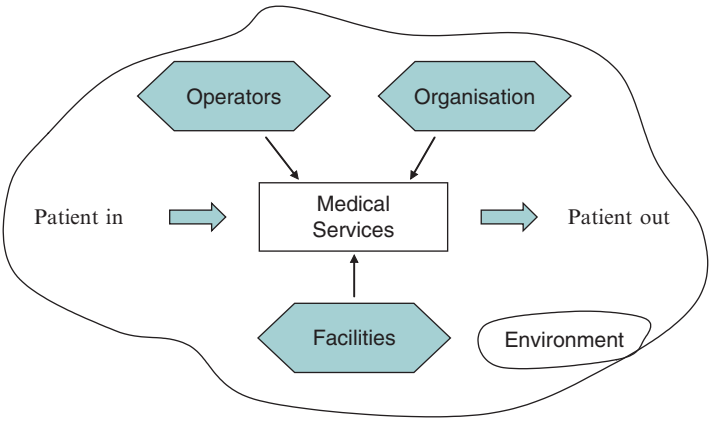

Fig. 12.1 System taxonomy of a hospital

From an engineering point of view, a hospital is a very complex system made of many components, of different nature, that jointly provide an output, namely, the medical services.

The taxonomy proposed by Bea (2003) for the so-called "complex-social" systems may be applied to hospitals as well. It identifies five major components: procedures, organization, operators, physical (structures and hardware) and environment. This taxonomy applied to hospitals is illustrated by the figure above (Fig. 12.1).

At the core of the system there are the *medical services*, which consist of standardized procedures established to guarantee an adequate treatment of patients. The medical services are delivered to patients by a joint contribution of the following three "active" components of the system:

- The *facility* (physical component), where the medical services are delivered. The physical component of a hospital system consists of *structural elements* and *non-structural elements* (architectural elements, basic contents and equipment). While the former are critical to preserve the life-safety of the building occupants, the latter are fundamental to preserve the hospital functionality.
- The *operators*, which are the doctors, nurses and in general whoever plays an active role in providing medical care;
- The *organisation*, which is responsible of setting up the adequate conditions so that the medical services can be delivered. In general, this is up to the hospital management through the development, the implementation and the supervision of the standardized procedures.

The *environment* includes all external influences to the functioning of a hospital system, which encompasses diverse factors from cultural background to soil properties. It acts on all the "active" components both directly, through characteristics such as accessibility, soil conditions, etc., and indirectly, through social context, economic pressures, standards, educational system, etc.

The assessment of the seismic performance of hospitals is an extremely complex task, significantly more demanding with respect to the case of, for example, residential buildings or bridges. A system performance measure has to be defined first, and then the contributions of all components, and their interactions, have to be appropriately accounted for the proper evaluation of the system performance.

12.1.2 Performance of Hospitals Under Emergency Conditions

An ad-hoc performance measure to evaluate the seismic response of a hospital has been derived on the basis of the analysis of the hospital's functioning under emergency condition (Lupoi et al. 2008).

The first result has been the identification of the sub-set of medical services that have to stay operative after a seismic event in order to guarantee the adequate treatment of patients and victims. They are classified as *essential* medical services and typically include: Emergency department, Operating theatres, Intensive care unit, Diagnostics, Blood bank; Hemodialysis, Urology; Neonatology, Gynecology, Obstetrics, Pediatrics, Laboratory, Pharmacy. In addition, one should carefully take into account the circumstance that the hospital emergency layout (i.e. the location of medical services) may differ from the everyday layout.

Previous experiences have shown that surgery is the bottleneck of medical care services after a mass-casualty event. Therefore, the number of surgical treatments that can be operated has been selected as the seismic performance measure of a hospital. While the number of functioning operating theatres is of primarily importance, the proper response of all other components is required to actually perform a surgery.

The above considerations have led to the development of a proposed performance measure called "Hospital Treatment Capacity", *HTC*, as defined by the following expression:

$$HTC = \alpha \cdot \beta \cdot \frac{\gamma_1 \cdot \gamma_2}{t_m}, \tag{12.1}$$

where: α accounts for the efficiency of the *organizational* component, β accounts for the quality, training and preparation of the operators (*human* component), t_m is the mean duration of a surgical operation, γ_1 is the number of operating theatres which remain operative after the hazardous event, γ_2 is a Boolean function equal to 1 if the (hospital) system "survives" and nil otherwise. The survival condition is defined as follows:

(a) the "operational" limit state has to be satisfied for the areas of the building devoted to the essential medical services;
(b) the "safeguard of human life" limit state has to be satisfied for all other areas.

Condition (a) depends on the response of both structural and non-structural elements, while condition (b) depends on the response of structural elements only.

At the current stage of development, the effects related to the *organizational* and the *human* components are empirically estimated by expert judgment, as illustrated in Sects. 12.3.1 and 12.3.2. Those relative to the *facility* are instead analytically evaluated by engineering-based method, which are illustrated in Sect. 12.2.

The demand on hospitals comparable to the *HTC* is the number of victims that required hospitalization. This figure largely depends on the area exposed to the earthquake. Types of construction, population density, population age, time of the day, medical facilities in the area, damage to road infrastructure, etc., are all influencing factors. The generic expression for the *Hospital Treatment Demand*, HTD, is then:

$$HTD = f(\delta) \tag{12.2}$$

where δ accounts for the *environment* component. It is made explicit in Sect. 12.3.3 by means of casualty models and epidemiologic studies.

12.2 Physical Component

12.2.1 Description of Elements

The physical component includes a large variety of elements different in nature and scope such as: structures, installations, furniture, equipment, etc. Elements are typically subdivided between structural and non-structural ones.

The structural elements are sub-systems, elements, or components that are part of the load-bearing system, such as beams, slabs, columns, joints and walls.

The non-structural elements are sub-systems, elements, or components that are not part of the load-bearing system, but nevertheless are part of the building dynamic environment caused by the earthquake. Typical classification subdivides the non-structural elements into three categories: *architectural* elements, *basic installations* and *equipment/contents*. The sub-elements of each category are listed in Table 12.1.

While the response of structural elements under the earthquake action has been the object of extensive studies in the past three decades, and well-established capacity models are now available, the situation is quite the opposite for the non-structural ones. In fact, few capacity models are available for a limited number of non-structural elements and these are all characterised by large uncertainties (Shinozuka 2001; Grigoriu and Waisman 1988).

12.2.2 Fault Tree Analysis of Physical Component

The relationship between the state of the elements and the state of the whole system is expressed by a fault-tree.

Table 12.1 Classification of sensitive non-structural elements in hospital systems

Architectural	Basic installations	Building content (equipment/ furnishing)
Stairs	Power system	Mechanical and electrical equipment
Exterior and partition walls	Water system	Shelves and rack systems
Doors	HVAC system	Kitchen appliances
Parapets and cornices	Medical gases	Vending machines
Ceilings	Fire protection	Medical and laboratory equipment
Windows	Communication system (internal and external)	Medicine containers
Cladding	Conveying system	...
...	Ductwork and piping systems	
	Lighting system	
	...	

The fault tree analysis schematically depicts the components and their functional interrelationship. A basic combination of components consists of a tree-like relationship where the top component is related to its contributing components by "AND" and "OR" gates. An "AND" gate means that the top component is functional (survival state) if all the contributing components are functional (series arrangement), whereas an "OR" gate indicates that the top component is functional if at least one of the contributing components is functional (parallel arrangement).

Since the fault-tree is hospital dependent, it has to be customized on a case-by-case basis. The starting point is the identification of areas of the hospital that will house the *essential* medical services in the emergency configuration. In fact, the emergency layout (i.e. spatial location of the medical services) of the hospital may differ from the everyday one. The required performance for these areas is the Operational Limit State; therefore, one has to evaluate the response of both structural and non-structural elements. For the remaining areas, a Life Safety performance level is required; the assessment is limited to structural elements.

A preliminary examination of the vulnerable elements is recommended in order to reduce as much as possible the branches of the system fault tree. For example, the principle of hierarchy of resistance may be employed to check the presence of a "week element" between columns, beams and joints; well-anchored non-structural elements may be eliminated from the fault-tree; etc.

The fault-tree analysis provides a failure/survival response on the state of the hospital: in the case of survival, $\gamma_2 = 1$ in Eq. (12.1); otherwise, $\gamma_2 = 0$.

12.2.3 Capacity Models for Assessment Purposes

Capacity and demand have to be expressed in terms of local response quantities well-correlated to damage in order to adequately represent the actual state of an

element. The selection of capacity models is a delicate task, since as stated in (LESSLOSS 2005) "capacity models developed and used for assessment purposes bear a conceptual difference with respect to those used in design. The latter generally tend to be simple of use and approximated in a conservative way, which makes them unsuitable for a consistent evaluation of risk. Risk assessment requires explicit consideration of all relevant uncertainties, aleatoric and epistemic, and probabilistic models that are unbiased. A conservative model does not comply with this requirement."

Capacity models may be derived on *empirical*, *theoretical* or *judgmental* basis. *Empirical* models are based on the statistical analysis of the performance of the element during past earthquakes and/or experimental tests. *Theoretical* models are based on analytical simulations (static and dynamic analysis) of a mechanical model of the element. *Judgmental* models represent the opinion of experts.

12.2.4 Reinforce Concrete Structural Elements

The structural failure of a RC building may occur due to the *local* collapse of a single element (beams, columns and joints) or due to the formation of a *global* mechanism (more elements involved, such as "weak-storey").

The response quantities are force-based or displacement/deformation-based: the former are employed to evaluate the state of elements with respect to the activation of force-controlled failure mechanisms, such as shear failure; the latter are used to evaluate the element's state with respect to displacement-related mechanisms, such as inter-storey drift ratios or chord-rotations.

The generic fault tree for RC structures is then represented in Fig. 12.2.

A vast literature is available on capacity models for RC structural elements. Those included in the Eurocode 8-Part3 are recommended for the estimation of member's shear strength. Deformation and drift capacity are described in the following sections. The Kowalsky and Priestley (2000) shear-strength model for *beams, columns and walls* as revised in fib (2003) can be employed for the shear capacity. The ultimate drift capacity is modelled after Panagiotakos and Fardis (2001). The well-known expressions of the mentioned capacity models are omitted for brevity.

Since the capacity formulas are generally based on relatively weak mechanical basis, eventually integrated with empirical knowledge, a model-error term accounting for scatter and (if necessary) for bias is introduced:

$$C_i(\mathbf{x}, \varepsilon_C) = \overline{C}_i(\mathbf{x})\varepsilon_{C_i}$$

where $\overline{C}_i(\mathbf{x})$ is the value obtained by the semi-empirical formulas available in the literature. The type of distribution of ε_{Ci} is based on expert judgment.

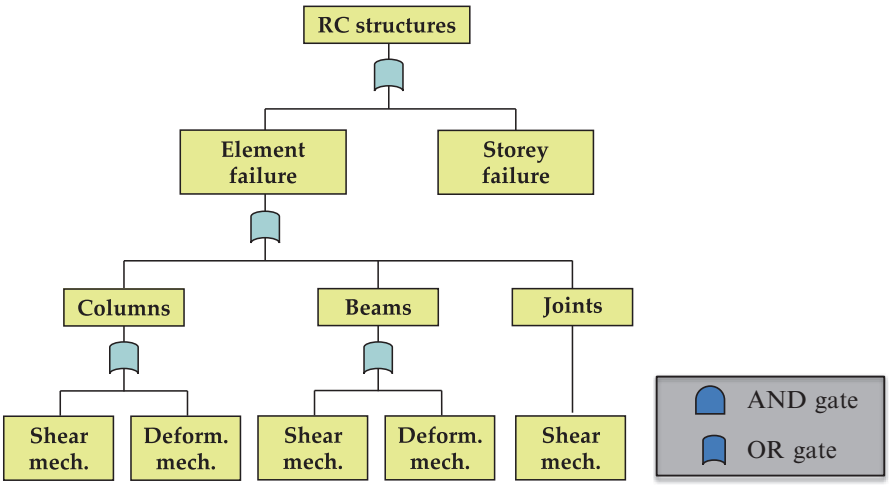

Fig. 12.2 Generic fault tree of structural failure for RC elements

12.2.5 Non-structural Elements

The response of *non-structural* elements is governed by one of the following parameters:

- local acceleration, which may cause the element sliding or overturning;
- structural deformation;
- relative movements (drift) between adjacent or connected structures.

In general, a *restrained* non-structural element is drift-sensitive, while a *free* non-structural element is acceleration-sensitive. Elements that provide a continuous link across a separation joint or between two different structures are sensitive to differential displacement.

Elements that hang from floor, such as many mechanical and electrical components, ceilings and contents, are examples of acceleration sensitive elements; glazing, doors and partition walls, which are tightly locked into the structure, are examples of structural deformation sensitive elements. Some components are sensitive to both inter-storey drift and peak floor acceleration. Elevators have rails, door and other components that are damaged primarily by inter-storey drift ratios, while others, such as the motor and counterweights, are damaged as a result of floor accelerations.

Items that are connected to objects with independent movement, i.e. utilities extended across the separation joints, should be capable of providing functional continuity and therefore are sensitive to differential displacements.

The generic fault tree for non-structural elements is represented in Fig. 12.3.

The definition of capacity models for non-structural elements is not straightforward; although the general working principles are the same for all elements, each

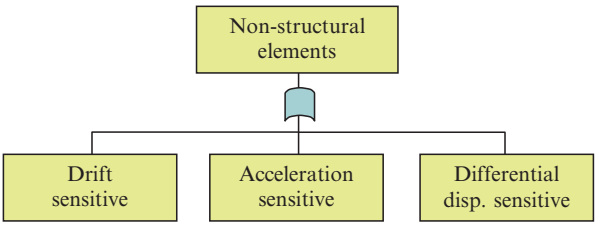

Fig. 12.3 Non-structural element classification by failure mechanism

Table 12.2 Median drift capacity (%) for non-structural elements

Slight	Moderate	Extensive	Complete
0.4	0.8	2.5	5.0

one has its own unique adaptation. For example, the element-structure interface can take different forms: elements can be fixed to the floor, supported by a layer of interposed material intended to isolate them from the floor motion, or placed securely in a rack fixed to the floor and wall. The importance of such details is pointed out in Porter et al. (1993).

Since the accurate modelling for all non-structural elements is not feasible in a real application, the strategy is to develop *specific* capacity models for critical elements only, while employing *generic* capacity models for the others.

12.2.6 Generic Capacity Model for Drift-Sensitive Elements

The median values of the capacity for a generic drift-sensitive non-structural element are reported in Table 12.2 for different states of increasing damage (NIBS 2004). The threshold for the operational limit state is "slight damage".

The dispersion of the damage thresholds is evaluated as the sum of two contributes:

- uncertainty in the damage state threshold of non-structural elements, $\beta_1 = 0.5$;
- variability in the capacity properties of the non-structural elements, $\beta_2 = 0.2$.

The resulting error term is thus described by a lognormal random variable with unit median and coefficient of variation $\beta = \beta_1 + \beta_2 = 0.7$. The resulting fragility curves are shown in Fig. 12.4.

12.2.7 Generic Capacity Model for Acceleration-Sensitive Elements

The median values of the capacity for an acceleration-sensitive non-structural element as a function of the type of seismic prescriptions enforced at the time of

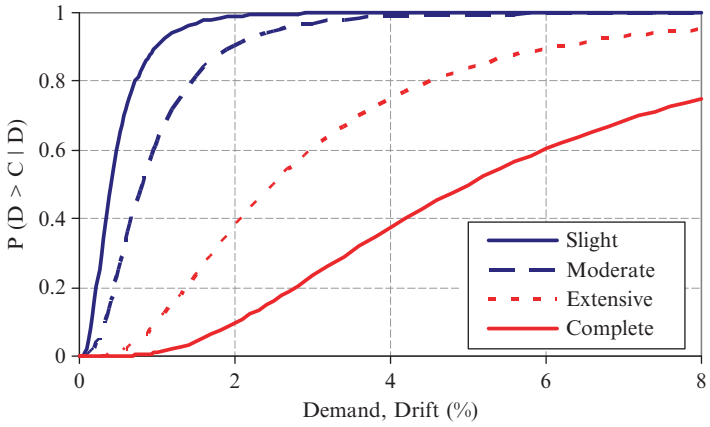

Fig. 12.4 Fragility curves for drift-sensitive non-structural elements

Table 12.3 Peak floor acceleration capacity (in *g*) for non-structural elements

Seismic design level	Slight	Moderate	Extensive	Complete
High-code	0.45	0.90	1.80	3.60
Moderate-code	0.375	0.75	1.50	3.00
Low-code	0.30	0.60	1.20	2.40
Pre-code	0.30	0.60	1.20	2.40

the design (denoted as seismic design level) are given for different states of increasing damage in Table 12.3 (NIBS 2004).

These values have been derived for the "Special Buildings" category, characterized by increased anchorage strength of non-structural elements. For a "General Building", where no special provisions for anchoring have been enforced, the values in Table 12.3 have to be divided by a factor of 1.5.

The operational limit state corresponds to the "slight damage" level.

The dispersion of each damage threshold can be evaluated as the sum of the following two contributions:

- uncertainty in the damage state threshold of non-structural elements, $\beta_1 = 0.6$;
- variability in capacity properties of the non-structural elements, $\beta_2 = 0.2$.

The resulting error term is thus described by a lognormal random variable with unit median and coefficient of variation $\beta = \beta_1 + \beta_2 = 0.8$.

The fragility curves for a Special Building designed according to a High-Code are shown in Fig. 12.5.

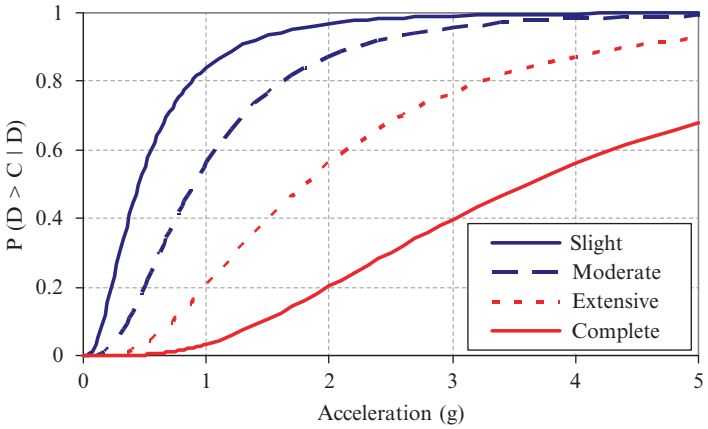

Fig. 12.5 Fragility curves for acceleration-sensitive non-structural elements (High-code)

12.2.8 Non-structural Elements: Architectural

The architectural elements are typically built-in components that form part of the building. The elements that have jeopardised the functionality of several hospitals in past earthquakes are:

- interior and exterior walls;
- ceilings;
- windows, glasses and doors.

Walls are made of masonry or other materials and are typically stiffer and more brittle than the structural frame; therefore, they tend to develop cracks when the building is subjected to earthquake shaking. Usually, the crack growth is initiated at (the corner of) an opening in the wall. The failure of either interior or exterior walls can be attributed to (a) excessive flexural out-of-plane stresses induced by floor accelerations or (b) excessive in-plane shear stresses induced by inter-storey drifts imposed on the building structure. The seismic performance of walls has been studied among others by Freeman (1977), Rihal (1982) and Cohen (1995).

Ceilings are non-structural elements that are sensitive to both deformation and acceleration. The deformation of the floor slabs can cause horizontal distortion and the deformation of the main structure, leading to possible loss of support and fall of the ceiling. Gates and McGavin (1998) point out the interaction between the ceiling system and both the fire sprinkler system and the lighting fixtures. References to this type of non-structural elements are, among others, Eidenger and Goettel (1998), Yao (2000), Badillo et al. (2003) and Gann et al. (2005).

Elements that are attached to the structure or to non-structural walls, such as doors, windows and glasses, can twist and buckle when they are subjected to large deformations. Most often, deformation of the structural frame can jam the element (as in the case of doors) or cause failure (as in the case of glasses) due to the

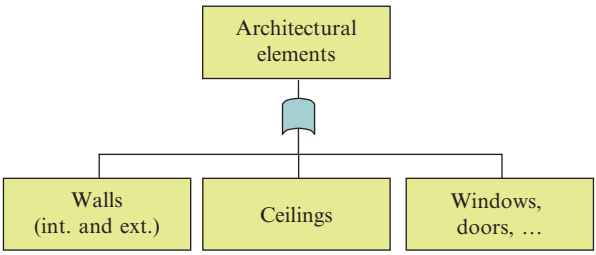

Fig. 12.6 Generic fault tree for architectural non-structural elements

Table 12.4 Probabilistic characterisation of capacity of architectural elements

Object	Demand	Distr.	Mean	CoV	References
Walls	Drift	LN	0.75 %	0.23	Rihal (1982)
Glazing, doors, windows, etc.	Drift	LN	4.60 %	0.33	Behr and Worrell (1998)
Ceilings	Acceleration	LN	0.90 g	0.30	Eidenger and Goettel (1998) and Badillo et al. (2003)

LN lognormal

inadequate edge clearance around the item (door, glass, windows, etc.). The performance of glass doors, windows and glazing during earthquakes is highly dependent on the deformation capacity provided to the brittle material with respect to it supporting frame. Failure of this kind of elements causes not only a problem for the functionality but could also produce injuries. Studies on this category have been conducted, among others, by Bouwkamp and Meehan (1960) and by Behr and Worrell (1998).

The generic fault tree for architectural elements is illustrated in Fig. 12.6.

The behavior of architectural elements has been extensively studied and is adequately understood. Nevertheless, well-defined limit state equations are not available due to the large variety of these elements. For this reason capacities are expressed as function of structural response quantities such as interstorey drift and floor acceleration.

The capacity parameters given in Table 12.4 refer to a moderate damage state of the components, which is the level beyond which functionality of the building is compromised.

12.2.9 Non-structural Elements: Building Content

Building contents include furniture, medical and industrial equipment, general supplies, shelves, etc. Equipment and supplies are essential for the functioning of the facility and for protecting the lives of its occupants, and yet they can represent a danger in case of an earthquake.

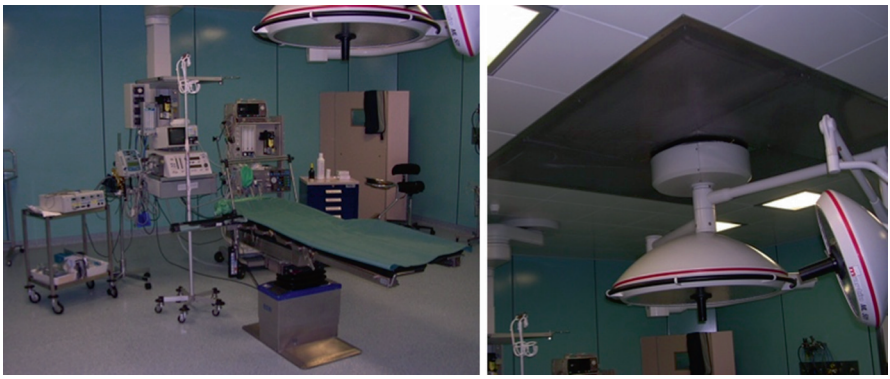

Fig. 12.7 Operating table and scialytic lamp

Examples of equipment and anchorage are shown in Fig. 12.7 for an operating theatre and a radiology room. A list of essential equipment and supplies for life-support of patients and for emergency care after an earthquake is given in Table 12.5.

In practice, however, the on-site verification of the anchorages of all the contents of a hospital is practically unfeasible, both for the excessive number of elements and for the limited possibility of investigation. As a result, it is customary to assume for the assessment that all items susceptible to moving are properly anchored and, consequently, their vulnerability is not explicitly considered in the analysis. Alternatively, a fragility curve based on engineering judgment may be derived on the basis of field investigation.

12.2.10 Non-structural Elements: Basic Installations

Across all occupancies, including essential facilities, the most disruptive kind of non-structural damage is the breakage of water lines inside buildings, including fire sprinklers, domestic water, and chilled-water systems. Leaked water can travel quickly throughout a building and disrupt its functionality.

Second in significance is failure of emergency power systems. The power outage is usually so extensive that reliable backup power is necessary for essential facilities to operate. Others frequently damaged installations, among those essential for the functioning of hospitals, are the conveying and the medical gas systems.

Each of such systems can be subdivided in two main components:

(a) **Generation:** it can be provided by an internal or an external source. However, in an emergency situation, all the essential systems have to be complemented with an internal source. Examples of internal sources are electrical generator,

Table 12.5 Essential equipment and supplies

Building content	Description
Essential diagnostic equipment:	Phonendoscopes, tensiometers, thermometers, otoscopes, ophthalmoscopes, reflex hammers and flashlights should always be available
Mobile carts	Carts used to move special equipment for crisis intervention are particularly important for saving lives and storing supplies. Objects must be secured to the trolley. When not in use the trolleys must have their brakes on and be parked against dividing walls
Respirators and suction equipment	This equipment should be secured in such a way that they do not be disconnected from the patients
Hazardous substances	Storage shelves containing medicines or chemicals, if overturned, can constitute a hazard by virtue of their toxicity, both in liquid and in gas form. On many occasions fires start by chemical action, overturned gas cylinders or ruptures in gas supply lines
Heavy articles	Heavy articles such as televisions, X-ray equipment, ceiling lamps, sub-stations can pose a threat ore be damaged if they fall
Filing cabinets	They store data and a large amount of information necessary for patient treatment
Computers	They must be well secured to desks to prevent them from falling and losing their function. Computer services should be backed up by the emergency power plant
Refrigerators	Particularly important for the blood bank, medicine and food refrigerator to maintain continuous cooling. They should be connected to the emergency power supply

water tank and gas tank. Their typical mode of failure is the damage of anchorages.

(b) **Distribution:** it includes pipes for water, wastewater, fuel, gas, and electrical conduits (lines) that run underground or above grade, inside and outside the building. Damage to above ground transmission lines typically occurs along unsupported line sections when lines crack, leak, or fail. Damage to underground transmission lines usually occurs in areas of soil failure where the line sections cannot accommodate soil movements or differential settlements. Damage can also occur when other equipment shifts or falls onto the line, or if a piece of equipment the line is connected to suffers damage. Lines that run across a seismic joint without an expansion joint may suffer damage to their connections or get torn apart. It is noted that electric power is necessary for the proper functioning of the distribution lines.

The generic fault tree for a basic installation is represented in Fig. 12.8.

12.2.11 Medical Gas

The medical gas system of a hospital typically consists of tanks and cylinders of the medical gases (oxygen, nitrogen, etc.), the distribution lines (pipes) and several

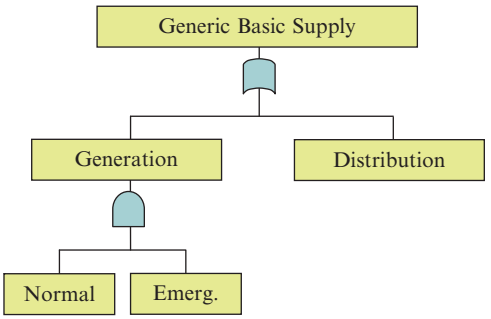

Fig. 12.8 Fault tree of a generic basic supply

other pieces of equipment, such as, for example, electric pumps, necessary to the normal functioning. The cylinders and the auxiliary equipments are usually located in a large room at the base floor of the building.

Examples for cylinders and the auxiliary equipment are shown in Fig. 12.9; for this case, a proper anchorage is noted. Examples for not properly anchored oxygen and nitrogen cylinders are shown in Fig. 12.10. A piping system and an oxygen bottle (tank) are shown in Fig. 12.11. It can be noted that the piping system is not provided by flexible couplings.

The generic fault tree for the medical gas system is shown in Fig. 12.12.

The probabilistic description of the vulnerable components for a medical gas system is given in Table 12.6.

12.2.12 Power System

The power system of a hospital building is typically composed of:

- MV-LV (Medium Voltage – Low Voltage) transformation station;
- Uninterruptible Power System (UPS);
- Emergency Power Generator (EPG);
- Transmission lines;
- Distribution stations.

The MV-LV transformation station is usually not included in the vulnerability analysis, since, according to the requirements of the majority of national regulations, a hospital should be able to generate power by means of the UPS and EPG systems for a number of days.

A UPS system is typically composed of battery-chargers, inverters, and batteries. By far the most vulnerable component is the battery system located in several cabinets, which may not be anchored to the floor. An example is shown in Fig. 12.13. Battery failure could occur due to overturning or to impact of adjacent cabinets.

Fig. 12.9 Examples for anchorages of different equipment of medical gases network

The EPG system typically consists of engines able to generate the necessary power for the functioning of all the essential equipment and furniture. Examples of EPG engines is shown in Fig. 12.14; a detail of the engine anchorage in shown in Fig. 12.15. The weakest components of EPG system are the fuel diesel conduits, which usually are not provided by flexible connections.

The transmission lines of the power network can be generally considered not vulnerable.

The distribution station, including the switchboard panel (Fig. 12.16), may be a cause of system failure if not properly anchored.

The generic fault tree of the power system is illustrated in Fig. 12.17.

The probabilistic description of the capacity of the vulnerable components is given in Table 12.7.

Fig. 12.10 Example of oxygen cylinders – detail of anchorage

Fig. 12.11 Examples for distribution lines (*left*) and for oxygen bottle tank (*right*)

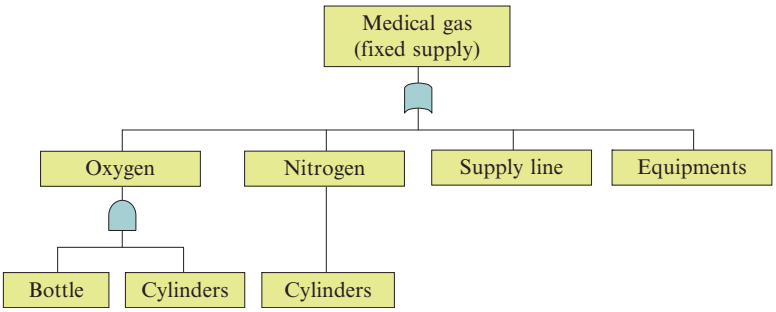

Fig. 12.12 Fault tree of medical gases network

Table 12.6 Probabilistic characterization of capacity of medical gas system

Object	Demand	Distr.	Mean	CoV	References
Cylinders	Acceleration	LN	0.50 g	0.25	Expert judgment
Pipes	Drift	LN	0.90 %	0.25	Kuwata and Takada (2003)

Fig. 12.13 Example of UPS: Battery cabinet

12.2.13 Water System

The water system of a hospital typically consists of the supplies, the distribution network (piping) and several equipment such as pumps and boilers. The emergency water supply consists of buried tanks capable of guaranteeing autonomy for a number of days. The equipment should be well anchored and the piping should be provided with flexible connections.

The generic fault tree of the water system is shown in Fig. 12.18.

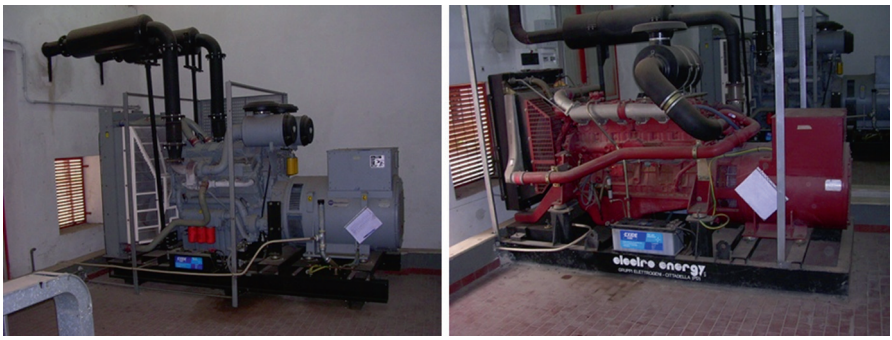

Fig. 12.14 Example of EPG engines

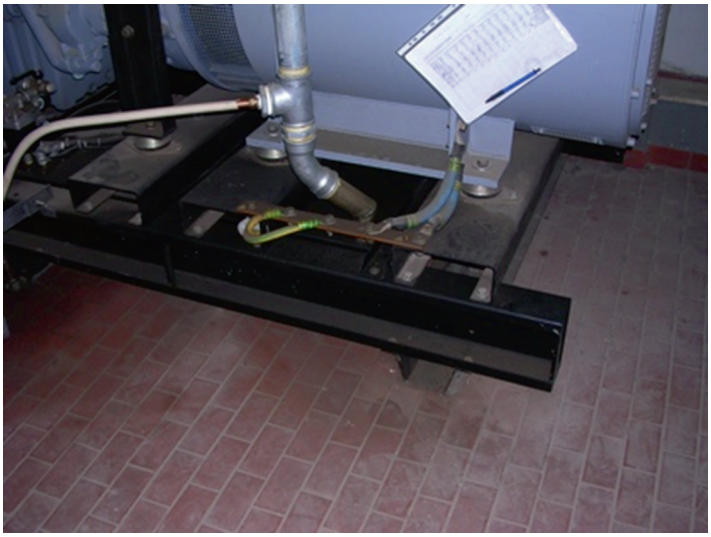

Fig. 12.15 Detail for the anchorage of an EPG engine

Past experiences indicate that pipelines are the real vulnerable component of the water system. An example of piping system is shown in Fig. 12.19. The probabilistic description of its capacity is given in Table 12.8.

12.2.14 Conveying System

The performance of elevators in past earthquakes has been satisfactory from the viewpoint of safeguarding passengers. However, damages to their components have often caused functional failure of the system. It is worth noting that the failure of the

Fig. 12.16 Example of general switchboard panel

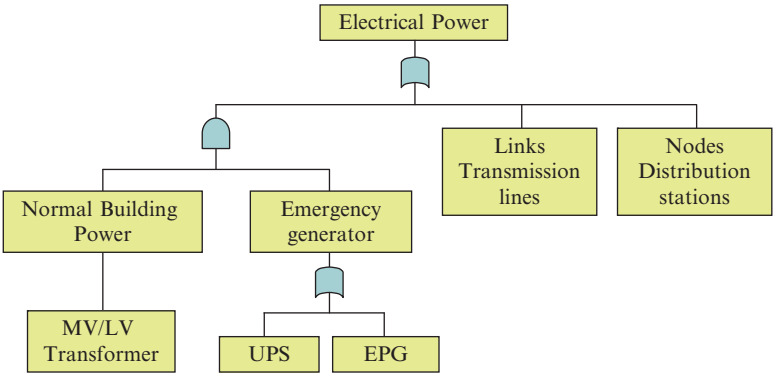

Fig. 12.17 Fault tree of electric power system

Table 12.7 Probabilistic characterization of capacity of electric power system

Object	Demand	Distr.	Mean	CoV	References
Diesel conduits	Drift	LN	0.90 %	0.25	Kuwata and Takada (2003)
Battery cabinet	Acceleration	LN	0.52 g	0.62	Swan and Kassawara (1998)
General switchboard panel	Acceleration	LN	1.12 g	0.64	Swan and Kassawara (1998)
Floor distribution panel	Acceleration	LN	1.75 g	0.68	Swan and Kassawara (1998)

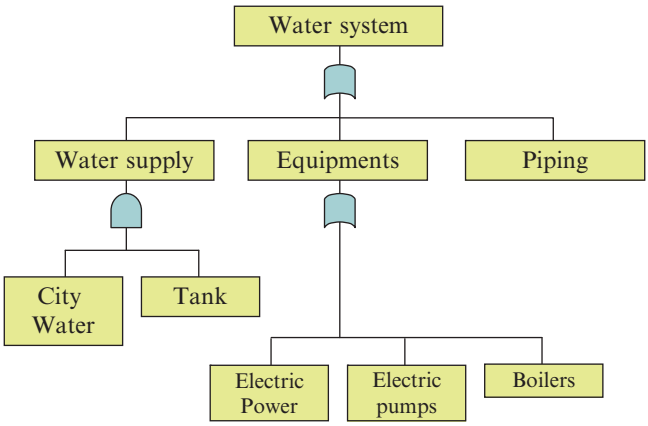

Fig. 12.18 Fault tree of water system

Fig. 12.19 Piping of water system

Table 12.8 Probabilistic characterization of capacity of water system

Object	Demand	Distr.	Mean	CoV	References
Piping	Drift	LN	0.90 %	0.25	Kuwata and Takada (2003)

vertical circulation systems (elevators, escalators and stairs) is particularly relevant since in practice it fatally impairs the functionality of the hospital.

Damage at the elevator systems typically occurs to mechanical components rather than the car itself. Guide rails, counterweights, controllers, machines,

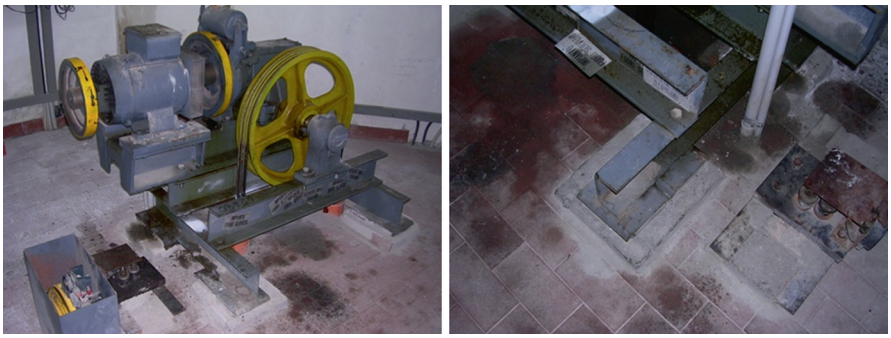

Fig. 12.20 Example of elevator's guide rail and anchorages

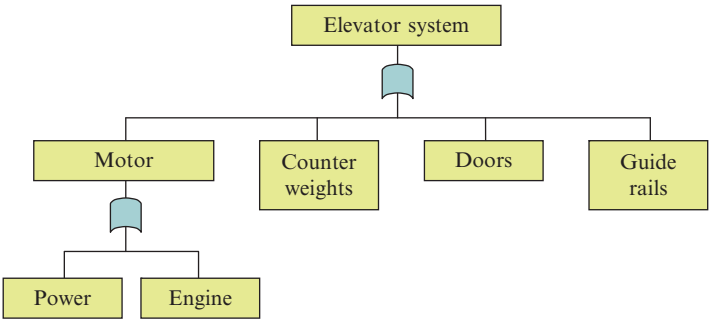

Fig. 12.21 Fault tree of elevators

Table 12.9 Probabilistic characterisation of the capacity of the elevator system

Object	Demand	Distr.	Mean	CoV	Reference
Elevator (global criteria)	PGA	LN	0.20 g	0.30	Nuti et al. (1999)

motor generators, stabilisers, and their supports and anchorages were the most damaged components during past earthquakes (Suarez and Singh 2000). An example of well-anchored engine is shown in Fig. 12.20.

The generic fault tree for elevators is shown in Fig. 12.21.

The capacities for these components are difficult to assess; therefore, the global criterion by Nuti et al. (1999) has been adopted. The probabilistic model of the elevator capacity is given in Table 12.9. The functionality of the whole conveying system of a hospital is jeopardised if more than half of the elevators fails.

12.2.15 Example of Fault Tree for a Hospital Facility

The generic fault-trees of the various elements illustrated in previous sections have to be appropriately assembled to build up the system fault-tree of the whole physical component.

The fault-tree developed for a RC hospital located in Italy is illustrated in Fig. 12.22, as an example. It is based on the distinction between essential and basic medical services.

Since the fault-tree is hospital dependent, it has to be customized on a case-by-case basis.

12.2.16 Computation of Fragility Curve

The γ_1 and γ_2 factors in Eq. (12.1) are analytically evaluated from the results of structural analysis.

The fragility curve is calculated employing the "advanced" structure-specific approach described in (Lupoi et al. 2005). Its peculiarity consists in splitting the reliability problem in two parts in order to reduce the computational burden (Pinto et al. 2004).

A relationship between the structural response quantities $\boldsymbol{D}$ (forces, displacements and deformations) and the ground motion intensity measure, *IM*, is established at first, by means of a reduced number of numerical analyses carried out for the mean values of the structural random variables.

Then, a standard Monte Carlo simulation is performed without carrying out any further structural analysis since, at each run, the structural demand is obtained from the $\boldsymbol{D}(IM)$ relationship. The capacity of the *basic* structural and non-structural elements is obtained for the sampled random variables (r.v.) by means of the fragility curves described in the previous section. At each run, the number of functioning operating theatres is checked and the state of the hospital system is evaluated by the fault-tree.

The final outcome is the relationship: $\gamma(IM) = \gamma_1(IM) \times \gamma_2(IM)$.

The complete fragility curve is obtained by repeating the simulation for a convenient number of levels of *IM*.

The approach in (Lupoi et al. 2005) takes into account the uncertainties related to seismic hazard as well as those relative to structural properties (strength of materials, amounts of reinforcement, capacity models, etc.).

12.3 Other Hospital Components

Some basic information on the assessment of the other components of a hospital system are provided in this section. A more detailed description can be found in Chapter 11 of Book 2.

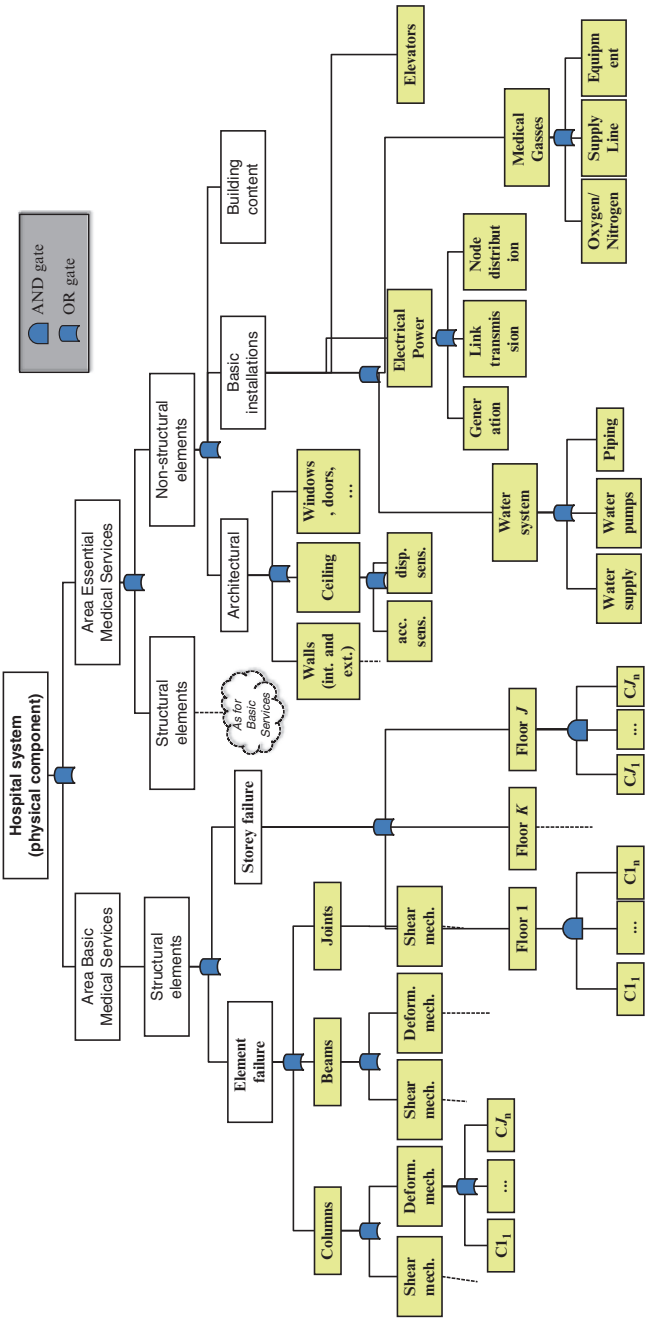

Fig. 12.22 Example of Fault-Tree for a physical component

12.3.1 Organisational Component: Emergency Plan

The organization of the hospital to a hazardous event must be regulated by an emergency plan. A vast literature is available on this subject: (PAHO 1995, 2000; PAHO/WHO 2000; Pidgeon 1991), among others.

The emergency plan should provide explicit procedures for immediate actions as well as awareness of responsibilities and identification of emergency roles. The evaluation of the emergency plan results in assigning a value to the α-factor in the *HTC* index (Eq. 12.1). At the current state of development, this is done according to engineering judgment. Typical values range between 0.5, for very poor emergency plan, up to 1, for an excellent and complete one. The lack of the emergency plan certified the inadequateness of the hospital to successfully cope with an emergency after a disaster: in this case, the factor α in the expression of the *HTC* index (Eq. 12.1) has to be taken equal to nil.

12.3.2 Human Component: Operators

The evaluation of the Human component involves the assessment of the *skill* and the *availability* of the operators (medical doctors and staffs).

It results in assigning a value to the β-factor in the *HTC* index (Eq. 12.1). At the current state of development, this is done according to engineering judgment. The typical value may range from 0.5, for poorly trained and understaffed operators, up to 1 for well-trained and adequately-staffed ones.

12.3.3 Environment Component: Hospital Treatment Demand

The *Hospital Treatment Demand*, *HTD*, provides an estimate of the number of people that requires surgical attention. It is therefore related to the number of casualties and to the epidemiology of the event.

Casualty models provide an estimate of the impact on population of an earthquake. They have been developed by engineers from limited, anecdotal, historical data (not from epidemiological studies nor involving health related researchers). Types and numbers of casualties vary with the characteristics of the earthquake, the building stock in the struck area, the demography and also with the time of the day when the earthquake occurs. In fact, these models are affected by large uncertainties, because there is no agreed definition of when victims may be classified as "injured" (Alexander 1996).

The model proposed by Coburn and Spence (1992) as simplified by Nuti and Vanzi (1998) can be adopted for the European context. It provides the casualties as a percentage of the population through the following expression:

$$C(IM) = k(IM - IM_{\min})^4 \tag{12.3}$$

where IM is the intensity measure of the seismic event, k and $IM_{\min}$ are the model parameters which take into account both the vulnerability of the building stock and the occupancy rate. Expression (12.3) accounts for the "severely injured" people (i.e. those to be hospitalised, labelled *T1* and *T2*) and for the deaths (labelled *T4*). The lightly injured people (labelled *T3*) are not accounted for.

The number of *all* casualties, $N_{Cas} = N_{T1} + N_{T2} + N_{T4}$, is given by the following expression:

$$N_{Cas}(IM) = N_{T1+T2+T4}(IM) = C(IM) \cdot \varepsilon_{Cas} \cdot N_{pop} \tag{12.4}$$

where N_{pop} is the population in the area affected and ε_{Cas} is a model error term that is included to account for the large uncertainties that affect the model. A log-normal distribution with unit median and coefficient of variation equal to 0.3 may be assumed for the model error term.

The hospital tributary area can be evaluated by assigning each municipality to the closest "main" hospital, i.e. one able to provide adequate medical assistance to the seriously injured people (T1 and T2).

Epidemiology studies the patterns of disease in human populations and identifies the causes and the severity of injuries due to hazardous events, including major earthquakes. This provides fundamental information for estimating the type and the amount of the resources needed to treat casualties.

The medical severity of an event as a function of the patients' conditions is commonly assessed by means of the two *severity* indexes:

- $S_1 = N_{T4}/(N_{T1} + N_{T2} + N_{T3})$ which represents the medical severity of the event itself;
- $S_2 = (N_{T1} + N_{T2})/N_{T3}$, which measures of the severity of the injuries caused by the event.

For the same number of casualties, the larger is the value of S_2, the greater is the amount of medical resources that are needed to treat the victims. In general, according to data from past earthquakes, the value of S_1 ranges between 0.1 and 0.5, while that of S_2 between 0.15 and 0.6. More information on this subject can be found in (Ramirez and Peek-Asa 2005; Shoaf et al. 2000; De Boer et al. 1989).

The number of seriously injured people, $N_{T1+T2} = (N_{T1} + N_{T2})$, is derived by combining the expression (12.4) with the severity indices S_1 and S_2. After some manipulation the following expression is obtained:

$$N_{T1+T2} = \frac{S_2 \cdot N_{Cas}}{S_1 + S_1 S_2 + S_2}, \tag{12.5}$$

The *HTD* index is given by the expression:

$$HTD = \zeta \cdot N_{T1+T2}, \tag{12.6}$$

where ζ is a factor accounting for the proportion of seriously injured people which requires surgical attention. The latter varies between 1/3 and 1/2; the actual value is defined on case-by-case basis by expert opinion.

The final expression for *HTD* is:

$$\begin{aligned} HTD &= \zeta \cdot S_2/(S_1 + S_1S_2 + S_2) \cdot N_{Cas} \\ &= \zeta \cdot S_2/(S_1 + S_1S_2 + S_2) \cdot C(IM) \cdot \varepsilon_{Cas} \cdot N_{pop} \end{aligned} \tag{12.7}$$

12.4 Summary of the Seismic Risk Analysis

The seismic risk for a hospital system is measured by the comparisons between treatment demand and capacity given by the following expressions:

$$HTD(IM) = \zeta \cdot S_2/(S_1 + S_1S_2 + S_2) \cdot C(IM) \cdot \varepsilon_{Cas} \cdot N_{pop} \tag{12.8}$$

$$HTC(IM) = \alpha \cdot \beta \cdot \frac{\gamma_1(IM) \cdot \gamma_2(IM)}{t_m} \tag{12.9}$$

The evaluation of the above performance measure is based on the analysis of all hospital components: *human*, *organizational*, *physical*, *environmental* and *medical services*.

Some "preliminary" activities have to be carried out at the beginning of the assessment:

- verifying that the hospital is provided of all the *essential* medical services, defined as those that have to be operative after the seismic event in order to guarantee the adequate treatment of patients and victims;
- assessing the quality of the emergency plan;
- verifying the existence of adequate resources to put into effect the emergency plan;
- assessing the quality of the human component and the availability of the operators to put in practice the emergency plan;
- examining the environment where the hospital is located.

These activities provide the data/information for:

1. the estimation of the coefficients α and β in (Eq. 12.1);
2. the identification of the areas where the *essential* medical services are going to be located and, consequently, the definition of limit states (*operational* or *life-safety*);

3. the set-up of the system fault tree;
4. the definition of the *basic* elements at risk (at the low-level of the fault-tree) for which a fragility curve/capacity model has to be obtained;
5. the estimation of the casualty model parameters k and IM_{min} in Eq. (12.3) and the computation of the severity indexes S_1 and S_2 in Eq. (12.7).

The second part of the assessment consists in the analytical evaluation of the fragility curve for the γ-factors. This is carried out according to the probabilistically-based procedure outlined in Sect. 12.2.16.

The probability of not being able to provide the medical care to the victims of the earthquake can easily be computed in the Monte Carlo simulation as:

$$P_f\left(HTD > HTD \middle| IM\right)$$

The risk is obtained by convolution of P_f with the hazard curve of the site of interest.

References

Alexander D (1996) The health effects of earthquakes in the mid-1990s. Disasters 20(3):231–247

Badillo H, Whittaker AS, Reinhorn AM (2003) Performance characterization of suspended ceiling systems. ATC-29-2, Redwood City, CA, pp 93–106

Bea R (2003) Lecture notes of CE290A. University of Berkeley, Berkeley

Behr RA, Worrel CL (1998) Limits states for architectural glass under simulated seismic loadings. ATC 29-1, Redwood City, CA, pp 229–240

Bouwkamp JG, Meehan JF (1960) Drift limitations imposed by glass. In: Proceedings of the 2nd world conference on earthquake engineering, Tokyo/Kyoto, Japan, , vol III, pp 1763–1778

Coburn A, Spence R (1992) Earthquake protection. Wiley, Chichester

Cohen JM (1995) Seismic performance of cladding: responsibility revisited. J Perform Constr Facil ASCE 9(4):254–270

De Boer J, Brismar B, Eldar R, Rutherford WH (1989) The medical severity index of disasters. J Emerg Med 7(3):269–273

Eidenger J, Goettel K (1998) The benefits and costs of seismic retrofits of nonstructural components for hospital, essential facilities, and schools. ATC 29-1, Redwood City, CA, pp 491–504

fib (2003) Seismic assessment and retrofit of reinforce concrete buildings. Federation internationale du beton, State-of-the-art report prepared by Task Group 7.1, Bulletin 24, Lausanne, Switzerland

Freeman SA (1977) Racking tests of high-rise building partitions. J Struct Div ASCE 103 (ST8):1673–1685

Gann RG, Riley MA, Repp JM, Whittaker AS, Reinhorn AM, Hough PA (2005) Reaction of ceiling tile systems to shocks (Draft). National Institute of Standards and Technology (NIST) NCSTAR 1-5D

Gates WE, McGavin G (1998) Lesson learned from the 1994 Northridge Earthquake on the vulnerability of non structural systems. ATC 29-1, Redwood City, pp 93–106

Grigoriu M, Waisman F (1988) Seismic reliability and performance of non-structural components. In: Proceedings of seminar on seismic design, retrofit and performance of nonstructural components, ATC 29-1, Applied Technology Council, Redwood City, CA

Kowalsky MJ, Priestley MJN (2000) Improved analytical model for shear strength of circular reinforced concrete columns in seismic regions. ACI Struct J 97(3):388–396

Kuwata Y, Takada S (2003) Seismic risk assessment and upgrade strategy of hospital lifeline performance. In: Proceedings of technical council on lifeline earthquake engineering, ASCE, Long Beach, CA, pp 82–91

LESSLOSS (2005) Practical methods for structure-specific probabilistic seismic risk assessment. LESSLOSS Risk Mitigation for Earthquake and Landslides, Integrated Project, Deliverable 74

Lupoi G, Franchin P, Lupoi A, Pinto PE (2005) Seismic fragility analysis of structural systems. ASCE J Eng Mech 132(4):385–395

Lupoi G, Franchin P, Lupoi A, Pinto PE, Calvi GM (2008) Probabilistic seismic assessment for hospitals and complex-social systems. Rose School Technical Report 2008/02,.IUSSPress, Pavia. ISBN 978-88-6198-017-4

NIBS (2004) HAZUS: Hazard US: earthquake loss estimation methodology. National Institute of Building Sciences, NIBS document 5200-03, Washington, DC

Nuti C, Vanzi I (1998) Assessment of post-earthquake availability of hospital system and upgrading strategies. Earthq Eng Struct Dyn 27(12):1403–1423

Nuti C, Santini S, Vanzi I (1999) Seismic risk of Italian hospitals. In: Proceedings of workshop on design and retrofitting of hospitals in seismic areas, Florence, Italy, 21–22 Oct 1999

PAHO (1995) Establishing a mass-casualty management system. Pan American Health Organisation/World Health Organisation, Washington, DC

PAHO (2000) Natural disasters – protecting the public's health. Pan American Health Organisation, Washington, DC

PAHO/WHO (2000) Principles of disaster mitigation in health facilities. Pan American Health Organisation/World Health Organisation, Washington, DC

Panagiotakos T, Fardis MN (2001) Deformation of R.C. members at yielding and ultimate. ACI Struct J 98(2):135–148

Pidgeon N (1991) Safety culture and risk management in organisations. J Cross Cult Psychol 22:129–141

Pinto PE, Giannini R, Franchin P (2004) Seismic reliability analysis of structures. IUSS Press, Pavia

Porter K, Johnson GS, Zadeh MM, Scawthorn CR, Eder SJ (1993) Seismic vulnerability of equipment in critical facilities: life-safety and operational consequences. Technical Report NCEER-93-0022. Multidisciplinary Center for Earthquake Engineering Research, State University of New York, Buffalo, NY, p 364

Ramirez M, Peek-Asa C (2005) Epidemiology of traumatic injuries from earthquakes. Epidemiol Rev 27:47–55

Rihal SS (1982) Behaviour of nonstructural building partitions during earthquakes. In: Proceedings of 7th symposium on earthquake engineering, Department of Earthquake Engineering, University of Roorke, Roorke, India, 10–12 Nov 1982

Shinozuka M (2001) Seismic risk assessment of non-structural components in hospitals. FEMA/USC Hospital Report No. 4, University of Southern California, Los Angeles

Shoaf K, Selingson H, Peek-Asa C, Giangreco MM (2000) Standardized injury categorization schemes for earthquake related injuries. Produced for the National Science Foundation by the UCLA Center for Public Health and Disaster Relief, p 43

Suarez LE, Singh MP (2000) Review of earthquake performance, seismic code, and dynamic analysis of elevators. Earthq Spectra 16(4):853–878

Swan SW, Kassawara R (1998) The use of earthquake experience data for estimates of the seismic fragility of standard industrial equipment. ATC 29-1, Redwood City, CA, pp 313–322

Yao GC (2000) Seismic performance of suspended ceiling systems. J Archit Eng 6(1)

Chapter 13
Fragility Function Manager Tool

Vitor Silva, Helen Crowley, and Miriam Colombi

Abstract This chapter describes the SYNER-G Fragility Function Manager, which has been developed to store, visualize and manage a large number of fragility function sets. The tool can store functions for a wide range of elements at risk, and has features that allow these functions to be harmonized (in terms of intensity measure type and limit state) and then compared. The tool is provided, together with a collection of European fragility functions, as an electronic supplement to this book.

13.1 Introduction

The SYNER-G Fragility Function Manager (FFM) has been developed to store, visualize and manage a large number of fragility function sets. It is clear that thousands of fragility functions have been proposed in the academic literature, many of which have been described, summarized and proposed within the chapters of this Book. Those that wish to use these functions will have to obtain the parameters of the functions (which are not always reported within the aforementioned publications, and thus need to be digitally extracted from figures) and format them in a way that allows them to be easily used in software. The FFM has been created such that users can easily obtain standardized sets of fragility functions that contain all the parameters required for their use in seismic risk calculations. Each fragility function is accompanied by metadata to allow the user to compare and select the functions that are of interest. Within the SYNER-G project, a large effort was made to compile and upload European fragility functions to the FFM, which are made available as an electronic supplement to this Book, together with the tool itself. The following section of this chapter describes in more detail the features of this useful tool.

V. Silva • H. Crowley (✉) • M. Colombi
European Centre for Training and Research in Earthquake Engineering (EUCENTRE),
Via Ferrata 1, 27100 Pavia, Italy
e-mail: vitor.silva@eucentre.it; helen.crowley@eucentre.it; miriam.colombi@eucentre.it

K. Pitilakis et al. (eds.), *SYNER-G: Typology Definition and Fragility Functions for Physical Elements at Seismic Risk*, Geotechnical, Geological and Earthquake Engineering 27,
DOI 10.1007/978-94-007-7872-6_13,

13.2 Uploading, Viewing, and Comparing Fragility Functions

Three interfaces are currently available for the FFM: buildings, bridges and other elements at risk. For all elements at risk, the general metadata provided for each study includes:

- Reference: reference papers, documents, deliverables;
- Region of applicability: this region represents the reference place for which structures and buildings have been analysed and fragility functions have been developed;
- Element at risk: list of the elements at risk considered by the fragility functions (i.e., buildings, bridges, lifelines, etc.);
- Typology of the element at risk considered: based on the original description provided in the references (i.e. RC – low rise – high code, masonry – simple stone, steel, etc.);
- Methodology: description of the method used to develop the fragility functions (e.g. empirical, analytical – nonlinear static, analytical nonlinear dynamic etc.);
- Intensity Measure Type: the reference ground motion parameter against which the probability of exceedance of a given limit state is plotted (i.e. Macroseismic Intensity, PGV, PGA, Spectral displacement, etc.);
- Damage scale: where applicable, the reference to the damage scale used in the development of the fragility functions;
- Notes: notes and comments on the analysed study.

For buildings and bridges, there is an additional possibility to input the SYNER-G taxonomies; the former has been presented and described in detail in SYNER-G Deliverables 3.1 and 3.2 (Crowley et al. 2011a, b), whilst the latter is presented in SYNER-G Deliverable 3.6 (Crowley et al. 2013). For the other elements at risk (such as pipelines, roadways, storage tanks and so on), the interface accepts custom taxonomies. The remaining features of the FFM are the same for each interface, and are described in the following sections of this chapter. The interface of the Fragility Function Manager for buildings is illustrated in Fig. 13.1.

13.2.1 Uploading and Viewing Functions

In order to add a set of fragility functions to the FFM, the taxonomy and metadata needs to be provided for each set as described previously. Once this information has been input, the last step of the upload procedure requires the user to input the parameters of each fragility function (Fig. 13.2).

Fragility functions can be discrete, where each intensity measure level input by the user requires a corresponding probability of exceedance for each limit state (see Fig. 13.3) or they can be continuous distributions, either normal or lognormal

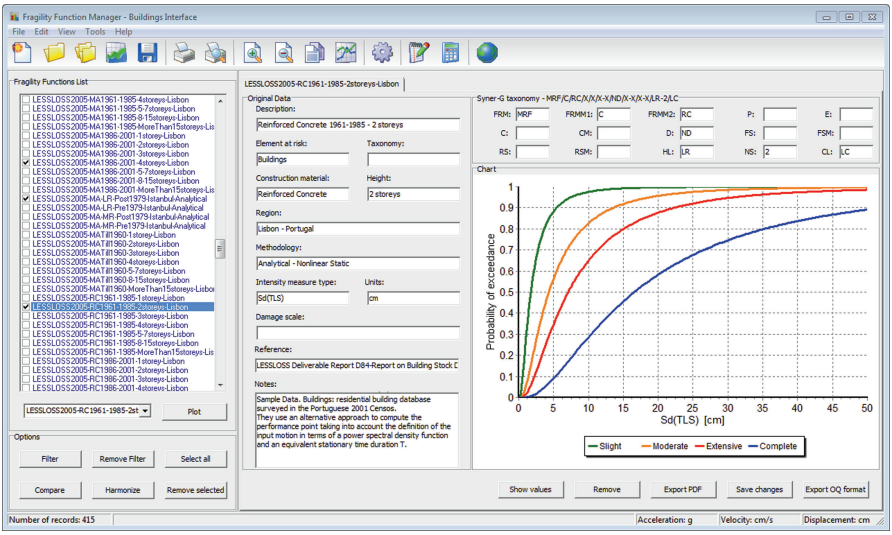

Fig. 13.1 Interface of the Fragility Function Manager for buildings

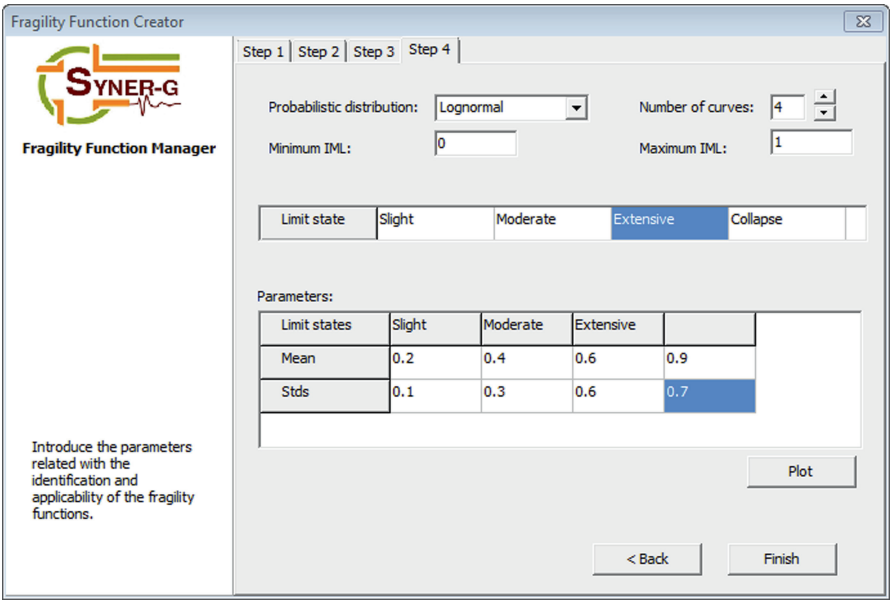

Fig. 13.2 Interface for uploading the parameters for the set of fragility functions

(see Fig. 13.4). In the case of normal or lognormal distributions (with the latter being the most common distribution found in the literature), the mean and standard deviation need to be provided for each limit state. There can be any number of limit

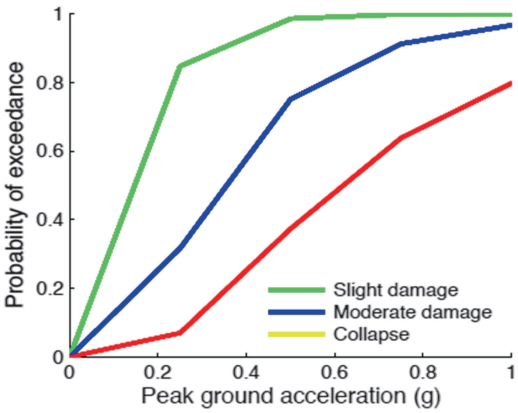

Fig. 13.3 Discrete fragility functions

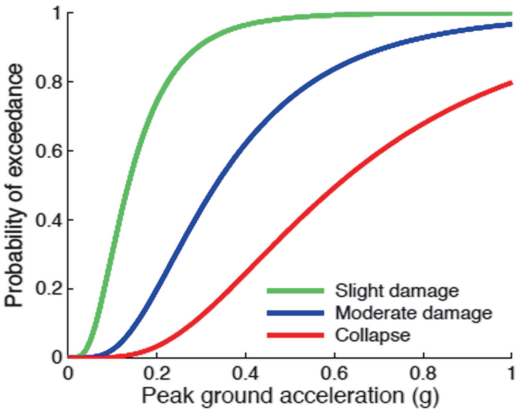

Fig. 13.4 Continuous fragility functions

states, each of which can be given a name by the user. In order to provide the range of intensity measure levels (IML) over which the functions are valid, the minimum and maximum IML need to also be input.

The tool produces an .XML file using the information provided by the user for the set of fragility functions. This .XML file can be used by software for seismic risk calculations, such as the OpenQuake engine of the Global Earthquake Model (Silva et al. 2013). The .XML format is has some attributes that are common to all of the fragility functions within the set which cover all of the metadata fields provided in Fig. 13.5.

For each building typology, a set of limit state curves needs to be stored within the field `ffs` (fragility function set), as shown in Fig. 13.6. The following attributes are currently being employed to define discrete fragility functions:

- `noDamageLimit`: this attribute defines the intensity measure level below which the probability of exceedance for all curves is zero;

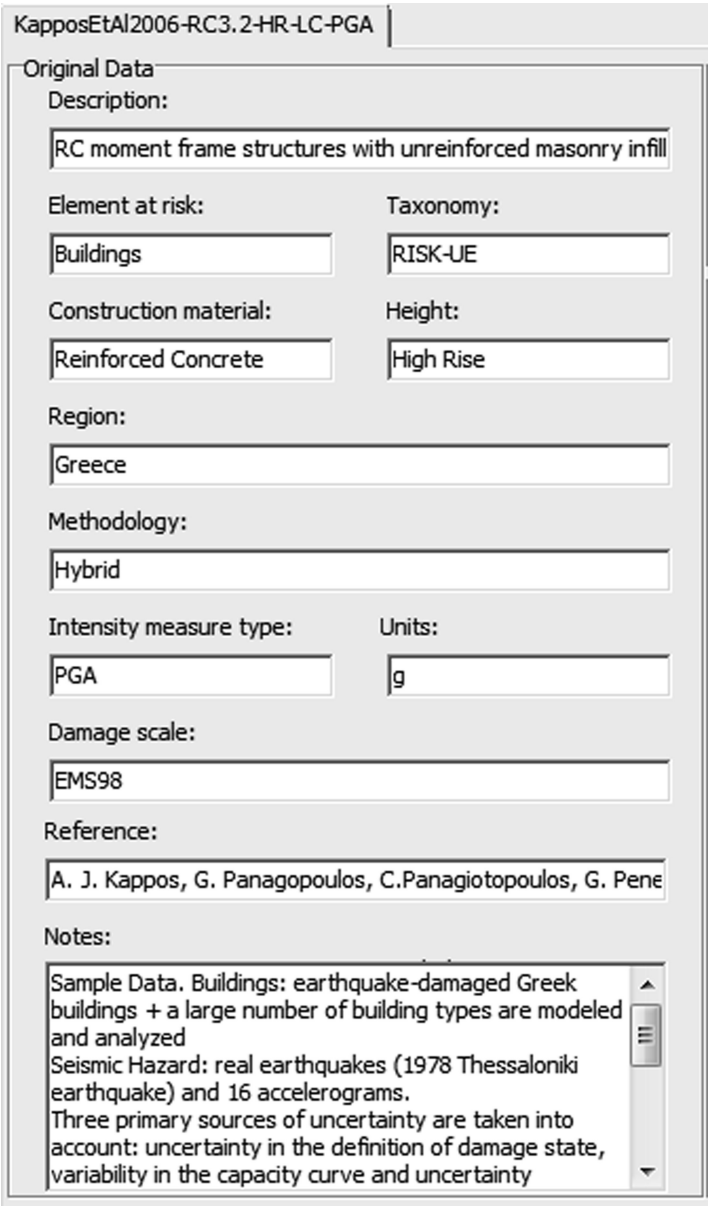

Fig. 13.5 Metadata which is stored at the beginning of the .XMLfile

- `taxonomy`: a unique key that is used to relate each fragility function with the relevant assets in the exposure model;
- `IML`: this attribute serves the purposes of defining the list of intensity measure levels for which the limit state curves are defined. In addition, it is also necessary

```
    ...
    <ffs noDamageLimit= 0.05>
        <taxonomy RC </taxonomy>
        <IML IMT="PGA" imlUnit="g"> 0.0 0.25 0.50 0.75 1.00 </IML>

        <ffd ls="slight damage">
            <poes> 0.0 0.85 0.98 0.99 1.00 < /poes>
        </ffd
        <ffd ls="moderate damage">
            <poes> 0.0 0.32 0.75 0.91 0.97 < /poes>
        </ffd
        <ffd ls="collapse">
            <poes> 0.0 0.07 0.37 0.64 0.80 < /poes>
        </ffd
    </ffs>
</fragilityModel>
</nrml>
```

Fig. 13.6 XML schema for fragility functions: parameters of discrete fragility functions

to define the intensity measure type (`IMT`) being used and the respective units (`imlUnit`);

- ffd: this field (fragility function discrete) is used to define the probabilities of exceedance (`poes`) of each limit state curve. It is also necessary to include which limit state is being defined in the attribute `ls`.

The .XML schema to store continuous functions has an initial structure similar to that described for the discrete fragility models. Then, the continuous limit state curves are stored as illustrated in Fig. 13.7.

Again, the set of limit state curves for each building typology needs to be stored within the field `ffs` (fragility function set), through the definition of the following attributes:

- `noDamageLimit`: this attribute defines the intensity measure level below which the probability of exceedance for all curves is zero;
- `type`: this parameter defines the type of probabilistic distribution being used to define the limit state curves;
- `taxonomy`: a unique key that is used to relate each fragility function with the relevant assets in the exposure model;
- `IML`: in this field, the intensity measure type (`IMT`) and associated units (`imlUnit`) for the limit state curves is defined, along with the minimum (`minIML`) and maximum (`maxIML`) intensity measure levels enclosing the range of applicability of the set of fragility functions;
- `ffc`: this field (fragility function continuous) is used to define the mean (`mean`) and standard deviation (`stddev`) of the cumulative lognormal function. In

```
    ...
    <ffs noDamageLimit= 0.05>
        <taxonomy RC </taxonomy>
        <IML IMT="PGA" minIML="0.0" maxIML="1.0" imlUnit="g" ></IML>
        <ffd ls="slight damage">
            <params mean="0.16" stddev="0.11" />
        </ffd
        <ffd ls="moderate damage">
            <params mean="0.40" stddev="0.26" />
        </ffd
        <ffd ls="collapse">
            <params mean="0.73" stddev="0.48" />
        </ffd
    </ffs>
</fragilityModel>
</nrml>
```

Fig. 13.7 XML schema for fragility functions: parameters of continuous fragility functions

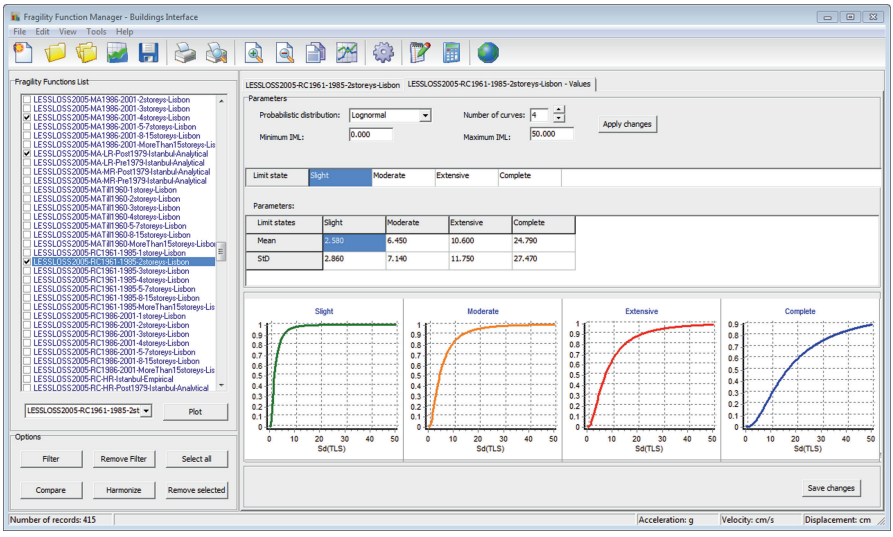

Fig. 13.8 Interface showing the parameters of each fragility function

addition, the limit state for the curve being defined needs to be specified in the attribute `ls`.

Once the functions have been uploaded and the .XML file created, the user is able to visualize the mean and the standard deviation of the fragility curves, the statistical distribution, the minimum and maximum IML, the number and the name of the limit states used, as shown in Fig. 13.8.

13.2.2 Harmonizing Intensity Measure Types

As presented in the various chapters of this Book, a number of different intensity measure types (IMT) are used for the various elements at risk (i.e. system components). In order to directly compare fragility functions from different studies, it may be necessary to convert the various intensity measure types to a common standard. The standard (or target) IMTs that can currently be selected with the tool are PGA, PGV and Sa(T), where T is the fundamental period of vibration selected by the user.

13.2.2.1 From Macroseismic Intensity to PGA and PGV

There are a number of different conversion equations that allow macroseismic intensity to be converted to PGA or PGV and a selection of these have been added to the FFM, considering the fact that the region of interest is Europe and considering the recommendations of Cua et al. (2010).

There are a number of studies that have dealt with the problem of estimating intensity from peak ground motion. The conversion equations in this direction, named GMICEs (Ground Motion to Intensity Conversion Equations), are used for example in the ShakeMap process of estimating intensity from the available peak ground motion observations (Wald et al. 1999a). On the contrary, conversion equations in the other direction, called IGMCEs (Intensity to Ground Motion Conversion Equations), are less common. They are usually necessary with historical earthquake studies, where intensity data are available, and it is of interest to estimate peak ground motion. It has to be noted that though it is common practice to simply invert a GMICE to get an IGMCE, it is not necessarily correct; they are usually not invertible. The Faenza and Michelini (2010) relationship represents an exception, since it is based on an orthogonal distance regression, and it is designed to be both a GMICE and an IGMCE. However, this relationship is not universally applicable because it is based on few high intensity data and most of the events are in a limited moderate magnitude range.

Within the FFM both GMICE and IGMCE have been used, even if the GMICEs relationships are not exactly invertible. However, in practise, these latter relationships are often used to estimate peak ground motion. Functional forms of GMICE from both active crustal and subduction zones have been selected. It is important to note that these conversion equations have a significant amount of scatter, which has not been currently considered in the tool.

The equations implemented in the tool are not presented here, due to space restrictions, but can be found in the following publications: Faenza and Michelini (2010), Margottini et al. (1992), Wald et al. (1999b), Tselentis and Danciu (2008), Murphy and O'Brien (1977), Sorensen et al. (2008).The following macroseismic intensity types are considered in the former equations: MCS, MSK-64, MMI, EMS.

Wald et al. (1999b) is tailored for California and USA. Notwithstanding that, in Cua et al. (2010) some validation efforts have been carried out which demonstrate

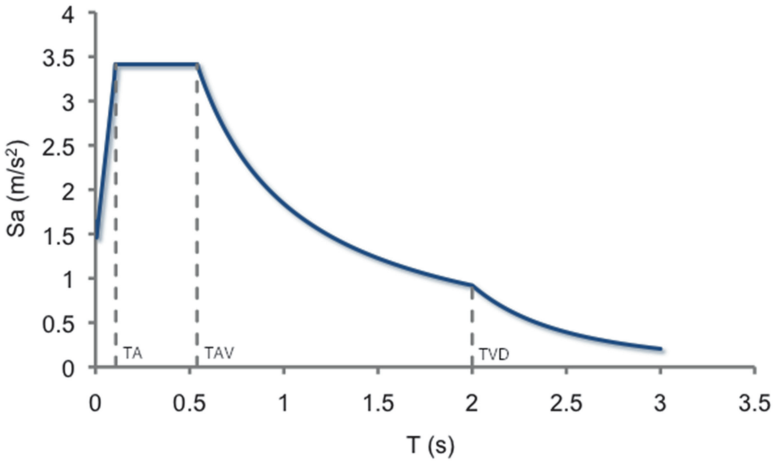

Fig. 13.9 IBC 2006 standardized spectral shape (ICC 2006)

that it is possible to adopt this relationship worldwide with good results. For this reason, this relationship is recommended as the default in the European context, as long as the fragility function sets are given in MMI.

13.2.2.2 From Spectral Acceleration to PGA and Vice Versa

In order to convert the Spectral acceleration (Sa) at the elastic period of vibration to the value of PGA, a standardized response spectrum shape is needed. Currently, the procedure of IBC-2006 (ICC 2006) is incorporated in the tool. It has been decided to use IBC-2006 instead of Eurocode 8 (CEN 2004) for the sake of simplicity. EC8 is identified by two different spectra (Type I and Type II) in accordance with the magnitude of the considered earthquake. This would lead to more complex system to estimate the conversion and would add further uncertainty to the results. The IBC-2006 spectrum can be divided into four parts (see Fig. 13.9): a region with a linear function for periods from zero (period corresponding to PGA) to T_A, a region with constant spectral acceleration for periods between T_A and T_{AV}, a region with constant spectral velocity between periods from T_{AV} to T_{VD} and a region with constant spectral displacement for periods of T_{VD} and beyond.

The elastic response spectrum is defined by the following equations:

$$Sa(T) = Sa(0.3)(0.4 + 0.6{}^{T}/_{T_A}) \quad \text{if } 0<T<T_A \tag{13.1}$$

$$Sa(T) = Sa(0.3) \quad \text{if } T_A < T < T_{AV} \tag{13.2}$$

$$Sa(T) = {}^{Sa(1)}\Big/_{T} \quad \text{if } T_{AV} < T < T_{VD} \tag{13.3}$$

$$Sa(T) = Sa(1){}^{T_{VD}}/_{T^2} \quad \text{if } T_{VD} < T < 10 \tag{13.4}$$

Table 13.1 NEHRP site classification as applied by IBC-2006 (ICC 2006)

Site class	Site class description	Shear wave velocity $V_{S,30}$ (m/s)
A	Hard rock, Eastern U.S. sites only	>1,500
B	Rock	760–1,500
C	Very dense soil and soft rock	360–760
D	Stiff soil	180–360
E	Soft soil, profile with >3 m of soft clay defined as soil with plasticity index PI > 20, moisture content w > 40 %	<180
F	Soils requiring site specific evaluations	–

Where the transition periods are defined as follows:

$$T_A = 0.2T_{AV} \tag{13.5}$$

$$T_{AV} = {Sa(1)}\Big/{Sa(0.3)} \tag{13.6}$$

$$T_{VD} = 10^{\left({M-5}/{2}\right)} \tag{13.7}$$

When the moment magnitude M is not known, the T_{VD} period is assumed to be 10 s (i.e. M = 7). It should be noted that in the case of rock site conditions (class B), the following expressions have to be considered:

$$Sa(0.3) = S_{AS} = 2.5PGA \tag{13.8}$$

$$Sa(1) = S_{Al} = PGA \tag{13.9}$$

Using this aforementioned formula, one can go from spectral acceleration Sa (T) to the value of PGA by simply inverting Eqs. (13.1), (13.2), (13.3) and (13.4). If different types of soil (such as those in Table 13.1) are to be considered, some more steps are needed in converting the spectral acceleration to PGA (and vice versa). In this case, the amplification of ground shaking to account for local site conditions has to be considered and the soil amplification factors given by IBC-2006 provisions are used. The methodology amplifies rock PGA according to the factors given in Table 13.2, as expressed by the following formula:

$$PGA_i = PGA \cdot F_{Ai} \tag{13.10}$$

in which PGA_i is the peak ground acceleration (in g) for site class *i*, PGA is the peak ground acceleration for rock soil (B) and F_{Ai} is the short period amplification factor for site class *i* for spectral acceleration S_{AS}. For what concerns $Sa(0.3)_i$ and $Sa(1)_i$ of different soil classes, the following equations have to be used:

$$Sa(0.3)_i = S_{ASi} = S_{AS} \cdot F_{Ai} \tag{13.11}$$

$$Sa(1)_i = S_{Ali} = S_{Al} \cdot F_{Vi} \tag{13.12}$$

Table 13.2 Site amplification factors as given in IBC-2006 (ICC 2006)

Site class B	Site class				
Spectral acceleration	A	B	C	D	E
Short period, S_{AS} (g)	Short-period amplification factor, F_A				
≤0.25	0.8	1.0	1.2	1.6	2.5
(0.25, 0.50]	0.8	1.0	1.2	1.4	1.7
(0.50, 0.75]	0.8	1.0	1.1	1.2	1.2
(0.75,1.0]	0.8	1.0	1.0	1.1	0.9
<1.0	0.8	1.0	1.0	1.0	0.9
1-second period, S_{Al} (g)	1-second period amplification factor, F_V				
≤0.10	0.8	1.0	1.7	2.4	3.5
(0.1, 0.2]	0.8	1.0	1.6	2.0	3.2
(0.2, 0.3]	0.8	1.0	1.5	1.8	2.8
(0.3, 0.4]	0.8	1.0	1.4	1.6	2.4
>0.4	0.8	1.0	1.3	1.5	2.4

S_{ASi} and S_{Ali} represent short-period spectral acceleration for site class i (in g) and 1 second-period spectral acceleration for site class i (in g), respectively. The values of the factors F_{Ai} and F_{Vi} are reported in Table 13.2. Moreover also the period T_{AV} that defines the transition period from constant spectral acceleration and constant spectral velocity is a function of the site class:

$$T_{AVi} = \left(\frac{S_{Al}}{S_{AS}}\right) \cdot \left(\frac{F_{Vi}}{F_{Ai}}\right) \tag{13.13}$$

Where:

S_{Al} is 1 second-period spectral acceleration for site class B;
S_{AS} is short-period spectral acceleration for site class B;
F_{Vi} is 1 second-period amplification factor for site class i and spectral acceleration S_{Al};
F_{Ai} is short-period amplification factor for site class i and spectral acceleration S_{AS}.

Using these formulae, the PGA for each class of soil and for each value of spectral acceleration can be estimated by the tool. The conversion starts from Sa (T_y) and for this reason, the user is asked to provide the value of the elastic period T_y of the considered structure that can be known or can be found using some empirical relationships that relate the height of a building to its elastic period. There are a number of empirical existing relationships that can be used for buildings e.g. Goel and Chopra (1997) and Crowley and Pinho (2004).

13.2.2.3 From Spectral Displacement to PGA and Vice Versa

If the fragility function is provided in terms of Sd(T_y), which is the spectral acceleration at the fundamental period of vibration, it is possible to convert it into Sa(T_y) and then, following the procedure described in Sect. 13.2.2, it is possible to

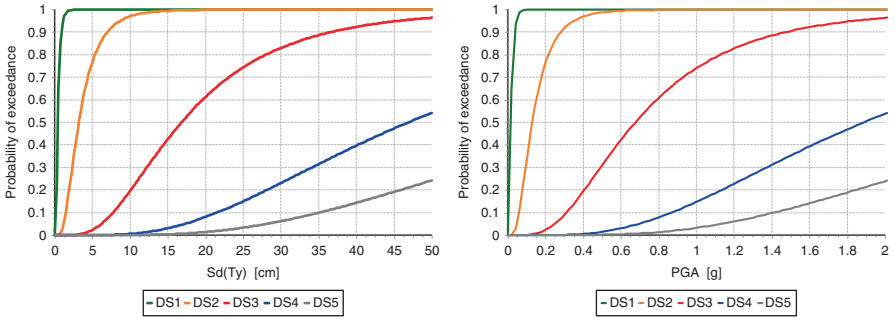

Fig. 13.10 Conversion of a set of fragility functions from spectral displacement at fundamental period to PGA

estimate PGA. The conversion equation from $Sd(T_y)$ to $Sa(T_y)$ is given by the following expression:

$$S_d(T_y) = \left(\frac{T_y}{2\pi}\right)^2 Sa(T_y) \tag{13.14}$$

In Fig 13.10, an example of fragility functions converted from spectral displacement, $Sd(T_y)$, to PGA is shown.

13.2.2.4 From PGV to PGA and Vice Versa

The peak ground velocity (PGV) is widely used for engineering applications and a number of existing fragility functions are based on this IMT. Bommer and Alarcon (2006) found that there is a good correlation between PGV and Sa(0.5). Based on this finding they proposed the following equation that has been implemented in the tool:

$$PGV\left(^{cm}/_{s}\right) = \frac{Sa(0.5)\left(^{m}/_{s2}\right)}{20} \tag{13.15}$$

It is possible to convert PGV into Sa(0.5) and then, following the procedure described in Sect. 13.2.2, it is possible to estimate any other spectral acceleration or PGA.

13.2.3 Harmonizing Limit States

Fragility functions from different authors generally feature distinct limit states, but when these functions are to be compared it is necessary to have the same limit

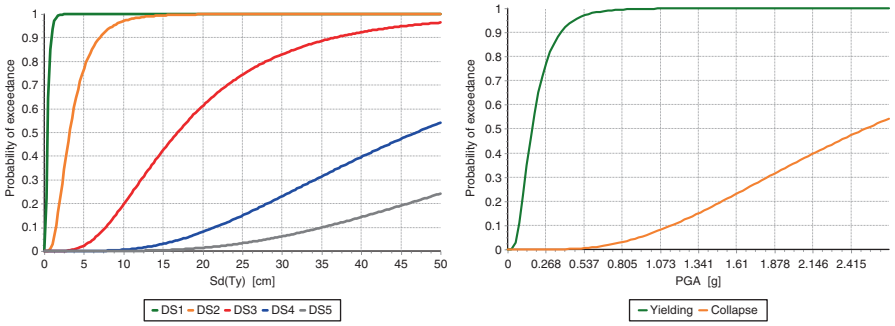

Fig. 13.11 Conversion of a set of fragility functions from five limit states to two limit states (yielding and collapse)

states. It is believed that using two limit states is the simplest way of harmonising the limit states for a large number of fragility functions, as nearly all sets of fragility functions already have the following two thresholds: damage limitation (or yielding) and collapse. Moreover, some curves have only these two limit states. The selection and the identification of the limit states when deriving fragility functions can be based on the results of experiments, engineering judgment or experience from previous earthquakes. When the limit state is defined quantitatively with terms such as "moderate damage" or "extensive damage" it becomes difficult to compare the functions from different studies; however, such comparison is slightly more straightforward for the threshold to yield and collapse. It is possible to say that the yielding limit state will almost always be either the first or the second curve from a set of fragility functions, whilst the collapse limit state is usually the last curve in the set.

The proposed tool allows functions to be harmonised also with regards to the limit states. In the 'Harmonize function' window it is possible to assign the original limit states of the fragility function to the yielding and collapse limit states. For instance, if three limit states are considered (LS1, LS2 and LS3), the user can decide to assign LS1 to yielding and LS3 to collapse.

In Fig 13.11, an example of a fragility function set with five limit states and its harmonized set with two limit states is shown. In this case, the tool converts $Sd(T_y)$ into PGA and then it harmonizes the limit states. The yielding is assigned to 'DS1' and collapse is assigned to 'DS5'.

13.2.4 Comparison of Fragility Functions

13.2.4.1 Comparison of Damage Distributions

Once a user has harmonised their fragility functions in terms of IMT and limit states, a number of features are available to allow the functions to be compared. The fragility functions (which may be a combination of discrete and continuous

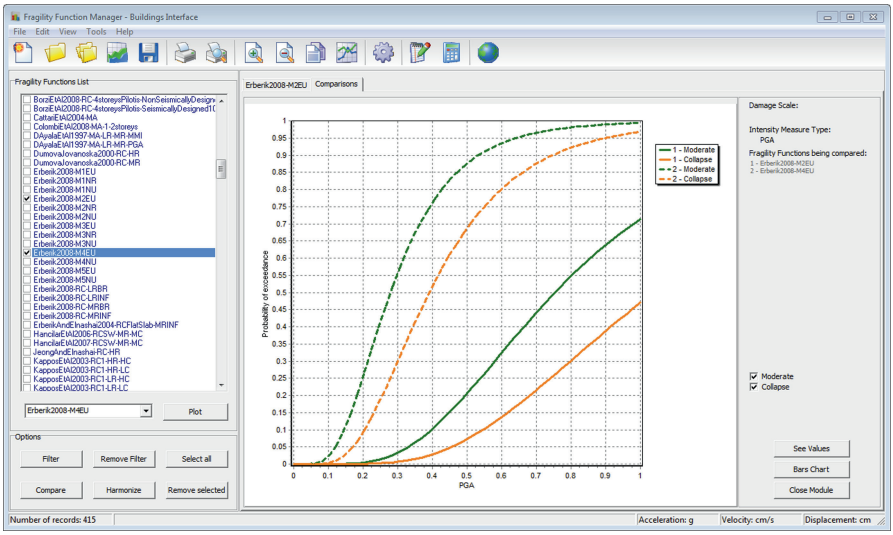

Fig. 13.12 Interface for comparing fragility functions

functions) are converted into discrete functions, and the values of IML versus probability of exceedance for each limit state can be extracted into tables. This allows the user to transfer the data into other applications, such as Microsoft Excel, for further processing. Once a user has harmonised their fragility functions in terms of IMT and limit states, a number of features are available to allow the functions to be compared, as illustrated in Fig. 13.12.

It is also possible to compare the damage distributions from different sets of fragility functions using the "bar chart" feature. The user can move the slider to different levels of intensity, and compare the damage distribution from set of each fragility function. One can thus immediately get an idea of the building typology that will lead to higher levels of extensive damage and collapse at a given level of ground motion (as shown in Fig. 13.13).

13.2.4.2 Modelling Epistemic Uncertainty of Fragility Functions

Figure 13.14 shows the variability that can be observed in the harmonized fragility functions for a user-selected class of buildings at the yield and collapse limit states. Provided the same sources of uncertainty have been modelled in the derivation of each fragility function, the variability between the functions can be considered epistemic uncertainty. It is noted that some of the variability will be due to the conversion of intensity measure types and limit states, and further scrutiny is needed to understand the impact of these uncertainties on the harmonized fragility functions. If we consider, however, that these fragility functions originally had the same IMT and limit state and are all lognormal distributions, then we can estimate

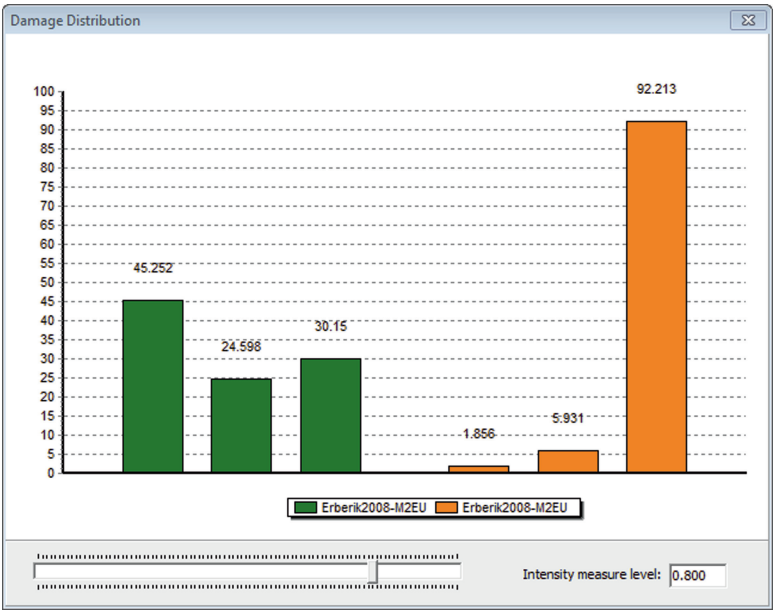

Fig. 13.13 Interface for comparing the damage distribution from different fragility functions

the epistemic uncertainty and model it using the mean and standard deviation of the parameters of the fragility functions (which each have a median and dispersion), as well as the correlation between these parameters (Fig. 13.14).

Figures 13.15a, b show how histograms of the median and dispersion values obtained by considering each of the individual fragility functions from a group of fragility functions (shown in Fig. 13.15d). The mean and standard deviation of the median and dispersion can then be estimated from these histograms. Figure 13.15c shows that there is a correlation between the median and dispersion.

By plotting different combinations of the computed parameters (mean of the median, standard deviation of the median, mean of the dispersion, standard deviation of the dispersion) for each limit state, it is possible to observe a correlation between the parameters (see Fig. 13.16). A correlation coefficient matrix can thus be computed, such as the one shown in Table 13.3. The computation of these parameters and the correlation coefficient matrix feature has not yet been added to the FFM, but is expected as a future development.

13.3 Final Comments

This chapter has presented a new tool for storing, viewing, harmonizing and comparing fragility functions. The tool provides users with fragility functions that can be directly extracted and used in seismic risk software applications. However, one limitation of the tool is that there is no mechanism for users to share their

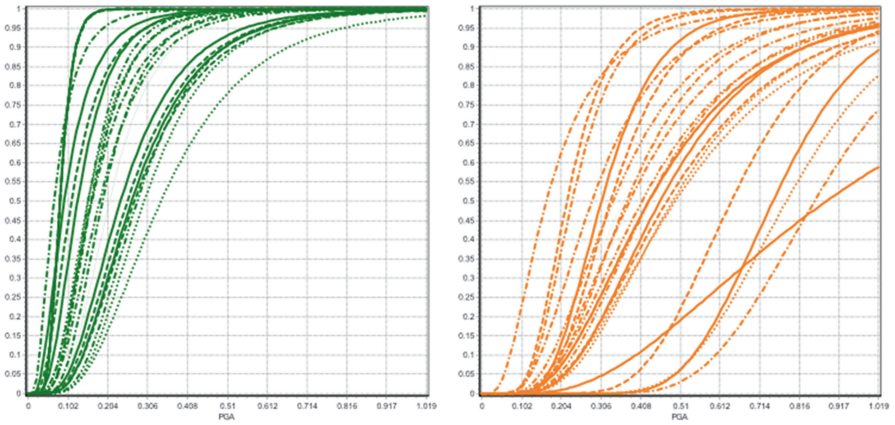

Fig. 13.14 Yield limit state (*left*) and collapse limit state (*right*) harmonized fragility functions for a user-selected building type

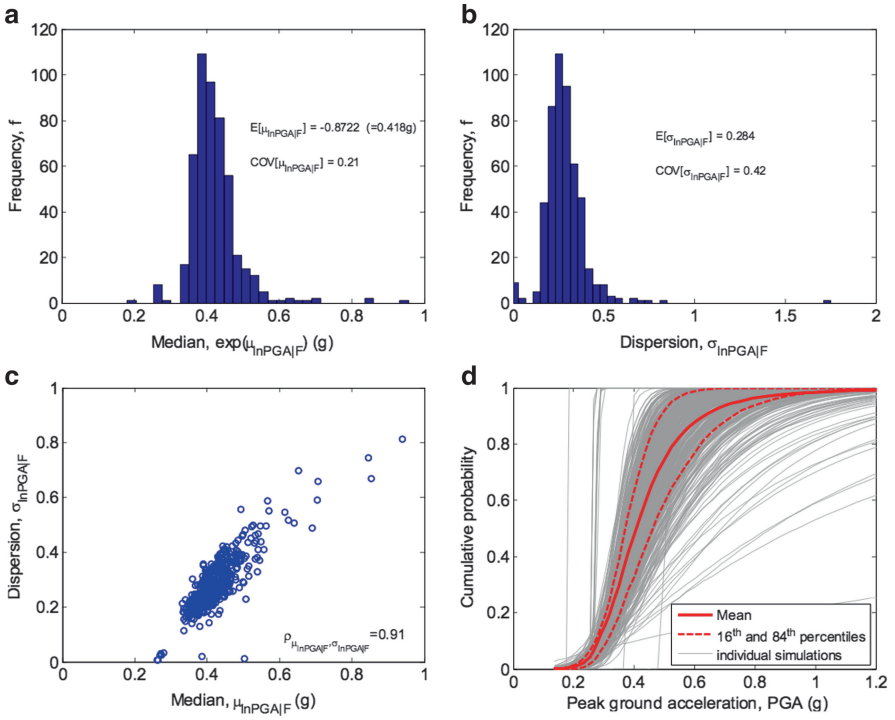

Fig. 13.15 (**a**) Histogram of median values (**b**) histogram of dispersion values (**c**) correlation between median and dispersion and (**d**) individual and mean ± one standard deviation fragilities (From Bradley 2010)

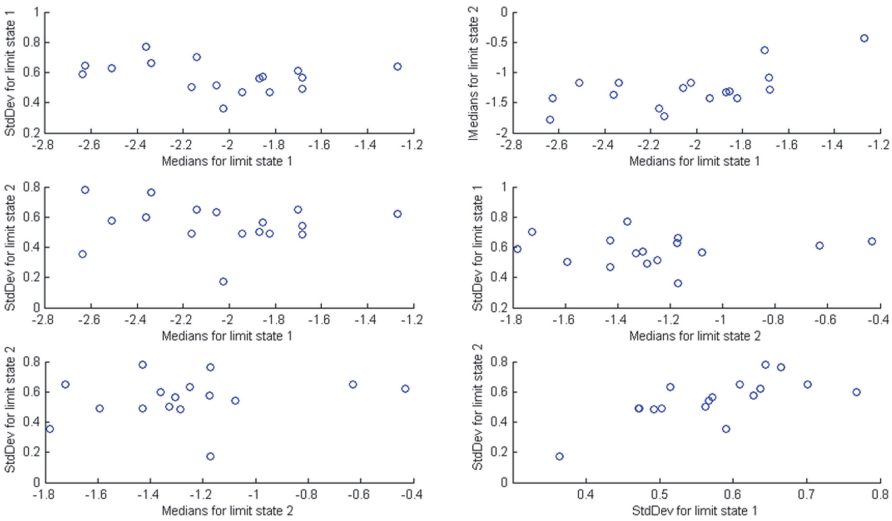

Fig. 13.16 Correlation between the individual fragility functions parameters

Table 13.3 Example of a correlation coefficient matrix

	Median (yield)	Dispersion (yield)	Median (collapse)	Dispersion (collapse)
Median (yield)	1	−0.302	0.642	−0.098
Dispersion (yield)		1	0.053	0.710
Median (collapse)	Symmetric		1	0.209
Dispersion (collapse)				1

uploaded fragility functions. Although a number of fragility functions have already been uploaded and are provided as an electronic supplement with this Book, it will be difficult to share additional fragility functions with the community. The Global Earthquake Model (GEM)[1] will attempt to address this gap by developing a global database of fragility functions that will be made available to the scientific community through the OpenQuake web-based platform. This database will build upon the work carried out in developing the Fragility Function Manager, using many of the parameters and features that have been included in this tool.

[1] www.globalquakemodel.org

References

Bradley BA (2010) Epistemic uncertainties in component fragility functions. Earthq Spectra 26(1):41–62

Bommer JJ, Alarcon JE (2006) The prediction and use of peak ground velocity. J Earthq Eng 10(1):1–31

CEN (2004) Eurocode 8: Design of structures for earthquake resistance – Part 1: General rules, seismic actions and rules for buildings. European Committee for Standardization. EN 1998–1, Brussels

Crowley H, Pinho R (2004) Period-height relationship for existing European reinforced concrete buildings. J Earthq Eng 8:93–119

Crowley H, Colombi M, Silva V, Ahmad N, Fardis M, Tsionis G, Papailia A, Taucer F, Hancilar U, Yakut A, Erberik MA (2011a) D3.1. Fragility functions for common RC building types in Europe, SYNER-G Deliverable 3.1. Available from URL: http://www.vce.at/SYNER-G/files/dissemination/deliverables.html

Crowley H, Colombi M, Silva V, Ahmad N, Fardis M, Tsionis G, Karatoni T, Lyrantazaki F, Taucer F, Hancilar U, Yakut A, Erberik MA (2011b) D3.2. Fragility functions for common masonry building types in Europe, SYNER-G Deliverable 3.2. Available from URL: http://www.vce.at/SYNER-G/files/dissemination/deliverables.html

Crowley H, Colombi M, Silva V, Monteiro R, Ozcebe S, Fardis M, Tsionis G, Askouni P (2013) D3.6. Fragility functions for roadway bridges, SYNER-G Deliverable 3.6. Available from URL: http://www.vce.at/SYNER-G/files/dissemination/deliverables.html

Cua G, Wald DT, Allen TI, Garcia D, Worden CB, Gerstenberger M, Lin K, Marano K (2010) "Best Practises" for using macroseismic intensity and ground motion-intensity conversion equations for hazard and loss models in GEM1. GEM technical report 2010-4, GEM Foundation, Pavia, Italy

Faenza L, Michelini A (2010) Regression analysis of MCS intensity and ground motion parameters in Italy and its application in ShakeMap. Geophys J Int 180:113–1152

Goel RK, Chopra AK (1997) Period formulas for moment-resisting frame buildings. ASCE 123 (11):1454–1461

International Code Council (2006) 2006 International Building Code (IBC-2006), United States

Margottini C, Molin D, Serva L (1992) Intensity versus ground motion: a new approach using Italian data. Eng Geol 33:45–58

Murphy JR, O'Brien LJ (1977) The correlation of peak ground acceleration amplitude with seismic intensity and other physical parameters. Bull Seismol Soc Am 67(3):877–915

Silva V, Crowley H, Pagani M, Monelli D, Pinho R (2013) Development of the OpenQuake engine, the Global Earthquake Model's open-source software for seismic risk assessment. Nat Hazards. doi:10.1007/s11069-013-0618-x

Sorensen MB, Stromeyer D and Grunthal G (2008) Estimation of macroseismic intensity – new attenuation and intensity vs. ground motion relations for different parts of Europe. In: Proceedings of the fourteenth world conference on earthquake engineering, Beijing, China

Tselentis GA, Danciu L (2008) Empirical relationships between Modified Mercalli Intensity and engineering ground-motion parameters in Greece. Bull Seismol Soc Am 98(4):1863–1875

Wald DJ, Quitoriano V, Heaton T, Kanamori H, Scrivner CW, Worden BC (1999a) TriNet "Shakemaps": rapid generation of peak ground-motion and intensity maps for earthquakes in southern California. Earthquake Spectra 15:537–556

Wald DJ, Quitoriano V, Heaton T, Kanamori H (1999b) Relationship between peak ground acceleration, peak ground velocity and Modified Mercalli Intensity in California. Earthquake Spectra 15:557–564

Chapter 14
Recommendations for Future Directions in Fragility Function Research

Kyriazis Pitilakis and Helen Crowley

Abstract This chapter outlines the main comments relevant to the compilation of fragility functions and highlights the main recommendations given in the different Chapters of this Book concerning the selection among existing fragility functions or the derivation of new ones for the most important elements at risk. Essential needs for future studies are also summarized.

14.1 Introduction

The objective of this Book, which also reflects a part of the work carried out in the SYNER-G project, is to present the state of the art on the fragility functions used in seismic risk assessment of buildings, lifelines, utility systems, transportation infrastructures and critical facilities, considering as much as possible the construction typologies in Europe. To this end, fragility curves from literature were collected, reviewed, harmonised and, where possible, validated against observed damage. In some cases, existing functions were modified and adapted, whereas in other cases, new fragility functions were developed.

Special attention is given to the methods used to derive the fragility curves and the various uncertainties associated with this topic. Different approaches can be used to compile fragility curves. Empirical curves, which are based on statistical damage data from past earthquakes, are more appropriate to the particular region and construction practice where the empirical data comes from and should be used with caution. They

K. Pitilakis (✉)
Department of Civil Engineering, Aristotle University, P.O.Box. 424,
54124 Thessaloniki, Greece
e-mail: kpitilak@civil.auth.gr

H. Crowley
European Centre for Training and Research in Earthquake Engineering (EUCENTRE),
Via Ferrata 1, 27100 Pavia, Italy
e-mail: helen.crowley@eucentre.it

K. Pitilakis et al. (eds.), *SYNER-G: Typology Definition and Fragility Functions for Physical Elements at Seismic Risk*, Geotechnical, Geological and Earthquake Engineering 27,
DOI 10.1007/978-94-007-7872-6_14,

are also useful for the validation of functions based on other methods. Their main weaknesses are the lack of adequate and well documented data for all typologies of structures and the poor correlation of the observed damage with records of strong ground motion. Judgmental or expert elicitation methods depend on the experience of the individual experts consulted. They are approximate and highly subjective methods. Analytical methods, based on numerical models of structures subject to increasing level ground motion, and hybrid approaches which combine the results from different methods lead to reduced bias and are becoming more attractive, in particular due to the recent development of computing capabilities.

Whatever the approach is, crucial choices must be made regarding the definition of damage states and the associated damage indexes, together with their threshold values, as well as the intensity measure adequate to capture the seismic response of each element at risk. A wide range of options is available in the literature and only general recommendations may be put forward, based on effectiveness, efficiency, sufficiency, robustness and computability of the selected parameters. In principle, the use of a particular damage or intensity measure should be guided by the extent to which it corresponds and correlates to damage, but in practice it is often more related to the approach followed for the derivation of fragility curves.

The treatment of uncertainties is of major importance both in the derivation of fragility curves and in risk assessment in general. In Chap. 2 a comprehensive presentation of the way that the problem may be tackled has been provided. In the risk analyses that have been carried out within SYNER-G, aleatory and epistemic uncertainties are practically coexisting, and there is no conceptual difference between the two, except that the aleatory uncertainties are describable, in the majority of cases, by means of a continuous probability distributions, while on the other hand, the epistemic ones are often of the discrete type, and the associated probabilities are to be assigned subjectively, on the basis of experience.

There are several approximate techniques for dealing with this problem, starting from the simple but rather inadequate First Order Second Moment (FOSM) method, to the approach based on the use of a Response Surface in the space of the structural variables. In Chap. 2, Latin Hypercube Sampling is recommended for accuracy, however its practical limits, due to the demanding computational effort when modelling a large number of uncertain quantities, are underlined (P. E. Pinto in Chap. 2). In the different Chapters of this Book this issue is extensively discussed, providing the reader with a good overview of how uncertainties should be or have been modelled in the derivation of fragility functions.

The work performed within SYNER-G allows the identification of topics that require refinement and could be the subject of future research. In particular:

- Validation of existing fragility curves against observed damage will enable better rating of their quality and will potentially improve their reliability. However, such damage data is scarce for some elements at risk. The development of robust field measurement techniques that might help to better define the real condition of a building or a structure with regard to its vulnerability rating should be also an important improvement to the fragility analysis. Another essential step towards the improvement of damage estimation models is the establishment of a commonly

accepted format for the systematic documentation and compilation of both damaged and undamaged structures as well as of nonstructural components. Moreover, advances in information technologies now permit rapid, cost-effective collection and analysis of virtually exhaustive data sets, which should be appropriately archived and made available to the engineering community.

- Fragility curves are not available and should be developed for several structures not included in the SYNER-G typologies, such as high-rise reinforced concrete frame buildings with infills, masonry buildings with seismic design, HDPE pipelines that are used in European cities, waterfront structures other than of gravity type, various components of EPN, industrial facilities and others.
- The uncertainty of the most important parameters that are introduced in the fragility curves (i.e. capacity and demand assessment of the element at risk and definition of damage states) needs to be further investigated so as to confirm the default values that describe the variability of these parameters that have been adopted in many studies, or to propose new ones.

In the following, an attempt is made to summarize essential comments relevant to the compilation of fragility functions and to highlight once more the main recommendations given in the different Chapters concerning the selection among existing fragility functions or the derivation of new ones. Important needs for future studies are also grouped for the most important elements at risk.

14.2 Fragility Functions for Reinforced Concrete Buildings

The review of existing fragility curves for reinforced concrete buildings shows a variety of methodologies, damage states, and intensity measures. It also becomes clear that existing taxonomies could leave out a large number of characteristics that could be used to distinguish the seismic performance of buildings. Hence, a modular classification scheme was developed. This collapsible and expandable scheme gives the flexibility to describe a building with as much information as can be collected, and allows one to expand the taxonomy when more detailed information is available, by adding new categories or sub-categories so as to describe all types of buildings, or by adding new sets of fragility curves considering other modelling hypothesis. For example in the frame of SYNER-G University of Patras in Greece (Fardis et al. 2012) has developed new fragility curves for RC frame and wall-frame buildings designed according to Eurocode 2 alone or for the three ductility classes of Eurocode 8. The curves were established point-by-point, from the probability that the (random variable) demand for given intensity measure exceeds the (random variable) capacity and consider shear failures, which are normally ignored in most of the existing analytical fragility studies.

The dynamic tool that has been developed and described in Chap. 13 provides a set of fragility functions for the most important RC building typologies in Europe, which are stored into the Fragility Function Manager. This dynamic tool was used

for the harmonisation of the fragility curves and for the estimation of the associated epistemic uncertainty in the mean and standard deviation values for a set of curves, which was applied to buildings but could be used for other elements at risk. For simplicity, fragility curves were harmonised for the yielding and ultimate damage states, as it is difficult to compare the functions for the intermediate damage states.

The selection of the most appropriate fragility curves for the exposed assets is discussed in detail mainly for RC and masonry buildings in Chap. 3. On the basis of this discussion a rating system is proposed for empirical and analytical fragility functions and then a procedure is proposed for rationally selecting the most appropriate fragility curves from the literature for application in seismic risk assessment. Given that it is often very difficult to decide which existing fragility function is the "best" for a particular asset and location, within Chap. 3 possible methods for combining fragility functions, in cases where more than one set of suitable fragility curves exist, are explored.

14.2.1 Future Needs

Given the large number of approaches that have been applied in the past for developing fragility and vulnerability functions, especially within the branch of analytical methods, standard guidelines for the future development of these functions are needed. This important issue needs a coordinating effort at a global scale. To this respect the Global Earthquake Model provides one possible framework. It will release guidelines at the end of 2013 for empirical, analytical and expert-opinion development of physical vulnerability functions, which should be then reviewed and tested by the engineering community such that they may attain a general level of consensus. By having vulnerability functions that are developed using standard procedures accepted by the engineering community, the selection of functions by non-expert users will be easier, which should promote the use of seismic risk assessment in risk mitigation policy making.

Besides the permanent need to standardize procedures, to improve existing fragility functions and to validate them with empirical and experimental data, there are some specific challenges, which need further investigation. Among them are the following:

- Development of fragility curves for irregular RC buildings and buildings, which are not comprised in the taxonomy of SYNER-G, like for example prefabricated buildings of variable size and use.
- Traditionally, in seismic vulnerability assessment, it is implicitly assumed that structures are optimally maintained during their lifetime, thus neglecting any deterioration mechanism that may adversely affect their structural performance. On this basis, the impact of progressive deterioration of the material properties caused by aggressive environmental conditions, as for example the corrosion due to chloride penetration leading to the variation of the mechanical properties

of steel and concrete over time, is not accounted for. The safety and serviceability of RC structures may then be affected under the action of seismic loading, compromising the ability of the structures to withstand the loads they are designed for. Consequently, fragility functions are not constant in time and should account for aging effects introducing the time-variant vulnerability assessment. Among the recent efforts on this subject the reader is referred to the following: Ghosh and Padgett (2010), Choe et al. (2010), Fotopoulou et al. (2012), Karapetrou et al. (2013a, b, c) and Pitilakis et al. (2013).

- The effects of soil-foundation-structure interaction (SFSI) in the derivation of fragility functions for RC buildings are not explicitly taken into account so far in any of the currently available sets of fragility functions. In several cases these SFSI effects may modify considerably and sometimes in a detrimental way the analytical fragility functions (Pitilakis et al. 2013; Saez et al 2011).
- Development of damage-state-dependent fragility functions, which can be used to estimate the likelihood of a structure to suffer further damage in the event of an earthquake, while accounting for the increased vulnerability due to the fact that the building was previously damaged in a past earthquake. Cumulative damages from multiple seismic events on a building are actually a critical factor, which usually increase considerably the physical losses and the resulted casualty rate. In this context if the damaged building suffers further damage from aftershocks or/and new seismic events before repairs can take place, then its fragility is dependent on the accumulation of damage. A whole new set of fragility curves should be developed to account for this important issue (Luco et al. 2011; Iervolino et al. 2012; Réveillère et al. 2012).
- Development of fragility curves for reinforced concrete buildings in landslide prone areas triggered by earthquakes. An attempt to tackle this topic for few common building typologies is provided by Fotopoulou and Pitilakis (2012, 2013).

14.3 Fragility Functions for Masonry Buildings

In Chap. 5 a method for the vulnerability assessment of ordinary masonry buildings at territorial scale has been proposed in the framework of a probabilistic seismic risk assessment. The classification of the built environment is based on the SYNER-G taxonomy, which is dependent on the available data mainly from Europe. The general definition of fragility functions is recalled, through the use of static non-linear analysis for the evaluation of the capacity spectrum and the calculation of the response displacement using the demand spectrum. The selection of proper intensity measures for masonry buildings is treated, as well as the definition of damage and performance limit states. A detailed procedure for the propagation of uncertainties is proposed, which is able to single out the contribution of each independent component of uncertainty. Recommendations for deriving fragility functions with different approaches are given. In particular, it is shown how the macroseismic vulnerability method, derived from EMS98, can be used with expert elicitation or if empirical data are available. Moreover, the DBV-masonry

(Displacement Based Vulnerability) method is proposed as a powerful tool for the derivation of fragility function by an analytical approach. Finally, fragility functions are derived for ten different classes of masonry buildings, defined by a list of tags from the taxonomy, in order to show the capabilities of the proposed methods and their cross-validation.

14.3.1 Future Needs

- Analytical models for masonry buildings are now reliable enough to be used for the development of fragility functions, provided that results are compared with empirical/experimental data and/or checked by experts.
- Analytical models can be very useful in the near future to distinguish the influence on vulnerability of single specific characteristics of buildings, moving from a macro-classification to a subdivision into sub-classes, through a proper taxonomy.
- The definition of a proper intensity measure for masonry buildings and the validation of the capacity spectrum method, currently frequently used for the development of fragility functions, would require an extensive use of incremental non-linear analysis (IDA).
- The mechanical models for masonry, the failure mechanisms and the dynamic properties, stiffness and strength of the masonry need further improvement and implementation in software tools to be used for the analytical derivation of fragility functions.
- There is a need to develop fragility curves for masonry buildings in landslide prone areas triggered by earthquakes, eventually combining this with hydrogeological hazards.

14.4 Fragility Functions for Electric Power Networks

A modern electric power network (EPN) is a complex interconnected system designed to generate, transform and transfer electric energy from generating units to various locations. Based on the review of the main recent works on fragility functions of EPN components, standard damage scales for micro- and macro-components were proposed together with the most appropriate fragility functions for the components that are of interest in SYNER-G. Several updates and improvements are needed especially in the European context, such as:

- Update of the taxonomy to include not only typologies for USA and Italy, but also those present to date in other European power networks.
- In case the fragility curves for these components are not available or not up to date, development of new fragility functions is needed.
- Since the SYNER-G methodology already accounts for the substation's internal logic, an update is needed of the typical layouts which are present to date in European power networks. The layouts are required not only for substations but

also for generation plants, for which today only the HAZUS curves (considering a power plant as a whole) are available.

14.5 Fragility Functions for Water Wastewater, Gas and Oil Systems

Water and wastewater systems are complex networks, prone to damage, which may result in extended direct and indirect losses and possibly in pollution of the environment. In this Book the most appropriate fragility functions for the main components and subcomponents have been collected, reviewed and, if possible, validated with empirical data. Fragility functions have been recommended mostly based on the validation of existing empirical curves from observed damage in different parts of the world; sometimes the recommended fragility functions have been compiled from numerical and fault tree analyses. The uncertainties are generally quite high, which is a determinant fact that should be taken into account in any risk assessment.

Fragility functions for gas and oil pipelines, storage tanks and support facilities are also collected and reviewed. It is recognized that existing fragility curves developed in the USA are mainly empirical, while those developed in Europe are based on numerical or fault-tree analysis. Appropriate functions were recommended in this Book based on their ability to cover all the important elements and typologies in Europe.

14.5.1 Future Needs

- There is a serious lack of empirical data, especially in Europe, on damage to all kinds of pipes and pipelines for water, wastewater, gas and oil. As a result, empirical relations that have been derived from observational data in USA, Japan and recently in New Zealand are not always adequate for Europe. There is an urgent need in Europe, and elsewhere, to organize good documentation of the damage to utility and gas/oil systems following future earthquakes. A minimum requirement for this is the detailed survey and documentation in GIS of the existing networks, at least in the most vulnerable cities in seismic prone areas.
- It is often proposed to end-users to apply the same fragility functions for water and gas pipes; it is then necessary that the analogy between water and gas/oil network should be made more carefully, especially due to the differences in flow pressure and viscosity of the different fluids.
- More research should be engaged to assess the vulnerability of polyethylene (MDPE/HDPE) pipelines, which seem to behave well in earthquakes (O'Rourke et al. 2012).

- The use of generic fragility curves for gas/oil stations or reservoirs is probably irrelevant, mainly due to the large variability of the typologies and the construction materials. Large discrepancies are observed in the different typologies, based on the network type (high or low-pressure), or even from country to country. Further research on fragility curves for subcomponents (pumps, motors, electrical equipment, etc.) is advised, followed by fault-tree analyses to develop specific fragility functions whenever it is needed.

14.6 Fragility Functions for Bridges

The existing fragility curves for road and railway bridges were reviewed, stored in the Fragility Function Manager and used to identify the key parameters of a new taxonomy. It is noted that relatively few studies exist on the seismic fragility of European bridges, and for this reason, the fragility curves developed for bridges in other parts of the world are often adjusted for use in Europe. Except for few recent studies, shear failure of the piers is often disregarded in existing fragility studies. New fragility curves were produced in SYNER-G and have been described in this Book for road and railway bridges with continuous deck, monolithically connected to the piers or supported on elastomeric bearings, where the damage states are defined by the flexural and shear failure modes together with the deformation of the deck and the bearings.

14.6.1 Future Needs

Among the most important needs for further improvement, refinement and development of the fragility analysis are the following:

- Validation of numerical fragility curves against earthquake damage data and experimental results.
- Development of fragility curves for irregular bridges and bridges beyond the SYNER-G typologies.
- Further study of the fragility of bridges designed with low-level seismic codes.
- Further development of parameterized fragility curves and eventually field noise measurements to easily obtain bridge-specific curves using only basic information.
- Consideration of particular structural characteristics and performance requirements for railway bridges.
- Better understanding of special issues, such as soil-structure interaction, asynchronous excitation, aging effects and cumulative damage and multiple hazards (i.e. earthquake, liquefaction, scour, corrosion), and incorporation in the standard procedures for fragility analysis.

14.7 Fragility Functions for Roadways and Railways

Experience from past earthquakes reveals that in roadway and railway systems, the most vulnerable components are usually the bridges. However, other components may also affect seriously the vulnerability of these important systems, vital in any modern society and economy. Their damage can be greatly disruptive for the whole urban or regional transportation network due to lack of redundancy, lengthy repair time or re-routing difficulties.

Road and railway elements, except bridges, such as tunnels, embankments, road pavements, slopes, trenches, railway tracks and bridge abutments, are basically "geotechnical" structures that need special attention in the fragility analysis. An extensive review is made in this Book on the available fragility functions for all these components. For several elements where the available fragility functions, mostly empirical or based on expert elicitation, were not considered reliable enough, new analytical curves have been proposed for a few common typologies; for example, for shallow tunnels in alluvial deposits, embankments, cuts/trenches and bridge abutments.

The existing fragility functions for railway elements are limited and are mainly based on data for road elements. New fragility curves were developed based on those for road elements and considering appropriate (lower) threshold values for the definition of the damage states.

14.7.1 Future Needs

- Fragility functions are needed for several transportation network components (i.e. road and railway slopes, trenches, cuts, embankments, retaining/gravity walls, bridge abutments, tunnels) for earthquake-triggered landslides (eventually combined with hydrogeological hazards as well) and ground failures (i.e. liquefaction, lateral spreading, fault rupture).
- Further research is deemed necessary for tunnels of different geometries, and underground structures in the urban environment. It is also important that stakeholders/authorities are involved in the evaluation and verification of the fragility models, the definitions of damage states and serviceability thresholds for all components of the networks.
- More empirical data are needed as well as further validation of the present and future analytically derived fragility functions with experimental and empirical data.
- As for the above ground structures, aging effects for time dependent vulnerability assessment should also be considered, in particular for shallow tunnels in alluvial deposits with high water table and for bridge abutments.

14.8 Fragility Functions for Harbours

Damage to waterfront structures is usually attributed to ground failure and to a lesser degree to ground shaking alone, while damage to cargo handling and storage components is due to both ground shaking and permanent deformations. An extensive review of the existing fragility curves has been carried out for the most important elements of harbour systems based on the SYNER-G taxonomy. The available fragility functions are developed using all possible approaches i.e. use of empirical data from past earthquakes, expert judgement and analytical studies, while a fault-tree analysis is recommended for the complex components. Among them, the most appropriate for the European typologies were selected and recommended.

14.8.1 Future Needs

- Development of fragility functions for different typologies of waterfront structures other than gravity walls for ground shaking and permanent ground displacements due to liquefaction.
- Development of fragility functions for different typologies of cargo handling facilities.

14.9 Fragility Functions for Hospitals

Hospital facilities are complex systems comprising several components (human, organizational, physical, environmental and medical services), each including a large variety of elements. Their behaviour has been studied, but capacity models and fragility curves are not available for all of them. A general methodology for the evaluation of the "probability of failure" of hospital systems has been proposed. It uses the fault-tree technique to establish the relationship between the state of the elements and the state of the system and a probabilistic approach to account for the large uncertainties characterising most of the quantities that contribute to the system response. Uncertainties are related, among others, to the external hazard, the evaluation of the structural response, the knowledge of system properties, the modelling of the capacities, and definition of damage levels. It is noted that each hospital needs to be modelled separately, as the layout is totally facility-dependent, and for this reason, a detailed analysis is necessary for each system.

References

Choe DE, Gardoni P, Rosowsky D (2010) Fragility increment functions for deteriorating reinforced concrete bridge columns. Eng Mech 136(8):969–978

Fardis MN, Papailia A, Tsionis G (2012) Seismic fragility of RC framed and wall-frame buildings designed to the EN-Eurocodes. Bull Earthq Eng 10(6):1767–1793

Fotopoulou S, Pitilakis K (2012) Vulnerability assessment of reinforced concrete buildings subjected to seismically triggered slow-moving earth slides. Landslides 10(5):563–582. doi:10.1007/s10346-012-0345-5

Fotopoulou S, Pitilakis K (2013) Fragility curves for reinforced concrete buildings to seismically triggered slow-moving slides. Soil Dyn Earthq Eng 48:143–161

Fotopoulou SD, Karapetrou ST, Pitilakis KD (2012) Seismic vulnerability of RC buildings considering SSI and aging effects. In: Proceedings of the 15WCEE international conference, Lisbon, Portugal, 24–28 Sept 2012

Ghosh J, Padgett JE (2010) Aging considerations in the development of time-dependent seismic fragility curves. J Struct Eng 136(12):1497–1511

Iervolino I, Chioccarelli E, Giorgio M (2012) Time-dependent seismic reliability of damage-cumulating non-evolutionary bilinear systems. In: Proceedings of the 15th WCEE, Lisboa, September 2012

Karapetrou S, Fotopoulou S, Pitilakis K (2013a) Consideration of aging and SSI on the time-variant seismic vulnerability assessment of R/C buildings. In: Proceedings of the 11th international conference on structural safety and reliability (ICOSSAR 2013), Columbia University, New York, 16–20 June 2013

Karapetrou S, Fotopoulou S, Pitilakis K (2013b) Consideration of aging effects on the time-dependent seismic vulnerability assessment of RC buildings. In: Adam C, Heuer R, Lenhardt W Schranz C (eds) Vienna congress on recent advances in earthquake engineering and structural dynamics 2013 (VEESD 2013), Vienna, Austria, 28–30 Aug 2013

Karapetrou S, Filippa A, Fotopoulou S, Pitilakis K (2013c) Time-dependent vulnerability assessment of RC buildings considering SSI and aging effects, COMPDYN 2013. In: Proceedings of the 4th international conference on computational methods in structural dynamics and earthquake engineering, Kos, Greece, 12–14 June 2013

Luco N, Gerstenberger MC, Uma SR, Ryu H, Liel AB, Raghunandan M (2011) A methodology for post-mainshock probabilistic assessment of building collapse risk. In: Proceedings of the Ninth Pacific conference on earthquake engineering, Auckland, New Zealand

O'Rourke TD, Jeon SS, Toprak S, Cubrinovski M, Jung JK (2012) Underground lifeline system performance during the Canterbury earthquake sequence. In: Proceedings of the 15th world conference on earthquake engineering, Lisbon, Portugal

Pitilakis KD, Karapetrou ST, Fotopoulou SD (2013) Consideration of aging and SSI effects on seismic vulnerability assessment of RC buildings. Bull Earthq Eng (accepted)

Réveillère A, Gehl P, Seyedi D, Modaressi H (2012) Development of seismic fragility curves for mainshock-damaged reinforced-concrete structures. In: Proceedings of the 15th WCEE, Lisboa, September 2012

Saez E, Lopez-Caballero F, Modaressi-Farahmand-Razavi A (2011) Effect of the inelastic dynamic soil-structure interaction on the seismic vulnerability assessment. Struct Saf 33:51–63

Subject Index

A
Abutments, 9, 19, 25, 56, 227, 245, 246, 260, 263, 265, 268, 270, 271, 279–281, 283, 284, 287–289, 291, 301–303, 305, 308, 311, 315–320, 323, 324, 411
Acceleration-displacement curve, 53
Acceleration-displacement response spectrum (ADRS), 119
Acceleration spectrum intensity (ASI), 267, 268
Aging effects, 19, 164, 407, 410, 411
Analysis
  dynamic, 15, 19–22, 35, 42, 44, 54, 87, 144, 166, 315, 317, 318, 323, 336, 362
  elastic, 285
  modal, 12, 338
  nonlinear dynamic, 19, 22, 64, 87, 265–268, 270, 275, 279, 337–339, 386
  non-linear static, 17, 22, 53, 64, 73, 87, 119, 141, 164–165, 275, 386
  nonlinear time-history, 35, 53, 265, 336, 339
  probabilistic, 31
  pushover, 16, 21, 53, 123, 135, 144, 264–266, 275
  static, 73, 122, 144, 280, 314, 362
Approach fills, 302, 305, 307–309, 315
Architectural components, 37, 366
ASI. *See* Acceleration spectrum intensity (ASI)
Autotransformer, 8, 164, 180–182

B
Backfill soil, 329, 333
Back-up power, 196, 202, 203, 223, 224, 235–237, 250, 340, 341, 349, 351, 353, 368
Bayesian approach, 59, 206, 232, 233
Bayesian networks (BN), 56
Bearings
  elastomeric, 261–263, 269, 275, 281, 283, 286, 410
  expansion, 261, 262, 269, 273, 274, 277
  fixed, 261–263, 266, 269, 274, 280, 282, 292
Binomial distribution, 125, 130, 131
Boundary conditions, 7, 140
Bridge
  abutments, 9, 19, 25, 56, 227, 245, 246, 291, 301, 302, 305, 308, 311, 315–319, 323, 411
  continuous, 260, 263, 275–278, 280, 410
  highway, 52, 227, 246, 262, 263, 265, 268, 271, 272, 275, 279
  irregular, 275, 281, 410
  multi-span, 260, 265, 272, 275–279
  railway, 25, 259–293, 311, 410
  regular, 25, 260, 266, 270, 274, 275, 281–292
  retrofitted, 25, 263, 278–279
  road, 4, 25, 259–293, 410, 411
  simply-supported, 260, 263, 265, 272, 274, 278, 279
  straight, 279

C
Canal, 8, 222, 223, 225, 227, 230–232, 244–246, 252, 253
Capacity
  curve, 16, 17, 53–55, 64, 67, 87, 88, 119, 120, 122–124, 127–129, 131, 135–138, 140, 142–144, 146, 264, 269
  model, 273, 276, 360–366, 378, 383, 412
  spectrum, 53, 407

K. Pitilakis et al. (eds.), *SYNER-G: Typology Definition and Fragility Functions for Physical Elements at Seismic Risk*, Geotechnical, Geological and Earthquake Engineering 27, DOI 10.1007/978-94-007-7872-6,

Capacity spectrum method (CSM), 15–18, 119, 264–266, 408
Cargo handling, 9, 25, 327, 329–330, 332, 335, 336, 340, 343–348, 352, 412
Chord rotation, 41, 285, 286, 362
Circuit-breaker, 8, 159, 164–168, 171, 173–176, 180–182
Column curvature, 268
Columns, 37, 41, 44, 101, 128, 135, 195, 225, 243, 260, 263, 268, 270, 271, 273, 275, 278–282, 285, 334, 352, 360–362
Connectivity loss, 176, 178, 179
Corrosion, 25, 189, 194, 224, 228, 260, 276–278, 293, 406, 410
Critical acceleration, 307
Cuts, 19, 225, 301–304, 306, 307, 310, 311, 313, 316, 318–324, 411

D
Damage
  data, 15, 23, 50–52, 60–63, 79, 81, 83, 88, 89, 134, 222, 246, 263, 264, 307, 403, 404, 410
  function, 168, 250
  in pipes, 200, 203, 227, 232, 251
  in tunnels, 301, 304
Damage state, 2, 37, 61, 117, 165, 188, 222, 260, 303, 338, 364, 404
Damping
  equivalent viscous, 119, 123, 124
  hysteretic, 73, 119, 123
  initial, 123
  ratio, 19, 264, 280, 314
Deck displacement, 268, 284
Deformation capacity, 21, 40, 286, 303, 367
Delphi method, 58
Displacement-based assessment/design, 54
Displacement capacity curve, 53, 264
Distribution stations, 160, 370, 371
Drift
  capacity, 55, 128, 362, 364
  interstorey, 37, 82, 87, 117, 122, 123, 137, 143, 148, 362, 363, 366, 367
  ratio, 16, 17, 21, 37, 97, 268, 269, 362, 363
  sensitive, 198, 364, 365
Ductility, 54, 89, 113, 115, 130, 131, 147, 194, 268, 269, 273, 274, 405
Dynamic response, 33, 36, 336

E
Earthquake action, 360
Earthquake intensity, 2, 10, 232, 267, 307, 312, 328
Elastic spectral acceleration, 67
Embankments, 4, 9, 14, 19, 25, 52, 56, 225, 227, 245, 246, 300–305, 307, 310, 311, 318–324, 333, 334, 411
Emergency plan, 380, 382
Engineering demand parameter (EDP), 11, 20, 21, 33, 55, 73, 82, 87
Equivalent Frame (EF) behavior, 113, 135, 141, 145
Equivalent SDOF system, 16, 139, 266, 267, 274
Eurocode 2 (EC2), 99, 260, 283, 284, 286–291, 405
Eurocode 8 (EC8), 54, 143, 148, 260, 283, 284, 286–291, 300, 313, 316, 317, 319, 323, 337, 339, 344, 362, 393, 405
European buildings, 96–100, 105
European macroseismic scale (EMS), 11, 97, 121, 130, 392
Expert elicitation, 13, 49, 57–58, 68, 69, 116, 121, 130, 150, 404, 411

F
Facilities
  critical, 4, 6, 23, 56, 179, 403
  fuel, 336, 340, 341, 348–353
  health care, 25, 357–383
  processing, 25, 188, 217
  support, 196, 198, 202, 409
Failure modes, 14, 25, 81, 139–141, 143, 166, 189, 194–196, 201, 222, 227, 228, 270, 273, 276, 287, 328, 330–332, 344, 349, 410
Fault rupture, 12, 300, 303, 323, 411
Fault-tree analysis, 23, 25, 56, 188, 207, 214, 217, 234, 249, 340, 360–361, 409, 412
FFM. *See* Fragility function manager (FFM)
Finite element, 314, 317, 318, 320, 336, 337, 339, 342
First order second moment (FOSM) method, 31, 41–43, 404
Force resisting mechanism (FRM), 8, 14, 16, 98, 99, 113, 114, 134, 145
Force resisting mechanism material (FRMM), 8, 98, 99, 113, 114, 134

Foundations
deep, 301
surface, 331
Fragility function manager (FFM), 23–25, 76, 100, 106, 385–401, 405, 410
Fragility functions
analytical, 6, 11, 13, 48, 53, 55–57, 63–68, 71, 72, 96, 121, 137, 205, 407
empirical, 6, 11, 13, 14, 50–52, 57, 60–62, 96, 117, 121, 122, 217, 233, 234, 339, 341
expert elicitation, 6, 13, 57–58, 68, 121, 411
hybrid, 6, 11, 13, 22, 23, 58–59, 68, 96, 117, 121
numerical, 23, 57, 63, 96, 181, 188, 216, 409

G
Generators, 158, 162, 170, 182, 196, 202, 351, 368, 377
Geographical information systems (GIS), 3, 222, 409
Global Earthquake Model (GEM), 15, 57, 59, 69, 76–78, 100, 105, 388, 401, 406
Ground
failure, 6, 9, 12, 193, 197, 199, 200, 203, 205, 208, 210–212, 227, 228, 230, 242, 244, 247–249, 252, 253, 260, 301, 302, 304, 305, 310, 311, 323, 324, 328, 329, 336, 340, 342, 344, 345, 347–349, 351, 352, 411, 412
motion, 2, 6, 10–12, 19–21, 36, 42, 47, 48, 50, 51, 53, 54, 61–66, 71, 73, 76, 79, 81, 86–88, 119, 121, 188, 194, 197, 203, 204, 206, 208, 210, 211, 224, 248, 252, 265, 268, 272, 311, 312, 316, 323, 341, 378, 386, 392, 398, 404
Ground motion prediction equations (GMPE), 32, 51–53, 61, 62, 65, 199

H
Hazard curve, 34, 55, 118, 119, 122, 126, 127, 383
Hospital, 4, 13, 32, 37, 172, 357–361, 366, 368–370, 373, 376–382, 412
Hospital Treatment Capacity (HTC), 359, 360, 380
Hospital Treatment Demand (HTD), 360, 380–382
Hysteretic models, 66, 67

I
Incremental dynamic analysis (IDA), 15, 20–22, 42, 54, 57, 144, 408
Intensity measure, 6, 10–12, 15, 17, 20, 21, 23, 24, 33, 34, 50–52, 55, 60–62, 64, 65, 68, 71, 76, 79, 81, 86, 88, 96–98, 102, 103, 117, 118, 120–123, 167, 188, 192, 193, 198–200, 203, 229–230, 232, 252, 260–262, 264–268, 271, 274, 275, 285, 303, 311, 312, 341, 342, 350, 378, 381, 386, 404, 405, 407, 408
Inter-story drift ratio, 87

L
Landslide, 12, 193, 221, 227, 228, 245, 246, 300, 302, 303, 309–311, 323, 331, 407, 408, 411
Lateral spreading, 193, 280, 300, 303, 332, 337–339, 342, 411
Latin hypercube sampling (LHS), 19, 43, 44, 64, 87, 404
Life safety, 117, 327, 343, 361
Lift station, 224, 228, 230, 232–234, 250–252, 254
Limit state
collapse, 21, 57, 103–107, 397, 398, 400
harmonizing, 396–397
operational, 359, 361, 364, 365
threshold, 7, 10, 118, 121–124, 128–129, 131, 149, 397
yielding, 105–107, 397
Lines
autotransformer, 8, 164, 180, 182
distribution, 8, 160, 209, 211, 369, 372
transmission, 8, 158, 160, 190, 209, 211, 369–371
Liquefaction, 12, 193–195, 210, 221, 224, 227–229, 245–247, 260, 262, 273, 275, 280–281, 293, 301, 302, 309, 323, 328–331, 336–339, 342, 352, 410–412
Load, 13, 36, 40, 53, 56, 104–109, 135, 137, 145, 146, 157–163, 182, 184, 195, 280, 283–285, 287, 301, 316, 332, 333, 335, 407
Logic tree, 31, 32, 34, 36, 44, 48, 74–76, 130, 136, 207
Lognormal distribution, 22, 55, 62, 66, 118, 148, 168, 206, 207, 311, 315, 337, 387, 398

M
Macro-component, 8, 159, 163–167, 175, 179, 180, 182
Macroseismic intensity, 11, 13, 14, 51, 53, 96, 97, 117, 121, 122, 130, 131, 133, 147, 199, 230, 392–393
Macroseismic vulnerability method, 134, 147, 149, 150, 407
Markov chain, 32
Masonry buildings
  confined, 112
  mixed masonry-RC buildings, 112
  with RC framed structures, 112
  reinforced, 100, 112
  traditional, 117
  unreinforced, 22, 80, 84, 112–114
Matrix-based system reliability (MBSR), 56
Medical gas, 9, 361, 368–371, 373
Metering/pressure reduction stations (M/R stations), 190, 191
Micro-component, 8, 159, 163–167, 172, 175, 178–184
Mohr-Coulomb model, 312
Moment-curvature analysis, 284
Monte-Carlo, 31, 64, 87, 128, 204, 263, 276, 305, 376, 381
Monumental structures, 122
Multi degree of freedom, 64, 119, 262

N
Non-linear
  dynamic analysis, 87, 265–266, 268, 270, 280, 338, 339
  simplified analysis, 116
  spectral displacements, 264
  static analysis, 53, 87, 119–120, 264–265, 275
  structural response, 265
Non-structural elements, 9, 14, 33, 39, 100, 113, 117, 122, 360, 361, 363–369, 378

P
PBVA. *See* Performance Based Vulnerability Assessment (PBVA)
Peak ground acceleration (PGA), 2, 11, 14, 15, 17, 21, 33, 51, 53, 57, 61, 62, 64, 65, 76–79, 82, 83, 97, 117, 120–122, 126, 127, 131–133, 148, 150, 165, 168, 169, 173–178, 180, 181, 193, 199, 200, 204, 205, 229, 230, 233, 234, 236–238, 240–244, 249, 251, 252, 254, 261, 262, 264, 266–268, 275, 280, 283, 285–287, 301, 304–308, 311, 313–315, 318–320, 323, 337–342, 346, 347, 349, 350, 353, 377, 392–397
Peak ground strain (PGS), 199, 205, 230
Peak ground velocity (PGV), 2, 11, 15, 51, 61, 97, 121, 193, 197, 199, 204, 205, 207–210, 222, 229, 230, 232, 233, 245–248, 252, 261, 262, 267, 268, 305, 307, 386, 392–393, 396
Performance-based assessment/design, 54, 340
Performance Based Vulnerability Assessment (PBVA), 56–57
Performance indicators (PI), 10, 23, 117, 341–343, 394
Performance point, 16, 17, 53, 54
Permanent ground deformation (PGD), 6, 11, 12, 23, 61, 121, 122, 188, 193–194, 197, 199, 205, 207, 211, 216, 221, 222, 224, 227–230, 232, 233, 242–244, 246–248, 252, 262, 301, 303–305, 307–310, 317, 320, 323, 328–330, 336, 338–342, 345, 347, 349, 350, 352
PGA. *See* Peak ground acceleration (PGA)
PGS. *See* Peak ground strain (PGS)
PGV. *See* Peak ground velocity (PGV)
Piers, 9, 10, 57, 122, 135–137, 139–141, 143, 145–147, 260–263, 265, 266, 268–270, 273–276, 278, 280–292, 329, 331, 333, 334, 345, 410
Pipelines/pipes
  brittle, 188, 204, 205, 208, 216, 244, 247
  buried, 25, 188, 189, 193–194, 196–199, 205, 209, 216, 222, 223, 227, 228, 230, 331
  cast-iron, 204, 205, 209, 225, 227, 228, 248, 249
  ductile, 188, 189, 205, 207–209, 216, 244, 247–249
  flexible, 204, 225, 244
  gas, 7, 25, 189, 203, 207, 208, 210, 212, 227, 228, 246, 409
  PVC, 189, 190, 204, 205, 207, 210, 211, 225, 244, 247–249
  steel, 188, 189, 193, 194, 225
  transmission, 189
  waste-water, 229, 230, 255
  water, 228–230, 247
  welded-steel, 190, 194, 205, 207, 210, 211, 216
Plant
  generation, 8, 163, 164, 166, 168–170, 172, 179, 182, 409

processing, 190–192, 196–198, 200, 202, 207, 213–216
pumping, 8, 13, 207, 214, 215, 250
treatment, 8, 13, 222–228, 230–234, 236–239, 249–253
Plastic hinge, 15, 285, 332
PLAXIS, 314, 317, 320
Poisson distribution, 200
Port infrastructures, 330, 335, 336, 340–341, 347–348
Prototype building, 55, 144, 145
Pumping stations, 8, 9, 13, 192, 196, 217, 222–227, 230–233, 237–241, 252
Pushover curve, 119, 143, 265
Push over static analysis (POSA), 57

R
Railway track, 302, 303, 309–310, 323, 324, 411
Reduction groups, 191–192, 215, 216
Reinforced concrete (RC)
members, 44
structures, 100, 362, 363, 407
Repair costs, 2, 9, 37, 38, 55, 117, 201, 259, 270, 302, 308, 327
Repair rate, 23, 199, 200, 203, 208–212, 222, 231, 232, 244, 245, 247, 248
Response spectrum
elastic, 268, 393
inelastic, 15
Restoration, 10, 226, 231, 235, 237, 240, 250, 251, 254, 255, 264, 271, 272, 337
Risk, 1–7, 10–12, 14, 16, 19, 21, 30–32, 34–37, 40–41, 47, 48, 52, 54–57, 60, 65, 67, 69, 73, 84, 95, 105, 106, 115–118, 120–122, 126, 129, 134, 137, 147, 169, 173, 174, 176–178, 180, 181, 259, 260, 278, 293, 300, 304, 327, 338, 350, 362, 382–383, 385, 386, 388, 392, 399, 403–407, 409
Road pavements, 9, 301–303, 305, 308–310, 323, 324, 411
Roads, 4, 7, 9, 10, 14, 25, 56, 229, 259–293, 300–302, 304, 305, 307–309, 319, 321–324, 327, 332, 360, 410, 411
Rotation, 41, 139, 145, 194, 195, 228, 268–270, 283, 285, 286, 330, 344

S
Safety factor, 283
Sampling, 19, 29, 36, 38, 43, 60, 63, 64, 73, 87, 88, 106, 168, 404
SCADA. *See* Supervisory control and data acquisition (SCADA)
Seismic
assessment, 54, 359
codes, 16, 88, 100, 115, 126, 207, 275, 329, 336, 410
design, 7, 9, 54, 108, 116, 223, 225, 233–235, 240, 243, 249, 250, 252, 254, 261, 263–265, 281, 283, 284, 288, 291, 336, 337, 341, 349, 365, 405
hazard, 1, 3, 6, 31, 32, 34, 47, 48, 52, 57, 68, 115, 272, 280, 300, 378
joint, 369
provisions, 287
retrofit, 263
risk, 1–4, 6, 7, 10, 47, 48, 52, 55, 56, 60, 65, 69, 84, 95, 106, 120, 122, 126, 134, 259, 327, 338, 382–383, 385, 388, 399, 403, 406
Sensitivity, 79, 81, 84, 273, 276, 293
Serviceability state, 23, 231, 232, 336, 340, 341, 344
Shear
modulus, 137, 286, 314
strain, 283, 314
stress, 366
Short-circuit, 159, 164, 182
Single degree of freedom, 64, 79, 119, 264
Site
amplification, 122, 395
effects, 14, 20, 65, 121
Slope, 9, 56, 223, 300–305, 307–310, 323, 324, 411
Soil
alluvial, 25, 227, 301, 302, 306, 307, 311, 323
liquefaction, 227, 247, 280, 302, 330
profile, 19, 311, 312, 314, 316, 317, 323, 394
Soil-structure interaction (SSI), 14, 19, 20, 274, 336–338, 410
Spectra
elastic demand, 54
inelastic response spectra, 15
nonlinear displacements, 264
uniform hazard displacement, 86
Spectral acceleration, 2, 16, 21, 33, 51, 61, 65, 97, 119, 127, 136, 139, 165, 229, 266, 268, 393–397
Spectrum
analysis, 284, 285
matching, 313, 316

SSI. *See* Soil-structure interaction (SSI)
SSWP. *See* Strong spandrels weak piers (SSWP)
Steel, 44, 59, 63, 66, 99, 114, 115, 136, 188–191, 193–195, 204–206, 210–213, 217, 223, 225, 227, 228, 232, 233, 242–244, 248, 249, 253, 262, 269, 273, 276–278, 280, 285, 287, 301, 302, 333, 334, 386, 407
Stiffness, 40, 41, 44, 53, 64, 113, 115, 128, 135, 137, 140, 146, 147, 266, 267, 273, 274, 276, 278, 283–285, 293, 316, 317, 328, 331, 336, 408
Story mechanism, 113, 115
Strains, 193, 194, 197, 199, 205, 212, 227, 229, 230, 232, 269, 283, 286, 314, 316, 317, 343
Strength, 6, 10, 16, 19, 36, 41, 44, 66, 67, 73, 99, 113–115, 128, 135, 137, 139, 140, 145, 189, 223, 225, 267, 269, 273, 280, 285, 293, 312, 328, 331, 332, 344, 362, 365, 378, 408
Stresses, 140, 146, 147, 194, 195, 227, 228, 313, 314, 338, 339, 342, 343, 366
Strong spandrels weak piers (SSWP), 113, 114, 135
Substation, 8, 10, 52, 159, 161–179, 182–184, 408–409
Supervisory control and data acquisition (SCADA), 8, 191, 196, 202, 223–226, 230–232
Surface waves, 197
Switch, 8, 159, 164, 166, 171, 172, 180–182
SYNER-G taxonomy, 7–9, 24, 95, 98–100, 105, 114, 225–226, 263, 300, 302, 386, 406, 407, 412

T
Tanks
  atmospheric, 190, 195, 206
  buried, 348, 349, 352, 373
  chlorination, 237, 251
  grade, 195, 206, 212, 217, 233, 242, 243
  steel, 63, 195, 206, 212, 213, 217, 232, 233, 242–244, 253
  storage, 8, 9, 25, 188, 190, 194–196, 198, 200–202, 206–207, 212–213, 223–225, 230–233, 239–244, 253, 335, 386, 409
  water, 242, 369
  wood, 242–244, 253
Taxonomy, 3, 4, 6–8, 17, 22–24, 77, 78, 95, 98–100, 103, 105, 113–116, 118, 121, 128, 134, 145, 147, 148, 157–165, 260, 263, 328, 358, 386, 389, 390, 405
Time history, 11, 15, 19–21, 35, 53, 265–267, 272–275, 277, 278, 280, 281, 316, 319, 336, 339
Transformer, 8, 158, 159, 164, 166, 168, 171–177, 180–182
Transient ground deformation (TGD), 6, 188, 193, 221, 222
Transient ground strain, 199
Transportation, 3, 4, 6, 23, 52, 56, 59, 188, 259, 300, 327, 330, 335, 336, 343, 347, 403, 411
Tunnels, 4, 7–9, 14, 25, 52, 56, 222–227, 230–234, 248–249, 252, 255, 300–302, 304–307, 311–316, 323, 324, 335, 411

U
Uncertainty
  aleatoric, 30, 31, 362
  epistemic, 6, 12, 30–32, 34, 36, 41–44, 55, 60, 64, 66, 75, 95–109, 127, 128, 148, 206, 272, 362, 398–399, 404, 406
  model, 41–44, 128, 283
  sources of, 10, 12, 17, 19, 35, 61, 64, 65, 67, 68, 72, 88, 126–129, 229, 274–275, 311, 398
  total, 35, 66, 67, 312

V
Vulnerability
  analysis, 128, 141, 178–184, 260
  curve, 69, 130–132, 134, 250, 337, 340, 344, 347
  index, 14, 15, 130, 131, 133, 134, 147

W
Waterfront structures, 25, 328–346, 348, 405, 412
Wave propagation, 193, 194, 197, 199, 208, 210, 216, 222, 227, 228, 230, 242–244, 246, 247, 253, 281
Weak spandrels strong piers (WSSP), 113–115, 135, 136, 139–141, 143, 145

Y
Yielding displacement, 141, 143